(NASA-CR-170188) THE FINITE ANALYTIC METHOD, VOLUME 5 Final Report (Iowa Univ.) 438 p HC A19/MF A01 CSCL 12A

N83-23089

Unclas
G3/64 09751

VOLUME V

THE FINITE ANALYTIC METHOD

by

Ching-Jen Chen

Kuo-San Ho

and

Wu-Sun Cheng

APR 1983
RECEIVED
NASA STI FACILITY
ACCESS DEPT.

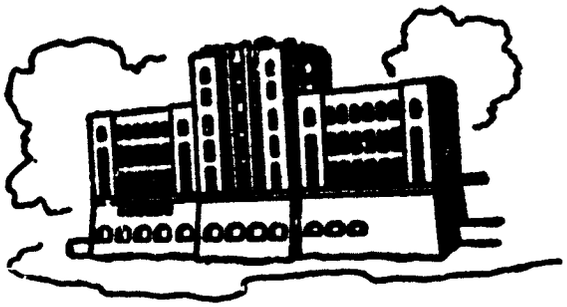

IIHR Report No. 232-V

Iowa Institute of Hydraulic Research
The University of Iowa
Iowa City, Iowa 52242

October 1982

FINAL REPORT
NASA NSG 3305

VOLUME 5

THE FINITE ANALYTIC METHOD

BY

CHING-JEN CHEN

KUO-SAN HO

WU-SUN CHENG

Energy Division
and
Iowa Institute of Hydraulic Research

THE UNIVERSITY OF IOWA
IOWA CITY, IOWA

OCTOBER 1982

THE FINITE ANALYTIC METHOD

CONTENTS OF VOLUMES 1-5

VOLUME 1 PART I : THE FINITE ANALYTIC SOLUTIONS FOR TWO-DIMENSIONAL NAVIER-STOKES EQUATIONS

PART II : THE FINITE ANALYTIC SOLUTIONS FOR LINEAR PARTIAL AND NONLINEAR ORDINARY DIFFERENTIAL EQUATIONS

VOLUME 2 PART I : FINITE ANALYTIC NUMERICAL SOLUTION OF HEAT TRANSFER FOR FLOW PAST A RECTANGULAR CAVITY

PART II : FINITE ANALYTIC NUMERICAL SOLUTIONS FOR STEADY TWO-DIMENSIONAL HEAT TRANSFER AND FLOW IN BENDS

VOLUME 3 PART I : APPLICATION OF FINITE ANALYTIC METHOD TO THE NUMERICAL SOLUTION OF TWO-POINT BOUNDARY VALUE PROBLEMS OF ORDINARY DIFFERENTIAL EQUATIONS

PART II : NUMERICAL SOLUTION OF TWO-DIMENSIONAL POISSON AND LAPLACE EQUATIONS BY FINITE ANALYTIC METHOD

PART III : FINITE ANALYTIC NUMERICAL SOLUTION OF TWO-DIMENSIONAL NAVIER-STOKES EQUATIONS IN PRIMITIVE VARIABLES

VOLUME 4 DEVELOPMENT OF FINITE ANALYTIC METHOD FOR UNSTEADY THREE DIMENSIONAL NAVIER-STOKES EQUATIONS

VOLUME 5 PART I : FINITE ANALYTIC METHOD FOR MOMENTUM AND HEAT TRANSFER PROBLEMS USING CARTESIAN AND BOUNDARY-FITTED COORDINATES

PART II : FINITE ANALYTIC NUMERICAL SOLUTION FOR TWO-DIMENSIONAL INCOMPRESSIBLE FLOWS OVER AN ARBITRARY BODY SHAPE

THE FINITE ANALYTIC METHOD (V)

PART I

FINITE ANALYTIC METHOD FOR MOMENTUM AND HEAT TRANSFER PROBLEMS USING CARTESIAN AND BOUNDARY-FITTED COORDINATES

PART II

FINITE ANALYTIC NUMERICAL SOLUTION FOR TWO-DIMENSIONAL INCOMPRESSIBLE FLOWS OVER AN ARBITRARY BODY SHAPE

ORIGINAL PAGE IS
OF POOR QUALITY

PREFACE

The Finite Analytic Method

This monograph contains the fundamental development of the new numerical method called the "Finite Analytic" method. The finite analytic method differs from the finite difference method and the finite element method. The basic idea of the finite analytic method is the incorporation of local analytic solutions in the numerical solution of linear or nonlinear partial differential equations. In the finite analytic method, the total problem is subdivided into a number of small elements. The local analytic solution is obtained for the small element in which the governing equation, if nonlinear, is linearized. The local analytic solutions are then expressed in algebraic form and are overlapped to cover the entire region of the problem. The assembly of these local analytic solutions, which still preserves the overall nonlinearity of the governing equation, results in a system of linear algebraic equations. The system of algebraic equations is then solved to provide the numerical solutions of the total problem.

Unlike the finite difference method, the finite analytic method does not tamper with the differentials or the derivatives of the governing equation, nor does the analytic method need the shape function which is made to satisfy the integral form of the governing equation, as in the finite element method. The finite analytic solution obtained from the finite analytic method is differentiable. As a result, the derivative of the solution obtained analytically is much more reliable. In this monograph the finite analytic solution is shown to be stable, even when the highest derivative term of the partial differential equation is multiplied by a small factor, such as one over Reynolds number. It is also shown that the finite analytic solution for Navier-Stokes equations at high Reynolds numbers automatically provides a gradual shift of the upwinding effect. Therefore the finite analytic solution accurately simulates the effect of convection and eliminates the false numerical diffusion that would occur in the upwinding difference or unidirection difference used in the finite difference or the finite element methods. The computational time for the finite anayltic solution is shown to be about equal to that of the finite difference method. In certain cases, due to the stability of the system of algebraic equations derived in the finite analyitc method, the overall computational time can be even less. The finite analytic solution derived in

ORIGINAL PAGE IS
OF POOR QUALITY

the present analytic mehtod is in its most elementary form in terms of accuracy. But it has already been shown to be sufficient for the problems under consideration. Further accurate finite analytic formulae can be derived and are indicated in the monograph.

The finite anlytic method was developed in early 1977, when Dr. Peter Li was then a graduate student working on his doctoral dissertation with me. He had been having difficulty in obtaining convergence of a system of finite difference algebraic equations derived from the Navier-Stokes equations for two-dimensional turbulent flow with a second-order turbulent model. I conceived the finite analytic method one night and solved the simple two-dimensional Laplace equation. Li then carried the finite analytic method to the unsteady diffusion equation and nonlinear ordinary differential equations and compltted his Ph.D. dissertation in 1978. In 1982, Dr. Kuo-San Ho developed the finite analytic method by solving momentum and heat transfer problems with complex geometries. This bound volume contains the research results of Dr. Ho and myself, extended further by Mr. Wu-Sun Cheng to the problem of vortex shedding behind an arbitrary obstacle.

ORIGINAL PAGE IS
OF POOR QUALITY

ACKNOWLEDGEMENT

I would like to acknowledge Dr. Kuo-San Ho and Mr. W. S. Cheng for tak.ng the finite analytic method as their doctoral dissertation and thesis. Without them, the finite analytic method could not have been developed and understood as it is today.

I would also like to thank my colleagues, Professors V. C. Patel, David C. Chou, T. F. Smith, Allen Chwang, and K. Atkinson, for their encouragement and criticisms of the method. I would also like to thank Drs. William D. Mcnally, Peter M. Sockol, Gary Johnson, and J. J. Adamczyk of NASA Lewis Center for taking a keen interest in and supporting the continuation of the development of the finite analytic method. My thanks also go to Dr. Melvyn Ciment, of the Applied Mathematical Division, and Dr. Ronald W. Davis, of the Fluid Engineering Division, of the National Bureau of Standards, for their in-deep discussion of the method and to Drs. Oscar P. Manley of the U. S. Department of Energy and P.C. Lu of the University of Nebraska for their discussion and encouragement. This work is, in part, supported by NASA Grant No. N.S.G. 3305 and U. S. Department of Energy Grant No. DE-AC02-79ER-10515.A000. The support of the University of Iowa Computer Center and Division of Energy Engineering, The University of Iowa, is also acknowledged.

Ching-Jen Chen
Professor and Senior Research Scientist
Division of Energy Engineering and Iowa Institute of Hydraulic Research
The University of Iowa
Iowa City, Iowa 52240
(319) 353-4473

October 1982

PART I

Finite Analytic Method For Momentum And Heat Transfer Problems Using Cartesian And Boundary-Fitted Coordinates

ABSTRACT

A numerical scheme, called the "Finite Analytic Method" is used to solve the two-dimensional incompressible momentum and energy equations. The basic idea of the finite anytic (FA) solutions is the incorporation of local analytic solutions in the numerical solutions of linear or nonlinear partial differential equations. In the FA method, the flow region is subdivided into a number of small rectangular elements, in which the governing equation is locally linearized . Hence, by specifing suitable boundary and initial conditions for each element, the local analytic solution for an element can be obtained. When the local analytic solution is evaluated at a given nodal point, it results in a system of linear algebraic equations which are solved iteratively to provide the numerical solution of the total problem for the flow region.

In order to solve more practical engineering problems, an FA method capable of solving flow and heat transfer problems involving complex geometries is developed. In this study, the boundary-fitted coordinate transformation is incorpo ted into the FA mrthod.

The A method is employed to solve several flow and heat transfer problems. The problem of "convective heat

ORIGINAL PAGE IS
OF POOR QUALITY

transfer in a cavity" is studied with the Reynolds number ranging from 100 to 2,000 and the Peclet number ranging from 10 to 20,000 by using an equal size grid in the physical plane. The "separation of channel flow" is examined at different Reynolds numbers over the range 25 to 229 with both equal and unequal size grids in the physical plane. For problems with complex geometries, "flow past an airfoil" and "convective heat transfer in tube bundles", both are solved with the FA method for the boundary-fitted coordinate system . The FA results are compared with the experimental data, the theoretical calculation, and predictions by other numerical schemes. In all these problems, the FA solutions converge rapidly and are stable, and accurate.

TABLE OF CONTENTS

Page

LIST OF FIGURES vi

LIST OF SYMBOLS ix

CHAPTER

I. INTRODUCTION 1

II. PRINCIPLE OF THE FINITE ANALYTIC METHOD 10

III. BOUNDARY-FITTED CURVILINEAR COORDINATE SYSTEM . . 14

3.1 Introduction 14
3.2 The Basic Idea Of Boundary-Fitted Coordinate System 15
3.3 Boundary-Fitted Coordinate System For Two-Dimensional Problem 19
3.4 Numerical Solution And Examples 23

IV. FINITE ANALYTIC NUMERICAL SOLUTION 27

4.1 Formulation Of The Problems 27
4.2 Initial And Boundary Conditions 30
4.3 Finite Analytic Solutions 34
4.3.1 Vorticity Function 34
4.3.2 Stream Function 43
4.3.3 Temperature Function 45
4.4 Computational Procedure 46
4.4.1 Computational Procedures Of The $\psi - \omega$ Equation 47
4.4.2 Computational Procedures Of The θ Equation 49
4.4.3 Remarks On Time Marching And Iterative Procedures 49

V. CONVECTIVE HEAT TRANSFER IN CAVITY 53

5.1 General Remarks 53
5.2 Formultion Of Problem 55
5.3 FA Solution Of The Cavity Flow 57

PRECEDING PAGE BLANK NOT FILMED

I, II

Page

5.4 Stream Function And Vorticity Distribution 59
5.5 Temperature Distribution And Heat Transfer 61
5.6 Conclusion 66

VI. SEPARATION OF CHANNEL FLOW 68

6.1 General Remarks 68
6.2 Formulation of Problem 71
6.3 FA Solution 74
6.4 Results And Discussion 76
6.5 Special Case Of Channel Flow 80
6.5.1 Boundary Conditions 80
6.5.2 Recovery Of Pressure 83
6.5.3 Results And Discussion 83
6.6 Conclusion 87

VII. FLOW PAST A SINGLE AIRFOIL 88

7.1 General Remarks 88
7.2 Formulation Of The Potential Flow 89
7.3 Implementation Of Kutta Condition 92
7.4 FA Numerical Solution 97
7.5 Numerical Results And Discussion 98

VIII. HEAT TRANSFER PROBLEM OF TUBE BUNDLES 101

8.1 General Remarks 101
8.2 Governing Equation 105
8.3 Initial And Boundary Conditions 107
8.4 FA Solutions Of Tube Bundles Problem . 115
8.5 Results And Discussion 117
8.5.1 Conversion Of The Reynolds Numbers 117
8.5.2 Stream Function And Vorticity Distribution 121
8.5.3 Distribution Of Temperature And Heat Transfer 125
8.6 Conclusions 132

IX. CONCLUSION AND RECOMMENDATION 134

REFERENCES 139

APPENDIX A. RELATIONS BETWEEN PHYSICAL AND TRANSFORMED PLANES 144

Page

APPENDIX B. FA FORMULATION OF UNSTEADY 2-D CONVECTIVE EQUATION 148

APPENDIX C. COMPUTER PROGRAMS 164

LIST OF FIGURES

Figure		page
1.	Domain and local element for finite analytic formulations of unsteady two-dimensional convective transport equation	201
2.	Coordinate transformation	202
3.	Effect of source term in one-dimensional Poisson equation	203
4.	Infinite rows of tubes	204
5.	Coordinate systems of the infinite rows of tubes	205
6.	NACA-0018 and Karmann-Trefftz airfoils	208
7.	Contracted coordinate system -- NACA-0018 airfoil	211
8.	Contracted coordinate system -- Karmann-Trefftz airfoil	212
9.	Coordinates and boundary conditions of cavity flow	213
10.	Stream function of cavity flow	214
11.	Vorticity distribution of cavity flow	215
12.	Temperature distribution for Re = 100	216
13.	Temperature distribution for Re = 1000	217
14.	Temperature distribution for Re = 2000	218
15.	Local Nusselt number of moving wall for Re = 100	219
16.	Local Nusselt number of moving wall for Re = 1000	219
17.	Local Nusselt number of moving wall for Re = 2000	220
18.	Mean Nusselt number of moving wall	220
19.	Definition sketch of channel flow geometries	221

ORIGINAL PAGE IS
OF POOR QUALITY

20. Coordinate and description of flow over a step . .222

21. Stream function of laminar channel flow over a step, numerical values are of dimensionless stream function ψ/ψ_0 222

22. Vorticity distribution of laminar flow over a step 224

23. Variation of recirculation zone length with Reynolds number (Re) -- FA and measured 226

24. Variation of recirculation zone length with Reynolds number (Re) -- FA and FD 227

25. Variation of recirculation zone length with Reynolds number (Re) -- FA and FE 228

26. Comparison of measured and predicted total mass flow rate within the recirculation region 229

27. Similarity in the recirculation region flow -- path of the separation streamline and position of vortex center 230

28. Comparison of measured and predicted velocity profiles for laminar channel flow over a single step at Re = 125 231

29. Coordinate and description of suddenly expanded channel flow 232

30. Stream function contours of channel flow $\Delta\psi = 0.1$ .233

31. Vorticity contours of channel flow for $Re_s = 200$, $\Delta\omega = 1$ 235

32. Velocity profiles of channel flow for $Re_s = 200$ at different locations, h = k = 0.2 (81x11) 236

33. Pressure distribution of channel flow for $Re_s = 200$, $\Delta P = 0.01$, h=k= 0.2 237

34. Velocity extrapolation at airfoil trailing edge . .238

35. Stream function of uniform potential flow over NACA-0018 airfoil, (80x25) 239

36. Stream function of uniform potential flow over Karmann-Trefftz airfoil, (68x25) 242

37. Pressure curves of NACA-0018 245

38. Lifting curves of NACA-0018, Karmann-Trefftz and thin wing theory 246

39. Possible choices of grid for finite difference studies of tube banks 247

40. Field transformation of tube bundles flow problem . 248

41. Field transformation of tube bundles for heat transfer problem 249

42. Stream function of tube bundles flow 250

43. Vorticity distribution of tube bundles flow . . . 252

44. Comparison of stream function for $Re_m = 50$ 254

45. Comparison of stream function for $Re_m = 44.7$ . . . 255

46. Length of separation zone behind a tube in tube banks 255

47. Temperature distribution for $Re_m = 16$ 256

48. Temperature distribution for $Re_m = 160$ 257

49. Temperature distribution for $Re_m = 320$ 258

50. Local Nusselt number of the heated tube in tube banks for $Re_m = 16$ 259

51. Local Nusselt number of the heated tube in tube banks for $Re_m = 160$ 260

52. Local Nusselt number of the heated tube in tube banks for $Re_m = 320$ 261

53. Comparison of local Nusselt number of the heated tube in tube banks and in uniform flow 262

LIST OF SYMBOLS

Alphabetical Symbols

A, B	Linearlized convection coefficients in convective transport equation
A_n	Fourier series coefficients in FA formulations
C_n, C'_n	FA coefficients for unsteady convective transport equations based on nonuniform grid spacing local elements (n = EC, NE, ...)
F	Source function (inhomogeneous term) in convective transport equation
f	A constant in a small local element to approximate the source function F
g	A constant in a local element to approximate the source function, higher order correction term and unsteady term
h, k	grid sizes in x and y direction respectively
H, L	Reference length scale
m, n	Indices in series summation
P	Dimensionless pressure
Pr	Prandtl number
R	Dimensionless parameter in convective transport equation
Re	Reynolds number
t	Dimensionless time
u, v	Dimensionless velocity components

ORIGINAL PAGE IS
OF POOR QUALITY

U_0	Reference velocity scale
T	Temperature
x, y	Dimensionless Cartesian coordinate system

Greek Symbols

$\alpha, \beta, \gamma, \sigma, \tau$	Transformed coefficients between Cartesian and transformed coordinate systems
λ_m, λ'_m	Eigenvalues
μ_m, μ'_m	Eigenvalues
ϕ	Indenpendent variable of convective transport equations
$\tilde{\phi}$	Independent variable of homogeneous convective transport equations
ψ	Streamfunction
ψ_x, ψ_y	Components of vector potential $\vec{\psi}$
ξ, η	Dimensionless transformed coordinate system
∇	Gradient
∇^2	Laplacian
∇	Divergence
ρ	density
ν	Kinematic viscosity
θ	Dimensionles temperature
Δ	Difference
π	3.141592654
γ	reluxation factor

ORIGINAL PAGE IS
OF POOR QUALITY

Subscripts

E, W, N, S	East, West, North, South boundaries
EC	East Center (same to the WC, SE, etc.)
P	Center node for two-dimensional local elements
i, j	Nodal point location in the flow domain
r, R	Reference scale
w	Reference scale on the wall
x, y, t	First derivatives with respect to x, y and t
xx, yy,	Second derivatives with respect to x and y

Superscripts

k	k^{th} time step
E, W, N, S	East, West, North, South boundaries

Abbreviations

FA	Finite Analytic
FD	Finite Difference
FE	Finite Element
2D	Two-dimensional

CHAPTER I

INTRODUCTION

In many practical engineering problems, the best reliable information often comes from actual measurements with appropriate instruments. The on site measurement is not a prediction since the equipment or the facility is already built. Although a full scale model can be constructed before expensive equipment is built, this approach is still expensive and time consuming. Therefore, it is more economical and convenient to simulate the problem in a suitable scale which, in many engineering problems, is a small scale. However, the reduced scale approach often has difficulty in simulating the features of the full scale equipment. For example, radiation, combustion and boiling phenomena are difficult to simulate in a small scale. Measurement in a model simulation sometimes has difficulty also due to (1) smallness of the model, (2) instrumental restriction, and (3) disturbance created by insertion of instruments.

Due to difficulties in the experimental study the theoretical approach, when the phenomena can be simulated by a mathematical model, is an attractive alternative to an

experiment. For example, the Navier-Stokes equations are known to simulate flows of a Newtonian fluid. Unfortunately, there are only a handful of exact solutions of the Navier-Stokes equations due to the existence of the non-linearity and the coupling of many variables through the continuity and momentum equations. For such partial differential equations which cannot be solved analytically, numerical methods are often employed. Many numerical methods for solving partial differential equations bear the following similarities. First, the computational region is subdivided into a number of small elements and grid points, so that the boundary and/or initial conditions are replaced by the discretized values at a finite number of grid points or elements. Secondly, an algebraic equation that approximates the partial differential equation is derived with proper approximation function for dependent variables between nodal points in the local element. Finally, the resulting system of algebraic equation is solved with given boundary and/or initial conditions to obtain the numerical solutions for all of the grid points.

Among the available numerical methods, two of the most widely used methods are the finite difference (FD) and the finite element (FE) methods. In the FD method either forward, backward, or central difference formula is used to replace derivatives in the governing equations. Of these

three different formulae, the central difference formula has a better accuracy and is preferred over the other two. However, it cannot be used near the boundary as an extra node has to be located outside the boundary of the flow. It is also found that the use of the central difference formula for the convective transport equation for high Reynolds number flows may create numerical instability [1] in solving the system of finite difference equations. This difficulty is partly overcome by introducing the upwind scheme which shifts the difference scheme toward the upstream. If the upwind difference scheme is used improperly, it produces large numerical errors which are normally termed as numerical diffusion. Also the FD upwind scheme must be made judiciously at a given Reynolds number.

Another numerical method widely used is the finite element method. This method considers an approximation function which is often a polynomial of low degree in a small element of the flow which in general cannot satisfy the governing equation exactly. Therefore, the approximation functions are made to satisfy the governing equation in an integral sense by either a weighted residue method or a variational principle. The FE method also results in algebraic equations which are then solved. This method at present is more widely used in solid mechanics problems but when applied to fluid mechanics problems some

difficulties surface. Problems of accuracy and stability experienced by the FD method are also experienced by the FE method, particularly when the flow at high Reynolds number is considered.

In order to improve the FD and FE numerical methods, the finite analytic (FA) method was conceived. The FA method was first developed by Chen and Li [2] for the Laplace and heat diffusion equations. Later Chen et al. [3,4] extended the method to the Navier-Stokes equations. Unlike the FD or the FE method, in the FA formulation the algebraic equation which approximates the partial differential equation in an element is obtained from the analytic solution in each local element. Details of the principle and procedures in obtaining the FA solution are presented in Chapter II.

In earlier development of the FA method, the local analytic solutions for both steady and unsteady two-dimensional Navier-Stokes equations in a small element were obtained by Chen et al. [3,4] by locally linearizing the governing equation. They obtained the analytic solution for an element by adopting a second-order polynomial to approximate the boundary condition for all boundaries surrounding the local element. When the local analytic solution is evaluated at a given nodal point, a 9-point FA algebraic equation is obtained. The FA solution exhibits a

gradual and proper skew upwind shift of bounding nodal influence on the interior nodal value. This FA skewed upwind differs from the upwind scheme given by the FD and FE methods [5,6] since the skew upwind shift is automatic and analytic. The FA solution given by Chen et al. [7,8,9] was shown to be stable and accurate. Recently, Chen and Chen [10] in an attempt to improve the FA method employed linear and exponential functions as the boundary function along the boundaries of a local element. The reason for the improvement is because the linear and exponential functions specified along the boundary of an element also satisfy the convective transport equation considered. The FA coefficients obtained thus exhibit the correct asymptotic behavior at high Reynolds numbers and Peclet numbers. In addition, the computational time is also greatly reduced and thus the FA method is considered a viable numerical tool for solving practical engineering problems. However, as the numerical methods and computer technology advance the engineering problems that demand numerical solutions also become more complex. Therefore, in the present study the FA method capable of solving flow and heat transfer problems involving complex geometries is developed. In order to achieve this goal, the boundary-fitted coordinate transformation [11] is incorporated into the FA solution in the present investigation. More discussion on the boundary-fitted coordinate transformation is given in Chapter III.

The main purpose of this study is thus to extend and to apply the FA method to laminar two-dimensional flows and heat transfer problems in complex geometries. The detailed objectives are

1. to develop a computer program for grid generation based on the boundary-fitted coordinate transformation.
2. to transform the governing equation from the physical plane into the transformed plane and then derive the FA solution for the governing equation in the transformed plane.
3. to obtain FA solutions for internal flows with equal or unequal grid sizes in the physical plane.
4. to obtain FA solutions for external flows with complex geometries.

In the present study, the Navier-Stokes equations in the stream function-vorticity formulation are used. In such a formulation the boundary vorticities are unknown and must be solved as a part of the problem. The difficulties of specifying vorticity boundaries in this formulation is offsetting the assurance of the conservation of mass in the numerical solution and elimination of the pressure variable. Although some authors prefer to use the velocity-pressure formulation in which the difficulties of the unknown boundary vorticities can be avoided, it requires the

solution of the velocity and pressure variables simultaneously and needs careful treatment in satisfying the mass conservation [1].

In Chapter II, the principle of the FA method is briefly outlined. Since the FA method is employed to solve the given problem with complex geometry, in Chapter III the idea of boundary-fitted coordinate system is presented and the boundary-fitted transformation is obtained. Details of the relations of the coordinates between the physical plane and the transformed plane are given in Appendix A. Chapter III also presents the generation of three boundary-fitted coordinate systems to be used in later chapters.

In Chapter IV, the FA solution for unsteady two-dimensional convective transport equations in the transformed plane is derived. Details of the derivation are given in the Appendix B. A linerization scheme associated with the higher order correction of convective terms is outlined. The relation between the unsteady time marching and the steady iterative procedure is also discussed.

The FA numerical solution of steady and unsteady two-dimensional flow and heat transfer problems is given in the ensuing chapters. The survey of the problem considered is presented separately at the begining of each chapter.

In Chapter V, the problem of convective heat transfer in a cavity is investigated. The temperature distribution

and the heat transfer are studied with the Reynolds number ranging from 100 to 2000 and the Peclet number ranging from 10 to 20,000 by using equal-size grids in the physical plane.

In Chapter VI, the separation of channel flow is examined at several different Reynolds numbers over the range of 25 to 229. In this problem, the FA solutions are evaluated with both equal and unequal grid sizes in the physical plane. These FA results are compared with reported experimental measurments and the numerical results by the FD and FE methods. The computer program is appended in Appendix C-2.

In chapter VII, flow passing a single airfoil is solved with the FA method for the boundary-fitted coordinate systems. The FA solutions of these potential flow problems are compared with the experimental data and the theoretical calculations. The computer program is appended in Appendix C-3.

The most complex problem considered in the present investigation is contained in Chapter VIII. The FA method with the boundary-fitted coordinate system is employed to solve the viscous flow through tube bundles and heat transfer between a heated tube and the surrounding fluid. The FA solutions for the streamline pattern, vorticity distribution, temperature distribution and heat transfer of

a tube are presented for different Reynolds numbers. For the given configuration of the tube bundles, the critical Reynolds number for the predominantly laminar flow is predicted. The FA results using the boundary-fitted coordinate system are compared with the experimental and empirical results and also with the numerical predictions obtained by the FD method with different grid systems. The computer program is appended in Appendex C-5 and C-6.

The last chapter summarizes the key findings and conclusions and suggests future studies.

ORIGINAL PAGE IS
OF POOR QUALITY

CHAPTER II

PRINCIPLE OF THE FINITE ANALYTIC METHOD

The basic idea of the finite analytic (FA) method is the incorporation of analytic solutions in the numerical solutions of partial differential equations (PDE). The FA method, unlike the finite difference (FD) and the finite element (FE) method, is based on the composition of analytic solutions obtained in the small elements which make up the total problem.

To illustrate briefly the basic principles [2] of the FA method an elliptic PDE, $L(\phi)=g$, is considered, where L can be a linear or nonlinear partial differential operator and g is the inhomogeneous term depending on the independent variables, x, y and t. If the boundary and initial conditions of the problem are properly specified, then the PDE is well posed. In order to solve the problem with the FA method, the whole domain of the problem is subdivided into a number of elements where analytic solutions can be obtained. A typical element of size 2h*2k in a time interval $\Delta t=t^k-t^{k-1}$ is shown in Fig. (1) where the center point, P(i,j), at a given time t^k or t^{k-1} is surrounded by eight neighboring nodal points, EC(east center), WC(west center), SC(south

ORIGINAL PAGE IS
OF POOR QUALITY

center), NC(north center), NE(northeast), NW(northwest), SE(southeast) and SW(southwest), which correspond to points (i+1,j), (i-1,j), (i,j-1), (i,j+1), (i+1,j+1), (i-1,j+1), (i+1,j-1) and (i-1,j-1) respectively in general indexing. Once the whole domain is subdivided into small elements, an analytic solution for the PDE in each element may be obtained. In the case when the PDE is nonlinear, the nonlinear equation may be locally linearized in the small element. In this fashion the overall nonlinear effect can still be approximately preserved by the assembly of local analytic solutions which constitute the numerical solution of the PDE over the whole domain. The problem is now reduced into one with many finite elements where analytic solutions can be obtained.

Let the linear or linearized governing equation in an element be $L(\phi)=g$. If in the small element the inhomogeneous term g is considered to be a constant then a simple analytic solution can be obtained at t^k when proper boundary and initial conditions are specified, or

$$\phi = f(f_N, f_S, f_E, f_W, h, k, x, y, t, g) \qquad (2\text{-}1)$$

where the f_N, f_S, f_E and f_W are respectively the northern, southern, eastern and western boundary conditions of the element. The boundary conditions f_N and f_S of the element

ORIGINAL PAGE IS
OF POOR QUALITY

are functions of x and t while f_E and f_W are functions of y and t. The boundary functions f_N, f_S, f_E and f_W for numerical purpose may be approximately expressed in the implicit formulation in terms of the nodal values along the boundaries of the element at time t^k. For example

$$f_N = f(\phi^k_{NE}, \phi^k_{NC}, \phi^k_{NW}, x) \tag{2-2}$$

where ϕ_{NE}, ϕ_{NC} and ϕ_{NW} are the nodal values of ϕ at nodal points NE, NC and NW at time t^k. Boundary conditions for f_S, f_E and f_W can be similarly expressed. The initial condition at t^{k-1} may be approximately taken to be ϕ^{k-1}_P. With the boundary conditions in equation (2-2) and the initial condition ϕ^{k-1}_P, equation (2-1) becomes

$$\begin{aligned}\phi = f(&\phi^k_{EC}, \phi^k_{WC}, \phi^k_{NC}, \phi^k_{SC}, \phi^k_{NE}, \phi^k_{NW}, \phi^k_{SW}, \\ &\phi^k_{SE}, \phi^{k-1}_P, h, k, x, y, t, g)\end{aligned} \tag{2-3}$$

Evaluating equation(2-3) at point P of time t^k in the element, one has the FA formula for the element as

$$\begin{aligned}\phi^k_P = {} & C_{EC}\phi^k_{EC} + C_{WC}\phi^k_{WC} + C_{NC}\phi^k_{NC} + \text{-----} + \\ & C_{SW}\phi^k_{SW} + C_{SE}\phi^k_{SE} + C_P g_P + C_I \phi^{k-1}_P\end{aligned} \tag{2-4}$$

Here the C's are known analytic coefficients representing the weightage of the boundary and initial nodal values , etc., ϕ^{k-1}_P and the inhomogeneous term g_P for the point P.

In general, equation (2-4) may be derived for each unknown nodal point (i,j) in the problem. For all interior ith and jth points

$$\phi^k(i,j) = C_{EC}(i,j,)\phi^k_{EC} + C_{WC}(i,j)\phi^k_{WC} + ----- +$$

$$C_p(i,j)g_p(i,j) + C_I(i,j)\phi^{k-1}_p(i,j) \qquad (2\text{-}5)$$

The system of algebraic equations, equation (2-5) thus is generated for all elements. It can be solved with the given boundary and initial conditions to provide the FA numerical solution of the given problem.

This is the principle of the FA method. The FA method can be applied to any partial differential equation such as the Navier-Stokes equations for laminar or turbulent flows, or the energy equation. In the present study the FA method is employed to solve the two-dimensional laminar flows and heat transfer problems for both simple and complex geometries.

ORIGINAL PAGE IS
OF POOR QUALITY

CHAPTER III

BOUNDARY-FITTED CURVILINEAR COORDINATE SYSTEM

3.1 Introduction

It is imperative in the numerical solution of partial differential equations that the boundary conditions be represented accurately in the numerical formulation. This is because the region in the immediate vicinity of solid surfaces is generally dominant in determining the characteristics of the fluid flow and energy exchange. The vorticity, shear stress and heat flux in the vicinity of the solid boundaries are directly dependent on the velocity and temperature gradients that prevail in the region near the surface. Accurate vorticity function, shear stress and heat flux can be determined provided that the velocity and temperature profiles are calculated accurately. The problem is acentuated at higher Reynolds numbers where the gradients of dependent variables become more severe. To overcome this difficulty, in the present study the boundary-fitted coordinate transformation is employed and incorporated into the FA method to solve problems involving irregular boundaries.

ORIGINAL PAGE IS
OF POOR QUALITY

3.2 The Basic Idea Of Boundary-Fitted Coordinate System

The boundary-fitted coordinate transformation is a method in which automatic numerical generation of a general curvilinear coordinate system can be made for a given problem. The method described below was first developed and applied to the fluid dynamic problem by Thompson et al. [12]. The basic idea of boundary-fitted coordinate system is most easily explained with an analogy to the cylindrical (or polar) coordinate system. For problems involving two concentric circular boundaries, the cylindrical coordinate system is the obvious choice. The reason for this choice is because a coordinate line, i.e., a line of constant radius, r, coincides with each boundary. Thus, the cylindrical coordinate system is fitted to the circular boundaries. The boundary-fitted system accomplishes precisely this feature regarless of the boundary shape ----- some particular coordinate lines are made to coincide with the arbitrarily shaped boundaries.

In Fig. (2), the curvilinear coordinate, η, is defined to be constant on the inner boundary in the same way that the curvilinear coordinate, r, is defined to be constant on the inner circle in the curvilinear coordinate system. Similarly, η is defined to be another constant of different value on the outer boundary. The other curvilinear

ORIGINAL PAGE IS
OF POOR QUALITY

coordinate, ξ, is defined to vary monotonically over the same range on both inner and outer boundaries, as the curvilinear coordinate, θ, varies from 0 to 2π around both inner and outer circles in cylindrical coordinates. It is noted that the actual values of coordinates, η and ξ, are irrelevant, just in the same way as r and θ may be expressed in different units in cylindrical coordinates. The question now is how to generate the boundary-fitted coordinate system.

Consider the general transformation from the physical plane (x,y) to the transformed plane (ξ,η) as shown in Fig. (2). It is required that Γ_1 map onto Γ_1^* Γ_2 map onto Γ_2^*, Γ_3 map onto Γ_3^* and Γ_4 map onto Γ_4^*. For identification purposes region D is referred as the physical plane, D^* as the transformed plane and Γ_1^* as the body-shaped contour. It is noted that the transformed boundaries (Γ_1^* and Γ_2^*) are made of constant coordinate lines (η-line) in the transformed plane. The contours Γ_3 & Γ_4 which connect the contours Γ_1 and Γ_2 are coincident in the physical plane and thus constitute re-entrant boundaries in the transformed plane. When the values of the coordinates ξ and η are chosen on all the boundaries of a closed field, the remaining work is to define the values in the interior of the transformed field in terms of these boundary values. To achieve this transformation, the elliptic partial differential equations

ORIGINAL PAGE IS
OF POOR QUALITY

with and as dependent variables can be used, since the solutions of

ξ and η from the elliptical PDE are completely defined in the interior of the region by its values on the boundaries of the region. In addition, an obvious condition is to require that the same pair of values (ξ,η) must not occur at more than one point in the field, otherwise the coordinate system is ambiguous. This condition can be met by choosing the elliptical PDE exhibiting extremum principles which require the occurence of extrema for ξ and η on the boundaries of the field.

An appropriate choice of the elliptical PDE for boundary-fitted coordinate system may be a Poisson equation. This can be illustrated with an example of one-dimensional Poisson problem for ξ. Consider a region $0<x<1$ having values at two ends $\xi=0$ and 1 respectively as shown in Fig. (3a). The function ξ in the interior of the region $0<x<1$ is described by the Poisson equation

$$\xi_{xx} = P \ , \qquad (3\text{-}1)$$

with the boundary conditions at two ends

$$\xi = 0 \quad \text{at } x = 0 \ ,$$
$$\xi = 1 \quad \text{at } x = 1 \ . \qquad (3\text{-}2)$$

The source (inhomogeneous) term, P, in equation (3-1) can be a function of dependent variables, but for simplicity it is

ORIGINAL PAGE IS
OF POOR QUALITY

assumed to be constant here. Thus, the analytic solution of equation (3-1) is obtained as

$$\xi = -\frac{p}{2}(x^2-x) + x \ . \qquad (3\text{-}3)$$

Equation (3-3) illustrates how a location in x-domain is transformed into ξ-domain. In order to show the effect of the source term (P) in the Poisson equation (3-1), three special cases, P=0, P=2>0 and P=-2<0 are considered. For the case P=0, equation (3-3) gives a linear relation between ξ and x. Thus, an equally spaced x interval maps into an equally spaced boundary-fitted coordinate. In other words, the corresponding ξ-lines are evenly distributed between two ends 0<x<1 as shown in Fig. (3-b). For the case p=2>0, the analytic solution in equation (3-3) is nonlinear relation, $\xi=x^2$, which causes the slope $d\xi/dx$ near x=1 to steepen as shown in Fig. (3c). This implies that the equally spaced ξ-lines represent unequally spaced interval of x in the physical domain with the x-lines more clusterd toward the boundary, x=1. On the other hand, for the case P=-2<0, the analytic solution in equation (3-3) becomes $\xi=2x-x^2$ which causes the evenly spaced ξ-lines to represent more dense x-lines at the other end x=0 as shown in Fig. (3d). It is seen that in the case of p=-2 the function $\xi=\xi(x)$ gives a one to one correspondence. If the source term P has a value larger

ORIGINAL PAGE IS
OF POOR QUALITY

than 2 or is a polynomial of sufficiently high degree in the range $0 \leq x \leq 1$, it is possible that the function $\xi = \xi(x)$ has an 'S' shaped profile as shown in Fig. (3e). In this situation a constant ξ may correspond to multiple locations of x. Consequently, the one to one correspondence between and x is invalidated. However, if a propery source function P is applied over the range $0 \leq x \leq 1$, the multi-valued relation between ξ and x does not occur as shown in Fig. (3f). Thus, the Poisson equation can be used as a vehicle for transforming the physical coordinate x into the transformed coordinate ξ with the great advantage of contracting more dense grid line of x at a desired location with evenly space ξ lines. This concept can be readily extended to two-dimensional and three-dimensional cases.

3.3 Boundary-Fitted Coordinate System For Two-Dimensional Problem

In view of the example given above, the Poisson equation may be considered as the coordinate generating equation. Therefore, let $\xi(x,y)$ and $\eta(x,y)$ be the coordinate system on the transformed plane as shown in Fig. (2). They are governed by

$$\xi_{xx} + \xi_{yy} = P(\xi,\eta) \quad , \tag{3-4a}$$

$$\eta_{xx} + \eta_{yy} = Q(\xi,\eta) \quad , \tag{3-4b}$$

with the boundary conditions

ORIGINAL PAGE IS
OF POOR QUALITY

$$\begin{aligned} \eta &= \eta_1 && \text{on } \Gamma_1(x,y) \ , \\ \eta &= \eta_2 && \text{on } \Gamma_2(x,y) \ , \\ \eta &= \eta_3(x,y) && \text{on } \Gamma_3(x,y) \ , \\ \eta &= \eta_4(x,y) && \text{on } \Gamma_4(x,y) \ , \end{aligned} \tag{3-5b}$$

and

$$\begin{aligned} \xi &= \xi_1(x,y) && \text{on } \Gamma_1(x,y) \\ \xi &= \xi_2(x,y) && \text{on } \Gamma_2(x,y) \ , \\ \xi &= \xi_3 && \text{on } \Gamma_3(x,y) \ , \\ \xi &= \xi_4 && \text{on } \Gamma_4(x,y) \ , \end{aligned} \tag{3-5a}$$

where the control functions P and Q in equation(3-4) may be chosen to cause the coordinate lines to concentrate as desired, in analogy with the coordinate lines shown in the one-dimensional example in Section III-2. As discussed in Section III-2, negative values of P causes ξ-lines to move toward the ξ-line having the lowest value of ξ, while positive values have the opposite effect. Similarly, the function Q may be used to shift the η-lines to be more dense toward one of the boundary lines according to the value of Q. In this study the following functions suggested by Thompson et al. [11,12] are used:

$$P(\xi) = -\sum_{i=1}^{n} a \, \mathrm{sgn}(\xi-\xi_i) \ e^{-d|\xi-\xi_i|} \ , \tag{3-6a}$$

ORIGINAL PAGE IS
OF POOR QUALITY

$$Q(\eta) = -\sum_{i=1}^{n} a \, \mathrm{sgn}(\eta-\eta_i) \, e^{-d|\eta-\eta_i|} , \qquad (3\text{-}6b)$$

where sgn(x) is simply the sign of x. In equation (3-6), 'a' and 'd' are attraction amplitude and decaying constants, while ξ_i is a specified ξ-line. For a given term in equation (3-6a) the function P reaches the local maximum magnitude on the ξ_i-line and decays exponentially from that line on either side at a rate controlled by 'd'. With the incorporation of the sign-changing function and the summation function in equation (3-6), not only the ξ-lines are dense on both sides of the ξ_i-line, but also that concentration near more than one line is possible. Furthermore, equation (3-6) has additional flexibility by varying the attraction amplitude and the decaying constants, 'a' and 'd', from one line to another. Control of η-lines is achieved by a similar form of the function Q provided in equation (3-6b). Next, consider the Dirichlet boundary conditions of equation (3-4). On the physical plane η_1 and η_2 given in equation (3-5b) are different constants ($\eta_2 > \eta_1$), and $\xi_1(x,y)$ and $\xi_2(x,y)$ given in equation (3-5a) are specified monotonic functions on Γ_1 and Γ_2, respectively. Furthermore, one can specify arbitrarily a branch cut to join Γ_1 and Γ_2 in the physical plane. Here the coincident coordinate lines ξ_3 and ξ_4 form a branch cut, which becomes

ORIGINAL PAGE IS
OF POOR QUALITY

re-entrant boundaries Γ_3 and Γ_4 on the left and right sides of the transformed plane (see Fig. (2)). All functions and their derivatives are continuous across Γ_4 to Γ_3 so that $\eta_3(x,y)$ and $\eta_4(x,y)$ in equation (3-5b) are exactly the same ($\eta_1 < \eta_3 = \eta_4 < \eta_2$). Therefore, boundary conditions are neither required nor allowed on Γ_3 and Γ_4. The values of η on Γ_3 & Γ_4 are, of course, analogous to the coincident $\theta=0$ and 2π lines in the cylindrical coordinate system and are set $\eta(\Gamma_3)=\eta(\Gamma_4)$.

Since it is desired to perform numerical calculation in uniform square grids in the transformed plane (ξ,η), it is necessary to rewrite equation (3-4) into the form of $x(\xi,\eta)$ and $y(\xi,\eta)$, that is to interchange the dependent and independent variables in equation (3-4) by the relations and Jocobian given in equation (A-8) of Appendix A. The coupled system of equation (3-4) written with (ξ,η) as independent variables is as follows :

$$\alpha x_{\xi\xi} - 2\beta x_{\xi\eta} + \gamma x_{\eta\eta} = J^2(x_\xi P + x_\eta Q) \quad , \tag{3-7a}$$

$$\alpha y_{\xi\xi} - 2\beta y_{\xi\eta} + \gamma y_{\eta\eta} = J^2(y_\xi P + y_\eta Q) \quad , \tag{3-7b}$$

where

$$\begin{aligned} \alpha &= x_\eta^2 + y_\eta^2 \ , \\ \beta &= x_\xi x_\eta + y_\xi y_\eta \ , \\ \gamma &= x_\xi^2 + y_\xi^2 \ , \\ J &= x_\xi y_\eta - x_\eta y_\xi \ , \end{aligned} \tag{3-8}$$

with the transformed boundary conditions

$$x = f_1(\xi,\eta_1) \quad \text{on } \Gamma_1^* ,$$
$$x = g_1(\xi,\eta_2) \quad \text{on } \Gamma_2^* , \qquad (3\text{-}9a)$$
$$x = h_1(\xi,\eta) \quad \text{on } \Gamma_3^* \text{ and } \Gamma_4^* ,$$
$$y = f_2(\xi,\eta_1) \quad \text{on } \Gamma_1^* ,$$
$$y = g_2(\xi,\eta_2) \quad \text{on } \Gamma_2^* , \qquad (3\text{-}9b)$$
$$y = h_2(\xi,\eta) \quad \text{on } \Gamma_3^* \text{ and } \Gamma_4^* .$$

The functions f_1, f_2, g_1 and g_2 are specified by the known shape of the contours Γ_1, Γ_2 and the specified distribution of ξ. As noted, the points outside the right side boundary Γ_4^* in the transformed plane (Fig. (2)) are the same as corresponding points on the same η-line inside the left side boundary Γ_3^* and vice versa. Therefore, boundary values, h_1 and h_2 in equation (3-9) are not specified along the re-entrant boundaries Γ_3^* and Γ_4^* in the transformed plane.

The elliptical governing equation (3-7) is now well posed so that the boundary-fitted coordinate system can be generated by solving the elliptic boundary value problem with the values of the transformed coordinate being specified along the contours in the physical plane.

3.4 Numerical Solution And Examples

In obtaining the solution of equation (3-7), all derivatives are approximated by the second-order central difference expressions. The resulting difference equations are coded in a computer program listed in Appendix C. The set of nonlinear simultaneous difference equations is then solved by the line-by-line implicit iterative method.

ORIGINAL PAGE IS
OF POOR QUALITY

In particular, it should be noted that the actual values of the transformed coordinates, ξ and η, are irrelevant to the subsequent use of the coordinate system in the numerical solution of partial differential equations. For the grid size in the transformed plane, $\Delta\xi$ and $\Delta\eta$ simply cancel out of all difference expressions for transformed derivatives. Therefore, $\Delta\xi$ and $\Delta\eta$ are both taken as unity for convenience, with ξ and η each ranging from unity to the total number of coordinate lines.

In the present study, equation (3-7) is solved numerically and applied to several geometries with single and multi-body regions. The transformations selected for presentation here are chosen to verify the generality of the method as well as to introduce the boundary-fitted coordinate systems for numerical analysis of fluid flows and heat transfer problems to be discussed in Chapter VII and VIII.

As the first example, the configuration of infinite rows of tubes shown in Fig. (4) is considered for the boundary-fitted coordinates. Considering symmetry and periodicity of the flow field, the transformation is made only for one quadrant. The plots in Fig. (5) show the uniformly spaced ξ=constant and η=constant lines with various contracting functions P and Q in the physical plane. The coordinate system given in Fig. (5a) is the case of zero

contraction in which P and Q of equation (3-7) are set equal to zero. For the contracted forms shown in Fig. (5), the choice of the decaying factor 'd' is found to be more sensitive than that of the attraction amplitude 'a'. For example, setting a=20 and d=0.2, an over-contracted form with rather strong wide-spread effect is obtained as shown in Fig. (5b). Next, using a=20 and d=0.75, a better contracted form is obtained as shown in Fig. (5c). The coordinate system shown in Fig. (5c) is employed for the numerical calculation in Chapter VIII. Because it creates more dense grids near the tube in the physical domain, in this transformation 22 ξ-lines and 21 η-lines are used and the contraction toward both solid boundaries of tubes is demonstrated.

As a second example, the boundary-fitted coordinates arround a single airfoil is considered. Figures (6a,6b) show two typical airfoils, NACA-0018 and Karmann-Trefftz airfoils. Their coordinate data defining the body contours are given in Figs. (6c,6d). The outer boundary for the coordinate transformation is taken to be a circle having a diameter of three to four body lengths. The number of coordinate lines used and the factors of control functions are 80 ξ-lines, 25 η-lines and a=200, d=0.5 for NACA-0018 airfoil and 68 ξ-lines, 25 η-lines and a=200, d=0.3 for Karmann-Trefftz airfoil. The desired effect of the

ORIGINAL PAGE IS
OF POOR QUALITY

contracted transformation is demonstrated for both airfoils in Figs. (7,8). These figures exhibit the effect of contraction of the equi-spaced η-lines to the airfoil. It should also be noted that grid spacing is significantly clustered near both leading edge and trailing edge of airfoils in the contracted transformation. As is discussed in Chapter VII, the contracted mesh spacing near solid body boundaries of airfoils may help to minimize the numerical error caused from the severe geometric change.

In this study the convergent solution of the transformation in equation (3-7) is obtained if the maximum differnce of all values of (x,y) in the computational field between two successive iterations is of accuracy 10^{-6}. The convergent solutions for the above examples can be obtained within 250 iterations which requires about five to eight minutes of CPU time on PRIME 750 to generate the boundary-fitted coordinate.

CHAPTER IV

FINITE ANALYTIC NUMERICAL SOLUTION

In this chapter, the FA solutions of the unsteady two-dimensional Navier-Stokes equations cast in the stream function-vorticity formulation and the energy equation are derived. If the flow and heat transfer problems involve complex geometry, the boundary-fitted coordinate system described in Chapter III is employed to cast the governing equations and the physical geometry into the transformed coordinates before the problem is solved. The boundary-fitted coordinates cooresponding to each problem are obtained numerically by solving the partial differential equation (3-7) outlined in Chapter III. In this chapter only the FA solutions for the governing equations are presented while the details of boundary and initial conditions for each problem solved are given separately in the Chapters V, VI, VII and VIII.

4.1 Formulation Of The Problems

It is assumed that the fluid is Newtonian and incompressible with constant transport properties. The two-dimensional Navier-Stokes equations cast in the stream

ORIGINAL PAGE IS
OF POOR QUALITY

funtion-vorticity formulation and energy equation are given below.

Vorticity Transport Equation :

$$Re\left[\omega_t + (u\omega)_x + (v\omega)_y\right] - \omega_{xx} - \omega_{yy} = 0 \ , \qquad (4\text{-}1)$$

where the vorticity, ω is defined by

$$\omega = v_x - u_y = -\nabla^2\psi \ , \qquad (4\text{-}2)$$

and velocity components

$$u = \psi_y \ , \quad v = -\psi_x \ . \qquad (4\text{-}3)$$

Here space and time variables x, y, t, are dimensionless and normalized by a reference length H and a reference time H/U. The velocity u and v are normalized by the reference velocity U. $Re=UH/\nu$ is the Reynolds numbers.

Energy Equation :

$$Pe\left[\theta_t + (u\theta)_x + (v\theta)_y\right] - \theta_{xx} - \theta_{yy} = 0 \ . \qquad (4\text{-}4)$$

In equation (4-4) temperature θ is normalized as $(T-T_w)/(T_0-T_w)$ where T_0 and T_w $(T_w \neq T_0)$ are the constant inlet or free stream temperature of fluid and the isothermal wall temperature. The Peclet number, Pe, is Pr*Re where Pr is the

ORIGINAL PAGE IS
OF POOR QUALITY

Prandtl number. The frictional heating (Eckert number) due to the viscosity dissipation is assumed small in this present study.

In order that a problem with complex geometry be solved on the boundary-fitted coordinate system, equations (4-1), (4-2) and (4-4) must be transformed into the boundary-fitted coordinates. Utilizing the relations given in Appendix A, the governing equations (4-1) through (4-4) become

$$\frac{J^2 Re}{\alpha}\omega_t + \left(\frac{J\,Re}{\alpha}\psi_\eta - \frac{\tau}{\alpha}\right)\omega_\xi + \left(-\frac{J\,Re}{\alpha}\psi_\xi - \frac{\sigma}{\alpha}\right)\omega_\eta$$

$$-\omega_{\xi\xi} - \frac{\gamma}{\alpha}\omega_{\eta\eta} = \frac{-2\beta}{\alpha}\omega_{\xi\eta} \quad , \tag{4-5}$$

$$\frac{\tau}{\alpha}\psi_\xi + \frac{\sigma}{\alpha}\psi_\eta + \psi_{\xi\xi} + \frac{\gamma}{\alpha}\psi_{\eta\eta} = \frac{2\beta}{\alpha}\psi_{\xi\eta} - \frac{J^2}{\alpha}\omega \quad , \tag{4-6}$$

$$\frac{J^2 Re}{\alpha}\theta_t + \left(\frac{J\,Re}{\alpha}\psi_\eta - \frac{\tau}{\alpha}\right)\theta_\xi + \left(-\frac{J\,Re}{\alpha}\psi_\xi - \frac{\sigma}{\alpha}\right)\theta_\eta$$

$$-\theta_{\xi\xi} - \frac{\gamma}{\alpha}\theta_{\eta\eta} = \frac{-2\beta}{\alpha}\theta_{\xi\eta} \quad , \tag{4-7}$$

where ψ, ω, Re and Pe are stream function, vorticity, Reynolds number and Peclet number, respectively, as defined before. α, β, γ, J, σ and τ are functions related to the boundary-fitted coordinates transformation, namely,

$$\alpha = x_\eta^2 + y_\eta^2 \quad , \tag{4-8a}$$

$$\beta = x_\xi x_\eta + y_\xi y_\eta \quad , \tag{4-8b}$$

$$\gamma = x_\xi^2 + y_\xi^2 \quad , \tag{4-8c}$$

$$J = x_\xi y_\eta - x_\eta y_\xi \quad , \tag{4-8d}$$

ORIGINAL PAGE IS
OF POOR QUALITY

$$\sigma = \frac{1}{J} y_\xi D_x - x_\xi D_y \quad , \tag{4-9a}$$

$$\tau = \frac{1}{J} x_\eta D_y - y_\eta D_x \quad , \tag{4-9b}$$

where

$$D_x = \alpha x_{\xi\xi} - 2\beta X_{\xi\eta} + \gamma X_{\eta\eta} \quad , \tag{4-10a}$$

$$D_y = \alpha x_{\xi\xi} - 2\beta x_{\xi\eta} + \gamma x_{\eta\eta} \quad . \tag{4-10b}$$

Examining equation (4-10) and equation (3-7) , it is noted that Dx, Dy and the parameters σ and τ vanish if non-contracting control functions (i.e. P=Q=0) in equation (4-4) are employed. Also it is noted that the coefficients of transformation (α, β, γ, J, σ and τ) at each point of the computational domain can be calculated when the boundaries of the physical plane and the control functions P and Q are defined. Thus these coefficients at each node can be tabulated and stored for later use in the solutions of equations (4-5), (4-6) and (4-7).

4.2 Initial And Boundary Conditions

In order to make the problem well posed, the initial and boundary conditions associated with the particular example are given in Chapters V, VI, VII and VIII. In this section only provide a general discussion about the coordinates needed to be specified for an arbitrary body shape as shown in Fig. (2). In Fig. (2a), the computational

ORIGINAL PAGE IS
OF POOR QUALITY

region, D, is bounded by the body contour Γ_1 and the outer boundary Γ_2 . The boundary and initial conditions for the governing equations (4-1), (4-2) and (4-4) in the physical plane are given below.

Boundary Conditions:

For [x,y] Γ_1(body contour),

$$\omega(x,y,t) = \omega_0(x,y,t) \quad , \tag{4-11a}$$

$$\psi(x,y,t) = \text{constant} \quad , \tag{4-11b}$$

$$\theta(x,y,t) = \theta_0(x,y,t) \quad , \tag{4-11c}$$

$$\frac{\partial\psi(x,y,t)}{\partial n(\Gamma_1)} = 0 \quad . \tag{4-11d}$$

For [x,y] Γ_2 (remote boundary),

$$\omega(x,y,t) = \omega_\infty(x,y,t) \quad , \tag{4-12a}$$

$$\psi(x,y,t) = \psi_\infty(x,y,t) \quad , \tag{4-12b}$$

$$\theta(x,y,t) = \theta_\infty(x,y,t) \quad . \tag{4-12c}$$

Initial Conditions:

For [x,y] D (computational domain)

$$\omega(x,y,0) = 0 \quad , \tag{4-12d}$$

$$\theta(x,y,0) = 0 \quad . \tag{4-12e}$$

Here $\hat{n}(\Gamma_1)$ of equation (4-11a) is the unit vector normal to the contour Γ_1 at all points and ψ_∞ and θ_∞ are prescribed boundary functions. The boundary condition in equation (4-11d) specifies the no slip condition on the body, while that in equation (4-11b) stipulates the impermeable condition on the body. The vorticity boundary condition on the body contour Γ_1 in equation (4-11a), $\omega_0(x,y,t)$, is needed in solving the vorticity equation (4-1), but it indeed is unknown and has to be calculated as a part of the solution of equations (4-1) and (4-2). Therefore, $\partial\psi/\partial n$ of equation (4-11d) is used instead of ω_0. Further detail of this replacement is discussed later. The initial conditions for ω and θ are specified in equations (4-12a,b). The initial condition for stream function is not necessary since there is no time derivative term in equation (4-6) and (4-2). The fact that vorticity ω is initially set equal to zero implies that the flow initially is impulsively started as the flow is irrotational. In this study the initial temperature is considered to be uniform.

Boundary and initial calculations given in equations (4-11) and (4-12) written in (x,y,t) coordinate system may be expressed in the boundary-fitted coordinate system (ξ, η, t). It is recalled that the boundary Γ_1 is transformed to Γ_1^*, Γ_2 to Γ_2^*, Γ_3 to Γ_3^*, Γ_4 to Γ_4^* and D to D^*, and that the right and left boundaries of the transformed plane (shown in Fig.

ORIGINAL PAGE IS
OF POOR QUALITY

(2b)), Γ_3^* and Γ_4^*, are coincident in the physical plane. Then the boundary and initial conditions for the equation (4-5), (4-6) and (4-7) in the transformed plane are given below.

Boundary Conditions:

For $[\xi, \eta]$ Γ_2^*

$$\omega(\xi,\eta_1,t) = \omega_0(\xi,\eta_1,t) \quad , \tag{4-13a}$$

$$\psi(\xi,\eta_1,t) = \text{constant} \quad , \tag{4-13b}$$

$$\theta(\xi,\eta_1,t) = \theta_0(\xi,\eta_1,t) \quad , \tag{4-13c}$$

$$\frac{\partial\psi(\xi,\eta_1,t)}{\partial n(\eta_1)} = 0 \quad . \tag{4-13d}$$

For $[\xi, \eta]$ Γ_2^*

$$\omega(\xi,\eta_2,t) = \omega_\infty(\xi,\eta_2,t) \quad , \tag{4-14a}$$

$$\psi(\xi,\eta_2,t) = \psi_\infty(\xi,\eta_2,t) \quad , \tag{4-14b}$$

$$\theta(\xi,\eta_2,t) = \theta_\infty(\xi,\eta_2,t) \quad . \tag{4-14c}$$

Initial Conditions:

For $[\xi,\eta]$ D^*

$$\omega(\xi,\eta,0) = 0 \quad , \tag{4-14d}$$

$$\theta(\xi,\eta,0) = 0 \quad . \tag{4-14e}$$

ORIGINAL PAGE IS
OF POOR QUALITY

where η_1 and η_2 are the values of the η-coordinate for contours Γ_1^* and Γ_2^*, and D^* is the computational region in the transformed plane as shown in Fig. (2b).

4.3 Finite Analytic Solutions

In the following, the FA solutions of governing equations (4-5), (4-6) and (4-7) are obtained in each element and the corresponding FA algebraic equations are formed. The system of these FA algebraic equations is eventually solved numerically to provide the approximate solution of the problem.

4.3.1 Vorticity Function

At first, the Navier-Stokes equations (4-5) and (4-6) in the stream function-vorticity formulation in (ξ, η, t) plane are considered. Since equation (4-5) is a nonlinear equation, the general analytic solution of the equations (4-5) and (4-6) is not available. Thus the FA numerical method is used to obtain an approximate solution. To impliment the FA method, first locally linearize the vorticity transport equation (4-5) in the element as shown in Fig. (1).

Let

$$\psi_\eta = \bar{\psi}_\eta + \psi'_\eta \quad , \qquad \psi_\xi = \bar{\psi}_\xi + \psi'_\xi \tag{4-15}$$

and

$$A = 0.5\left[\frac{J\ Re}{\alpha}\ \bar{\psi}_\eta - \frac{\tau}{\alpha}\right] \quad , \tag{4-16a}$$

$$B = 0.5\left[-\ \frac{J\ Re}{\alpha}\ \bar{\psi}_\xi - \frac{\sigma}{\gamma}\right] , \tag{4-16b}$$

$$C = \frac{\gamma}{\alpha} \quad , \tag{4-16c}$$

where $\bar{\psi}_\eta$ and $\bar{\psi}_\xi$ are constants representing the average convective velocity in the element. They may be taken as the integral average of ψ_η and ψ_ξ in the element

$$\bar{\psi}_\eta = \frac{\int \psi_\eta dA}{\int dA} \quad , \qquad \bar{\psi}_\xi = \frac{\int \psi_\xi dA}{\int dA} \quad , \tag{4-17}$$

or simply the convective value at the interior node, P, given in Fig. (1). The ψ'_η and ψ'_ξ are then respectively the deviation of the convective velocities ψ'_η and ψ'_ξ from those of $\bar{\psi}_\eta$ and $\bar{\psi}_\xi$ in the element. In general ψ'_η and ψ'_ξ are small if the element is reasonably small. Substituting equation (4-16) into equation (4-5) and assuming that α, β, γ, σ, τ and J take the values at the node P, the vorticity transport equation (4-5) becomes

$$2A\omega_\xi + 2BC\omega_\eta - \omega_{\xi\xi} - C\omega_{\eta\eta} = g \quad , \tag{4-18a}$$

$$g = \frac{-J\ Re}{\alpha}\left[(\psi'_\eta\omega)_\xi + (\psi'_\xi\omega)_\eta\right] - \frac{2\beta}{\alpha}\omega_{\xi\eta} - \frac{J^2 Re}{\alpha}\omega_t \quad . \tag{4-18b}$$

ORIGINAL PAGE IS
OF POOR QUALITY

The function g in equation (4-18b) consists of three terms namely, unsteady, cross derivative, and higher order correction terms. In order to simplify the derivation of the analytic solution of equation (4-18a), the finite difference approximation is employed to approximate the unsteady term, ω_t, and cross derivative term, $\omega_{\xi\eta}$ and the higher order correction term. These terms when expressed in the finite difference are no longer function of x, y and t variables. Therefore, their variation from one element to another can be approximated by a representative constant value in the local element. From the description given above, the term g is considered as a constant in the local element. Thus equation (4-18) becomes a linear partial differential equation with constant coefficients. Hence the FA solution for (4-18) can be obtained analytically.

Because of the ellipticity of equation (4-18a) in space, it can be solved uniquely if the boundary conditions $\omega_N(x)$, $\omega_S(x)$, $\omega_E(y)$ and $\omega_W(y)$ are specified. Various functions can be used to approximate the boundary conditions where three nodal values are available for each boundary (see Fig. (1)). In this investigation, two different approximate functions are considered. One is a second order polynomial employed by Chen et al. [4] in solving the heat transfer problem of the cavity flow. This work is presented in Chapter V. The other boundary approximation used is the

combination of a linear and exponential function proposed by Chen and Chen [10] which is also employed in the present investigation of flow and heat transfer problems in Chapter VI, VII, and VIII. This choice of a linear and exponential function is because it satisfies the governing equation (4-18). As an example of a linear and exponential boundary function, the western boundary condition of the vorticity transport equation (4-18) in the transformed domain may be approximated by

$$a_W(\eta) = a_0 + a_1\eta + a_2(e^{2B\eta} - 1) \tag{4-19}$$

where the constants a_0, a_1 and a_2 can be determined by the three nodal values of vorticity on the western boundary, namely

$$\begin{aligned} a_0 &= \omega_{WC} \quad , \\ a_1 &= \frac{1}{2k}\left[\omega_{NW} - \omega_{SW} - \coth Bk(\omega_{NW} + \omega_{SW} - 2\omega_{WC})\right] , \\ a_2 &= \frac{\omega_{NW} + \omega_{SW} - 2\omega_{WC}}{4 \sinh^2 Bk} \quad . \end{aligned} \tag{4-20}$$

The boundary conditions for north, south, and east sides (i.e., $\omega_N(\xi)$, $\omega_S(\xi)$ and $\omega_E(\eta)$) can be similarly approximated by the combination of a linear and exponential functions. It should be remarked that one may transfer all complex and non-uniform grid spacing in physical plane

ORIGINAL PAGE IS
OF POOR QUALITY

(x,y,t) into a rectangular uniform grid spacing in boundary-fitted coordinates. Thus on the boundary-fitted coordinate one may make all the numerical computation in the equal grid size (i.e. $h=k=\Delta\xi=\Delta\eta=1$).

The linearized vorticity transport equation (4-18) in the transformed plane (ξ,η,t) with its boundary conditions $\omega_E(\eta)$, $\omega_W(\eta)$, $\omega_S(\xi)$ and $\omega_N(\xi)$ can now be solved analytically by the method of separation of variables to give the analytic solution of equation (4-18) in an element. Details of derivation of the FA solution are summarized in Appendix B. When the analytic solution is evaluated at the interior node P(i,j) of the element as outlined in chapter II, it gives the FA 9-point algebraic equation (see Appendix B) as

$$\omega_P = \sum_{n=1}^{8} C_n \omega_n + C_P g_P = C_{EC}\,\omega_{EC} + C_{NC}\,\omega_{NC} + C_{WC}\,\omega_{WC} + C_{SC}\,\omega_{SC}$$

$$+C_{NE}\,\omega_{NE} + C_{NW}\,\omega_{NW} + C_{SW}\,\omega_{SW} + C_{SE}\,\omega_{SE} + C_P\,g_P \quad , \qquad (4\text{-}21)$$

where the coefficients C_{EC}, C_{NC}, ----, etc. are derived from the analytic solution. The FA coefficients are given below.

$$\begin{aligned}
C_{EC} &= EB\cdot\exp(-Ah) \quad , & C_{NE} &= E\exp(-Ah-Bk) \quad , \\
C_{WC} &= EB\exp(Ah) \quad , & C_{NW} &= E\exp(Ah-Bk) \quad , \\
C_{NC} &= EA\exp(-Bk) \quad , & C_{SE} &= E\exp(-Ah+Bk) \quad , \\
C_{SC} &= EA\exp(Bk) \quad , & C_{SW} &= E\exp(Ah+Bk) \quad ,
\end{aligned} \qquad (4\text{-}22)$$

$$C_P = \frac{Ah}{2(A^2 + B^2C)} (C_{NW} + C_{WC} + C_{SW} - C_{NE} - C_{EC} - C_{SE})$$

$$+ \frac{Bk}{2(A^2 + B^2C)} (C_{SE} + C_{SW} + C_{SC} - C_{NE} - C_{NW} - C_{NC}) \tag{4-23}$$

$$E = \frac{1}{4 \cosh Ah \cosh Bk} - Ah \coth Ah\, E_2 - Bk \coth Bk\, E_2' \quad ,$$

$$EA = 2\, Ah \cosh Ah \coth Ah\, E_2 \quad , \tag{4-24}$$

$$EB = 2\, Bk \cosh Bk \coth Bk\, E_2' \quad ,$$

$$E_2 = \sum_{m=1}^{\infty} \frac{-(-1)^m \lambda_m h}{\left[(Ah)^2 + (\lambda_m h)^2\right]^2 \cosh \mu_m h}$$

$$E_2' = \sum_{m=1}^{\infty} \frac{-(-1)^m \lambda_m' k}{\left[(Bk)^2 + (\lambda_m' h)^2\right]^2 \cosh \mu_m' k} \tag{4-25}$$

$$\lambda_m = \frac{(2m-1)\pi}{2h} \quad , \quad \mu_m = \sqrt{(A^2 + B^2C + \lambda_m^2)\frac{1}{C}}$$

$$\lambda_m' = \frac{(2m-1)\pi}{2k} \quad , \quad \mu_m' = \sqrt{A^2 + B^2C + \lambda_m'^2 C} \quad . \tag{4-26}$$

A relationship between E_2 and E_2' can be found to be

$$Ch^2 E_2 - k^2 E_2' = \frac{BCh \tanh Ah - Ah \tanh Bk}{4AB \cosh Ah \cosh Bk} \quad . \tag{4-27}$$

The evaluation of inhomogeneous term g_P, which contains the unsteady term ω_t, cross derivative term $\omega_{\xi\eta}$ and the high order correction term, is approximated as follows :

$$(\omega_t)_P = (\omega_P^k - \omega_P^{k-1}) \frac{1}{\Delta t} \quad , \tag{4-28}$$

$$G_P = \frac{J\, Re}{\alpha} (\psi_\eta' \omega)_\xi + (\psi_\xi' \omega)_\eta + \frac{2\beta}{\alpha} \omega_\xi \quad . \tag{4-29}$$

ORIGINAL PAGE IS
OF POOR QUALITY

Substituting equation (4-28) and (4-29) for g in equation (4-21), one has the equation for vorticity at the kth time step in terms of time step k-1 as

$$\omega_P^k = \frac{1}{1 + \frac{C_P \, Re \, J^2}{\alpha \Delta t}} \left[\sum_{n=1}^{8} C_n \, \omega_n^k + C_P \, G_P^{k-1} - \frac{C_P \, Re \, J^2}{\alpha \Delta t} \, \omega_P^{k-1} \right], \qquad (4\text{-}30)$$

where n denotes the neighboring boundary nodes, EC, WC, NC, SC, NE, SE, NW, and SW.

Examining equations (4-23) and (4-24) through (4-27), one finds that only one series summation is needed to calculate eight FA coefficients for each element. For example, if E_2 (or E_2') is calculated from equation (4-25), then E_2 (or E_2') is obtained from equation (4-27). It follows that EA, EB of equation (4-24) and all FA coefficients are calculated. The choice of calculating either E_2 or E_2' in equation (4-25) can be best made based on the value of the coefficient C in equation (4-18). It is found that E_2' series converges faster when c>1 because cosh $\mu_m h$ in the denominator of E_2' is larger than that of E_2. On the other hand, when c<1, E_2 is tabulated and E_2' is obtained through equation (4-27). Hence the number of terms needed in calculating E_2 or E_2' for the FA coefficients in equation (4-25) can be reduced according to the value of C. For example, for C=9, one generally needs only 6 term summation

to achieve an accuracy for E_2' to within 10^{-5} and for C=4, 9 term summation is needed to achieve the same accuracy.

The FA coefficients, C_{NC}, C_{NW}, ---- etc., in general, are functions of local cell Reynolds number, 2Ah and 2BCk and C which are differnt from one element to another. A typical FA solution of equation (4-18) written in equation (4-21) with g=0, C=1 and h=k is schematically illustrated in equation (4-31) for a skewed convective vector

$$\omega_p = (2Ah = 2) \begin{matrix} 0.0430 & 0.1850 & 0.0362 \\ 0.2260 & P & 0.1850 \\ 0.0541 & 0.2260 & 0.0430 \end{matrix} * \omega_n, \quad (4\text{-}31a)$$

$$(2BCk = 2)$$

$$\omega_p = (2Ah = 100) \begin{matrix} 10^{-6} & 10^{-8} & 10^{-9} \\ 0.07956 & P & 10^{-8} \\ 0.84088 & 0.07956 & 10^{-6} \end{matrix} * \omega_n. \quad (4\text{-}31b)$$

$$(2BCk = 100)$$

In equation (4-31a) the values in the block are the FA coefficients of the corresponding node to be multiplied by the nodal value ω_n. The summation of these products provides the FA solution of ω_p for the element given in equation (4-21). The FA coefficients can be interpreted as the

ORIGINAL PAGE IS
OF POOR QUALITY

percentage influence of the boundary node ω_n on the interior node ω_P under the given convective vector with components of 2Ah and 2BCk. Equation (4-31a) shows that the convection comes from the southeast corner with cell Reynolds number of 2Ah=2BCk=2. The cell Reynolds number is quite small that the effect of the diffusion between the center node P and the surrounding points is felt at all neighboring nodes. It can be seen that all four middle coefficients on the boundaries, C_{NC}, C_{WC}, C_{SC}, and C_{EC}, have the same order of magnitude. It is noted that the influence of the nodal value at the upstream side of the convection is slightly larger than that at the downstream side (i.e., $C_{WC}>C_{EC}$, $C_{SC}>C_{NC}$, $C_{SW}>C_{NE}$). However, the FA coefficient for the SW node, C_{SW}, is still smaller than the C_{WC} and C_{SC} since the SW node is further away from the center node, P. Therefore, C_{SW} has a smaller effect of diffusion on the node P than the node C_{SC} or C_{WC}.

On the other hand, equation (4-31b) gives the FA solution of larger cell Reynolds number (2Ah=2Bck=100) with the convection vector approaching the element from the southwest corner. Since a large cell Reynolds number implies that the flow involves small diffusion, the FA analytic solution predicts that the influence of the southwest boundary node, ω_{SW}, on the interior ω_P is the strongest while the downstream node, NE, has practically zero influence at 10^{-9}.

ORIGINAL PAGE IS
OF POOR QUALITY

The virtue of the FA solution derived here is that it does not tamper with the derivatives of the governing equation (4-18) and it is valid for all range of the Reynolds number without the need of upwind schemes. Further discussion of the FA coefficients for different cell Reynolds numbers with different direction of convective vectors can be found in Ref. [13].

4.3.2 Stream Function

The stream function in an element can be similarly solved from equation (4-6). When the FA solution for vorticity is known from equation (4-21), the FA solution of the stream function in an element of 2h*2k can be easily obtained. We note that the equation for the stream function in equation (4-6) is a special case of vorticity equation (4-5). In other words, equation (4-6) can be cast into the same form of equation (4-18) by replacing ω by ψ and letting

$$A = \frac{-\tau}{2\alpha} \quad , \qquad B = \frac{-\sigma}{2\gamma} \quad , \tag{4-32a}$$

and

$$g = \frac{-2\beta}{\alpha} \psi_{\xi\eta} + \frac{J^2}{\alpha} \omega \quad . \tag{4-32b}$$

ORIGINAL PAGE IS
OF POOR QUALITY

Equation (4-6) unlike equation (4-5) does not have convective terms. However the terms, A and B, shown in equation (4-32a) which contains functional relation between (x,y,t) and (ξ,η,t) coordinates varies from an element to the other element on the transformed plane (ξ,η,t). The function g in equation (4-32b) for stream function equation (4-18) consists of the cross derivative term $\psi_{\xi\eta}$ and the source term ω only. The finite anlytic algebraic representation of the stream function ψ_p at the node, P, in an element is thus

$$\psi_P = \sum_{n=1}^{8} C'_n \psi_n + C'_P g_P \quad . \tag{4-33}$$

Here C'_n and C'_P are the FA coefficients given in equation (4-22) and equation (4-23) with the values of A and B and the function g_p is replaced by those given in equation (4-32).

Some special problems, for example, the cavity flow and the channel flow shown in Chapter V and VI, are desired to perform the numerical calculation directly on the physical plane (x,y,t) with uniform rectangular grid ($\Delta x=h=\Delta y=k$). The coefficients of transformation in equations (4-8) through (4-10) can be simply set as

$$\begin{aligned} \alpha = \gamma = J = 1 \quad , \\ \beta = \sigma = \tau = D_x = D_y = 0 \quad . \end{aligned} \tag{4-44}$$

ORIGINAL PAGE IS
OF POOR QUALITY

In this case, the convective terms in equation (4-6) vanish due to A=B=0 in equation (4-32a). Thus the FA coefficients in the physical plane are simply invariant and are given below :

$$
\begin{aligned}
C'_{EC} &= C'_{WC} = C'_{NC} = C'_{SC} = 0.205315 \quad , \\
C'_{NE} &= C'_{NW} = C'_{SE} = C'_{SW} = 0.044685 \quad . \\
C'_{P} &= 0.294685 \frac{1}{h^2}
\end{aligned}
\tag{4-34}
$$

4.3.3 Temperature Function

The energy equation given in equation (4-7) has an identical form as that in the vorticity transport equation (4-5) if θ is identified with ω and the Peclet number, Pe, is identified with the Reynolds number, Re. Therefore, the FA solution of equation (4-7) in an element is similar to that of equation (4-18), if we set

$$
\begin{aligned}
A &= 0.5 \left(\frac{J\,Pe}{\alpha} \bar{\psi}_{\eta} - \frac{\tau}{\alpha} \right) \quad , \\
B &= 0.5 \left(\frac{-J\,Pe}{\alpha} \bar{\psi}_{\xi} - \frac{\sigma}{\gamma} \right) \quad .
\end{aligned}
\tag{4-35}
$$

As a result, the FA solution of the temperture at the center node, θ_P, can be expressed in the FA equation relating to its surrounding θ_n (i.e., θ_{EC}, θ_{SE}, -----) as in equation (4-21) which is

ORIGINAL PAGE IS
OF POOR QUALITY

$$\theta_P = \sum_{n=1}^{8} C_n^* \theta_n + C_P^* g_P \quad . \tag{4-36}$$

Here C_n^* and C_P^* are identical to equations (4-21) and (4-22) except that A and B are given in equation (4-35) and g_P is same as in equation (4-18) except that ω is replaced by θ .

4.4 Computational Procedure

As mentioned earlier, if the flow and the heat transfer problem involve complex geometries, the boundary-fitted coordinate system mentioned in Chapter III must be generated before solving the governing equations. The calculation of the boundary-fitted coordinate system from the physical plane (x,y) to the transformed plane (ξ,η), the line-by-line implicit iterative method is employed to solve the difference approximation of equation (3-7) subject to boundary conditions of equation (3-9) as described in Chapter III. The results of transfomed coefficients α, β, γ, J, σ and τ calculated in equation (4-9) are stored and ultilized for solving the governing equations (4-5) through (4-7) in the transformed plane. In the present study, because the fluid is assumed to be incompressible and has constant viscosity ν , the stream function (ψ) and vorticity (ω) equations (4-5) and (4-6) are uncoupled from the temperature (θ) equation (4-7). Thus equations (4-5) and (4-6) can be solved for ψ and ω independent of θ . The

ORIGINAL PAGE IS
OF POOR QUALITY

temperature (θ) can be solved from equation (4-7) when ψ and ω are known. The computational procedures of stream function-vorticity equations and the energy equation are described in the following.

4.4.1 Computational Procedures Of The ψ-ω Equation

The aim of the present investigation is to obtain the steady solutions of the Navier-Stokes equations (4-5) and (4-6) and the energy equation (4-7). It can be obtained by the time marching procedure instead of the iterative method. This casts the problem from steady state into unsteady state with the initial guess for the steady problem as the initial condition for the unsteady problem. This time marching procedure has a certain advantage over the iterative method which is to be discussed in the last section of this chapter. The time marching procedure is briefly outlined here.

1. Assign a proper marching time step Δt, and input the boundary conditions of stream function ψ.
2. Start with some initial guess of the vorticity, ω^k, at kth time step for all unknown nodes of the problem including the unknown boundaries. Typically, one may, at the beginning, assume zero or a constant value for ω^k.

ORIGINAL PAGE IS
OF POOR QUALITY

3. Calculate FA coefficients for the stream function as defined by equations (4-22) and (4-32a).
4. Solve the system of FA algebraic equation (4-33) by the line-by-line implicit iterative method to obtain the new solution ψ^{k+1} at (k+1)th time step. The iterative process in obtaining the stream function for ψ^{k+1} is termed as 'the inner iteration for the stream function ψ'.
5. Calculate the FA coefficients for the vorticity transport equation (4-5) defined by equations (4-22) and (4-16).
6. Determine the vorticity value on the boundaries from the vorticity boundary equations, such as equation (4-11a). Details of the the derivation of these equations are to be discussed later in each problem.
7. Solve the system of the FA algebraic equations for vorticity defined in equation (4-21) by the line-by-line implicit iterative method to obtain the new solution, ω^{k+1}, at (k+1)th time step. The iterative process in obtaining the vorticity for ω^{k+1} is termed as 'the inner iteration for the vorticity, ω'.
8. Repeat steps (4) to (7) for the marching time step k=1,2,3,----- until the convergence criterion (to be specified in each problem later) of steady state solution is met. The marching procedure from (4) to (8) is called an outer iteration.

ORIGINAL PAGE IS
OF POOR QUALITY

This computational procedure step (1) to (8) described above is referred to the computer program given in Appendix C.

4.4.2 Computational Procedures Of The θ Equation

For an incompressible, two-dimensional flow with constant viscosity, the Navier-Stokes equations are uncoupled from the energy equation so that (x,y,t) can be solved from equation (4-7) after equations (4-6) and (4-6) have been solved. The FA solution of equation (4-7) is given in equation (4-35). Since the convection terms of the energy equation (4-7) are determined from equation (4-16) of the Navier-Stokes equations, the temperature distribution, θ, for the problem can be solved with proper boundary conditions. Therefore, the computational procedure of the energy equation (see Appendix C-6) is similar to that of the stream function-vorticity equations given in Section (4-4-1) except without the outer iteration.

4.4.3 Remarks On Time Marching And Iterative Procedures

In this section the relation between the unsteady time marching computational procedure and the steady iterative procedure is discussed. It is often asked which procedure, the time marching procedure or the steady iterative procedure, is best for calculating the steady flow solution.

ORIGINAL PAGE IS
OF POOR QUALITY

It is shown in this section that these two procedures are closely related if the relaxation parameter used in the iterative procedure is allowed to vary in a certain way. The solution of vorticity as an example is discussed now. In order to stablize the numerical computation for the steady vorticity transport equation (4-5), the under-relaxation factor, γ, is often used, where γ is defined as :

$$\omega^{k} = \omega^{k-1} + \gamma (\bar{\omega}^{k} - \omega^{k-1}) \quad . \tag{4-37}$$

Here k-1 denotes the (k-1)th iteration of the variable. is the relaxed funtional value of ω after the kth iteration and is used in the next iteration. $\bar{\omega}^{k}$ is the value of ω just calculated from the kth iteration. It should be remarked that for the under-relaxation, γ , is normally chosen to be a constant between 0 and 1 during the iterative calculation for the steady solution of ω. In the present formulation the problem is cast in the unsteady time marching procedure in equation (4-30). The question becomes how this unsteady time marching problem is related to the iterative procedure of equation (4-37). By examining the unsteady solution given in equation (4-30), the first two terms in the right hand side of equation (4-30) can be redefined as

$$\bar{\omega}_{P}^{k} = \sum_{n=1}^{8} C_n \, \omega_n^{k} + C_P \, G_P^{k-1} \quad , \tag{4-38}$$

ORIGINAL PAGE IS
OF POOR QUALITY

which can be considered to be the value of vorticity just calculated from the kth iteration. With the expression of equation (4-38), equation (4-30) can be written as

$$\omega_p^k = \omega^{k-1} + \frac{1}{1+\dfrac{C_p\, Re\, J^2}{\alpha \Delta t}} \left(\bar{\omega}^k - \omega^{k-1} \right) \quad . \tag{4-39}$$

By comparison of equations (4-39) and (4-37), one finds that if the relaxation factor γ of equation (4-37) is identified as

$$\gamma = \frac{1}{1+\dfrac{C_p\, Re\, J^2}{\alpha \Delta t}} \quad , \tag{4-40}$$

then equations (4-38) and (4-36) are identical even though the superscript k in equation (4-38) denotes the time step while in equation (4-36) denotes the iteration step. It is noted that the value of γ in the present analysis is always smaller than one, since $(C_p Re J^2)/(\Delta t \alpha)$ in equation (4-40) is a positive quantity. It should be noted that γ expressed in equation (4-39) is dependent on the time step, the Reynolds number, curvilinear coordinate parameters J and α, and the FA coefficient C_p. Further, C_p (see equation(4-23)) is a function of local convection terms A and B and grid size. Therefore, one may conclude that the relaxation parameter γ, (or rather a relaxation function) derived in

ORIGINAL PAGE IS
OF POOR QUALITY

the present analysis varies from one node to another depending on the grid size, Reynolds number, and local convective terms. This leads to the conclusion that if the relaxation parameter γ is identified as equation (4-40) the calculation of steady flow solution equation (4-37) or equation (4-39) is essentially identical. Thus, in this investigation the steady problems are solved by the unsteady time marching procedure. In the following chapters, several problems are solved by the FA method with and without boundary-fitted coordinate system. In Chapters V and VI, because the problem boundaries are specified on the Cartesian coordinates, there is no need to make for boundary-fitted coordinate transformation. Therefore, the accuracy of the FA solutions can be examined without the adoptation of the boundary-fitted coordinates. In Chapters VII and VIII more complex geometries are treated. There, the FA solutions are solved on the boundary-fitted coordinate system.

ORIGINAL PAGE IS
OF POOR QUALITY

CHAPTER V

CONVECTIVE HEAT TRANSFER IN CAVITY

5.1 General Remarks

The cavity flow problem considered in this investigation is a two-dimensional square cavity where three walls are stationary while the fourth wall moves at a uniform velocity along its own plane. Because the wall boundaries coincide with the Cartesian coordinates, the problem can be solved by the FA method on the Cartesian coordinates without involving further boundary-fitted coordinates.

The cavity problem is of theoretical importance, because first it is a part of the larger class of steady separated flows and secondly it is a flow where the transport properties and the nonlinear convection affect the entire flow region.

The finite difference and the finite element numerical methods have been used extensively for the evaluation of low and high Reynolds number problems in the cavity flows. Early attempts using second-order central difference approximations to the terms in the governing equations representing convection [14] were found difficult to produce

ORIGINAL PAGE IS
OF POOR QUALITY

stable solutions for the Reynolds number above 400 at which the experiments of Mill [15] and Pan and Acrivos [16] indicated that the flow remains stable and laminar. Later solution for high Reynolds number flows have been obtained by Greenspan [17], Gosman, et al. [18], de Vahl Davis and Mallinson [19], Nallasarmy and Prasaa [20], and Olson and Tuann [21]. It is, however, known that the upwind differencing not only produces significant truncation errors, but also the numerical diffusive effect which augments the effects of viscosity [22,23]. Considerable controversy has ensued over the significance of the false diffusion [23], especially in the case of the high Reynolds number flow when the physical diffusion is weak.

Although many numerical solutions by the finite difference or the finite element methods are available for the cavity flow problem, little work is available for solutions of the heat transfer in the cavity flow. Therefore, in the present investigation, the temperature distribution and heat transfer characteristic in the cavity are studied. Formulation of the cavity flow problem is given in the next section where a brief review of the FA solutions for stream function and vorticity in the cavity flow as proposed by Chen et al. [4] is made. In this study the FA solutions for Peclet numbers ranging from 10 to 20,000 and Reynolds numbers from 100 to 2,000 are then obtained.

ORIGINAL PAGE IS
OF POOR QUALITY

5.2 Formultion Of Problem

Consider a square cavity as shown in Fig. (9) where the cavity depth and width have a length L. The bottom wall at a temperature T moves with a speed U_r in the positive x-direction. The other walls are at rest and at an isothermal temperature T_w. The flow is assumed to be two-dimensional, incompressible, laminar and steady. The characteristic velocity and length are taken to be U_r and L_r respectively and the dimensionless temperature θ is defined as $(T-T_w)/(T_m-T_w)$. The dimensionless Navier-Stokes equations in the stream function-vorticity formulation and the energy equation given in (4-1), (4-2) and (4-4) are rewritten as below :

$$Re\,(\psi_y\,\omega_x - \psi_x\,\omega_y) = \omega_{xx} + \omega_{yy} \quad , \tag{5-1}$$

$$\nabla^2\psi = -\omega \quad , \tag{5-2}$$

$$Pe\,(\psi_y\,\theta_x - \psi_x\,\theta_y) = \theta_{xx} + \theta_{yy} \quad . \tag{5-3}$$

These equations are written in the Cartesian coordinates due to the geometric simplicity of the cavity. The boundary conditions to be satisfied are the non-slip and impermeable conditions and the isothermal wall conditions, i.e.

On the bottom wall, $y=0$, $0<x<1$

$$\psi = 0,\ \psi_y = 1,\ \theta = 1. \tag{5-4}$$

ORIGINAL PAGE IS
OF POOR QUALITY

On the left and right walls, x=0 and x=1, 0<y<1

$$\psi = 0, \ \psi_y = 0, \ \theta = 0. \tag{5-5}$$

On the top wall, y=1, 0<x<1

$$\psi = 0, \ \psi_y = 0, \ \theta = 0. \tag{5-6}$$

The vorticity boundary conditions for equation (5-1) may be approximately derived from the above boundary conditions using the Taylor series expansion of the stream function from the wall to an interior point normal to the wall [1]. the vorticity boundary functions are approximated as follows :

$$\omega(x,0) = \frac{-2\ \psi(x,\Delta y)}{\Delta y^2} + \frac{2}{\Delta y} \quad , \tag{5-7a}$$

$$\omega(0,y) = \frac{-2\ \psi(\Delta x,y)}{\Delta x^2} \quad , \tag{5-7b}$$

$$\omega(1,y) = \frac{-2\ \psi(1-\Delta x,y)}{\Delta x^2} \quad , \tag{5-7c}$$

$$\omega(x,1) = \frac{-2\ \psi(x,\ 1-\Delta y)}{\Delta y^2} \quad . \tag{5-7d}$$

At the four corners, they are

$$\omega(1,1) = \omega(0,1) = 0 \quad , \tag{5-7e}$$

$$\omega(0,0) = \omega(1,0) = \frac{2}{\Delta y} \quad . \tag{5-7f}$$

ORIGINAL PAGE IS
OF POOR QUALITY

In this investigation, the cavity flow region is discretized with 41*41 nodes for calculation for the Reynolds number of 100 and 1,000, and 61*61 nodes for Re= 2,000. For each Reynolds number three different Prandtl numbers, 0.1, 1 and 10 are considered. Temperature profiles in the cavity as well as heat flux at the moving wall are also studied.

5.3 FA Solution Of The Cavity Flow

In Chapter IV, the FA solutions of stream function (ψ), vorticity (ω) and temperature (θ) are derived in the transformed plane (ξ,η,t). However, in the cavity flow problem, because of the simplicity in geometry, the Cartesian coordinate system is obviously the best choice. Therefore, the FA solution in equation (4-5) for general boundary-fitted coordinates can be easily reverted back to the physical plane. This can be done by letting the coefficients relating the transformation to be

$$\alpha=\gamma=J=1,$$

and $\beta=\sigma=\tau=0.$

The FA solutions of equations (5-1) through (5-3) for ω, ψ and θ can be obtained by substituting the above coefficients into the equations (4-21), (4-33) and (4-36). In obtaining these FA solutions of the cavity flow, several simplifications are made because the problem was solved at the early stage of the present investigation.

ORIGINAL PAGE IS
OF POOR QUALITY

1. The boundary function for an element is approximated by a simple second-order polynomial rather than the function which combines the linear and exponential function.

2. For simplicity, the velocities in the convection term are linearized by the area average of the velocity distribution in the element, i.e.,

$$\bar{U} = \frac{1}{36} (u_{NW} + u_{NE} + u_{SW} + u_{SE}) + 4 (u_{EC} + u_{WC} + u_{NC} + u_{SC}) + 16\, u_P \quad ,$$

$$\bar{V} = \frac{1}{36} (v_{NW} + v_{NE} + v_{SW} + v_{SE}) + 4 (v_{EC} + v_{WC} + v_{NC} + v_{SC}) + 16\, v_P \quad .$$

3. The inhomogeneous terms, ω , of the equation (5-2) based on Naseri-Nashat [3] is approximated by a second order polynomial of x and y. When the FA solution of equation (5-2) is evaluated at the center node, P, the algebraic equation obtained involves the values of ψ_P at the 9 points of the element. For details see Ref. [4].

4. The line-by-line implicit iterative method is used for solving the stream function and vorticity equations (5-1) and (5-2), instead of the time marching method.

ORIGINAL PAGE IS
OF POOR QUALITY

Further analysis of the cavity flow problem can be found in Chen, Naseri-Nashat and Ho [4].

In this investigation, the convergence criterions for computing ψ, ω and θ between two iterations are $|\Delta\psi_{max}| < 10^{-5}$, $|\Delta\omega_{max}| < 10^{-4}$ and $|\Delta\theta_{max}| < 10^{-4}$.

5.4 Stream Function And Vorticity Distribution

The stream function and vorticity distributions of the two-dimensional steady square cavity flow are calculated by the FA method [3] and plotted in Fig. (10) and (11). Figure (10) gives the contour of the stream function for Re=100, 1000 and 2000, at an interval increment of $\Delta\psi=10^{-2}$. It is seen that at the low Reynolds number of 100 the stream pattern is only slightly distorted by convection such that the center of the primary vortex is located close to the moving wall at (0.66, 0.30). For Re=100, the present calculation shows that the flow separates at the two upper corners of the cavity. This is in agreement with the experiments of Mill [15]. When the Reynolds number is 1000 as shown in Fig. (10), the primary vortex moves away from the moving wall toward the geometric center of the cavity. The streamlines become more circular near the center while the two secondary vortices at two upper corners grow much larger than those for Re=100. The right-hand secondary vortex is distinctively larger than the left-hand secondary

ORIGINAL PAGE IS
OF POOR QUALITY

vortex. When the Renolds number is 2000, the primary vortex is almost positioned at the center of the cavity. This is also in agreement with experiments [24] which show that in the flow of high Reynolds number, 10^5, the primary vortex is almost located at the center of the cavity. In the present calculation a third secondary vortex is predicted near the upstream corner where the moving wall and the stationary wall meet. This third secondary vortex can be vaguely seen from Mill's experiment [24] and is in agreemwnt with Olson and Tuann's calculation [21] with the finite element method. They predicted that the third secondary vortex comes to exist at Re= 1500-2000.

The vorticity contour is shown in Fig. (11). It shows that at low Reynolds number of 100 the diffusion is so strong that the vorticity generated by the moving wall is readily diffused into the cavity. The vorticity strength is largest at two lower corners where the moving wall and the stationary wall meet. As the Reynolds number is increased to 1000 and 2000, the vorticity is pretty much confined to the near wall region particularly near the moving wall and the right wall where the flow does not separate from the wall and exhibits the boundary layer phenomena. Once the flow separates at the upper corner the vorticity penetrates slightly more into the cavity but still is confined largely to the corner. In general, the central region of the cavity

ORIGINAL PAGE IS
OF POOR QUALITY

is occupied by the primary vortex with a constant vorticity ω_{vc}. For example, ω_{vc}=1.62 for Re=1000 and ω_{vc}=1.59 for Re=2000.

5.5 Temperature Distribution And Heat Transfer

The temperature distribution and heat transfer across the moving wall are calculated by the FA method and plotted in Fig. (12) through (16). Fluids with Prandtl numbers of 0.1, 1.0 and 10 are considered for Reynolds numbers of 100, 1000 and 2000. This combination gives the range of Peclet numbers from 10 to 20,000. The calculation of Pe=20,000 normally is difficult for both the finite difference method and the finite element method. However, in the present finite analytic method the same FA solution is used for Pe= 10 to 20,000 without difficulty.

Figure (12) shows the isothermal lines for Re= 100 and Prandtl numbers of 0.1, 1.0 and 10. It is noted that the isothemal lines for the three Prandtl numbers are quite different even though the velocity field is identical at Re= 100. At Pr=0.1 or Pe= 10, the fluid convection does not seem to distort much of the temperature profile as the isotherms remain fairly symmetric about the vertical central plane. This is because for Pr=0.1 the thermal diffusion is ten times stronger than the momentum diffusion so that at a

ORIGINAL PAGE IS
OF POOR QUALITY

moderate Reynolds number of 100 the convection of fluid has a weak influence on the heat diffusion process. When Pr= 1.0 and Re= 100 the temperature profile as shown in Fig. (12) gives close resemblance to the vorticity plot for Re= 100 in Fig. (11). This is because the governing equations for ω and θ are identical except that the boundary conditions for vorticity and temperature are different. Burggraf [14] has calculated the temperature profile for Re= 100 and Pr= 1.0. The present result in Fig. (12) for this case is almost identical to the Burggraf results. Figure (12) also shows the effect of convection on temperature. That is since the primary vortex convects the fluid in the counterclockwise direction the fluid absorbs heat from the moving wall and then is convected upward along the right wall. As a result the isotherms are distorted toward the right. For fluids of Pr= 10, Fig. (12) shows the existence of closed isotherms. This implies that near the primary vortex center there exists a constant temperature core just as the constant vorticity core at the vortex center. With Pr= 10 and Re= 100, the Peclet number is 1000. Except for the boundary conditon the temperature solution from the energy equation (5-3) for Pe= 1000 is similar to the vorticity solution from the vorticity transport equation (5-1) at Re= 1000. Examining the vorticity plot for Re= 1000 in Fig. (11) and the temperature plot for Re= 100 and

ORIGINAL PAGE IS
OF POOR QUALITY

Pr= 10 in Fig. (12), one finds that there is similarity between ω and θ profiles except near the wall where boundary conditons for ω and θ are different. Figure (13) shows the isotherms for Re= 1000 and Pr= 0.1, 1.0 and 10. It is seen that the isotherms in Fig. (13) for Re= 1000 and Pr= 0.1 are quite similar to the isotherms in Fig. (12) for Re=100 and Pr= 1. Figure (13) shows that as the Prandtl number is increased to Pr= 1.0 and 10 the temperature distribution starts to show the phenomenon of boundary layer development near the moving wall and the right-hand wall. The region of constant temperature core is gradually enlarged and occupies a large portion of the cavity. When Re= 2000 the isotherms for Pr= 0.1, 1.0 and 10 are plotted in Fig. (14). In addition to the temperature boundary development and the spread of constant temperature core, the strong circulation in the secondary vortices begins to distort the temperature distribution at the upper corners particularly for the case of Pr= 10. The calculation of isotherms for Pe= 20,000 can be done with the FA method without difficulty of instability or the need of upwinding approximation.

The local and mean Nusselt number i.e., Nu and $\overline{Nu}$ may be expressed from the local heat transfer coefficient h(x) as

$$Nu = \frac{h(x)\ L}{k} = -\left.\frac{\partial\theta}{\partial y}\right|_{y=0} , \tag{5-8}$$

$$\overline{Nu} = \int_0^1 Nu\ dx \quad . \tag{5-9}$$

ORIGINAL PAGE IS
OF POOR QUALITY

They are tabulated and shown in Fig. (15), (16), (17) and (18). Figures (15), (16) and (17) plot the local Nusselt number along the moving wall. It is noted that at both lower corners of the cavity the temperature jumps from $\theta = 0$ on the stationary wall to $\theta = 1$ on the moving wall. Therefore, the local Nusselt number theoretically becomes infinite and is avoided in the calculation. Figure (15) shows the local Nusselt number for Re= 100 with Pr= 0.1, 1.0 and 10. The general trend is that heat transfer is strong near the upstream corner x= 0, and gradually decreases till near the downstream corner x= 1.0, where the heat transfer is increased again. Physically, this is because the fluid near the moving wall is heated up at the upstream so that there is less heat transferred from the moving wall to the fluid at the downstream. When the moving wall comes close to the right stationary wall, which serves as a thermal sink, then a large heat flux can again be transferred from the moving wall to the stationary wall. At large Reynolds numbers of 1000 and 2000, because of strong convection in general, the Nusselt number for a given Prandtl number is larger than that for the low Reynolds number of 100 as shown in Fig. (15), (16) and (17). From these figures it can be seen that since the flow patterns are different for each Reynolds number the correlation of local Nusselt number with Reynolds number cannot be made into a simple equation as done in

ORIGINAL PAGE IS
OF POOR QUALITY

boundary layer flow. For given Reynolds numbers of 1000 and 2000, the larger the Prandtl number is the larger is the Nusselt number. When Pr= 10, both flows for Re= 1000 and 2000 show the Nusselt number decreases near the corner and then increases again in the central portion of the moving wall. This may be explained as follows. Near the central portion of the moving wall the convection is strong and the Nusselt number is obviously large. It should be remarked that since the thermal diffusivity for the fluid of Pr= 10 is small, the thermal energy transferred to the fluid from the moving wall is convected around the constant temperature core at the cavity center and eventually conducted through the stationary wall. Near both lower corners where the convection is weak and the thermal diffusivity is also small for fluid of Pr= 10, the heat transfer and hence the Nusselt number decreases. However, at the extreme corner because the large temperature gradient exists between the moving wall and the stationary wall, the heat transfer and the Nusselt number increase again.

The average Nusselt number for each fluid of Pr= 0.1, 1.0 and 10 is plotted in Fig. (18). It shows that the heat transfer can be enhanced if the Reynolds number is increased and that the different value of Prandtl number can affect markedly the heat transfer particularly at the high Reynolds number cavity flow. The correlation of mean Nusselt number

ORIGINAL PAGE IS
OF POOR QUALITY

with the Reynolds and Prandtl numbers can be approximately expressed as

$$Nu = 0.71\ Re^{1/2}\ Pr^{1/3}\ . \qquad (5\text{-}10)$$

5.6 Conclusion

The FA method is developed here based on the assembly of the local analytic solution obtained in small elements of the problem. The FA solution is derived for the two-dimensional Navier-Stokes equations in the stream function - vorticity formulation and the energy equation. The FA solution is shown to be stable from small Reynolds number (or Peclect number) to large Reynolds number (or Peclet number), i.e., Re= 100 - 2000 (or Pe= 10 - 20,000). The heat transfer and flow problem considered is a square cavity flow with the moving wall held at an isothermal temperature and the stationary walls held at another isothermal temperature. The temperature distribution, heat transfer, stream function and vorticity distribution are predicted for Reynolds numbers of 100, 1000 and 2000, and Prandtl numbers of 0.1, 1.0 and 10.

It is shown that the FA method does not require the upwind approximation as needed in the finite difference method or the finite element method for the calculation with the Peclect number varying from 10 to 20,000. It is found

ORIGINAL PAGE IS
OF POOR QUALITY

that for the range of Reynolds numbers calculated if the Peclet number is 1000 or larger there exists a constant temperature core in the cavity.

ORIGINAL PAGE IS
OF POOR QUALITY

CHAPTER VI

SEPARATION OF CHANNEL FLOW

6.1 General Remarks

The ability to predict accurately the flow separation and subsequent re-attachment has been challenging fluid dynamicists for many years and is considered important in industrial designs and applications. In many instances separation of flow is undesirable and leads to unwanted pressure drops and energy losses which require additional power to overcome them. However, in other circumstances, flow separation may be advantageous. For example, tubulence induced by flow separation may promote and enhance heat and mass transfer rates. In this chapter , flow separation in a channel is investigated by the FA numerical method. Again, since the channel boundaries are specified on the Cartesian coordinates, no further boundary-fitted transformation is necessary in obtaining the FA solutions.

In the previous related works on laminar separated flows, several channel geometries shown in Fig. (19) were considered. For example, Macagno and Hung [25] and Iribarne et al. [26] solved the flow through an axi-symmetric sudden pipe expansion (Fig. (19-a)). Goldstein et al. [27]

ORIGINAL PAGE IS
OF POOR QUALITY

measured the flow structure associated with a downstream-facing step in a flat wall adjacent to an essentially free stream as shown in Fig. (19-b). Durst at el. [28] conducted mesurements in a rectangular duct with downstream-facing steps on both walls (Fig.(19-c)). Denham and Patrick [29] measured the flow over a backward facing step placed in a flow channel (Fig. (19-d)). In the present chapter, the problem chosen is channel flow over a backward facing step as shown in Fig. (19-d).

There are several reasons for this selection. First, Denham and Patrick provided extensive experimental data at four different Reynolds numbers (Re=73, 125, 191 and 229) by dye and laser anemometer measurements for comparison with computational results. The Reynolds number, Re, in the study [29] is defined as $Re=\bar{U}h/\nu$, where $\bar{U}$ is the mean velocity in the inlet section and h is the height of the step. Secondly, the calculation of flow over a backward facing step demands less computational domain than that of the symmetrical plane expansion. One may argue that the latter case can be solved with either top or bottom half from the symmetrical line. However, the relatively high momentum fluid near the center-line for the latter case tends to elongate the separation zone and hence requires longer computational domain than that proposed in the present study. Finally, both the FD and the FE solutions were available for the proposed laminar

ORIGINAL PAGE IS
OF POOR QUALITY

channel flow. They serve as a basis for comparision with the FA numerical solution.

In the previous numerical works of this proposed laminar channel flow, Atkins [29] considered both the fully developed inlet profile and the experimental inlet profile in the FD calculation. Atkins [30] also repeated the same numerical calculation with both upwind and central difference schemes six years later. He showed that better results were obtained and in agreement with experimental measurements if the experimentally measured inlet profiles were used. However, little discussions about the grid size and the numerical scheme were given. The FE solution was obtained by Hutton and Smith [31] and Thomas, Morgan and Taylor [32]. Hutton et al. and Thomas et al. predicted longer lengths of separation zone than those of experimental measurements mentioned in [29]. In order to stablize the numerical computation they had to use the upwind technique and a special outlet boundary condition ($\partial v/\partial x = 0$). Unfortunately, details of the grid size and the numerical scheme for the numerical calculation at different Reynolds numbers were not given.

From these studies, one finds that the available numerical schemes still have difficulty in obtaining accurate and stable results in flow with separation. Thus, the FA method is applied to solve this problem in an attempt

ORIGINAL PAGE IS
OF POOR QUALITY

to obtain better numerical predictions. In this chapter, the FA solution is compared with the best available numerical and experimental results. Details are presented in the ensuing sections.

6.2 Formulation of Problem

The dimensions of the single plane duct expansion is shown in Fig. (20). The height of the step, h, is one half of the height of the upstream channel, H (i.e. the expansion ratio is 1.5). The ratio of the entry length (EF) of the upstream channel to the step is 4/3. The direction of the flow is in the positive x-direction.

Due to the simple geometry of this channel flow, the Cartesian coordinate system is used. If the upstream channel height, H and the maximum velocity, U_{max}, in the inlet section are selected as the characteristic length and the characteristic velocity, the dimensionless Navier-Stokes equations in stream function-vorticity formulation are

$$Re_H(u\omega_x + v\omega_y) = \omega_{xx} + \omega_{yy} \quad , \tag{6-1}$$

where

$$\omega = v_x - u_y = -\nabla^2\psi \quad , \tag{6-2}$$

and

$$u = \psi_y \quad , \quad v = -\psi_x \quad . \tag{6-3}$$

ORIGINAL PAGE IS
OF POOR QUALITY

In equation (6-1), Re is the Reynolds number and is defined as $U_{max}H/\nu$. It should be remarked that in order to compare the numerical results with the experimental measurements of [29] in which a different definition of the Reynolds number Re is used, the present Reynolds number Re is related to Re as

$$Re_H = U_{max}\ H/\nu = 1.5\bar{U}\ 2h/\nu = 3Re \qquad (6\text{-}4)$$

The elliptic partial differential equations (6-1) and (6-2) are coupled. They can be solved uniquely if the proper boundary conditions are specified for ω, and ψ. With the aid of Fig. (20), the boundary conditions at the inlet, outlet and boundary walls are given as follows :

at y=1, i.e. the upper wall AB,

$$\psi = \psi_0 = Q, \quad \psi_x = 0, \quad \psi_y = 0. \qquad (6\text{-}5)$$

at the bottom wall DC and the step FFD

$$\psi = 0, \quad \psi_x = 0, \quad \psi_y = 0. \qquad (6\text{-}6)$$

at the inlet, the fully developed velocity profile is assumed, or

$$u = \psi_y = 4y(1-y)$$
$$v = -\psi_x = 0 \qquad (6\text{-}7a)$$
$$\text{or} \quad \psi = (2-4y/3)y^2 .$$

This gives a discharge Q=2/3 at the inlet. The vorticity at the inlet is obtained from equation (6-2) and the velocity at the inlet. Thus

ORIGINAL PAGE IS
OF POOR QUALITY

$$\omega = -4+8y+\frac{\partial v}{\partial x} \quad , \tag{6-7b}$$

where $\partial v/\partial x$ can be approximated by the backward difference formula.

At the far downstream where x=L the velocity in the channel is assumed to be fully developed, or a Poiseuille velocity profile given by

$$\begin{aligned} u &= \psi_y = \frac{16}{27}(1+y-2y^2) \ , \\ v &= -\psi_x = 0 \ , \end{aligned} \tag{6-8a}$$

where the numerical value 16/27 is needed to conserve the mass flow of Q=2/3 which is obtained from the inlet velocity profile. The stream function and vorticity boundary conditions at the far downstream position are obtained from this velocity distribution. This gives

$$\begin{aligned} \psi &= \frac{2}{27}(7/3+8y+4y^2-16/3y^3) \ , \\ \omega &= \frac{16}{27}(4y-1) \ . \end{aligned} \tag{6-8b}$$

The vorticity boundary condition at the solid wall can be evaluated from equation (6-2) when the stream function is known. Taking a Taylor series expansion of the stream function normal to the wall and involving the non-slip condition and the stream function at the wall, one has the vorticity boundary functions as follows :

at the upper wall $\overline{AB}$, y=1

ORIGINAL PAGE IS
OF POOR QUALITY

$$\omega(x,1) = -2\ [Q-\psi(x,1-\Delta y)]/\Delta y^2 . \tag{6-9}$$

at the bottom wall $\overline{DC}$, y=-0.5

$$\omega(x,-0.5) = -2\ \psi(x,-0.5+\Delta y)/\Delta y^2 . \tag{6-10}$$

at the step $\overline{FE}$ and $\overline{ED}$,

$$\begin{aligned} (x,0) &= -2\ \psi(x,\Delta y)/\Delta y^2 , \\ (0,y) &= -2\ \psi(0,y)/\Delta x^2 . \end{aligned} \tag{6-11}$$

For the corner points, the vorticity can be obtained again by using a Taylor series expansion for the stream function in both x and y directions. This gives

$$\begin{aligned} \omega(-2/3,1) &= 2\ [Q-\psi(-2/3,1-\Delta y)]/\Delta y^2 , \\ \omega(L,1) &= 2\ [Q-\ (L,1-\Delta y)]/\Delta y^2 , \\ \omega(L,-0.5) &= -2\ \psi(L,-0.5+\Delta y)/\Delta y^2 , \\ \omega(0,-0.5) &= 0 , \\ \omega(0,0) &= -2\ [\psi(\Delta x,0)/\Delta x^2 + \psi(0,\Delta y)/\Delta y^2] , \\ \omega(-2/3,0) &= -2\ \psi(-2/3,\Delta y)/\Delta y^2 . \end{aligned} \tag{6-12}$$

6.3 FA Solution

As mentioned before, because the geometry of the backward facing step and the channel is relatively simple, the Cartesian coordinate system is employed to solve this channel flow problem. The governing equations derived in equations (6-1) and (6-2) and their corresponding FA

ORIGINAL PAGE IS
OF POOR QUALITY

solutions in an element obtained in equations (4-21) and (4-33) in the transformed plane can be easily reverted to the physical plane. This is done by simply considering (ξ,η) as (x,y) and let

$$\alpha = \gamma = J = 1 \tag{6-13}$$

and $\beta = \sigma = \tau = 0$.

In other words, the FA solutions evaluated at the center node, P, of an element for the stream function and vorticity in equations (6-1) and (6-2) are identical to those of equations (4-21) and (4-33) in the transformed plane. They are

$$\omega_P = \sum_{n=1}^{8} C_n \omega_n + C_P g_P \quad , \tag{6-14}$$

$$\psi_P = \sum_{n=1}^{8} C'_n \psi_n + C'_P g_P \quad . \tag{6-15}$$

Here C'_n, C'_P, C'_n and C'_P are identical to those in equations (4-21) and (4-33) except that the transformed coefficients are given in equation (6-13) and g_P is without the unsteady term.

Furthermore, in the present study the unequal grid size of $\Delta x=h=5/3$ and $\Delta y=k=0.1$ is used for the main series of computations. Under this consideration, the FA coefficients C'_n of the FA solution in equation (6-15) for the stream function performed in the physical plane become invariants, namely

ORIGINAL PAGE IS
OF POOR QUALITY

$$
\begin{aligned}
&C'_{EC} = C'_{NC} = 0.07488, \\
&C'_{NW} = C'_{SW} = C'_{SE} = C'_{NE} = 0.03909, \\
&C'_{NC} = C'_{SC} = 0.34695, \\
&C_P = 0.00425.
\end{aligned}
\tag{6-16}
$$

6.4 Results And Discussion

In the computation, the length L from the step to the downstream boundary is chosen as 205 which is 13.66 times the height of the step. In this study, Re=25, 50, 73, 125, 191 and 229 (where experimental data ceased) are considered. The unequal grid size 0.166*0.1 is used. The results of the FA solutions of the stream function and vorticity for the two-dimensional channel over a backward facing step are shown in Figs. (21) and (22). Figure (21) gives the contour of stream function ψ/ψ_0 for Re=25, 50, 73, 125, 191 and 229 at an increment of $\psi/\psi_0 = 0.1$. It is seen from these figures that separation occurs at the step edge and the re-attachment point is shifted to downstream as the Reynolds number is increased over the range considered. The recirculation zone length, L_R, (i.e. the distance from the step to the re-attachment point) is an important parameter to characterize the flow in the separation region. This quantity is plotted against the Reynolds number (Re) in Figs. (23 - 24). In Fig. (23), the results of the present

ORIGINAL PAGE IS
OF POOR QUALITY

study are compared with the experimental measurments of Denham and Patrick [29] who made dye-tracer observations and laser anemometer measurements. It is shown that the recirculation zone lengths obtained by the FA method are slightly longer than those of experiments at the low Reynolds number (Re<75). However, at the higher Reynolds number (Re>200) the predictions are in excellent agreement with the experimental results. The reason for over-prediction of recirculation length at low Reynolds number may be due to the fact that the location of the outlet boundary is specified at only x = 13.66 h from the step. Therefore, the parabolic velocity profile specified at the downstream boundary may significantly influence the flow in the upstream at the low Reynolds number (Re<75).

The recirculation lengths computed by the FA method are compared with those by the FD and the FE methods as shown in Figs. (24) and (25). In Fig. (24), it is shown that Atkins [30] calculated with the FD method using the fully developed inlet profile predicted a much longer recirculation zone length for Reynolds numbers greater than 150, and that using the experimental inlet profile yielded better results. The velocity profile at the inlet section does have a strong influence on Atkins' numerical results. This is not found in the present calculations with the FA method in the range of the Reynolds numbers considered. Figure (25) compares the FA

ORIGINAL PAGE IS
OF POOR QUALITY

solution with the numerical results of Hutton and Smith [31] and Thomas et al. [32] obtained by the FE method. Hutton and Smith employed the special boundary elements in the wall region close to the step, and the best numerical results of Thomas et al. were obtained by using the upwind scheme and specifying the outlet boundary conditions as $\partial v/\partial x = 0$. It is evident in Fig. (25) that although the upwind scheme and use of the special boundary element predict reasonable results at the low Reynolds number (Re), the predicted separation length for high Reynolds number (Re) overpredicts that measured by the experiment by a substantial error. From the comparison given in Figs. (23 - 25), It is concluded conclude that the separation lengths obtained by the FA method are closer to the experimental measurements than those of the FD and FE methods.

The recirculating mass flow rate is another important parameter of separated flows. In Fig. (26), the total recirculating mass flow rate relative to that in the mainstream is denoted by the minimum value of ψ/ψ_0 which has a negative value in this problem. $-\psi_{min}/\psi_0$ is plotted against the Reynolds number in Fig. (26). In accordance with the present FA calculation the minimum value of ψ_{min}/ψ_0 remains approximately constant over the range of the Reynolds numbers considered (Re= 73 to 229) at a value of -0.027 which is larger than -0.023 predicted by Akins [29].

ORIGINAL PAGE IS
OF POOR QUALITY

However, Akins does not provide the recirculating mass flow in his latter work [30]. The present FA prediction of recirculating mass flow rate at the higher Reynolds number (Re>200) is in agreement with the experimental data, although at Re<200, the FA prediction is somewhat less than the experimental measurement. This again may be interpreted as the effect of the location of the oulet boundary and the velocity profile assumed.

The similarity of the recirculation region flows at the six Reynolds numbers is illustrated in Fig. (27). Figure (27) shows the position of the separation streamline with the downstream distances normalized by the recirculation zone length. The points of numerical results by the FA method lie close to a single curve, and the position of the center of the recirculation region (the point where minimum ψ/ψ_0 occurs) also remains nearly constant. This position of the vortex center may be given by the coordinates, $x_C = 0.3$ L_R and $y_C = 0.6$ h.

Finally the comparison between the measured velocity profile at Re=125 and the predicted velocity profile using the fully developed parabolic profile, is shown in Fig. (28). The agreement is good as far as the re-attachment is concerned, but further downstream a slight difference is observed. This may be due to the fact that in reality the flow requires longer distances to become fully developed.

C-2

ORIGINAL PAGE IS
OF POOR QUALITY

6.5 Special Case Of Channel Flow

If, for the problem of laminar flow over a backward facing step shown in Fig. (27) it is assumed that the length (EF) upstream of the step vanishes, the problem that of a suddenly expanded channel flow. The IAHR (International Association of Hyaudraulic Research) working group on refined modeling of flows adopted this problem as a working problem at the fourth meeting of refined modeling of flows in the winter of 1981. The configuration of the suddenly expanded channel flow with expansion ratio 2 is shown in Fig. (27). The height of the channel at the inlet is one half of the height of the channel and the downstream length L is 16 (it is eight times the height of the channel). In this study, the characteristic length and velocity are the height of the step, h, and the maximum velocity at the inlet, U_{max}, respectively. The Reynolds number in this special case, Re_s, is defined as $U_{max}h/\nu$.

6.5.1 Boundary Conditions

The boundary conditions of the suddenly expanded channel flow are similar to that given in Section VI-2 and are

at y = 0, i.e. the bottom wall,

$$\psi = 0, \quad \psi_x = 0, \quad \psi_y = 0. \tag{6-17}$$

ORIGINAL PAGE IS
OF POOR QUALITY

at y = 2, i.e. the upper wall,

$$\psi = 0, \quad \psi_x = 0, \quad \psi_y = 0. \tag{6-18}$$

at the inlet station, the follwing velocity profile is used :

$$u = \psi_y = \begin{cases} \tanh\,[30(y-1)] & \text{for } 1<y<1.5\,, \\ \tanh\,[30(2-y)] & \text{for } 1.5<y<2\,, \end{cases} \tag{6-19a}$$

$$v = -\,\psi_x = 0\ .$$

The velocity at the vertical wall is zero. The stream function at the inlet is expressed as

$$\psi = \begin{cases} 1/30\ \log[\cosh\,(30(y-1)] & \text{for } 1<y<1.5\,, \\ -1/30\ \log[\cosh\,(30(2-y)] & \text{for } 1.5<y<2. \end{cases} \tag{6-19b}$$

This gives a discharge mass flux Q=0.95379 at the inlet. The vorticity at the inlet is obtained from the definition of the vorticity equation (6-2) by taking the derivatives of the velocities and is

$$\omega = \begin{cases} -30\ \mathrm{sech}^2\,[30(y-1)] + v_x & \text{for } 1<y<1.5\,, \\ 30\ \mathrm{sech}^2\,[30(2-y)] + v_x & \text{for } 1.5<y<2\,, \end{cases} \tag{6-19c}$$

ORIGINAL PAGE IS
OF POOR QUALITY

where v_x can be approximated by the second order backward difference formula.

At a downstream distance of x=L, a Poiseuille velocity profile is again assumed as follows

$$\psi_y = u(L,y) = 0.75\ Q\ y(2-y),$$
$$\psi_x = -v(L,y) = 0\ .$$

The stream function and vorticity boundary conditions at x=L are obtained by integrating the above velocity distribution. This gives

$$\psi = 0.25\ y^2\ (3-y),$$
$$\omega = 1.5\ Q\ (y-1)\ .$$

The vorticity boundary conditions at the solid walls and their corners are derived from the Taylor series expansion of the stream function either normal to the wall or in both x and y direction. They are given below :

$$\omega(x,0) = -2\ \psi\ (x,\Delta y)/\Delta y^2\ ,$$
$$\omega(x,2) = 2[Q - \psi\ (x,2-\Delta y)]/\Delta y^2\ ,$$
$$\omega(0,y) = -2\ \psi\ (\Delta x,y)/\Delta x^2\ ,$$
$$\omega(0,0) = 0\ ,$$
$$\omega(L,0) = -2\ \psi\ (L,\Delta y)/\Delta y^2\ ,$$
$$\omega(0,2) = -2[Q - \psi(0,2-\Delta y)]/\Delta y^2\ ,$$
$$\omega(L,2) = 2[Q - \psi(L,2-\Delta y)]/\Delta y^2\ ,$$
$$\omega(0,1) = -2[\psi\ (\Delta X,1)/\Delta x^2 + \ (0,1+\Delta y)/\Delta y^2]\ .$$

ORIGINAL PAGE IS
OF POOR QUALITY

6.5.2 Recovery Of Pressure

When the stream function-vorticity equations (6-1) and (6-2) are solved, the velocity can be easily obtained from differentiation of the stream function given by equation (6-3). The pressure distribution can be computed from the Poisson equation (6-22) which can be deduced from the momentum equations by taking the divergence.

$$P_{xx} + P_{yy} = 2(u_x v_y - v_x u_y) = f \quad . \tag{6-22}$$

It should be noted that equation (6-22) is similar to equation (6-2) for the stream function. The pressure boundary condition can be obtained by using the Taylor series expansion of pressure about the pressure at the interior nodes. The algebraic equation for the pressure evaluated at the center node P of an element is the same as that of the stream function in equation (6-15) except replacing ψ by P and ψ_P by f_P. It is

$$P_P = \sum_{n=1}^{8} C_n' P_n + C_P' f_P \ . \tag{6-23}$$

6.5.3 Results And Discussion

In computing the channel flow with a sudden expansion, both Re_s=200 and 400 are considered. For Re_s=200, an equal grid 0.2*0.2 and an unequal grid 0.5*0.2 are used. For Re_s =400, the grid size used is 0.1*0.1.

ORIGINAL PAGE IS
OF POOR QUALITY

The algorithm of the FA solution is the same as that in Section VI-3 by casting the steady state problem as an unsteady one. Thus time marching procedure and internal iterations are needed for calculating stream function and vorticity. In the present FA calculation 20 and 12 internal iterations are respectively used for calculating the stream function and vorticity. As mentioned before in Chapter IV, since the time marching procedure is used in this channel flow problem, it does not need to consider the relaxation factor. The time step becomes the only parameter to be controlled. In this study, all of the results are obtained with a time step of 0.2.

For the cases $Re_s=200$ and $Re_s=400$, after 151 time steps of computation the maximum difference of $|\Delta\psi_{max}|<10^{-5}$ for ψ and $|\Delta\omega_{max}|<10^{-4}$ for ω between two time steps are found and the steady state condition is assumed to be established. In the case of $Re_s=200$ (0.5*0.2) only 120 time steps are required to achieve the same accuracy.

The results of the FA solution for the suddenly expanded channel flow are plotted in Figs. (30) through (33). The stream function and vorticity distribution for the channel flow are shown in Figs. (30) and (31). Figure (30) gives the contours of the stream function for $Re_s=200$ and $Re_s=400$ at an increment of $\Delta\psi=0.1$. It appears that the recirculation zone exists at the entrance corner and the re-

ORIGINAL PAGE IS
OF POOR QUALITY

attachment point is shifted to downstream as the Reynolds number (Re_s) increases from 200 to 400. From Figs. (30a) and (30b), one finds that the recirculation zone developed at Re=200 is almost same for two different grid sizes (0.5*0.2 and 0.2*0.2) used in computing the same flow. The flow enters the channel with a maximum velocity of 1 at the inlet. Because separation occurs at the lower left corner, the flow near the center line of the channel is thus accelerated. Here the maximum velocity behind the inlet is likely to be larger than the maximum velocity of 1 at the entrance region. When the flow goes downstream the streamlines gradually expand, thereby decelerating the flow and increasing the pressure near the upper wall. This increase of pressure produces an adverse pressure gradient (dP/dx) which tends to reduce the momentum of the flow. When the re-attachment occurs at the lower wall, there is a tendency for the streamlines near the upper wall to diverge which is indicated by the distribution of zero vorticity in Fig. (31). However, no evidence for actual separation is obtained. Deham and Patrick [29] also particularly noted this phenomenon in their experimental measurments by the inflection in the velocity profiles at the upper wall.

The velocity profiles u(x,y) for Re_s=200 at x=0, 1, 2, 3, 4, 5 and 16 are given in Fig. (32). The tendency of separation at the upper wall is detected from the velocity

ORIGINAL PAGE IS
OF POOR QUALITY

profiles at stations x=4 and 5 where the re-attachment point occurred. Furthermore, it is observed that the maximum velocity at the stations x=0 through x=5 shifts downward gradually as the flow goes downstream. Beyond the station x=5, the maximum velocity of the flow gradually shifts back to the center (y=1.0) to meet the fully developed condition at the outlet. This observation of the maximum velocity shifting down and then up is not found in the investigation of channel flow with a backward facing step shown in Section VI-4 in which the maximum velocity just gradually goes down to meet the outlet boundary condition. This difference probably is due to the different expansion ratios and the inlet velocity profiles considered.

The pressure distribution for Re_s=200 using equal grid size 0.2*0.2 is shown in Fig. (33). In the region of recirculation, a constant core is formed with a value of -0.23, if the center of the outlet station is chosen as the reference point with a value of zero. Further downstream, the pressure in the recirculation zone increases to 0 near the re-attachment point. At the lower wall, the concentration of the isobars around the re-attachment point indicates that a large pressure gradient occurs. At the upper wall, an interesting phenomenon is observed. Between station x=2 and x=8, the pressure gradually increases due to the diverging nature of the stream lines. The adverse

ORIGINAL PAGE IS
OF POOR QUALITY

pressure gradient thus creates a tendency toward separation at the upper wall. This observation has already been shown in the distribution of vorticity of Fig. (31) and in the velocity profile of Fig. (32). Beyond x=13, the pressure distribution becomes almost uniform. This is expected from a Poiseuille flow assumed. Therefore, the assumption of uniform pressure at the outlet station (x=16) is a reasonable boundary condition for this problem.

6.6 Conclusion

The FA method is used to solve for the flow over a backward facing step and its special case of a suddenly expanded channel flow. The FA solutions of the channel flow over a step predict the recirculation zone lengths and the recirculated mass flow rates for Reynolds numbers of 25, 50, 73, 125, 191 and 229 which correlate well with experimental measurements. The general flow field bears similarity of the recirculation region flows over the range of the Reynolds numbers considered. In the special case of the suddenly expanded channel flow, the FA solutions at Re_s=200 and 400 show the separation tendency at the upper wall. This tendency is observed from the distribution of vorticity and velocity pro' 'es and distribution of isobars which is in agreement with xperimental observations.

ORIGINAL PAGE IS
OF POOR QUALITY

CHAPTER VII

FLOW PAST A SINGLE AIRFOIL

7.1 General Remarks

In Chapters V and VI, the FA solution is derived in the Cartesian coordinate system and applied to obtain the numerical solution for viscous flow and heat transfer problems. Both equal and unequal grid sizes are considered. In the following two chapters, the FA method with the boundary-fitted coordinates is employed to solve the problems involving the complex boundaries. In this chapter the potential flow past a single airfoil is studied and the numerical prediction of viscous flow and heat transfer in tube bundles is presented in Chapter VIII.

As the first application of the FA method with the boundary-fitted coordinates, the incompressible inviscid irrotational flow is solved numerically. There are several reasons for this choice. First, the FA solution is of interest in itself as it provides another potential flow method for airfoil sections. Secondly, the applicability of the FA method using the boundary-fitted coordinate system can be verified since the FA solution can be compared with the theoretical potential solution. Finally, the invicid

ORIGINAL PAGE IS
OF POOR QUALITY

potential flow is governed by Laplace equation which appears in many engineering fields. Thus, if we can demonstrate the ability of the FA method in solving this equation for complex boundaries, the FA solution may be readily extended to other engineering problems.

In the first study of the FA method incorporated with boundary-fitted coordinate system, two airfoils, the symmetric NACA-0018 and the Karmann-Trefftz airfoil, are examined. These two airfoil sections are plotted in Fig. (6a) and (6b) and the corresponding boundary-fitted coordinates (ξ, η) are shown in Figs. (7,8).

7.2 Formulation Of The Potential Flow

The two dimensional irrotational flow in the dimensionless stream function formulation is

$$\nabla^2\psi = \psi_{xx} + \psi_{yy} = 0 \quad . \tag{7-1}$$

As indicated in chapter IV, the first step to solve the problem involved complex boundaries is to transform the governing equation (7-1) into the transformed plane (ξ, η). Using the transformation relations (from A-1 to A-8) derived in Appendix A, the Laplace equation becomes

$$\alpha\psi_{\xi\xi} - 2\beta\psi_{\xi\eta} + \gamma\psi_{\eta\eta} + \sigma\psi_{\eta} + \tau\psi_{\xi} = 0 \quad . \tag{7-2}$$

ORIGINAL PAGE IS
OF POOR QUALITY

The transformed coefficients $\alpha, \beta, \gamma, \sigma$, and τ defined in equations (4-8) and (4-9) are functions of the transformed coordinate variables and may be calculated and stored one for all as this coordinate system is generated. It is recalled that if the non-contracting transformed coordinate system is employed, the quantities σ and τ vanish which reduces equation (7-2) to

$$\alpha\psi_{\xi\xi} - 2\beta\psi_{\xi\eta} + \gamma\psi_{\eta\eta} = 0 \quad . \tag{7-3}$$

The boundary conditions (see Fig. (2)) for a uniform flow passing an airfoil for either equation (7-2) or equation (7-3) are given as below :

$$\begin{aligned} \psi(\xi,\eta_1) &= \psi_0 = \text{constant} && \text{in } (\xi,\eta_1)\in\Gamma_1^*, \\ \psi(\xi,\eta_2) &= f(\xi,\eta_2) && \text{in } (\xi,\eta_2)\in\Gamma_2^*, \\ \psi(\xi_1,\eta) &= \psi(\xi_2,\eta) && \text{in } (\xi_1,\eta)\in\Gamma_3^* \\ & && \text{or } (\xi_2,\eta)\in\Gamma_4^* \quad . \end{aligned} \tag{7-4}$$

Here $f(\xi,\eta_2)$ is a prescribed function for the outer boundary of the computational field shown in Fig. (2). η_1 and η_2 are the values of the coordinate η on the boundary contours Γ_1^* and Γ_2^*. Γ_3^* and Γ_4^* are the transformed re-entrant boundaries.

Since the equation (7-3) is linear in ψ, the problem can be decomposed into three simple problem each with their own boundary conditions. The three problems are

ORIGINAL PAGE IS
OF POOR QUALITY

1. A zero circulation solution at zero degree angle of attack, denoted $\psi^1(\xi,\eta)$, and the boundary conditions are

$$\begin{aligned} \psi^1(\xi,\eta_1) &= 0 \quad \text{in } (\xi,\eta_1)\in \Gamma_1^* \ , \\ \psi^1(\xi,\eta_2) &= U_0\, y(\xi,\eta_2) \quad \text{in } (\xi,\eta_2)\in \Gamma_2^* \ , \end{aligned} \tag{7-5}$$

2. A zero circulation solution at 90 degrees of angle of attack, denoted $\psi^2(\xi,\eta)$, and the boundary conditions are

$$\begin{aligned} \psi^2(\xi,\eta_1) &= 0 \quad \text{in } (\xi,\eta_1)\in \Gamma_1^* \ , \\ \psi^2(\xi,\eta_2) &= U_0\, x(\xi,\eta_2) \quad \text{in } (\xi,\eta_2)\in \Gamma_2^* \ . \end{aligned} \tag{7-6}$$

3. A solution with circulation without free stream velocity, denoted $\psi^3(\xi,\eta)$, and the boundary conditions are

$$\begin{aligned} \psi^3(\xi,\eta_1) &= 1 \quad \text{in } (\xi,\eta_1)\in \Gamma_1^* \ , \\ \psi^3(\xi,\eta_2) &= 0 \quad \text{in } (\xi,\eta_2)\in \Gamma_2^* \end{aligned} \tag{7-7}$$

where U_0 is the dimensionless free stream velocity.

After these three solutions ψ^1, ψ^2 and ψ^3 are obtained, the total solution of equation (7-3) can be given by superposing these three solutions. The final result is

ORIGINAL PAGE IS
OF POOR QUALITY

$$\psi(\xi,\eta) = \cos\alpha\ \psi^1(\xi,\eta) + \sin\alpha\ \psi^2(\xi,\eta) + \mu\ \psi^3(\xi,\eta) \quad . \tag{7-8}$$

Here α is the angle of attack and μ is a constant or a circulation strength which is to be determined by satisfying the Kutta condition. Because the periodic boundary condition is applied to the re-entrant boundaries of Γ_3^* and Γ_4^* shown in Fig. (2), it is expected that the solution of equation (7-2) is determined uniquely.

7.3 Implementation Of Kutta Condition

As discussed above, after obtaing the solutions, ψ^1 , ψ^2 and ψ^3, the constant μ may be determined so that the Kutta condition is satisfied. The Kutta condition originated from the physical necessity that required the flow to leave the trailing edge of an airfoil in a smooth fashion. Mathematically, the smoothness condition implies that the velocity on the surface of the airfoil is continuous. Thus, if the trailing edge angle is finite as shown in Fig. (32), the velocity at the tip of the trailing edge must be zero. Otherwise this discontinuity will occur at the edge. On the other hand, if the cusped trailing edge is considered, at such an edge the velocity need not be zero but of finite magnitude. However, from the view point of numerical calculation, one finds that no matter how the trailing edge is, the stipulation of the same velocity magnitude at the

ORIGINAL PAGE IS
OF POOR QUALITY

edge on either side is sufficient to meet the requirement of the Kutta condition. This interpretation of the Kutta condition has been applied in the studies of Giesing [33] and Thompson et al. [12].

Because the airfoil is considered to have the impermeable solid surface, the normal velocity component on the airfoil surface vanishes. Thus in deriving the Kutta condition only the tangential velocity along the surface is examined. If the velocity in the physical plane is denoted as

$$\vec{v} = u\,\hat{i} + v\,\hat{j} \quad ,$$

then using equation (A-21), the tangential velocity in terms of the transformed coordinates (ξ,η) along a constant η-line is expressed as

$$v_{t_\eta} = \hat{t}\Big|_\eta \vec{v} = (x_\xi u + y_\xi v)\,\frac{1}{\sqrt{\gamma}} \tag{7-9}$$

where $\hat{t}\big|_\eta$ is the unit vector tangent to a constant η-line. From the definition of the stream line in equation (4-2), u and v in equation (7-9) can be replaced by ψ_y and $-\psi_x$, respectively. These derivatives of stream function in coordinates (x,y) can be transformed into the coordinates (ξ,η) by the Jacobian given in equation (A-8). Substituting the above results into equation (7-9), one has

ORIGINAL PAGE IS
OF POOR QUALITY

$$v_t\Big|_{\eta} = \frac{1}{J\sqrt{\gamma}} \left(\gamma\psi_{\eta} - \beta\psi_{\xi}\right) \quad . \tag{7-10}$$

If this tangential velocity is evaluated at an airfoil surface ($\eta = \eta_1 = 1$), the component ψ_{ξ} is eliminated. Thus the tangential velocity along the airfoil is

$$v_t(\xi,1) = \frac{\sqrt{\gamma}}{J}\, \psi_{\eta}(\xi,1) \quad . \tag{7-11}$$

For futher simplicity, the derivative ψ_{η} in equation (7-11) can be approximated by a second order forward difference formulation. The final expression of the tangential velocity along an airfoil becomes

$$v_t(\xi,1) = \frac{\sqrt{\gamma}}{J}\left[-3\psi(\xi,1) + 4\psi(\xi,2) - \psi(\xi,3)\right] \quad . \tag{7-12}$$

In order to obtain the explict expression for the constant α, equation (7-8) is substituted into equation (7-12). After rearrangement, equation (7-12) becomes

$$v_t(\xi,1) = \Psi_{12}(\xi,1) + \Psi_{13}(\xi,1) \quad , \tag{7-13}$$

where

$$\begin{aligned} \Psi_{12}(\xi,1) &= 4\frac{\sqrt{\gamma}}{J}\Big[\cos\alpha\, \psi^1(\xi,2) + \sin\alpha\, \psi^2(\xi,2) \\ &\qquad -\cos\alpha\, \psi^1(\xi,3) + \sin\alpha\, \psi^2(\xi,3)\Big] \quad , \\ \Psi_3(\xi,1) &= \frac{\sqrt{\gamma}}{J}\left[-3 + 4\psi^3(\xi,2) - 4\psi^3(\xi,3)\right] \quad . \end{aligned} \tag{7-14}$$

ORIGINAL PAGE IS
OF POOR QUALITY

It is noted that the boundary conditions in equations (7-5), (7-6) and (7-7), $\psi^1(\xi, \eta_1) = \psi^2(\xi, \eta_1)$ and $\psi^3(\xi, \eta_1) = 1$ have been applied in the above manipulation. In evaluating the tangential velocities at the edge point on the both sides of the airfoil, the quadratic extrapolation is employed in this study. For example, on the upper surface, the extrapolated function is assumed to be

$$v_t^u(\xi,1) = a\xi^2 + b\xi + c \quad , \tag{7-15a}$$

with three conditions

$$\begin{aligned} v_t^u(\xi,1) &= v_t(1,1) \qquad \text{at } \xi = 1 \quad , \\ v_t^u(\xi,1) &= v_t(2,1) \qquad \text{at } \xi = 2 \quad , \\ v_t^u(\xi,1) &= v_t(3,1) \qquad \text{at } \xi = 3 \quad . \end{aligned} \tag{7-15b}$$

This extrapolation is illustrated in Fig. (34). A similar extrapolated function can be obtained for the lower surface according to the equation (7-15).

Consequently, the extrapolated tangential velocity at the edge point on upper side and lower side as shown in Fig. (1) are

$$v_t^u(0,1) = 3v_t(1,1) - 3v_t(2,1) + v_t(3,1) \quad , \tag{7-16a}$$

$$v_t^L(0,1) = 3v_t(-1,1) - 3v_t(-2,1) + v_t(-3,1) \quad . \tag{7-16b}$$

ORIGINAL PAGE IS
OF POOR QUALITY

Here the locations $(\xi,1)$ for $\xi=0$, 1, 2, 3, -1, -2 and -3 are shown in Fig. (34) and the value of $v_t(\xi,1)$ can be calculated from equation (7-13). Therefore, numerically the Kutta condition implies that

$$v_t^u(0,1) = v_t^L(0,1) \quad , \tag{7-17}$$

From equations (7-14), (7-16) and (7-17), the expression to the constant μ is obtained as

$$\mu = -\frac{\Psi_{12}^u - \Psi_{12}^L}{\Psi_3^u - \Psi_3^L} \quad , \tag{7-18}$$

where

$$\begin{aligned}
\Psi_{12}^u &= 3\Psi_{12}(1,1) - 3\Psi_{12}(2,1) + \Psi_{12}(3,1) \quad , \\
\Psi_3^u &= 3\Psi_3(1,1) - 3\Psi_3(2,1) + \Psi_3(3,1) \quad , \\
\Psi_{12}^L &= 3\Psi_{12}(-1,1) - 3\Psi_{12}(-2,1) + \Psi_{12}(-3,1) \quad , \\
\Psi_{12}^L &= 3\Psi_3(-1,1) - 3\Psi_3(-2,1) + \Psi_3(-3,1) \quad ,
\end{aligned} \tag{7-19}$$

which $\Psi_{12}(\xi,1)$ and $\Psi_3(\xi,1)$ for $\xi = 1$, 2, 3, -1, -2 and -3 can be calculated from equation (7-14). It is remarked that if the denominator of equation (7-18) vanishes, the numerator $\Psi_{12}^u - \Psi_{12}^L$ must vanish, too. Thus, the constant μ is set to zero. This situation may occur in the nonlifting airfoil, for example, the symmetry airfoil NACA-0018 at zero angle of attack.

ORIGINAL PAGE IS
OF POOR QUALITY

7.4 FA Numerical Solution

The numerical solution of equation (7-2) is obtained by the FA method. In this potential flow problem, the FA algebraic equation of the stream function evaluated at the center point P of an element is exactly the same as equation (4-33) except that the vorticity ω vanishes. It is

$$\psi_P = \sum_{n=1}^{8} C'_n \psi_n \quad , \tag{7-20}$$

where C'_n are the FA coefficients surrounding the center node, which can be calculated from equation (4-22). For the computational field appearing in Fig. (2) the system of algebraic equation can be expressed as

$$\psi_P(\xi,\eta) = \sum_{n=1}^{8} C'_n(\xi,\eta)\, \psi_n(\xi,\eta) \quad , \tag{7-21}$$

for all $\xi_1 \le \xi \le \xi_2$ and $\eta_1 \le \eta \le \eta_2$.

In this investigation, the line-by-line implicit iteration method is employed to solve the system of the algebraic equation (7-21). The criterion of convergence is that the maximum difference of the stream function for all the point in the computatuional field is $|\Delta\psi_{max}| < 10^{-5}$ between two iterations. The computer program for solving this potential problem is listed in Appendix C-1.

ORIGINAL PAGE IS
OF POOR QUALITY

7.5 Numerical Results And Discussion

The numerical solutions of the uniform flow passing the NACA-0018 and the Karmann-Treftz airfoils at three different angles of attack, 0, 5 and 10, are presented. The stream function contours for these two airfoil sections are shown in Fig. (35) and (36). It is shown that the Kutta condition is satisfied so that the divided stream line smoothly leaves the trailing edge.

The pressure cofficient C_p is an important parameter in the potential flow, which may be obtained at any point in the field by application of Bernoulli equation. It is

$$C_p = \Delta p/(0.5\rho U_0^2) = 1-(u/U_0)^2 .$$

For the case of the symmetric NACA-0018 airfoil at zero angle attack, the calculated distribution of $(u/U_0)^2$ (or $1-C_p$) along the airfoil surface is compared with the experimental results from [34]. In Fig. (37), it is shown that the FA results is in agreement with the experimental measurements (at average Reynolds number of 3,100,000) near the leading edge, while a slight difference exists near the trailing edge. This is because the thickness of the trailing edge of the experimental model is not zero but with a definite thickness of 0.189 percent of the chord length.

In this study, the lifting coefficient is another important parameter and the discussion is given below. The

ORIGINAL PAGE IS
OF POOR QUALITY

lifting coefficient for the two-dimensional flow, C_L, is defined as

$$C_L = F_L/(0.5\ \rho\ U_0^2\ L)\ ,$$

where L is the characteristic length and F_L is lifting force. Utilizing the Kutta-Joukowski theorem, $F_L = \rho\, U_0\, \Gamma$, one obtains the simple relationship between C_L and the circulation Γ, or

$$C_L = 2\Gamma/U_0\, L.$$

The computer program for calculating the circulation around an airfoil is given in Appendix C-2. The results of lifting coefficients for both the NACA-0018 and the Karmann-Trefftz airfoils at different angles of attack considered are exhibited in Fig. (38). The lifting coefficients are linearly related to the angles of attack over the range considered. Due to the effect of the camber, the C_L of the Karmann-Trefftz airfoil is larger than that of NACA-0018 for the angles of attack considered. This trend is shown in Fig. (38). It is noted that all of the values of the C_L lie above the theoretical value for thin wings, 2π per radian. This result is in accordance with the thin wings theory that C_L tends to increase with increasing thickness of an airfoil.

ORIGINAL PAGE IS
OF POOR QUALITY

In this potential problem with arbitrary boundaries, the FA method with the boundary-fitted coordinate system is employed to solve the Laplace equation. The numerical solutions calculated are in good agreement with those of theoretical and experimental results. Hence, in the next chapter, the FA method with the boundary-fitted coordinate system is extended to solve the viscous flow and heat transfer problem involving complex boundaries.

ORIGINAL PAGE IS
OF POOR QUALITY

CHAPTER VIII

HEAT TRANSFER PROBLEM OF TUBE BUNDLES

8.1 General Remarks

In this chapter convective heat transfer for two-dimensional incompressible flow past tube bundles is investigated. The study of heat transfer in tube bundles has attracted great interest in the past mainly because of the importance of the flow configuration in the design of heat exchangers [35,36,37]. In addition, when the tubes are densely compact, the problem can serve as a basic model of the flow through a porous medium [38]. Because of the difficulty in making theoretical or numerical predictions of flow and heat transfer in this complex geometry, previous studies of the problem are mostly experimental [35,39], that is, building a scale model of the tube bundles under consideration. In general, experiments are carried out in a tunnel [35]. Hot fluid is blown over the tubes in which cooling fluid is circulated so that measurements can be made. The empirical correlations thus are obtained for variation of flow patterns, relating heat transfer coefficients and pressure losses with the Reynolds number and the geometry. Details of work are given by Zukauskas

ORIGINAL PAGE IS
OF POOR QUALITY

[39]. However, experimental approaches not only cost money but also consume time, since for each new geometry considered a new model must be constructed . An alternative approach is computer simulation by solving the partial differential equation numerically. To date, for a typical two-dimensional laminar recirculating flow problem with reasonably simple and confined boundaries, the prediction of heat transfer and flow patterns can be obtained in about twenty minutes computational time on a PRIME 750 computer. Therefore, the cost of such an exploration is usually a small fraction of the cost of a experiment. The comprehensive account of numerical studies up to 1978 is reviewed in [40]. However, an obstacle to the use of numerical methods in this problem of tube bundles is the irregular boundaries. In order to make the problem more tractable , numerical handling of the irregular geometries must be first addressed. Several possible choices of grid systems in finite difference studies of tube bundles have been carried out. They are briefly described below.

1. Thom and Apelt [41] employed the conformal mapping technique to transform the boundaries of the staggered tubes such that they coincide with equi-valued surfaces of one of the independent variables, as shown in Fig. (39a). This coordinate transformation that maps the irregular curved surface

ORIGINAL PAGE IS
OF POOR QUALITY

onto coordinate lines is excellent since it produces a low density of grid lines near the surface precisely where an accurate numerical solution demands a fine grid.

2. In another numerical work, Le Feuvre [42] adopted a Cartesian grid in which the spacing between nodes is adjusted so that all the near-wall nodes fall on the in-line surfaces of tubes, as indicated in Fig. (39b). This grid was also adopted earlier by Thoman and Szewczyk [43] to study the flow past a single tube. This grid coordinate is far from ideal since it produces high densities of nodes in regions outside the wall where they are not needed. Le Feuvre also found that the numerical solution obtained on this coordinate system was particularly susceptible to numerical diffusion because of the streamline near the tube cutting diagonally across the grid.

3. Launder and Massey [40] used two coordinate systems as illustrated in Fig (39c). The cylindrical grid system is used near the tube while the Cartesian grid is filled in the remaining region between the tubes. The idea of adopting two coordinates systems comes from the fact that close to each tube the steepest gradients of flow properties are in the radial direction. However at the overlapped region between

ORIGINAL PAGE IS
OF POOR QUALITY

the cylindrical and Cartesian grids, a false row of nodes is introduced to provide a connection between the Cartesian and polar regions. The disadvantage of this two coordinates systems is that the cylindrical coordinate system cannot be applied for non-circular tubes.

In the present study, the boundary-fitted coordinate system described in Chapter III is employed to generate a curvilinear coordinate system (ξ,η). The transformed coordinate system for the problem of staggered tube bundles is developed in Chapter III and is plotted in Fig. (5c). For completeness, the boundary-fitted curvilinear coordinate system that is on the physical plane is given in Fig. (40). It is observed that not only the boundaries of tubes are mapped onto constant η-lines, but also the η-lines become dense near the tube boundaries. Thus, in the following study, the boundary-fitted coordinate system illustrated in Fig. (40) or (41) is adopted. After the governing equations for the stream function, vorticity and temperature function are transformed into (ξ,η) coordinates and the corresponding initial and boundary conditions are introduced, the FA solutions can be obtained. The FA numerical procedures are dicussed below.

ORIGINAL PAGE IS
OF POOR QUALITY

8.2 Governing Equation

In the present study the atttenis forcused on fully-developed region of flow in tube bundles, i.e., the situation where the flow pattern is exactly repeated from one row to the next. The configuration for tube bundles chosen is illustrated in Fig. (40), which was used in the works of Thom and Apelt [41] and Launder and Massey [40]. The reason for choosing this geometry is to reduce the difficulty in making comparisons.

The stream function-vorticity formulation of the two-dimensional incompressible viscous flow equations in dimensionless form is

$$Re\ (\omega_t + \psi_y \omega_x - \psi_x \omega_y) = \omega_{xx} + \omega_{yy} \quad , \tag{8-1}$$

$$\psi_{xx} + \psi_{yy} = -\omega \quad , \tag{8-2}$$

and the energy equation is

$$Pe\ (\theta_t + \psi_y \theta_x - \psi_x \theta_y) = \theta_{xx} + \theta_{yy} \quad . \tag{8-3}$$

where ψ , ω and θ are dimensionless and are the stream function , vorticity and temperature, respectively, which are normalized by $U_r L_r$, U_r/L_r and $(T_w - T_0)$. Re is the Reynolds number $U_r L_r/\nu$ and the Peclet number is Pe = Pr Re. Here U_r and L_r are taken to be unit characteristic velocity and length respectively. The reference temperature is taken

ORIGINAL PAGE IS
OF POOR QUALITY

to be the difference between the constant inlet temperature of fluid T_0 and the isothermal temperature on the tube T_w.

Since the dimensionless governing equations (8-1) through (8-3) are given in the physical plane with the Cartesian coordinates (x,y), these equations must be transformed and expressed in boundary-fitted coordinates (ξ,η) as illustrated in Figs. (40) or (41). Ultilizing the operators given in from Appendix (A-1 to A-18), the transformed governing equations are

$$\frac{J^2 Re}{\alpha}\omega_t + \left(\frac{J\ Re}{\alpha}\psi_\eta - \frac{\tau}{\alpha}\right)\omega_\xi + \left(\frac{-J\ Re}{\alpha}\psi_\xi - \frac{\sigma}{\alpha}\right)\omega_\eta - \omega_{\xi\xi} - \frac{\gamma}{\alpha}\omega_{\eta\eta} = -\frac{2\beta}{\alpha}\omega_{\xi\eta}\ , \tag{8-4}$$

$$\frac{\tau}{\alpha}\psi_\xi + \frac{\sigma}{\alpha}\psi_\eta + \psi_{\xi\xi} = \frac{2\beta}{\alpha}\psi_{\xi\eta} - \frac{J^2}{\alpha}\omega\ . \tag{8-5}$$

$$\frac{J^2 Pe}{\alpha}\omega_t + \left(\frac{J\ Pe}{\alpha}\psi_\eta - \frac{\tau}{\alpha}\right)\theta_\xi + \left(\frac{-J\ Re}{\alpha}\psi_\xi - \frac{\sigma}{\alpha}\right)\theta_\eta - \theta_{\xi\xi} - \frac{\gamma}{\alpha}\theta_{\eta\eta} = \frac{-2\beta}{\alpha}\theta_{\xi\eta}\ , \tag{8-6}$$

where ψ, ω, Re and Pe are as defined above and the coefficients of coordinates transformation α, β, γ, J, σ and τ are introduced in equations (4-8) and (4-9), respectively. It is noted that since the boundary-fitted coordinate system is stationary and independent of time in this study, the coefficients of coordinate transformation defined above are fixed and can be calculated once and for all.

ORIGINAL PAGE IS
OF POOR QUALITY

8.3 Initial And Boundary Conditions

With reference to Fig. (40a), the initial and boundary conditions for the governing equations (8-1) and (8-2) for the stream function and vorticity in the physical plane (x,y) are given below.

At t>0, on the contour Γ_1 of upper boundary $\overline{BC}$ (symmetry line)

$$\omega(x,y,t) = 0 ,$$
$$\psi(x,y,t) = 4 .$$

On the contour Γ_4 of the lower boundary $\overline{EF}$ (symmetry line)

$$\omega(x,y,t) = 0 ,$$
$$\psi(x,y,t) = 0 .$$

Along the upper boundary contour Γ_2 of the tube $\overline{CD}$

$$\omega(x,y,t) = \omega_u(x,y,t) ,$$
$$\psi(x,y,t) = 4 ,$$
$$\partial\psi(x,y,t)/\partial\vec{n} = 0 .$$

Along the lower boundary contour Γ_5 of the tube $\overline{AF}$

$$\omega(x,y,t) = \omega_L(x,y,t) ,$$
$$\psi(x,y,t) = 0 ,$$
$$\partial\psi(x,y,t)/\partial\vec{n} = 0 .$$

ORIGINAL PAGE IS
OF POOR QUALITY

And at t=0 the initial conditions for fluid is taken to be rest

$$\omega\ (x,y,t) = 0\ ,$$

$$\psi\ (x,y,t) = 0\ .$$

In equations (8-7c) and (8-7d) n denotes the unit vector which is normal to the boundaries at all points. The vorticity boundary functions on the tubes $\omega_u(x,y,t)$ and $\omega_L(x,y,t)$ are unknown and must be calculated as parts of the governing equations (8-1) and (8-2). Therefore, two alternate but natural boundary conditions (impermeable condition) are given in equation (8-7c) and (8-7d). To complete the specification of the boundary conditions one must specify the conditions on boundaries $\overline{AB}$ and $\overline{DE}$. Because the fully developed flow is considered in this study, the flow pattern is expected to repeat from a row to the next. Therefore, the re-entrant (or vertical) boundary conditions at the inlet (contour $\overline{AB}$ or Γ_6) and the outlet (contour $\overline{DE}$ or Γ_3) stations are treated as periodic. This implies that the values of the dependent variables along $\overline{AB}$ are identical with those along $\overline{DE}$. Specially referring to Fig. (40a), with distances $\overline{EH}=\overline{BG}$ and $\overline{HD}=\overline{GA}$ one may set

$$\omega_D = -\omega_A \quad , \quad \omega_H = -\omega_G \quad , \quad \omega_E = -\omega_B \quad , \qquad \text{(8-8a)}$$

also

$$\psi_A + \psi_D = \psi_G + \psi_H = \psi_B + \psi_E = 4 \quad , \tag{8-8b}$$

where from equation (8-7a) one has

$$\psi_{B-C-D} = 4 \quad , \quad \psi_{A-F-E} = 0 \quad , \quad \psi_G = \psi_H \quad . \tag{8-8c}$$

In computations, the values of the dependent variables are taken from the outlet boundary (contour Γ_3) and placed on the inlet boundary (contour Γ_6) as described in equation (8-8) to serve as boundary conditions during the next cycle of the iteratrion.

In the case of the temperature, the scheme described above is modified to account for the fact that due to the heat transfer from tubes, the inlet and outlet temperatures are not the same. Hence, in the computation of the temperature distribution, the computational field Fig. (40a) is extended twice that of the flow calculation as shown in Fig. (41a). With reference to Fig. (41a), the initial and boundary conditions of temperature in the energy equation (8-3) are as follows.

At t>0, along the inlet boundary $\overline{AB}$, tube boundaries (unheated tubes) $\overline{AH}$ and $\overline{FG}$ (i.e., contours Γ_8, Γ_7 and Γ_5)

$$\theta\,(x,y,t) = 0 \ . \tag{8-9a}$$

On the contour Γ_2 of tube boundary $\overline{CD}$ (heated tube)

ORIGINAL PAGE IS
OF POOR QUALITY

$$\theta(x,y,t) = 1 \ . \tag{8-9b}$$

On the symmetry planes $\overline{BC}$ and $\overline{DE}$ (i.e., contours Γ_1, Γ_3)

$$\theta(x,y,t)/\partial\hat{n} = 0 \ . \tag{8-9c}$$

On the contour Γ_4 of the outlet boundary $\overline{EF}$

$$\theta(x,y,t) = \theta_e = \text{constant} \ . \tag{8-9d}$$

For the contour Γ_6 along $\overline{GH}$ it is assumed no or negligible heat flux passing through the boundary or

$$\theta(x,y,t)/\partial\hat{n} = 0 \ . \tag{8-9e}$$

At t=0, the initial condition is

$$\theta(x,y,0) = 0 \ , \tag{8-9f}$$

where θ_e taken as a constant equal to the averaged temperatue at the outlet boundary $\overline{EF}$. This constant temperature θ_e may be obtained by making an energy balance over the computational domain. This will be discussed in detail later.

Physically, the initial and boundary conditions specified for the temperature simulate a heat exchanger with staggered tube bundles where one particular tube is heated while the others are unheated. When the problem is solved it may reveal the difference of the heat transfer

ORIGINAL PAGE IS
OF POOR QUALITY

coefficient between a single tube in a uniform flow and that in a flow past staggered tube bundles.

Since the governing equations (8-4) through (8-6) are given on the transformed plane (ξ,η), the initial and boundary conditions of equations (8-7) through (8-9) have to be transformed into the same plane. As shown in Fig. (40b), this coordinate transformation for the stream function ψ and vorticity ω yields the relations as follows.

At t>0

$$
\begin{aligned}
&\omega(\xi, JMAX, t) = 0 && \text{in } [\xi, JMAX] \in \Gamma_1^*, \\
&\omega(\xi, JMAX, t) = \omega_u(\xi, JMAX, t), && \text{in } [\xi, JMAX] \in \Gamma_2^*, \\
&\omega(\xi, 1, t) = 0 && \text{in } [\xi, 1] \in \Gamma_4^*, \\
&\omega(\xi, 1, t) = \omega_L(\xi, 1, t) && \text{in } [\xi, 1] \in \Gamma_5^*,
\end{aligned}
\tag{8-10a}
$$

$$
\begin{aligned}
&\psi(\xi, JMAX, t) = 4 && \text{in } [\xi, JMAX] \in \Gamma_1^* \text{ or } \Gamma_2^*, \\
&\psi(\xi, 1, t) = 0 && \text{in } [\xi, 1] \in \Gamma_4^* \text{ or } \Gamma_5^*, \\
&\partial\psi(\xi, JMAX, t)/\partial n = 0 && \text{in } [\xi, JMAX] \in \Gamma_2^*, \\
&\partial\psi(\xi, 1, t)/\partial n = 0 && \text{in } [\xi, 1] \in \Gamma_5^*,
\end{aligned}
\tag{8-10b}
$$

and at t=0, the initial condition is

$$
\begin{aligned}
&\omega(\xi, \eta, 0) = 0, \\
&\psi(\xi, \eta, 0) = 0.
\end{aligned}
\tag{8-10c}
$$

The initial and boundary conditions in equation (8-9) for temperature illustrated in Fig. (41b) are transformed and become

ORIGINAL PAGE IS
OF POOR QUALITY

At t>0

$$\theta(1,\eta,t) = 0 \qquad \text{in } [1,\eta] \in \Gamma_8^* ,$$
$$\theta(\xi,1,t) = 0 \qquad \text{in } [\xi,1] \in \Gamma_7^* \text{ or } \Gamma_5^* ,$$
$$\theta(\xi,JMAX,t) = 1 \qquad \text{in } [\xi,JMAX] \in \Gamma_2^* ,$$
$$\partial\theta(\xi,Jmax,t)/\partial\hat{n} = 0 \qquad \text{in } [\xi,JMAX] \in \Gamma_1^* \text{ or } \Gamma_3^* ,$$
$$\partial\theta(\xi,1,t)/\partial\hat{n} = 0 \qquad \text{in } [\xi,1] \in \Gamma_6^* , \qquad (8\text{-}11a)$$
$$\theta(IMAX,\eta,t) = \theta_e = \text{const.}, \qquad \text{in } [IMAX,\eta] \in \Gamma_2^* ,$$

and at t=0, the initail temperature condition for the computational field is

$$\theta(\xi,\eta,0) = 0 , \qquad (8\text{-}11b)$$

where IMAX and JMAX are the maximum node numbers on the ξ- and η- coordinates in the transformed plane shown in the Figs. (40b) and (41b), respectively.

It should be remarked that in the calculation of the stream function-vorticity formulation in equations (8-4) and (8-5), both the accurate determination of the unknows on tube boundaries $\omega_u(\xi,JMAX,t)$ and $\omega_L(\xi,1,t)$, and the satisfication of the no-slip condition on tubes as stated in equation (8-10b) are very important. Although vorticity function on the tubes are readily defined by equation (8-5) when the stream function is solved from equation (8-5) and the impermeable condition in equation (8-10a). During numerical iterations, one should realize that the no-slip

ORIGINAL PAGE IS
OF POOR QUALITY

condition (8-10b) which is the alternative boundary condition for vorticity is not satisfied. In order to incorporate the no-slip condition (8-10b) in evaluation of vorticity boundary conditions, some modification of equation (8-5) on the boundaries ω_u and ω_L must be introduced. This modification is introduced in an attempt to insure that the alternative vorticity condition or no-slip condition (8-10b) is satisfied. A variety of numerical procedures approximating the equation (8-5) and satisfying the no-slip condition are documented in [1]. Several approaches suggested by Roache [1] are tested in the present study. Numerical results are found either inaccurate or even divergent. The main reason is perhaps the assumption that no-slip condition is automatically assumed for the solution of the stream function during numerical iterations when it is solved only to satisfy the impermeable condition. Israeli [44] thus suggests that ω_u and ω_L be calculated with an iterative algorithm including a correlation of the slip velocity $\partial\psi/\partial\eta$ on the wall which is obtained during the iterative procedure as follow

$$\omega_u^{k+1}(\xi_i, JMAX, t_n) = \omega_u^{k}(\xi_i, JMAX, t_n) - \gamma\left[\frac{\partial\psi}{\partial\eta}(\xi_i, JMAX, t_n)\right]^k \quad . \qquad (8\text{-}12)$$

ORIGINAL PAGE IS
OF POOR QUALITY

Here $\partial\psi/\partial\hat{n}$ is the no-slip velocity in the wall boundary. denotes the ξ - position along the tube wall. JMAX is the η - value for the tube, t_n is the current time, k is the iteration counter at time t_n and γ is an under-relaxation factor (γ=1 in this study) for the slip velocity correction. A similar expression like equation (8-12) may be obtained for ω_L. The direction derivative $\partial\psi/\partial\hat{n}$ of equation (8-12) in boundary-fitted coordinates is given by equation (A-21), in which the second-order forward difference is approximated for the η - derivative and central difference for the ξ - derivative. Obviously, the procedure of equation (8-12) is written implicity in time which required iterations at each time step. It is important to note that convergence of the sequence $[\partial\psi(\xi_i, JMAX, t_n)/\partial\hat{n}]$ to zero implies convergence of and the satisfication of the no-slip condition. Equation (8-12) is adopted in the present study.

Temperature boundary conditions are given in equation (8-11) for the energy equation (8-6). Detail expression for the temperature derivative $\partial\theta/\partial\hat{n}$ is given by equation (A-21). The constant temperature θ_e of the outlet boundary Γ_4 shown in Fig. (41a) is determined by balancing the energy in the flow field and is

$$\int_{\Gamma_3} K \left.\frac{\partial T}{\partial n}\right|_w d\bar{s} = \int_{\Gamma_4} C_p (T_e - T_0) \rho u \, dy \quad , \qquad (8\text{-}13)$$

ORIGINAL PAGE IS
OF POOR QUALITY

where k is the conductivity and C_p is specific heat of the fluid. If equation (8-13) is non-dimensionlized, the isothermal temperature $\theta_e=(T_e-T_0)/(T_w-T_0)$ of the outlet boundary of Γ_4 becomes

$$\theta_e = \frac{q}{Pe\ Q} \quad , \tag{8-14a}$$

where

$$Q = \int_{\Gamma_4} u\ dy \quad , \tag{8-14b}$$

$$q = \int_{\Gamma_2} \frac{\partial\theta}{\partial n}\bigg|_w d\bar{s} \quad , \tag{8-14c}$$

where Pe is the Peclet number defined as before, and $\bar{s}$ is an element of arc lengtn along the tube wall. In equation (8-13), Q is total mass flow rate across the outlet contour Γ_4 (Q=4 in this study), and q denotes the heat flux along the contour Γ_2 of the tube. This heat flux q can be calculated from equation (8-14c) by any numerical integration method, for example, the trapezoidal rule.

8.4 FA Solutions Of Tube Bundles Problem

The governing equations (8-4) through (8-6) for the flow and heat transfer in the tube bundles problem are for the two-dimensional incompressible flow with constant properties. Thus, the flow pattern is uncoupled from temperature. The stream function and vorticity equations

ORIGINAL PAGE IS
OF POOR QUALITY

(8-4) and (8-5), can be solved first and then the temperature distribution obtained from the energy equation (8-6) afterward.

The FA method described in Chapter IV is employed to obtain the numerical solution for this problem. The FA algebraic equation for vorticity, stream fucction and temperature in each element have already been cited separately in equations (4-21), (4-33) and (4-36). They are summaried below for completeness.

$$\omega_P = \sum_{n=1}^{8} C_n \, \omega_n + C_P \, g_P \quad , \tag{8-14}$$

and

$$\psi_P = \sum_{n=1}^{8} C'_n \, \psi_n + C'_P \, g_P \quad , \tag{8-15}$$

where the FA coefficients C_n and C_P are calculated from equations (4-22) and (4-23), and the source term g_P is given by equations (4-18) and (4-32), respectively. Temperature equation can be similarly given as

$$\theta_P = \sum_{n=1}^{8} C_n \, \theta_n + C_P \, g_P \quad , \tag{8-16}$$

where C_n and g_P correspond to the FA coefficients and the source term, are similar to equation (8-14) except that the

ORIGINAL PAGE IS
OF POOR QUALITY

Reynolds number is replaced by the Peclet number and ω replaced by θ. The iterative calculation procedure is treated as a time marching method in the present study. Details have already been discussed in Section (4-4-3). The computer programs for calculating the stream function, vorticity and temperature are given in Appendex C-5 and C-6.

8.5 Results And Discussion

In this section, the results of the FA solutions for the flow past tube bundles are presented. In addition to the stream function and vorticity distribution, the heat transfer problem is also investigated. The comparison of the FA solutions with experimental measurements and earlier numerical predictions is made.

8.5.1 Conversion Of The Reynolds Numbers

In different references, different characteristic scales are used in defining the Reynolds number. Therefore, in order to avoid confusion in comparing the present FA solutions with those given in references, the Reynolds numbers used in these references must be first converted into that of the present study.

As mentioned before, the configuration of tube bundles chosen in this study is the same as that of Thom and Apelt [41] and shown in Fig. (40a). This staggered arrangement of

ORIGINAL PAGE IS
OF POOR QUALITY

tubes is defined by the transverse and longitudinal center to center distances (or called transverse and longitudinal pitches) which are 13.08 and 8.9 respectively. Between two symmetric planes BC and EF the mass flow rate is assigned as $(\psi_B - \psi_A) = 4$. There are several Reynolds numbers used in previous investigations. In order to relate these different Reynolds numbers, a reference Reynolds number is defined as

$$Re = \frac{L_r U_r}{\nu} , \tag{8-17a}$$

where L_r and U_r are unit characteristic length and velocity. In case of Fig. (40a), the diameter of the tube D is

$$D = 5.34 L_r , \tag{8-17b}$$

and both the mean velocity U_m across the line $\overline{MN}$ (the largest fluid cross section) and the averaged inlet velocity U_i across $\overline{AB}$ (the smallest fluid cross section) are found to be

$$U_m = \frac{1}{|\overline{MN}|} \int_{y_N}^{y_M} u \, dy = \frac{\psi_M - \psi_N}{6.54} = \frac{4}{6.54} U_r , \tag{8-17c}$$

$$U_i = \frac{1}{|\overline{AB}|} \int_{y_A}^{y_B} u \, dy = \frac{4}{3.87} U_r . \tag{8-17d}$$

ORIGINAL PAGE IS
OF POOR QUALITY

Based on equation (8-16) and (8-17), the conversions of the Reynolds number appearing in references are summarized as follows.

1. Re_m defined in [41] by Thom and Apelt is

$$Re_m = \frac{U_m D}{\nu} = \left(\frac{4}{6.54} 5.34 \right) \frac{U_r L_r}{\nu} = 3.26 \, Re \, . \tag{8-18a}$$

2. Re_i defined in [40] by Launder and Massey is

$$Re_i = \frac{U_i D}{\nu} = \left(\frac{4}{3.88} 5.34 \right) \frac{U_r L_r}{\nu} = 5.5 \, Re \, . \tag{8-18b}$$

3. Re_c defined in [35,36,37] by Bergelin et al.

In series of experimental works by Bergelin et al. [35,36,37], the Reynolds number is defined as $Re_c = G_m D_v / \mu$ where G_m denotes mass velocity through minimum cross section $\overline{AB}$ and D_v denotes the volumetric hydraulic diameter, or

$$G_m = \rho U_i \quad \text{and} \quad D_v = 4 r_h \, ,$$

where ρ is the density and r_h is the hydraulic radius defined as cross-sectional area (i.e., rectangular area 8.9*6.54 subtracted by one half circle area $\pi D^2/8$) divided by a wetted perimeter. The value of D calculated for this configuration is 8.15 L_r. This gives

ORIGINAL PAGE IS
OF POOR QUALITY

$$Re_c = \frac{G_m D_v}{\mu} = \left(\frac{4}{3.88} 8.15 \right) \frac{U_r L_r}{\nu} = 8.4 \ Re \quad . \qquad (8\text{-}18c)$$

4. Re_d defined in the uniform flow passing a single tube

For the uniform flow passing a single tube with an approaching velocity U, the Reynolds number is commonly defined as $Re_d = UD/\nu$. If the velocity U is set equal to the mean velocity U_m across $\overline{MN}$, then the Reynolds number Re_d becomes

$$Re_d = \frac{U D}{\nu} = \frac{U_m D}{\nu} = Re_m = 3.26 \ Re \quad . \qquad (8\text{-}18d)$$

which is the same as Re_m shown in case 1.

With these relationships and classification of various Reynolds numbers defined in previous works, the Reynold number $Re_m = U_m D/\nu$ is used in the following discussion. It should be remarked that the computer program presented in Appendix C-5 is for dimensionless formulation with unit velocity U_r, unit length L_r and $Re = U_r L_r/\nu$. The reason for this choice is to make the program flexible to adopt different tube diameters or/and longitudinal and transverse pitches.

ORIGINAL PAGE IS
OF POOR QUALITY

8.5.2 Stream Function And Vorticity Distribution

The stream function and vorticity distributions of the two-dimensional incompressible flow past the staggered tube bundles are plotted in Figs. (42,43). Fig. (42) gives the contours of the stream function for Re_m = 16, 98, 160 and 320 at an interval increment of $\Delta\psi$ =0.5. It is seen that variation of the flow pattern arround a tube is a strong function of the Reynolds number. It is symmetric with respect to the horizontal axis and periodic from a row to the next or from a column to another. Therefore, the unsteady vortex shedding phenomena behind a tube is not considered in this study.

For a small Reynolds number of 16, Fig. (42a) shows that the stream approaches the front of a tube like a stagnation point flow, and then is deflected side ways around the tube to the downstream. Although no eddies or separation is found, the streamlines tend to move away from the rear of the tube. This implies that the flow is decelerated and the boundary layer becomes thick. For larger Reynolds numbers of 98, 160 and 320, there are two attached eddies behind each tube shown in Figs. (42b,c,d). These eddies grow larger with increasing Re_m. As illustrated in Fig. (42d) at Re_m=320, the front part of the tube is enclosed by the elongated eddy induced by the tube ahead of

ORIGINAL PAGE IS
OF POOR QUALITY

the tube. There are no experimental mesurements of separation eddies known for the present geometry in laminar flow. However, Zukauskas [39] observed in turbulent flow that the elongated flow separation reattaching at the latter tube is possible under an appropriate longitudinal pitch between the tubes at a large Reynolds number of 3200. Observing Fig. (42d), one may realize that when elongated eddies are filled between tubes, the remaining flow passes the tube banks as if it flows through a curved channel of periodically convergent and divergent cross sections.

Contours of constant vorticity are shown in Fig. (43). The concentration of the vorticity is seen to persist for a long distance downstream at large Reynolds numbers. Another feature exhibited in Fig. (43) is the existence of the flow zone in the rear part of a tube where the vorticity changes sign. Further detail of changing sign of the vorticity in the separation zones is discussed in [45]. Fig. (43) also shows that at the low Reynolds number Re_m=16, the boundary layer begins to develop near the front part of the tube so that the vorticity concentration is essentially confined there. When the Reynolds number is greater than 50, the contours of constant vorticity begin to swing downstream, while the separation zone behind the tube lengthens. The streamlines of the through-flow that passes among the staggered tubes begin to look like an wavy 'S' shape. At an

even larger Reynolds number of 98, Fig. (43) shows that the strong vorticity generated along the front part of a tube is mostly confined to a thin boundary layer. The vorticity behind the tube begins to diffuse away due to the flow separation as shown in Figs. (43b,c). For the flow of Re_m =320 shown in Fig. (43d), the eddy regions behind a tube are so elongated as to touch and enclose the front part of the downstream tube. As a result, a constant vorticity core seems to be formed. A comparision is made with an earlier prediction by Thom and Apelt [41] for flows past the same staggered tube banks shown in Fig. (44) at Re_m=50. The distribution of the stream function predicted by the present study (solid line) shows excellent agreement with the results of Thom and Apelt dotted lines. This comparison implies that for this case of Re_m=50 the FA method with the nonorthogonal boundary-fitted coordinate systems is as good as the orthogonal coordinate systems generated by the conformal mapping technique. Launder and Massey [40] also predicted this flow field for Thom and Apelt's geometry at Reynolds number Re_m=50. In [40], Launder and Massey compared their result at Re_i=75 (Re_m=45.5) with that of Thom and Apelt at Re_m=50 and indicated a significant difference between the two. However, according to the conversion derived in equations (8-18a,b), Re_m=50 of Thom and Apelt is equivalent to Re_i=84 and not 75. It is the error in

ORIGINAL PAGE IS
OF POOR QUALITY

converting different definitions of the Reynolds number that led to the incompatible comparison and the criticism by Launder and Massey of Thom and Apelt's results. Fig. (45) compares the predictions of Launder and Massey [40] (in dotted lines) and the present study (in solid lines) at Re_m =44.7 (Re_i =75). The discrepancy between the two results probably is because of the Launder and Massey's linear interpolation scheme in the overlapped regions between the polar coordinate and the Cartesian coordinate systems where coordinate lines are not smooth and continuous.

Fig. (46) illustrates the relationship between the length of the eddy and the Reynolds number for the single tube and the staggered banks. It is observed that the blocked effect of the staggered bank has substantially suppressed the initial formulation of eddies behind the tube. In this study, the eddies still do not appear at Re_m =16, while for the single tube, the eddies appear around Re_m =5. From Fig. (46), one may interpolate from the present prediction that the eddies may be elongated and touch the downstream tube at around Re_m =310.

From experimental study [36], Bergelin et al. indicated that the transition from laminar to turbulent flow for in-line tube banks is shown to be in the range of Reynolds number Re_m of 7 to 18. Launder and Massey [40] also reported that the transition regime for tube banks

ORIGINAL PAGE IS
OF POOR QUALITY

frequently begins at Reynolds number Re_m below 18. However, it is noted that even at the transitional Reynolds number, the flow in tube banks is still predominantly laminar with large scale eddies in the recirculation regions. Furthermore, the disturbances created from the flow over a tube may tend to be eliminated by viscous forces and acceleration of flow around the downstream tube maintaining the laminar flow in the boundary layer. Thus, Zukauskas [39] suggested that the flow be predominantly laminar pattern at Re_m<1000. According to this description, one may conclude that the critical Reynolds number for the geometric configuration studied in Fig. (40) is Re_m<310. Beyond Reynolds number 310, the higher degree of disturbance may exist in the eddies and the flow is no longer predominantly laminar.

8.5.3 Distribution Of Temperature And Heat Transfer

The temperature distribution and heat transfer around a tube in staggered tube banks are obtained by using the FA method with boundary-fitted coordinate systems also. These results are plotted in Figs. (47,48,49). In this investigation, fluids with Prandtl numbers of 0.1, 1 and 10 are considered for three Reynolds numbers 16, 160 and 320. This combination gives the range of the Peclet number ($Pe=Re_m Pr$) from 1.6 to 3200. The configuration used for computation

ORIGINAL PAGE IS
OF POOR QUALITY

of the temperature field is shown in Fig. (41). The isothermal lines for Pe=1.6 to 3200 at a temperature increment of $\Delta\theta=0.1$ are shown in Figs.(47-49). In Fig. (47) it is observed that the isothermal lines for three Prandtl numbers 0.1, 1 and 10 are quite different even though the velocity field at $Re_m=16$ is identical. In the case of Pr=10 which implies that the thermal diffusion is ten times smaller than the momentum diffusion, the heat is readily convected along with the fluid, as shown in Fig. (47). However, in the other case of Pr=0.1, the thermal diffusion effect becomes significantly large, ten times larger than the viscous diffusion. Thus the isothermal lines around the tube do not seem to be distorted by the fluid convection. In Fig. (47), it is also observed that the thermal boundary layer is gradually developing from Pr=0.1 to 10, where the fluid absorbs heat from the front part of the tube and then convects it to the downstream within the thermal boundary layer. For a larger Reynolds number $Re_m=160$, Fig. (48) shows that the thermal diffusion effect is not so dominant even for Pr=0.1. It is seen that there is a similar trend for the flow at $Re_m=160$ with Pr=0.1 and Pr=1 shown in Fig. (48) and the flow at $Re_m=16$ with Pr=1 and Pr=10 shown in Fig. (47). This is because the Peclet number and the thermal boundary conditions are the same in the energy equation (8-6) except the velocity field.

ORIGINAL PAGE IS
OF POOR QUALITY

At larger Reynolds numbers Re_m=160 or 320, three stagnation points on a tube can be identified which are denoted by A, B and C shown in Figs. (47,48). The stagnation points A and C are inward stagnation points to where the fluid rushes, while the point B is the outward stagnation point where the fluid departs. Due to the curve boundary between two stagnation points, the flow velocity is accelerated and then decelerated. This results in convergence and divergence of the isotherms between A and B or B and C around the tube as shown in Figs. (48,49). The influence of separation zones on the temperature distribution behind the tube can be readily realized by the isothermal contours. Figs. (48,49) show this influence for the cases of Re_m=160 and 320.

From Figs. (47-49), it can be seen that the assumption of constant outlet temperature distorts the temperature field near the outlet region. However, this distortion is only confined to the last two ξ-coordinate lines near the outlet boundary. Therefore, it is believed that the choice of these thermal boundary conditions in equation (8-11) will not affect the temperature distribution around the tube.

In the heat transfer calculation, it is convenient to use the local and the mean Nusselt numbers (Nu and $\overline{Nu}$) which are easily derived from the temperature distribution. They are defined as

ORIGINAL PAGE IS
OF POOR QUALITY

$$Nu = \frac{h(\xi)\ L_r}{k} = -\left.\frac{\partial\theta}{\partial n}\right|_{\Gamma_2} \tag{8-19a}$$

$$\overline{Nu} = \int_{\Gamma_2} Nu\ ds \quad , \tag{8-19b}$$

where $h(\xi)$ is the local heat transfer coefficient and is the contour of the tube shown in Fig. (41). The local Nusselt numbers for the heated tube in the staggered tube banks are plotted in Figs. (50-52). From these figures, it can be found that for given Reynolds numbers of 16, 160 and 320, the local Nusselt number Nu increases with increasing the Prandtl number. At low Reynolds number Re_m=16, where the flow does not separate, the local Nusselt numbers of the tube with Pr=0.1, 1 and 10 are shown in Fig. (50). The general trend is that heat transfer is strong near the front stagnation point. Physically this is because there are no eddies behind a tube at Re_m=16. Thus the fluid convected around the tube is already heated up in the front part of the tube so that there will be less heat transferred from the tube to the fluid in the rear part. At larger Reynolds numbers of Re_m=160 and 320, due to their strong convection, the local Nusselt number for a given Prandtl number is generally larger than that at low Reynolds number Re_m= 16 as shown in Figs. (50-52). Due to strong convection and the existence of eddies behind the tube for flow at Re_m=160 and 320, the general trends of local Nusselt numbers illustrated

ORIGINAL PAGE IS
OF POOR QUALITY

in Figs. (51,52) are different from that of Re_m=16 in Fig. (50). Observing the flow pattern from Figs. (47,48), one can see that the acceleration and deceleration of the flow occurs between stagnation points A and B (due to the main flow) and between B and C (due to the reverse flow in separation zone). This results in high heat transfer from tube to fluid at the region where flow is accelerating than that where it is decelerating. Therefore, in Figs. (51,52) two peaks and two valleys of Nu are seen, especially for the cases of larger Prandtl numbers. The minimum Nusselt number occurs at the separation point B, where the flow departs from the tube surface. Zukauskas [39] also indicated this phenomenon for flow at high Reynolds number (Re_m=O(10^3)).

From the above study, one finds that the flow in the tube banks is relatively complex and the flow pattern is affected by the tube diameter and the configuration of the tube banks. Thus a comparison of different configurations is not attempted. In addition, the details of experimental measurement for flow passing tube banks and the information of heat transfer are not available, such as, the local Nusselt number. Hence comparison of heat transfer predicted in the present study with other studies is not possible. However, a comparison is made in Fig. (53) of the local Nusselt number obtained from the experimental measurements [46] of a single tube with the present results. At low

ORIGINAL PAGE IS
OF POOR QUALITY

Reynolds number (Re_m=16 for staggered tube banks and Re_m=23 for a single tube), the comparison shows that the Nusselt number of the tube in the staggered tube bank is larger than that of a single tube. Furthermore, the general tendency is true except that the Nu of a single tube in the rear part slightly decreases and then increases. This is because at Re_m =23 large scale of eddies are observed to appear behind a single tube but not in the tube banks. In the Fig. (53), it is noted that the heat transfer of the tube in the staggered tube bank can be enhanced if the Reynolds number is increased, epecially in the front part.

In this study, the predominantly laminar flow for Re_m <310 is considered. The mean Nusselt numbers for each fluid of Pr=0.1, 1 and 10 are given in the following table.

staggered tube banks				single cylinder
Re	Pr	$\overline{Nu}$	$\overline{Nu} = 0.166\ Re_m^{1/2}\ Pr^{1/3}$	
5	0.1	0.358		
	1.0	0.678		0.434
	10.	1.477		
50	0.1	0.787		
	1.0	2.080		1.2
	10.	5.60		
100	0.1	1.224	1.39	
	1.0	3.812	3.0	1.66
	10.	9.248	6.46	

ORIGINAL PAGE IS
OF POOR QUALITY

From this table, it is seen that the heat transfer can be significantly affected if the Reynolds number and the Prandtl number are increased. In the range of predominantly laminar flow (Re_m<310), the correlation of the mean Nusselt number with the Reynolds number and the Prandtl number is approximately expressed as :

$$\overline{Nu} = 0.166\ Re_m^{1/2}\ Pr^{1/3} \quad . \tag{8-20}$$

According to the recommendation by Morgan [47], the mean Nusselt number of a single tube for air may be expressed as follows :

$$\overline{Nu} = 0.795\ Re_m^{0.384} \quad \text{for } 1<Re<35 \quad ,$$
$$\overline{Nu} = 0.583\ Re_m^{0.471} \quad \text{for } 35<Re<5000 \quad .$$

Three mean Nusselt numbers for a single tube at Re_m =16, 160 and 320 are calculated by equation (8-21) and listed in the above table. Comparison among these three mean Nusselt numbers with those of staggered tube banks at Pr=1.0, leads to a conclusion that the heat transfer from the tube to the fluid in the staggered banks is larger than that in the single tube.

ORIGINAL PAGE IS
OF POOR QUALITY

8.6 Conclusions

In this chapter, the FA method combined with the boundary-fitted coordinate system is used to predict the flow and heat transfer in tube bundles. The FA solution is obtained for the two-dimensional Navier-Stokes equations and the energy equation in the transformed plane. This FA solution is obtained for the cases of $16<Re_m<320$ or $1.6<Pe<3200$. The results of the stream function, vorticity and temperature are plotted and the heat transfer is discussed. The comparison of these results with other predictions is made whenever possible, and the physical trend of flow and heat transfer are illustrated and explained.

It is shown that the boundary-fitted coordinate transformation can be successfully employed in the FA method to solve flow and heat transfer problems with complex geometries. The computational procedure for boundary-fitted coordinates is not only systematic, but also can be adjusted and contracted so that dense grid lines near the boundary can be used. It is also shown that the FA method contains the automatic upwinding influence of neighboring nodes. The solution is relatively stable. In this study, it is found that the flow pattern is affected by the tube bank and the predominantly laminar flow may exist up to the Reynolds number of 310. When one tube in the tube banks is heated

ORIGINAL PAGE IS
OF POOR QUALITY

with a higher isothermal wall temperature, the heat transfer is larger than that from a single tube in uniform flow.

ORIGINAL PAGE IS
OF POOR QUALITY

CHAPTER IX

CONCLUSION AND RECOMMENDATION

At the present time, although the FA numerical method is still in its developmental and evolution stage, it has already demonstrated the advantage of invoking the local analytic solution of the partial differential equation in constructing the numerical solution of the linear or non-linear partial differential equation.

Chen et al. have successfully solved many fluid and heat transfer problems with the FA method in the physical plane employing the Navier-Stokes equations in either the stream function-vorticity formulation [3,4,7,8,10] or the velocity-pressure formulation [9,13]. Furthermore, the FA solutions in the Cartesian coordinates for three-dimensional Navier-Stokes equations have also been investigated by Chen [13]. From these studies it is realized that the FA method is accurate and has smaller numerical diffusion than the other numerical methods. Further, the system of the FA algebraic equation converges well and is stable in iterative process or time marching procedure. It is , therefore, natural to extend the FA solution of unsteady two-dimensional Navier-Stokes equations in the stream function-

ORIGINAL PAGE IS
OF POOR QUALITY

vorticity formulation to the problem of flow and heat transfer with complex geometries in this study.

For problems with simple geometries, the FA solution may be directly applied in the physical plane (x,y), either with an equal grid size or a unequal grid size. Two such examples, heat transfer in cavity and separation of channel flow, are examined in Chapters V and VI. For problems with complex geometries, the FA method is applied to the governing equations on a boundary-fitted coordinate system. Again, two examples, potential flow passing over an airfoil and viscous flow and heat transfer in tube bundles are presented in Chapter VII and VIII. In all of the four problems considered, the FA numerical solutions are shown to be accurate and stable during computation. Significant results are summarized in the following.

In the problem of heat transfer in square cavity driven by a moving wall, the FA solution for flow in the cavity is first solved for the Reynolds number ranging from 100 to 2000. The temperature distribution and the heat transfer along the heated moving wall are given over the range from Pe=10 to 20,000. It is found that there exists a constant temperature core in the cavity if Pe>1000 for the Reynolds numbers considered, in addition to the vorticity core formulation at Re>1000.

ORIGINAL PAGE IS
OF POOR QUALITY

In the problem of a two-dimensional channel flow with sudden expansion, the FA solution with a unequal grid size and the linear and exponential boundary approximation is obtained. The stream function and vorticity distributions are plotted for Re = 25, 50, 73, 125, 191 and 229. The lengths of separation zone calculated over the range of the Reynolds numbers considered are in good agreement with the experimental measurements, and better than those predicted by the FD and the FE methods. The similarity relation for the separation length and the center of the separation eddies are found for the Reynolds numbers considered.

In the problem of the potential flow passing an airfoil, the boundary-fitted coordinate transformation is used to generate coordinates systems for the NACA-0018 and Karmann-Trefftz airfoils. The FA solution of the Laplace equation in the transformed plane is obtained. The streamlines over the airfoils are plotted at three different angles of attack, 0, 5 and 10. The FA prediction of pressure distribution and lift coefficients is compared with the experimental measurements and the theorectical calculations.

In solving the viscous flow and heat transfer problem in tube bundles, the boundary-fitted coordinate system is generated for a region bounded by the symmetric and periodic condition. Then the steady FA solution is obtained the boundary-fitted coordinates. For the configuration

ORIGINAL PAGE IS
OF POOR QUALITY

considered the critical Reynolds number of the predominantly laminar flow is known at around 310. Thus the flow patterns, vorticity and temperature distributions and the heat transfer of a tube wall are plotted and discussed over the range of Re<320. It is found that in the tube bundles flow when only one tube is heated while the other tubes are kept at the fluid temperature, the heat transfer between the heated tube and fluid is larger than that of a single heated tube in the uniform flow.

Although the FA solutions of the convective transport equation are shown to be accurate and stable in the above problems, some improvements can be made in future studies.

First, for high Reynolds number flows, one should investigate a boundary-fitted coordinate system such that close to the boundary the grid near the boundary wall can be made as fine as required while maintaining a coarse grid outside the boundary. It is found in the present investigation that if a grid near the boundary is severely distorted and nonorthogonal in the physical plane the truncation error due to the grid generation may increase by a factor of about $1/\sin\theta$ for first derivatives and $(1/\sin\theta)^2$ for second derivatives [48] when the coordinate transformation is solved by the FD method. Here the angle denotes the internal angle of the element. It is suggested that the governing equation (3-7) for boundary-fitted

coordinates be treated with the FA method so that the numerical error in the distorted grid may be minimized.

Secondly, since the computation of the FA coefficients still involve one series summation given in equation (4-25), the computational time required by the FA method is still large. In order to reduce the computational time, an alternative analytic solution technique of obtaining the analytic solution should be studied.

Finally, for future application of the FA method the three dimensional boundary-fitted coordinate transformation and the turbulent flow should be considered.

REFERENCES

1. Roache, P. J., Computational Fluid Mechanics, Hermosa Publishers, 1972.

2. Chen, C. J. and Li, P., " Finite Differential Method in Heat Conduction - Application of Analytic Solution Technique", ASME Paper 79-WA/HT-50, December 2-7, 1979. ASME Winter Annual Meeting, New York, N.Y., 1979.

3. Naseri-Neshat, H., "The Finite Analytic Solutions for Two-Dimensional Navier-Stokes Equations", Ph. D. Dissertation, Mechanical Engineering Program, 1980, University of Iowa, Iowa City, Iowa.

4. Chen, C. J., Naseri-Nashat, H. and Ho, K. S., "Finite Analytic Numerical Solution of Heat Transfer in Two-Dimensional Cavity Flow", ASME Paper,HTD, Vol. 13, ASME Winter Annual Meeting, November, 1980, Chicago,Ill. pp.49-61. Also J. of Numerical Heat Transfer, vol. 4, 1981, pp.179-197.

5. Heinrich, J. C., Huyakorn, P. S., Zienkiewicz, O. C. and Mitchell, A. R., "An 'Upwind' Finite Element Scheme for Two-Dimensional Convective Transport Equation", International J. for Numerical Methods in Engineering, vol. 11, 1977, pp. 131-143.

6. Gallagher, R. H., Oden, J. T., Taylor, C. and Zienkiewicz, O. C., "Finite Element in Fluid - vol. 3" pp. 1-22, John Wiley & Sons, 1978.

7. Chang, C. M., "Finite Analytic Numerical Solutions for Steady Two-Dimensional Heat Transfer and Flow in Bends", M. S. Thesis, Mechanical Engineering Program, 1981, University of Iowa, Iowa City, Iowa.

8. Chen, C. J. and Obasih, K., "Finite Analytic Numerical Solution of Heat Transfer and Flow Past a Square Channel Cavity", 82-IHTC-43. The 7th International Heat Transfer Conference, Munchen. Sept. 6-10, 1982.

9. Singh, K., "Finite Analytic Numrical Solution of Two-Dimensional Navier-Stokes Equations in Primitive Variables", M. S. Thesis, Mechanical Engineering Program, 1981, University of Iowa, Iowa City, Iowa.

10. Chen, C. J. and Chen, H. C., "Development of Finite Analytic Numerical Method for Unsteady Two-Dimensional Convective Transport Equation", Simposium on Refined Modelling of Flows International Association for Hydraulic Research, Paris, Sept 7-10, 1982

11. Thompson, J. F., "Numerical Solution of Flow Problems Using Body-Fitted Coordinate System", Computational Fluid Dynamics, Von Karmann Institute Book, 1980.

12. Thompson, J. F., Thames, F. C., Mastin, C.W. and Shank, S. P., "Use of Numerically Generated Body-Fitted Coordinate Systems for Solution of Navier-Stokes Equations", AIAA Computational Fluid Dynamics Conference Proceeding, 2nd, 1975.

13. Chen, H. C., " Development of Finite Analytic Method for Unsteady Three-Dimensional Navier-Stokes Equations", Ph.D. Dissertation, Mechanical Engineering Program, 1982, University of Iowa, Iowa City, Iowa.

14. Burggraf, D. E., "Analytical and Numerical Studies of Structure of Steady Separated Flows", J. Fluid Mechanics, vol. 24, Part I, 1966, pp 113-151.

15. Mill, R. D., "Numerical Solution of the Viscous Flow Equations for a class of Closed Flows", J. of Royal Aeronautical Society, vol. 69, 1968, pp. 714-718.

16. Pan, F. and Acrivos, A., "Steady Flows in Rectangular Cavities", J. Fluid Mechanics, vol. 28, Part 4, 1967, pp. 653-655.

17. Grennspan, D., "Lectures on the Numerical Solution of Linear, Singular and Nonlinear Differential Equation", Prentice-Hall, Englewood Cliffs, New Jersey, 1968.

18. Gosman, A. D., Pun, W. M., Runchal, A. k, Spalding, D. E. and Woilshtein, M., "Heat Transfer in Recirculating Flows", Academic Press, London, 1969.

19. de Vahl Davis, G. and Mallinson, C. D., "An Evaluation of Upwind and Central Difference Approximations by a study of Recirculating Flow", Computers and Fluids, vol. 4, 1976, pp. 29-43.

20. Nallasamy, M. and Prasad, K. K, "On Cavity Flow at High Reynolds Numbers,", J. Fluid Mechanics, vol. 79, part 2, 1977, pp-391-414.

21. Olson, M. D. and Tuann,s. Yu, "New Finite Element Result for the Square Cavity", Computers and Fluids, vol. 7, 1979, pp. 123-135.

22. Raithby, G. C., "Skew Upstream Difference Schemes for Problems Involving Fluid Flow Computer Method", Applied Mechanics and Engineering, vol. 9, 1976, pp. 153-164.

23. Hughes, T. R., Jr., ed., "Finite Element Methods for Convection Dominated Flow", AMD, vol. 34, Dec. 2-7, 1979, ASME Winter Annual Meeting, New York, New York.

24. Mill, R. D, "On the Closed Motion of a Fluid in a Square Cavity", J. of Royal Aeronautical Society, vol. 69, 1965, pp. 116-120.

25. Hung, T. and Macagno, E. O., Houille Blance, 1966, 21, 391.

26. Iribarne, A., Frantisak, F., Hummel, R. 1. and Smith, J. W., A. I. Ch. E. Jl., 1972, 18, 689.

27. Goldstein, R. J., Eriksen, V. L., Olson, R. M. and Eckert, E. R. G. J. Bas. Engng, 1970, 92, 732.

28. Durst, F., Melling, A. and Whitelaw, J. H., "Proceedings of DISA Conference -- Fluid Dynamics Measurements in the Industrial and Medical Enviornments" 1972, pp. 81 (Leicester: Leicester University Press).

29. Denham, M. K and Patrick, M. A., " Laminar Flow Over a Downstream Facing Step in a Two-Dimensional Flow Channel", Tran. Instit. Chem. Engrs, vol. 52, 1974, pp. 361-367.

30. Atkins, D. J., Maskell, S. J. and Patrick, N. A., "Numerical Prediction of Separated Flows", International j. for Numerical Methods Engineering, vol. 15, 1980, pp. 129-144.

31. Hutton, A. G. and Smith, R. M., "The Prediction of Laminar Flow over a downstream facing step", C.E.G.B. Report, RD/B/B 3600, 1979.

32. Thomas, C. E., Morgan, K. and Taylor C., Computers and Fluids, vol 9, 1981, pp. 265-278.

33. Giesing, J. P., "Potential Flow About Two-Dimensional Airfoils", Report No. LB 31946, Douglas Aircraft Division, 1965.

34. Abbott, I. H. and Doenhoff, A. E., Theory of Wing Section, Dover, 1958, pp. 325.

35. Bergelin, O. P., Davis, E. S. and Hull, H. L. "A study of three Arrangements in Unbaffled Tubular Heat Exchangers", Transactions of the ASME, May 1949.

36. Bergelin, O. P., Brown, G. A., Hull, H. L. and Sullivan, F. W., " heat Transfer and Fluid Friction Durning Viscous Flow Across Banks of Tubes ---III", Transactions of the ASME, Aug. 1950.

37. Bergelin, O. P., Brown, G. A. and Doberstein, S. C., "Heat Transfer and Fluid Friction During Flow across Banks of Tubes ---IV", Transaction Of the ASME, Aug. 1952.

38. Happel, J., "Viscous Flow Separate to Arrays of Cylinders", A.I.Ch.E. J., June 1959.

39. Zukauskas, A. "Advances in Heat Transfer", vol. 8, Academic, New York, 1972, pp 93-160.

40. Launder, B. E. and Massey, T. H., "The Numerical Prediction of Viscous Flow and Heat Transfer in Tube Banks", J. of Heat Transfer, Nov. 1978, vol. 100.

41. Thom, A. and Apelt, C. J., "Fliuid Computations in Engineering Physics" by D. Van Norstrand Company, 1961.

42. Le Feuvre, R.F., "Laminar and Turbulent Forced Convection Processes Through In-Line Tube Banks", Imperical college, London, Mechanical Engineering Department, HTS/74/5, 1973.

43. Thomas, D. C. and Szewcyzk, A. A., "Time-Dependent Viscous Flow Over a Circular Cylinder", Physics of Fluids, supplement II, 1969, pp. II 76-86.

44. Israeli, M., "A Fast Implicit Numerical Method for Time Dependent Viscous Flows", Studies in Applied Methmatics, 1970.

45. Apelt, C. J., "The Steady Flow Of a Viscous Flow Past a Circular Cylinder at Reynolds Numbers 40 and 44", Report and Memoranda No. 3175, University of Oxford, Oct. 1958.

46. Eckert, E. R. and Soengen, E., Tansaction of the ASME, vol. 74, 1952. pp 343

47. Morgan, V. T., "Advances in Heat Transfer", vol. 11, Academic, New York, 1975, pp 199-264.

48. Mastin, C.W., "Error Induced by Coordinate System", Symposium on Numerical Generation of Curvilinear Coordinate Systems and in the Numerical Solution of Partial Differential Equations, April 13-16, 1982. Nashville, Tennessee.

ORIGINAL PAGE IS
OF POOR QUALITY

APPENDIX A

RELATIONS BETWEEN PHYSICAL AND TRANSFORMED PLANES

This appendix contains the pertinent definitions and relations between the physical (x,y) plane and transformed (ξ,η) plane used in the present study. Basically the relations and the notation used in Ref. [11] is retained here. The function f(x,y,t) is defined as a twice continuously differentiable scalar function of x,y and t and the vector $F(x,y)=F_1(x,y)i+F_2(x,y)j$ is a continuously differentiable vector-valued function where i and j are the conventional cartesian coordinate unit vectors.

It should be noted that all derivative transformations given here are in the geometrically non-conservation form.

Definitions of the transformation relevent to the present study are

$$\alpha=x_\eta^{\ 2}+y_\eta^{\ 2} \tag{A-1}$$

$$\beta=x_\xi x_\eta+y_\xi y_\eta \tag{A-2}$$

$$\gamma=x_\xi^{\ 2}+y_\xi^{\ 2} \tag{A-3}$$

ORIGINAL PAGE IS
OF POOR QUALITY

$$D_x=\alpha x_{\xi\xi}-2\beta x_{\xi\eta}+\gamma x_{\eta\eta} \tag{A-4}$$

$$D_y=\alpha y_{\xi\xi}-2\beta y_{\xi\eta}+\gamma y_{\eta\eta} \tag{A-5}$$

$$\sigma=(y_\xi D_x-x_\xi D_y)/J \tag{A-6}$$

$$\tau=(x_\eta D_y-y_\eta D_x)/J \tag{A-7}$$

$$J=x_\xi y_\eta-x_\eta y_\xi \tag{A-8}$$

where J is the determinant of the Jacobian matrix.

Derivative transformations for function f between (x,y) and (ξ,η) coordinate are

$$f_x=(\partial f/\partial x)_{y,t}=(y_\eta f_\xi-y_\xi f_\eta)/J \tag{A-9}$$

$$f_y=(\partial f/\partial y)_{x,t}=(x_\xi f_\eta-x_\eta f_\xi)/J \tag{A-10}$$

$$\begin{aligned} f_{xx}=(\partial^2 f/\partial x^2)_{y,t}&=(y_\eta{}^2 f_{\xi\xi}-2y_\xi y_\eta f_{\xi\eta}+y_\xi{}^2 f_{\eta\eta})/J^2\\ &+(y_\eta{}^2 y_{\xi\xi}-2y_\xi y_\eta y_{\xi\eta}+y_\xi{}^2 y_{\eta\eta})(x_\eta f_\xi-x_\xi f_\eta)/J^3\\ &+(y_\eta{}^2 x_{\xi\xi}-2y_\xi y_\eta x_{\xi\eta}+y_\xi{}^2 x_{\eta\eta})(y_\xi f_\eta-y_\eta f_\xi)/J^3 \end{aligned} \tag{A-11}$$

$$\begin{aligned} f_{yy}=(\partial^2 f/\partial x^2)_{x,t}&=(x_\eta{}^2 f_{\xi\xi}-2x_\xi x_\eta f_{\xi\eta}+x_\xi{}^2 f_{\eta\eta})/J^2\\ &+(x_\eta{}^2 y_{\xi\xi}-2x_\xi x_\eta y_{\xi\eta}+x_\xi{}^2 y_{\eta\eta})(x_\eta f_\xi-x_\xi f_\eta)/J^3\\ &+(x_\eta{}^2 x_{\xi\xi}-2x_\xi x_\eta x_{\xi\eta}+x_\xi{}^2 x_{\eta\eta})(y_\xi f_\eta-y_\eta f_\xi)/J^3 \end{aligned} \tag{A-12}$$

$$\begin{aligned} f_{xy}=&((x_\xi y_\eta+x_\eta y_\xi)f_{\xi\eta}-x_\xi y_\xi f_{\eta\eta}-x_\eta y_\eta f_{\xi\xi})/J^2\\ &+(x_\eta y_\eta x_{\xi\xi}-(x_\xi y_\eta+x_\eta y_\xi)x_{\xi\eta}+x_\xi y_\xi x_{\eta\eta})(y_\eta f_\xi-y_\xi f_\eta)/J^3\\ &+(x_\eta y_\eta y_{\xi\xi}-(x_\xi y_\eta+x_\eta y_\xi)y_{\xi\eta}+x_\xi y_\xi y_{\eta\eta})(x_\xi f_\eta-x_\eta f_\xi)/J^3 \end{aligned} \tag{A-13}$$

ORIGINAL PAGE IS
OF POOR QUALITY

Vector Derivative Transformations for function f and F are

Laplacian:

$$\nabla^2 f=(\alpha f_{\xi\xi}-2\beta f_{\xi\eta}+\gamma f_{\eta\eta})/J^2+((\alpha x_{\xi\xi}-2\beta x_{\xi\eta}+\gamma x_{\eta\eta})(y_\xi f_\eta-y_\eta f_\xi)$$
$$+(\alpha y_{\xi\xi}-2\beta y_{\xi\eta}+\gamma y_{\eta\eta})(x_\eta f_\xi-x_\xi f_\eta))/J^3 \qquad \text{(A-14)}$$

or $$\nabla^2 f=(\alpha f_{\xi\xi}-2\beta f_{\xi\eta}+\gamma f_{\eta\eta}+\sigma f_\eta+\tau f_\xi)/J^2 \qquad \text{(A-15)}$$

Gradient:

$$\nabla f=((y_\eta f_\xi-y_\xi f_\eta)i+(x_\xi f_\eta-x_\eta f_\xi)j)/J \qquad \text{(A-16)}$$

Divergence:

$$\nabla\cdot F=(y_\eta(F_1)_\xi-y_\xi(F_1)_\eta+x_\xi(F_2)_\eta-x_\eta(F_2)_\xi)/J \qquad \text{(A-17)}$$

Curl:

$$\nabla\, xF=k(y_\eta(F_2)_\xi-y_\xi(F_2)_\eta-x_\xi(F_1)_\eta+x_\eta(F_1)_\xi)/J \qquad \text{(A-18)}$$

Unit Tangent and Normal Vectors

Normal to η-line

$$n^{(\eta)}=\nabla\eta/|\nabla\eta|=(-y_\xi i+x_\xi j)/\sqrt{\gamma} \qquad \text{(A-19)}$$

Normal to ξ-line

$$n^{(\xi)}=\nabla\xi/|\nabla\xi|=(y_\eta i-x_\eta j)/\sqrt{\alpha} \qquad \text{(A-20)}$$

Tangent to η-line

$$t^{(\eta)}=n^{(\eta)}\times k=(x_\xi i+y_\xi j)/\sqrt{\gamma} \qquad \text{(A-21)}$$

Tangent to ξ-line

$$t^{(\xi)}=n^{(\xi)}\times k=-(x_\eta i+y_\eta j)/\sqrt{\alpha} \qquad \text{(A-22)}$$

ORIGINAL PAGE IS
OF POOR QUALITY

Vector Components Tangent and Normal to ξ and η lines

$$F_n^{(\eta)} = n^{(\eta)} \cdot F = (-y_\xi F_1 + x_\xi F_2)/\sqrt{\gamma} \tag{A-23}$$

$$F_t^{(\eta)} = t^{(\eta)} \cdot F = (x_\xi F_1 + y_\xi F_2)/\sqrt{\gamma} \tag{A-24}$$

$$F_n^{(\xi)} = n^{(\xi)} \cdot F = (y_\eta F_1 - x_\eta F_2)/\sqrt{\alpha} \tag{A-25}$$

$$F_t^{(\xi)} = t^{(\xi)} \cdot F = -(x_\eta F_1 + y_\eta F_2)/\sqrt{\alpha} \tag{A-26}$$

Directional Derivatives:

$$\partial f/\partial n^{(\eta)} = n^{(\eta)} \cdot \nabla f = (\gamma f_\eta - \beta f_\xi)/J\sqrt{\gamma} \tag{A-27}$$

$$\partial f/\partial t^{(\eta)} = t^{(\eta)} \cdot \nabla f = f_\xi/\sqrt{\gamma} \tag{A-28}$$

$$\partial f/\partial n^{(\xi)} = n^{(\xi)} \cdot \nabla f = (\alpha f_\xi - \beta f_\eta)/J\sqrt{\alpha} \tag{A-29}$$

$$\partial f/\partial t^{(\xi)} = t^{(\xi)} \cdot \nabla f = -f_\eta/\sqrt{\alpha} \tag{A-30}$$

ORIGINAL PAGE IS
OF POOR QUALITY

APPENDIX B

FA FORMULATION OF UNSTEADY 2-D CONVECTIVE EQUATION

In this appendix, the analytic solution for unsteady two-dimensional convective transport equation in the transformed plane is derived in a local element as shown in Fig. (1).

First, consider a dimensionless unsteady two-dimensional convective transport equation in the physical plane (x,y) of the form

$$\phi_{xx} + \phi_{yy} = R\,(\phi_t + u\phi_x + v\phi_y) + F \quad , \qquad \text{(B-1)}$$

where ϕ may represent any one of convective transport quantities, ϕ_j, such as vorticity, velocity, concentration or temperature. The coefficients u, v and F may be fuctions of independent variables x, y and t, and dependent variables ϕ_j. R is a dimensionless parameter, and is Reynolds number when ϕ represents vorticity or velocity.

In order that a problem with complex geometries be solved with the boundary-fitted coordinate system in the transformed plane (ξ,η), equation (B-1) must be transformed into the boundary-fitted coordinates. Utilizing the

ORIGINAL PAGE IS
OF POOR QUALITY

relations given in Appendix A, the governing equation (B-1) becomes

$$\phi_{\xi\xi} + \frac{\gamma}{\alpha}\phi_{\eta\eta} = \frac{J^2 Re}{\alpha}\phi_t + \left(\frac{J\ Re}{\alpha}u - \frac{\tau}{\alpha}\right)\phi_\xi + \left(\frac{J\ Re}{\alpha}v - \frac{\sigma}{\alpha}\right)\phi_\eta + \frac{2\beta}{\alpha}\phi_{\xi\eta} + F \quad , \qquad \text{(B-1a)}$$

where α, β, γ, J, σ and τ are functions related to the boundary-fitted coordinates transformation, they are given in equations (A-1) to (A-8).

Since, in general, an analytic solution of equation (B-1) in the local element is not available due to variable coefficients and/or nonlinearity, the FA numerical method is used to obtain the local analytic solution. Therefore in order to solve the convective transport equation (B-1a) analytically in the local element on the transformed plane(ξ,η), equation (B-1a) is first rearranged to be

$$\phi_{\xi\xi} + \frac{\gamma}{\alpha}\phi_{\eta\eta} = \frac{J^2 Re}{\alpha}\phi_t + \left(\frac{J\ Re}{\alpha}\bar{\psi}_\eta - \frac{\tau}{\alpha}\right)\phi_\xi + \left(\frac{-J\ Re}{\alpha}\psi_\xi - \frac{\sigma}{\alpha}\right)\phi_\eta + F + \left(\frac{J\ Re}{\alpha}\psi'_\eta\phi_\xi + \frac{J\ Re}{\alpha}\psi'_\xi\phi_\eta\right), \qquad \text{(B-2)}$$

with

$$\psi_\xi = \bar{\psi}_\xi + \psi'_\xi \quad , \qquad \text{(B-2a)}$$

$$\psi_\eta = \bar{\psi}_\eta + \psi'_\eta \quad ,$$

ORIGINAL PAGE IS
OF POOR QUALITY

where $\overline{\psi}_\xi$ and $\overline{\psi}_\eta$ are representative constant values in the local element, for example, the velocities at the interior point P or the area-averaged velocities over the small element.

When the local element is small enough, the deviations ψ'_ξ and ψ'_η from the $\overline{\psi}_\xi$ and $\overline{\psi}_\eta$ should be small also. Therefore, the term $JRe(\psi'_\eta\phi_\xi+\psi'_\xi\phi_\eta)/\alpha$ may be considered as a high order correction term. Denoting two time steps t^{k-1} and t^k, one may locally linearized the convective transport equation (B-1a) by approximating the inhomogeneous term, the higher order correction term and the cross derivative term as a function known from previous time step t^{k-1}, it is

$$\phi_{\xi\xi} + \frac{\gamma}{\alpha}\phi_{\eta\eta}{}^{k} = \frac{J^2Re}{\alpha}\phi_t + \left(\frac{J\ Re}{\alpha}\overline{\psi}_\eta - \frac{\tau}{\alpha}\right)\phi_\xi + \left(\frac{-J\ Re}{\alpha}\psi_\xi - \frac{\sigma}{\alpha}\right)\overline{\phi}_\eta{}^{k} + f^{k-1} \quad , \qquad \text{(B-3)}$$

where

$$f^{k-1} = \frac{2\beta}{\alpha}\phi_{\xi\eta} + F + \frac{J\ Re}{\alpha}\left(\psi_\eta\phi_\xi + \psi_\xi\phi_\eta\right) \quad . \qquad \text{(B-3a)}$$

Equation (B-3) is a linearized PDE with constant coefficients at kth time step. In order to reduce the complexity of the deviation and to save the computational time, the hybrid FA method will be employed in this appendix to approximate the unsteady term as follows :

$$\frac{J^2Re}{\alpha}\phi_t = \frac{J^2Re}{\alpha} \cdot \frac{\phi_P^k - \phi_P^{k-1}}{\Delta t} = \text{constant} \quad . \qquad \text{(B-4)}$$

ORIGINAL PAGE IS
OF POOR QUALITY

Furthermore, the nonhomogeneous part $f^{k-1}(\xi,\eta,\phi_j)$ can be approximated by a representative constant value in the element to further reduce the manupulation effort and computational time needed. Under these approximations, the unsteady two-dimensional convective transport equation (B-1a) is simplified to be

$$\phi_{\xi\xi} + C\phi_{\eta\eta} = 2A\phi_{\xi} + 2BC\phi_{\eta} + g \quad , \tag{B-5}$$

with

$$A = \frac{1}{2}\left(\frac{J\ Re}{\alpha}\bar{\psi}_{\eta} - \frac{\tau}{\alpha} \right) \quad ,$$

$$B = \frac{1}{2}\left(\frac{J\ Re}{\alpha}\bar{\psi}_{\xi} - \frac{\sigma}{\alpha} \right) \quad ,$$

and

$$g = \frac{J^2 Re}{\alpha} \frac{\phi_P^k - \phi_P^{k-1}}{\Delta t} + f_P \quad . \tag{B-5a}$$

The constant inhomogeneous term in equation (B-5) can be taken care of by introducing a new variable

$$\tilde{\phi} = \phi + \frac{g}{2(A^2 + B^2 C)}(A\xi + B\eta) \quad , \tag{B-6}$$

such that the new variable satisfies the homogeneous governing equation

$$\tilde{\phi}_{\xi\xi} + C\tilde{\phi}_{\eta\eta} = 2A\tilde{\phi}_{\xi} + 2BC\tilde{\phi}_{\eta} \quad , \tag{B-7}$$

in the local element.

ORIGINAL PAGE IS
OF POOR QUALITY

For the problem to be well posed, four boundary conditions are specified on east, west, south and north boundaries in terms of the eight surrounding nodes of the local element. Depending on the local element and boundary functions chosen, different local analytic solution can be derived. In this appendix, the uniform grid spacing local element ($\Delta\xi = h = \Delta\eta = k$) with the exponential and linear boundary approximation is considered. For further information see [13].

Under this consideration, the local analytic solution for steady or unsteady two-dimensional convective transport equation is derived on a rectangular local element of unform grid spacing on the transformed plane (ξ,η). For the linear homogeneous partial differential equation (B-7) to be well posed in the local element shown in Fig. (1), the exponential and linear boundary functions based on the natural solution of equation (B-7) are specified on four boundaries in terms of the eight boundary nodes of the local element. For example, the boundary condition on north side can be approximated by

$$\tilde{\phi}_N(\xi) = a_N\,(e^{2A\xi} - 1) + b_N\xi + c_N \qquad \text{(B-8a)}$$

where

$$a_N = \frac{\tilde{\phi}_{NE} + \tilde{\phi}_{NW} - 2\tilde{\phi}_{NC}}{4\sinh^2 Ah},$$

$$b_N = \frac{\tilde{\phi}_{NE} - \tilde{\phi}_{NW} - \coth Ah(\tilde{\phi}_{NE} + \tilde{\phi}_{NW} - 2\tilde{\phi}_{NC})}{2h}, \qquad c_N = \tilde{\phi}_{NC}$$

ORIGINAL PAGE IS
OF POOR QUALITY

and the other three boundary conditons for south, east and west sides, i.e., $\tilde{\phi}_S(\xi)$, $\tilde{\phi}_E(\eta)$ and $\tilde{\phi}_W(\eta)$ can be similarly approximated.

$$\tilde{\phi}_S(\xi) = a_S(e^{2A\xi} - 1) + b_S\xi + c_S \quad , \tag{B-8b}$$

$$\tilde{\phi}_E(\eta) = a_E(e^{2B\eta} - 1) + b_E\eta + c_E \quad , \tag{B-8c}$$

$$\tilde{\phi}_W(\eta) = a_W(e^{2B\eta} - 1) + b_W\eta + c_W \quad . \tag{B-8d}$$

With the introduction of a change of variable

$$\tilde{\phi} = w\, e^{A\xi + B\eta} \quad . \tag{B-9}$$

Equation (B-7) and boundary conditions (B-8) are transformed into

$$w_{\xi\xi} + w_{\eta\eta} = (A^2 + B^2)\, w \quad , \tag{B-10}$$

$$w(\xi,k) = e^{-Bk}[a_N e^{A\xi} + b_N x e^{-A\xi} + (c_N - a_N)e^{-A\xi}] = w_1(\xi), \tag{B-10a}$$

$$w(\xi,-k) = e^{Bk}[a_S e^{A\xi} + b_S x e^{-A\xi} + (c_S - a_S)e^{-A\xi}] = w_2(\xi), \tag{B-10b}$$

$$w(h,\eta) = e^{-Ah}[a_E e^{B\eta} + b_E y e^{-B\eta} + (c_E - a_E)e^{-B\eta}] = w_3(\eta), \tag{B-10c}$$

$$w(-h,\eta) = e^{Ah}[a_W e^{B\eta} + b_W y e^{-B\eta} + (c_W - a_W)e^{-B\eta}] = w_4(\eta). \tag{B-10d}$$

Utilizing the method of superposition for the linear equation (B-10), this problem can be solved analytically by

ORIGINAL PAGE IS
OF POOR QUALITY

further dividing it into four simpler problems with each of them contains one inhomogeneous and three homogeneous boundary conditions, it is

$$w = w^E + w^W + w^N + w^S \quad . \tag{B-11}$$

Problem (1)

$$w^N_{\xi\xi} + w^N_{\eta\eta} = (A^2 + B^2)\, w^N \quad , \tag{B-12}$$

$$w^N(\xi,k) = w_1(\xi) \quad , \tag{B-12a}$$

$$w^N(\xi,-k) = w^N(h,\eta) = w^N(-h,\eta) = 0 \quad . \tag{B-12b}$$

Problem (2)

$$w^S_{\xi\xi} + w^S_{\eta\eta} = (A^2 + B^2)\, w^S \quad , \tag{B-13}$$

$$w^S(\xi,-k) = w_2(\xi) \quad , \tag{B-13a}$$

$$w^S(\xi,k) = w^S(h,\eta) = w^S(-h,\eta) = 0 \quad . \tag{B-13b}$$

Problem (3)

$$w^E_{\xi\xi} + w^E_{\eta\eta} = (A^2 + B^2)\, w^E \quad , \tag{B-14}$$

$$w^E(h,\eta) = w_3(\eta) \quad , \tag{B-14a}$$

$$w^E(-h,\eta) = w^E(\xi,k) = w^E(\xi,-k) = 0 \quad . \tag{B-14b}$$

Problem (4)

$$w^W_{\xi\xi} + w^W_{\eta\eta} = (A^2 + B^2)\, w^W \quad , \tag{B-15}$$

$$w^W(-h,\eta) = w_4(\eta) \quad , \tag{B-15a}$$

$$w^W(h,\eta) = w^W(\xi,k) = w^W(\xi,-k) = 0 \quad . \tag{B-15b}$$

Problems (1) to (4) can be solved analytically by the method of separation of variables. For example, let $\omega^N = X(\xi)Y(\eta)$ and substituting it into equation (b-12), the linear PDE is then separated into two ordinary differential equations. They are

$$X' + \lambda^2 X = 0 \quad , \tag{B-16}$$

$$X(-h) = X(h) = 0 \quad , \tag{B-16a}$$

and

$$Y' - (A^2 + B^2C + \lambda^2)Y = 0 \quad , \tag{B-17}$$

$$Y(-k) = 0 \quad . \tag{B-17a}$$

The two boundary conditions in the ξ-direction, $\xi = h$, in this case can be used to find the eigenvalues λ_n . And the series solution ω^N can be written as

$$w^N(\xi,\eta) = \sum_{n=1}^{\infty} A_n \sinh\mu_n(\eta+k)\, \sin\lambda_n(\xi+h) \tag{B-18}$$

with

$$\lambda_n = \frac{n\pi}{2h} \quad , \quad \mu_n = \sqrt{A^2 + B^2C + \lambda_n^2} \quad , \; n = 1, 2, 3 \text{ --- } .$$

ORIGINAL PAGE IS
OF POOR QUALITY

The coefficients A in equation (B-18) can be easily obtained by applying the nonhomogeneous boundary condition in equation (B-12a), it is

$$w^N(\xi,k) = w_1(x) = \sum_{n=1}^{\infty} A_n \sinh 2\mu_n k \sin\lambda_n(\xi+h) \quad \text{(B-19)}$$

where

$$A_n = \frac{1}{h} \int_{-h}^{h} w_1(\xi) \sin\lambda_n(\xi+h)\, d\xi$$

$$= \frac{e^{-Bk}}{\sinh 2\mu_n k} [\, a_N e_{0n} + b_N h\, e_{1n} + (c_N - a_N) e_{2n}] \quad \text{(B-20)}$$

and

$$e_{0n} = \frac{1}{h} \int_{-h}^{h} e^{A\xi} \sin\lambda_n(\xi+h)\, d\xi$$

$$= \frac{\lambda_n h}{(Ah)^2 + (\lambda_n h)^2} [e^{-Ah} - (-1)^n e^{Ah}] \quad , \quad \text{(B-20a)}$$

$$e_{1n} = \frac{1}{h^2} \int_{-h}^{h} \xi e^{-A\xi} \sin\lambda_n(\xi+n)\, d\xi$$

$$= \frac{2(Ah)(\lambda_n h)}{[(Ah)^2+(\lambda_n h)^2]^2} [\, e^{Ah} - (-1)^n e^{-Ah}] -$$

$$\frac{\lambda_n h}{(Ah)^2+(\lambda_n h)^2} [\, e^{Ah} - (-1)^n e^{-Ah}] \quad , \quad \text{(B-20b)}$$

$$e_{2n} = \frac{1}{h} \int_{-h}^{h} e^{-A\xi} \sin\lambda_n(\xi+h)\, d\xi$$

$$= \frac{\lambda_n h}{(Ah)^2 + (\lambda_n h)^2} [\, e^{Ah} - (-1)^n e^{-Ah}] \quad . \quad \text{(B-20c)}$$

ORIGINAL PAGE IS
OF POOR QUALITY

The local analytic solution (B-19) evaluated at the interior node P(0,0) of the local element gives the FA algebraic equation relating the interior nodal value to the eight surrounding nodal values as

$$w_P^N = w^N(0,0) = \sum_{n=1}^{\infty} A_n \sinh\mu_n k \sin\lambda_n h \quad . \qquad \text{(B-21)}$$

Since $\sin\lambda_n h = \sin\frac{n\pi}{2} = \begin{matrix} 0 , & n=2m \\ -(-1)^m , & n=2m-1 \end{matrix} \quad m=1, 2, 3, \ldots ,$

equation (B-21) can be further simplified to be

$$w_P^N = \sum_{m=1}^{\infty} \frac{-(-1)^m e^{-Bk} \sinh\lambda_m k}{\sinh 2\mu_m k} [a_N e_{0m} + b_N h\, e_{1m} + (c_N - a_N) e_{2m}]$$

$$= e^{-Bk} \sum_{m=1}^{\infty} \frac{-(-1)^m}{2\cosh\mu_m k} [a_N e_{0m} + b_N h\, e_{1m} + (c_N - a_N) e_{2m}]. \qquad \text{(B-22)}$$

and defining

$$E_i = \sum_{m=1}^{\infty} \frac{-(-1)^m \lambda_m h}{[(Ah)^2 + (\lambda_m h)^2]^i \cosh\mu_m k} \quad , \quad i = 1,2 \quad , \text{(B-22a)}$$

we have

$$\sum_{m=1}^{\infty} \frac{-(-1)^m}{\cosh\mu_m k} e_{0m} = (e^{Ah} + e^{-Ah}) \sum_{m=1}^{\infty} \frac{-(-1)^m \lambda_m h}{[(Ah)^2 + (\lambda_m h)^2] \cosh\mu_m k}$$

$$= 2\cosh Ah\; E_1 \quad , \qquad \text{(B-22b)}$$

ORIGINAL PAGE IS
OF POOR QUALITY

$$\sum_{m=1}^{\infty} \frac{-(-1)^m}{\cosh\mu_m k} e_{1m} = -(e^{Ah}-e^{-Ah}) \sum_{m=1}^{\infty} \frac{-(-1)^m \lambda_m h}{[(Ah)^2+(\lambda_m h)^2]\cosh\mu_m k}$$

$$+ 2(Ah)(e^{Ah}+e^{-Ah}) \sum_{m=1}^{\infty} \frac{-(-1)^m \lambda_m h}{[(Ah)^2+(\lambda_m h)^2]^2\cosh\mu_m k}$$

$$= 4Ah \cosh Ah\ E_2 - 2\sinh Ah\ E_1 \quad , \qquad \text{(B-22c)}$$

$$\sum_{m=1}^{\infty} \frac{-(-1)^m}{\cosh\mu_m k} e_{2m} = (e^{Ah}+e^{-Ah}) \sum_{m=1}^{\infty} \frac{-(-1)^m \lambda_m h}{[(Ah)^2+(\lambda_m h)^2]\cosh\mu_m k}$$

$$= 2\cosh Ah\ E_1 \quad . \qquad \text{(B-22d)}$$

Substituting a_N, b_N and c_N into equation (B-22), the local analytic solution becomes

$$\tilde{\phi}_P^N = e^{-Ah-Bk}\left(\frac{1}{2}E_1 - Ah \coth Ah\ E_2 \right)\tilde{\phi}_{NE} +$$
$$e^{Ah-Bk}\left(\frac{1}{2}E_1 - Ah \coth Ah\ E_2 \right)\tilde{\phi}_{NW} +$$
$$e^{-Bk}(2Ah \cosh Ah \coth Ah\ E_2)\tilde{\phi}_{NC} \quad . \qquad \text{(B-23a)}$$

Similarly, $\tilde{\phi}_P^S$, $\tilde{\phi}_P^E$ and $\tilde{\phi}_P^W$ can be solved in terms of the nodal values at the south, east and west boundaries, respectively.

ORIGINAL PAGE IS
OF POOR QUALITY

$$\tilde{\phi}_P^N = e^{-Ah+Bk}\left(\frac{1}{2}E_1 - Ah \coth Ah\, E_2\right)\tilde{\phi}_{SE} + e^{Ah+Bk}\left(\frac{1}{2}E_1 - Ah \coth Ah\, E_2\right)\tilde{\phi}_{SW} + e^{Bk}\left(aAh \cosh Ah \coth Ah\, E_2\right)\tilde{\phi}_{SC} \quad , \tag{B-23b}$$

$$\tilde{\phi}_P^E = e^{-Ah+Bk}\left(\frac{1}{2}E_1' - Bk \coth Bk\, E_2'\right)\tilde{\phi}_{NE} + e^{-Ah+Bk}\left(\frac{1}{2}E_1' - Bk \coth Bk\, E_2'\right)\tilde{\phi}_{SE} + e^{-Ah}\left(2Bk \cosh Bk \coth Bk\, E_2'\right)\tilde{\phi}_{WC} \quad , \tag{B-23c}$$

$$\tilde{\phi}_P^W = e^{Ah-Bk}\left(\frac{1}{2}E_1' - Bk \coth Bk\, E_2'\right)\tilde{\phi}_{NW} + e^{Ah+Bk}\left(\frac{1}{2}E_1' - Bk \coth Bk\, E_2'\right)\tilde{\phi}_{SW} + e^{Ah}\left(2Bk \cosh Bk \coth Bk\, E_2'\right)\tilde{\phi}_{WC} \quad , \tag{B-23d}$$

where

$$E_i' = \sum_{m=1}^{\infty} \frac{-(-1)^m(\lambda_m' k)}{[(Bk)^2 + (\lambda_m' k)^2]^1 \cosh \mu_m' h} \, , \quad i = 1, 2$$

and

$$\lambda_m' = \frac{(2m-1)\pi}{2k} \quad , \qquad \mu_m' = \sqrt{A^2 + B^2 C + \lambda_m'^2} \quad .$$

The 9-point FA formula relating the center value and its neighboring nodal values can thus be obtained by superimposing the four solutions of the linear problems (1) through (4), or

$$\tilde{\phi}_P = \tilde{\phi}_P^N + \tilde{\phi}_P^S + \tilde{\phi}_P^E + \tilde{\phi}_P^W$$

ORIGINAL PAGE IS
OF POOR QUALITY

$$= (e^{-Ah-Bk}\tilde{\phi}_{NE} + e^{Ah-Bk}\tilde{\phi}_{NW} + e^{-Ah+Bk}\tilde{\phi}_{SE} +$$

$$e^{Ah+Bk}\tilde{\phi}_{SW})[\ \tfrac{1}{2}(E_1 + E_1') - Ah\ \coth Ah\ E_2 - Bk\ \coth Bk\ E_2']$$

$$+2Ah\ \cosh Ah\ \coth Ah\ E_2\ (e^{-Bk}\tilde{\phi}_{NC} + e^{Bk}\tilde{\phi}_{SC}) +$$

$$2Bk\ \cosh Bk\ \coth Bk\ E_2'\ (e^{-Ah}\tilde{\phi}_{EC} + e^{Ah}\tilde{\phi}_{WC})\ . \quad \text{(B-24)}$$

Since $\tilde{\phi}=1$ and $\tilde{\phi}=-BC\xi + A\eta$ are two particular solutions of this convective transport equation (B-7), and both of them can be represented by the exponential and linear boundary functions (B-10), it is instructive to utilize these exact summation terms E_1, E_1', E_2 and E_2' as follows

(I) For $\tilde{\phi} = 1$

Since $\tilde{\phi}=1$ is an analytic solution of equation (B-7) and can be represented by boundary fuctions (B-10), it should satisfy the FA formula (B-24) also. By substituting

$$\tilde{\phi}_P = \tilde{\phi}_{EC} = \tilde{\phi}_{WC} = \tilde{\phi}_{NC} = \tilde{\phi}_{SC} = \tilde{\phi}_{NE} = \tilde{\phi}_{NW} = \tilde{\phi}_{SE} = \tilde{\phi}_{SW} = 1$$

into equation (B-24), an analytic relation between E_1 and E_1' can be obtained

ORIGINAL PAGE IS
OF POOR QUALITY

$$\tilde{\phi}_P = 1 = (e^{-Ah}+e^{Ah})(e^{-Bk}+e^{Bk})\left[\tfrac{1}{2}(E_1+E_1') - Ah\ \coth Ah\ E_2 - Bk\ \coth Bk\ E_2'\right] + 2Ah\ \cosh Ah\ \coth Ah\ E_2(e^{-Bk}+e^{Bk}) + 2Bk\ \cosh Bk\ \coth Bk\ E_2'(e^{-Ah}+e^{Ah})$$

$$= 2\cosh Ah\ \cosh Bk(E_1+E_1')$$

or

$$E_1 + E_1' = \frac{1}{2\cosh Ah\ \cosh Bk} \quad . \tag{B-25}$$

(II) For $\tilde{\phi} = -BC\,\xi + A\eta$

Similarly, $\tilde{\phi}=-BC\xi + A\eta$ satisfies the FA formula (B-24) also. It gives $\tilde{\phi}_P=0$, $\tilde{\phi}_{EC}=-BCh$, $\tilde{\phi}_{NC}=Ak$ etc. By substituting these values into equation (B-24), an analytic expression between E_2 and E_2' is obtained as below

$$\tilde{\phi}_P = 0 = [Ak(e^{-Ah-Bk}+e^{Ah-Bk}-e^{-Ah+Bk}-e^{Ah+Bk}) + Bh(e^{Ah-Bk}+e^{Ah+Bk}-e^{-Ah-Bk}-e^{-Ah+Bk})]\left[\tfrac{1}{2}(E_1+E_1') - Ah\ \coth Ah\ E_2 - Bk\ \coth Bk\ E_2'\right] + 2Ah\ \cosh Ah\ \coth Ah\ E_2\ Ak\,(e^{-Bk}-e^{Bk}) + 2Bk\ \cosh Bk\ \coth Bk\ E_2'\ Bk(e^{Ah}-e^{-Ah})$$

$$= \frac{1}{\cosh Ah\ \cosh Bk}(Bh\ \sinh Ah\ \cosh Bk - Ak\ \cosh Ah\ \sinh Bk) + 4(Ak)(Bk)\cosh Ah\ \sinh Bk\ \coth Bk\ E_2' - 4(Ah)(Bh)\cosh Bk\ \sinh Ah\ \coth Ah\ E_2 \quad ,$$

or

$$E_2 - \frac{k^2}{Ch^2}E_2' = \frac{BCh\ \tanh Ah - Ak\ \tanh Bk}{4Ah\ BCh\ \cosh Ah\ \cosh Bk} \quad . \tag{B-26a}$$

ORIGINAL PAGE IS
OF POOR QUALITY

Defining

$$E = \frac{1}{2}(E_1 + E_1') - Ah \coth Ah \; E_2 - Bk \coth Bk \; E_2' \;, \qquad \text{(B-26c)}$$

$$EA = 2Ah \cosh Ah \coth Ah \; E_2 \;, \qquad \text{(B-26d)}$$

$$EB = 2Bk \cosh Bk \coth Bk \; E_2' \;, \qquad \text{(B-26e)}$$

then the 9-point FA solution (B-24) can be summarized as

$$\tilde{\phi}_P = C_{NE}\tilde{\phi}_{NE} + C_{NW}\tilde{\phi}_{NW} + C_{SE}\tilde{\phi}_{SE} + C_{EC}\tilde{\phi}_{EC} + C_{WC}\tilde{\phi}_{WC} + C_{EC}\tilde{\phi}_{EC} + C_{SC}\tilde{\phi}_{SC} + C_{NC}\tilde{\phi}_{NC} \;, \qquad \text{(B-27)}$$

where

$$C_{NE} = e^{-Ah-Bk} E \;, \qquad C_{NW} = e^{Ah-Bk} E \;,$$

$$C_{SE} = e^{-Ah+Bk} E \;, \qquad C_{SW} = e^{Ah+Bk} E \;,$$

$$C_{NC} = e^{-Bk}(EA) \;, \qquad C_{SC} = e^{Bk}(EA) \;,$$

$$C_{EC} = e^{-Ah}(EB) \;, \qquad C_{WC} = e^{Ah}(EB) \;,$$

After applying the analytic expressions (B-25) and (B-26), only one series summation term in E_2 or E_2' is to be evaluated In most of the applications, ten terms of summation for calculating E_2 or E_2' are enough to achieve an accuracy of 10^{-6}.

ORIGINAL PAGE IS
OF POOR QUALITY

For the unsteady, inhomogeneous convective transport equation (B-5) with high order correction term, i.e., $g \neq 0$, the local analytic solution can be obtained by substituting of equation (B-6) into equation (B-24) for $\tilde{\phi}$, which gives

$$\phi_P = C_{NF}\phi_{NE} + C_{NW}\phi_{NW} + C_{SE}\phi_{SE} + C_{SW}\phi_{SW} + C_{EC}\phi_{EC} + C_{WC}\phi_{WC} + C_{NC}\phi_{NC} + C_{SC}\phi_{SC} - C_P g_P \quad . \tag{B-28}$$

where

$$C_P = \frac{1}{2(A^2+B^2)} [\, Ah(C_{NW} + C_{SW} + C_{WC} - C_{NE} - C_{SE} - C_{EC}) + Bk(C_{SE} + C_{SW} + C_{SC} - C_{NE} - C_{NW} - C_{NC})] \cdot \tag{B-28a}$$

By substituting g of equation (B-5a) into equation (B-28), a 10-point FA formula for steady inhomogeneous convective transport equation with higher order correction term can be obtained

$$\phi_P = \frac{1}{1 + \frac{R}{\tau} C_P} (C_{NE}\phi_{NE} + C_{NW}\phi_{NW} + C_{SE}\phi_{SE} + C_{SW}\phi_{SW} + C_{EC}\phi_{EC} + C_{WC}\phi_{WC} + C_{NC}\phi_{NC} + C_{SC}\phi_{SC} + \frac{R}{\tau} C_P \phi_P^{n-1} - C_P f_P) \quad , \tag{B-29}$$

where

$$f_P = f^{n-1}(x,y,\phi_j)|_{P(0,0)}$$

Here the nodal values without superscript denote those values evaluated at kth time step, while ϕ_P^{n-1} denotes the nodal value of interior point at (k-1)th step.

ORIGINAL PAGE IS
OF POOR QUALITY


```
C
C     ********************************************************
C      APPENDIX C-1
C     ********************************************************
C
C
C     ********************************************************
      GENERATION OF BOUNDARY-FITTED COORDINATES
      FOR KARMANN-TREFFTZ AIRFOIL
C     ********************************************************
C
$INSERT SYSCOM½ERRD.F
$INSERT SYSCOM½KEYS.F
$INSERT SYSCOM½A$KEYS
      IMPLICIT REAL*8 (A-H,O-Z)
      COMMON/ABC/A(68),B(68),X(68,25),Y(68,25),Q(68),P(68),
     $X1(68),Y1(68)
      COMMON/EEF/VA(68,25),VC(68,25),VB(68,25),VABW(68,25),
     $VF1(68,25),VF2(68,25)
      DATA X1/-.5027,-.5027,-.4973,-.4867,-.4711,-.4508,
     1-.4259,-.3969,.3640,-.3276,-.2879,-.2455,-.2006,-.1538
     2,-.1053,-.0558,-.0056,.0447,.0948,.1440,.1920,.2393,
     3 .2823,.3235,.3515,.3958,.4256,.4515,.4720,.4871,.4964
     5,.4980,.4990,.4994,.4995,.4994,.4991,.4980,.4961,.4863
     6,.4705,.4489,.4220,.3901,.3538,.3134,.2596,.2228,.1736
     7,.1227,.0706,.0179,-.0348,-.0870,-.1380,-.1875,-.2348,
     8,-.2795,-.3211,-.3593,-.3937,-.4239,-.4496,-.4705,
     $-.4865,-.4973,-.5027,-.5027/
      DATA Y1/.0036,.0112,.0187,.0264,.0341,.0416,.0486,
     1 .0552,.0611,.0661,.0702,.0733,.0753,.0762,.0759,
     $,.0745,.0721,.0687,.0644,.0593,.0536,.0475,.0411,.0346
     2,.0283,.0221,.0154,.0113,.0068,.0030,.0019,.0009,.0004
     3,.0000,-.0005,-.0009,-.0019,-.0028,-.0056,-.0085,
     4-.0117,-.0150,-.0186,-.0223,-.0261,-.0300,-.0338,
     5 -.0374,-.0408,-.0438,-.0464,-.0485,-.0499,-.0506,
     6 -.0505,.0497,-.0480,-.0456,-.0424,-.0384,-.0337,
     7 -.0285,-.0227,-.0165,.0100,-.0032,.0036/
      CALL SRCH$$(K$WRIT,'OUT3',4,2,TYPE,CODE)
C
C     ********************************************************
      INITIAL AND BOUNDARY CONDITIONS
C     ********************************************************
C
      IMAX=68
      JMAX=25
      IMAX1=IMAX-1
      JMAX1=JMAX-1
      RD=3.141592653589793D0
      D33=RD/33.
      R=2.0
      DO 31 I=1,IMAX
```

```
      DEG=RD-(I-2)*D33
      X(I,JMAX)=R*DCOS(DEG)
      Y(I,JMAX)=R*DSIN(DEG)
 31   CONTINUE
      DO 32 I=1,IMAX
      X(I,1)=X1(I)
      Y(I,1)=Y1(I)
 32   CONTINUE
      DO 40 J=2,JMAX1
      DO 50 I=2,IMAX1
      X(I,J)=X(I,1)+((X(I,JMAX)-X(I,1))*(J-1)*.7)/JMAX1
      Y(I,J)=Y(I,1)+((Y(I,JMAX)-Y(I,1))*(J-1)*.7)/JMAX1
   50 CONTINUE
   40 CONTINUE
      DO 52 I=1,IMAX
      WRITE(6,51)I,X(I,1),Y(I,1)
 52   CONTINUE
 51   FORMAT(4X,I2,3X,F6.4,3X,F6.4)
C
C    ********************************************************
      CALCULATION OF COORDINATE TANSFORMATION
C    ********************************************************
C
      DO 15 J=2,JMAX1
      Q(J)=CON(J,1,1)
      WRITE(6,200)Q(J)
   15 CONTINUE
      DO 25 I=2,IMAX1
      P(I)=0.0
      WRITE(6,200)P(I)
   25 CONTINUE
      N=1
   80 DO 65 J=2,JMAX1
      K=J
      X(1,K)=X(IMAX1,K)
      Y(1,K)=Y(IMAX1,K)
      X(IMAX,K)=X(2,K)
      Y(IMAX,K)=Y(2,K)
    7 DO 70 I=2,IMAX1
      XET=X(I,J+1)-X(I,J-1)
      XXI=X(I+1,J)-X(I-1,J)
      YET=Y(I,J+1)-Y(I,J-1)
      YXI=Y(I+1,J)-Y(I-1,J)
      XXIET=X(I+1,J+1)-X(I+1,J-1)+X(I-1,J-1)-X(I-1,J+1)
      YXIET=Y(I+1,J+1)-Y(I+1,J-1)+Y(I-1,J-1)-Y(I-1,J+1)
      AF=(XET)**2+(YET)**2
      BT=XXI*XET+YXI*YET
      GM=(XXI)**2+(YXI)**2
      FX=(AF*(X(I-1,J)+X(I+1,J))-(BT*XXIET/2.)
     1+GM*(X(I,J+1)+X(I,J-1)))/(2.*(AF+GM))
```

ORIGINAL PAGE IS
OF POOR QUALITY


```
      FY=(AF*(Y(I-1,J)+Y(I+1,J))-(BT*YXIET/2.)
     1+GM*(Y(I,J+1)+Y(I,J-1)))/(2.*(AF+GM))
      XYJ=.25*(XXI*YET-XET*YXI)
      XAD=((XYJ)**2*(XET*Q(J)+XXI*P(I)))/(AF+GM)
      YAD=((XYJ)**2*(YET*Q(J)+YXI*P(I)))/(AF+GM)
      FX=FX+XAD
      FY=FY+YAD
   75 X(I,J)=X(I,J)+(FX-X(I,J))*1.5
      Y(I,J)=Y(I,J)+(FY-Y(I,J))*1.5
   70 CONTINUE
   65 CONTINUE
      IF(N.GT.300) GO TO 85
      EPS=0.0
      DO 77 J=2,JMAX1
      EPS1=X(1,J)-X(IMAX1,J)
      IF(DABS(EPS1).GT.DABS(EPS))EPS=EPS1
      EPS2=X(2,J)-X(IMAX,J)
      IF(DABS(EPS2).GT.DABS(EPS))EPS=EPS2
      EPS3=Y(1,J)-Y(IMAX1,J)
      IF(DABS(EPS3).GT.DABS(EPS))EPS=EPS3
      EPS4=Y(2,J)-Y(IMAX,J)
      IF(DABS(EPS4).GT.DABS(EPS))EPS=EPS4
 77   CONTINUE
      N=N+1
      WRITE(6,202)N,EPS
 202  FORMAT(1X,'ITERATION AND EPS ARE',I4,F13.7)
      IF(DABS(EPS).LT.0.0000001)GO TO 85
      GO TO 80
C
C    ************************************************************
C     PRINT THE COORDINATES GENERATED IN THE
C         TRANSFORMED PLANE
C    ************************************************************
C
   85 WRITE(6,500) N
      DO 90 I=1,IMAX
      WRITE(6,100) I
      WRITE(6,200)(X(I,J),J=1,JMAX)
   90 WRITE(6,200)(Y(I,J),J=1,JMAX)
  100 FORMAT('I=',I2,,50X,'** X-COORDINATE **')
  200 FORMAT(8F10.5)
  400 FORMAT(9F5.2)
  500 FORMAT(50X,'***** N=',I3,' *****')
C
C    ************************************************************
C     CALCULATION OF TRANSFORMED COEFFICIENTS
C    ************************************************************
C
      DO 411 IX=2,IMAX1
      DO 411 IY=2,JMAX1
      XZ=0.5*(X(IX+1,IY)-X(IX-1,IY))
```

ORIGINAL PAGE IS
OF POOR QUALITY


```
      XZZ=X(IX+1,IY)-2.0*X(IX,IY)+X(IX-1,IY)
      XE=0.5*(X(IX,IY+1)-X(IX,IY-1))
      XEE=X(IX,IY+1)-2.0*X(IX,IY)+X(IX,IY-1)
      YZ=0.5*(Y(IX+1,IY)-Y(IX-1,IY))
      YZZ=Y(IX+1,IY)-2.0*Y(IX,IY)+Y(IX-1,IY)
      YE=0.5*(Y(IX,IY+1)-Y(IX,IY-1))
      YEE=Y(IX,IY+1)-2.0*Y(IX,IY)+Y(IX,IY-1)
      XZE=0.25*(X(IX+1,IY+1)-X(IX+1,IY-1)+X(IX-1,IY-1)
     1          -X(IX-1,IY+1))
      YZE=0.25*(Y(IX+1,IY+1)-Y(IX+1,IY-1)+Y(IX-1,IY-1)
     1          -Y(IX-1,IY+1))
      ARFA=XE*XE+YE*YE
      BETA=XZ*XE+YZ*YE
      GAMA=XZ*XZ+YZ*YZ
      BINJ=XZ*YE-XE*YZ
      CODX=ARFA*XZZ-2.0*BETA*XZE
     1          +GAMA*XEE
      CODY=ARFA*YZZ-2.0*BETA*YZE
     1          +GAMA*YEE
      COZE=(YZ*CODX-XZ*CODY)/BINJ
      COTA=(XE*CODY-YE*CODX)/BINJ
      VA(IX,IY)=-0.5*COTA/ARFA
      VC(IX,IY)=GAMA/ARFA
      VB(IX,IY)=-0.5*COZE/GAMA
      VABW(IX,IY)=0.5*BINJ/ARFA
      VF1(IX,IY)=BINJ*BINJ/ARFA
      VF2(IX,IY)=BETA/ARFA
 411  CONTINUE
C
C     ***********************************************************
C      PRINT THE TRANSFORMED COEFFICIENTS
C     ***********************************************************
C
      DO 91 I=2,IMAX1
      WRITE(6,201)I
 91   WRITE(6,200)(VA(I,J),J=2,JMAX1)
      DO 92 I=2,IMAX1
      WRITE(6,201)I
 92   WRITE(6,200)(VB(I,J),J=2,JMAX1)
      DO 93 I=2,IMAX1
      WRITE(6,201)I
 93   WRITE(6,200)(VC(I,J),J=2,JMAX1)
      DO 94 I=2,IMAX1
      WRITE(6,201)I
 94   WRITE(6,200)(VABW(I,J),J=2,JMAX1)
      DO 95 I=2,IMAX1
      WRITE(6,201)I
 95   WRITE(6,200)(VF1(I,J),J=2,JMAX1)
      DO 96 I=2,IMAX1
      WRITE(6,201)I
 96   WRITE(6,200)(VF2(I,J),J=2,JMAX1)
```

ORIGINAL PAGE IS
OF POOR QUALITY


```
 201  FORMAT(1X,'ZETA=',I3)
      CALL EXIT
      END
C
C     ***********************************************************
C     FUNCTION SUBROUTINE TO CALCULATE THE CONTRACTION FACTOR
C     ***********************************************************
C
      FUNCTION CON(I,J1,J2)
      IMPLICIT REAL*8 (A-H,O-Z)
      DIMENSION AK(74),CK(74)
      CON=0.
      C1=100.
      C2=0.5
      DO 10 J=J1,J2
      AK(J)=C1-(J-J1)*1.
      CK(J)=C2
   10 CONTINUE
      DO 20 J=J1,J2
      M=I-J
      IF(M)1,2,3
    1 SIG=-1.
      L=-M
      GO TO 4
    3 SIG=1.
      L=M
    4 GP=CK(J)*L
      XM=DEXP(GP)
      CON1=(-1.*AK(J)*SIG)/(XM)
      GO TO 6
    2 CON1=0.
    6 CON=CON+CON1
   20 CONTINUE
      RETURN
      END
```

ORIGINAL PAGE IS
OF POOR QUALITY


```
C
C     ********************************************************
C      APPENDIX C-2
C     ********************************************************
C
C
C     ********************************************************
C      SEPARATION OF CHANNEL FLOW OVER A
C      BACKWARD FACING STEP
C     ********************************************************
C
$INSERT SYSCOM½ERRD.F
$INSERT SYSCOM½KEYS.F
$INSERT SYSCOM½A$KEYS
      IMPLICIT REAL*8(A-H,O-Z)
      COMMON/AAA/ AA(46),BB(46),CC(46),DD(46),U(46,16),
     $V(46,16),T(46),PSIN(46,16),DZTX(46,16),DZTY(46,16),
     $F(46,16),ZETAN(46,16,2),PSIO(46,16)
      COMMON/COEF/CM1P1(46,16),CP0P1(46,16),CP1P1(46,16),
     $P0(46,16),
     $CM1P0(46,16),CP0P0(46,16),CP1P0(46,16),CM1M1(46,16),
     $CP0M1(46,16),CP1M1(46,16)
      CALL SRCH$$(K$READ,'AAAA',4,7,TYPE,CODE)
      CALL SRCH$$(K$WRIT,'ZZZZ',4,2,TYPE,CODE)
C
C     ********************************************************
C      INPUT GIVEN DATA
C     ********************************************************
C
      IXMAX=46
      IYMAX=16
      IZMAX=IXMAX
      IRMAX=IYMAX
      IXM1=IXMAX-1
      IYM1=IYMAX-1
      IZM1=IXM1
      IRM1=IYM1
      ITERP=15
      ITERZ=6
      IEND=250
      L=1
      NM=20
      EPE=0.000001
      HX=0.1*5.0/3.0
      HY=0.5/5.
      DX=HX
      DY=HY
      DXX=HX*HX
      DYY=HY*HY
      TAU=0.3
      Q=2./3.
```

ORIGINAL PAGE IS
OF POOR QUALITY

```
      RE=73.
      DKY=16.0/27.0
      WRITE(6,50)RE,HX,HY,TAU
50    FORMAT(//5X,4E12.4)
C
C     ********************************************************
C     INITIAL AND BOUNDARY CONDITIONS
C     ********************************************************
C
      DO 105 IZ=1,IZMAX
      PSIN(IZ,IRMAX)=Q
C     PSIO(IZ,IRMAX)=Q
      U(IZ,IRMAX)=0.0
      V(IZ,IRMAX)=0.0
      PSIN(IZ,1)=0.0
C     PSIO(IZ,1)=0.0
      U(IZ,1)=0.0
  105 V(IZ,1)=0.0
      DO 106 IR=2,6
      PSIN(5,IR)=0.0
C     PSIO(5,IR)=0.0
      U(1,IR)=0.0
  106 V(1,IR)=0.0
      DO 104 IZ=1,5
      PSIN(IZ,6)=0.
      U(IZ,6)=0.
 104  V(IZ,6)=0.
      DO 107 IR=7,15
      YI=DY*(IR-6)
      U(1,IR)=4.0*YI*(1.0-YI)
      PSIN(1,IR)=2.0*YI*YI-4.0*YI*YI*YI/3.0
 107  V(1,IR)=0.
      DO 109 IR=1,IRMAX
      YI=DY*(IR-1)-0.5
      PSIN(IZMAX,IR)=DKY*YI+0.5*DKY*YI*YI-2.0*DKY*YI*YI*YI/
     $3.+14./81.
      U(IZMAX,IR)=DKY+DKY*YI-2.0*DKY*YI*YI
      ZETAN(IZMAX,IR,2)=-DKY+4.0*DKY*YI
109   V(IZMAX,IR)=0.0
      MM=0
      DO 1200 IT=1,IEND
      MM=MM+1
      SMZET=0.
      SMPSI=0.
      DO 156 IX=1,IXMAX
      DO 156 IY=1,IYMAX
 156  PSIO(IX,IY)=PSIN(IX,IY)
C
C     ********************************************************
C      CALCULATION OF STREAM FUNCTION EQUATION
C     ********************************************************
```

ORIGINAL PAGE IS
OF POOR QUALITY

```
C
      DO 159 ITER=1,ITERP
      DO 155 IY=2,IYM1
      IXB=2
      IF(IY.LE.6)IXB=6
      DO 160 IX=IXB,IXM1
      AA(IX)=-0.07488
      BB(IX)=1.0
      CC(IX)=-0.07488
  160 DD(IX)=0.34695*(PSIN(IX,IY+1)+PSIN(IX,IY-1))+0.03909*
     $PSIN(IX+1,
     $(PSIN(IX+1,IY+1)+PSIN(IX+1,IY-1)+PSIN(IX-1,IY+1)+
     $PSIN(IX-1,IY-1))+0.00425*ZETAN(IX,IY,1)
      DD(IXB)=DD(IXB)+0.07488*PSIN(IXB-1,IY)
      DD(IXM1)=DD(IXM1)+0.07488*PSIN(IXMAX,IY)
      CALL TRIDAG(IXB,IXM1,AA,BB,CC,DD,T)
      DO 170 IX=IXB,IXM1
      PSIN(IX,IY)=T(IX)
      DEPSI=PSIN(IX,IY)-PSIO(IX,IY)
      IF(DABS(DEPSI).GT.DABS(SMPSI))GO TO 438
      GO TO 170
 438  SMPSI=DEPSI
      IXSMP=IX
      IYSMP=IY
 170  CONTINUE
  155 CONTINUE
      IF(DABS(SMPSI).LT.0.0001)GO TO 157
 159  CONTINUE
 157  CONTINUE
  111 FORMAT(11F9.4)
C
C    ************************************************************
C     CALCULATION OF VELOCITY (FROM STREAM FUNCTION)
C    ************************************************************
C
      DO 175 IX=6,IXM1
      DO 175 IY=2,IYM1
      U(IX,IY)=(PSIN(IX,IY+1)-PSIN(IX,IY-1))/2.0/HY
  175 V(IX,IY)=(PSIN(IX-1,IY)-PSIN(IX+1,IY))/2.0/HX
      DO 176 IX=2,5
      DO 176 IY=7,IYM1
      U(IX,IY)=(PSIN(IX,IY+1)-PSIN(IX,IY-1))/2.0/HY
  176 V(IX,IY)=(PSIN(IX-1,IY)-PSIN(IX+1,IY))/2.0/HX
C
C    ************************************************************
C     CALCULATION OF HIGH ORDER CORRECTION TERM
C    ************************************************************
C
      DO 180 IX=6,IXM1
      DO 180 IY=1,IYMAX
      AH=0.5*RE*U(IX,IY)*HX
```

```
      BK=0.5*RE*V(IX,IY)*HY
      IF(DABS(AH).LT.EPE) AH=EPE
      IF(DABS(BK).LT.EPE) BK=EPE
      EPAH=DEXP(AH)
      EPBK=DEXP(BK)
      COSHA=0.5*EPAH+0.5/EPAH
      SINHA=0.5*EPAH-0.5/EPAH
      COSHB=0.5*EPBK+0.5/EPBK
      SINHB=0.5*EPBK-0.5/EPBK
      IF(IX.NE.6) GO TO 181
      DZTX(IX-1,IY)=(ZETAN(IX+1,IY,1)-ZETAN(IX-1,IY,1))/2.0/
     $HX+(AH/EPAH/EPAH-SINHA*COSHA)/2.0/HX/SINHA/SINHA*
     $(ZETAN(IX+1,IY,1)+ZETAN(IX-1,IY,1)-2.0*ZETAN(IX,IY,1))
      IF(IY.EQ.1) GO TO 181
      IF(IY.EQ.IYMAX) GO TO 181
      DZTY(IX-1,IY)=(ZETAN(IX-1,IY+1,1)-ZETAN(IX-1,IY-1,1))/
     $2.0/HY
181   IF(IX.NE.IXM1) GO TO 182
      DZTX(IX+1,IY)=(ZETAN(IX+1,IY,1)-ZETAN(IX-1,IY,1))/2.0/
     $HX+(AH*EPAH*EPAH-SINHA*COSHA)/2.0/HX/SINHA/SINHA*
     $(ZETAN(IX+1,IY,1)+ZETAN(IX-1,IY,1)-2.0*ZETAN(IX,IY,1))
      IF(IY.EQ.1) GO TO 182
      IF(IY.EQ.IYMAX) GO TO 182
      DZTY(IX+1,IY)=(ZETAN(IX+1,IY+1,1)-ZETAN(IX+1,IY-1,1))/
     $2.0/HY
182   IF(IY.NE.2) GO TO 183
      DZTY(IX,IY-1)=(ZETAN(IX,IY+1,1)-ZETAN(IX,IY-1,1))/2.0/
     $HY+(BK/EPBK/EPBK-SINHB*COSHB)/2.0/HY/SINHB/SINHB*
     $(ZETAN(IX,IY+1,1)+ZETAN(IX,IY-1,1)-2.0*ZETAN(IX,IY,1))
183   IF(IY.NE.IYM1) GO TO 184
      DZTY(IX,IY+1)=(ZETAN(IX,IY+1,1)-ZETAN(IX,IY-1,1))/2.0/
     $HY+(BK*EPBK*EPBK-SINHB*COSHB)/2.0/HY/SINHB/SINHB*
     $(ZETAN(IX,IY+1,1)+ZETAN(IX,IY-1,1)-2.0*ZETAN(IX,IY,1))
184   DZTX(IX,IY)=(ZETAN(IX+1,IY,1)-ZETAN(IX-1,IY,1))/2.0/HX
     $+(AH-SINHA*COSHA)/2.0/HX/SINHA/SINHA*(ZETAN(IX+1,IY,1)
     $+ZETAN(IX-1,IY,1)-2.0*ZETAN(IX,IY,1))
      IF(IY.EQ.1) GO TO 180
      IF(IY.EQ.IYMAX) GO TO 180
      DZTY(IX,IY)=(ZETAN(IX,IY+1,1)-ZETAN(IX,IY-1,1))/2.0/HY
     $+(BK-SINHB*COSHB)/2.0/HY/SINHB/SINHB*(ZETAN(IX,IY+1,1)
     $+ZETAN(IX,IY-1,1)-2.0*ZETAN(IX,IY,1))
180   CONTINUE
      DZTY(5,1)=(2.0*ZETAN(5,2,1)-1.5*ZETAN(5,1,1)-0.5*
      ZETAN(5,3,1))/HY
      DZTY(5,IYMAX)=(1.5*ZETAN(5,IYMAX,1)+0.5*
     $ZETAN(5,IYMAX-2,1)-2.0*ZETAN(5,IYMAX-1,1))/HY
      DZTY(IXMAX,1)=(2.0*ZETAN(IXMAX,2,1)-1.5*
     $ZETAN(IXMAX,1,1)-0.5*ZETAN(IXMAX,3,1))/HY
      DZTY(IXMAX,IYMAX)=(1.5*ZETAN(IXMAX,IYMAX,1)+0.5*
     $ZETAN(IXMAX,IYMAX-2,1)-2.0*ZETAN(IXMAX,IYMAX-1,1))/HY
```

ORIGINAL PAGE IS
OF POOR QUALITY

```
      DO 200 IX=6,IXM1
      DO 200 IY=2,IYM1
      AU=0.5*RE*U(IX,IY)
      BV=0.5*RE*V(IX,IY)
  200 CALL COEFF(AU,BV,HX,HY,IX,IY)
      DO 202 IX=2,5
      DO 202 IY=7,IYM1
      AU=0.5*RE*U(IX,IY)
      BV=0.5*RE*V(IX,IY)
  202 CALL COEFF(AU,BV,HX,HY,IX,IY)
      DO 1190 IX=6,IXM1
      DO 1190 IY=2,IYM1
      F(IX,IY)=RE*(CM1P1(IX,IY)*((U(IX-1,IY+1)-U(IX,IY))*
     $DZTX(IX-1,IY+1)+(V(IX-1,IY+1)-V(IX,IY))*DZTY(IX-1,IY+1)
     $+CP0P1(IX,IY)*((U(IX,IY+1)-U(IX,IY))*DZTX(IX,IY+1)+
     $(V(IX,IY+1)-V(IX,IY))*DZTY(IX,IY+1))
     $+CP1P1(IX,IY)*((U(IX+1,IY+1)-U(IX,IY))*DZTX(IX+1,IY+1)
     $+(V(IX+1,IY+1)-V(IX,IY))*DZTY(IX+1,IY+1))+CM1P0(IX,IY)
     $*((U(IX-1,IY)-U(IX,IY))*DZTX(IX-1,IY)+(V(IX-1,IY)-
     $V(IX,IY))*DZTY(IX-1,IY))+CP1P0(IX,IY)*
     $((U(IX+1,IY)-U(IX,IY))*DZTX(IX+1,IY)+(V(IX+1,IY)-
     $V(IX,IY))*DZTY(IX+1,IY)))
      F(IX,IY)=F(IX,IY)+RE*(CM1M1(IX,IY)*((U(IX-1,IY-1)-
     $U(IX,IY))*DZTXIX-1,IY-1)+(V(IX-1,IY-1)-V(IX,IY))*
     $DZTY(IX-1,IY-1))+CP0M1(IX,IY)*((U(IX,IY-1)-U(IX,IY))*
     $DZTX(IX,IY-1)+(V(IX,IY-1)-V(IX,IY))*DZTY(IX,IY-1))
     $+CP1M1(IX,IY)*((U(IX+1,IY-1)-U(IX,IY))*DZTX(IX+1,IY-1)
     $+(V(IX+1,IY-1)-V(IX,IY))*DZTY(IX+1,IY-1)))
      F(IX,IY)=F(IX,IY)*5.0/9.0
 1190 CONTINUE
      DO 1191 IX=2,5
      DO 1191 IY=2,IYM1
 1191 F(IX,IY)=0.
C
C    ************************************************************
C     CALCULATION OF BOUNDARY CONDITIONS FOR VORTICITY.
C     ************************************************************
C
      DO 210 IZ=2,IZM1
      ZETAN(IZ,IRMAX,2)=2.0*(Q-PSIN(IZ,IRM1))/DYY
      ZETAN(IZ,1,2)=-2.0*PSIN(IZ,2)/DYY
  210 CONTINUE
      DO 220 IR=2,5
      ZETAN(5,IR,2)=(-2.0*PSIN(6,IR)/DXX)
  220 CONTINUE
      DO 207 IR=7,15
      YI=DY*(IR-6)
      ZETAN(1,IR,2)=-4.0+8.0*YI+(4.0*V(2,IR)-V(3,IR))/(2.0*
     $DX)
  207 CONTINUE
```

ORIGINAL PAGE IS
OF POOR QUALITY


```
      DO 208 IZ=2,4
 208  ZETAN(IZ,6,2)=-2.0*PSIN(IZ,7)/DYY
      ZETAN(5,1,2)=0.0
      ZETAN(1,6,2)=-2.0*PSIN(1,7)/DYY
      ZETAN(5,6,2)=-2.0*(PSIN(6,6)/DXX+PSIN(5,7)/DYY)
      ZETAN(1,IRMAX,2)=2.0*(Q-PSIN(1,IRM1))/DYY
      ZETAN(IZMAX,IRMAX,2)=2.0*(Q-PSIN(IZMAX,IRM1))/DYY
      ZETAN(IZMAX,1,2)=-2.0*PSIN(IZMAX,2)/DYY
C
C    ********************************************************
C     CALCULATION OF VORTICITY TRANSPORT EQ.
C    ********************************************************
C
      DO 309 ITER=1,ITERZ
      DO 305 IY=2,IYM1
      IXB=2
      IF(IY.LE.6)IXB=6
      DO 320 IX=IXB,IXM1
      AA(IX)=-CM1P0(IX,IY)/(1.0+CP0P0(IX,IY)*RE/TAU)
      BB(IX)=1.0
      CC(IX)=-CP1P0(IX,IY)/(1.0+CP0P0(IX,IY)*RE/TAU)
  320 DD(IX)=(CP0P1(IX,IY)*ZETAN(IX,IY+1,2)+CP0M1(IX,IY)*
     $ZETAN(IX,IY-1,2)+CP1P1(IX,IY)*ZETAN(IX+1,IY+1,2)+

     $CP1M1(IX,IY)*ZETAN(IX+1,IY-1,2)+CM1P1(IX,IY)*
     $ZTAN(IX-1,IY+1,2)+CM1M1(IX,IY)*ZETAN(IX-1,IY-1,2)
     $+CP0P0(IX,IY)*(RE/TAU*ZETAN(IX,IY,1)-F(IX,IY)))/(1.0
     $+RE/TAU*CP0P0(IX,IY))
      DD(IXB)=DD(IXB)-AA(IXB)*ZETAN(IXB-1,IY,2)
      DD(IXM1)=DD(IXM1)-CC(IXM1)*ZETAN(IXMAX,IY,2)
      CALL TRIDAG(IXB,IXM1,AA,BB,CC,DD,T)
      DO 330 IX=IXB,IXM1
      ZETAN(IX,IY,2)=T(IX)
      DEZET=ZETAN(IX,IY,2)-ZETAN(IX,IY,1)
      IF(DABS(DEZET).GT.DABS(SMZET))GO TO 338
      GO TO 330
 338  SMZET=DEZET
      IXSMZ=IX
      IYSMZ=IY
 330  CONTINUE
  305 CONTINUE
      IF(DABS(SMZET).LT.0.001)GO TO 337
      GO TO 309
 337  IF(DABS(SMPSI).LT.0.0001)GO TO 1201
 309  CONTINUE
      DO 500 IX=1,IXMAX
      DO 500 IY=1,IYMAX
  500 ZETAN(IX,IY,1)=ZETAN(IX,IY,2)
      IF(MM.LT.NM) GO TO 999
      MM=0
```

ORIGINAL PAGE IS
OF POOR QUALITY

```
      WRITE(6,600)IT
  600 FORMAT(//5X,'NO. OF TIME STEPS =',I5)
      DO 700 IX=1,IXMAX,L
      WRITE(6,112)IX
112   FORMAT(1X,'IZ=',I3)
  700 WRITE(6,111)(PSIN(IX,IY),IY=1,IYMAX,L)
      DO 800 IX=1,IXMAX,L
      WRITE(6,112)IX
  800 WRITE(6,111)(ZETAN(IX,IY,2),IY=1,IYMAX,1)
  999 CIRCUL=0.0
      DO 1000 IX=6,IXMAX
      DO 1000 IY=2,IYMAX
 1000 CIRCUL=CIRCUL+(ZETAN(IX,IY,2)+ZETAN(IX,IY-1,2)+
     $ZETAN(IX-1,IY,2)+ZETAN(IX-1,IY-1,2))/4.0
      DO 1002 IX=2,5
      DO 1002 IY=7,IYMAX
 1002 CIRCUL=CIRCUL+(ZETAN(IX,IY,2)+ZETAN(IX,IY-1,2)+
     $ZETAN(IX-1,IY,2)+ZETAN(IX-1,IY-1,2))/4.0
      WRITE(6,1001)IT,CIRCUL,SMPSI,IXSMP,IYSMP,SMZET,IXSMZ,
     $IYSMZ
 1001 FORMAT(/1X,I3,1X,'CIR=',F10.6,1X,F10.6,1X,2I3,1X,
     $ F10.6,1X,2I3)
 1200 CONTINUE
 1201 CONTINUE
      DO 1101 IX=1,IXMAX,L
      WRITE(6,112)IX
 1101 WRITE(6,111)(U(IX,IY),IY=1,IYMAX,L)
      DO 1102 IX=1,IXMAX,L
      WRITE(6,112)IX
 1102 WRITE(6,111)(V(IX,IY),IY=1,IYMAX,L)
      DO 1299 IX=1,IXMAX
      WRITE(6,112)IX
 1299 WRITE(6,1350)(PSIN(IX,IY),IY=1,IYMAX)
      DO 1300 IX=1,IXMAX
      WRITE(6,112)IX
 1300 WRITE(6,1350)(ZETAN(IX,IY,1),IY=1,IYMAX)
 1350 FORMAT(7F11.6)
      CALL EXIT
      END
C
C     ******************************************************
C      SUBROUTINE TO SOLVE THE SYSTEM OF ALGEBRAIC EQUATIONS
C     ******************************************************
C
      SUBROUTINE TRIDAG(IF,L,A,B,C,D,V)
      IMPLICIT REAL*8(A-H,O-Z)
      DIMENSION A(46),B(46),C(46),D(46),V(46),BETA(46),
     $GAMA(46)
      BETA(IF)=B(IF)
      GAMMA(IF)=D(IF)/BETA(IF)
      IFP1=IF+1
```

ORIGINAL PAGE IS
OF POOR QUALITY

```
      DO 1 I=IFP1,L
      BETA(I)=B(I)-A(I)*C(I-1)/BETA(I-1)
    1 GAMMA(I)=(D(I)-A(I)*GAMMA(I-1))/BETA(I)
      V(L)=GAMMA(L)
      LAST=L-IF
      DO 2 K=1,LAST
      I=L-K
    2 V(I)=GAMMA(I)-C(I)*V(I+1)/BETA(I)
      RETURN
      END
C
C     ***********************************************************
C      SUROUTINE TO CALCULATE THE FA COEFFICIENTS FOR
C      UNEQUAL SIZE GRID
C     ***********************************************************
C
      SUBROUTINE COEFF(A,B,HX,HY,IX,IY)
      IMPLICIT REAL*8(A-H,O-Z)
      COMMON/COEF/CM1P1(46,16),CP0P1(46,16),CP1P1(46,16),
     $P0(46,16),
     $CM1P0(46,16),P0P0(46,16),CP1P0(46,16),CM1M1(46,16),
     $CP0M1(46,16),CP1M1(46,16)
      PI=3.141592653589793D0
      EPE=0.000001
      AH=A*HX
      BH=B*HX
      HXY=HY/HX
      IF(AH.LT.0.0) EPA=-EPE
      EPA=EPE
      IF(BH.LT.0.0) EPB=-EPE
      EPB=EPE
      IF(DABS(AH).LT.EPE) AH=EPA
      IF(DABS(BH).LT.EPE) BH=EPB
      AK=AH*HXY
      BK=BH*HXY
      EY2=0.0
      DO 10 I=1,11
      PWR=(-1.0)**I
      ZA=(I-0.5)*PI
      AB=(AK*AK+BK*BK+ZA*ZA)**0.5/HXY
      COSH=PWR*ZA*2.0/(DEXP(AB)+DEXP(-AB))
   10 EY2=EY2-COSH/(BK*BK+ZA*ZA)**2
      EPAH=DEXP(-AH)
      EPBK=DEXP(-BK)
      COSHA=0.5*EPAH+0.5/EPAH
      COSHB=0.5*EPBK+0.5/EPBK
      COTHA=(1.0+EPAH*EPAH)/(1.0-EPAH*EPAH)
      COTHB=(1.0+EPBK*EPBK)/(1.0-EPBK*EPBK)
      EX2=EY2*HXY*HXY+(BK/COTHA-AH*HXY*HXY/COTHB)/
     1     (4.0*AH*BK*COSHA*COSHB)
```

ORIGINAL PAGE IS
OF POOR QUALITY


```
      E=0.25/COSHA/COSHB-AH*COTHA*EX2-BK*COTHB*EY2
      EA=2.0*AH*COSHA*COTHA*EX2
      EB=2.0*BK*COSHB*COTHB*EY2
      CM1P1(IX,IY)=E/EPAH*EPBK
      CP1P1(IX,IY)=E*EPAH*EPBK
      CM1M1(IX,IY)=E/EPAH/EPBK
      CP1M1(IX,IY)=E*EPAH/EPBK
      CP0P1(IX,IY)=EA*EPBK
      CP0M1(IX,IY)=EA/EPBK
      CM1P0(IX,IY)=EB/EPAH
      CP1P0(IX,IY)=EB*EPAH
      CP0P0(IX,IY)=(0.5*A*HX*(CM1P1(IX,IY)+CM1P0(IX,IY)+
     1 CM1M1(IX,IY)-CP1P1(IX,IY)-CP1P0(IX,IY)-CP1M1(IX,IY))
     2 +0.5*B*HY*(CM1M1(IX,IY)+CP0M1(IX,IY)+CP1M1(IX,IY)-
     3 CP1P1(IX,IY)-CP1P1(IX,IY)-CP0P1(IX,IY)+CM1P1(IX,IY)))
     $ /(A*A+B*B)
      RETURN
      END
```

ORIGINAL PAGE IS
OF POOR QUALITY


```
C
C     ******************************************************
C      APPENDIX C-3
C     ******************************************************
C
C
C      ******************************************************
C      POTENTIAL FLOW OVER AN AIRFOIL
C      USING THE FA METHOD WITH THE BOUNDARY-FITTED
C      COORDINATE SYSTEMS
C      ******************************************************
C
$INSERT SYSCOM½ERRD.F
$INSERT SYSCOM½KEYS.F
$INSERT SYSCOM½A$KEYS
      IMPLICIT REAL*8(A-H,O-Z)
      COMMON/AAA/ AA(68),BB(68),CC(68),DD(68),U(68,58),
     $V(68,58),T(68),
     $PSIN(68,58,3),PSIB(68,58),PSIT(68,58),PSIL(68,58)
      COMMON/BBB/SIA(68,58),SIB(68,58),SIC(68,58),ABW(68,58)
     $      ,F1(68,58),F2(68,58),GAMAJ(68,1)
      COMMON/PSIC/PCM1P1(68,58),PCM1P0(68,58),PCM1M1(68,58),
     1 PCP0P1(68,58),PCP0M1(68,58),PCP1P1(68,58),
     2 PCP1P0(68,58),PCP1M1(68,58),PCP0P0(68,58)
      CALL SRCH$$(K$READ,'KAIN',4,7,TYPE,CODE)
      CALL SRCH$$(K$WRIT,'POOL',4,2,TYPE,CODE)
C
C      ******************************************************
C      INPUT GIVEN DATA AND BOUNDARY-FITTED COORDINATES
C      ******************************************************
C
      IXMAX=68
      IYMAX=58
      IXM1=IXMAX-1
      IYM1=IYMAX-1
      L=1
      EPE=0.000001
      HX=1.0
      HY=1.0
      TAU=0.1
      DELTA=0.3
      PAI=3.141592653589793D0
      ATTA=-PAI/36.
C     ATTA=0.
      D33=2.0*PAI/66.
  113 FORMAT(8F10.5)
      DO 122 IX=2,IXM1
  122 READ(11,113)(SIA(IX,IY),IY=2,IYM1)
      DO 123 IX=2,IXM1
  123 READ(11,113)(SIB(IX,IY),IY=2,IYM1)
```

ORIGINAL PAGE IS
OF POOR QUALITY


```
      DO 124 IX=2,IXM1
 124  READ(11,113)(SIC(IX,IY),IY=2,IYM1)
      DO 125 IX=2,IXM1
 125  READ(11,113)(ABW(IX,IY),IY=2,IYM1)
      DO 126 IX=2,IXM1
 126  READ(11,113)(F1(IX,IY),IY=2,IYM1)
      DO 127 IX=2,IXM1
 127  READ(11,113)(F2(IX,IY),IY=2,IYM1)
      READ(11,113)(GAMAJ(IX,1),IX=2,IXM1)
 50   FORMAT(//5X,6F8.3)
 52   FORMAT(5X,'NO. OF ITER.= ',I4,1X,'SMPSI=',F10.6)
C
C     ****************************************************
C     INPUT BOUNDARY AND INITIAL CONDITIONS
C     ****************************************************
C
      DO 100 IX=1,IXMAX
      DO 100 IY=1,IYMAX
      PSIB(IX,IY)=0.
      PSIN(IX,IY,1)=0.
      PSIN(IX,IY,2)=0.
100   PSIN(IX,IY,3)=0.
      DO 101 IX=1,IXMAX
      PSIN(IX,1,1)=0.0
      PSIN(IX,1,2)=0.0
 101  PSIN(IX,1,3)=1.0
      DO 102 IX=1,IXMAX
      DEG=PAI-(IX-2)*D33
      XR=10.*DCOS(DEG)
      YR=10.*DSIN(DEG)
      PSIN(IX,IYMAX,1)=YR
      PSIN(IX,IYMAX,2)=-XR
 102  PSIN(IX,IYMAX,3)=0.0
      WRITE(6,50)RE,HX,HY,TAU,ATTA
C
C     *****************************************************
C     CALCULATION THE FA COEFFICIENTS FOR STREAM
C     FUNCTION IN THE TRANSFORMED PLANE
C     *****************************************************
C
      MM=0
      DO 256 IX=2,IXM1
      DO 256 IY=2,IYM1
      AU=SIA(IX,IY)
      BV=SIB(IX,IY)
      CSI=SIC(IX,IY)
  256 CALL PSICOE(AU,BV,CSI,HX,HY,IX,IY)
C
C     *****************************************************
C     CALCULATION OF THE STREAM FUNCION (I)
C     *****************************************************
```

ORIGINAL PAGE IS
OF POOR QUALITY


```
C
      NM=0
 301  SMPSI=0.0
      DO 305 IY=2,IYM1
      DO 321 IX=2,IXM1
      PSIEZ=0.25*(PSIN(IX+1,IY+1,1)-PSIN(IX-1,IY+1,1)+
     1          PSIN(IX-1,IY-1,1)-PSIN(IX+1,IY-1,1))
      AA(IX)=-PCM1P0(IX,IY)
      BB(IX)=1.0
      CC(IX)=-PCP1P0(IX,IY)
  321 DD(IX)=PCP0P1(IX,IY)*PSIN(IX,IY+1,1)+PCP0M1(IX,IY)*
     $PSIN(IX,IY-1,1)+PCP1P1(IX,IY)*PSIN(IX+1,IY+1,1)+
     $PCP1M1(IX,IY)*PSIN(IX+1,IY-1,1)+PCM1P1(IX,IY)*
     $PSIN(IX-1,IY+1,1)+PCM1M1(IX,IY)*PSIN(IX-1,IY-1,1)
     $ +PCP0P0(IX,IY)*(-2.0*F2(IX,IY)*PSIEZ)
      DD(2)=DD(2)-AA(2)*PSIN(1,IY,1)
      DD(IXM1)=DD(IXM1)-CC(IXM1)*PSIN(IXMAX,IY,1)
      CALL TRIDAG(2,IXM1,AA,BB,CC,DD,T)
      DO 331 IX=2,IXM1
      PSIN(IX,IY,1)=T(IX)
      DEPSI=PSIN(IX,IY,1)-PSIB(IX,IY)
      IF(DABS(DEPSI).GT.DABS(SMPSI))SMPSI=DEPSI
  331 CONTINUE
  305 CONTINUE
      DO 332 IY=1,IYMAX
      PSIN(IXMAX,IY,1)=PSIN(2,IY,1)
 332  PSIN(1,IY,1)=PSIN(IXM1,IY,1)
      DO 307 IX=1,IXMAX
      DO 307 IY=1,IYMAX
  307 PSIB(IX,IY)=PSIN(IX,IY,1)
      NM=NM+1
      IF(DABS(SMPSI).GT.0.0001)GO TO 301
C
C     ************************************************************
C     CALCULATION OF THE STREAM FUNCTION (II)
C     ************************************************************
C
      NM=0
 401  SMPSI=0.0
      DO 405 IY=2,IYM1
      DO 421 IX=2,IXM1
      PSIEZ=0.25*(PSIN(IX+1,IY+1,2)-PSIN(IX-1,IY+1,2)+
     1          PSIN(IX-1,IY-1,2)-PSIN(IX+1,IY-1,2))
      AA(IX)=-PCM1P0(IX,IY)
      BB(IX)=1.0
      CC(IX)=-PCP1P0(IX,IY)
  421 DD(IX)=PCP0P1(IX,IY)*PSIN(IX,IY+1,2)+PCP0M1(IX,IY)*
     $PSIN(IX,IY-1,2)+PCP1P1(IX,IY)*PSIN(IX+1,IY+1,2)+
     $PCP1M1(IX,IY)*PSIN(IX+1,IY-1,2)+
     $PCM1P1(IX,IY)*PSIN(IX-1,IY+1,2)+PCM1M1(IX,IY)*
     $PSIN(IX-1,IY-1,2)+PCP0P0(IX,IY)*(-2.0*F2(IX,IY)*PSIEZ)
```

ORIGINAL PAGE IS
OF POOR QUALITY


```
      DD(2)=DD(2)-AA(2)*PSIN(1,IY,2)
      DD(IXM1)=DD(IXM1)-CC(IXM1)*PSIN(IXMAX,IY,2)
      CALL TRIDAG(2,IXM1,AA,BB,CC,DD,T)
      DO 431 IX=2,IXM1
      PSIN(IX,IY,2)=T(IX)
      DEPSI=PSIN(IX,IY,2)-PSIB(IX,IY)
      IF(DABS(DEPSI).GT.DABS(SMPSI))SMPSI=DEPSI
  431 CONTINUE
  405 CONTINUE
      DO 432 IY=1,IYMAX
      PSIN(IXMAX,IY,2)=PSIN(2,IY,2)
 432  PSIN(1,IY,2)=PSIN(IXM1,IY,2)
      DO 407 IX=1,IXMAX
      DO 407 IY=1,IYMAX
  407 PSIB(IX,IY)=PSIN(IX,IY,2)
      NM=NM+1
C     WRITE(1,52)NM,SMPSI
      IF(DABS(SMPSI).GT.0.0001)GO TO 401
C
C     ******************************************************
C     CALCULATION OF THE STREAM FUNCTION (III)
C     ******************************************************
C
      NM=0.0
 501  SMPSI=0.
      DO 505 IY=2,IYM1
      DO 521 IX=2,IXM1
      PSIEZ=0.25*(PSIN(IX+1,IY+1,3)-PSIN(IX-1,IY+1,3)+
     1          PSIN(IX-1,IY-1,3)-PSIN(IX+1,IY-1,3))
      AA(IX)=-PCM1P0(IX,IY)
      BB(IX)=1.0
      CC(IX)=-PCP1P0(IX,IY)
  521 DD(IX)=PCP0P1(IX,IY)*PSIN(IX,IY+1,3)+PCP0M1(IX,IY)*
     $PSIN(IX,IY-1,3)+PCP1P1(IX,IY)*PSIN(IX+1,IY+1,3)+
     $PCP1M1(IX,IY)*PSIN(IX+1,IY-1,3)+PCM1P1(IX,IY)*
     $PSIN(IX-1,IY+1,3)+PCM1M1(IX,IY)*PSIN(IX-1,IY-1,3)
     $   +PCP0P0(IX,IY)*(-2.0*F2(IX,IY)*PSIEZ)
      DD(2)=DD(2)-AA(2)*PSIN(1,IY,3)
      DD(IXM1)=DD(IXM1)-CC(IXM1)*PSIN(IXMAX,IY,3)
      CALL TRIDAG(2,IXM1,AA,BB,CC,DD,T)
      DO 531 IX=2,IXM1
      PSIN(IX,IY,3)=T(IX)
      DEPSI=PSIN(IX,IY,3)-PSIB(IX,IY)
      IF(DABS(DEPSI).GT.DABS(SMPSI))SMPSI=DEPSI
  531 CONTINUE
  505 CONTINUE
      DO 532 IY=1,IYMAX
      PSIN(IXMAX,IY,3)=PSIN(2,IY,3)
 532  PSIN(1,IY,3)=PSIN(IXM1,IY,3)
      DO 507 IX=1,IXMAX
      DO 507 IY=1,IYMAX
```

```
  507 PSIB(IX,IY)=PSIN(IX,IY,3)
      NM=NM+1
C     WRITE(1,52)NM,SMPSI
      IF(DABS(SMPSI).GT.0.0001)GO TO 501
C     ***********************************************************
C     APPLY KUTTA CONDITION
C     ***********************************************************
      COS=DCOS(ATTA)
      SIN=DSIN(ATTA)
      PS1U3=COS*PSIN(34,3,1)-SIN*PSIN(34,3,2)
      PS1U2=COS*PSIN(34,2,1)-SIN*PSIN(34,2,2)
      PS2U3=COS*PSIN(33,3,1)-SIN*PSIN(33,3,2)
      PS2U2=COS*PSIN(33,2,1)-SIN*PSIN(33,2,2)
      PS3U3=COS*PSIN(32,3,1)-SIN*PSIN(32,3,2)
      PS3U2=COS*PSIN(32,2,1)-SIN*PSIN(32,2,2)
      PS1L3=COS*PSIN(36,3,1)-SIN*PSIN(36,3,2)
      PS1L2=COS*PSIN(36,2,1)-SIN*PSIN(36,2,2)
      PS2L3=COS*PSIN(37,3,1)-SIN*PSIN(37,3,2)
      PS2L2=COS*PSIN(37,2,1)-SIN*PSIN(37,2,2)
      PS3L3=COS*PSIN(38,3,1)-SIN*PSIN(38,3,2)
      PS3L2=COS*PSIN(38,2,1)-SIN*PSIN(38,2,2)
      VT12U=3.0*GAMAJ(34,1)*(-PS1U3+4.0*PS1U2)-3.0*
     $GAMAJ(33,1)*
     1  (-PS2U3+4.0*PS2U2)+GAMAJ(32,1)*(-PS3U3+4.0*PS3U2)
      VT12L=3.0*GAMAJ(36,1)*(-PS1L3+4.0*PS1L2)-3.0*
     $GAMAJ(37,1)*
     1 (-PS2L3+4.0*PS2L2)+GAMAJ(38,1)*(-PS3L3+4.0*PS3L2)
      VT3U=3.0*GAMAJ(34,1)*(-PSIN(34,3,3)+4.0*PSIN(34,2,3)-
     1 3.0)-3.0*GAMAJ(33,1)*(-PSIN(33,3,3)+4.0*PSIN(33,2,3)-
     2 3.0)+GAMAJ(32,1)*(-PSIN(32,3,3)+4.0*PSIN(32,2,3)-3.0)
      VT3L=3.0*GAMAJ(36,1)*(-PSIN(36,3,3)+4.0*PSIN(36,2,3)-
     1 3.0)-3.0*GAMAJ(37,1)*(-PSIN(37,3,3)+4.0*PSIN(37,2,3)-
     2 3.0)+GAMAJ(38,1)*(-PSIN(38,3,3)+4.0*PSIN(38,2,3)-3.0)
      V3UL=VT3U+VT3L
      IF(DABS(V3UL).LT.0.00001)GO TO 801
      ALAM=-(VT12U+VT12L)/(VT3U+VT3L)
      GO TO 802
  801 ALAM=0.
  802 WRITE(6,50)ALAM
      WRITE(6,1350)VT12U,VT12L,VT3U,VT3L
      WRITE(1,1350)ALAM
```

ORIGINAL PAGE IS
OF POOR QUALITY


```
C
C     ********************************************************
C     SUPERPOSE THE SOLUTIONS OF THE THREE SUBPROBLEMS
C     ********************************************************
C
      DO 800 IX=1,IXMAX
      DO 800 IY=1,IYMAX
      PSIT(IX,IY)=DCOS(ATTA)*PSIN(IX,IY,1)-DSIN(ATTA)*
     1            PSIN(IX,IY,2)+ALAM*PSIN(IX,IY,3)
      PSIL(IX,IY)=DCOS(ATTA)*PSIN(IX,IY,1)-DSIN(ATTA)*
     $ PSIN(IX,IY,2)
 800  CONTINUE
      WRITE(6,1350)(PSIT(66,IY),IY=1,IYMAX)
      DO 700 IX=1,IXMAX
      WRITE(6,112)IX
112   FORMAT(1X,'IZ=',I3)
  700 WRITE(6,1350)(PSIT(IX,IY),IY=1,IYMAX)
      DO 702 IX=1,IXMAX
      WRITE(6,112)IX
 702  WRITE(6,1350)(PSIL(IX,IY),IY=1,IYMAX)
 1350 FORMAT(7F11.6)
      CALL EXIT
      END
C
C     ********************************************************
C     SUBROUTINE TO SOLVE THE SYSYTEM OF ALGEBRAIC EQS.
C     ********************************************************
C
      SUBROUTINE TRIDAG(IF,L,A,B,C,D,V)
      IMPLICIT REAL*8(A-H,O-Z)
      DIMENSION A(68),B(68),C(68),D(68),V(68),BETA(68),
     $ GAMMA(68)
      BETA(IF)=B(IF)
      GAMMA(IF)=D(IF)/BETA(IF)
      IFP1=IF+1
      DO 1 I=IFP1,L
      BETA(I)=B(I)-A(I)*C(I-1)/BETA(I-1)
    1 GAMMA(I)=(D(I)-A(I)*GAMMA(I-1))/BETA(I)
      V(L)=GAMMA(L)
      LAST=L-IF
      DO 2 K=1,LAST
      I=L-K
    2 V(I)=GAMMA(I)-C(I)*V(I+1)/BETA(I)
      RETURN
      END
```

ORIGINAL PAGE IS
OF POOR QUALITY


```
C
C     ******************************************************
C     SUBRIUTINE TO CALCULATE THE FA COEFFICIENTS
C     ******************************************************
C
      SUBROUTINE PSICOE(A,B,C,DH,DK,IX,IY)
      IMPLICIT REAL*8(A-H,O-Z)
      COMMON/PSIC/PCM1P1(68,58),PCM1P0(68,58),PCM1M1(68,58),
     1 PCP0P1(68,58),PCP0M1(68,58),PCP1P1(68,58),
     2 PCP1P0(68,58),PCP1M1(68,58),PCP0P0(68,58)
      PI=3.141592653589793D0
      EPE=0.000001
      AH=A*DH
      BK=B*DK
      IF(AH.LT.0.)EPA=-EPE
      EPA=EPE
      IF(BK.LT.0.)EPB=-EPE
      EPB=EPE
      IF(DABS(AH).LT.EPE)AH=EPA
      IF(DABS(BK).LT.EPE)BK=EPB
      AHS=AH*AH
      BKS=BK*BK
      BKSC=BKS*C
      MM=10
      IF(C.LT.1.0)GO TO 33
      E2P=0.
      DO 20 M=1,MM
      N=2*M-1
      PWR=(-1.)**M
      AN=FLOAT(N)
      ELAH=AN*PI*0.5
      ELAH2=ELAH*ELAH
      EMUPK=(AHS+BKSC+ELAH2*C)**0.5
      COSHP=.5*(DEXP(EMUPK)+DEXP(-EMUPK))
      E2P=-PWR*ELAH/((BKS+ELAH2)**2.0)/COSHP+E2P
 20   CONTINUE
      EXPAH=DEXP(AH)
      EXPBK=DEXP(BK)
      COSAH=0.5*EXPAH+0.5/EXPAH
      COSBK=0.5*EXPBK+0.5/EXPBK
      COTAH=(EXPAH*EXPAH+1.0)/(EXPAH*EXPAH-1.0)
      COTBK=(EXPBK*EXPBK+1.0)/(EXPBK*EXPBK-1.0)
      E2=  2P+(BK*C/COTAH-AH/COTBK)/(4.0*AH*BK*COSAH*COSBK))
     $/C
      GO TO  4
   33 E2=0.
```

ORIGINAL PAGE IS
OF POOR QUALITY


```
      DO 30 M=1,MM
      N=2*M-1
      PWR=(-1.)**M
      AN=FLOAT(N)
      ELAH=AN*PI*0.5
      ELAH2=ELAH*ELAH
      EMUK=((AHS+BKSC+ELAH2)/C)**0.5
      COSH=.5*(DEXP(EMUK)+DEXP(-EMUK))
      E2=-PWR*ELAH/((AHS+ELAH2)**2.0)/COSH+E2
30    CONTINUE
      EXPAH=DEXP(AH)
      EXPBK=DEXP(BK)
      COSAH=0.5*EXPAH+0.5/EXPAH
      COSBK=0.5*EXPBK+0.5/EXPBK
      COTAH=(EXPAH*EXPAH+1.0)/(EXPAH*EXPAH-1.0)
      COTBK=(EXPBK*EXPBK+1.0)/(EXPBK*EXPBK-1.0)
      E2P=C*E2-(BK*C/COTAH-AH/COTBK)/(4.0*AH*BK*COSAH*COSBK)
   44 EA=2.0*AH*COSAH*COTAH*E2
      EB=2.0*BK*COSBK*COTBK*E2P
      E=0.25/(COSAH*COSBK)-AH*COTAH*E2-BK*COTBK*E2P
      PCM1P1(IX,IY)=E*EXPAH/EXPBK
      PCM1P0(IX,IY)=EB*EXPAH
      PCM1M1(IX,IY)=E*EXPAH*EXPBK
      PCP0P1(IX,IY)=EA/EXPBK
      PCP0M1(IX,IY)=EA*EXPBK
      PCP1P1(IX,IY)=E/EXPAH/EXPBK
      PCP1P0(IX,IY)=EB/EXPAH
      PCP1M1(IX,IY)=E/EXPAH*EXPBK
      PCP0P0(IX,IY)=(0.5*AH*(PCM1P1(IX,IY)+PCM1P0(IX,IY)+
     1 PCM1M1(IX,IY)-PCP1P1(IX,IY)-PCP1P0(IX,IY)-
     2 PCP1M1(IX,IY))+0.5*BK*(PCM1M1(IX,IY)+PCP0M1(IX,IY)+
     3 PCP1M1(IX,IY)-PCP1P1(IX,IY)-PCP0P1(IX,IY)-
     4 PCM1P1(IX,IY)))/(AH*AH+BK*BK*C)
      RETURN
      END
```

ORIGINAL PAGE IS
OF POOR QUALITY

```
C
C     ******************************************************
C      APPENDIX C-4
C     ******************************************************
C
C
C      ####################################################
C      CALCULATE THE LIFTING COEFFICIENTS FROM
C      THE CIRCULATION BY INTEGRATING THE
C      VELOCITY ON THE AIRFOIL SURFACE
C      ####################################################
C
$INSERT SYSCOM½ERRD.F
$INSERT SYSCOM½KEYS.F
$INSERT SYSCOM½A$KEYS
      IMPLICIT REAL*8(A-H,O-Z)
      COMMON/AA/X(68,25),Y(68,25),PSIN(68,25),GAMAJ(68,1),
     $VT(68,1)
      CALL SRCH$$(K$READ,'LFIN',4,7,TYPE,CODE)
      CALL SRCH$$(K$WRIT,'LFOU',4,2,TYPE,CODE)
      IXMAX=68
      IYMAX=25
      IXM1=IXMAX-1
      IYM1=IYMAX-1
      DO 11 IX=1,IXMAX
      READ(11,113)(X(IX,IY),IY=1,IYMAX)
 11   READ(11,113)(Y(IX,IY),IY=1,IYMAX)
      READ(11,113)(GAMAJ(IX,1),IX=2,IXM1)
      DO 13 IX=1,IXMAX
 13   READ(11,1350)(PSIN(IX,IY),IY=1,IYMAX)
      DO 14 IX=1,34
      IB=IX+34
 14   WRITE(6,112)IX,X(IX,1),Y(IX,1),IB,X(IB,1),Y(IB,1)
C
C     ####################################################
C     CALCULATION OF TANGENTIAL VELOCITY OF THE AIRFOIL
C     ####################################################
C
      DO 21 IX=2,IXM1
 21   VT(IX,1)=0.5*GAMAJ(IX,1)*(-PSIN(IX,3)+4.0*PSIN(IX,2)
     1          -3.0*PSIN(IX,1))
      VT(1,1)=VT(IXM1,1)
      VT(IXMAX,1)=VT(2,1)
      WRITE(6,1350)(VT(IX,1),IX=1,IXMAX)
      SUMU=0.
```

ORIGINAL PAGE IS
OF POOR QUALITY

```
C
C     ##################################################
C     CALCULATE THE CIRCULATIN    CIR=SUM(V*dL)
C     WHICH IS HALF OF LIFT COEFFICIENT CL
C     ##################################################
C
      DO 31 IX=2,IXM1
      VLU=0.5*(VT(IX,1)+VT(IX+1,1))*((X(IX,1)-X(IX+1,1))**2
     1     +(Y(IX,1)-Y(IX+1,1))**2)**0.5
      SUMU=SUMU+VLU
      WRITE(6,1350)IX,VLU,SUMU
 31   CONTINUE
 1350 FORMAT(7F11.6)
 112  FORMAT(4X,I2,2X,F8.5,2X,F8.5,4X,I2,2X,F8.5,2X,F8.5)
 113  FORMAT(8F10.5)
      CALL EXIT
      END
```

ORIGINAL PAGE IS
OF POOR QUALITY


```
C
C     ********************************************************
C      APPENDIX C-5
C     ********************************************************
C
C
C     ********************************************************
C      FLOW PAST TUBE BUNDLES
C     ********************************************************
C
$INSERT SYSCOM½ERRD.F
$INSERT SYSCOM½KEYS.F
$INSERT SYSCOM½A$KEYS
      IMPLICIT REAL*8(A-H,O-Z)
      COMMON/AAA/ AA(22),BB(22),CC(22),DD(22),U(22,21),
     $V(21),T(22),PSIN(22,21,2),ZETAN(22,21,2),F(22,21)
      COMMON/BBB/SIA(22,21),SIB(22,21),SIC(22,21),ABW(22,21)
     $,
     $    ,F1(22,21),F2(22,21),GAMAJ(22,21)
      COMMON/COEF/CM1P1(22,21),CP0P1(22,21),CP1P1(22,21),CM1
     $P0(22,21),
     $CM1P0(22,21),CP0P0(22,21),CP1P0(22,21),CM1M1(22,21),
     $CP0M1(22,21),CP1M1(22,21)
      COMMON/PSIC/PCM1P1(22,21),PCM1P0(22,21),PCM1M1(22,21),
     1 PCP0P1(22,21),PCP0M1(22,21),PCP1P1(22,21),
     2 PCP1P0(22,21),PCP1M1(22,21),PCP0P0(22,21)
      CALL SRCH$$(K$READ,'ONLY',4,7,TYPE,CODE)
      CALL SRCH$$(K$WRIT,'ZZZW',4,2,TYPE,CODE)
C
C     ********************************************************
C      INPUT GIVEN DATA
C     ********************************************************
C
      IXMAX=22
      IYMAX=21
      IXM1=IXMAX-1
      IYM1=IYMAX-1
      ITERP=20
      ITERZ=12
      IEND=200
      L=1
      NM=20
      EPE=0.000001
      HX=1.0
      HY=1.0
      TAU=0.2
      DELTA=1.0
      RE=13.6
  113 FORMAT(8F10.5)
      DO 122 IX=2,IXM1
  122 READ(11,113)(SIA(IX,IY),IY=2,IYM1)
```

ORIGINAL PAGE IS
OF POOR QUALITY


```
      DO 123 IX=2,IXM1
 123  READ(11,113)(SIB(IX,IY),IY=2,IYM1)
      DO 124 IX=2,IXM1
 124  READ(11,113)(SIC(IX,IY),IY=2,IYM1)
      DO 125 IX=2,IXM1
 125  READ(11,113)(ABW(IX,IY),IY=2,IYM1)
      DO 126 IX=2,IXM1
 126  READ(11,113)(F1(IX,IY),IY=2,IYM1)
      DO 127 IX=2,IXM1
 127  READ(11,113)(F2(IX,IY),IY=2,IYM1)
      READ(11,113)(GAMAJ(IX,1),IX=2,10)
      READ(11,113)(GAMAJ(IX,IYMAX),IX=12,21)
50    FORMAT(//5X,4F12.6)
C
C    ***********************************************************
C     BOUNDARY AND INITIAL CONDITIONS
C    ***********************************************************
C
      DO 100 IX=1,IXMAX
      DO 100 IY=1,IYMAX
      ZETAN(IX,IY,1)=0.
      ZETAN(IX,IY,2)=0.
100   PSIN(IX,IY,2)=0.0
      DO 101 IX=1,IXMAX
 101  PSIN(IX,1,2)=0.0
      DO 102 IX=1,IXMAX
 102  PSIN(IX,IYMAX,2)=4.0
      DO 108 IX=11,IXMAX
 108  ZETAN(IX,1,2)=0.
      DO 109 IX=1,11
 109  ZETAN(IX,IYMAX,2)=0.
      WRITE(6,50)RE,HX,HY,TAU
C*************************************************** B.C. A
     $ND.INITIAL Q
      MM=0
      DO 256 IX=2,IXM1
      DO 256 IY=2,IYM1
      AU=SIA(IX,IY)
      BV=SIB(IX,IY)
      CSI=SIC(IX,IY)
  256 CALL PSICOE(AU,BV,CSI,HX,HY,IX,IY)
C
C    ***********************************************************
C     CALCULATION OF STREAM FUNCTION EQ
C    ***********************************************************
C
      DO 1200 IT=1,IEND
      MM=MM+1
      SMZET=0.0
      SMPSI=0.0
```

```
      DO 406 ITER=1,ITERP
      DO 405 IY=2,IYM1
      DO 421 IX=2,IXM1
      PSIEZ=0.25*(PSIN(IX+1,IY+1,2)-PSIN(IX-1,IY+1,2)+
     1                    PSIN(IX-1,IY-1,2)-PSIN(IX+1,IY-1,2)
     $)
      AA(IX)=-PCM1P0(IX,IY)
      BB(IX)=1.0
      CC(IX)=-PCP1P0(IX,IY)
  421 DD(IX)=PCP0P1(IX,IY)*PSIN(IX,IY+1,2)+PCP0M1(IX,IY)*
     $PSIN(IX,IY-1,2)+PCP1P1(IX,IY)*PSIN(IX+1,IY+1,2)+
     $PCP1M1(IX,IY)*PSIN(IX+1,IY-1,2)+PCM1P1(IX,IY)*
     $PSIN(IX-1,IY+1,2)+PCM1M1(IX,IY)*PSIN(IX-1,IY-1,2)
     $ +PCP0P0(IX,IY)*(F1(IX,IY)*ZETAN(IX,IY,1)-2.0*
     $ F2(IX,IY)*PSIEZ)
      DD(2)=DD(2)-AA(2)*PSIN(1,IY,2)
      DD(IXM1)=DD(IXM1)-CC(IXM1)*PSIN(IXMAX,IY,2)
      CALL TRIDAG(2,IXM1,AA,BB,CC,DD,T)
      DO 431 IX=2,IXM1
      PSIN(IX,IY,2)=T(IX)
      DEPSI=PSIN(IX,IY,2)-PSIN(IX,IY,1)
      IF(DABS(DEPSI).GT.DABS(SMPSI))SMPSI=DEPSI
  431 CONTINUE
  405 CONTINUE
      DO 432 IY=1,IYMAX
      PSIN(IXMAX,IY,2)=4.0-PSIN(2,IYMAX+1-IY,2)
  432 PSIN(1,IY,2)=4.0-PSIN(IXM1,IYMAX+1-IY,2)
  406 CONTINUE
      DO 505 IX=1,IXMAX
      DO 505 IY=1,IYMAX
  505 PSIN(IX,IY,1)=PSIN(IX,IY,2)
C
C     ********************************************************
C      CALCULATION OF VELOVITY (FROM STREAM FUNCTION)
C     ********************************************************
C
  111 FORMAT(11F9.4)
      DO 175 IX=2,IXM1
      DO 175 IY=2,IYM1
      U(IX,IY)=(PSIN(IX,IY+1,2)-PSIN(IX,IY-1,2))/2.0/HY
  175 V(IX,IY)=(PSIN(IX-1,IY,2)-PSIN(IX+1,IY,2))/2.0/HX
C
C     ********************************************************
C      CALCULATION OF VORTICITY TRANSPORT EQ.
C     ********************************************************
C
      DO 200 IX=2,IXM1
      DO 200 IY=2,IYM1
      AU=RE*ABW(IX,IY)*U(IX,IY)
      BV=RE*ABW(IX,IY)*V(IX,IY)/SIC(IX,IY)
      CSI=SIC(IX,IY)
```

ORIGINAL PAGE IS
OF POOR QUALITY


```
  200 CALL COEFF(AU,BV,CSI,HX,HY,IX,IY)
      DO 250 IX=2,10
      DPSIE=GAMAJ(IX,1)*(-PSIN(IX,3,2)+4.0*PSIN(IX,2,2))*0.5
 250  ZETAN(IX,1,2)=ZETAN(IX,1,1)-DELTA*DPSIE
      DO 251 IX=12,21
      DPSIE=GAMAJ(IX,IYMAX)*(PSIN(IX,IYMAX-2,2)-4.0*
     1       PSIN(IX,IYMAX-1,2)+3.0*PSIN(IX,IYMAX,2))*0.5
 251  ZETAN(IX,IYMAX,2)=ZETAN(IX,IYMAX,1)+DELTA*DPSIE
C
C     ***********************************************************
C      HIGH ORDER CORRECTION TERM
C     ***********************************************************
C
      DO 1190 IX=2,IXM1
      DO 1190 IY=2,IYM1
      VORZ=0.5*(ZETAN(IX+1,IY,1)-ZETAN(IX-1,IY,1))
      VORE=0.5*(ZETAN(IX,IY+1,1)-ZETAN(IX,IY-1,1))
      F(IX,IY)=2.*ABW(IX,IY)*RE*(CM1P1(IX,IY)*((U(IX-1,IY+1)
     $-U(IX,IY))
     $-U(IX,IY))*VORZ+(V(IX-1,IY+1)-V(IX,IY))*VORE)+
     $CP0P1(IX,IY)*((U(IX,IY+1)
     $-U(IX,IY))*VORZ+(V(IX,IY+1)-V(IX,IY))*VORE)
     $+CP1P1(IX,IY)*((U(IX+1,IY+1)-U(IX,IY))*VORZ+
     $(V(IX+1,IY+1)-V(IX,IY))*VORE)+CM1P0(IX,IY)*
     $((U(IX-1,IY)-U(IX,IY))*VORZ+(V(IX-1,IY)-V(IX,IY))*
     $VORE)+CP1P0(IX,IY)*((U(IX+1,IY)-U(IX,IY))*VORZ+
     $(V(IX+1,IY)-V(IX,IY))*VORE))
      F(IX,IY)=F(IX,IY)+2.*ABW(IX,IY)*RE*(CM1M1(IX,IY)*
     $((U(IX-1,IY-1)-U(IX,IY))*VORZ+(V(IX-1,IY-1)-V(IX,IY))*
     $VORE)+CP0M1(IX,IY)*((U(IX,IY-1)-U(IX,IY))*VORZ+
     $(V(IX,IY-1)-V(IX,IY))*VORE)+CP1M1(IX,IY)*
     $((U(IX+1,IY-1)-U(IX,IY))*VORZ+(V(IX+1,IY-1)-V(IX,IY))
     $ *VORE))
      F(IX,IY)=F(IX,IY)*5.0/9.0
 1190 CONTINUE
      DO 306 ITER=1,ITERZ
      DO 305 IY=2,IYM1
      DO 320 IX=2,IXM1
      ZETEZ=0.25*(ZETAN(IX+1,IY+1,2)-ZETAN(IX-1,IY+1,2)+
     1         ZETAN(IX-1,IY-1,2)-ZETAN(IX+1,IY-1,2))
      VORZ=0.5*(ZETAN(IX+1,IY,1)-ZETAN(IX-1,IY,1))
      VORE=0.5*(ZETAN(IX,IY+1,1)-ZETAN(IX,IY-1,1))
      AA(IX)=-CM1P0(IX,IY)/(1.0+CP0P0(IX,IY)*F1(IX,IY)*RE/
     $TAU)
      BB(IX)=1.0
      CC(IX)=-CP1P0(IX,IY)/(1.0+CP0P0(IX,IY)*F1(IX,IY)*RE/
     $TAU)
```

ORIGINAL PAGE IS
OF POOR QUALITY


```
  320 DD(IX)=(CP0P1(IX,IY)*ZETAN(IX,IY+1,2)+CP0M1(IX,IY)*
     $ZETAN(IX,IY-1,2)+CP1P1(IX,IY)*ZETAN(IX+1,IY+1,2)+
     $CP1M1(IX,IY)*ZETAN(IX+1,IY-1,2)+CM1P1(IX,IY)*
     $ZETAN(IX-1,IY+1,2)+CM1M1(IX,IY)*ZETANIX-1,IY-1,2)+
     $CP0P0(IX,IY)*(F1(IX,IY)*RE/TAU*ZETAN(IX,IY,1))
     &   -2.0*SIA(IX,IY)*VORZ-2.0*SIB(IX,IY)*SIC(IX,IY)*VORE
     1 -2.0*F2(IX,IY)*ZETEZ-F(IX,IY)))/(1.0+F1(IX,IY)*RE/TAU
     2        *CP0P0(IX,IY))
      DD(2)=DD(2)-AA(2)*ZETAN(1,IY,2)
      DD(IXM1)=DD(IXM1)-CC(IXM1)*ZETAN(IXMAX,IY,2)
      CALL TRIDAG(2,IXM1,AA,BB,CC,DD,T)
      DO 330 IX=2,IXM1
      ZETAN(IX,IY,2)=T(IX)
      DEZET=ZETAN(IX,IY,2)-ZETAN(IX,IY,1)
      IF(DABS(DEZET).GT.DABS(SMZET))SMZET=DEZET
 330  CONTINUE
  305 CONTINUE
      DO 331 IY=1,IYMAX
      ZETAN(IXMAX,IY,2)=-ZETAN(2,IYMAX+1-IY,2)
 331  ZETAN(1,IY,2)=-ZETAN(IXM1,IYMAX+1-IY,2)
 306  CONTINUE
      DO 500 IX=1,IXMAX
      DO 500 IY=1,IYMAX
  500 ZETAN(IX,IY,1)=ZETAN(IX,IY,2)
      IF(MM.LT.NM) GO TO 999
      MM=0
C      TAU=TAU*2.0
      WRITE(6,600)IT
  600 FORMAT(//5X,'NO. OF TIME STEPS =',I5)
      DO 700 IX=1,IXMAX,L
      WRITE(6,112)IX
112   FORMAT(1X,'IZ=',I3)
  700 WRITE(6,1350)(PSIN(IX,IY,2),IY=1,IYMAX,L)
      DO 800 IX=1,IXMAX,L
      WRITE(6,112)IX
  800 WRITE(6,1350)(ZETAN(IX,IY,2),IY=1,IYMAX,1)
  999 CIRCUL=0.0
      DO 1000 IX=2,IXM1
      DO 1000 IY=2,IYMAX
 1000 CIRCUL=CIRCUL+(ZETAN(IX,IY,2)+ZETAN(IX,IY-1,2)+ZETAN(I
     $X-1,IY,2)
     $+ZETAN(IX-1,IY-1,2))/4.0
      WRITE(6,1001)IT,TAU,CIRCUL,SMPSI,SMZET
 1001 FORMAT(2X,I3,1X,F5.3,1X,'CIRCUL=',F12.7,'MAX.DPSI=',F1
     $2.8,
     #      'MAX.DZET=',F12.8)
 1200 CONTINUE
      DO 1299 IX=1,IXMAX
      WRITE(6,112)IX
 1299 WRITE(6,1350)(PSIN(IX,IY,1),IY=1,IYMAX)
```

ORIGINAL PAGE IS
OF POOR QUALITY


```
      DO 1300 IX=1,IXMAX
      WRITE(6,112)IX
 1300 WRITE(6,1350)(ZETAN(IX,IY,1),IY=1,IYMAX)
 1350 FORMAT(7F11.6)
      CALL EXIT
      END
C
C     ************************************************************
C      SUBROUTINE TO SOLVE THE SYSTEM OF ALGEBRAIC EQS.
C     ************************************************************
C
      SUBROUTINE TRIDAG(IF,L,A,B,C,D,V)
      IMPLICIT REAL*8(A-H,O-Z)
      DIMENSION A(22),B(22),C(22),D(22),V(22),BETA(22),GAMMA
     $(22)
      BETA(IF)=B(IF)
      GAMMA(IF)=D(IF)/BETA(IF)
      IFP1=IF+1
      DO 1 I=IFP1,L
      BETA(I)=B(I)-A(I)*C(I-1)/BETA(I-1)
    1 GAMMA(I)=(D(I)-A(I)*GAMMA(I-1))/BETA(I)
      V(L)=GAMMA(L)
      LAST=L-IF
      DO 2 K=1,LAST
      I=L-K
    2 V(I)=GAMMA(I)-C(I)*V(I+1)/BETA(I)
      RETURN
      END
C
C     ************************************************************
C      SUBROUTINE TO CALCULATE THE FINITE ANALYTIC
C      COEFFICIENTS FOR GENERAL UNEQUAL SIZE GRID
C     ************************************************************
C
      SUBROUTINE PSICOE(A,B,C,DH,DK,IX,IY)
      IMPLICIT REAL*8(A-H,O-Z)
      COMMON/PSIC/PCM1P1(22,21),PCM1P0(22,21),PCM1M1(22,21),
     1PCP0P1(22,21),PCP0M1(22,21),PCP1P1(22,21),PCP1P0(22,21
     $),
     2PCP1M1(22,21),PCP0P0(22,21)
      PI=3.1415926535897 93D0
      EPE=0.00001
      IF(A.LT.0.)EPA=-EPE
      EPA=EPE
      IF(B.LT.0.)EPB=-EPE
      EPB=EPE
      IF(DABS(A).LT.EPE)A=EPA
      IF(DABS(B).LT.EPE)B=EPB
      AH=A*DH
      BK=B*DK
      AHS=AH*AH
```

ORIGINAL PAGE IS
OF POOR QUALITY


```
      BKS=BK*BK
      BKSC=BKS*C
      MM=10.
      IF(C.LT.1.0)GO TO 33
      E2P=0.
      DO 20 M=1,MM
      N=2*M-1
      PWR=(-1.)**M
      AN=FLOAT(N)
      ELAH=AN*PI*0.5
      ELAH2=ELAH*ELAH
      EMUPK=(AHS+BKSC+ELAH2*C)**0.5
      COSHP=.5*(DEXP(EMUPK)+DEXP(-EMUPK))
      E2P=-PWR*ELAH/((BKS+ELAH2)**2.0)/COSHP+E2P
20    CONTINUE
      EXPAH=DEXP(AH)
      EXPBK=DEXP(BK)
      COSAH=0.5*EXPAH+0.5/EXPAH
      COSBK=0.5*EXPBK+0.5/EXPBK
      COTAH=(EXPAH*EXPAH+1.0)/(EXPAH*EXPAH-1.0)
      COTBK=(EXPBK*EXPBK+1.0)/(EXPBK*EXPBK-1.0)
      E2=(E2P+(BK*C/COTAH-AH/COTBK)/(4.0*AH*BK*COSAH*COSBK))
     $/C
      GO TO 44
   33 E2=0.
      DO 30 M=1,MM
      N=2*M-1
      PWR=(-1.)**M
      AN=FLOAT(N)
      ELAH=AN*PI*0.5
      ELAH2=ELAH*ELAH
      EMUK=((AHS+BKSC+ELAH2)/C)**0.5
      COSH=.5*(DEXP(EMUK)+DEXP(-EMUK))
      E2=-PWR*ELAH/((AHS+ELAH2)**2.0)/COSH+E2
30    CONTINUE
      EXPAH=DEXP(AH)
      EXPBK=DEXP(BK)
      COSAH=0.5*EXPAH+0.5/EXPAH
      COSBK=0.5*EXPBK+0.5/EXPBK
      COTAH=(EXPAH*EXPAH+1.0)/(EXPAH*EXPAH-1.0)
      COTBK=(EXPBK*EXPBK+1.0)/(EXPBK*EXPBK-1.0)
      E2P=C*E2-(BK*C/COTAH-AH/COTBK)/(4.0*AH*BK*COSAH*COSBK)
   44 EA=2.0*AH*COSAH*COTAH*E2
      EB=2.0*BK*COSBK*COTBK*E2P
      E=0.25/(COSAH*COSBK)-AH*COTAH*E2-BK*COTBK*E2P
```

ORIGINAL PAGE IS
OF POOR QUALITY

```
      PCM1P1(IX,IY)=E*EXPAH/EXPBK
      PCM1P0(IX,IY)=EB*EXPAH
      PCM1M1(IX,IY)=E*EXPAH*EXPBK
      PCP0P1(IX,IY)=EA/EXPBK
      PCP0M1(IX,IY)=EA*EXPBK
      PCP1P1(IX,IY)=E/EXPAH/EXPBK
      PCP1P0(IX,IY)=EB/EXPAH
      PCP1M1(IX,IY)=E/EXPAH*EXPBK
      PCP0P0(IX,IY)=(0.5*AH*(PCM1P1(IX,IY)+PCM1P0(IX,IY)+
     $ PCM1M1(IX,IY)
     1       -PCP1P1(IX,IY)-PCP1P0(IX,IY)-PCP1M1(IX,IY))+
     2    0.5*BK*(PCM1M1(IX,IY)+PCP0M1(IX,IY)+PCP1M1(IX,IY)
     3    -PCP1P1(IX,IY)-PCP0P1(IX,IY)-PCM1P1(IX,IY)))/
     4    (AH*AH+BK*BK*C)
      RETURN
      END
C     ************************************************************
C      SUBROUTINE COEFF IS EXACTLY SAME TO SUBROUTINE
C      PSICOE MENTIONED ABOVE
C     ************************************************************
```

ORIGINAL PAGE IS
OF POOR QUALITY


```
C
C     ********************************************************
C      APPENDIX C-6
C     ********************************************************
C
C     ********************************************************
C      CONVECTIVE HEAT TRANSFER IN TUBE BUNDLES
C     ********************************************************
C
$INSERT SYSCOM½ERRD.F
$INSERT SYSCOM½KEYS.F
$INSERT SYSCOM½A$KEYS
      IMPLICIT REAL*8(A-H,O-Z)
      COMMON/AAA/ AA(41),BB(41),CC(41),DD(41),U(41,21),
     $V(41,21),T(41),PSIN(41,21,2),ZETAN(41,21,2),F(41,21)
      COMMON/BBB/SIA(41,21),SIB(41,21),SIC(41,21),ABW(41,21)
     $ ,F1(41,21),F2(41,21),GAMAJ(41,21),Q(41,21),
     $ BETAJ(41,21)
      COMMON/COEF/CM1P1(41,21),CP0P1(41,21),CP1P1(41,21),
     $CM1P0(41,21),CP0P0(41,21),CP1P0(41,21),CM1M1(41,21),
     $CP0M1(41,21),CP1M1(41,21)
      CALL SRCH$$(K$READ,'AAAA',4,7,TYPE,CODE)
      CALL SRCH$$(K$WRIT,'ZZZT',4,2,TYPE,CODE)
C
C     ********************************************************
C      INPUT GIVEN DATA
C     ********************************************************
C
      IXMAX=41
      IYMAX=21
      IXM1=IXMAX-1
      IYM1=IYMAX-1
      IEND=100
      L=1
      NM=10
      EPE=0.000001
      HX=1.0
      HY=1.0
      TAU=0.01
      PAIS=3.141592653589793D0
      D9=PAIS/2.0/10.0
      ARC9=2.67*D9
      PE=1000.
  113 FORMAT(8F10.5)
      DO 122 IX=2,IXM1
  122 READ(11,113)(SIA(IX,IY),IY=2,IYM1)
      DO 123 IX=2,IXM1
  123 READ(11,113)(SIB(IX,IY),IY=2,IYM1)
      DO 124 IX=2,IXM1
  124 READ(11,113)(SIC(IX,IY),IY=2,IYM1)
```

ORIGINAL PAGE IS
OF POOR QUALITY


```
      DO 125 IX=2,IXM1
 125  READ(11,113)(ABW(IX,IY),IY=2,IYM1)
      DO 126 IX=2,IXM1
 126  READ(11,113)(F1(IX,IY),IY=2,IYM1)
      DO 127 IX=2,IXM1
 127  READ(11,113)(F2(IX,IY),IY=2,IYM1)
      READ(11,113)(GAMAJ(IX,1),IX=2,40)
      READ(11,113)(GAMAJ(IX,IYMAX),IX=2,40)
      READ(11,113)(BETAJ(IX,1),IX=2,40)
      READ(11,113)(BETAJ(IX,IYMAX),IX=2,40)
50    FORMAT(//5X,4F12.6)
C
C    ***********************************************************
C     INPUT INITIAL AND BOUNDARY CONDITIONS
C    ***********************************************************
C
      DO 100 IX=1,IXMAX
      DO 100 IY=1,IYMAX
      ZETAN(IX,IY,1)=0.
 100  ZETAN(IX,IY,2)=0.
      DO 1302 IX=1,22
 1302 READ(11,1350)(PSIN(IX,IY,2),IY=1,IYMAX)
      DO 1303 IX=2,21
      DO 1303 IY=1,IYMAX
 1303 PSIN(IX+20,IY,2)=4.0-PSIN(IX,IYMAX+1-IY,2)
      DO 107 IX=11,31
 107  ZETAN(IX,IYMAX,2)=1.0
      WRITE(6,50)PE,HX,HY,TAU
      DO 175 IX=2,IXM1
      DO 175 IY=2,IYM1
      U(IX,IY)=(PSIN(IX,IY+1,2)-PSIN(IX,IY-1,2))/2.0/HY
  175 V(IX,IY)=(PSIN(IX-1,IY,2)-PSIN(IX+1,IY,2))/2.0/HX
C
C    ***********************************************************
C     CALCULATION OF THE FA COEFFICIENTS IN
C     THE ENERGY EQUATION
C    ***********************************************************
C
      DO 200 IX=2,IXM1
      DO 200 IY=2,IYM1
      AU=PE*ABW(IX,IY)*U(IX,IY)
      BV=PE*ABW(IX,IY)*V(IX,IY)/SIC(IX,IY)
      CSI=SIC(IX,IY)
  200 CALL COEFF(AU,BV,CSI,HX,HY,IX,IY)
      DO 1200 IT=1,IEND
      DO 251 IX=2,10
 251  ZETAN(IX,IYMAX,2)=BETAJ(IX,IYMAX)*(ZETAN(IX+1,IYMAX,2)
     1 -ZETAN(IX-1,IYMAX,2))/(3.0*GAMAJ(IX,IYMAX))-
     2 (ZETAN(IX,IYMAX-2,2)-4.0*ZETAN(IX,IYMAX-1,2))/3.0
```

ORIGINAL PAGE IS
OF POOR QUALITY


```
      DO 252 IX=32,40
252   ZETAN(IX,IYMAX,2)=BETAJ(IX,IYMAX)*(ZETAN(IX+1,IYMAX,2)
     1 -ZETAN(IX-1,IYMAX,2))/(3.0*GAMAJ(IX,IYMAX))-
     2 (ZETAN(IX,IYMAX-2,2)-4.0*ZETAN(IX,IYMAX-1,2))/3.0
      DO 253 IX=11,31
253   Q(IX,IYMAX)=GAMAJ(IX,IYMAX)*(ZETAN(IX,IYMAX-2,2)-4.0*
     1 ZETAN(IX,IYMAX-1,2)+3.0*ZETAN(IX,IYMAX,2))/2.0-
     $ BETAJ(IX,IYMAX)*
     2 (ZETAN(IX+1,IYMAX,2)-ZETAN(IX-1,IYMAX,2))/2.0
      QOUT=0.
      DO 254 IX=12,30
254   QOUT=QOUT+Q(IX,IYMAX)
      QOUT=QOUT+(Q(11,IYMAX)+Q(31,IYMAX))/2.0
      QOUT=QOUT*ARC9
      DO 255 IX=11,31
255   Q(IX,1)=GAMAJ(IX,1)*(-ZETAN(IX,3,2)+4.0*ZETAN(IX,2,2)-
     1 3.0*ZETAN(IX,1,2))/2.0
      QIN=0.
      DO 258 IX=12,30
258   QIN=QIN+Q(IX,1)
      QIN=(QIN+(Q(11,1)+Q(31,1))/2.0)*6.23/10.
      TO=DABS(QOUT-QIN)
      DO 257 IY=1,IYMAX
257   ZETAN(IXMAX,IY,2)=TO/(4.0*PE)
      WRITE(6,1350)QOUT,QIN,ZETAN(IXMAX,10,2)
C
C     ************************************************************
C      CALCULATION OF HIGH ORDER CORRECTION TERM
C     ************************************************************
C
      DO 1190 IX=2,IXM1
      DO 1190 IY=2,IYM1
      VORZ=0.5*(ZETAN(IX+1,IY,1)-ZETAN(IX-1,IY,1))
      VORE=0.5*(ZETAN(IX,IY+1,1)-ZETAN(IX,IY-1,1))
      F(IX,IY)=2.*ABW(IX,IY)*PE*(CM1P1(IX,IY)*((U(IX-1,IY+1)
     $ -U(IX,IY))*VORZ+(V(IX-1,IY+1)-V(IX,IY))*VORE)+
     $ CP0P1(IX,IY)*((U(IX,IY+1)-U(IX,IY))*VORZ+(V(IX,IY+1)
     $ -V(IX,IY))*VORE)+CP1P1(IX,IY)*((U(IX+1,IY+1)-
     $ U(IX,IY))*VORZ+(V(IX+1,IY+1)-V(IX,IY))*VORE)
     $ +CM1P0(IX,IY)*((U(IX-1,IY)-U(IX,IY))*VORZ
     $ +(V(IX-1,IY)-V(IX,IY))*VORE)+CP1P0(IX,IY)*((
     $U(IX+1,IY)-U(IX,IY))*VORZ+(V(IX+1,IY)-V(IX,IY))*VORE))
      F(IX,IY)=F(IX,IY)+2.*ABW(IX,IY)*PE*(CM1M1(IX,IY)*((
     $ U(IX-1,IY-1)-U(IX,IY))*VORZ+(V(IX-1,IY-1)-V(IX,IY))*
     $ VORE)+CP0M1(IX,IY)*((U(IX,IY-1)-U(IX,IY))*VORZ
     $ +(V(IX,IY-1)-V(IX,IY))*VORE)+
     $ CP1M1(IX,IY)*((U(IX+1,IY-1)-U(IX,IY))*VORZ+(
     $ V(IX+1,IY-1)-V(IX,IY))*VORE))
      F(IX,IY)=F(IX,IY)*5.0/9.0
1190  CONTINUE
```

ORIGINAL PAGE IS
OF POOR QUALITY

```
      DO 305 IY=2,IYM1
      DO 320 IX=2,IXM1
      ZETEZ=0.25*(ZETAN(IX+1,IY+1,2)-ZETAN(IX-1,IY+1,2)+
     1     ZETAN(IX-1,IY-1,2)-ZETAN(IX+1,IY-1,2))
      VORZ=0.5*(ZETAN(IX+1,IY,1)-ZETAN(IX-1,IY,1))
      VORE=0.5*(ZETAN(IX,IY+1,1)-ZETAN(IX,IY-1,1))
      AA(IX)=-CM1P0(IX,IY)/(1.0+CP0P0(IX,IY)*F1(IX,IY)*PE/
     $TAU)
      BB(IX)=1.0
      CC(IX)=-CP1P0(IX,IY)/(1.0+CP0P0(IX,IY)*F1(IX,IY)*PE/
     $TAU)
  320 DD(IX)=(CP0P1(IX,IY)*ZETAN(IX,IY+1,2)+CP0M1(IX,IY)*
     $ZETAN(IX,IY-1,2)+CP1P1(IX,IY)*ZETAN(IX+1,IY+1,2)+
     $+CP1M1(IX,IY)*ZETAN(IX+1,IY-1,2)+CM1P1(IX,IY)*
     $ZETAN(IX-1,IY+1,2)+CM1M1(IX,IY)*ZETAN(IX-1,IY-1,2)
     $  +CP0P0(IX,IY)*(F1(IX,IY)*PE/TAU*ZETAN(IX,IY,1)
     $ -2.0*SIA(IX,IY)*VORZ-2.0*SIB(IX,IY)*SIC(IX,IY)*VORE
     1 -2.0*F2(IX,IY)*ZETEZ-F(IX,IY)))/(1.0+F1(IX,IY)*PE/
     2 TAU*CP0P0(IX,IY))
      DD(2)=DD(2)-AA(2)*ZETAN(1,IY,2)
      DD(IXM1)=DD(IXM1)-CC(IXM1)*ZETAN(IXMAX,IY,2)
      CALL TRIDAG(2,IXM1,AA,BB,CC,DD,T)
      DO 330 IX=2,IXM1
      ZETAN(IX,IY,2)=T(IX)
  330 CONTINUE
  305 CONTINUE
      SMZET=0.
      DO 307 IX=1,IXMAX
      DO 307 IY=1,IYMAX
      DEZET=ZETAN(IX,IY,2)-ZETAN(IX,IY,1)
      IF(DABS(DEZET).GT.DABS(SMZET))SMZET=DEZET
  307 CONTINUE
      IF(DABS(SMZET).LT.0.001)GO TO 1330
      DO 500 IX=1,IXMAX
      DO 500 IY=1,IYMAX
  500 ZETAN(IX,IY,1)=ZETAN(IX,IY,2)
      WRITE(6,600)IT,SMZET
  600 FORMAT(//5X,'NO. OF TIME STEPS =',I5,1X,F10.6)
 1200 CONTINUE
 1330 DO 1300 IX=1,IXMAX
      WRITE(6,112)IX
 1300 WRITE(6,1350)(ZETAN(IX,IY,1),IY=1,IYMAX)
 1350 FORMAT(7F11.6)
  112 FORMAT(1X,'IZ= ',I2)
      CALL EXIT
      END
```

ORIGINAL PAGE IS
OF POOR QUALITY

```
C
C     ***********************************************************
C      SUBROUTINE TO SOLVE THE SYSTEM OF ALGEBRAIC EQUATIONS
C         THIS PROGRAM IS SAME TO THAT IN APPENDIX C-5
C     ***********************************************************
C
      SUBROUTINE TRIDAG(IF,L,A,B,C,D,V)
      IMPLICIT REAL*8(A-H,O-Z)
      DIMENSION A(41),B(41),C(41),D(41),V(41),BETA(41),GAMMA
     $GAMMA(41)
      RETURN
      END
C
C     ***********************************************************
C      SUBROUTINE TO CALCULATE THE FA COEFFICIENTS
C      THIS PROGRAM IS SAME TO THAT IN APPENDIX C-5
C     ***********************************************************
C
      SUBROUTINE COEFF(A,B,C,DH,DK,IX,IY)
      IMPLICIT REAL*8(A-H,O-Z)
      COMMON/COEF/CM1P1(41,21),CP0P1(41,21),CP1P1(41,21),CM1
     1 CM1P0(41,21),CP0P0(41,21),CP1P0(41,21),CM1M1(41,21),
     2 CP0M1(41,21),CP1M1(41,21)
      RETURN
      END
BOTTOM
```

ORIGINAL PAGE IS
OF POOR QUALITY

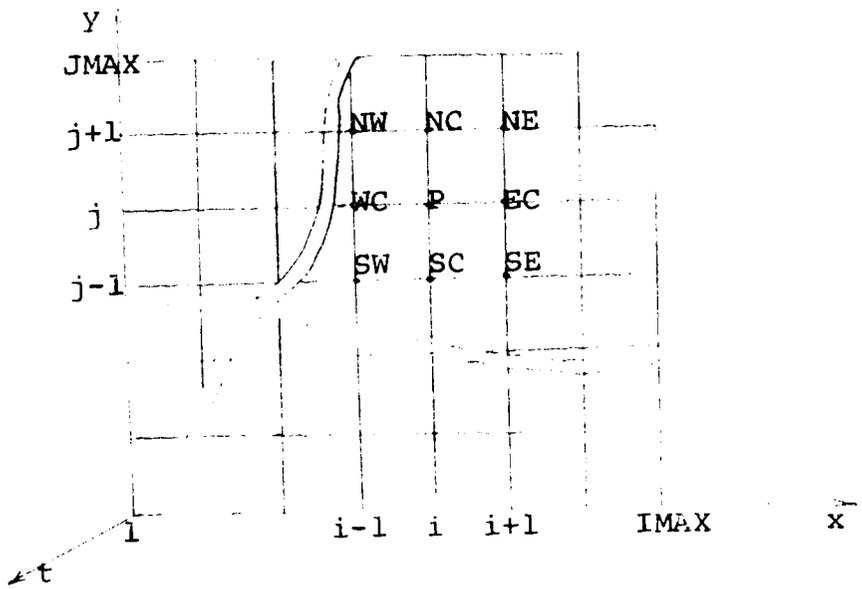

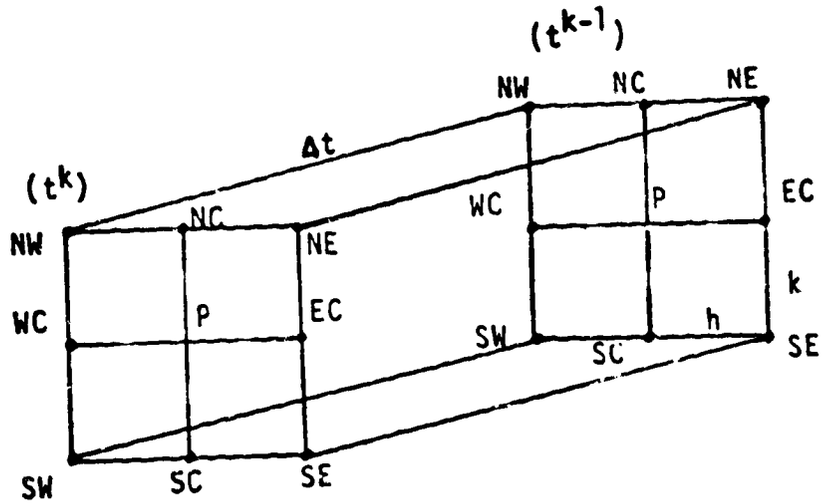

Figure 1 : Domain and local element for finite analytic formulations of unsteady two-dimensional convective transport equation

ORIGINAL PAGE IS
OF POOR QUALITY

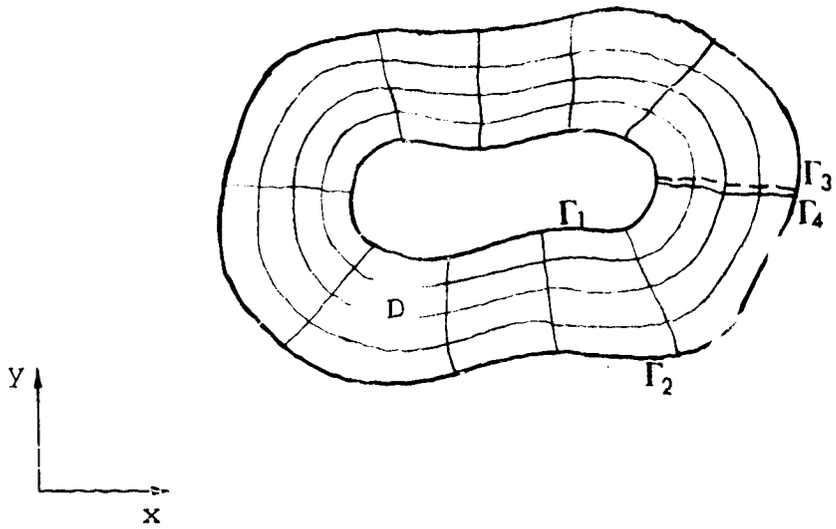

(a) Physical plane

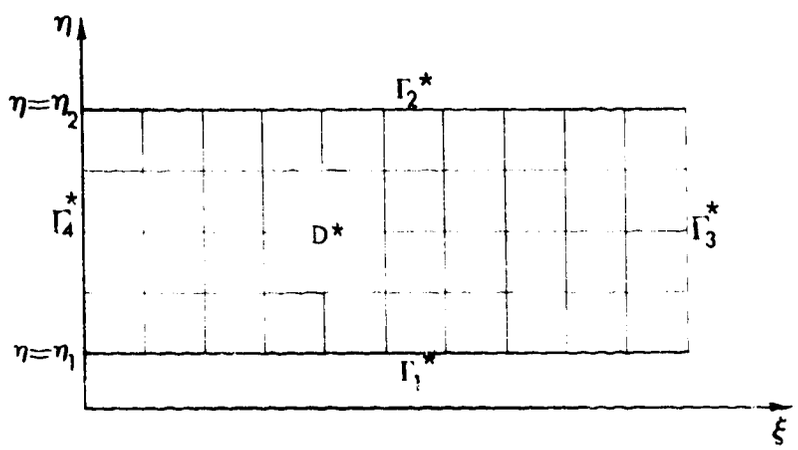

(b) Transformed plane

Figure 2 : Coordinate transformation .

ORIGINAL PAGE IS
OF POOR QUALITY

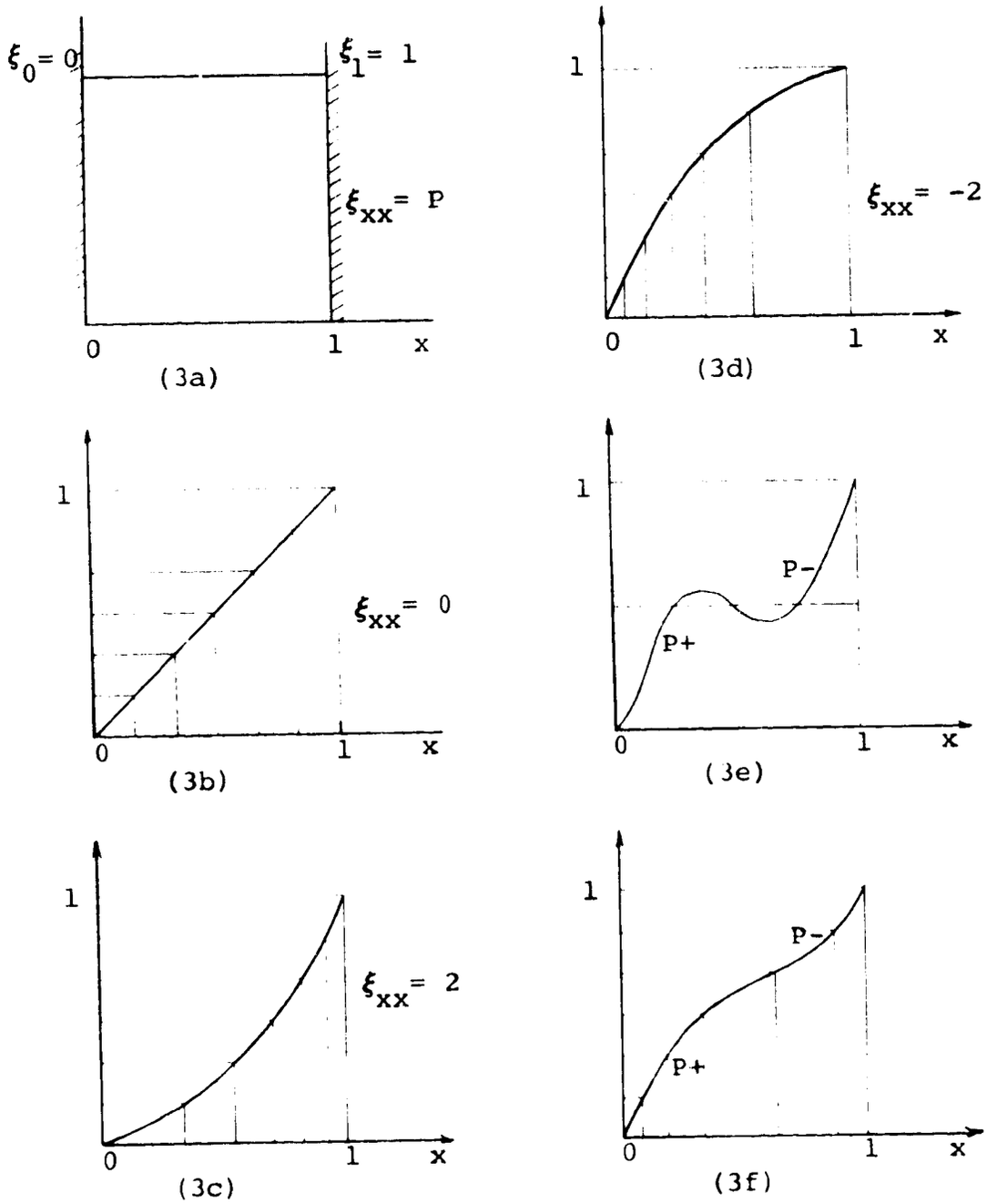

Figure 3 : Effect of source term in one-dimensional Poisson equation.

ORIGINAL PAGE IS
OF POOR QUALITY

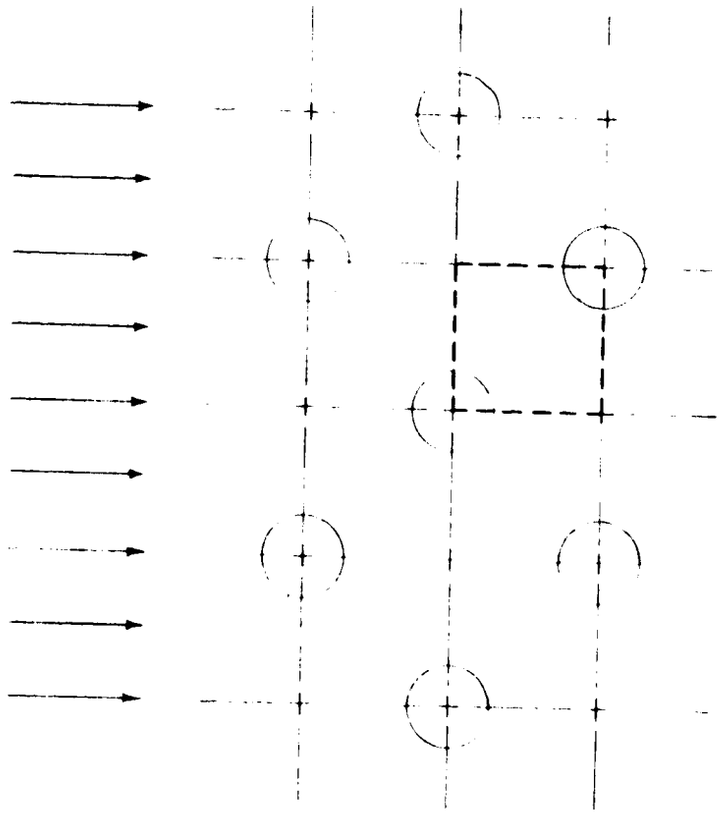

Figure 4 : Infinite rows of tubes.

ORIGINAL PAGE IS
OF POOR QUALITY

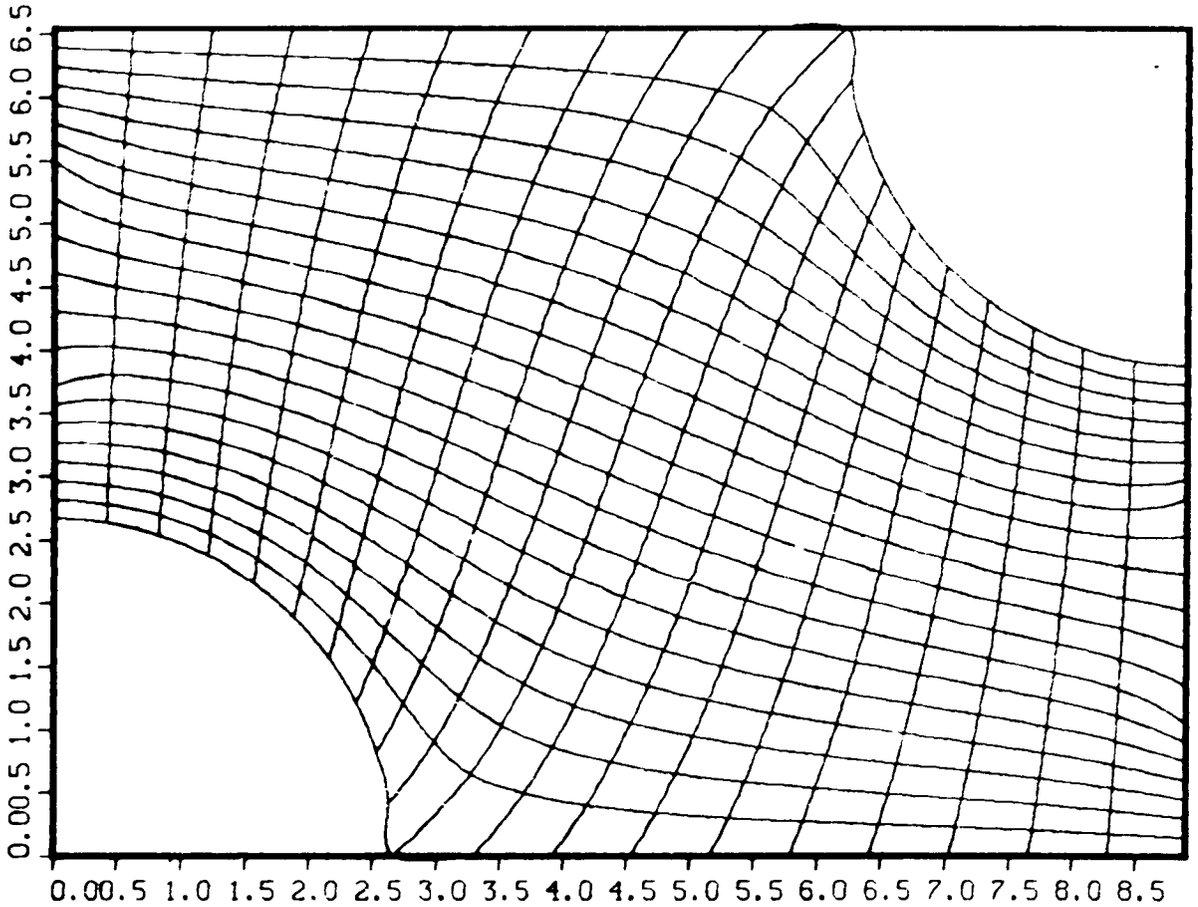

(a) Non-contraction P=Q=0

Figure 5 : Coordinate systems of the infinite rows of tubes.

ORIGINAL PAGE IS
OF POOR QUALITY

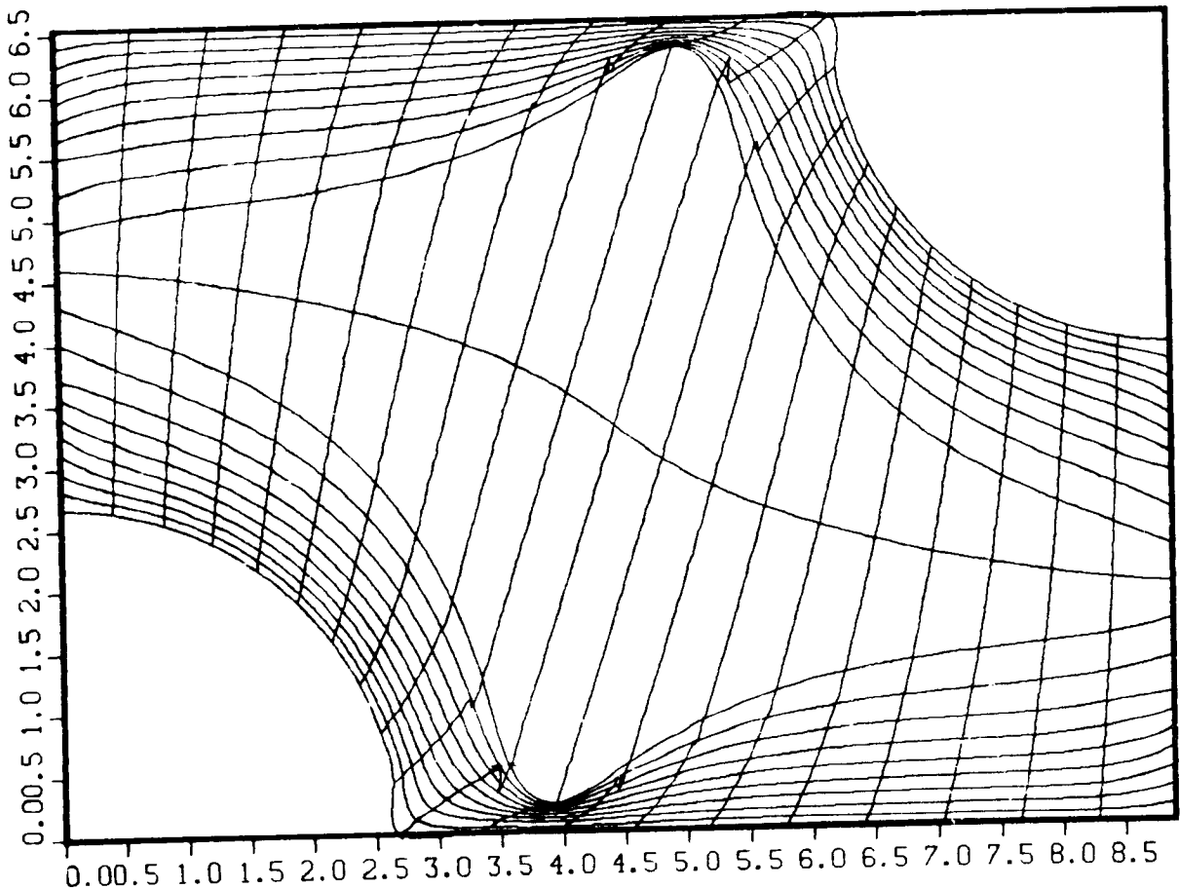

(b) Over-contraction a = 20 d = 0.2

Figure 5 (cont'd)

ORIGINAL PAGE IS
OF POOR QUALITY

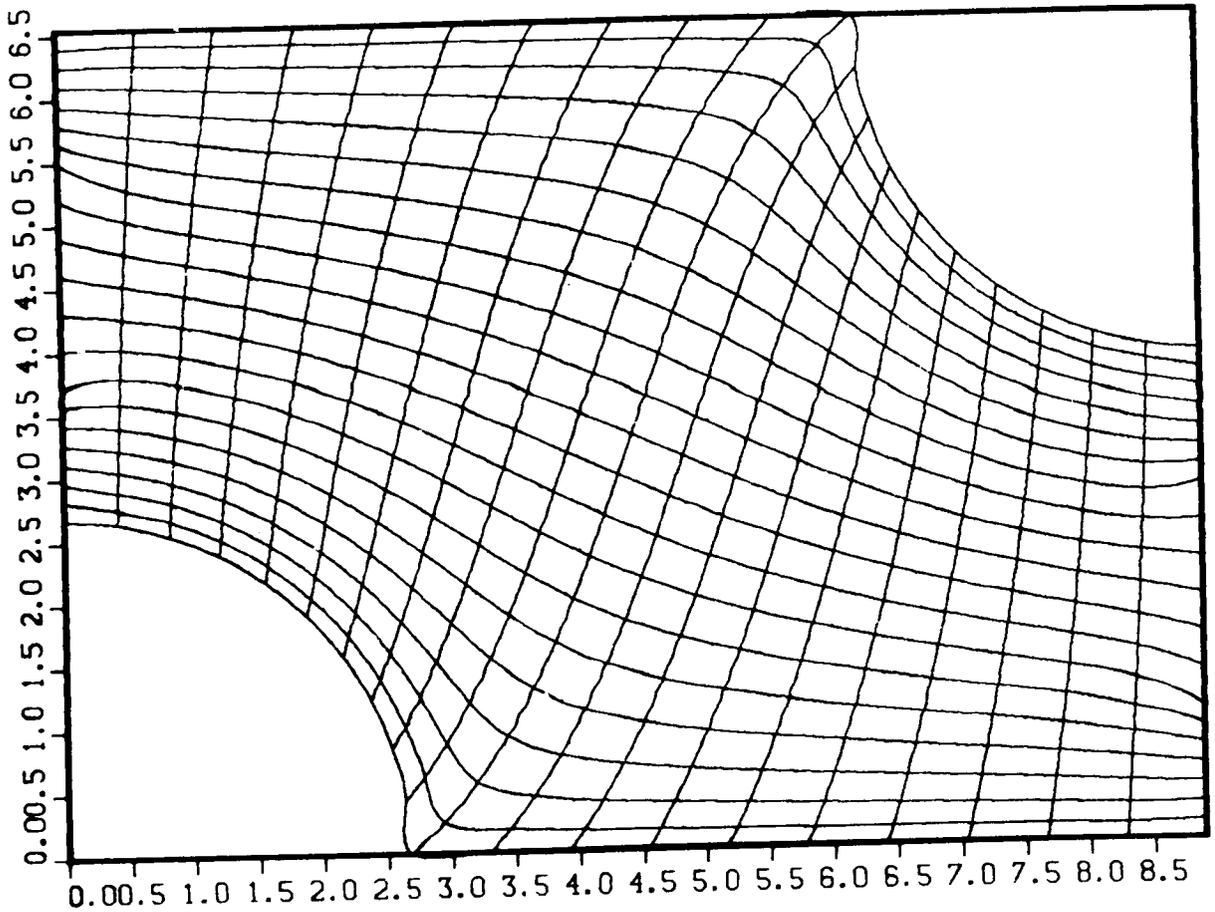

(c) Reasonable contraction a = 20 d = 0.75

Figure 5 (cont'd)

ORIGINAL PAGE IS
OF POOR QUALITY

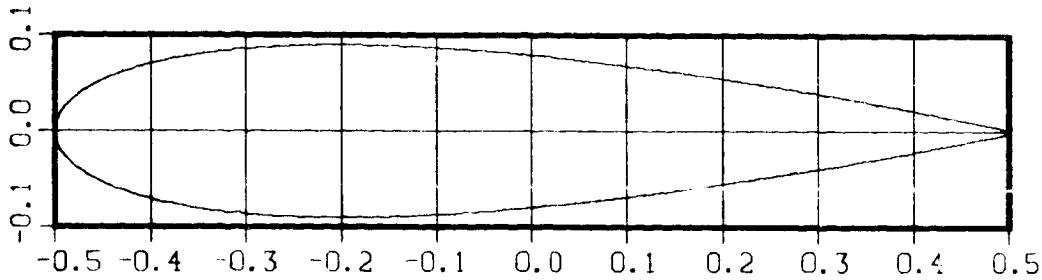

(a) NACA-0018 airfoil

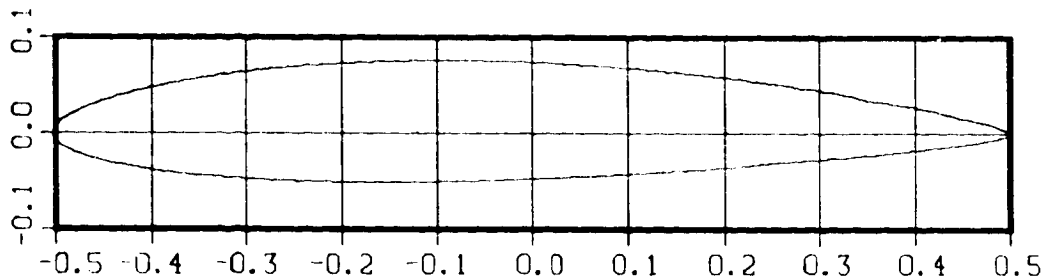

(b) Karmann-Trefftz airfoil

Figure 6 : NACA-0018 and Karmann-Trefftz airfoils.

ORIGINAL PAGE IS
OF POOR QUALITY

1	-0.49960	-0.00550	41	0.50000	0.00000
2	-0.50000	0.00000	42	0.49940	-0.00100
3	-0.49960	0.00550	43	0.49820	-0.00180
4	-0.49610	0.01630	44	0.49300	-0.00340
5	-0.48910	0.02670	45	0.48430	-0.00520
6	-0.47870	0.03650	46	0.47220	-0.00760
7	-0.46490	0.04570	47	0.45680	-0.01080
8	-0.44790	0.05430	48	0.43820	-0.01440
9	-0.42770	0.06210	49	0.41650	-0.01860
10	-0.40450	0.06910	50	0.39180	-0.02320
11	-0.37850	0.07510	51	0.36450	-0.02820
12	-0.34980	0.08020	52	0.33460	-0.03350
13	-0.31870	0.08420	53	0.30230	-0.03900
14	-0.28540	0.08720	54	0.26790	-0.04460
15	-0.25000	0.08910	55	0.23160	-0.05020
16	-0.21290	0.09000	56	0.19380	-0.05590
17	-0.17430	0.08980	57	0.15450	-0.06140
18	-0.13450	0.08870	58	0.11420	-0.06670
19	-0.09370	0.08670	59	0.07300	-0.07170
20	-0.05230	0.08390	60	0.03140	-0.07630
21	-0.01050	0.08040	61	-0.01050	-0.08040
22	0.03140	0.07630	62	-0.05230	-0.08390
23	0.07300	0.07170	63	-0.09370	-0.08670
24	0.11420	0.06670	64	-0.13450	-0.08870
25	0.15450	0.06140	65	-0.17430	-0.08980
26	0.19380	0.05590	66	-0.21290	-0.09000
27	0.23160	0.05020	67	-0.25000	-0.08910
28	0.26790	0.04460	68	-0.28540	-0.08720
29	0.30230	0.03900	69	-0.31870	-0.08420
30	0.33460	0.03350	70	-0.34980	-0.08020
31	0.36450	0.02820	71	-0.37850	-0.07510
32	0.39180	0.02320	72	-0.40450	-0.06910
33	0.41650	0.01860	73	-0.42770	-0.06210
34	0.43820	0.01440	74	-0.44790	-0.05430
35	0.45680	0.01080	75	-0.46490	-0.04570
36	0.47220	0.00760	76	-0.47870	-0.03650
37	0.48430	0.00520	77	-0.48910	-0.02670
38	0.49300	0.00340	78	-0.49610	-0.01630
39	0.49820	0.00180	79	-0.49960	-0.00550
40	0.49940	0.00100	80	-0.50000	0.00000

(c) Data of NACA-0018 airfoil

Figure 6 (cont'd)

ORIGINAL PAGE IS
OF POOR QUALITY

1	-0.50270	-0.00320	35	0.49950	0.00000
2	-0.50270	0.00360	36	0.49940	-0.00050
3	-0.49730	0.01120	37	0.49910	-0.00090
4	-0.48670	0.01870	38	0.49800	-0.00190
5	-0.47110	0.02640	39	0.49610	-0.00280
6	-0.45080	0.03410	40	0.48630	-0.00560
7	-0.42590	0.04160	41	0.47050	-0.00850
8	-0.39690	0.04860	42	0.44890	-0.01170
9	-0.36400	0.05520	43	0.42200	-0.01500
10	-0.32760	0.06110	44	0.39010	-0.01860
11	-0.28790	0.06610	45	0.35380	-0.02230
12	-0.24550	0.07020	46	0.31340	-0.02610
13	-0.20060	0.07330	47	0.25960	-0.03000
14	-0.15380	0.07530	48	0.22280	-0.03380
15	-0.10530	0.07620	49	0.17360	-0.03740
16	-0.05580	0.07590	50	0.12270	-0.04080
17	-0.00560	0.07450	51	0.07060	-0.04380
18	0.04470	0.07210	52	0.01790	-0.04640
19	0.09480	0.06870	53	-0.03480	-0.04850
20	0.14400	0.06440	54	-0.08700	-0.04990
21	0.19200	0.05930	55	-0.13800	-0.05060
22	0.23930	0.05360	56	-0.18750	-0.05050
23	0.28230	0.04750	57	-0.23480	-0.04970
24	0.32350	0.04110	58	-0.27950	-0.04800
25	0.35150	0.03460	59	-0.32110	-0.04560
26	0.39580	0.02830	60	-0.35930	-0.04240
27	0.42560	0.02210	61	-0.39370	-0.03840
28	0.45150	0.01540	62	-0.42390	-0.03370
29	0.47200	0.01130	63	-0.44960	-0.02850
30	0.48710	0.00680	64	-0.47050	-0.02270
31	0.49640	0.00300	65	-0.48650	-0.01650
32	0.49800	0.00190	66	-0.49730	-0.01000
33	0.49900	0.00090	67	-0.50270	-0.00320
34	0.49940	0.00040	68	-0.50270	0.00360

(d) Data of Karmann-Trefftz airfoil

Figure 6 (cont'd)

ORIGINAL PAGE IS
OF POOR QUALITY

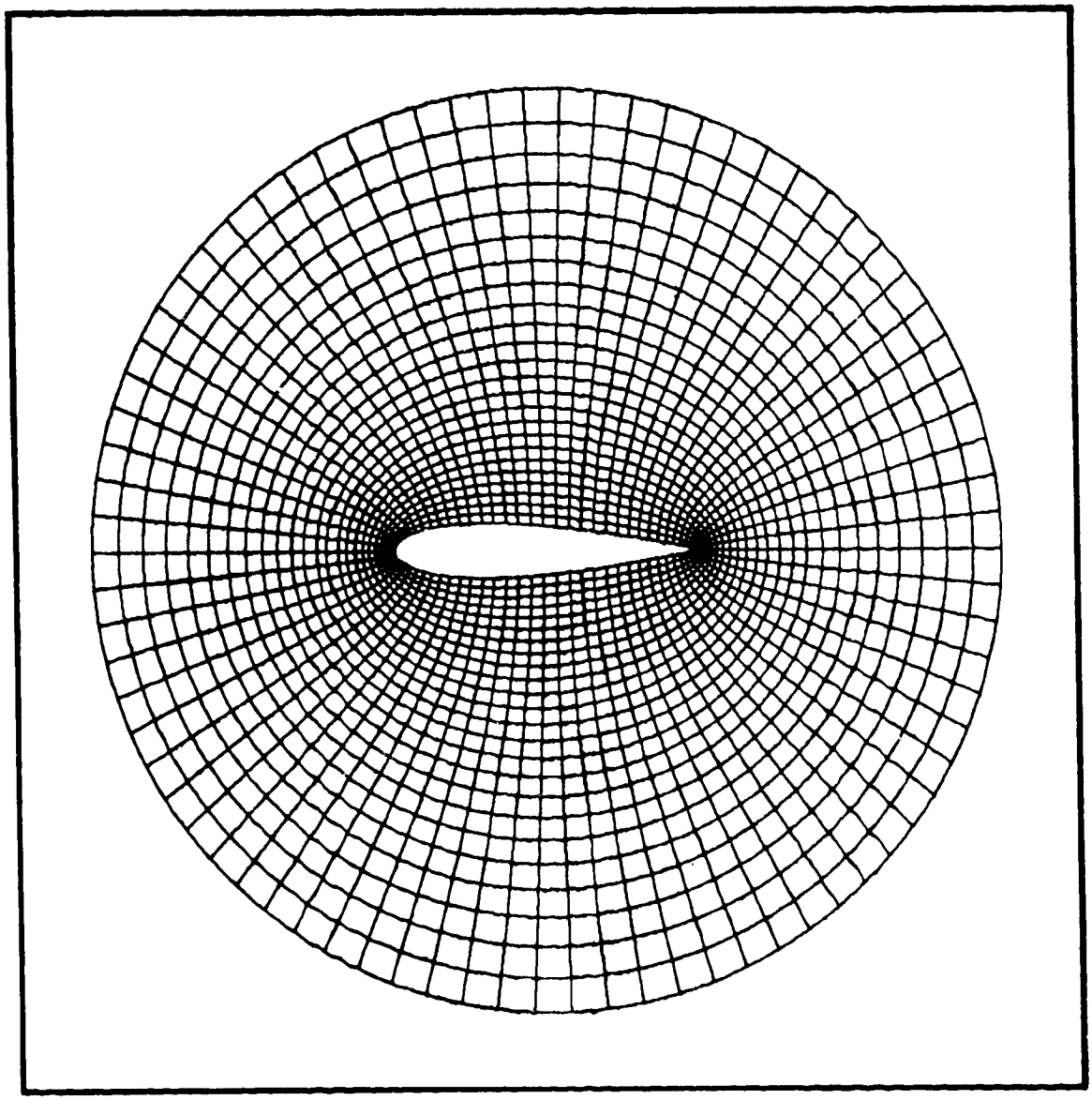

Figure 7 : Contracted coordinate system --
NACA-0018 airfoil.

ORIGINAL PAGE IS
OF POOR QUALITY

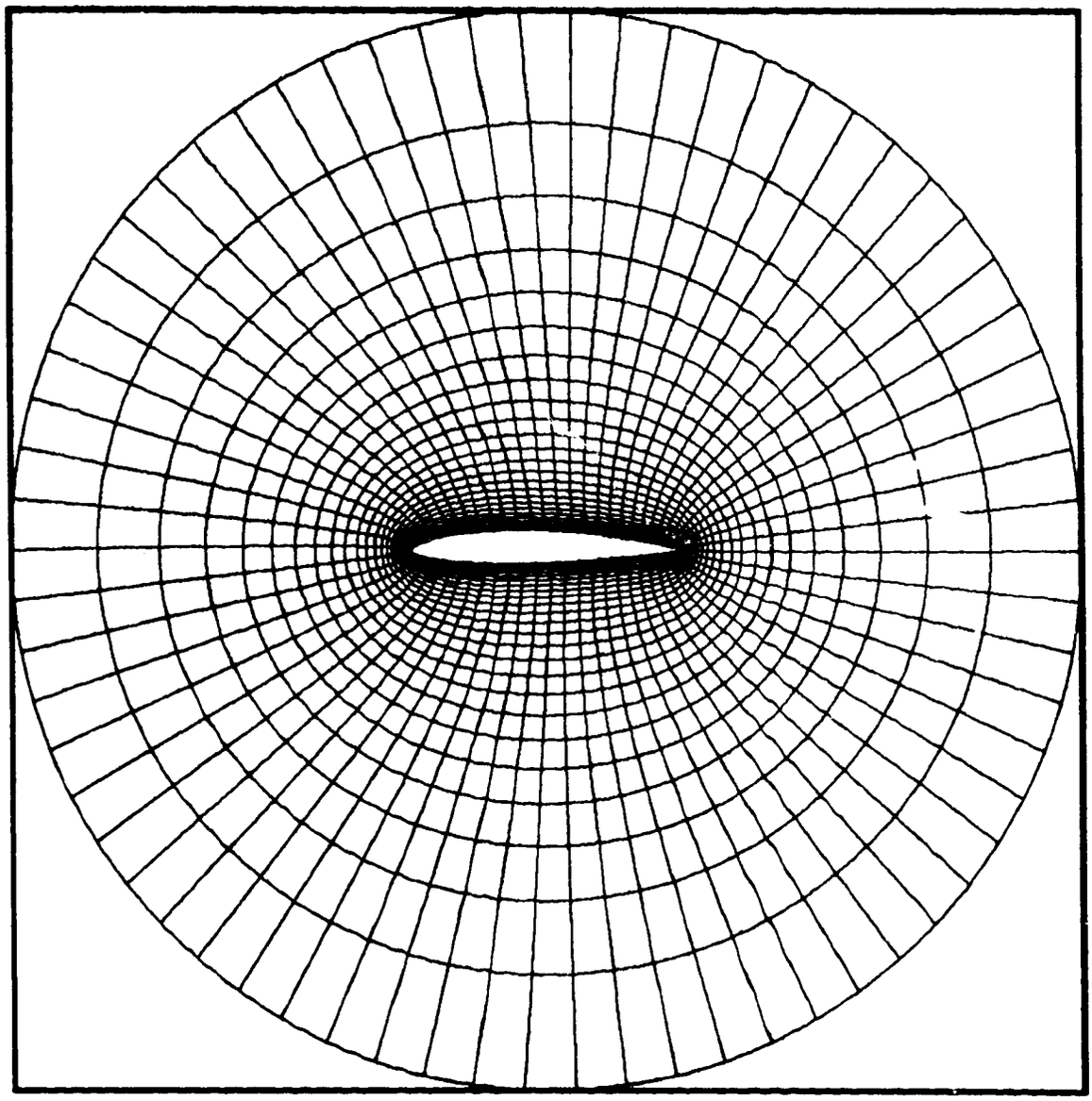

Figure 8 : Contracted coordinate system --
Karmann-Trefftz airfoil.

ORIGINAL PAGE IS
OF POOR QUALITY

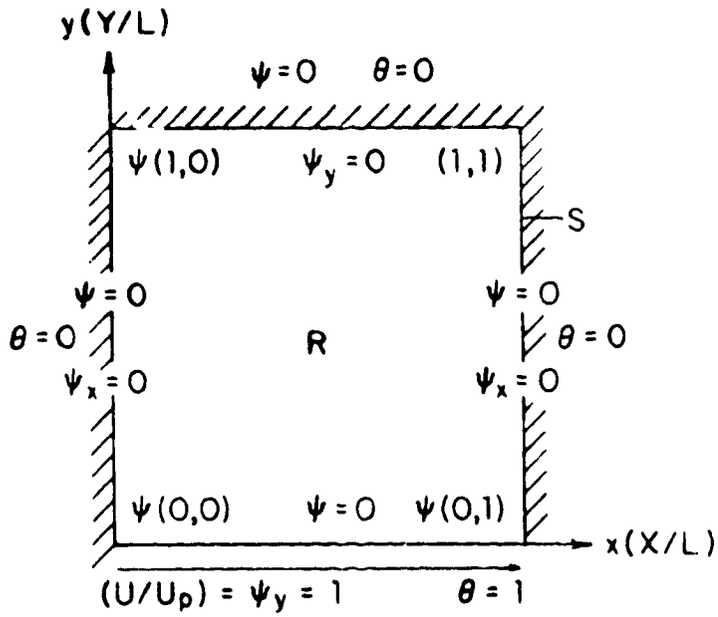

Figure 9 : Coordinates and boundary conditions of cavity flow.

ORIGINAL PAGE IS
OF POOR QUALITY

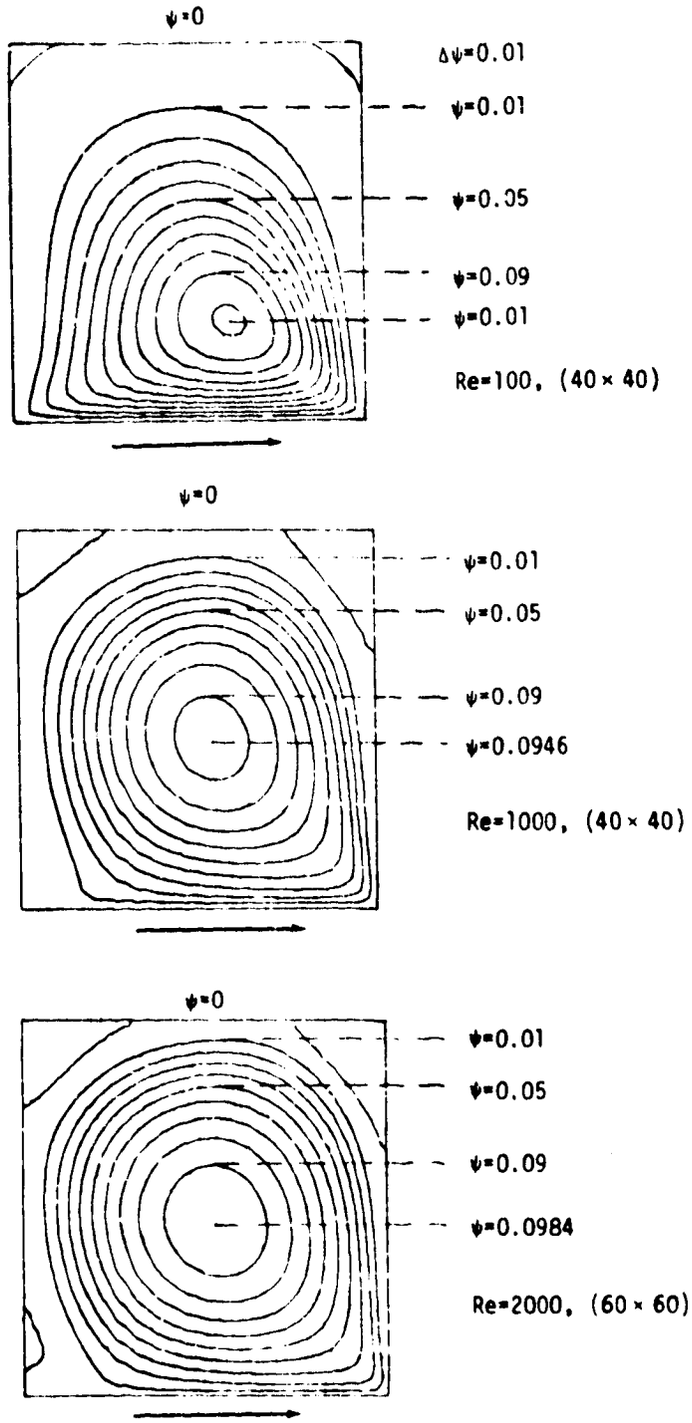

Figure 10 : Stream function of cavity flow.

ORIGINAL PAGE IS
OF POOR QUALITY

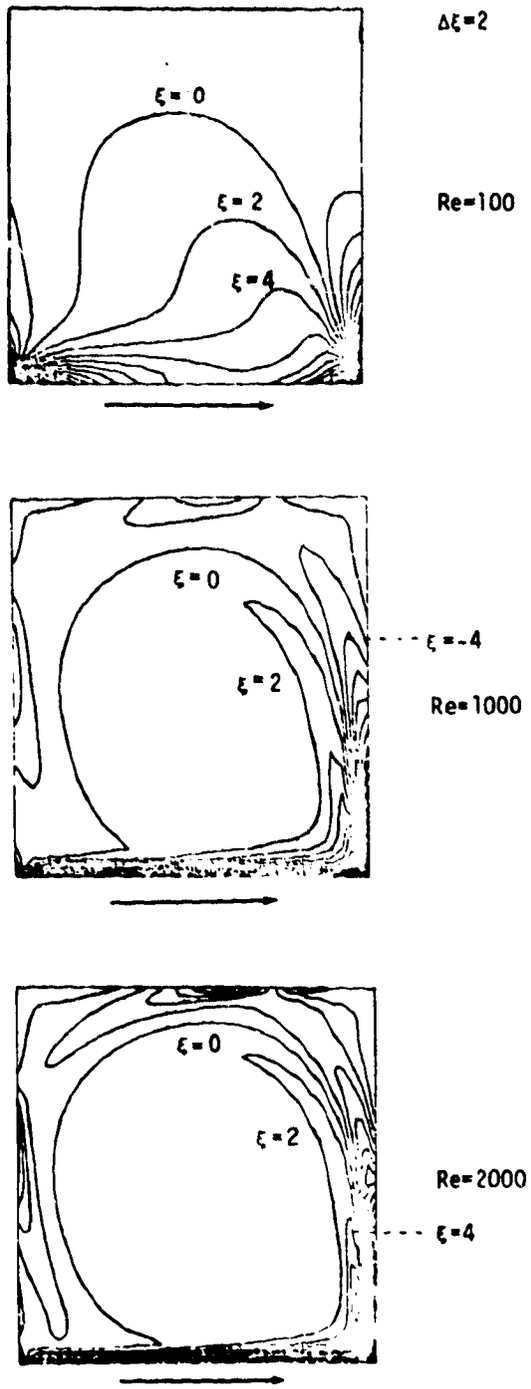

Figure 11 : Vorticity distribution of cavity flow.

ORIGINAL PAGE IS
OF POOR QUALITY

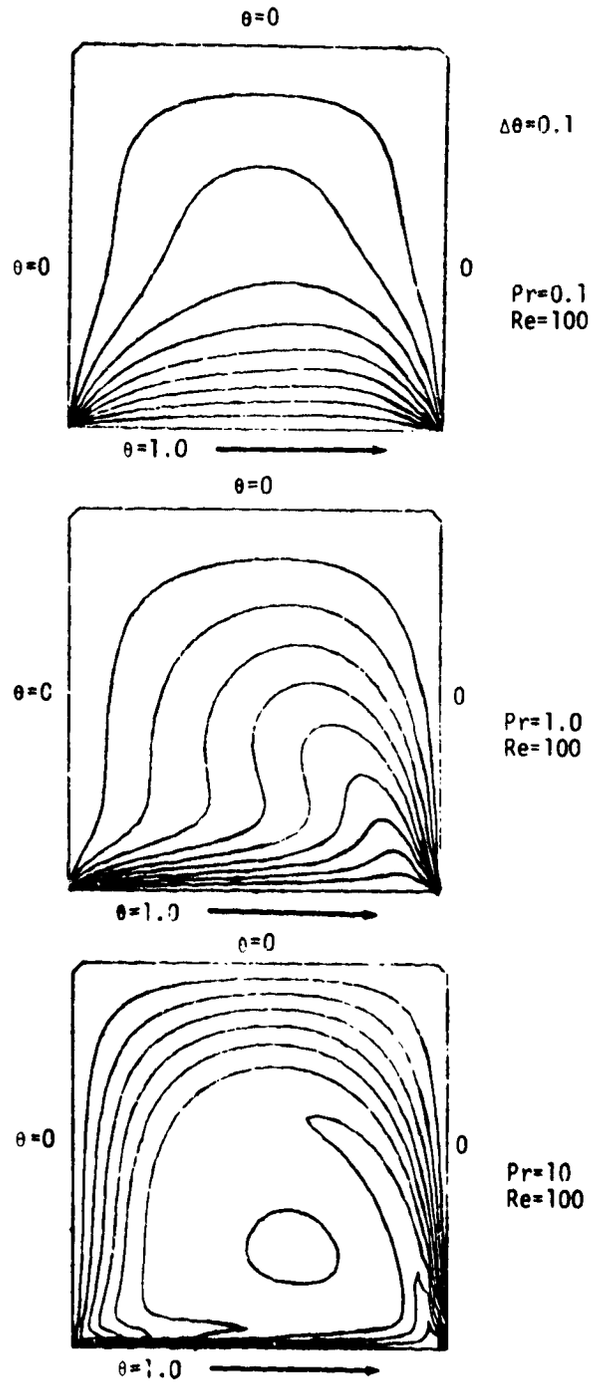

Figure 12 : Temperature distribution for Re = 100.

ORIGINAL PAGE IS
OF POOR QUALITY

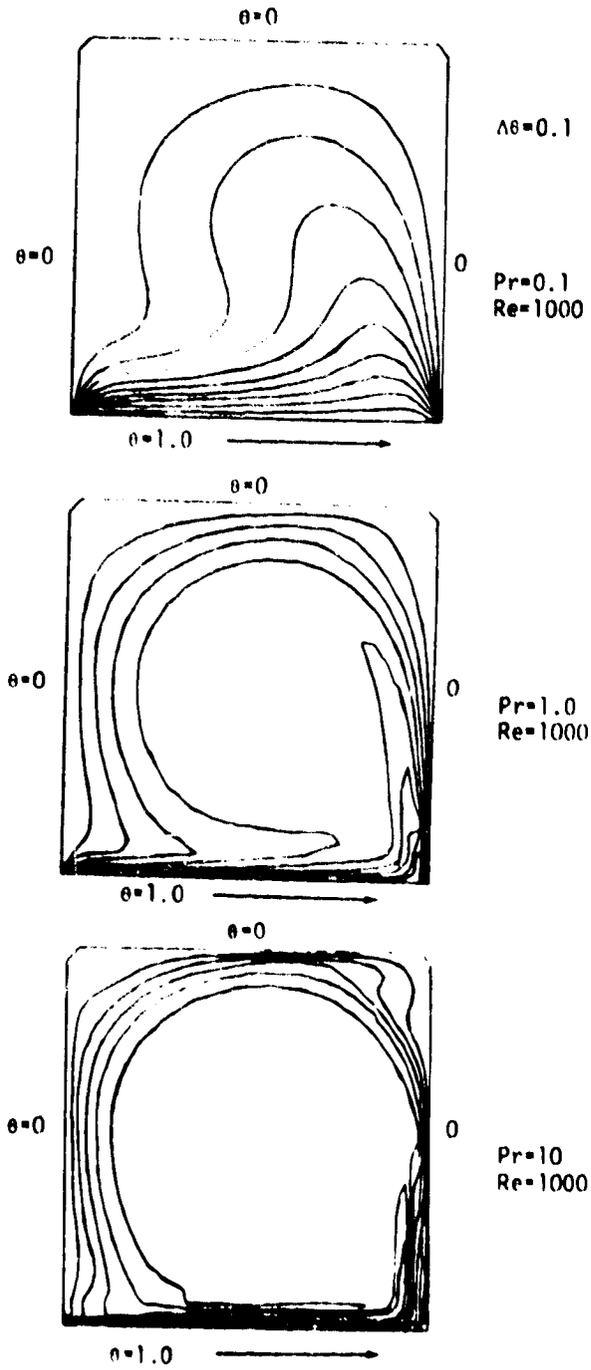

Figure 13 : Temperature distribution for Re = 1000.

ORIGINAL PAGE IS
OF POOR QUALITY

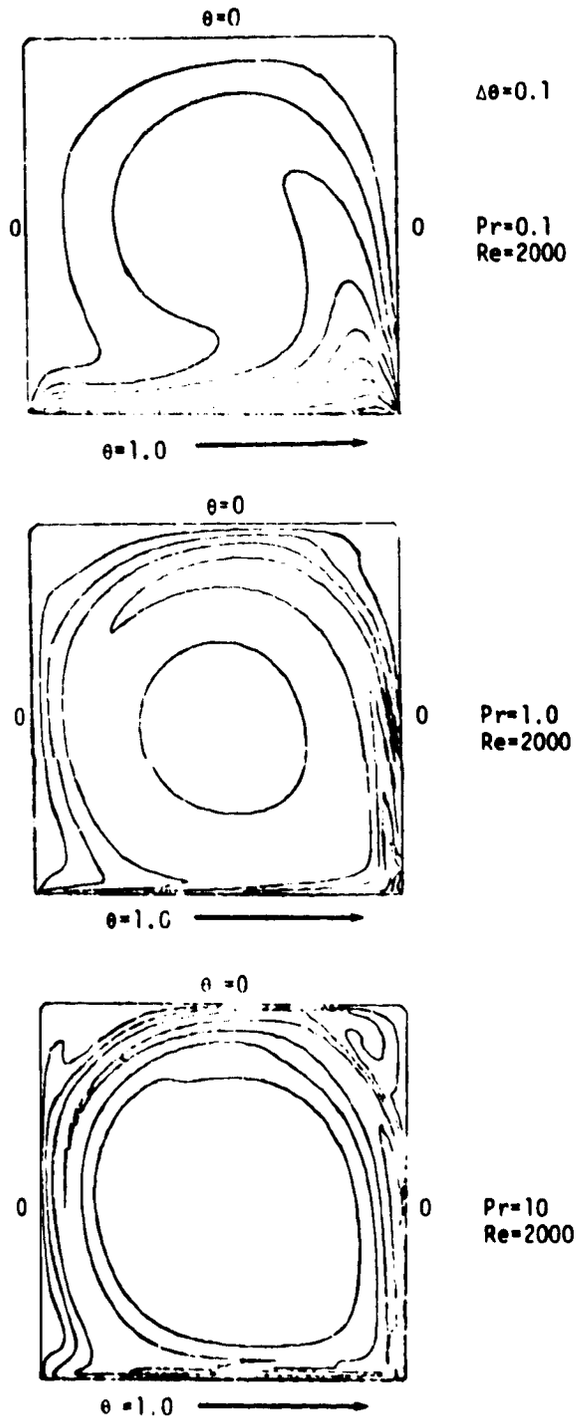

Figure 14 : Temperature distribution for Re = 2000.

ORIGINAL PAGE IS
OF POOR QUALITY

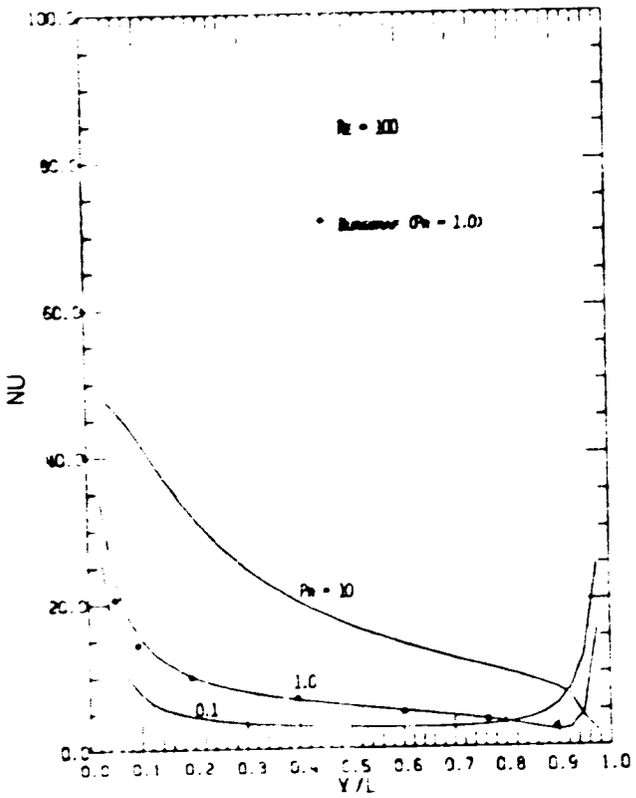

Figure 15 : Local Nusselt number of moving wall for Re = 100.

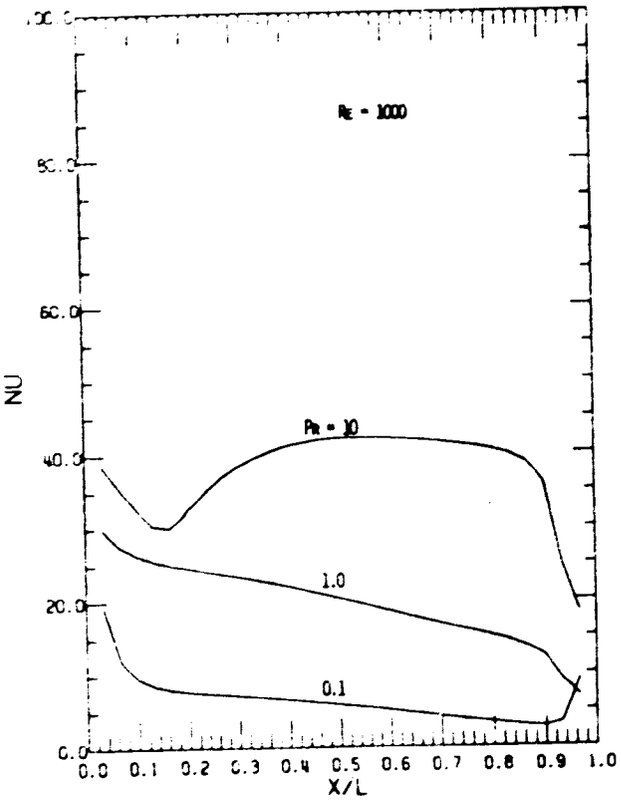

Figure 16 : Local Nusselt number of moving wall for Re = 1000.

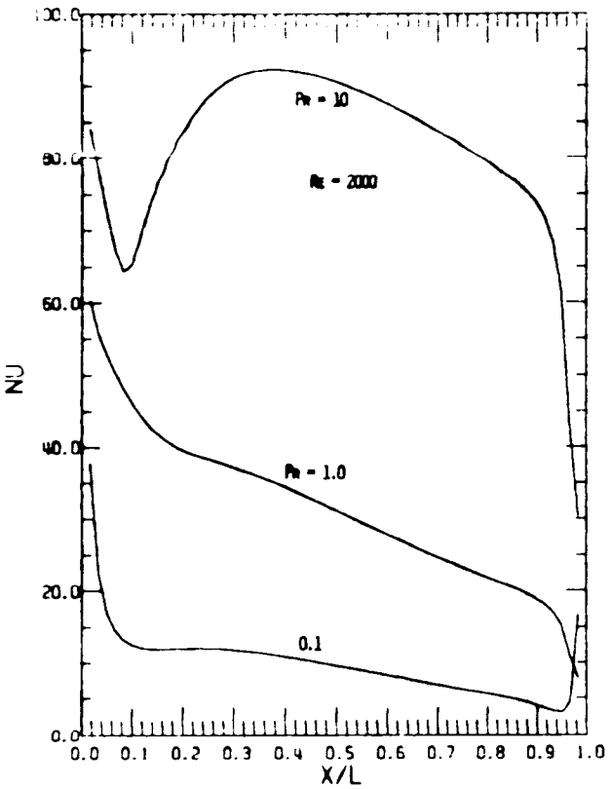

Figure 17 : Local Nusselt number of moving wall for Re = 2000.

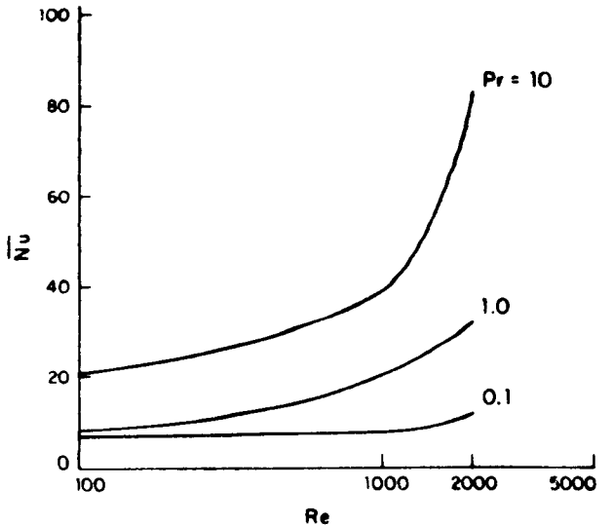

Figure 18 : Mean Nusselt number of moving wall.

ORIGINAL PAGE IS
OF POOR QUALITY

ORIGINAL PAGE IS
OF POOR QUALITY

(a) sudden pipe expansion

(b) step adjacent to a free stream

(c) double plane duct expansion

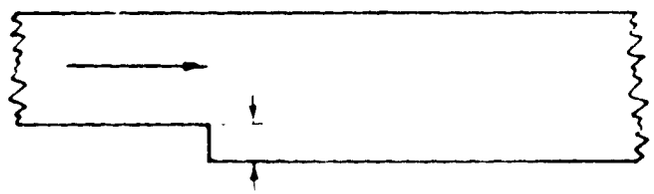

(d) single plane duct expansion

Figure 19 : Definition sketch of channel flow geometries.

ORIGINAL PAGE IS
OF POOR QUALITY

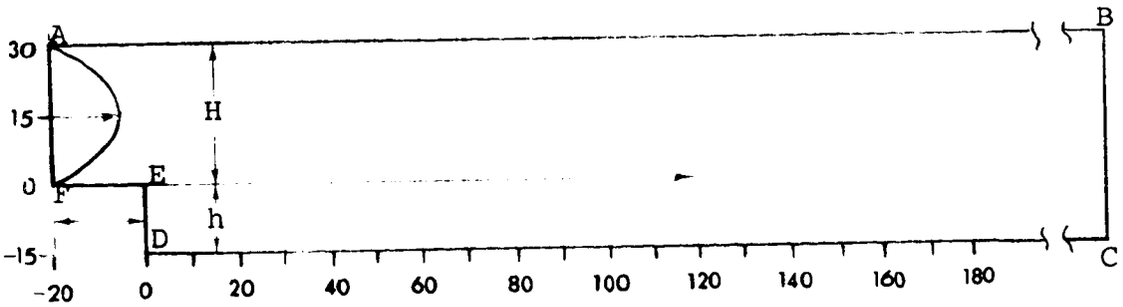

Figure 20 : Coordinate and description of flow over a step.

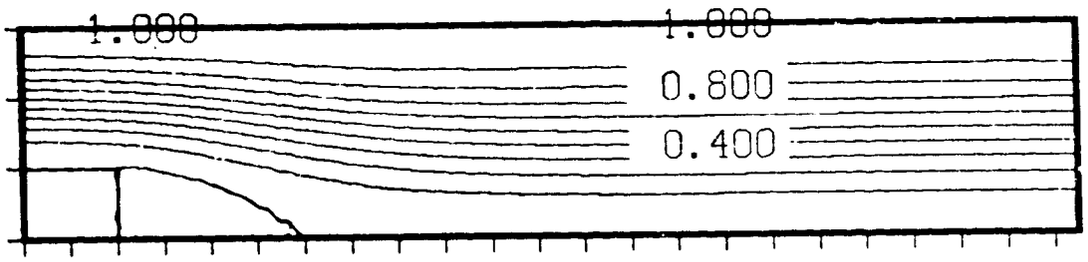

(a) Re = 25

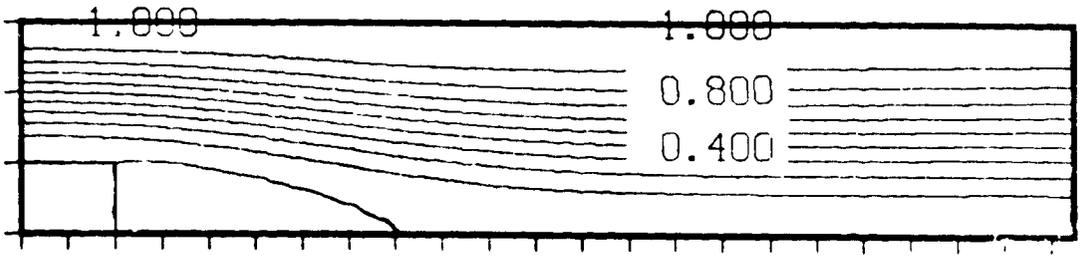

(b) Re= 50

Figure 21 : Stream function of laminar flow over a step, numerical values are of dimensionless stream function ψ/ψ_0.

ORIGINAL PAGE IS
OF POOR QUALITY

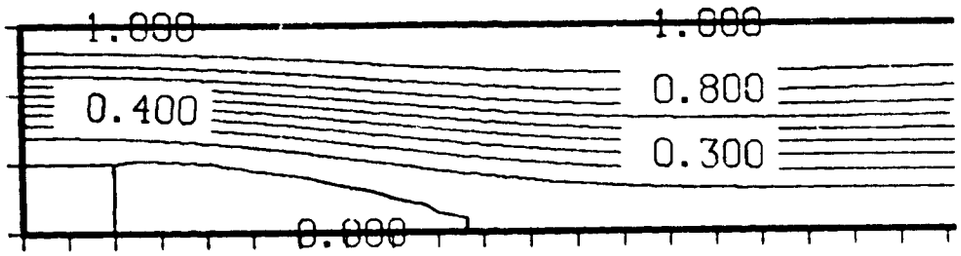

(c) Re = 73

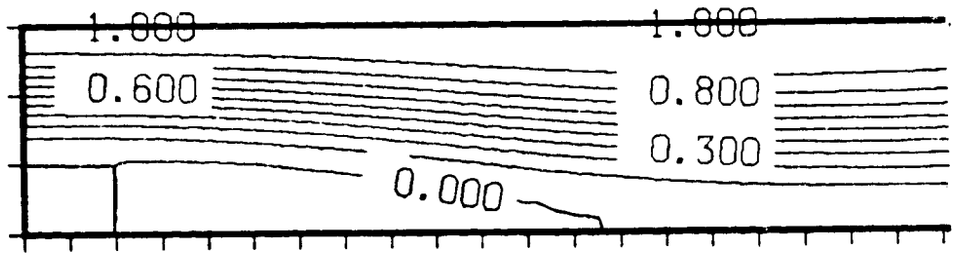

(d) Re =125

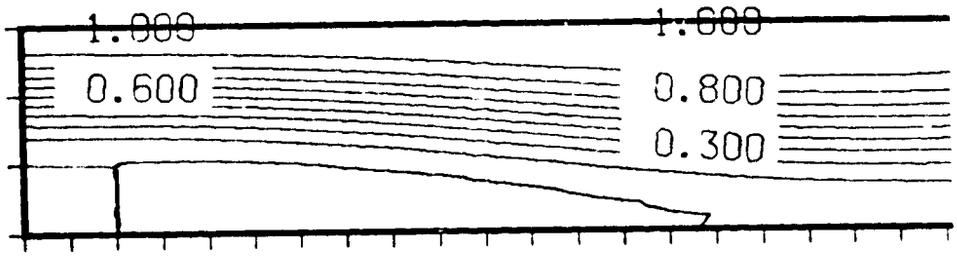

(e) Re = 191

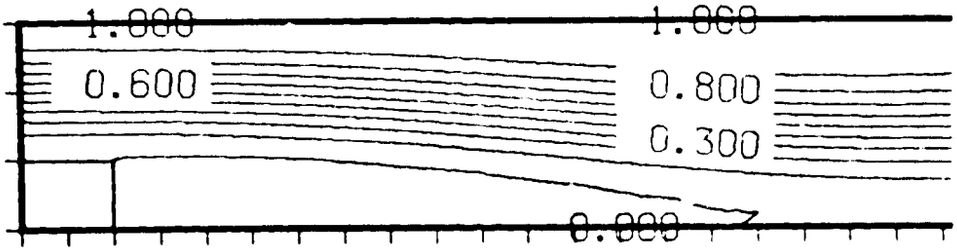

(f) Re = 229

Figure 21 (cont'd)

ORIGINAL PAGE IS
OF POOR QUALITY

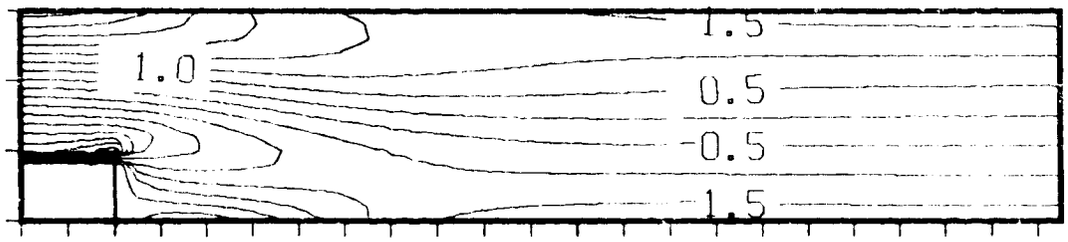

(a) Re = 25

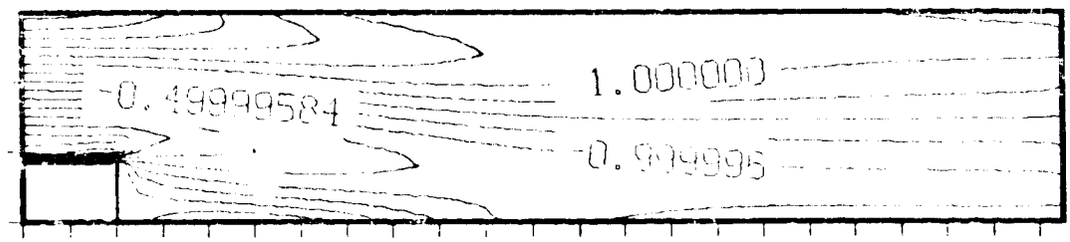

(b) Re = 50

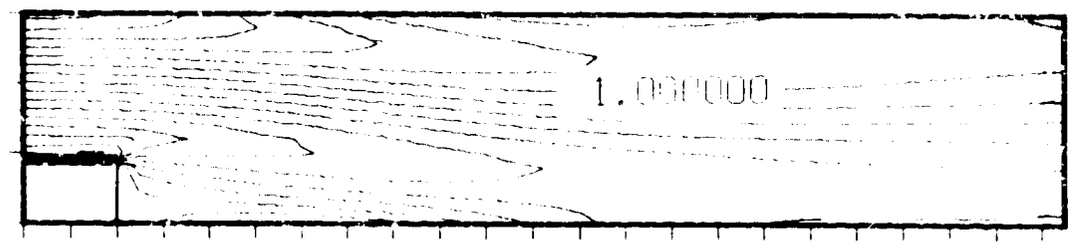

(c) Re = 73

Figure 22 : Vorticity distribution of laminar flow over a step

ORIGINAL PAGE IS
OF POOR QUALITY

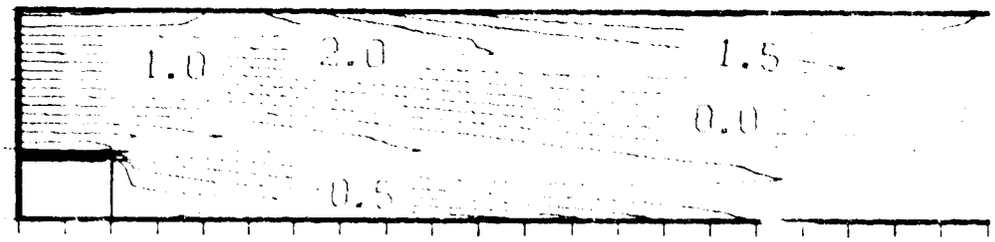

(d) Re = 125

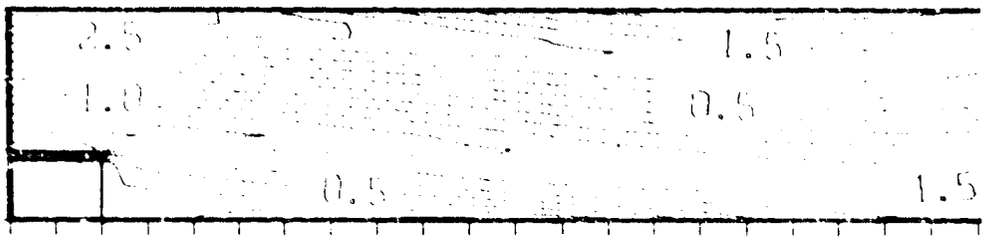

(e) Re = 191

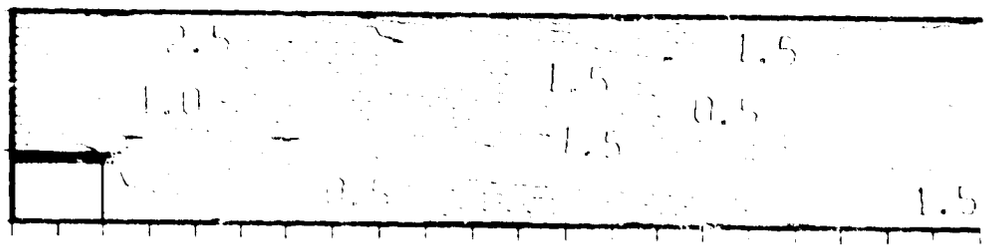

(f) Re = 229

Figure 22 (cont'd)

ORIGINAL PAGE IS
OF POOR QUALITY

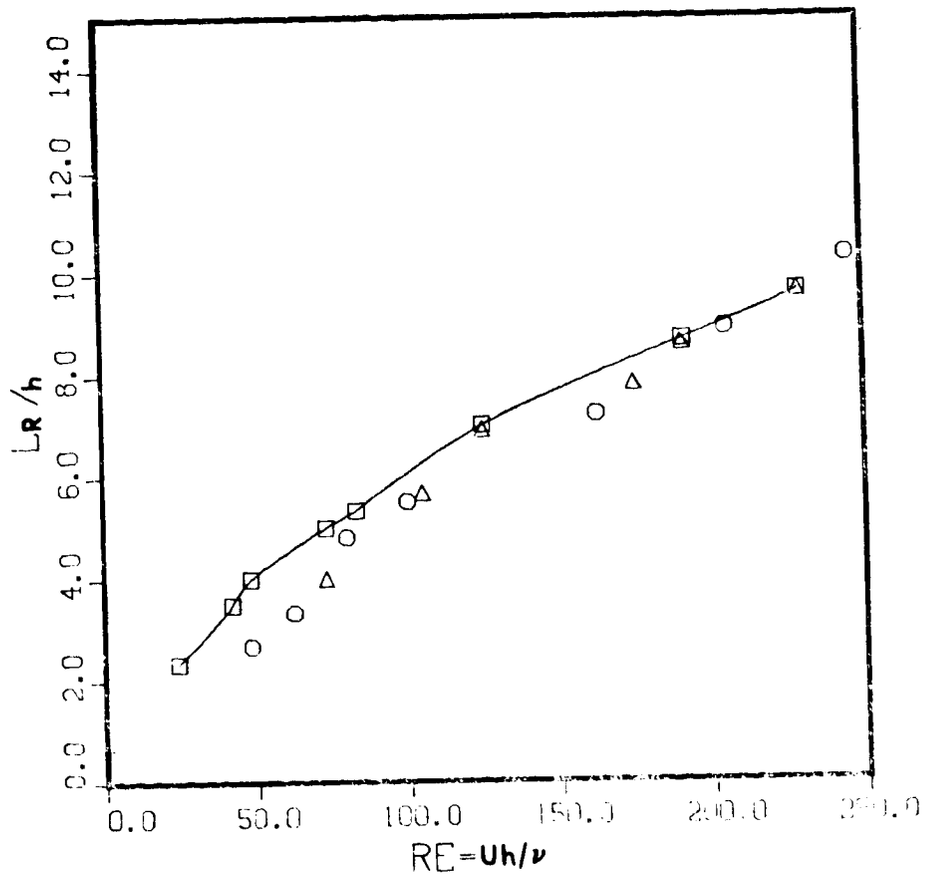

□ : present results, △ : laser anemometer,
○ : dye tracer.

Figure 23 : Variation of recirculation zone length with Reynolds number (Re) -- FA and measured.

ORIGINAL PAGE IS
OF POOR QUALITY

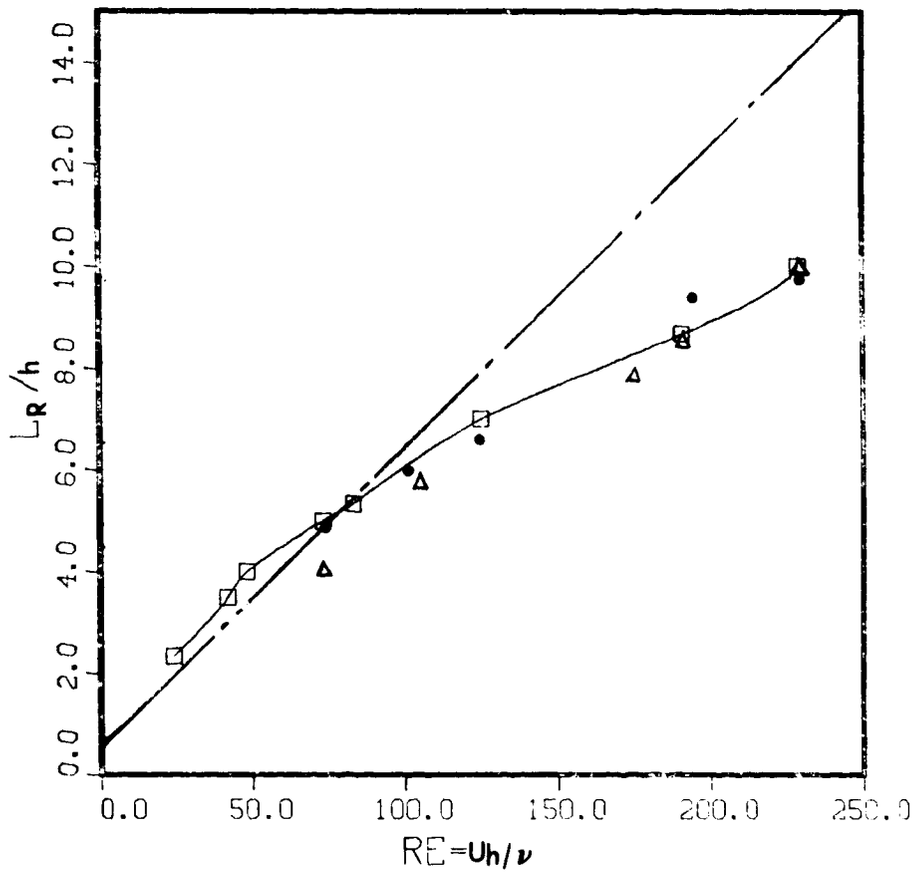

□: present results, . : FD with experimental inlet velocity profile, —.— : FD with fully developped velocity profile. △: laser anemometer

Figure 24 : Variation of recirculation zone length with Reynolds number(Re) -- FA and FD.

ORIGINAL PAGE IS
OF POOR QUALITY

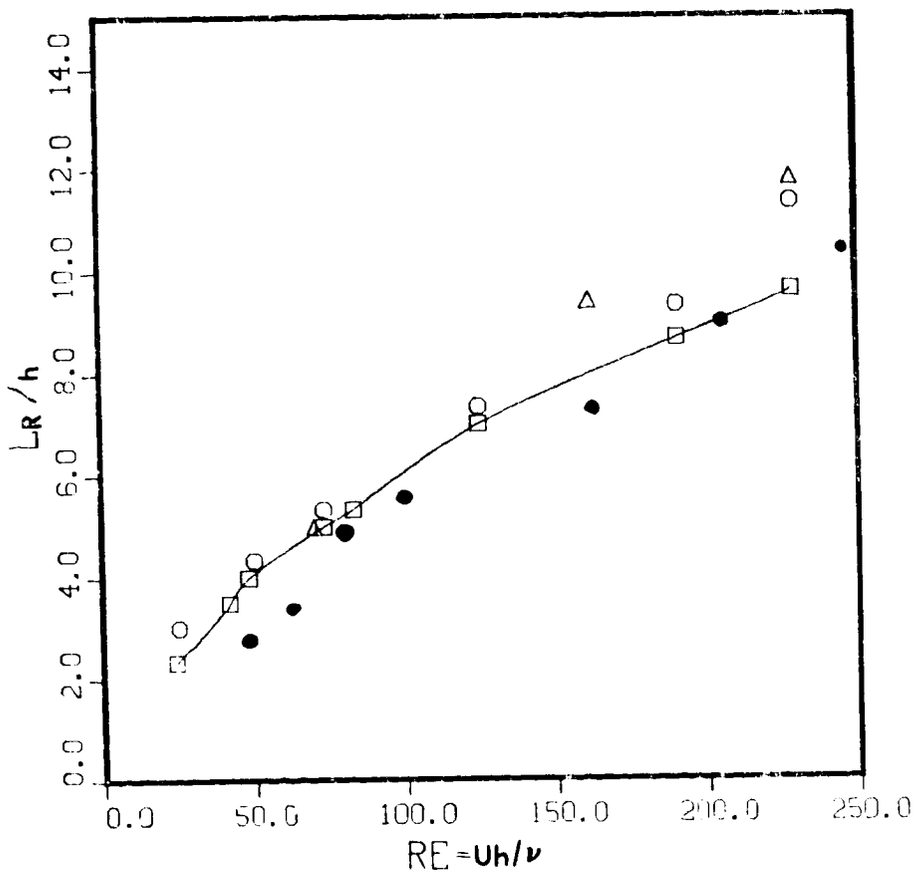

□ : present results, △ : by Hutton,
o : by Thomas. • : dye tracer.

Figure 25 : Variation of recirculation zone length with Reynolds number (Re) --FA and FE.

ORIGINAL PAGE IS
OF POOR QUALITY

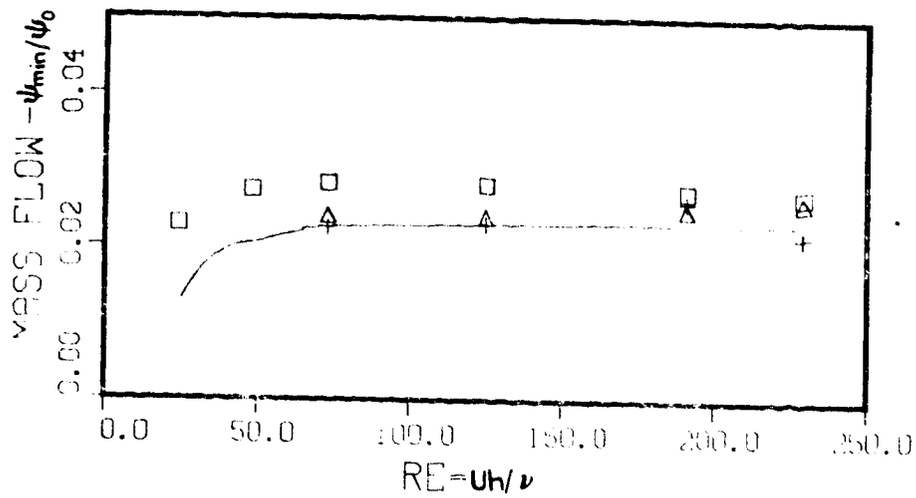

□ : present results

+ : experimental data

Δ : by Atkins

Figure 26 : Comparison of measured and predicted total mass flow rate within the recirculation region.

ORIGINAL PAGE IS
OF POOR QUALITY

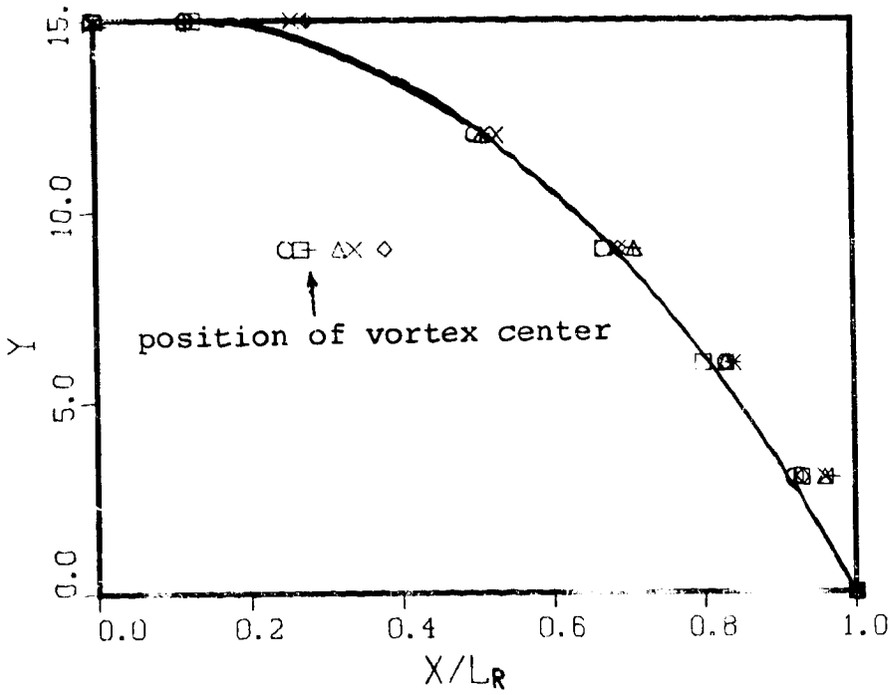

□ : Re = 25, ○ : Re = 50, △: Re = 73
+ : Re = 125, x : Re = 191, ◇ : Re = 229

Figure 27 : Similarity in the recirculation region flow -- path of the separation streamline and position of vortex center.

ORIGINAL PAGE IS
OF POOR QUALITY

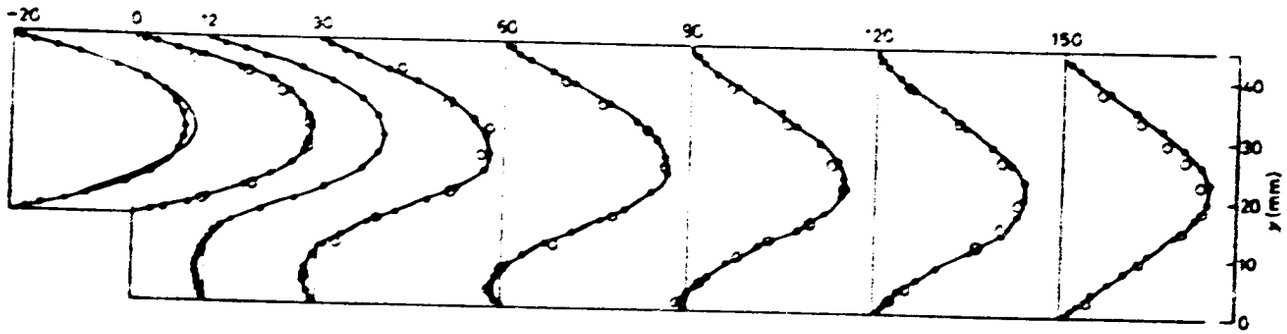

——— : measurement

○ : prediction

Figure 28 : Comparison of measured and predicted velocity profiles for laminar channel flow over a single step at Re = 125.

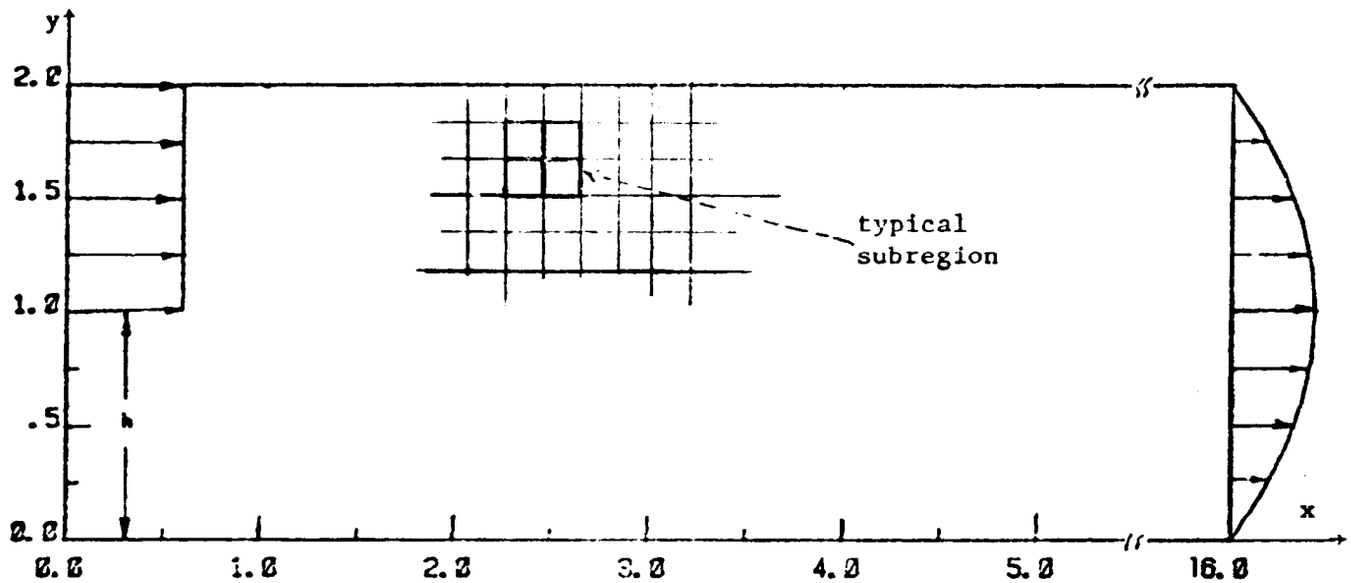

Figure 29 : Coordinate and description of suddenly expanded channel flow.

ORIGINAL PAGE IS
OF POOR QUALITY

ORIGINAL PAGE IS
OF POOR QUALITY

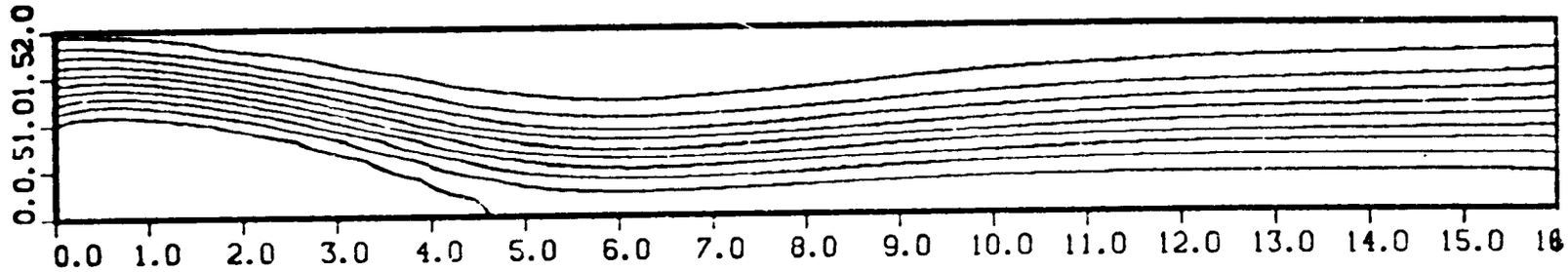

(a) h = k = 0.2 (81 x 11) for Re = 200

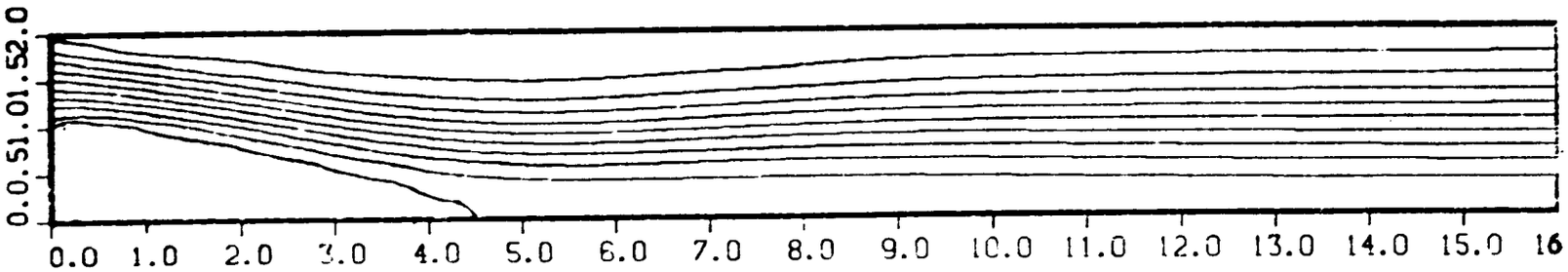

(b) h = 0.5, k = 0.2 (33 x 11) for Re = 200

Figure 30 : Stream function contours of channel flow $\Delta\psi = 0.1$

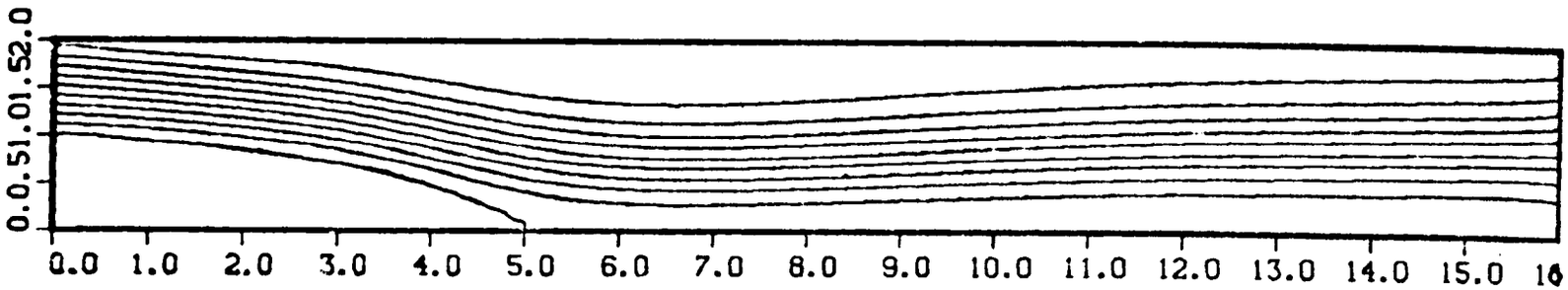

(c) h = k = 0.1 (161 x 21) for Re = 400

Figure 30 (cont'd)

ORIGINAL PAGE IS
OF POOR QUALITY

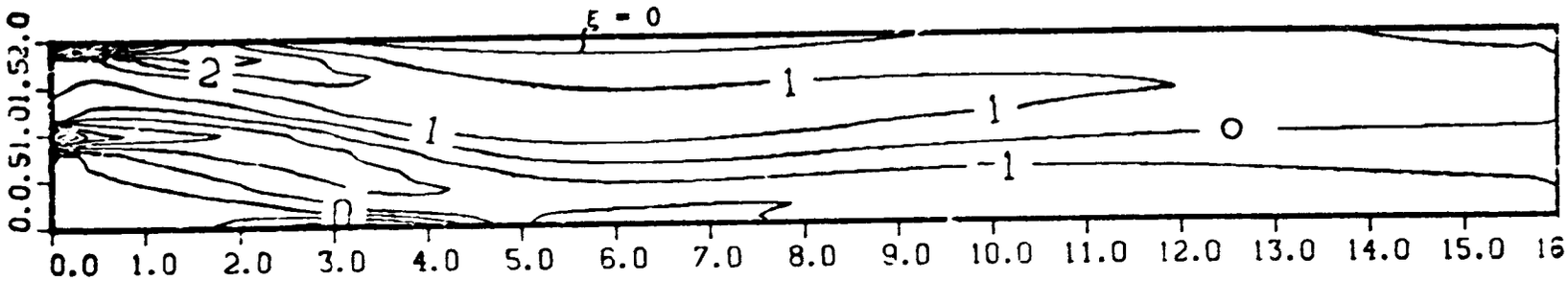

(a) h = k = 0.2 (81 x 11)

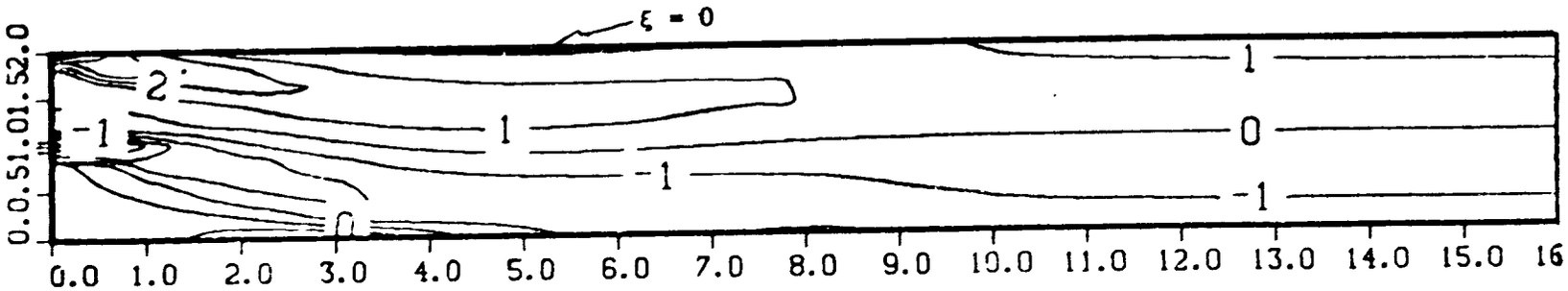

(b) h = 0.5, k = 0.2 (33 x 11)

Figure 31 : Vorticity contours of channel flow for $Re_s = 200$, $\Delta\omega = 1$.

ORIGINAL PAGE IS
OF POOR QUALITY

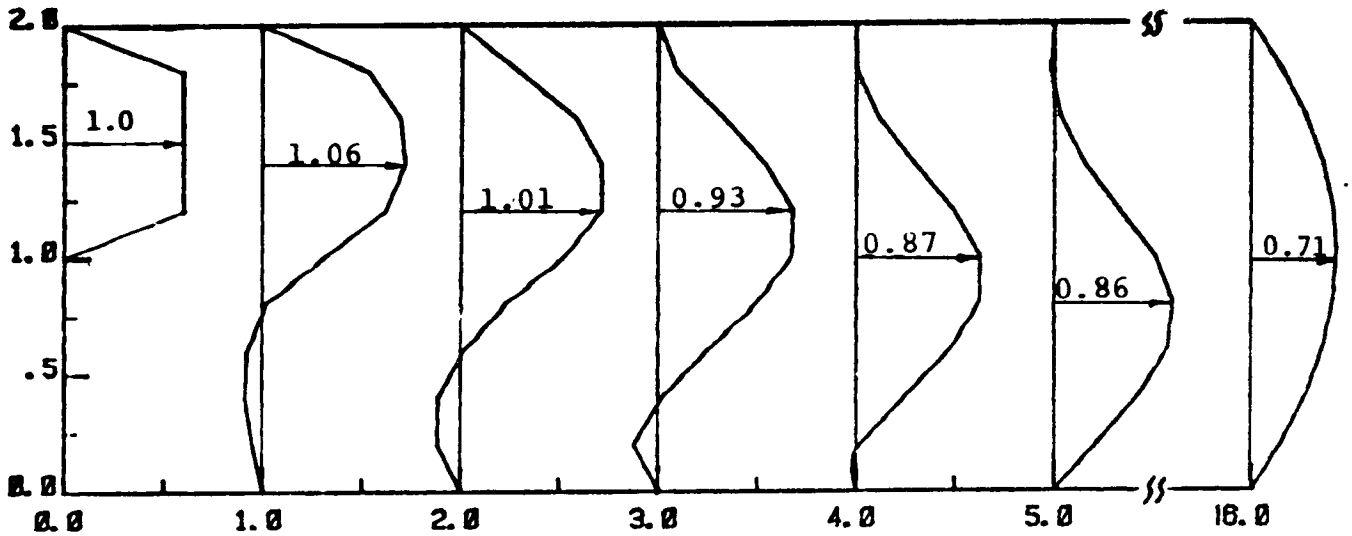

Figure 32 : Velocity profiles of channel flow for Re_s = 200 at different location, h = k = 0.2 (81 x 11).

ORIGINAL PAGE IS
OF POOR QUALITY

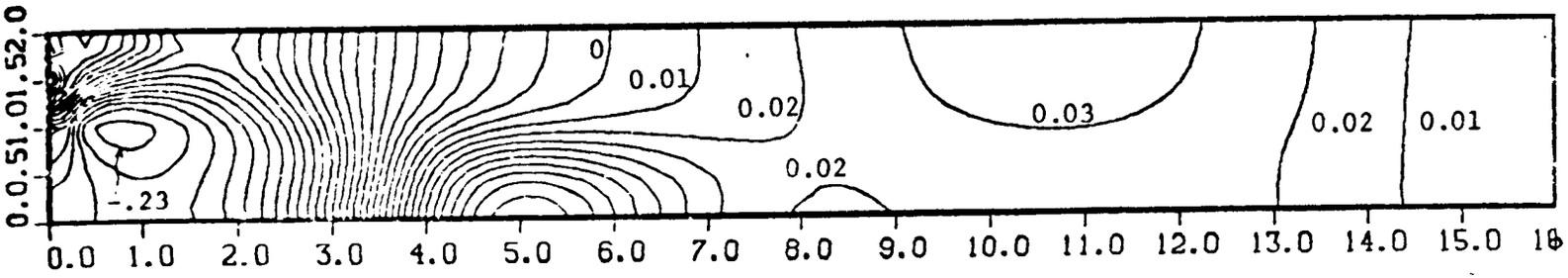

Figure 33 : Pressure distribution of channel flow for $Re_s = 200$, $\Delta p = 0.01$, $h = k = 0.2$.

ORIGINAL PAGE IS
OF POOR QUALITY

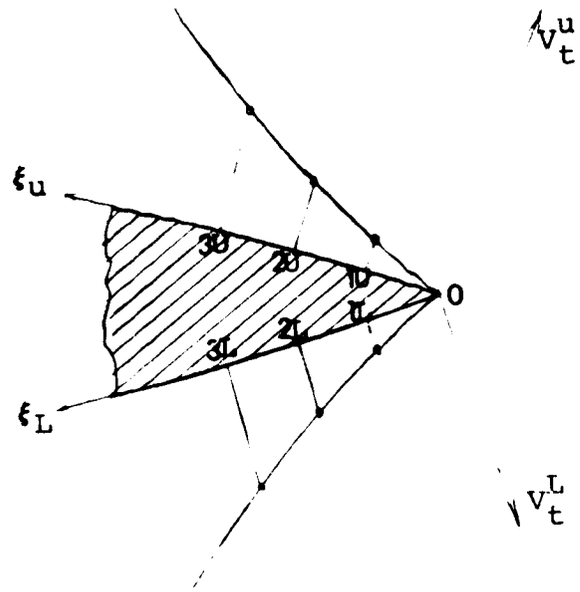

(a) trailing edge with a finite angle

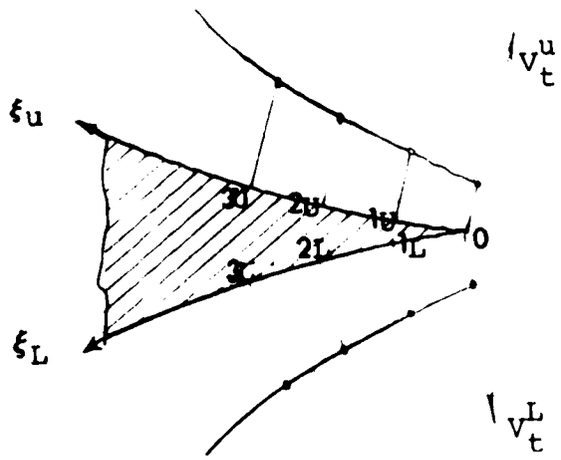

(b) cusped trailing edge

Figure 34 : Velocity extrapolation at airfoil trailing edge.

ORIGINAL PAGE IS
OF POOR QUALITY

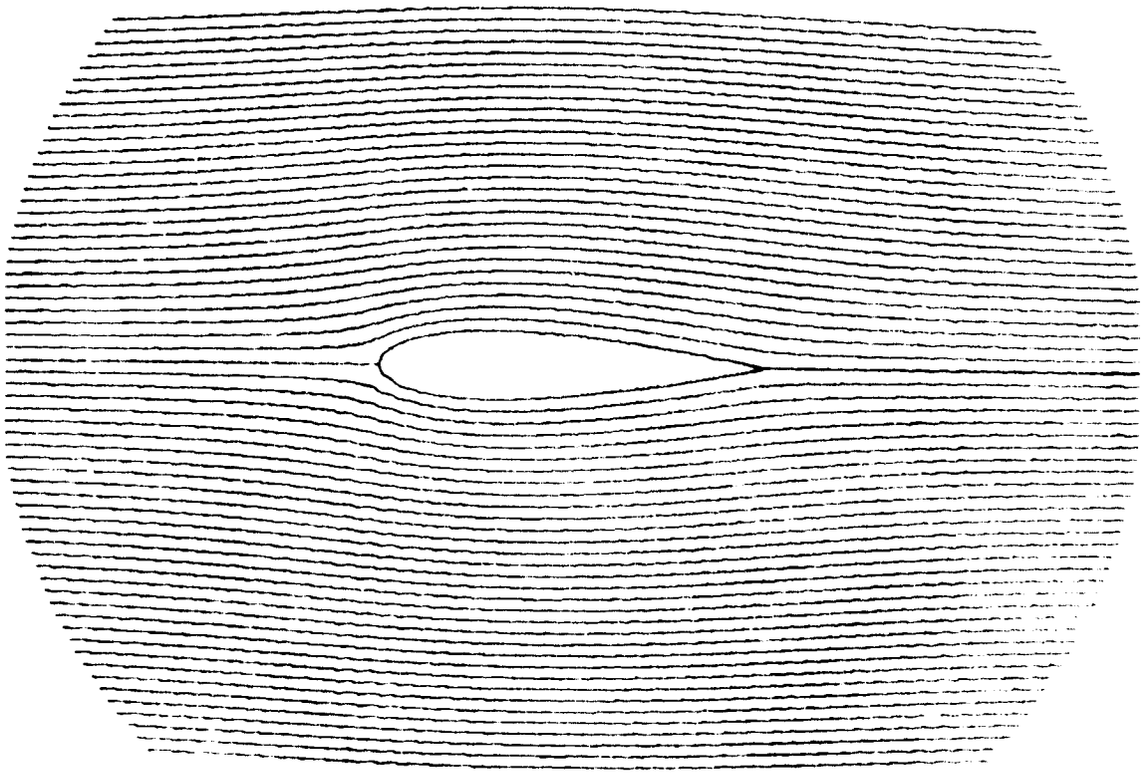

(a) 0° angle of attack

Figure 35 : Stream function of uniform potential flow over NACA-0018 airfoil, (80 x 25) .

ORIGINAL PAGE IS
OF POOR QUALITY

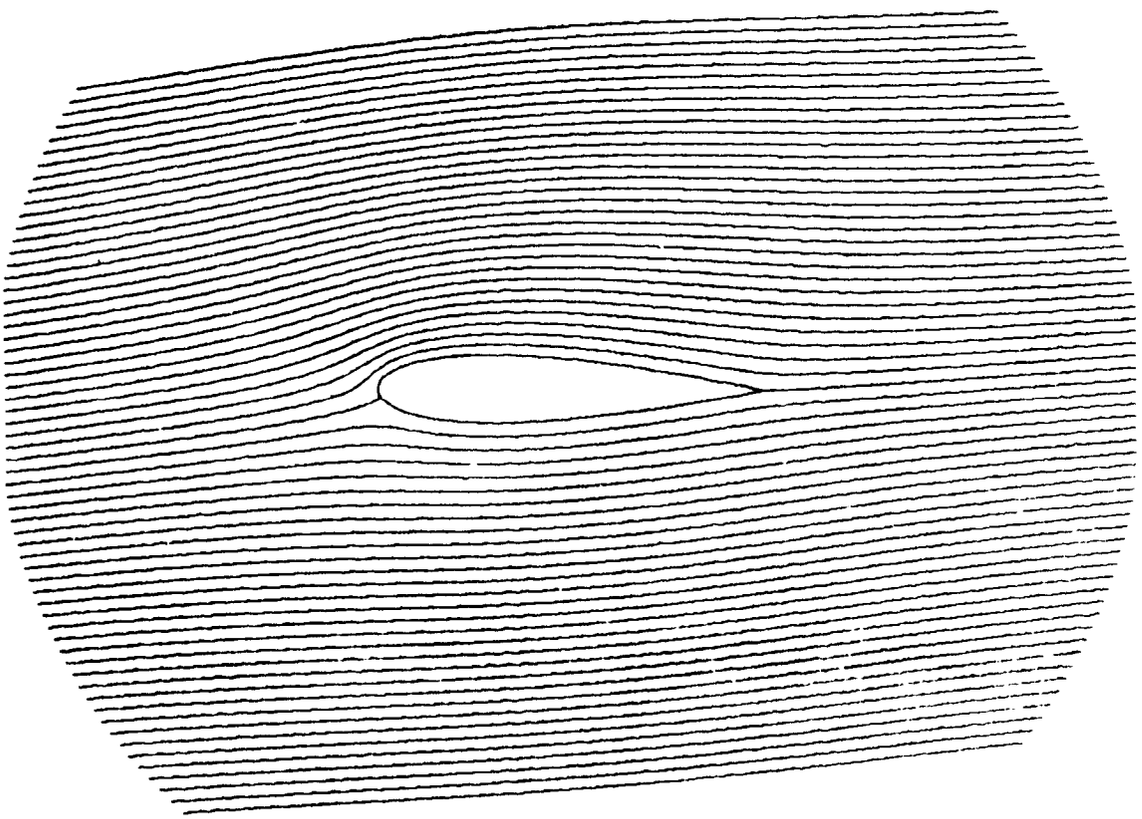

(b) 5° angle of attack

Figure 35 (cont'd)

ORIGINAL PAGE IS
OF POOR QUALITY

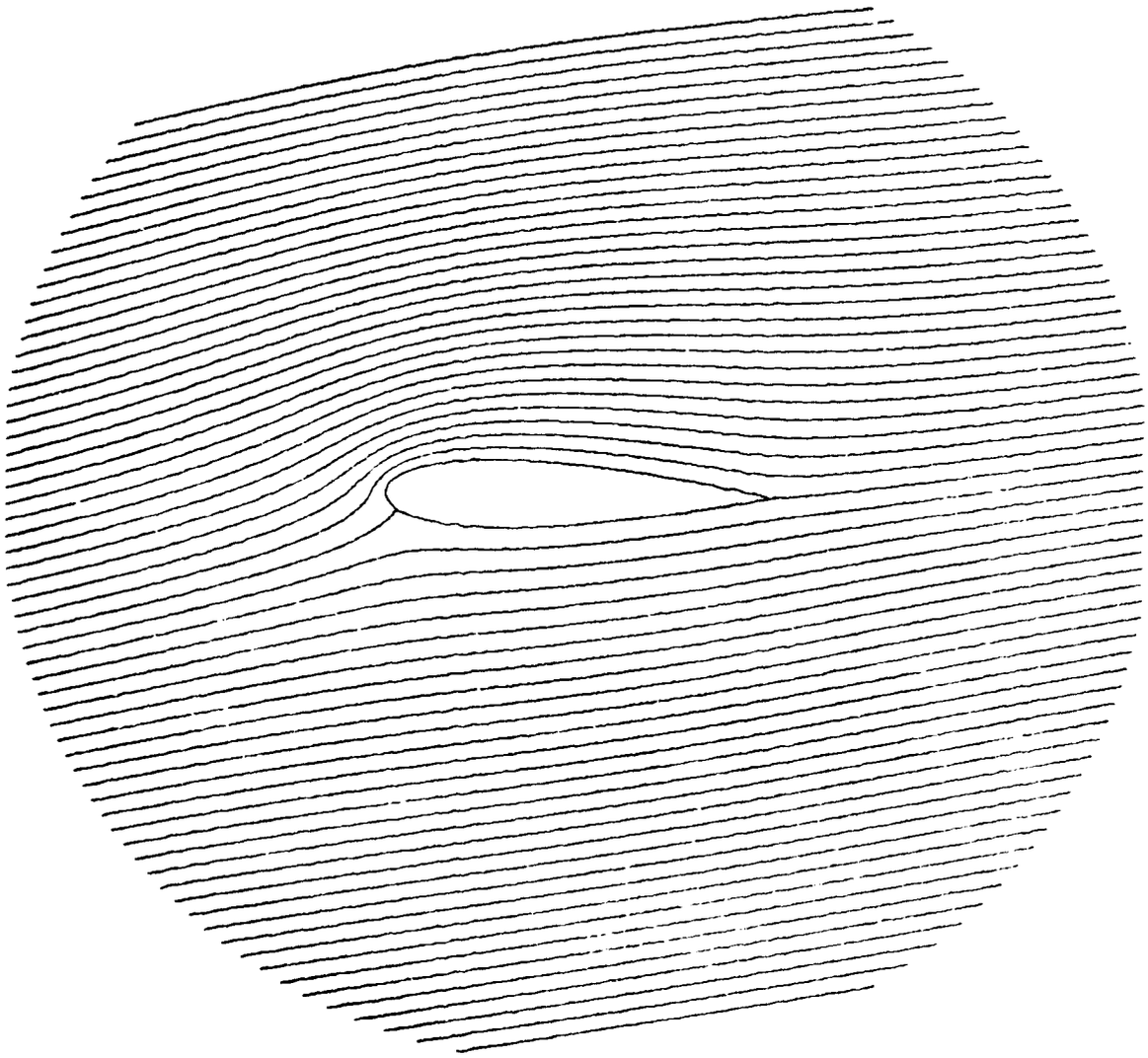

(c) 10° angle of attack

Figure 35 (cont'd)

ORIGINAL PAGE IS
OF POOR QUALITY

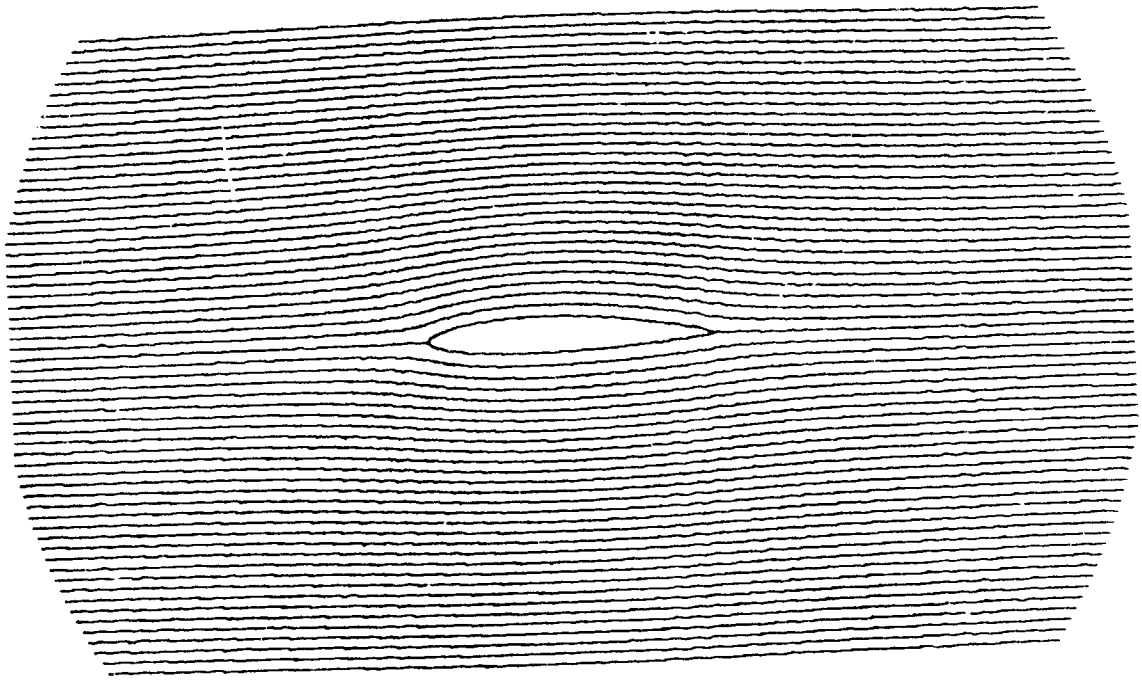

(a) 0° angle of attack

Figure 36 : Stream function of uniform potential flow over Karmann-Trefftz airfoil, (68 x 25).

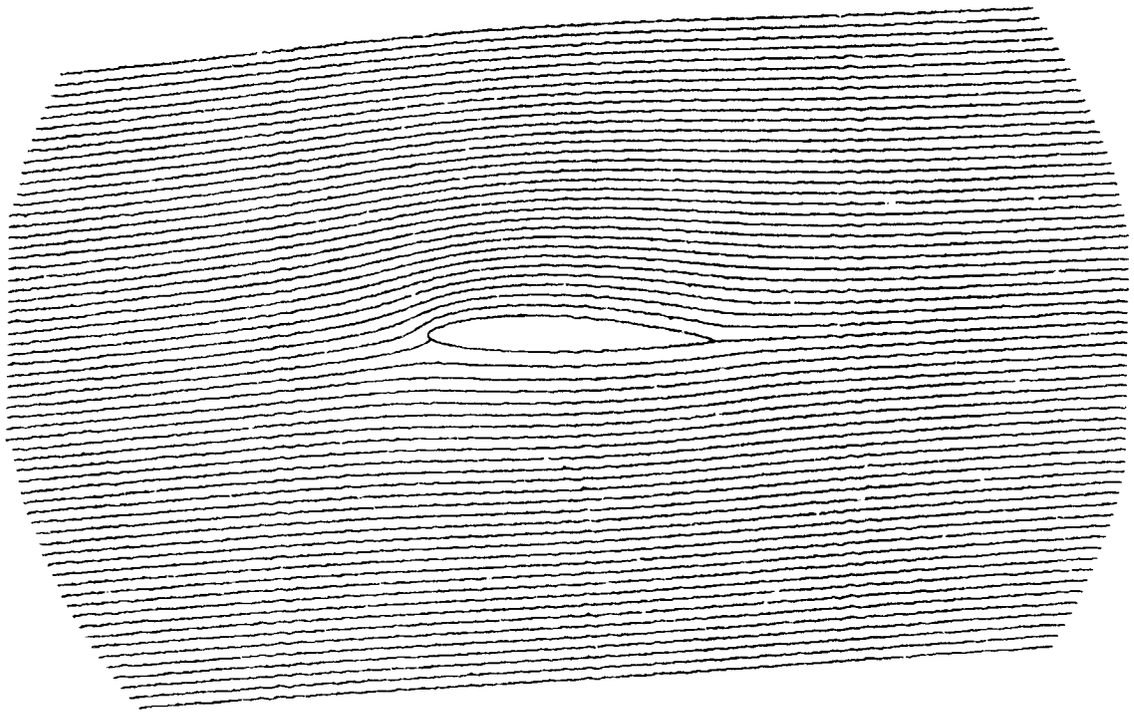

(b) 5° angle of attack

Figure 36 (cont'd)

ORIGINAL PAGE IS
OF POOR QUALITY

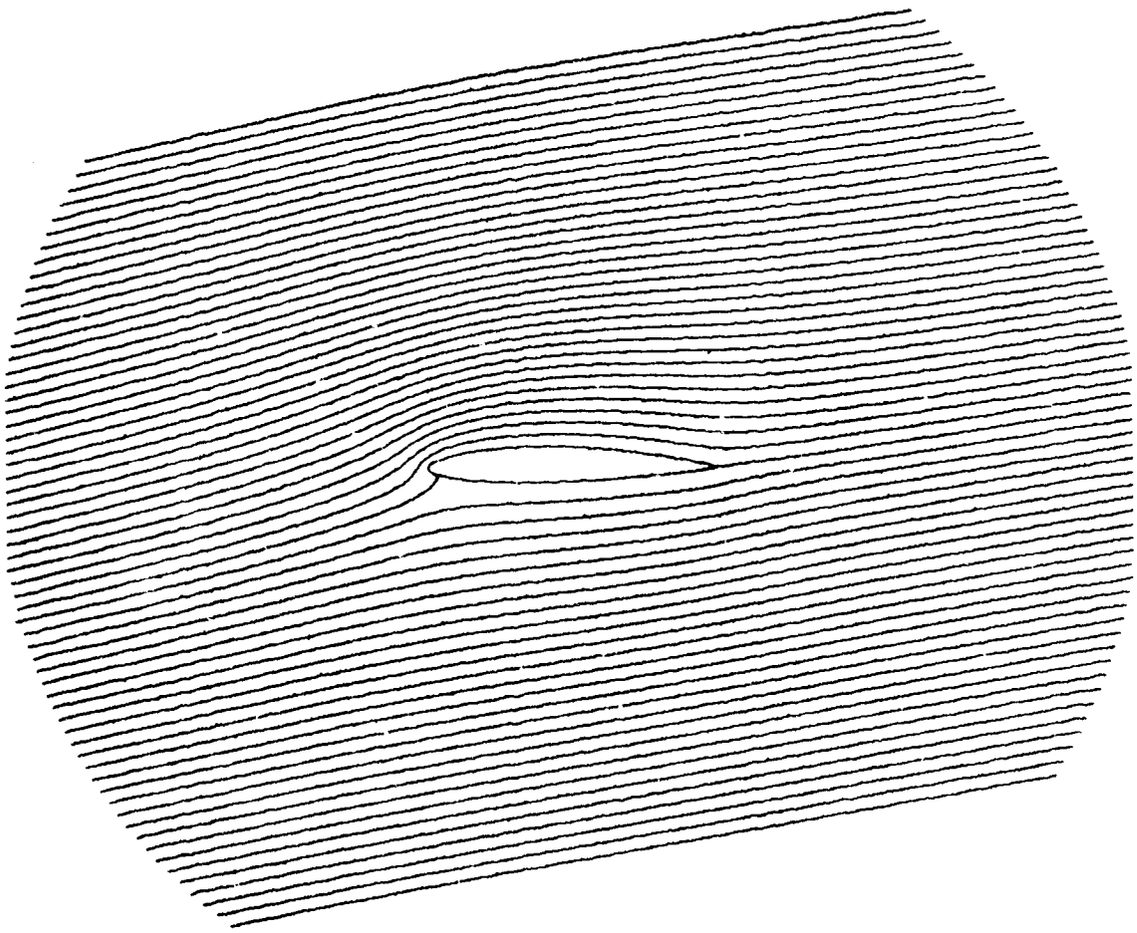

(c) 10° angle of attack

Figure 36 (cont'd)

ORIGINAL PAGE IS
OF POOR QUALITY

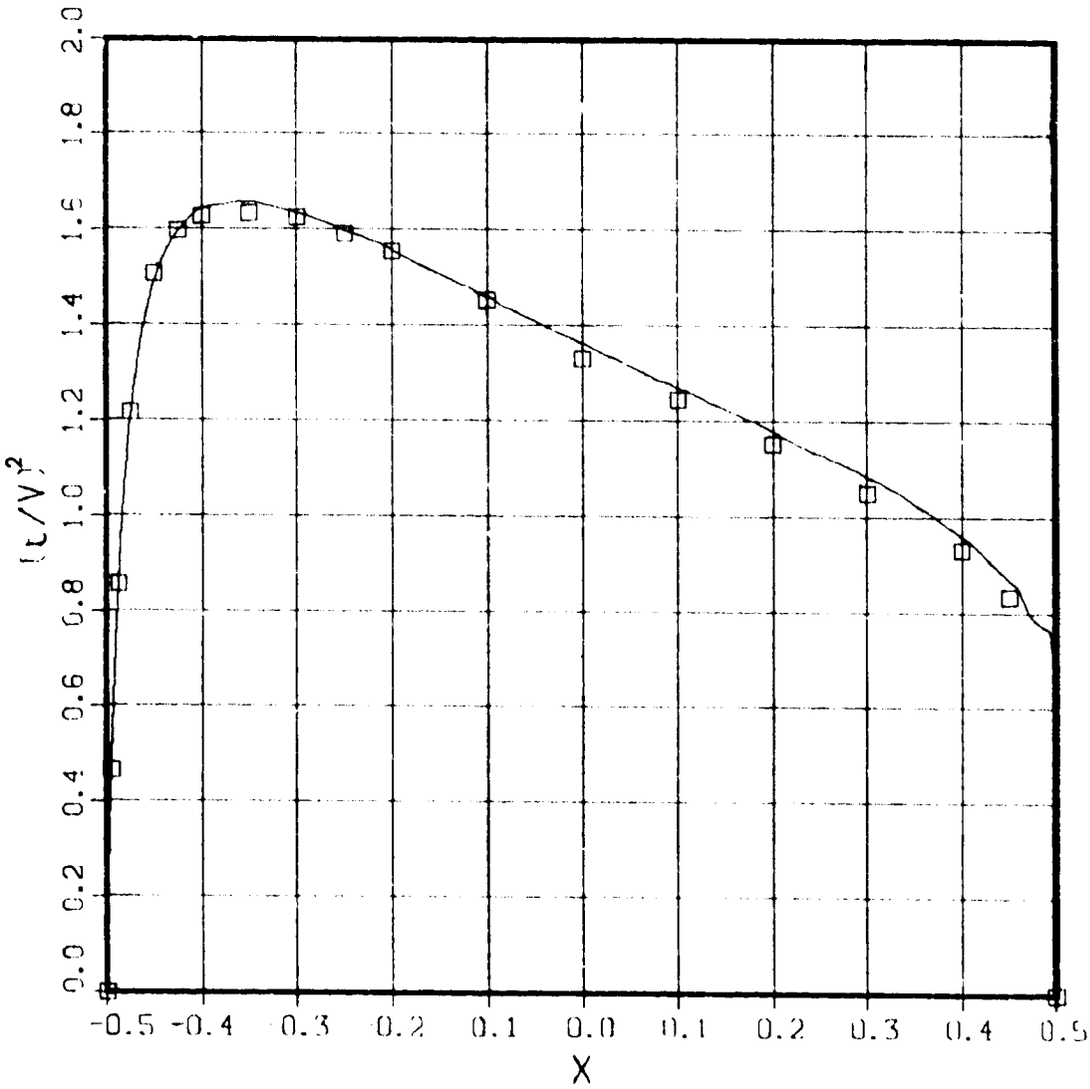

—— : measuement

□ : prediction

Figure 37 : Pressure curves of NACA-0018.

ORIGINAL PAGE IS
OF POOR QUALITY

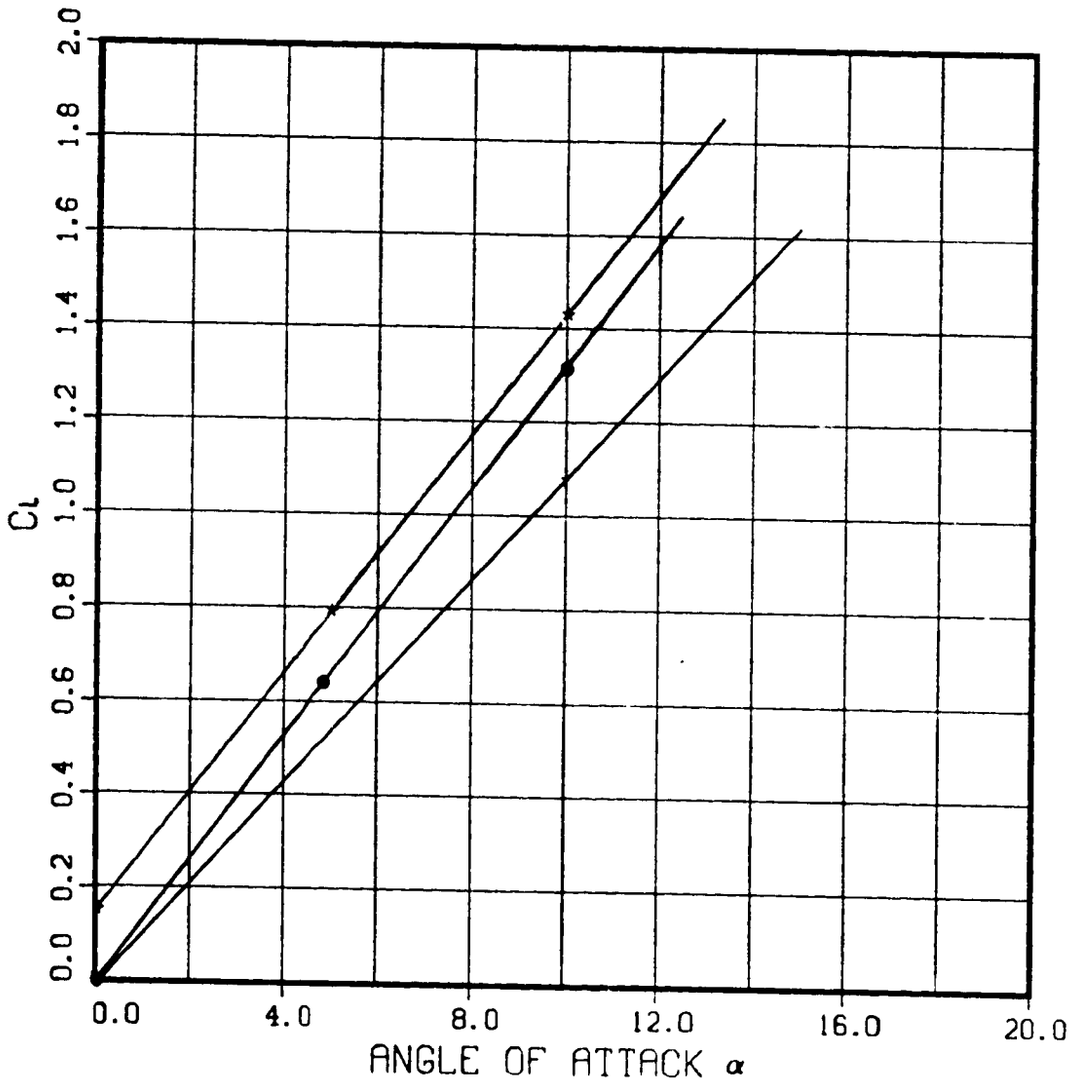

* : Karmann-Trefftz

-◆- : NACA-0018

— : thin wing theory

Figure 38 : Lift curves of NACA-0018, Karmann-Trefftz and thin wing theory.

ORIGINAL PAGE IS
OF POOR QUALITY

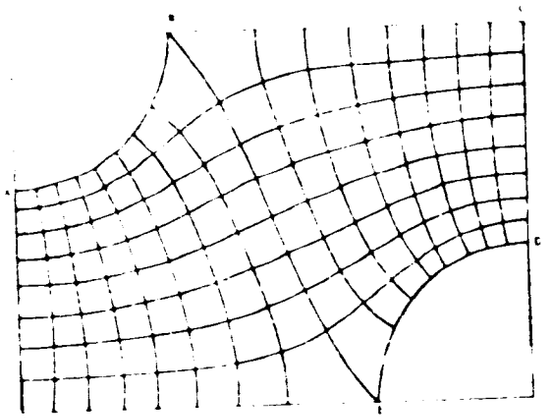

(a) Thom and Apelt

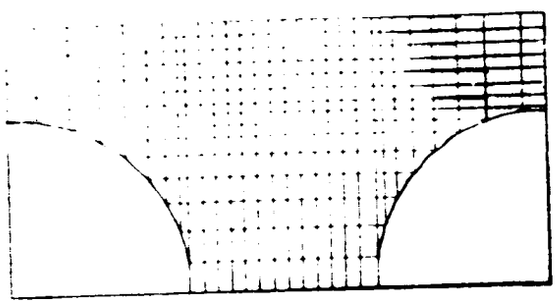

(b) Le Feuvre

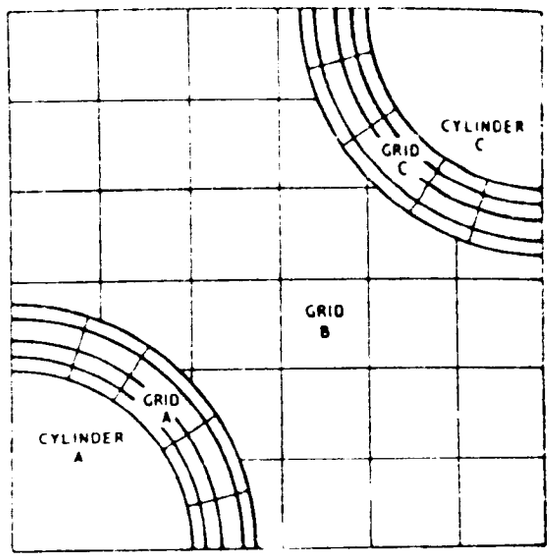

(c) Launder and Massey

Figure 39 : Possible choices of grid for finite difference studies of tube banks.

ORIGINAL PAGE IS
OF POOR QUALITY

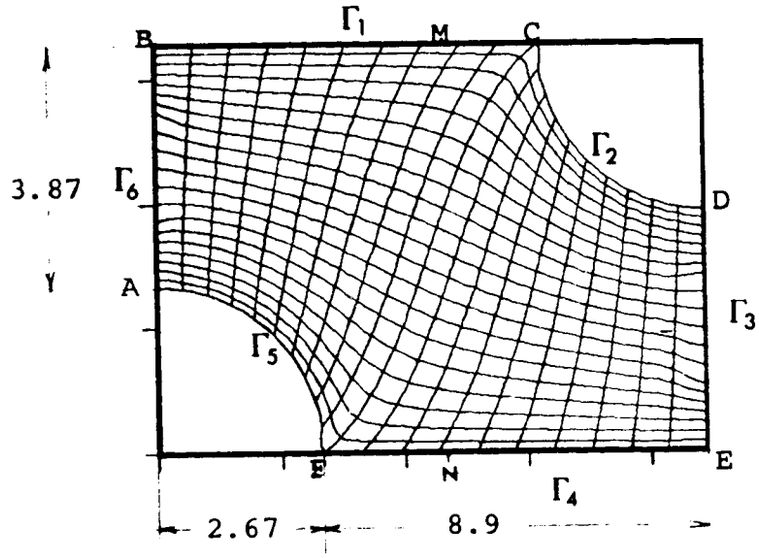

(a) physical plane

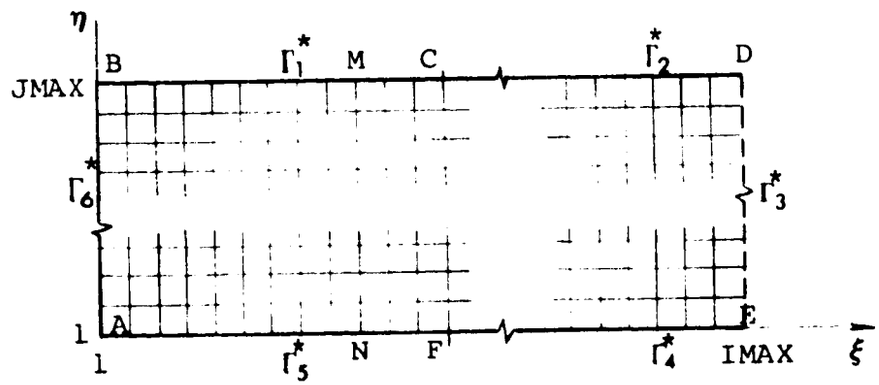

(b) transformed plane

Figure 40 : Field transformation of tube bundles flow problem.

ORIGINAL PAGE IS
OF POOR QUALITY

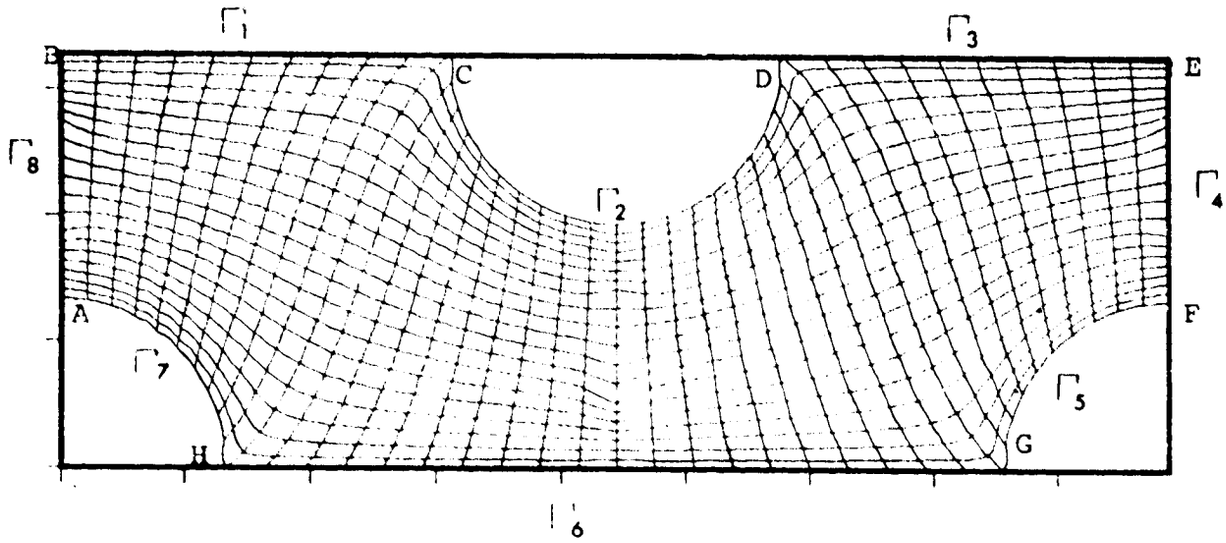

(a) physical plane

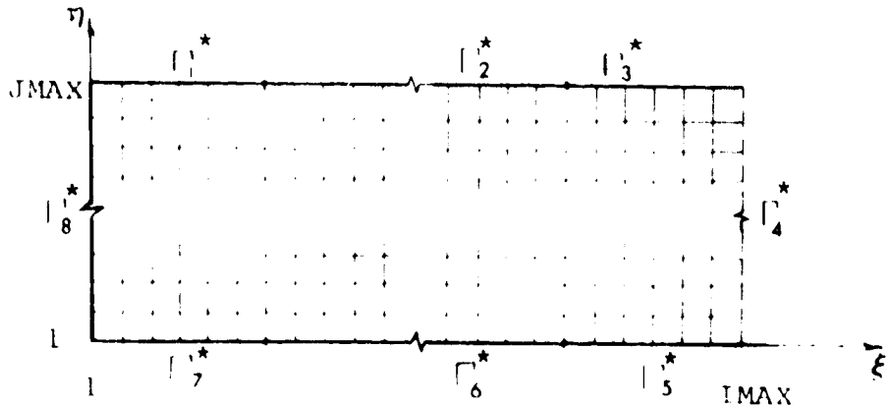

(b) transformed plane

Figure 41 : Field transformation of tube bundles for heat transfer problem.

ORIGINAL PAGE IS
OF POOR QUALITY

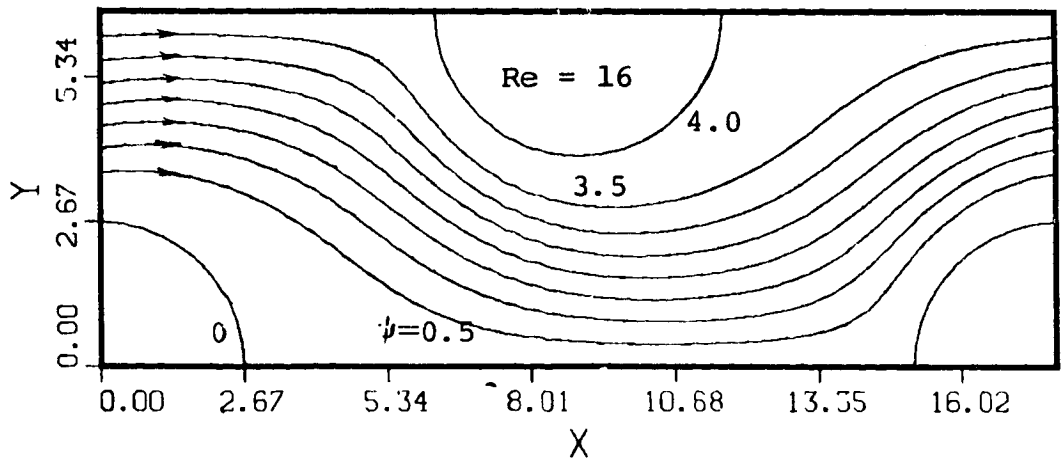

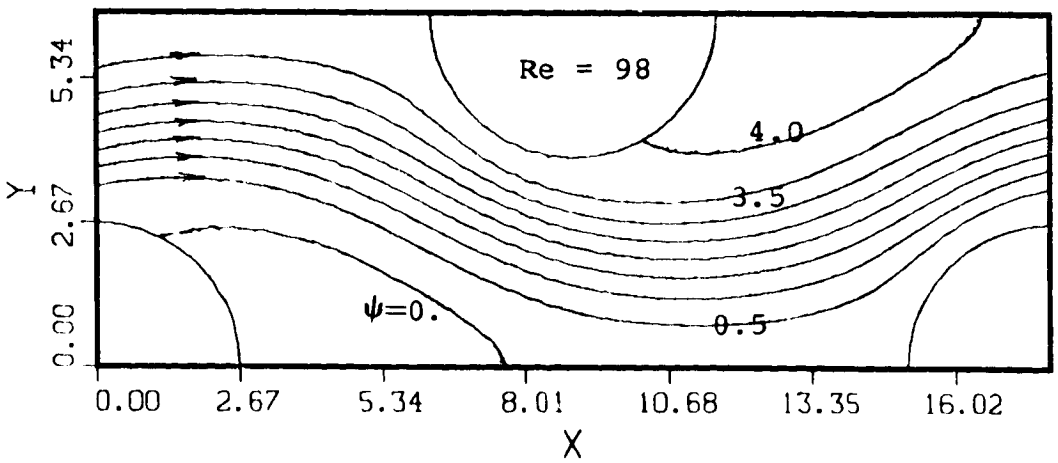

Figure 42 : Stream function of tube bundles flow.

ORIGINAL PAGE IS
OF POOR QUALITY

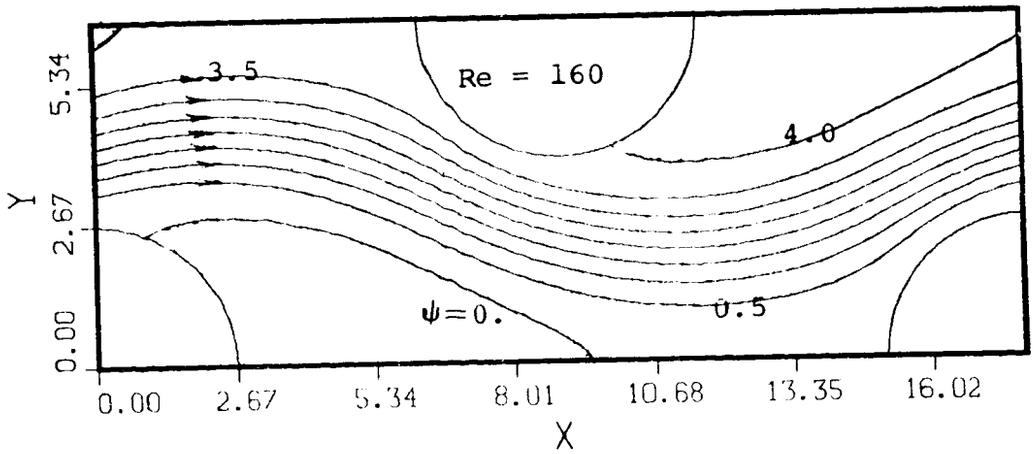

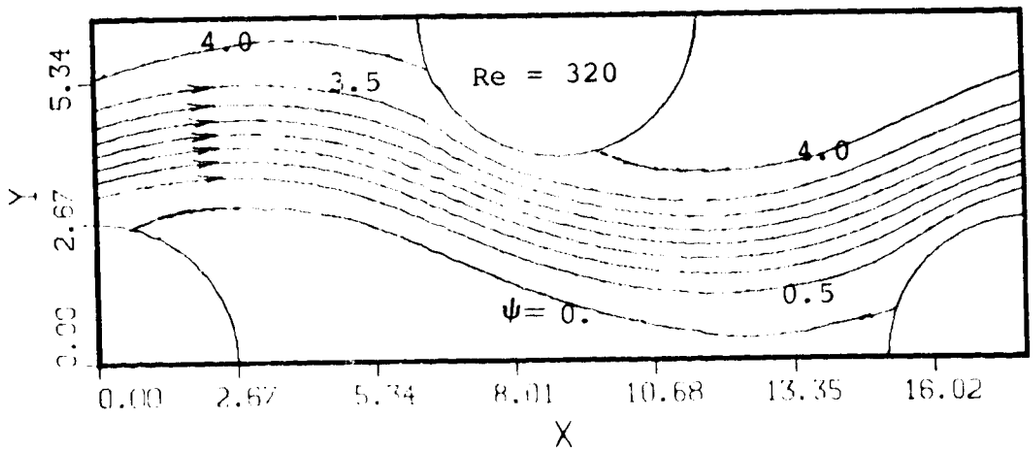

Figure 42 (cont'd)

ORIGINAL PAGE IS
OF POOR QUALITY

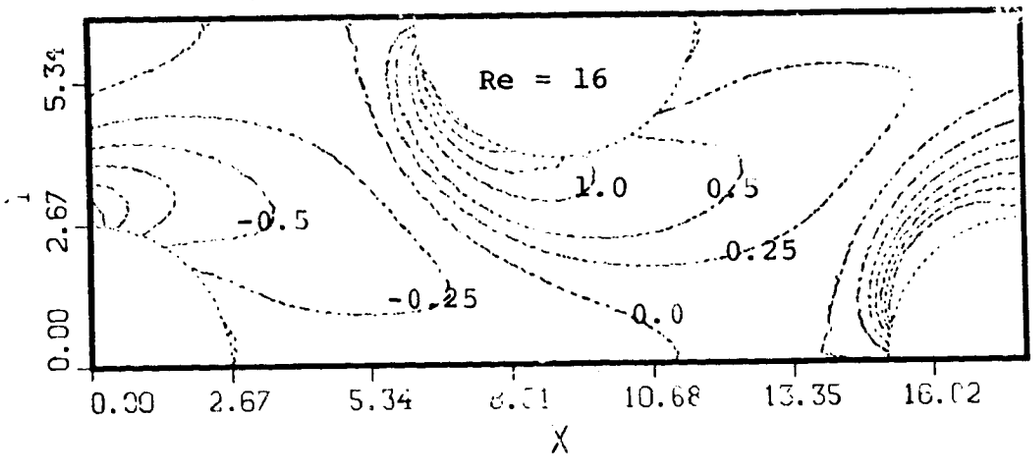

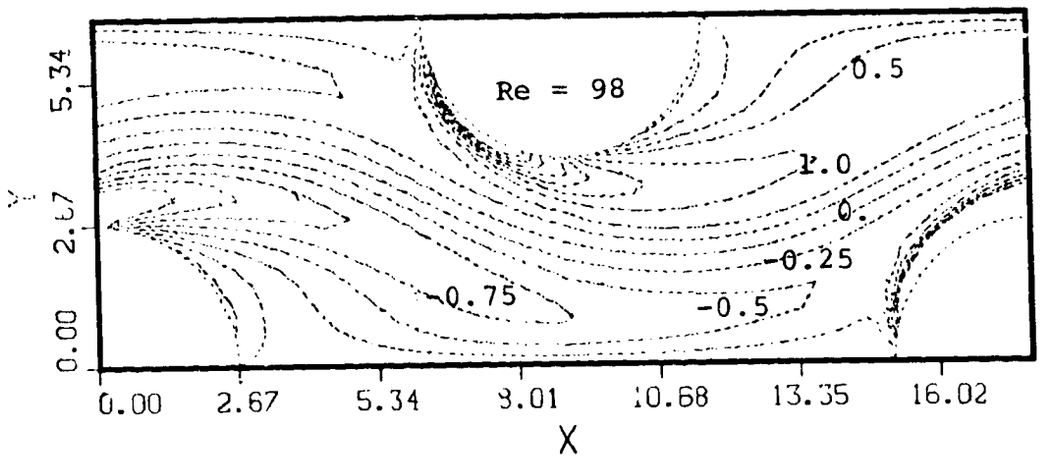

Figure 43 : Vorticity distribution of tube bundles flow.

ORIGINAL PAGE IS
OF POOR QUALITY

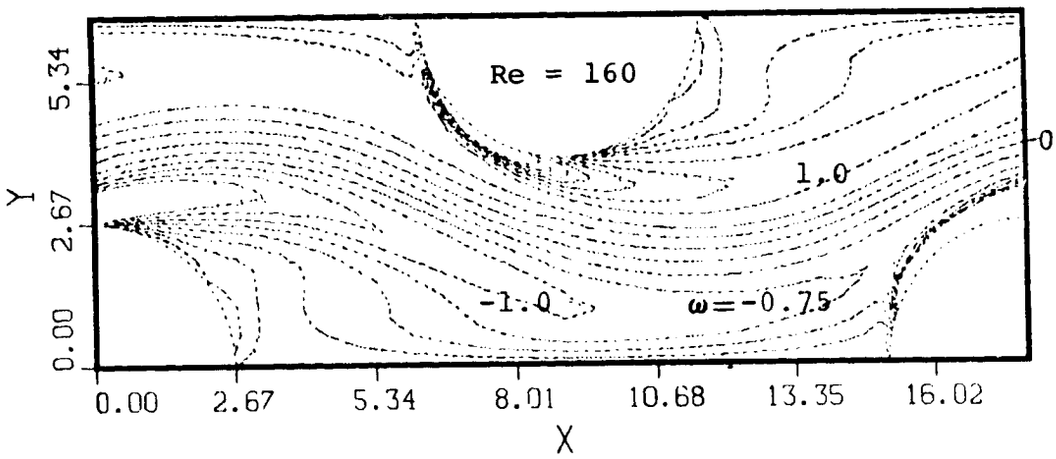

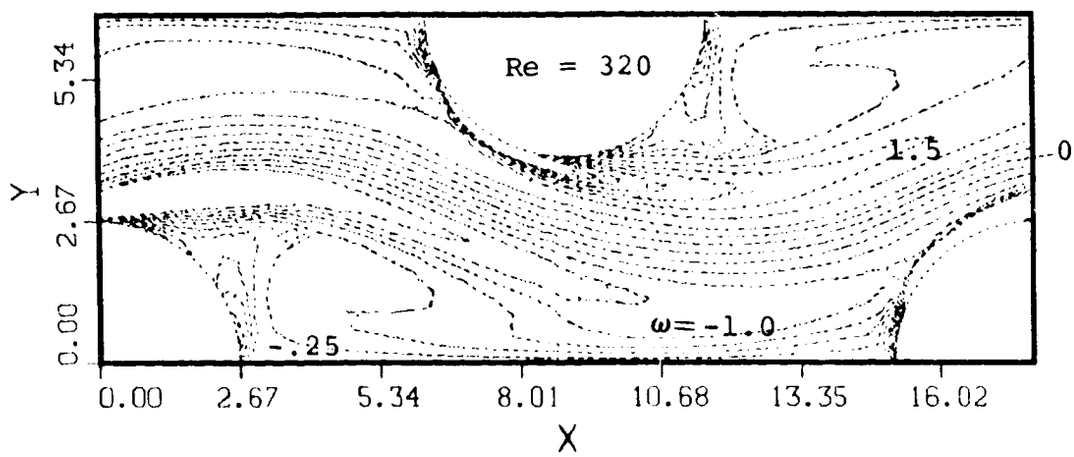

Figure 43 (cont'd)

ORIGINAL PAGE IS
OF POOR QUALITY

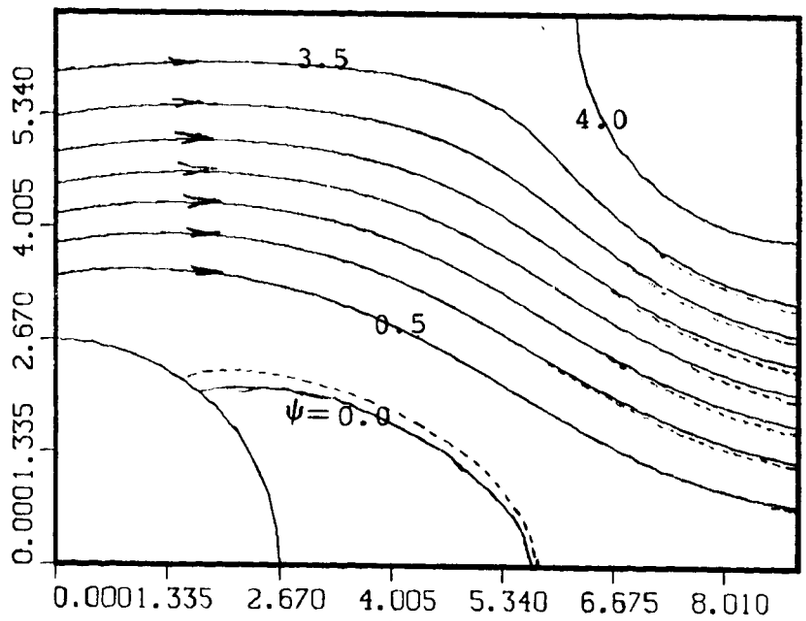

----- : Thom and Apelt

——— : present

Figure 44 : Comparison of stream function for Re_m = 50.

ORIGINAL PAGE IS
OF POOR QUALITY

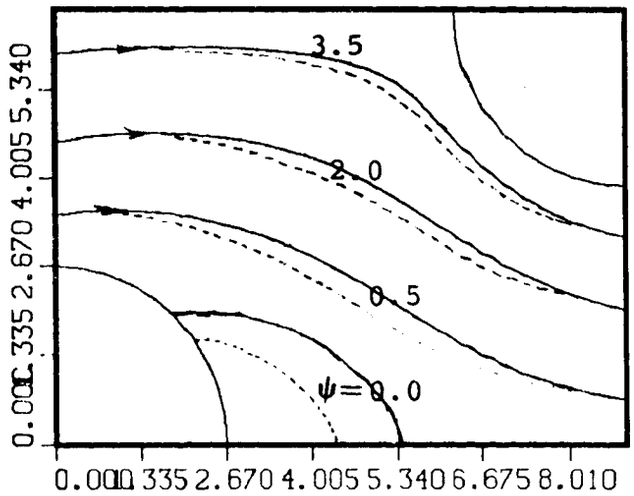

----- : Launder and Massey

——— : present

Figure 45 : Comparison of stream function for Re_m = 44.7

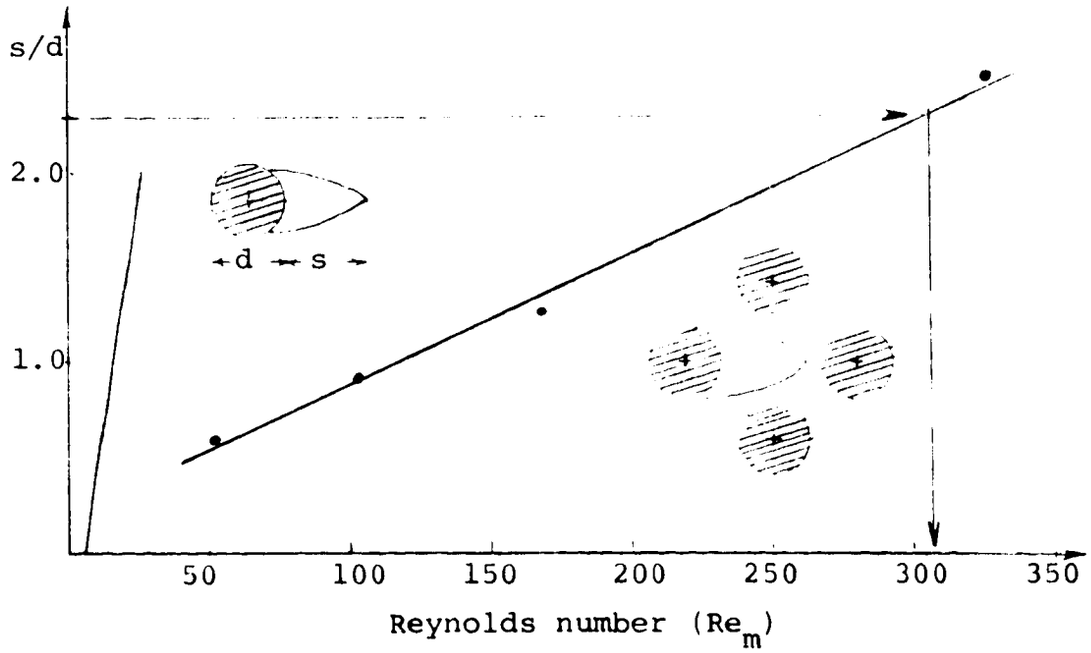

Figure 46 : Lengths of separation zone behind a tube in tube banks.

ORIGINAL PAGE IS
OF POOR QUALITY

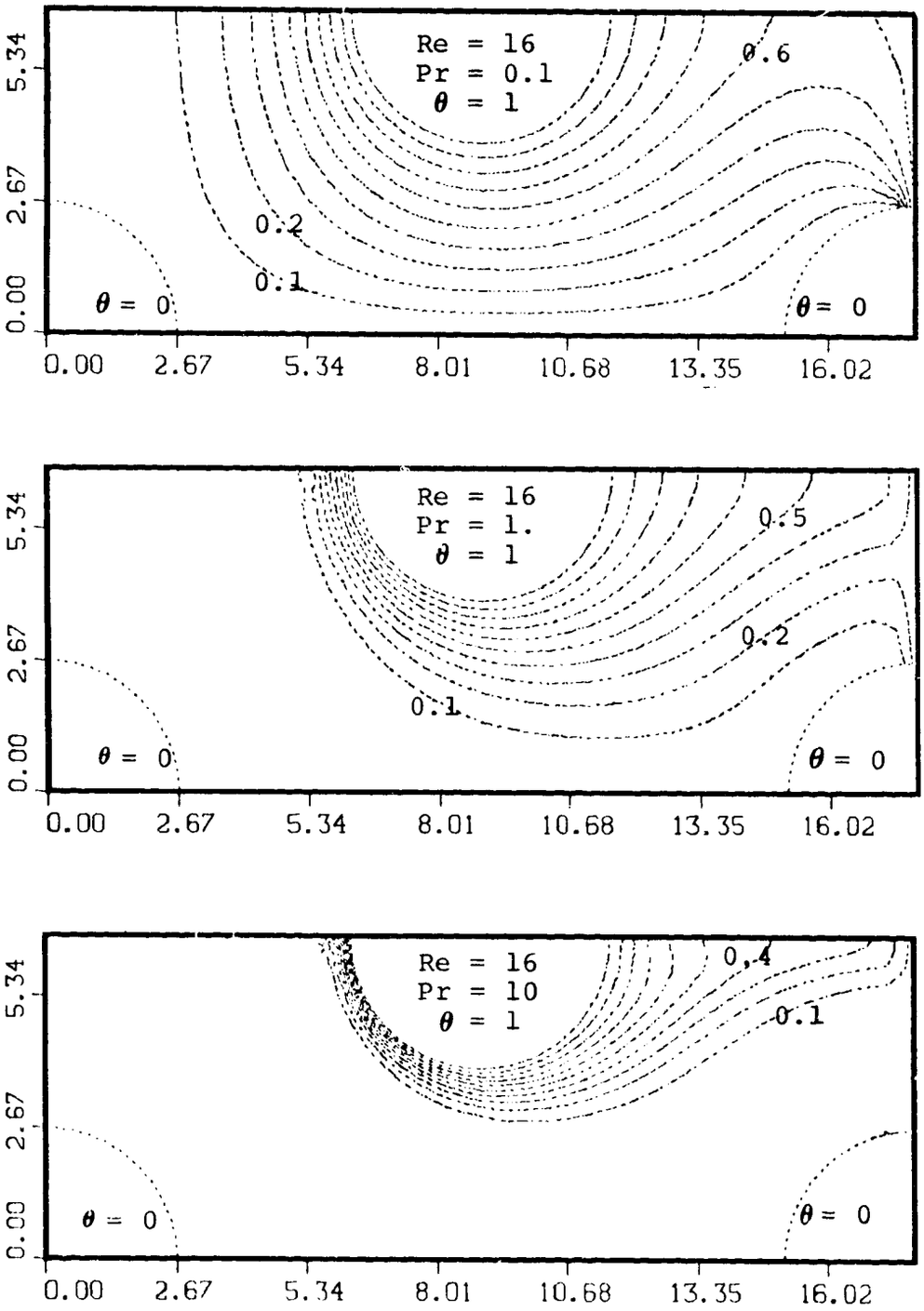

Figure 47 : Temperature distribution for Re_m = 16.

ORIGINAL PAGE IS
OF POOR QUALITY

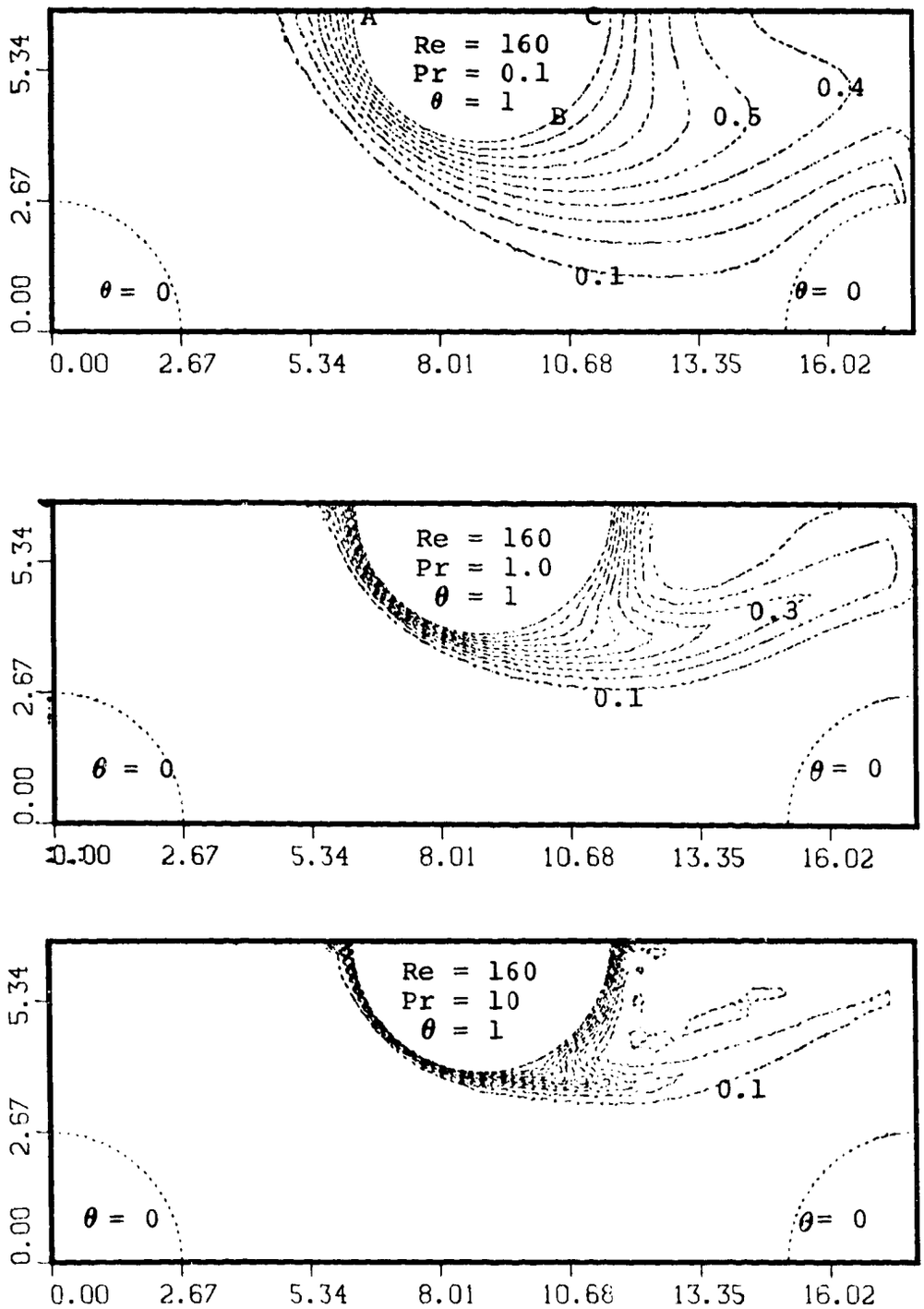

Figure 48 : Temperature distribution for $Re_m = 160$.

ORIGINAL PAGE IS
OF POOR QUALITY

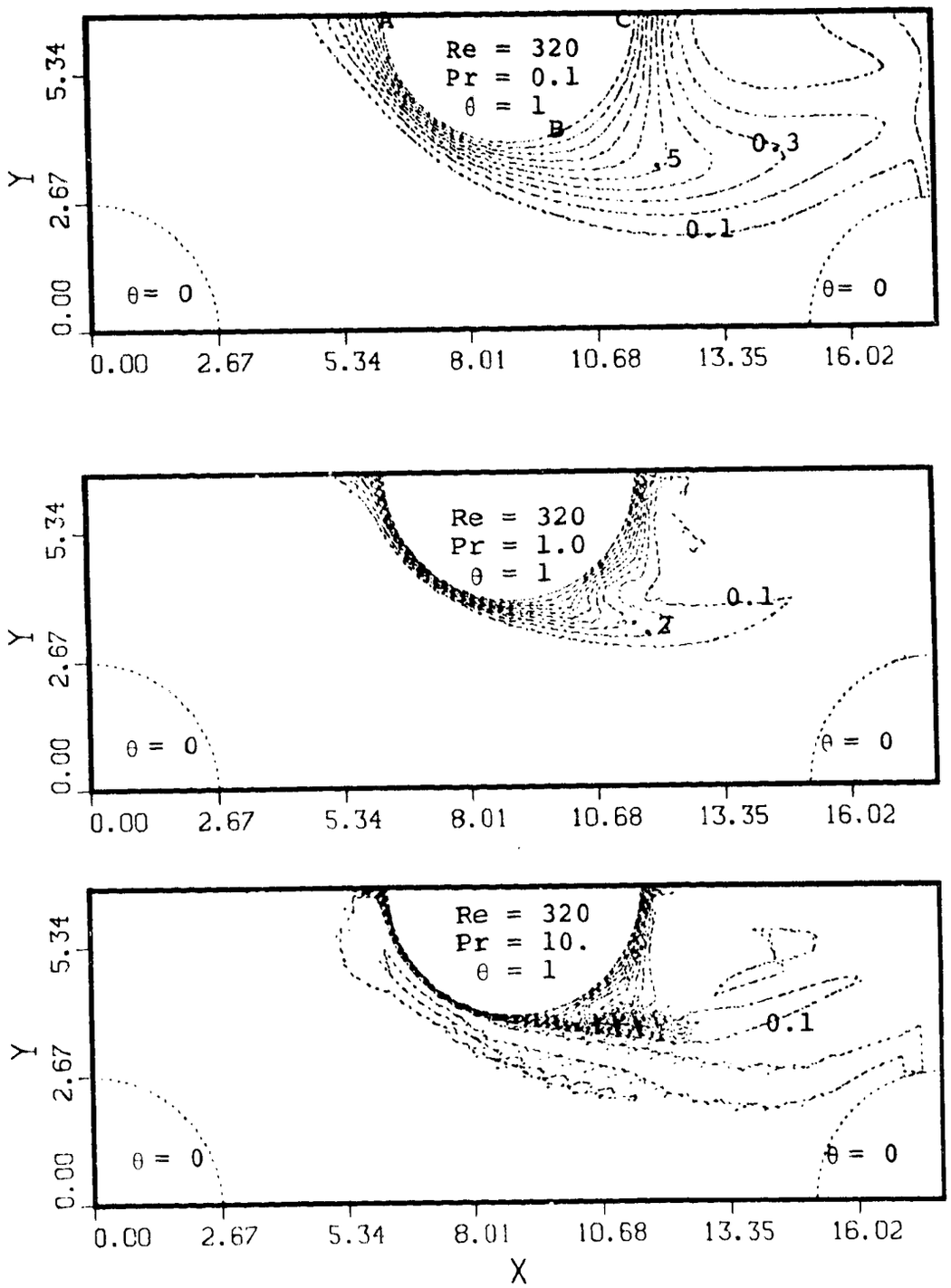

Figure 49 : Temperature distribution for Re_m = 320 .

ORIGINAL PAGE IS
OF POOR QUALITY

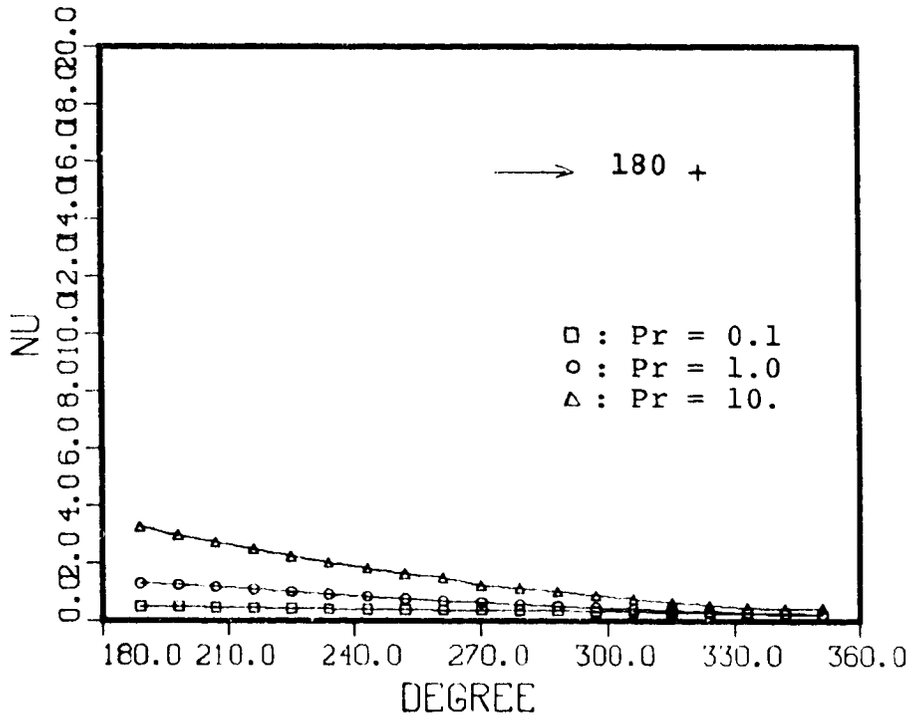

Figure 50 : Local Nusselt number of the heated tube in tube banks for $Re_m = 16$.

ORIGINAL PAGE IS
OF POOR QUALITY

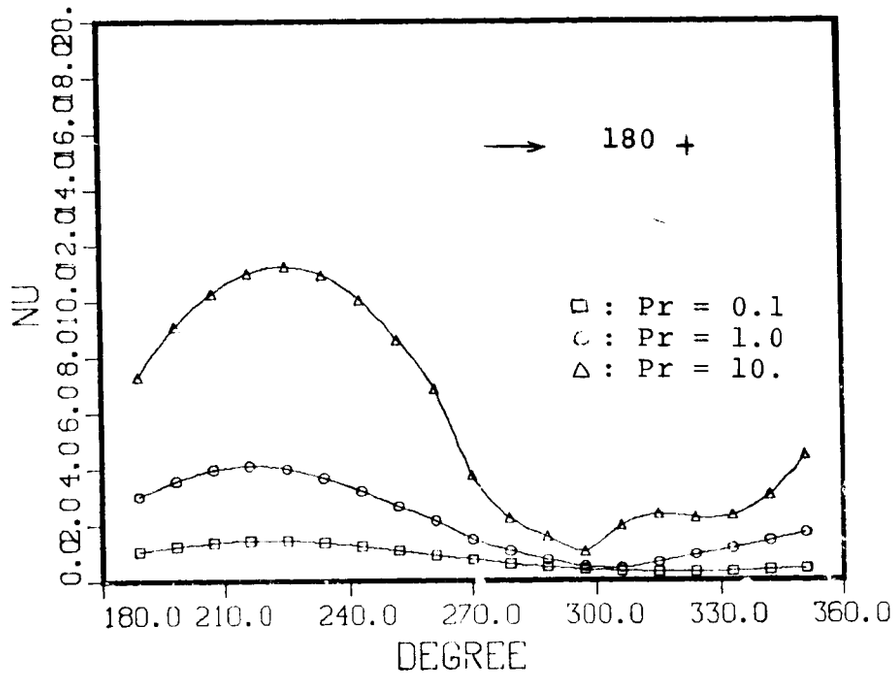

Figure 51 : Local Nusselt number of the heated tube in tube banks for Re_m = 160 .

ORIGINAL PAGE IS
OF POOR QUALITY

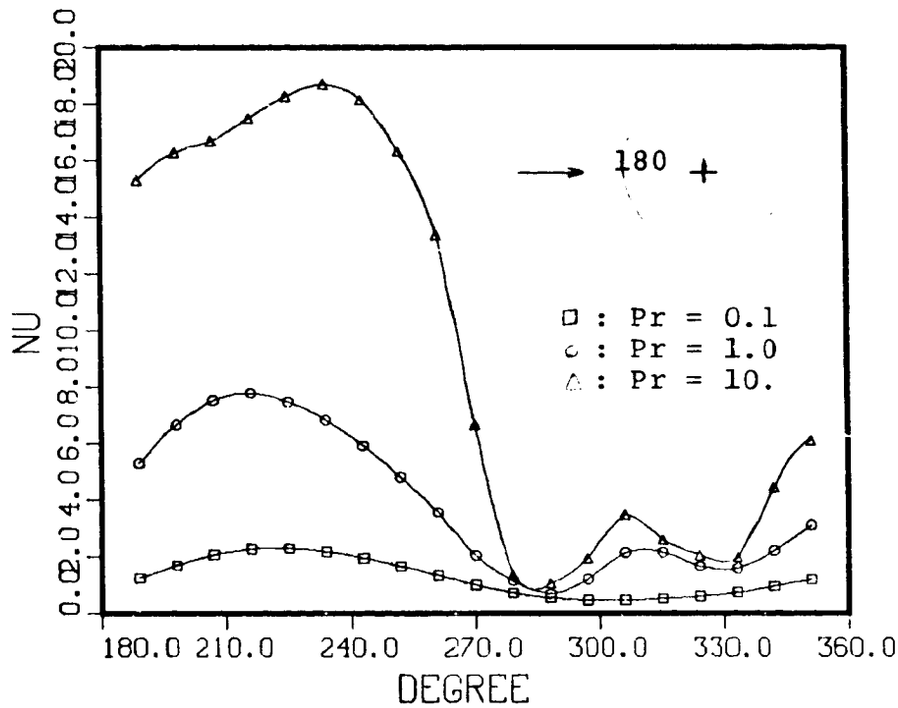

Figure 52 : Local Nusselt number of the heated tube in tube banks for $Re_m = 320$.

ORIGINAL PAGE IS
OF POOR QUALITY

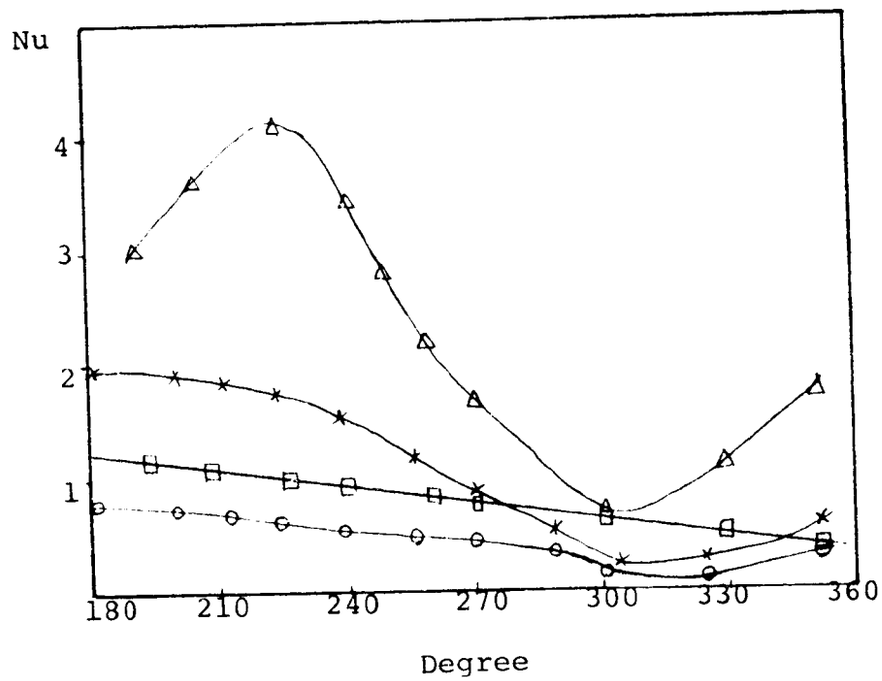

△ : Re_m = 160, Pr = 1.0, staggered tube banks.
× : Re_m = 120, gas flow, single tube [46].
□ : Re_m = 16, Pr = 1.0, staggered tube banks.
○ : Re_m = 23 , gas flow, single tube [46].

Figure 53 : Comparison of local Nusselt number of the heated tube in tube banks and in uniform flow.

PART II

Finite Analytic Numerical Solution For Two-Dimensional Incompressible Flows Over an Arbitrary Body Shape

TABLE OF CONTENTS

	Page
ACKNOWLEDGMENTS	ii
LIST OF TABLES	v
LIST OF FIGURES	vi
NOMENCLATURE	viii
CHAPTER	
I. INTRODUCTION	1
II. PRINCILPLE OF THE FINITE ANALYTIC NUMERICAL METHOD	5
III. THE BOUNDARY FITTED COORDINATE SYSTEM	11
IV. FORMULATION OF PROBLEM	20
4.1 Governing Equations	20
4.2 Boundary Conditions	21
4.3 In The Transformated Plane	25
V. PROCEDURE OF NUMERICAL SOLUTION	27
5.1 Boundary Fitted Coordinate System	27
5.2 The FA Numerical Solution In The Transformed Plane	31
VI. FLOW AROUND A CIRCULAR CYLINDER	35
6.1 Phenomenan of Vortex Shedding	35
6.2 Numerical Results at C-type Outer Boundary	38
6.3 Numerical Results at OC-type Outer Boundary	52
VII. VORTEX SHEDDING BEHIND THE NONCIRCULAR BODY SHAPE	70

PRECEDING PAGE BLANK NOT FILMED

7.1 Flow Over A Triangle Column 70
7.2 Flow Over An Irregular Body Shape 72

VIII. CONCLUSIONS AND SUGGESTIONS 88

REFERENCES 92

APPENDIX A. FINITE ANALYTIC SOLUTION OF TWO DIMENSIONAL ELLIPTIC PARTIAL DIFFERENTIAL EQUATION . 95

APPENDIX B. RELATIONSHIPS BETWEEN PHYSICAL AND TRANSFORMED PLANE 111

APPENDIX C. CONTOUR PLOT 115

APPENDIX D. COMPUTER PROGRAM 122

LIST OF TABLES

Table		Page
5-1	Flow Chart of Boundary Fitted Coordinate System	29
5-2	Flow Chart of Concentration Values of P & Q	30
5-3	Flow Chart of FA Numerical Method	33
A-1	Comparison of FA and FAP Coefficients	110
C-1	Flow Chart of Contour Plot	120

LIST OF FIGURES

Figure		Page
2-1	Typical local element	6
3-1	'C-type' outer boundary	12
3-2	'OC-type' outer boundary	12
3-3	Laplace equation	16
3-4	Poisson equation	17
4-1	'C-type' outer boundary	22
4-2	'OC-type' outer boundary	22
6-1	Regimes of fluid flow across circular cylinders	36
6-2	Small element	39
6-3	Potential flow	41
6-4	Re=5	41
6-5	Re=40	43
6-6	Observed lengths of the region of closed stream-lines behind a circular cylinder	43
6-7	Comparison between numerical calculations and measurements	44
6-8	Re=100 (Stream line)	45
6-9	Re=100 (Vorticity function)	46
6-10	The Strouhal-Reynolds number relationship for circular cylinder	48
6-11	Re=500 (Stream line)	49

6-12 Re=500 (Vorticity function) 50

6-13 Re=100 (Stream line) 55

6-14 Re=100 (Vorticity function) 56

6-15 Computational domain of 'OC-type' boundary fitted coordinates 57

6-16 Potential flow 57

6-17 Re=5 58

6-18 Re=40 59

6-19 Re=100 (Stream line) 60

6-20 Re=100 (Vorticity function) 64

7-1 Computational domain of a triangle body 71

7-2 Potential flow 71

7-3 Re=200 (Stream line) 73

7-4 Re=200 (Vorticity function) 75

7-5 Computational domain of an arbitrary body 77

7-6 Potential flow 77

7-7 Re=5 79

7-8 Re=40 (Stream line) 80

7-9 Re=40 (Vorticity function) 81

7-10 Re=100 (Stream line) 82

7-11 Re=100 (Vorticity function) 85

C-1 Contour of $\phi(\xi_i,\eta_j)$ 116

C-2 Simple grid in set D* 116

C-6 Local coordinate system for triangle 116

C-4 Interpolation for x and y 121

NOMENCLATURE

a_{sub}, b_{sub}, c_{sub}	(sub = E, W, N, S - 4 sides) coefficients used in boundary approximations for the Ellipitic partial differential equation.
C_{sub}	(sub - ne, ne, sw, etc. (eight nodal points) FA coefficients.
f	General function of ξ,η and t.
FA	Finite Analytic.
FD	Finite Difference.
h	Dimensionless grid spacing in the ξ-direction.
J	Jacobian determinate, Equation (B-8).
K	Dimensionless grid spacing in the η-direction.
L	Partial differential operator.
n,m	Index in series summation (=1,2,3,....,).
p	Center node of an FA element.
$P(\xi,\eta)$	ξ-line attraction function.
$Q(\xi,\eta)$	η-line attraction function.
Re	Reynold number based on chord length.
U	Dimension-less velocity component parallel to x-axis.

U_0	Reference velocity.
V	Dimensionless velocity component parrel to y-axis.
x	Physical cartesian coordinate.
y	Physical cartesian coordinate.

Greek Symbols

α	Coordinate transformation parameter, Equation (B-1).
β	Coordinate transformation parameter, Equation (B-2).
γ	Coordinate transformation parameter, Equation (B-3).
Γ_i	i^{th} contour in physical plane.
Γ_i^*	Contour in Transformed plane. corresponding to Γ_i.
η	Transformed coordinate.
ξ	Transformed coordinate.
σ	Coordinate transformation parameter, Equation (B-6).
τ	Coordinate transformation parameter, Equation (B-7).
ν	Kinematic viscosity.
ω	Vorticity.
μ, λ	Eigenvalues.

ϕ	Independent variable of a partial differential equation.
ψ	Stream function.
∇^2	Laplacian.

Subscripts

E	East boundary.
EC	East Central.
i,j	Nodal point location in the flow.
N	North boundary.
NC	North Central.
NE	North Eastern.
NW	North Western.
P	Values evaluated at the center node of an FA element.
S	South boundary.
SC	South Central.
SE	South Eastern.
SW	South Western.
W	West Central.
WC	West Central.
x	Derivative in the x-direction.
y	Derivative in the y-direction.
ξ	Derivative in the ξ-direction.
η	Derivative in the η-direction.

CHAPTER I

INTRODUCTION

This study applies the finite analytic (FA) method [1,2,3] to obtain the numerical solution of a uniform flow past a two dimensional obstacle of arbitrary shape. The fluid is assumed to be incompressible with constant viscosity. In order to solve the flow over an arbitrary body shape, the boundary fitted coordinate system [4,5,6,7] is adapted. This coordinate system transforms a physically complex geometry into a simple geometry on a transformed plane where an accurate numerical solution can be obtained by the finite analytic method. Furthermore in this study the finite analytic method is modified and improved.

Vortex formation behind bluff bodies is an important phenomena in fluid flows. Since von Karman (1912) elucidated theoretically the vortex street phenomena that formed far behind a body, numerous reports have been published [8,9,10,11,12] on theoretical and experimental aspects of the vortex street. However, theoretical analysis of viscous vortex shedding immediately behind the obstacle are not available. Because of computional difficulty the first numerical solution of stationary vortex formation

behind the cylinder was not obtained until Thom(1928), who was able to solve numerically for flow around a circular cylinder at a low Reynolds number Re=10. Later, Thom(1933) improved his numerical method and obtained a solution at Re=20. Kawaguti (1953) and Apelt(1961) used slightly modified versions of Thom's method to carry out calculations at Re=40. All these numerical studies at low Reynolds numbers produce only steady separation flow behind the circular cylinder. Experimentally, the flow pattern begins to oscillate behind a circular cylinder if the Reynolds number is greater than 40. Because of numerical difficulty in predicting the oscillating phenomena of vortex shedding, there are few published numerical solution of vortex shedding behind a circular cylinder which agree exactly with available experimental results to date. Examing the previous numerical studies, one finds that there are two major difficulties. The first difficulty comes from the nonlinear behavior of Navier-Stokes equations at high Reynolds number, which causes the numerical solution either to become unstable or inaccurate. The second difficulty is the numerical error associated in approximating the boundary geometry, especially for a complex non-linear boundary such as a circular cylinder. One may choose small grid size and small time step to reduce the error, but it demands too much computational time and storage to be economical and practical.

In order to tackle these two difficulties, following remedies are considered. The first one is to consider a numerical method which is more accurate and efficient in solving the Navier-Stokes equations at high Reynolds number. In this regard, the recently developed finite analytic (FA) method is adapted in this study. The FA method was introduced by Chen and Li [1], and was further developed by Chen, Naseri and Ho [2], Chen and Chen [3]. The basic idea of the FA method is to incorporate the local analytic solution of the governing partial differential equation in obtaining the numerical solution of the problem. More detail on the FA method is discussed in Chapter 2. The second means of resolving the computational difficulty in predicting the flow over an arbitrary shape body is to adapt the boundary fitted coordinate system which was introduced by Thompson, Thames and Mastin [4]. The integration of the FA method and the boundary fitted coordinate system represents a new approach in solving a vortex shedding phenomena behind an arbitrary body shape. More detail on the boundary fitted coordinate system is discussed in Chapter 3.

The two dimensional incompressible Navier-Stokes equations may be conveniently written in the stream function and vorticity form, because in this form one only has to solve two unknowns -- vorticity ω and stream function ψ. Thus in the present study the Navier-Stokes equations in the

stream function and vorticity form is numerically solved on the boundary fitted coordinates for flows past an obstacle of arbitrary shape body.

Chapter 5 describes the numerical procedures used in this study. In Chapter 6 the flow around a circular cylinder is predicted by the FA method with three different boundary fitted coordinates. Experimental data and several previous numerical investigations are compared with the FA solution. Once the FA solution for flow around a circular cylinder for the laminar range of Reynolds numbers is shown to agree well with the previous experimental data, flows past other shape body can be solved in the same way. In Chapter 7 two problems are considered. The first is the flow past a two dimensional triangle column with vertex facing the incoming flow. The second is the flow past a two dimensional complex irregular shape body. Conclusions of the present study and suggestions for the further work are given in Chapter 8.

CHAPTER II

PRINCIPLE OF THE FINITE ANALYTIC NUMERICAL METHOD

The basic idea of the FA method is the incorporation of analytic solutions in obtaining the numerical solutions of partial differential equations. To illustrate the basic principle of the FA method we consider a partial differential equation (PDE) $L\phi = f$. Where L is a linear or nonlinear partial differential operator and f is an inhomogeneous term that depends on the independent variables, such as x, y and t. The PDE is to be numerically solved with proper boundary and initial conditions. In the FA method the problem is first subdivided into small elements. For example, a typical local element in a given time interval $\Delta t = t^k - t^{k-1}$ is shown in Fig.2-1 where a node P(i,j) at given time t^k or t^{k-1} are surrounded by neighboring node points EC(east center), WC(west center), SC(south center), NC(north center), NE(northeast), NW(northwest), SE(southeast), and SW(southwest), which also correspond to points (i+1,j), (i-1,j), (i,j-1), (i,j+1), (i+1,j+1), (i-1,j+1), (i+1,j-1) and (i-1,j-1) respectively. Once the problem is subdivided into small elements,

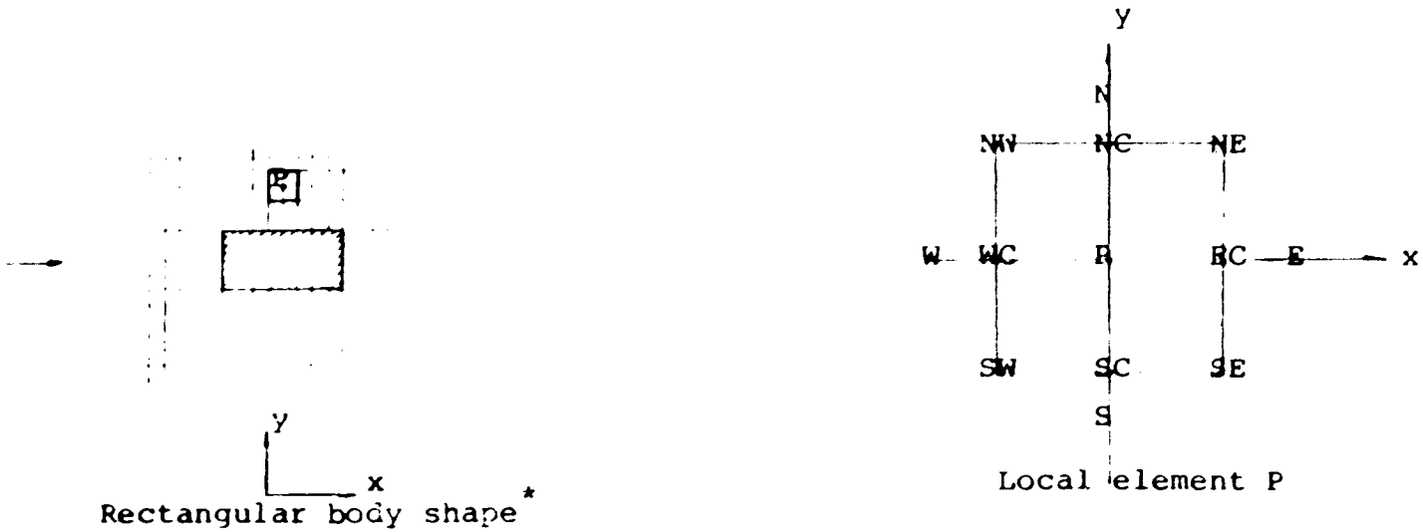

Fig. 2-1 Typical local element

*In this chapter a rectangular body in Cartesian coordinate system is choosen to illustrate the basic idea of FA method. The use of boundary fitted coordinate system will be discussed in the next chapter.

ORIGINAL PAGE IS
OF POOR QUALITY

ORIGINAL PAGE IS
OF POOR QUALITY

an analytic solution for the PDE in each element may be obtained.

In case when the PDE is nonlinear, such as Navier-Stokes equations, the nonlinear equation may be locally linearized in the element. In this fashion the overall nonlinear effect can still be approximately preserved by assembly of local analytic solutions. For example, we consider the incompressible two dimensional Nacier-Stokes equations cast in the dimensionless stream function and vorticity formulation.

$$Re(\omega_t+U\omega_x+V\omega_y)-(\omega_{xx}+\omega_{yy})=0 \qquad (2\text{-}1)$$

$$\nabla^2\psi=-\omega \qquad (2\text{-}2)$$

$$U=\psi_y\ , \quad V=-\psi_x\ , \quad \omega=V_x-U_y \qquad (2\text{-}3)$$

Here space and time variables x, y, t are dimensionless and normalized by a reference length quanity of L and a reference time quanity of L/U_0. The velocity U, V are normalized by the reference velocity U . Re is Reynolds number or LU_0/ν. To linearize Navier-Stokes equations in an element we may let

$$U=Up+u',\ V=Vp+v',\ 2A=ReUp,\ 2B=ReVp \qquad (2\text{-}4)$$

where Up and Vp are the velocity components at node P (see Fig. 2-1) and u' and v' are respectively the deviation of the velocity components in the element from those at node P. In general they are small if the element is reasonably small but can become significant when multiplied by large value of

ORIGINAL PAGE IS
OF POOR QUALITY

Reynolds number. Eq.(2-1) under this approximation can be written as

$$2A\omega_x+2B\omega_y-\omega_{xx}-\omega_{yy}=-Re(u'\omega_x+v'\omega_y+\omega_t)=f \qquad (2\text{-}5)$$

If the right hand side f is considered approximately to be a known value f_p from the solution at previous time t^k , then a simple analytic solution can be obtained for Eq.(2-5) at time t^k when proper element boundary conditions are specified or

$$\omega=F(\omega_n(x),\omega_s(x),\omega_e(y),\omega_w(y),\ h,k,x,y,t,f_p) \qquad (2\text{-}6)$$

where ω_n, ω_s, ω_e and ω_w are, respectively, the northern, southern, eastern and western boundary condition for the element 2hx2k at t^k.

For the numerical purpose the boundary conditions ω_n, ω_s, ω_e and ω_w may be specified in terms of nodal values along the bonudary (see Fig. 2-1), e.g., $\omega_s=G(\omega_{se},\omega_{sc},\omega_{sw},x)$. Substituting of the boundary condition into Eq.(2-6) and evaluating it at the point P(i,j) at time t one has the finite analytic formula for the interior nodal ω_p as

$$\omega_p=C_{ec}\omega_{ec}+C_{wc}\omega_{wc}+\ldots\ldots+C_{sw}\omega_{sw}+C_{se}\omega_{se}+C_pf_p \qquad (2\text{-}7)$$

Here C's are known analytic coefficients multiplying the corresponding boundary nodal values ω_{ec} etc. and the particular solution f_p representing the right hand side of Eq.(2-5). The system of finite analytic algebraic equations thus generated for all elements can be solved with proper boundary condition of the problem to provide FA solution for vorticity distribution.

ORIGINAL PAGE IS
OF POOR QUALITY

The treatment of unsteaty term and perturbed convection term in Eq.(2-5) can be achieved as follow:

$$\omega_t = \frac{\omega_p^k - \omega_p^{k-1}}{\Delta t} \qquad (2\text{-}8)$$

$$f_p = -Re(u'\omega_x - v'\omega_y)$$
$$= -Re((U_{ec}-U_p)\omega_{ec} - (U_{wc}-U_p)\omega_{wc})/4h$$
$$-Re((V_{nc}-V_p)\omega_{nc} - (V_{sc}-V_p)\omega_{sc})/4k \qquad (2\text{-}9)$$

Substituting Eqs. (2-8) and (2-9) for f_p in Eq.(2-7) one has

$$\omega_p^k = (\sum_{n=1}^{8} C_n\omega_n^k - C_p f_p^{k-1} + \frac{C_p Re\omega_p^{k-1}}{\Delta t})/(1+\frac{ReC_p}{\Delta t}) \qquad (2\text{-}10)$$

where n denotes the boundary nodes NE, EC, ... etc.

Similarly, Eq.(2-2) for stream function can be solved likewise by deriving the corresponding finite analytic representation with proper boundary conditions. For velocity components U and V one may derive from Eq.(2-3) directly, once the local analytic solution of stream function is known. Because the local analytic solution is differentiable up to the order of the PDE, so the derivatives of the ψ at P can be expressed as

$$-V = (\psi_x)_p = C_{ne}'\psi_{ne} + C_{se}'\psi_{se} + \cdots\cdots + C_p' f_p \qquad (2\text{-}11)$$

$$U = (\psi_y)_p = C_{ne}''\psi_{ne} + C_{se}''\psi_{se} + \cdots\cdots + C_p'' f_p \qquad (2\text{-}12)$$

Here the known analytic coefficients (C_{ne}' etc. and C_{ne}'' etc.) multiply the neighboring nodal values ψ_{ne}, ψ_{se}, ... etc. Alternatively, if one prefers, the velocity components U and V of Eq.(2-3) can also be derived with

finite difference approximation. More detail of derivation of these finite analytic algebraic equations is given in Appendix A.

CHAPTER III

THE BOUNDARY FITTED COORDINATE SYSTEM

The boundary fitted coordinate transformation was first presented by Thompson, Thames and Mastin [4]. Afterwards, many researches [6,7] have been devoted to the development of the techniques necessary for numerically generating boundary fitted coordinate system. Since the mathematical development and numerical implementation of these techniques is given in great detail by Thames [5], only overview is presented here.

The basic idea of the boundary fitted coordinate system is to generate a curvilinear coordinate system which has coordinate lines coincident with all the boundaries of a general multiply-connected region including the boundaries formed by solid walls and the external boundaries, which may be physically present or mathematically chosen to envelope the computational domain as shown in Fig. 3-1 and Fig. 3-2. Thus, on the transformed plane the numerical solution of the governing equations may be obtained on a fixed simple rectangular field without variation of the mesh size. Further, no interpolation of the boundary variables is required regardless of the shape of the physical

ORIGINAL PAGE IS
OF POOR QUALITY

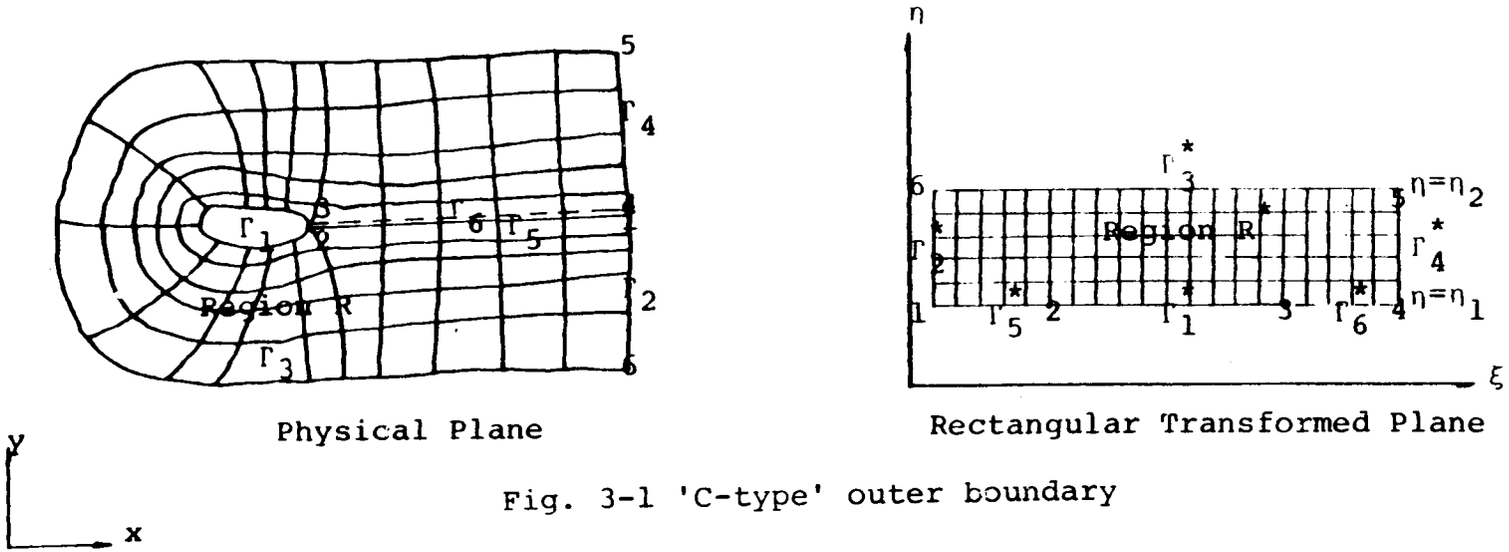

Fig. 3-1 'C-type' outer boundary

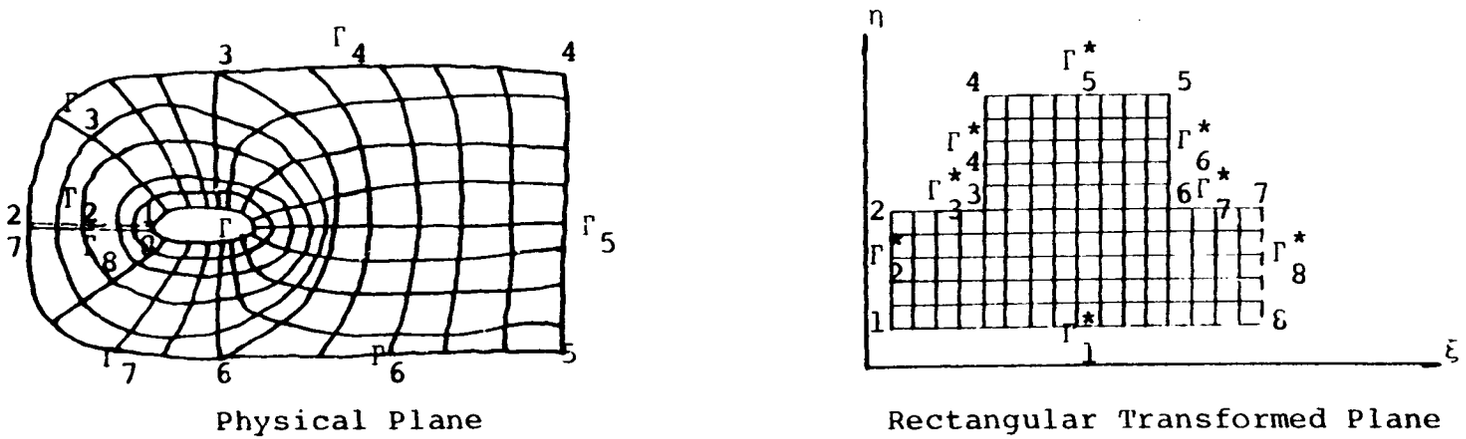

Fig. 3-2 'OC-type' outer boundary

boundaries or the spacing of the curvilinear coordinate lines in the physical plane.

For example, consider a two dimensional doubly connected region shown in Fig. 3-1. The general transformation is one which associates each point(x,y) in the physical plane with a corresponding point(ξ,η) in the transformed plane. Let the inner boundary of a physical body is presented by the closed contour Γ_1, and the 'C-type' outer boundary representing the desired external boundary of the computational domain is devoted by the contour Γ_3 and the downstream boundaries Γ_2 and Γ_4. For convenience in the transformation a cut in the physical plane can be made along the contours Γ_5 and Γ_6. In this configuration (Fig. 3-1) $\eta = \eta_1$ on the transformed plane may be identified with the contours Γ_5, Γ_1 and Γ_6, and $\eta = \eta_2$ with the contour Γ_3. ξ on the transformed plane may be made to vary monotonically from $\xi = \xi_1$ on Γ_2 to $\xi = \xi_2$ on Γ_4. Then the contour Γ_1 in the physical plane maps to the contour Γ_1^* in the transformed plane, Γ_2 maps to Γ_2^* etc. Since the value of η is constant along the contours Γ_5, Γ_1 and Γ_6, these contours must represent a line of constant η in the transformed plane. Also the cut made in the physical plane along the contours Γ_5 and Γ_6 is represented by the reentrant segments Γ_5^* and Γ_6^* in the transformed plane.

ORIGINAL PAGE IS
OF POOR QUALITY

Now ξ and η have been completely specified on all the boundaries of a closed field. It remains to define the values in the interior of the field in terms of these boundary values. This implies that elliptic partial differential equations can be used to generate the field points since the solution of an elliptic partial differential equation is completely defined in the interior of a region by its values on the boundaries of that region. However the elliptic system chosen must exhibit certain maximum principle which precludes the occurrence of extrema in the interior of the region and assures that a one-to-one correspondence exists between the physical and the transformed plane.

The elliptic system used to generate the boundary fitted coordinate system on the physical plane in this study is given by

$$\xi_{xx}+\xi_{yy}=-P(\xi,\eta) \qquad (3\text{-}1a)$$

$$\eta_{xx}+\eta_{yy}=-Q(\xi,\eta) \qquad (3\text{-}1b)$$

Subject to the following Dirichlet boundary conditions

$$\begin{vmatrix}\xi\\ \eta\end{vmatrix}=\begin{vmatrix}\xi_1(x,y)\\ \eta_1(x,y)\end{vmatrix} \qquad (x,y)E\Gamma_1 \qquad (3\text{-}2a)$$

$$\begin{vmatrix}\xi\\ \eta\end{vmatrix}=\begin{vmatrix}\xi_2(x,y)\\ \eta_2(x,y)\end{vmatrix} \qquad (x,y)E\Gamma_3 \qquad (3\text{-}2b)$$

where $P(\xi,\eta)$ and $Q(\xi,\eta)$ are the attraction functions for the ξ and η lines respectively. When $P=Q=0$ the Eq.(3-1) is

ORIGINAL PAGE IS
OF POOR QUALITY

Laplace equation which indeed assures that a one-to-one correspondence exists between the physical and the transformed plane because of the characteristics of the maximum principle (see Fig. 3-3). If P or Q are non-zero values Eq.(3-1) is Poisson equation, the source terms P or Q can be used for coordinate control to locate the lines of constant ξ or η toward either the inner boundary or external boundary creating a dense grid mesh in the physical plane (see Fig. 3-4). Thus, there are many ways of choosing the functions of P and Q [13,14,15] to get a desired shape in the physical plane. Here, we use the form suggested by Thames [5].

$$P(\xi,\eta)=-\sum_{k=1}^{n} A_k \frac{\xi(x,y)-\xi_k}{|\xi(x,y)-\xi_k|}\, e^{-C_k|\xi(x,y)-\xi_k|} \qquad (3\text{-}3a)$$

$$Q(\xi,\eta)=-\sum_{k=1}^{n'} A'_k \frac{\eta(x,y)-\eta_k}{|\eta(x,y)-\eta_k|}\, e^{-C'_k|\eta(x,y)-\eta_k|} \qquad (3\text{-}3b)$$

where $n(n')$ is the number of attraction ξ-lines(η-lines) to be affected, $A_k(A_k')$ is the amplitude factor, $C_k(C_k')$ is the decay factor, and $\xi(x,y)(\eta(x,y))$ are the concentrative lines. For detail, reader is referred to Thames's paper [5].

Since it is desired that all numerical computations be performed in the transformed plane with simple grid size $\Delta\xi$ and $\Delta\eta$. Eq.(3-1) is cumbersome to use. It is more convenient that the independent and dependent variables of Eq.(3-1) are interchanged. In the transformed plane the generating system

ORIGINAL PAGE IS
OF POOR QUALITY

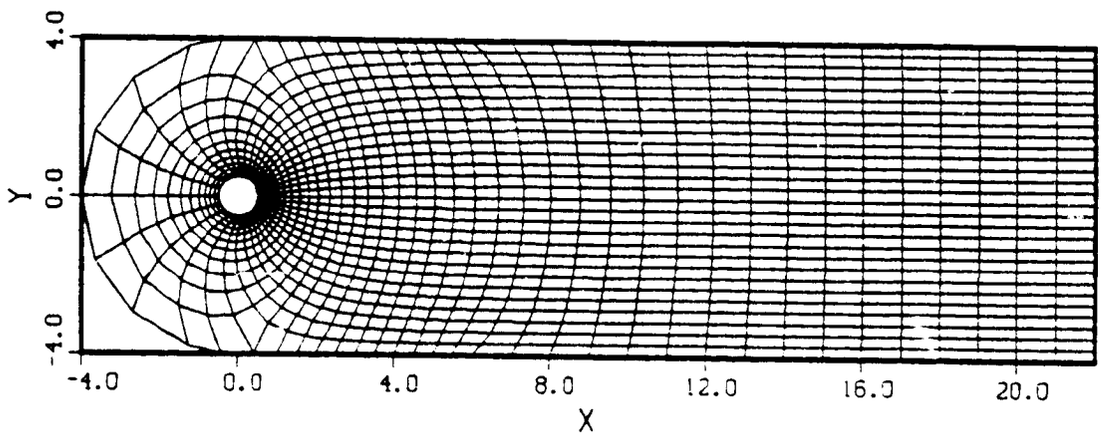

Fig. 3-3 Laplace equation

ORIGINAL PAGE IS
OF POOR QUALITY

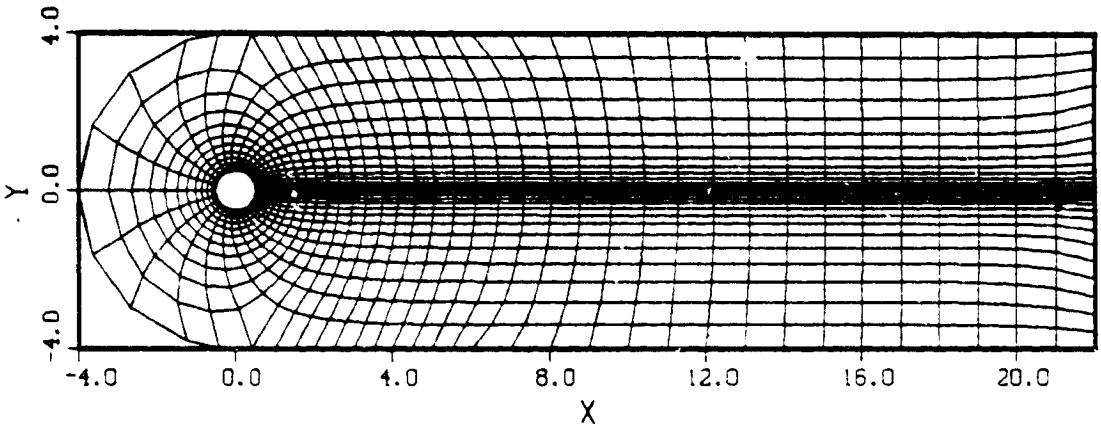

(a) P≠0, Q=0

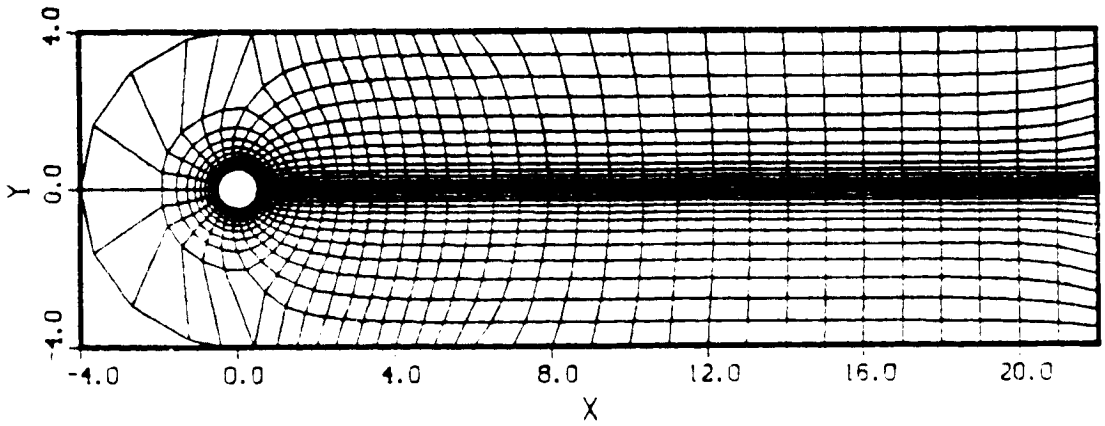

(b) P≠0, Q≠0

Fig. 3-4 Poisson equation

ORIGINAL PAGE IS
OF POOR QUALITY

Eq.(3-1) may be rewritten as, after interchange of independent (x,y) and dependent (ξ,η) variables,

$$\alpha x_{\xi\xi}-2\beta x_{\xi\eta}+\gamma x_{\eta\eta}=-J^2(x_\xi P+x_\eta Q) \qquad (3\text{-}4a)$$

$$\alpha y_{\xi\xi}-2\beta y_{\xi\eta}+\gamma y_{\eta\eta}=-J^2(y_\xi P+y_\eta Q) \qquad (3\text{-}4b)$$

with the transformed boundary conditions

$$\begin{vmatrix} x \\ y \end{vmatrix}=\begin{vmatrix} f_1(\xi,\eta_1) \\ f_2(\xi,\eta_1) \end{vmatrix} \qquad (\xi,\eta_1)E\Gamma_1^* \qquad (3\text{-}5a)$$

$$\begin{vmatrix} x \\ y \end{vmatrix}=\begin{vmatrix} g_1(\xi,\eta_2) \\ g_2(\xi,\eta_2) \end{vmatrix} \qquad (\xi,\eta_2)E\Gamma_2^* \qquad (3\text{-}5b)$$

where α, β, γ, J are the formations providing relationships between the physical and transformed plane (see Appendix B).

The functions $f_1(\xi,\eta_1)$, $f_2(\xi,\eta_1)$, $g_1(\xi,\eta_2)$ and $g_2(\xi,\eta_2)$ are specified by the known shape of the contours Γ_1 and Γ_3 respectively, and the specified ξ distribution thereon.

Although it is more difficulty to solve the system of quasi-linear partial differential equations Eq.(3-4) than to solve the original equations Eq.(3-1), the boundary conditions Eq.(3-5) are much easily specified along straight boundaries in the transformed plane. Also, since the computation of flow problem is first to be performed on the boundary fitted coordinate system it is desired that the transformed line spacing is uniform. That is one prefers to set $\Delta\xi = \Delta\eta$ =constant. Therefore, solving Eq.(3-4) with equal

ORIGINAL PAGE IS
OF POOR QUALITY

spacing $\Delta\xi$ and $\Delta\eta$, one has regular grids on (ξ,η) plane and irregular space in (x,y) plane. From previous works it seems to produce more advantages in using the boundary fitted coordinate system than the disadvantage it brings.

Eq.(3-4) can now be solved either by FD or FA method when the partial differential equations are approximated by a set of algebraic equations. The resulting set of simultaneous algebraic equations are thus solved to provide some coordinate relations between physical(x,y) plane and transformed(ξ,η) plane. For fixed boundary location the computation needs to be carried out only once.

It should be pointed out here that it is important to have an accurate solution in the coordinate transformation and evaluation of coefficients α, β, γ and J in Eq.(3-4). Inaccurate evaluation of these coefficients will add the errors to the numerical solution of the original problem. Indeed, this is the main disadvantage in using boundary fitted coordinate system. In this study two types of boundary fitted coordinate systems (Fig. 3-1 and Fig. 3-2) are investigated and compared.

ORIGINAL PAGE IS
OF POOR QUALITY

CHAPTER IV

FORMULATION OF PROBLEM

4.1 Governing Equations

In this study a two dimensional uniform flow over an arbitrary two dimensional obstacle is considered. The fluid is assumed to be incompressible with constant properties. The governing Navier-Stokes equations for two dimensional problem may be written in two formulations -- one with primitive equation and the other with stream function and vorticity form. Since the present study is only confined to the two dimensional problem, it is more advantageous to choose the stream function and vorticity formulation. The reason is there are only two equations for two unknowns -- vorticity ω and stream function ψ, while there are three equations for three primitive variables U, V and P in the primitive formulation.

The incompressible Navier-Stokes equations written in the stream function and vorticity form are

$$\omega_t+\psi_y\omega_x-\psi_x\omega_y=(\omega_{xx}+\omega_{yy})/Re \qquad (4\text{-}1a)$$

$$\psi_{xx}+\psi_{yy}=-\omega \qquad (4\text{-}1b)$$

where , is the nondimensional stream function defined from the continuity equation and the x and y velocity

ORIGINAL PAGE IS
OF POOR QUALITY

components are related to the stream function as $U=\psi_y$ and $V=-\psi_x$ when the nondimensional vorticity ω is defined as Eq.(4-1b). The reference length scale L used in normalization is the maximum width of the body, and the reference velocity scale U_0 is the uniform approaching velocity specified at the upstream boundary. Thus, the dimensionless stream function ψ is normalized by U_0L while the dimensionless vorticity ω is by U_0/L. Re in Eq.(4-1a) is the Reynolds number U_0L/ν , where ν is the constant viscosity coefficient of the fluid.

4.2 Boundary Conditions

Fig. 4-1 and Fig. 4-2 are two general types of computational domain we use in this study. The approximate boundary conditions for stream function and vorticity are derived as the following:

4.2.1 The body surface

Since there is no slip on the body surface and the body is impermeable, so $V_t=0$, $V_n=0$ where V_t is the tangential velocity along the body surface, V_n is the normal velocity on the body, then

$$\psi=\text{constant and} \quad \omega=-\partial V_t/\partial n \qquad (4\text{-}2a)$$

where ω and ψ are the stream function and vorticity value on the body surface, n is the outward direction normal

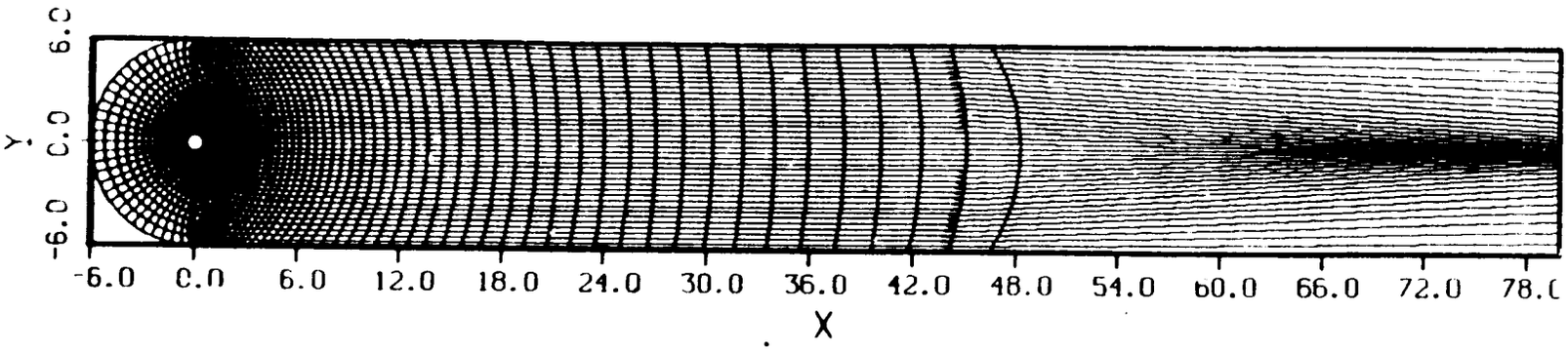

Fig. 4-1 'C-type' outer boundary

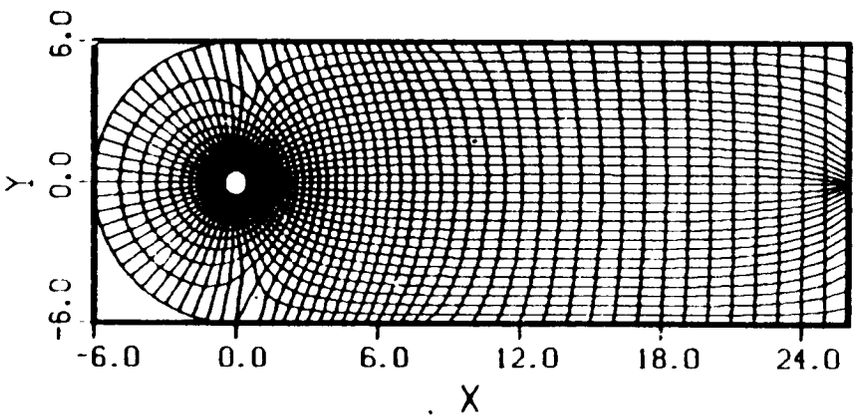

Fig. 4-2 'OC-type' outer boundary

ORIGINAL PAGE IS
OF POOR QUALITY

to the body surface. To simplify this study, we only select the symmetrical obstacle and put it at the center of the computational domain as shown in Fig. 4-1 and Fig. 4-2, say $\psi=0$. Strictly speaking, at the case while a periodic wake and staggered vortex street is formed, the stream function on the body surface no longer the fixed zero value (it is the value depends on the time). Since this change is difficult to figure it out and small, we still use $\psi=0$ on the body surface at each different time step.

4.2.2 The upstream boundary

Since the approaching flow is taken to be a two dimensional uniform flow, then U=1, V=0. Integrating the $U=\psi_y$, $V=-\psi_x$ and setting the approaching stream function at the center line to be zero we have

$$\psi = U*y = y, \qquad \omega = \frac{\partial V}{\partial x} - \frac{\partial U}{\partial y} = 0 \qquad (4\text{-}2b)$$

4.2.3 The upper and lower boundaries

As shown in Fig. 4-1 and Fig. 4-2 the distance from the center line to the upper or lower boundary is taken to be six times of the reference length (here, the reference length is the diameter of the circular cylinder). That this domain is assumed far enough to maintain U=1, V=0 on the upper and lower boundary, therefore

$\psi = 6 \quad \omega = 0$ on the upper boundary

$\psi = -6 \quad \omega = 0$ on the lower boundary (4-2c)

ORIGINAL PAGE IS
OF POOR QUALITY

4.2.4 The downstream boundary

As shown in Fig. 4-1 the downstream boundary behind the center of circular cylinder is taken to be a long distance. It is reasonable to assume that the condition posed at this boundary has minimum effect on the vortex shedding behind the cylinder. Therefore, the boundary condition is taken to be U=1, V=0 on the downstream boundary to preserve the continuity of mass flow. In other words the stream function and vorticity are set as

$$\psi = y, \qquad \omega = 0 \qquad (4\text{-}2d\text{-}1)$$

Alternatively, as shown in Fig. 4-2, if the distance from the downstream boundary to the center of circular cylinder is taken to be a short distance, some cares must be exercised in posing the boundary condition. In this case the boundary condition on the downstream boundary is taken to be the value on the grid line before the downstream boundary at the previous time step or

$$\psi_n^t = \psi_{n-1}^{t-1}, \qquad \omega_n^t = \omega_{n-1}^{t-1} \qquad (4\text{-}2d\text{-}2)$$

where the superscript t, t-1 denotes the time step, and the subscript n, n-1 denotes respectively the grid line on the downstream boundary and the one grid line before the downstream boundary.

ORIGINAL PAGE IS
OF POOR QUALITY

4.3 In The Transformed Plane

The governing equations and boundary conditions posed up to now are all in the physical plane, however, it is desired that all numerical computations be performed in the transformed plane. Thus, the transformation relationships in the Appendix B can be used to transform Eq.(4-1) to Eq.(4-3) and Eq.(4-2) to Eq.(4-4). The followings are governing equations Eq.(4-3) in the transformed plane.

$$\omega_t+(\psi_\eta\omega_\xi-\psi_\xi\omega_\eta)/J=(\alpha\omega_{\xi\xi}-2\beta\omega_{\xi\eta}+\gamma\omega_{\eta\eta}+\sigma\omega_\eta+\tau\omega_\xi)/J^2Re \qquad (4\text{-}3a)$$

$$\alpha\psi_{\xi\xi}-2\beta\psi_{\xi\eta}+\gamma\psi_{\eta\eta}+\sigma\psi_\eta+\tau\psi_\xi=-J^2\omega \qquad (4\text{-}3b)$$

where α, β, γ, σ, τ and J are the transformation relationships listed in the Appendix B.

The boundary conditions Eq.(4-4) in the transformed plane become

$\psi=0$	$\omega=\frac{\gamma}{J^2}\psi_{\eta\eta}$	on the body surface	(4-4a)
$\psi=y$	$\omega=0$	on the upstream boundary	(4-4b)
$\psi=6$	$\omega=0$	on the upper boundary	
$\psi=-6$	$\omega=0$	on the lower boundary	(4-4c)
$\psi=y$	$\omega=0$	on the downstream boundary	(4-4d-1)
or $\psi_n^t=\psi_{n-1}^{t-1}$	$\omega_n^t=\omega_{n-1}^{t-1}$	on the downstream boundary	(4-4d-2)

It should be remarked here that the vorticity values on the body surface $\omega=-\frac{\gamma}{J^2}\psi_{\eta\eta}$ are not known, because numerical evaluation of $\psi_{\eta\eta}$ requires the internal points of ψ ,

ORIGINAL PAGE IS
OF POOR QUALITY

several possible ways of computing vorticity boundary condition are discussed in Chapter 6.

Before the FA numerical method is implimented to solve Eq.(4-3) in the transformed plane (in Chapter 6), Eq.(4-3) can be rearranged in the suitable form which we had obtained an algebraic equation in the Appendix A or

$$\omega_{\xi\xi}+C\omega_{\eta\eta}-2BC\omega_{\eta}-2A\omega_{\xi}=f \qquad (4\text{-}5a)$$

where $A=(\psi_{\eta}JRe-\tau)/2\alpha$; $B=(-\psi_{\xi}JRe-\sigma)/2\gamma$; $C=\gamma/\alpha$;

$f=(\omega_{t}J^{2}Re+2\beta\omega_{\xi\eta})/\alpha$.

$$\psi_{\xi\xi}+C'\psi_{\eta\eta}-2B'C'\psi_{\eta}-2A'\psi_{\xi}=f' \qquad (4\text{-}5b)$$

where $A'=-\tau/2\alpha$; $B'=-\sigma/2\gamma$; $C'=\gamma/\alpha$;

$f'=(2\beta\psi_{\xi\eta}-J^{2}\omega)/\alpha$.

CHAPTER V

PROCEDURE OF NUMERICAL SOLUTION

In this study there are two major parts in the numerical procedures to obtain the final numerical result. The first one is the generation of the boundary fitted coordinate system. The second one is the FA numerical solution of the governing equation Eq.(4-3) with boundary conditions Eq.(4-4) in the boundary fitted coordinates. Details of numerical procedures are described below.

5.1 Boundary Fitted Coordinate System

In deciding a boundary fitted coordinate system for a particular problem, one should know which region of physical plane needs special attention, where detail and accurate result are desired then more dense discritization nodes should be placed. In this study we are especially intrested in examing the vortex shedding phenomena behind an obstacle, where the flow variations are expected to be most drastic. Therefore, the grid size for the region near the body surface and behind the body should be smaller than other parts to provide sufficient resolution of flow variables to capture the real character of flow. And the grid size in

ORIGINAL PAGE IS
OF POOR QUALITY

other region may be a bit coarser to save computational time and storage and not to influence the accurate of solution. To satisfy these requirements, we choose a 'C-type' outer boundary firstly as shown in Fig. 4-1 as the base for generating the boundary fitted coordinate system. In order to obtain accurate solutions at any given time, one must compute accurately the vorticity boundary values on the body surface at each time instance. Since for an arbitrary body shape the 'C-type' boundary fitted coordinate (Fig. 3-1) does not provide accurate evaluations of vorticity boundary values, because of nonorthogonal behavior of the coordinates, another 'OC-type' boundary fitted coordinate (Fig. 3-2) which provides nearly orthogonal coordinates and more accurate vorticity boundary values then was used. The flow chart for generating the boundary fitted coordinate system through Eqs.(3-4) to (3-5) is outlined in the Table 5-1.

The computation of attraction function P and Q are accomplished under computer code FUNCTION CONQ(I,J1,J2). Where I is the concentration line. J(J1¬J2) is the number of attraction line, A_k is the amplitude factor and C_k is the decay factor (see Eq.(3-3)). The flow chart for FUNCTION CONQ is shown in the Table 5-2.

Details of the computer program are listed in the Appendix D.

Table 5-1 Flow Chart of Boundary Fitted Coordinate System

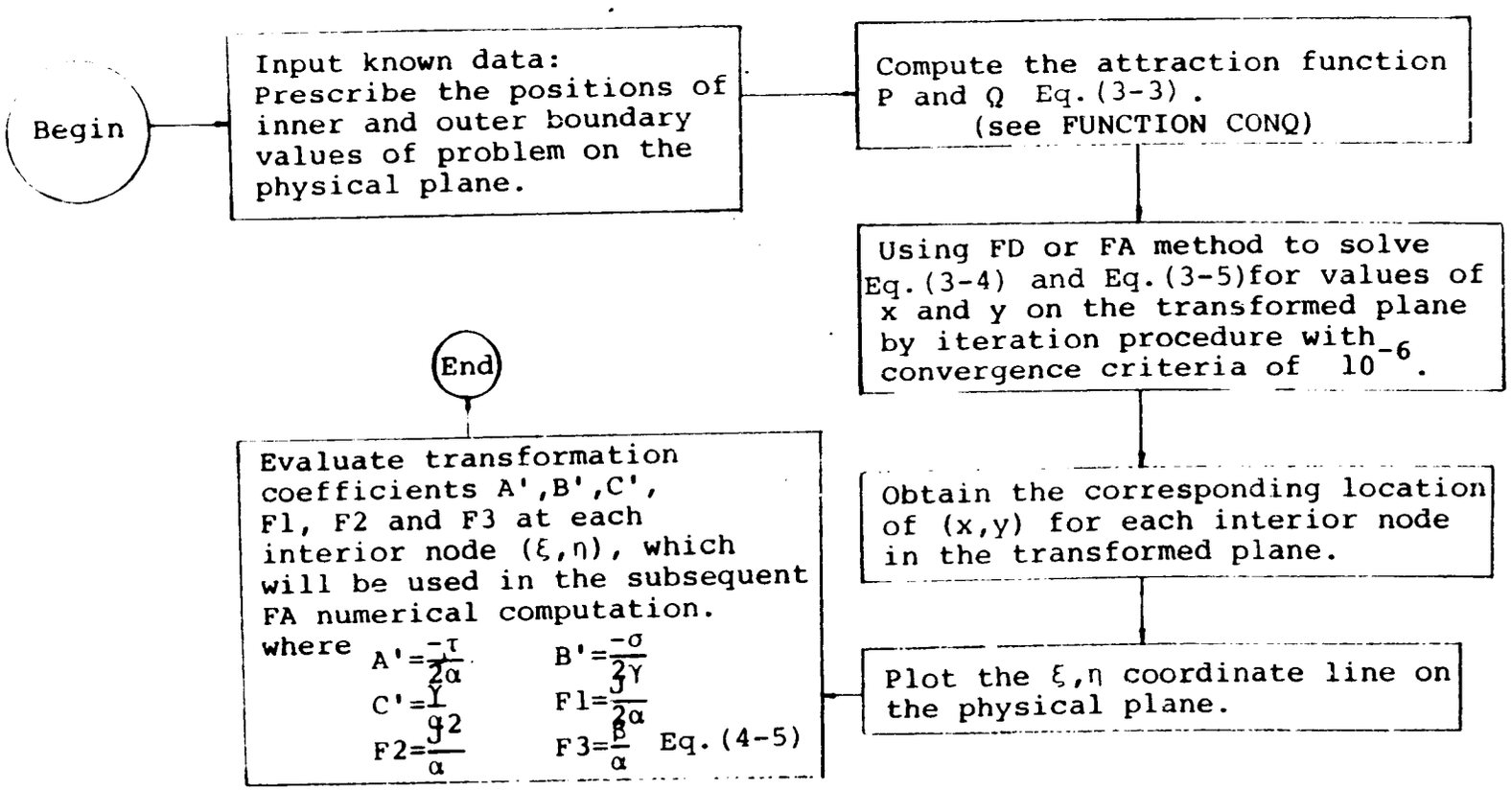

ORIGINAL PAGE IS
OF POOR QUALITY

ORIGINAL PAGE IS
OF POOR QUALITY

Table 5-2 Flow Chart of Concentration Values P & Q

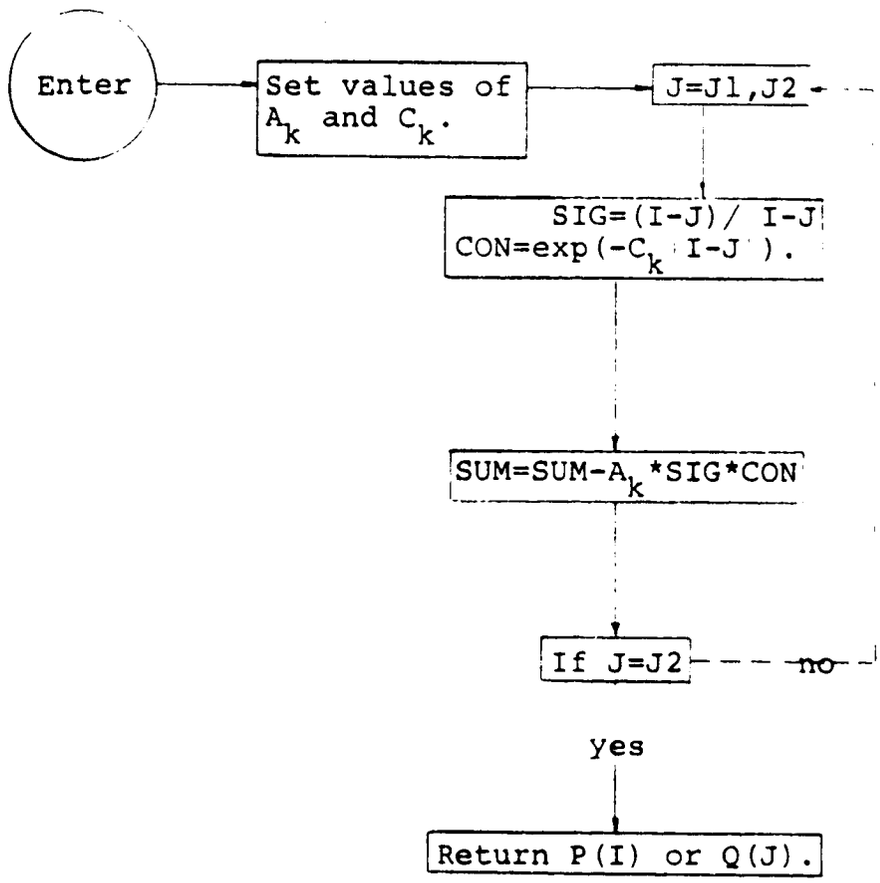

5.2 The FA Numerical Solution In The Transformed Plane

Since the governing equation Eq.(4-3) in the transformed plane is a unsteady problem, the computational procedure must march with time. The numerical calculation starts with the establishment of initial values of ψ, ω, everywhere, at time t=0. As pointed out earlier we are interested in the establishment of vortex shedding phenomena for uniform flow over the obstacle. Therefore, the initial condition in the computational domain can be arbitrarily chosen. In the present study the potential flow solution for ψ and zero vorticity is chosen to be the initial condition at the first calculation of problem at Reynplds number of 5. Physically, it means that initially the fluid is assumed to be inviscid and is moving passing the body with a uniform velocity U . In the later calculation for higher Reynolds numbers, it is decided to use the results of ψ and ω at the lower Reynolds number which has been solved as the initial condition at time t=0. Physically, it means that the approaching uniform velocity over the obstacle is suddenly increased.

After the initial values of ψ and ω are specified, the computational procedure begins with calculation of new vorticity boundary condition on the body surface from Eq.(4-4a) at k+1th time step. Theoretically, ω should

depend on the new values of ψ at the same k+1th time step, but in the iterative procedure the known values of ψ are only at previous kth time step. Several possible ways of approximately calculating ω for the k+1th time step are discussed in Chapter 6.

The next step in the computation is to use a line-by-line iterative method to solve the vorticity transport equation Eq.(4-5a), which is cast into the form given in Eq.(2-10), for all interior nodes of the problem. The new values of are calculated at a new k+1th time level. When is solved a line-by-line iterative method is again used to solve Eq.(4-5b) for new values of stream function ψ at k+1th time step with new vorticity values at k+1th time step. Then the computational cycle for one time step is completed. The same procedure is repeated until the desired time is reached. Schematically, the computational procedure is illustrated in the Table 5-3.

The equations for SUBROUTINE COEFF is given in Appendix A from Eq.(A-12) to Eq.(A-20). The program COEFF is listed in Appendix D.

Both the potential flow program which provides the initial guess of ψ in calculating Re=5, and the unsteady program for higher Re are listed in Appendix D.

Table 5-3 Flow Chart of FA Numerical Method

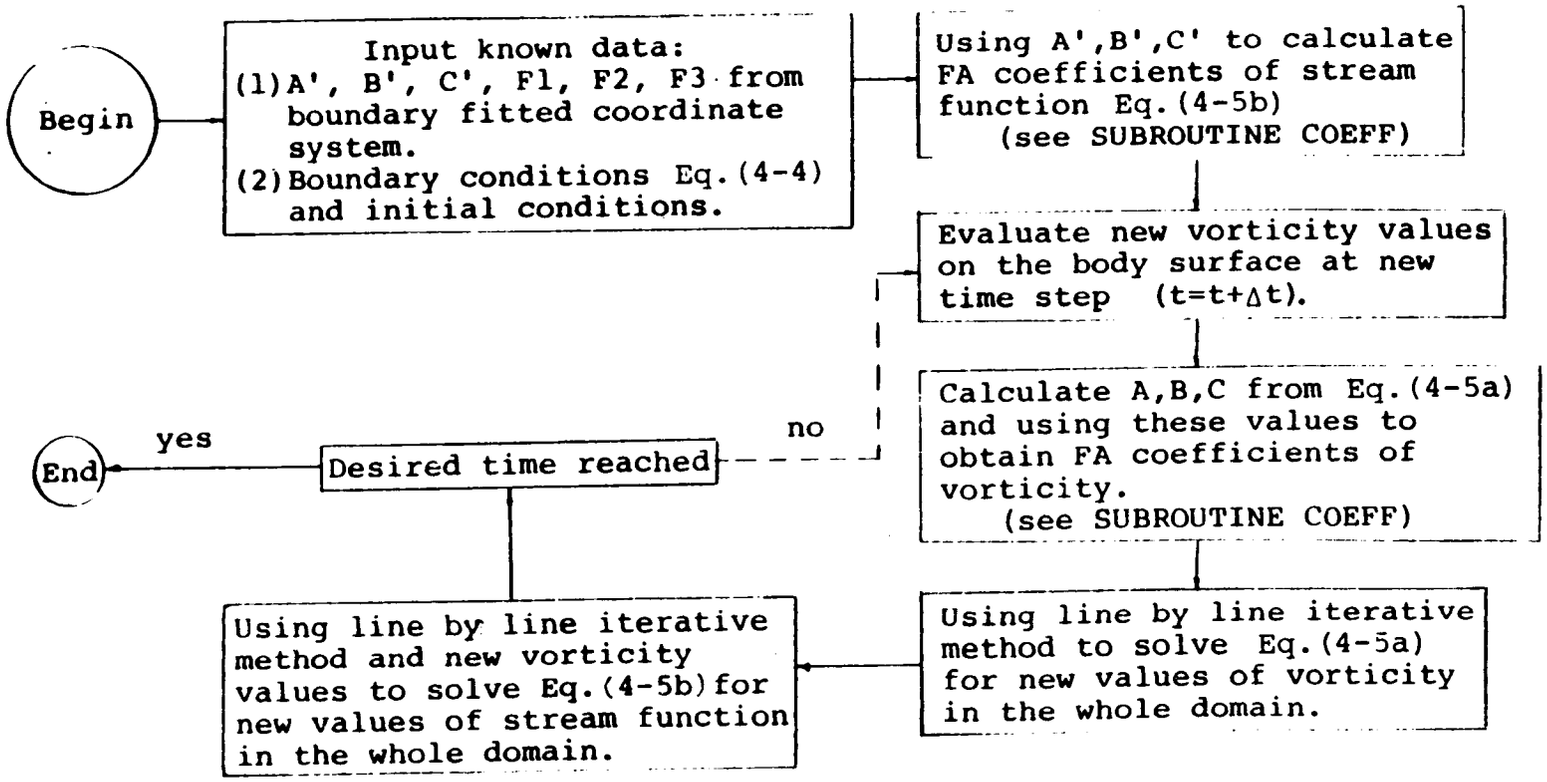

ORIGINAL PAGE IS
OF POOR QUALITY

All the above numerical procedures are excuted in the transformed plane. After obtaining the numerical results, one should be able to graph them back in the physical plane where the real pictures of the flow pattern are obtained. The numerical method to accomplish this requirement is shown in Appendix C, and computer program is listed in Appendix D.

CHAPTER VI

FLOW AROUND A CIRCULAR CYLINDER

6.1 Phenomenan of Vortex Shedding

The problem of the viscous flow around a circular cylinder is a classical one. There are a large number of experimental results. From these available results, the flow pattern at different Reynolds numbers are summarized by Blevins [16] as shown in Fig. 6-1. At very low Reynolds numbers based on cylinder diameter (Re<5), the flow around the cylinder is steady and does not separate and basically is a Stokes type flow. As Re is increased (5<Re<40), a pair of vortices is formed immediately behind the cylinder but the vortices are steady and stationary. As Re is further increased (40<Re<150), the vortices elongate until one of the vortices breaks away and a periodic wake and staggered vortex street is formed. The vortex street is known as Karman vortex street. Von Karman [17] is the first one to study the stability of vortex pair formed far behind the obstacle and predicted the stable pattern is a staggered pattern. Up to the Reynolds number of 150 the vortex street is laminar. At a Re of 300 the vortex street becomes turbulent and it degenerates into fully turbulent flow

ORIGINAL PAGE IS
OF POOR QUALITY

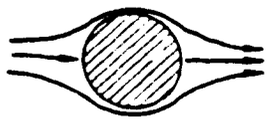

$Re<5$ Regime of unseparated flow.

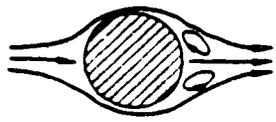

$5 \text{ to } 15 \leq Re < 40$ A fixed pair of foppl vortices in wake.

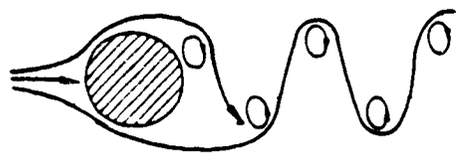

$40 \leq Re < 90$ and $90 \leq Re < 150$
Two regimes in which vortex street is laminar.

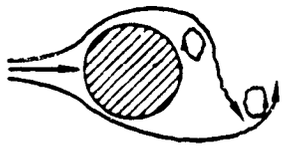

$150 \leq Re < 300$ Transition range to turbulence in vortex.

$300 \leq Re \lesssim 3x10^5$ Vortex street is fully turbulent.

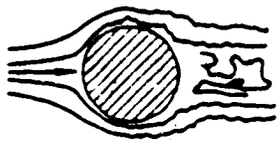

$3x10^5 \lesssim Re < 3.5x10^6$
Laminar boundary layer has undergone turbulent transition and wake is narrower and disorganized.

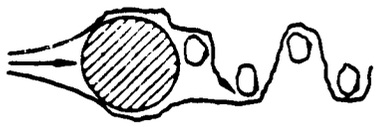

$3.5x10^6 \leq Re$
Re-establishment of turbulent vortex street.

Fig. 6-1 Regimes of fluid flow across circular cylinders.

beyond approximately 50 diameters downstream of the cylinder. The range of Re from 300 to approximately $3x10^5$ has been called the subcritical range where the vortex shedding occurs at a well defined frequency. At the transition range of $3x10^5<Re<3.5x10^6$ the flow separation point moves backwards, the vortex shedding is thus disorganized (with a broad band of shedding frequencies), and the cylinder drag drops sharply. At higher, supercritical range $Re>3.5x10^6$ the vortex street re-establishes itself.

Observing the flow pattern described above for different Reynolds numbers, it is obvious that in the present study of laminar vortex shedding, the Reynolds number should be below 300. However, in order to examine the proposed FA numerical solution it is decided to solve Re=5, Re=40, Re=100, Re=500. The reason of computing laminar solution at Re=500 is that one may want to know what kind of the flow pattern one might obtain if the flow be kept laminar at Re=500. In the future work some turbulence models may be incorporated to see what's the difference does it make at a high Re when the flow is laminar or turbulent. For each different region the comparison of the predicted separation points and Strouhal numbers with the experimental results is made, even though at Re=500 the flow is turbulent

ORIGINAL PAGE IS
OF POOR QUALITY

6.2 Numerical Results at C-type Outer Boundary

At C-type outer boundary (see Fig. 4-1), the computational domain has 129x20 nodes with a far downstream boundary and sufficiently dense grid matrix behind the circular cylinder, then boundary condition Eq.(4-4d-1) was chosen in this case. It should be remarked here the vorticity boundary formular Eq.(4-4a) $\omega=-\frac{\gamma}{J^2}\psi_{\eta\eta}$ was not adapted in this case, because the ξ lines have large curvature around the circular surface (see Fig. 6-2a). Then it is difficult using numerical method to evaluate the transformed values of γ/J^2 accurately on the body surface, where $\gamma=x_\xi^2+y_\xi^2$, $J=x_\xi y_\eta-x_\eta y_\xi$. An alternative approach was used to evaluate Eq.(4-4a) on the body surface. That is to compute ω in the physical (x,y) plane directly, and these vorticity values on the body surface is obtained from Eq.(4-2a) $\omega=-\frac{\partial V_t}{\partial n}$, where V_t is the tangential velocity along the body suface, and n is the outward direction normal to the body suface. Since $V_t=\frac{\partial\psi}{\partial n}$ then $\omega=-\frac{\partial^2\psi}{\partial n^2}$, using Taylor series expansion we obtained

$$\omega=-\frac{2(\psi_{w+1}-\psi_w)}{\Delta n^2}+\frac{2!}{\Delta n}\left.\frac{\partial\psi}{\partial n}\right|_w+O(\Delta n^3)$$

where subsript w means the wall value on the body surface. However, $\left.\frac{\partial\psi}{\partial n}\right|_w=0$ by the no-slip condition, thus

$$\omega=-\frac{2\psi_{w+1}}{\Delta n^2} \qquad (6\text{-}1)$$

ORIGINAL PAGE IS
OF POOR QUALITY

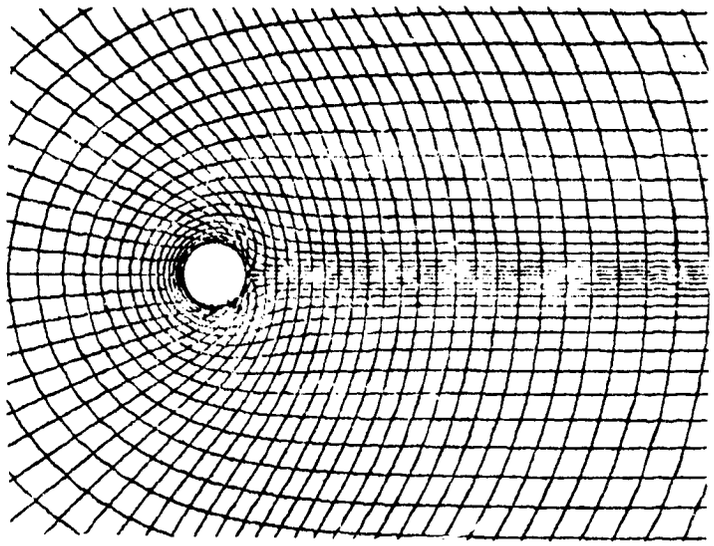

(a)

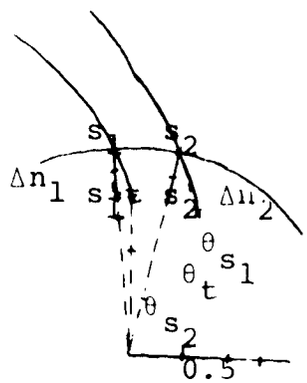

(b)

Fig. 6-2 Small element

ORIGINAL PAGE IS
OF POOR QUALITY

where Δn is the distance from the w+1-th η line normal to the body surface which is w-th η line. Fig. 6-2b shows the relative position of the following evaluations. Once the values of Δn_1 and Δn_2 are known, where

$$\left(\quad \Delta n_1=\sqrt{x_{s1}^2+y_{s1}^2}-0.5, \quad \Delta n_2=\sqrt{x_{s2}^2+y_{s2}^2}-0.5 \quad \right)$$

one may calculate vorticity values at points s1' and s2' from points s1 and s2 by Eq.(6-1). The vorticity value at point t can be obtained by interpolation between s1' and s2' after finding the relations between θ_{s1}, θ_{s2} and θ_t,

$$\text{where } \theta_{s1}=\mathrm{Tan}^{-1}\frac{y_{s1}}{x_{s1}}, \quad \theta_{s2}=\mathrm{Tan}^{-1}\frac{y_{s2}}{x_{s2}}, \quad \theta_t=\mathrm{Tan}^{-1}\frac{y_t}{x_t}.$$

With the known vorticity at points s1' and s2', the approximate vorticity value at point t is

$$\omega_t=\omega_{s1'}+\frac{\theta_t-\theta_{s1}}{\theta_{s2}-\theta_{s1}}(\omega_{s2'}-\omega_{s1'}) \qquad (6\text{-}2)$$

Followings are the FA numerical predictions of flow over a circular cylinder with the C-type boundary fitted coordinate system.

6.2.1 Potential Flow

Stream line of potential flow is shown in Fig. 6-3. The solution shows that streamlines are not only symmetrical with respect to the axial line but also with respect to the upstream and downstream. Then solution of potential flow is used as the initial guess for calculation of FA solution at low Reynolds number Re=5.

ORIGINAL PAGE IS
OF POOR QUALITY

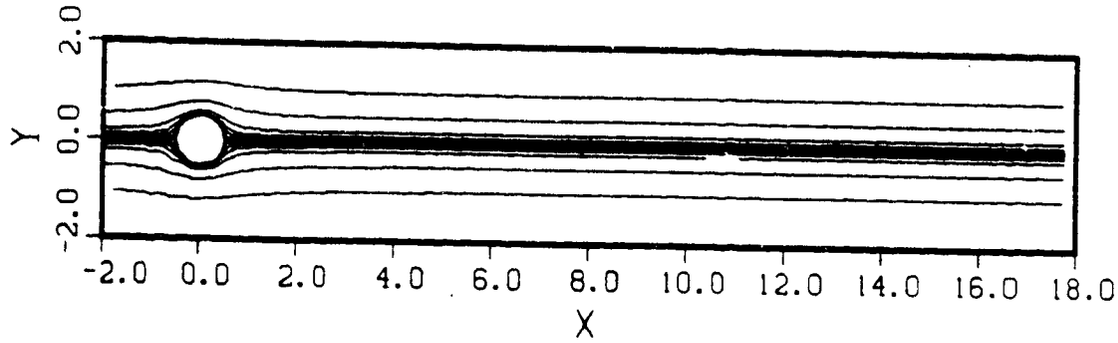

Fig. 6-3 Potential flow

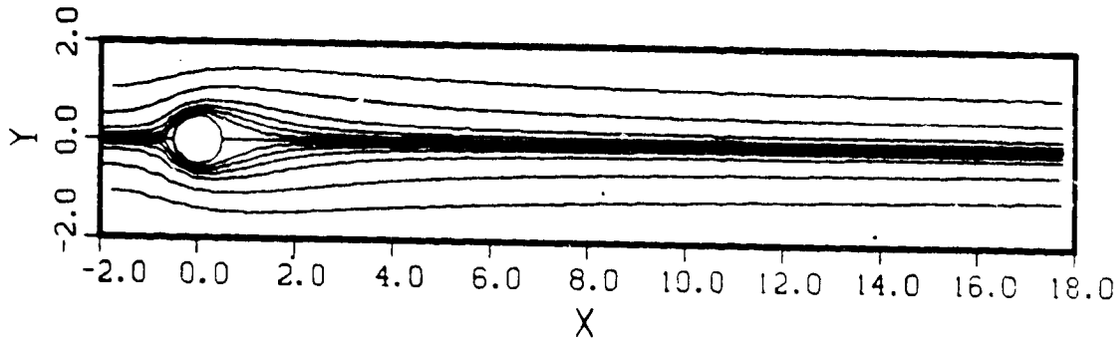

(a) Stream line

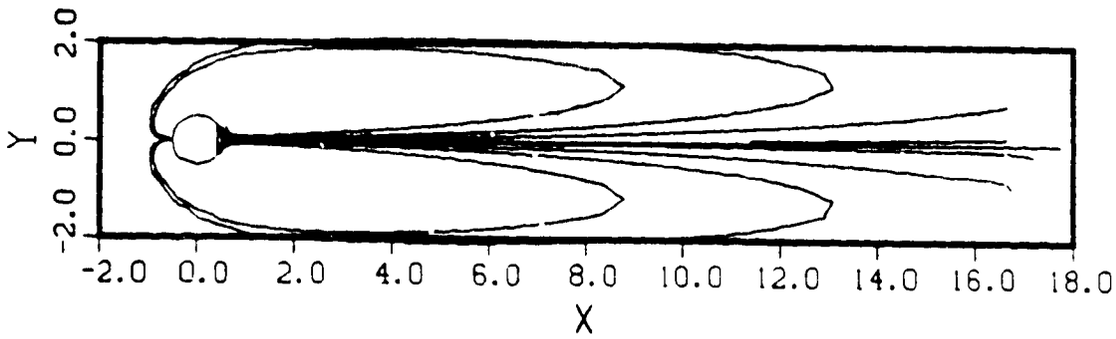

(b) Vorticity function

Fig. 6-4 Re=5

6.2.2 Re=5

Fig. 6-4 shows the stream line and equal vorticity value line at Re=5. The present FA solution predicts the same flow pattern as predicted by theoretical analysis and expremental measurement, which shows at this low Reynolds number the flow is still stationary and does not separate.

6.2.3 Re=40

Fig. 6-5 gives the stream line and equal vorticity value line at Re=40. At this Reynolds number the flow separates and forms a pair of stationary vortices behind the cylinder. The predicted length s of the region of closed stream lines behind a circular cylinder with diameter d is equal to 2.2d, which coincides with the experimental results presented by Taneda [18] at Fig. 6-6, and the angle of separation is about 55 , which also agrees with the others results [19] at Fig. 6-7.

6.2.4 Re=100

Fig. 6-8 gives the periodic stream pattern at Re=100. Fig. 6-9 is the equal vorticity value line at the corresponding time step. Since the flow manifests a vortex shedding, the flow must be considered no longer stationary. Therefore, in the computation the time step size and iteration error for each time step should be set carefully to get an unsteady program. In this study we are interested

ORIGINAL PAGE IS
OF POOR QUALITY

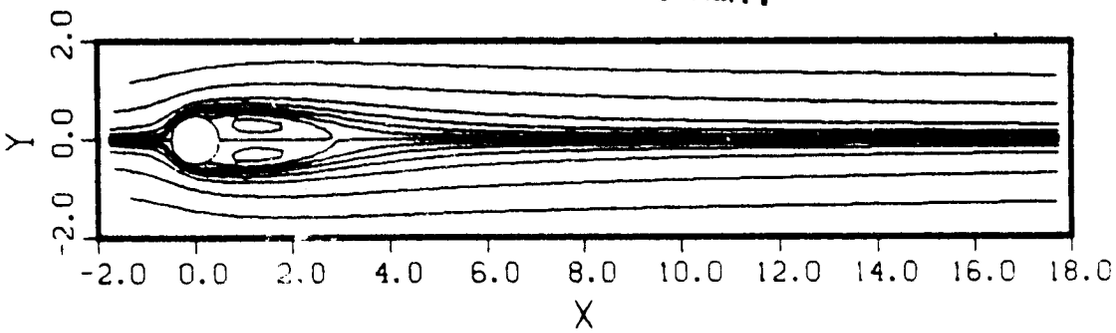

(a) Stream line

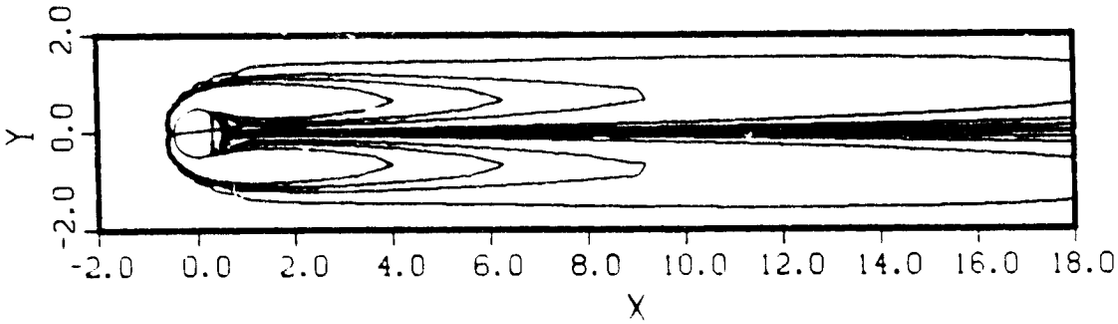

(b) Vorticity function

Fig. 6-5 Re=40

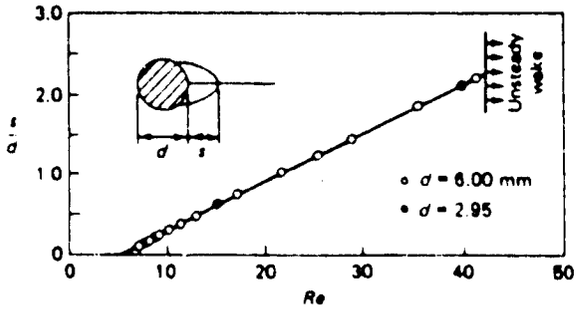

Fig. 6-6 Observed lengths of the region of closed streamlines behind a circular cylinder. (From Taneda;1956)

ORIGINAL PAGE IS
OF POOR QUALITY

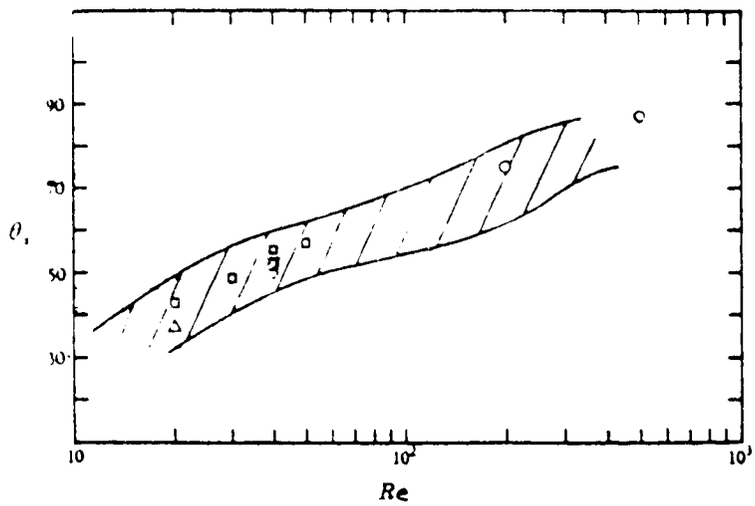

Fig. 6-7 Comparison between numerical calculations and measurements. Numerical solution ○, Jaime & Thomas(1969); □, Kawaguti & Jain(1966); ◇, Apelt (1961); ▽, Kawaguti(1953); △, Thom(1928). Measurements: shaded area, with and without splitter plate. (Ref. 19)

ORIGINAL PAGE IS
OF POOR QUALITY

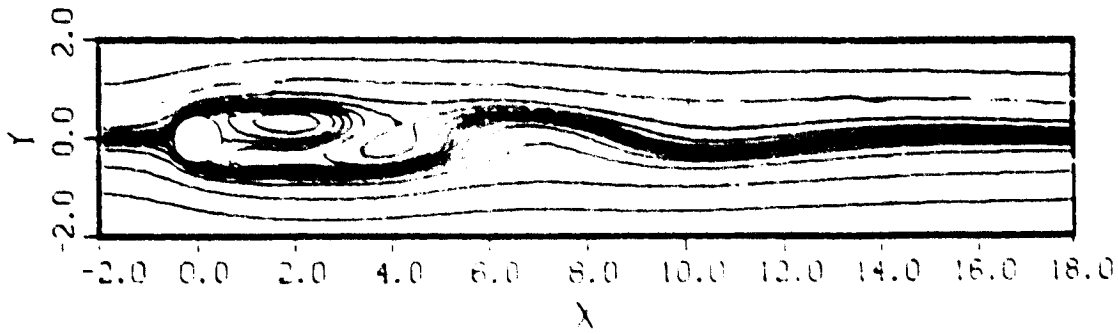

(a) T=27.0

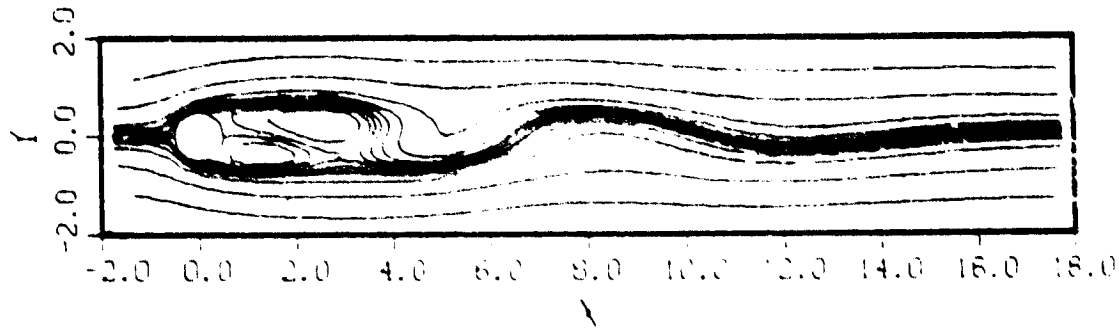

(b) T=29.0

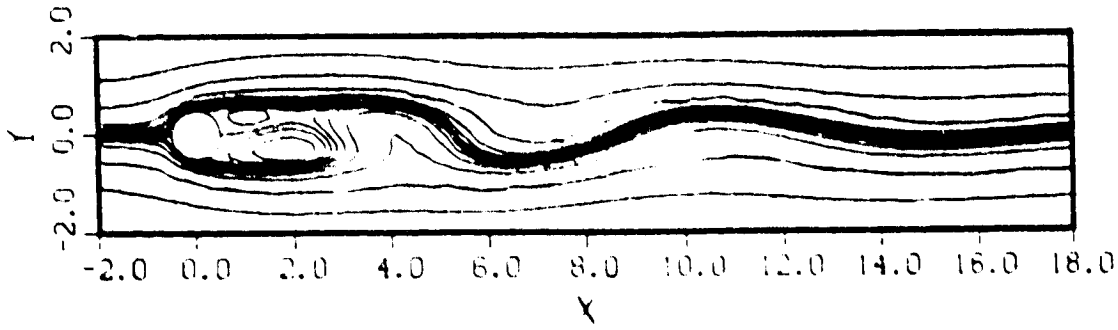

(c) T=32.0

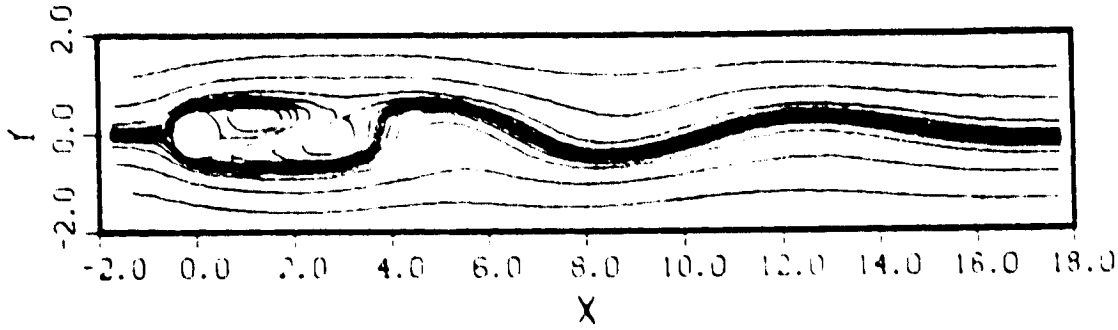

(d) T=33.8

Fig. 6-8 Re=100 (Stream line)

ORIGINAL PAGE IS
OF POOR QUALITY

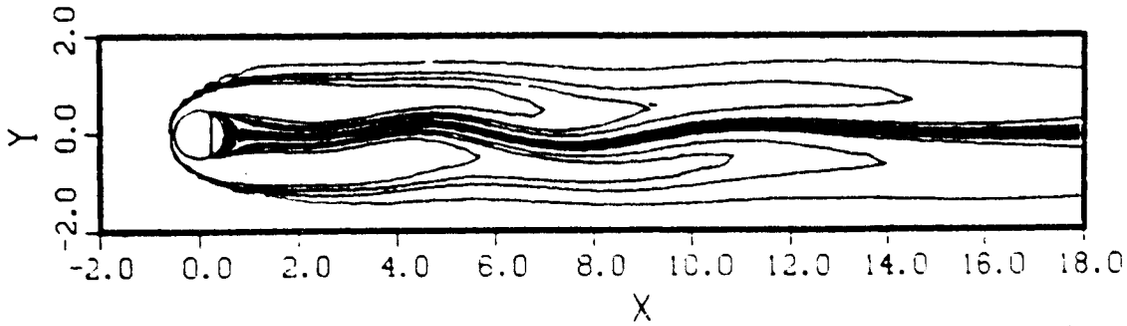

(a) T=27.0

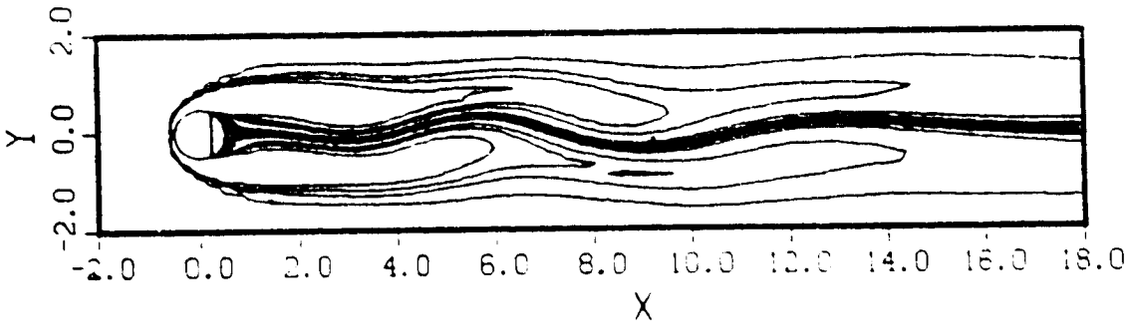

(b) T=29.0

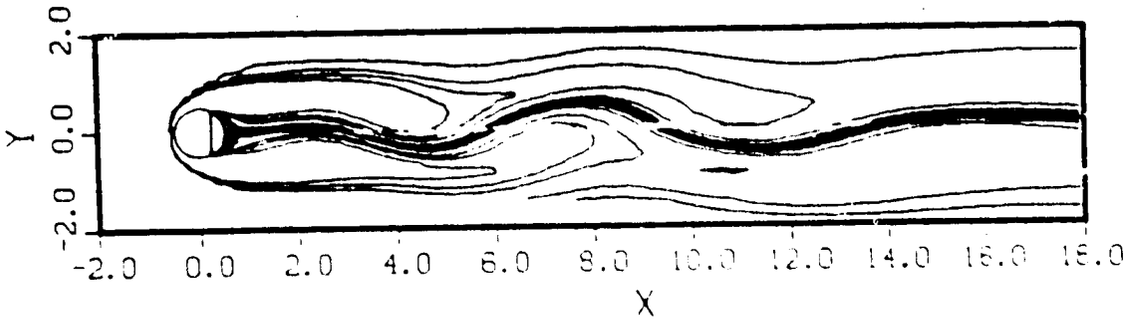

(c) T=32.0

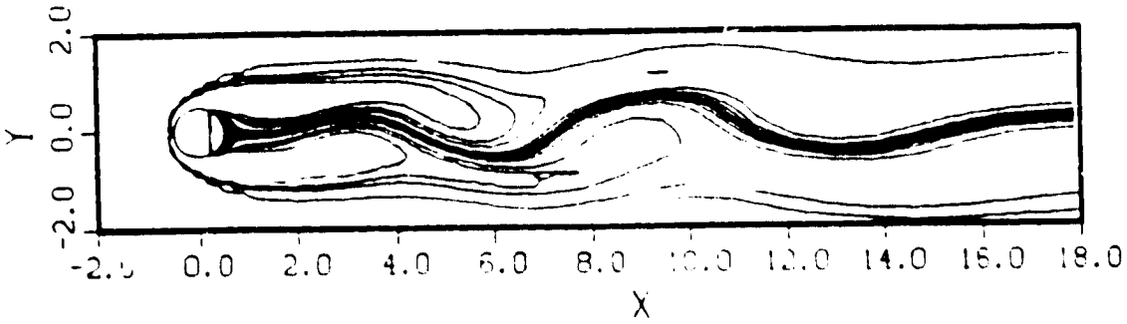

(d) T=33.8

Fig. 6-9 Re=100 (Vorticity function)

in finding whether the integration of the FA method and boundry fitted coordinate system can be used to solve the vortex shedding phenomena behind an arbitrary shape body and whether an accurate numerical result can be obtained with large time step Δt and few iterations at each time. In this case, the time step size is $\Delta t=0.2$ and the maximum iteration for each time step in solving stream function Eq.(4-5b) or vorticity function Eq.(4-5a) is 20. If the absolute error between two iteration is not larger than 10^{-6}, then the iteration is terminated automatically. Using the general numerical procedure outlined in Table 5-2, the FA solution predicts the separation angle at $\theta=64$, which agrees with results as shown in Fig. 6-7. A little lower Strouhal number S=0.15, as compared to experimental results [20] of 0.155 and 0.165, as shown in Fig. 6-10.

6.2.5 Re=500

Fig. 6-11 shows the prediction of the stream line in one half period of vortex shedding at Re=500, and Fig. 6-12 is the vorticity distribution at the corresponding time step. Although at Re=500 the flow is turbulent, the numerical procedure is the same as that for Re=100 except we decrease the time step Δt to 0.1 and increase the maximum number of iteration to 50 times. The FA solution for laminar vortex shedding at Re=500 shows that the separation angle is

ORIGINAL PAGE IS
OF POOR QUALITY

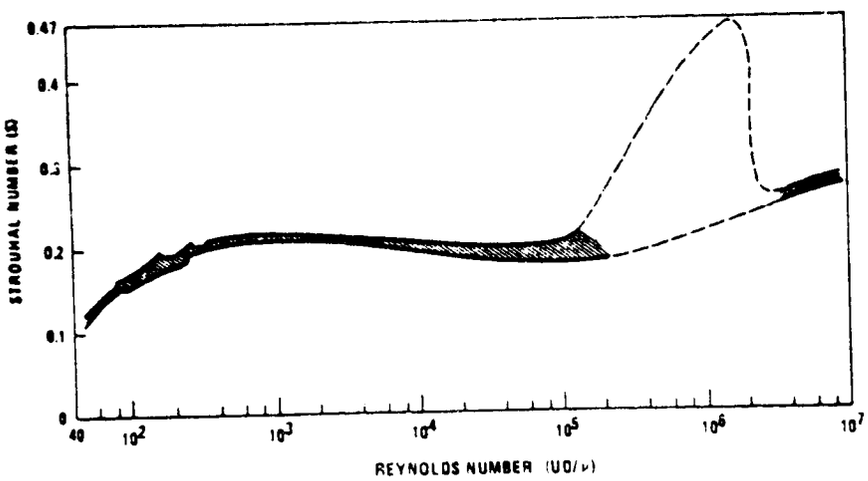

Fig. 6-10 The Strouhal-Reynolds number relationship for circular cylinders. (Ref.20)

ORIGINAL PAGE IS
OF POOR QUALITY

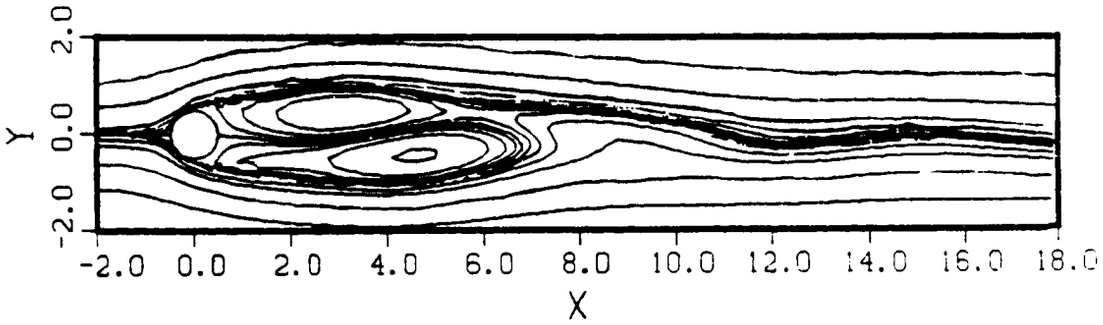

(a) T=15.2

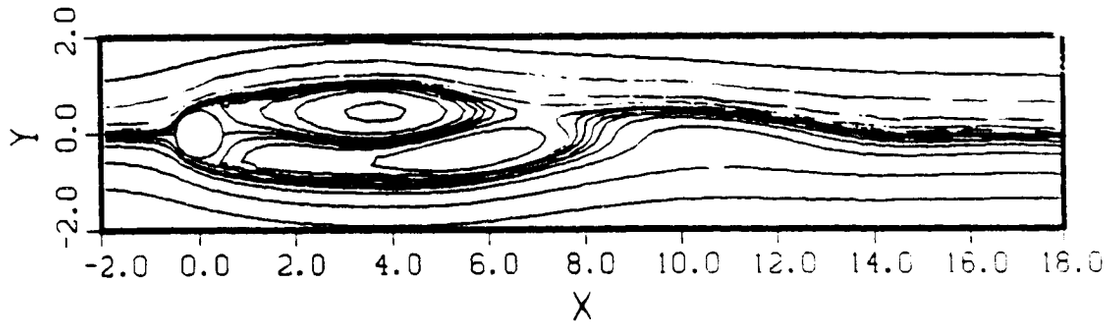

(b) T=17.6

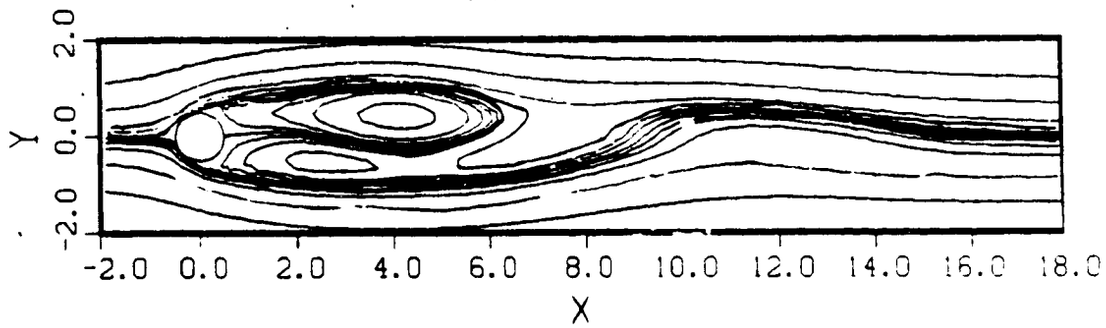

(c) T=19.2

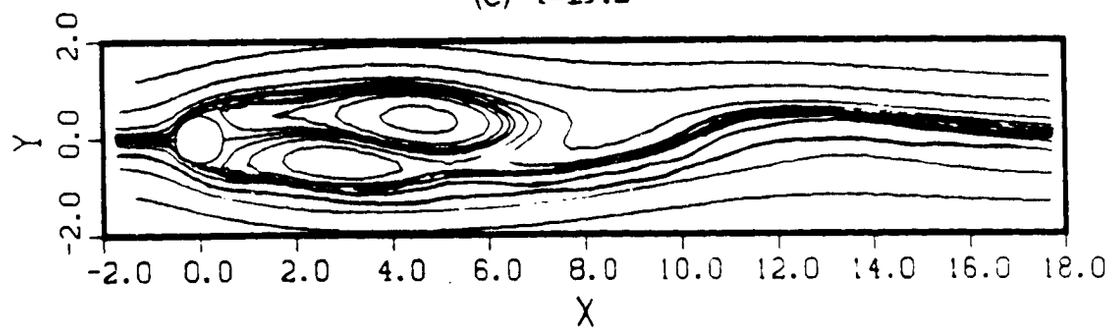

(d) T=20.8

Fig. 6-11 Re=500 (Stream line)

ORIGINAL PAGE IS
OF POOR QUALITY

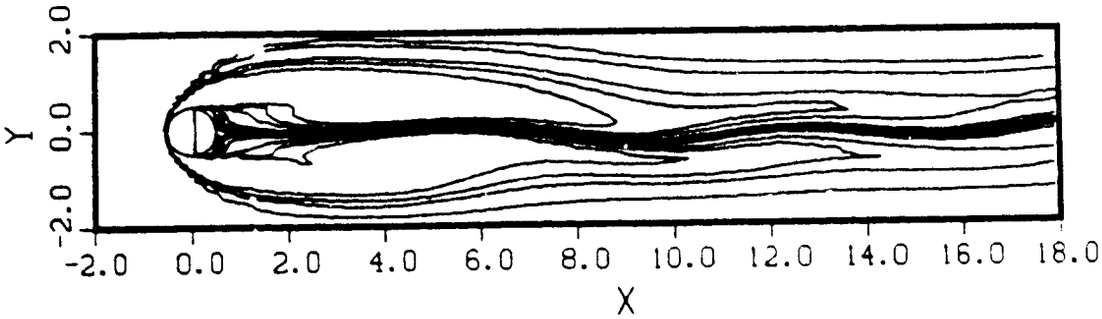

(a) T=15.2

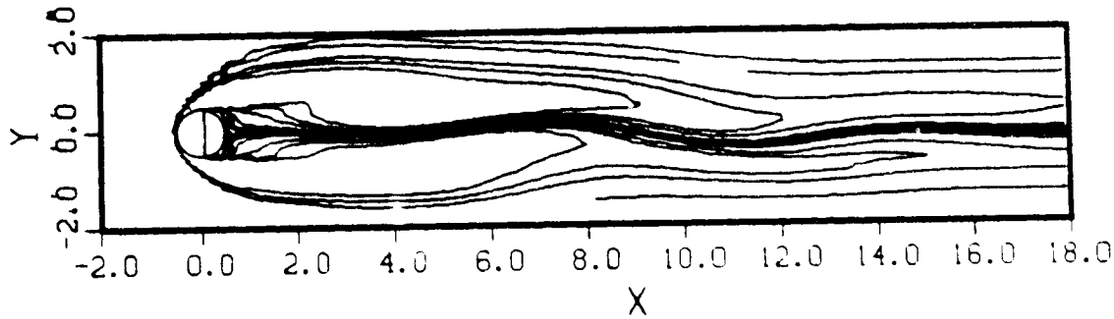

(b) T=17.6

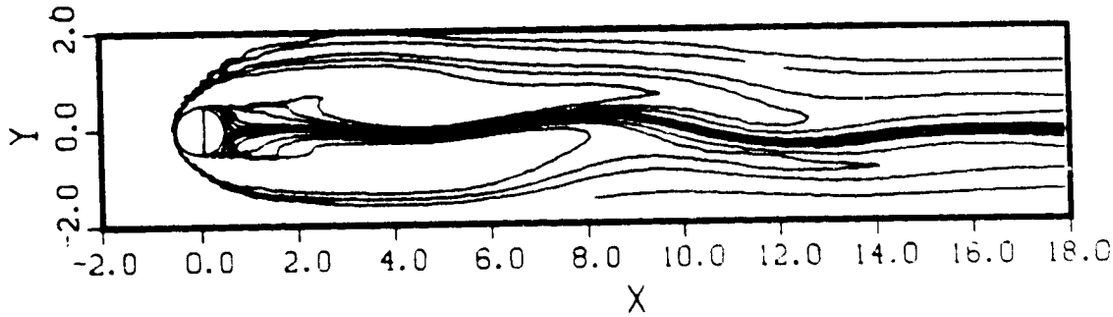

(c) T=19.2

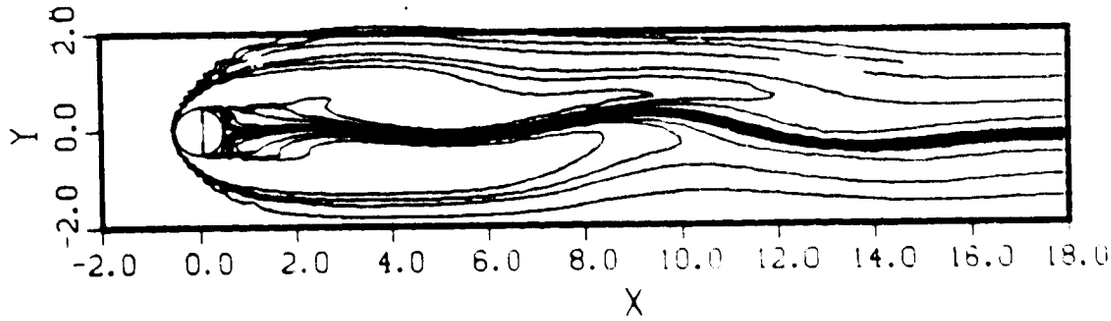

(d) T=20.8

Fig. 6-12 Re=500 (Vorticity function)

82.5 , which is in reasonable agreement with others measurements shown in Fig. 6-7, while the predicted Strouhal number S is 0.09, which is lower when compared with experimental data in Fig. 6-10.

6.2.6 Discussion

It should be remarked first that the separation angle is obtained from the zero vorticity value on the circular cylinder surface. This is because the stream function on the circular cylinder is zero at all time, and there is no other indication of how the zero stream function line in the field on the first η- coordinate line above the circular surface and that on circular surface can be connected. This seems always to lead plot machine to distort the separation point on the graph of stream line. On the other hand the separation point based on the zero vorticity values on the circular surface gives more consistent prediction. This is because the vorticity values at wall can be defined as $\omega=-\partial V_t/\partial n$, thus when the sign of the vorticity values at wall changes between two wall nodes, it means there exists a separation point there. An simple interpolation between these two wall nodes gives the degree of separation angle.

The fact that the separation angle is predicted satisfactorily by Eq.(6-2) on the body surface means the proper distribution of vorticity values on the body surface

is achieved. However, this method of evaluating vorticity values on the body surface may become more difficult if the obstacle has a complex shape, where accurate normal direction is difficult to evaluate. Therefore, it is desirable to have a boundary fitted coordinate system that is almost orthogonal near the body surface, so that Eq.(6-1) instead of Eq.(6-2) can be used. The 'OC-type' outer boundary (see Fig. 4-2 and Fig. 6-15) adopted in the next section provides a boundary fitted coordinate system which is nearly orthogonal near the body surface.

Examing the predicted results for laminar flow at Re=500, one realizes that the laminar model can't predict the turbulent flow. A turbulence model must be added in the governing equations in order to obtain the real flow pattern in this case.

It should be mentioned that thirteen streamlines of different increments ($\psi=\pm 1.0$, ± 0.5, ± 0.2, ± 0.1, ± 0.05, ± 0.02 and 0.00) are plotted in all the figures of stremline in this study, while nineteen equal-vorticity lines ($\omega=\pm 5.0$, ± 1.0, ± 0.5, ± 0.2, ± 0.1, ± 0.05, ± 0.02, and 0.00) are plotted in all the figures of vorticity function.

6.3 Numerical Results at OC-type Outer Boundary

In setting up an OC-type boundary fitted coordinate system (see Fig. 3-2) the computational domain was generated

by combining an O-type coordinate system around the body and a C-type coordinate system downstream of this O-type coordinate. Two boundary fitted coordinate systems are obtained as shown in Figs. 4-2 and 6-15. The former with a wide but a short computational domain (12x32) is generated with Laplace equation as the transformation equation, while the later with a narrow but a long computational domain (8x54) is generated with Poisson equation. In either case lines arround the circular cylinder is almost normal to the body surface, thus Eq.(6-1) is employed to evaluate the vorticity values on the body surface. In order to examine the effect of the boundary condition and the size of computational domain on the solution, two sets of the downstream boundary conditions are chosen. For the coordinate system with 60x48 nodes (see Fig. 4-2) in 12x32 domain, downstream boundary is not far behind the circular cylinder, thus Eq.(4-4d-2) was adapted as the boundary conditions for the downstream boundary. For the coordinate system with 38x41 nodes (see Fig. 6-15) in 8x54 domain, the downstream boundary is much farther behind the circular cylinder, thus Eq.(4-4d-1) instead of Eq.(4-4d-2) was used as the downstream boundary conditions.

Figs. 6-13 and 6-14 present the FA numerical solution of the streamline and vorticity function for one half period of vortex shedding at Re=100 for the coordinates with a short downstream boundary. The separation angle is predicted to be θ_s=68 and Strouhal number S=0.125 which are worse than the results obtained in the last section. Compare Figs 6-13 and 6-14 with Figs. 6-7 and 6-8 one sees that there are some differences between these two results.

Using the same numerical procedures in section 6-2, the numerical solutions were obtained at the second computational domain (Fig. 6-15) for Reynolds numbers 5, 40, and 100. Fig. 6-16 through Fig. 6-20 show all the FA numerical results at this case. At Re=100, the separation angle is now 66, and Strouhal number S=0.15. Compare with the results in the last section, one can find much similar between these two results.

6.3.1 Discussion

Before making the comparison of three numerical results, let us designate the numerical results obtained on the C-type boundary fitted coordinate as case 1, the numerical results on the OC-type boundary fitted coordinate (Fig. 4-2) with 12x32 computational domain as case 2, and the numerical results on the OC-type boundary fitted coordinate with 8x54 computational domain as case 3.

ORIGINAL PAGE IS
OF POOR QUALITY

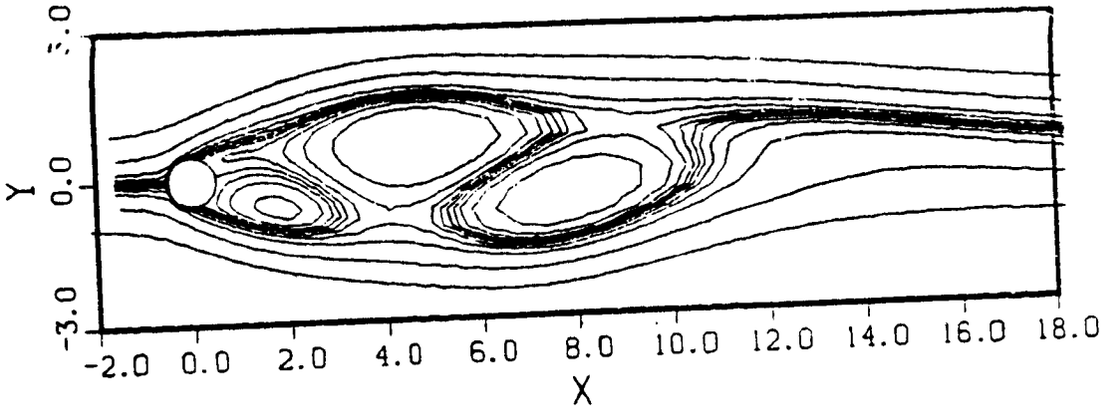

(a) T=20.0

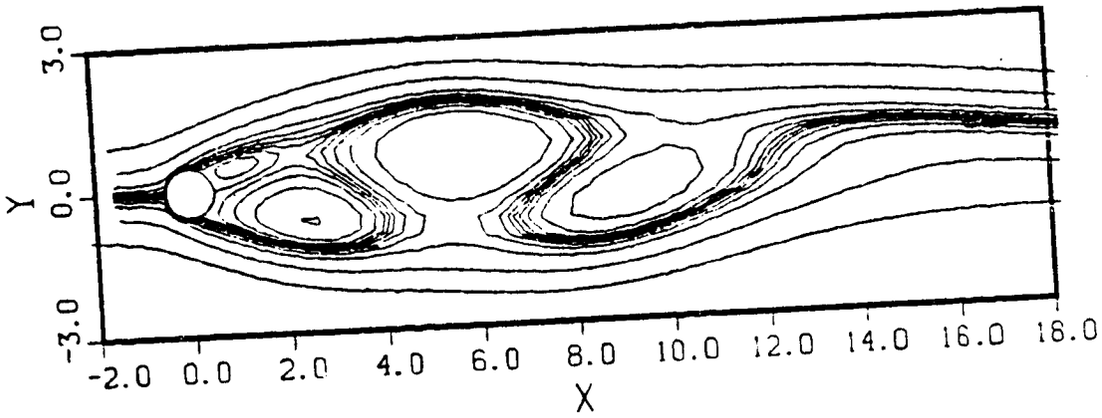

(b) T=22.0

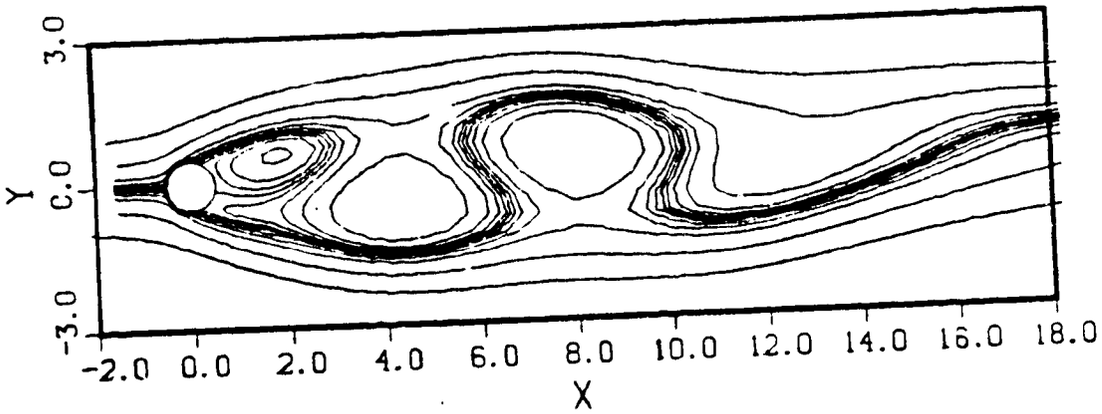

(c) T=24.0

Fig. 6-13 Re=100 (Stream line)

ORIGINAL PAGE IS
OF POOR QUALITY

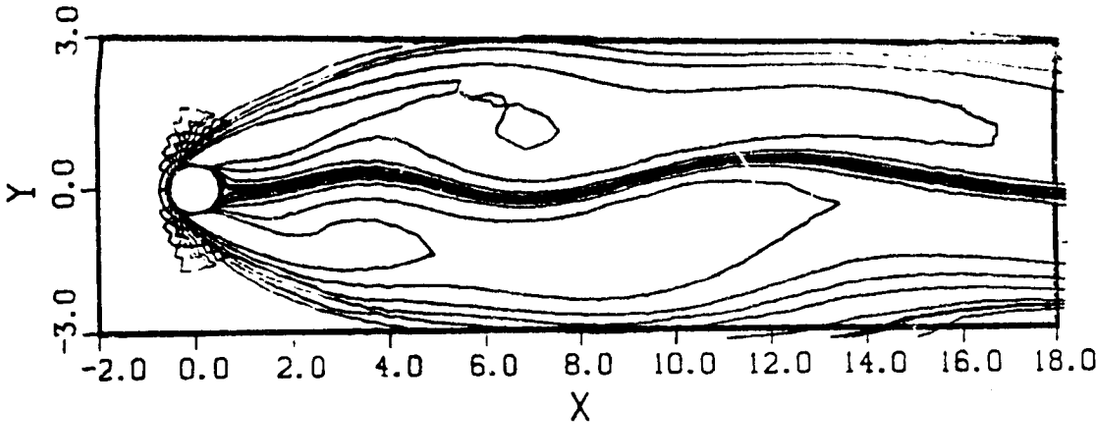

(a) T=20.0

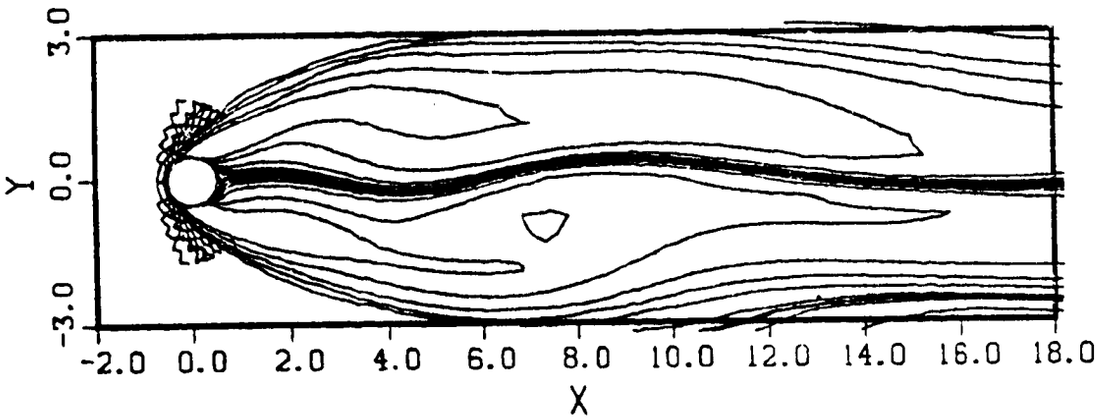

(b) T=22.0

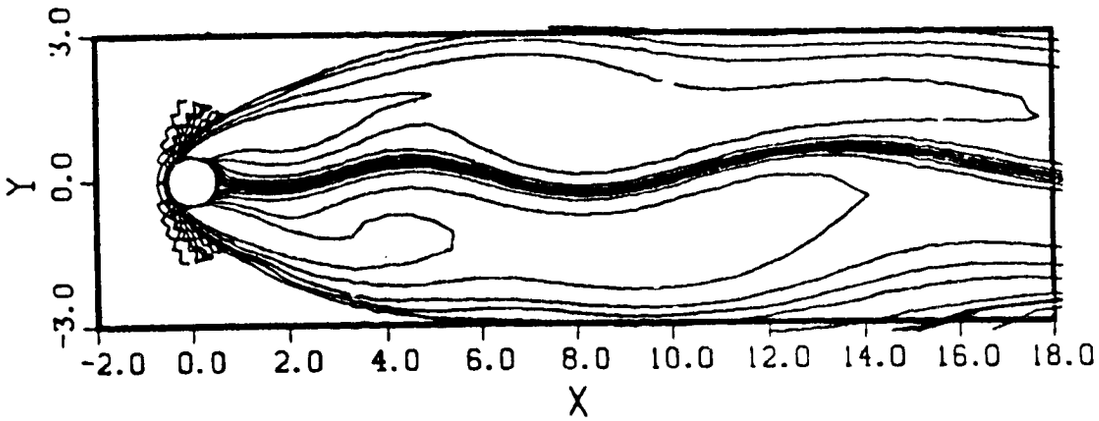

(c) T=24.0

Fig. 6-14 Re=100 (Vorticity function)

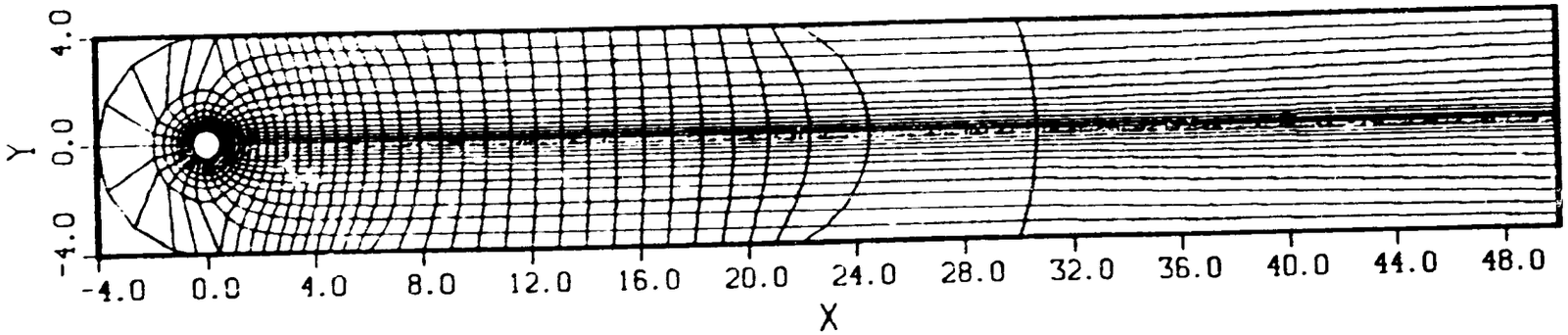

Fig. 6-15 Computational domain of 'OC-type' boundary fitted coordinates

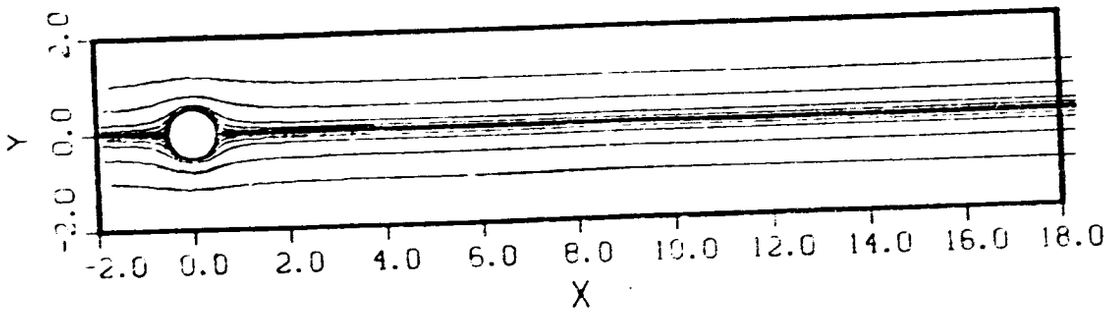

Fig. 6-16 Potential flow

ORIGINAL PAGE IS
OF POOR QUALITY

ORIGINAL PAGE IS
OF POOR QUALITY

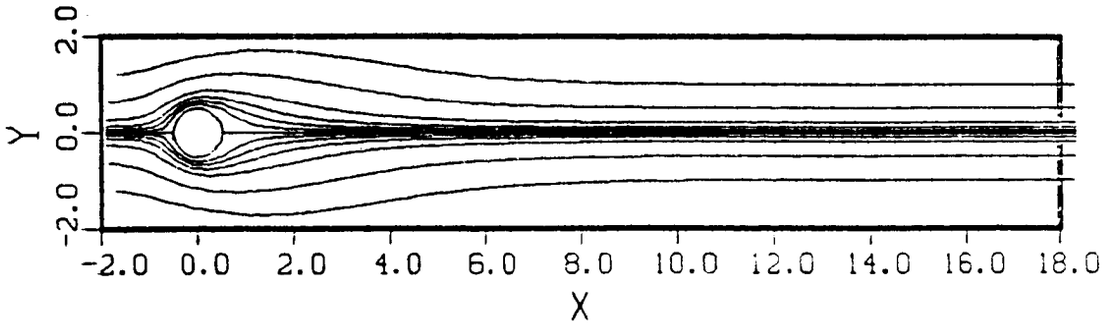

(a) Stream line

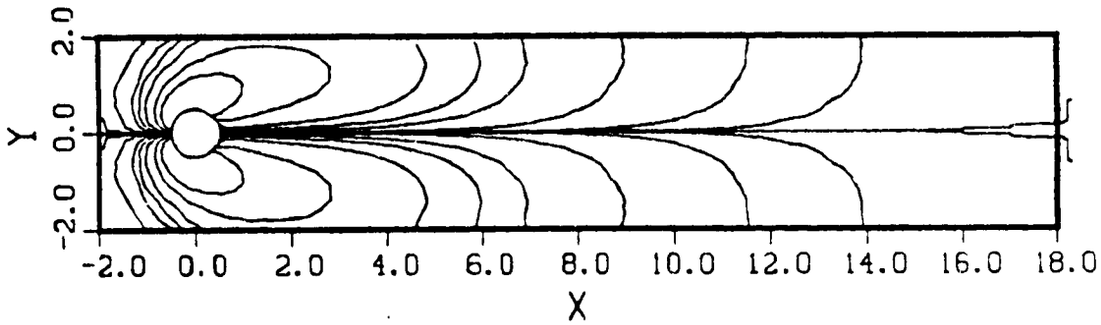

(b) Vorticity function

Fig. 6-17 Re=5

ORIGINAL PAGE IS
OF POOR QUALITY

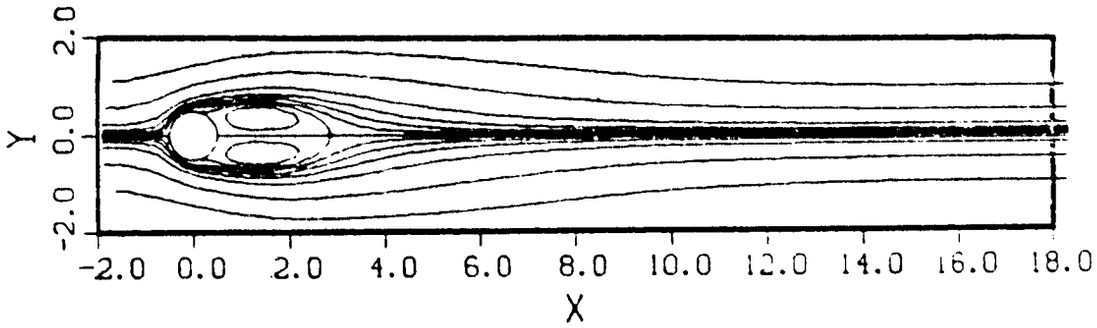

(a) Stream line

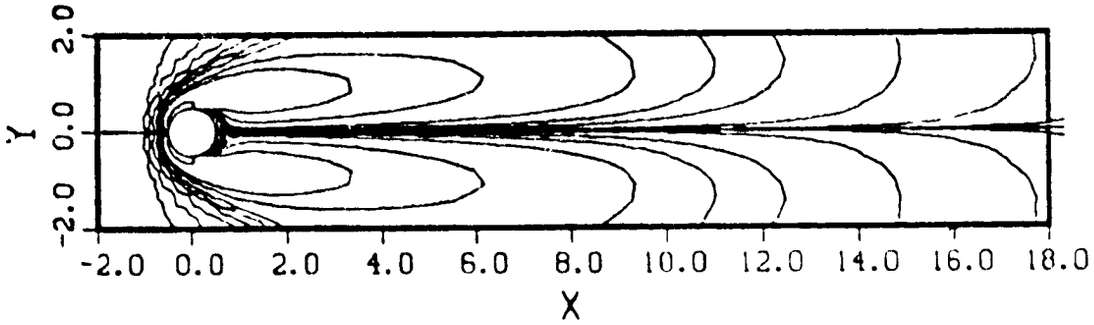

(b) Vorticity function

Fig. 6-18 Re=40

ORIGINAL PAGE IS
OF POOR QUALITY

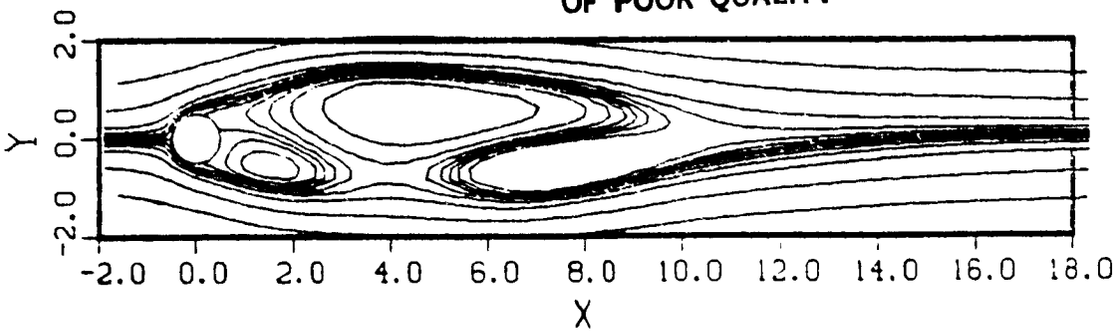

(a) T=1.8

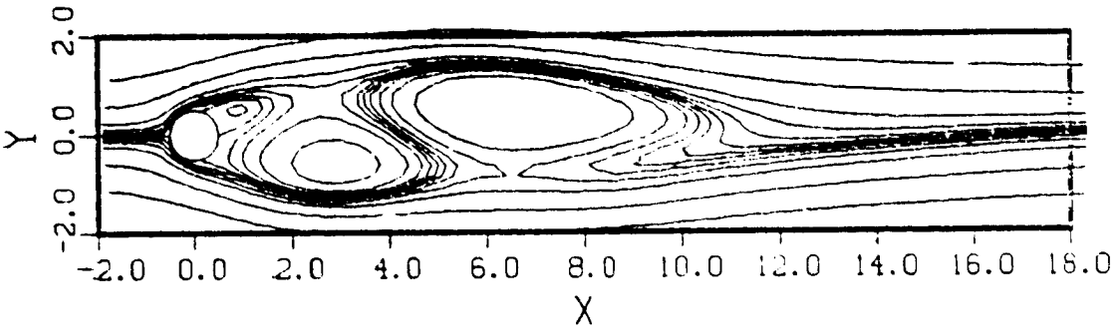

(b) T=4.4

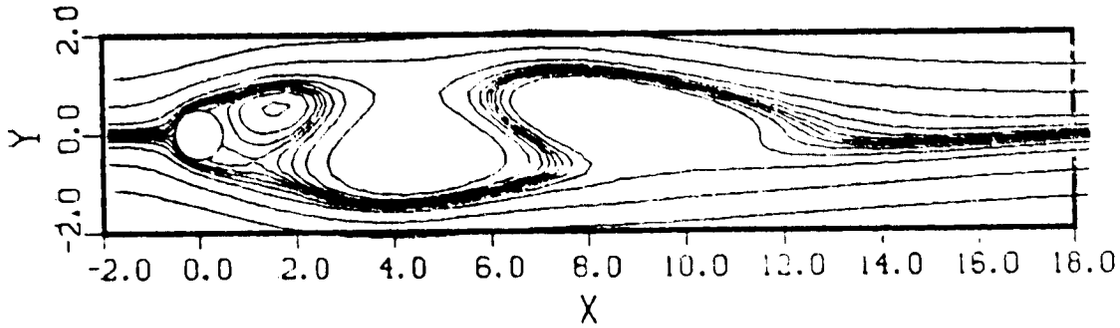

(c) T=6.6

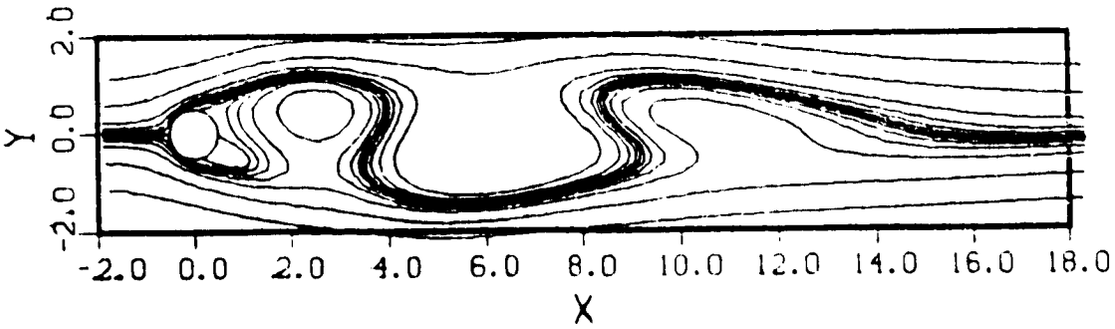

(d) T=8.6

Fig. 6-19 Re=100 (Stream line)

ORIGINAL PAGE IS
OF POOR QUALITY

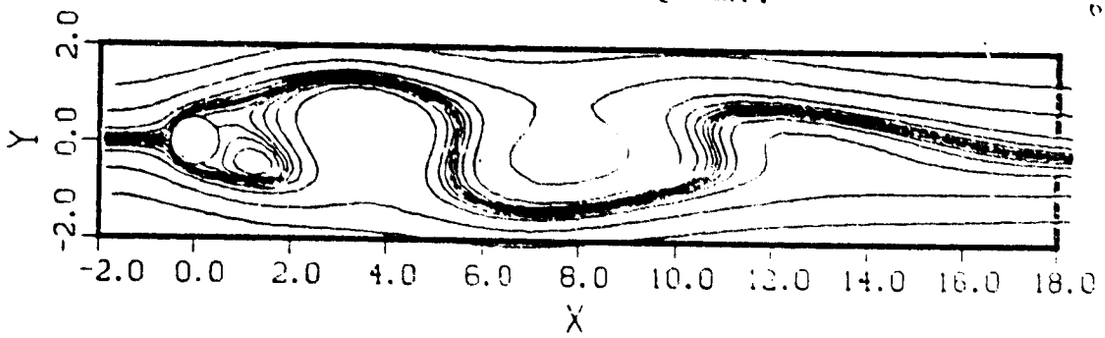

(e) T=10.0

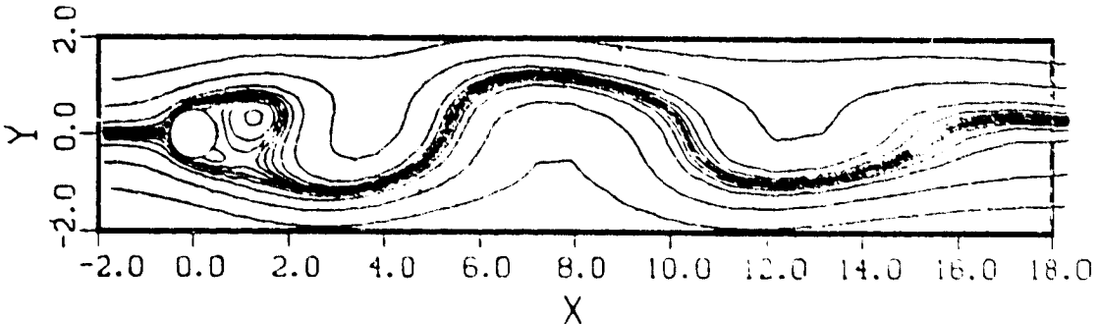

(f) T=13.0

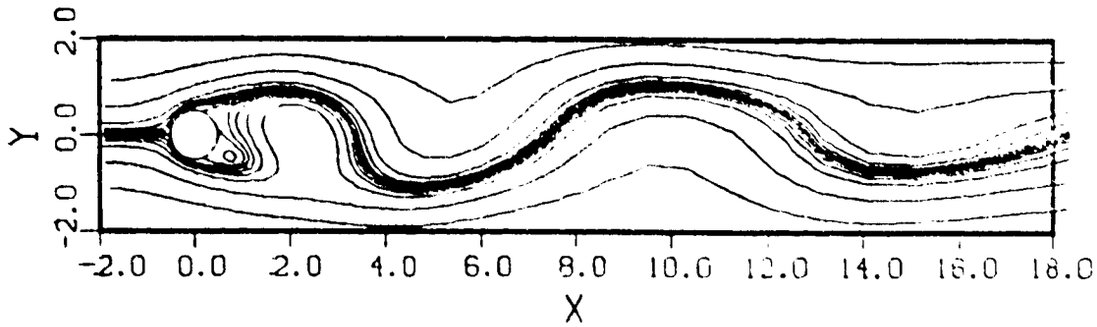

(g) T=15.0

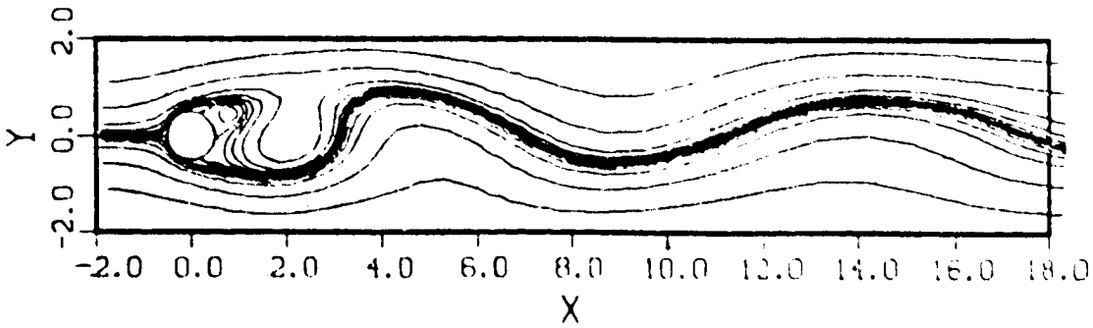

(h) T=17.0

Fig. 6-19 Continued

ORIGINAL PAGE IS
OF POOR QUALITY

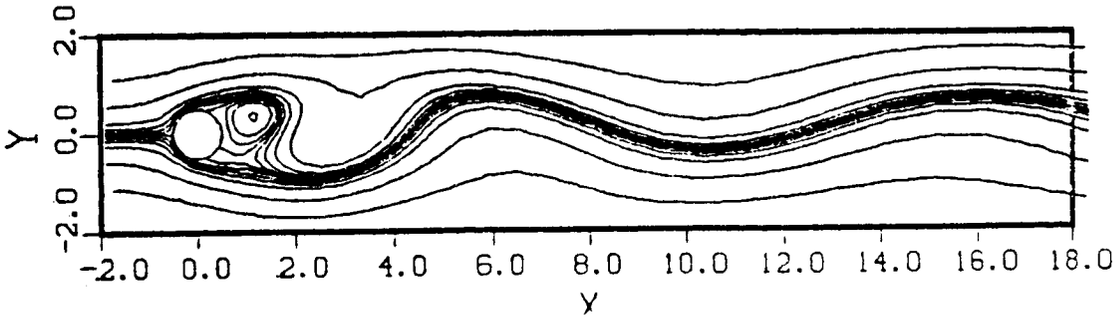

(i) T=18.0

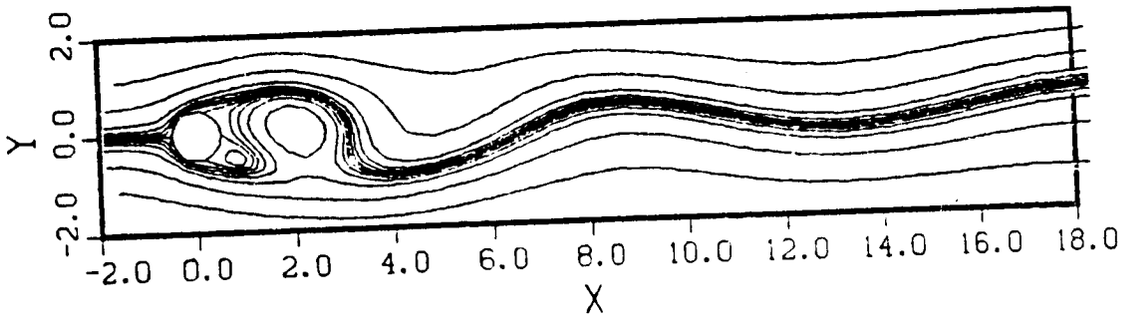

(j) T=19.8

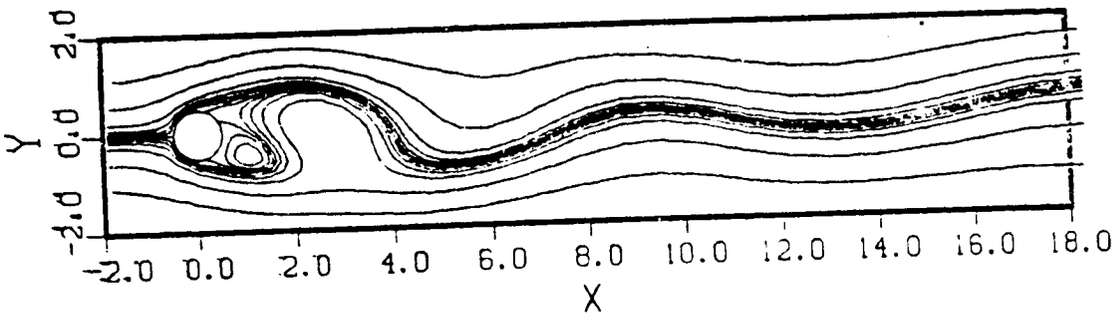

(k) T=21.0

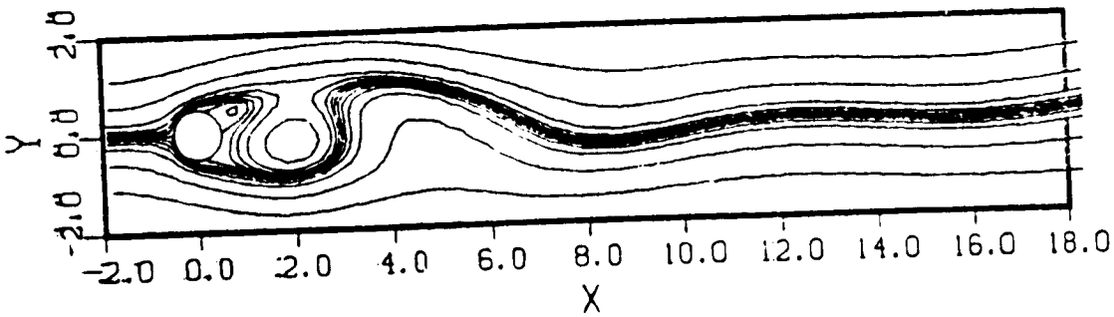

(l) T=23.0

Fig. 6-19 Continued

ORIGINAL PAGE IS
OF POOR QUALITY

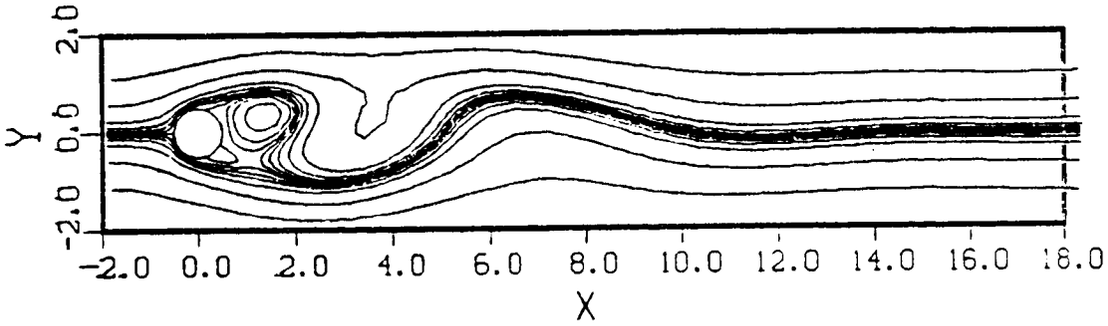

(m) T=24.8

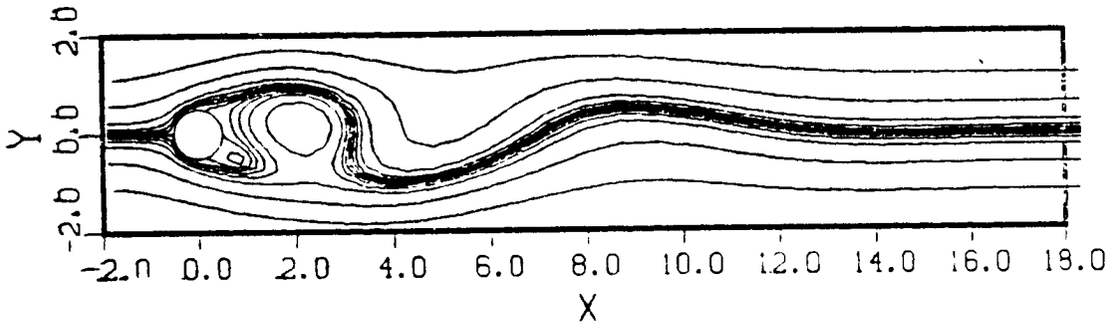

(n) T=26.4

Fig. 6-19 Continued

ORIGINAL PAGE IS
OF POOR QUALITY

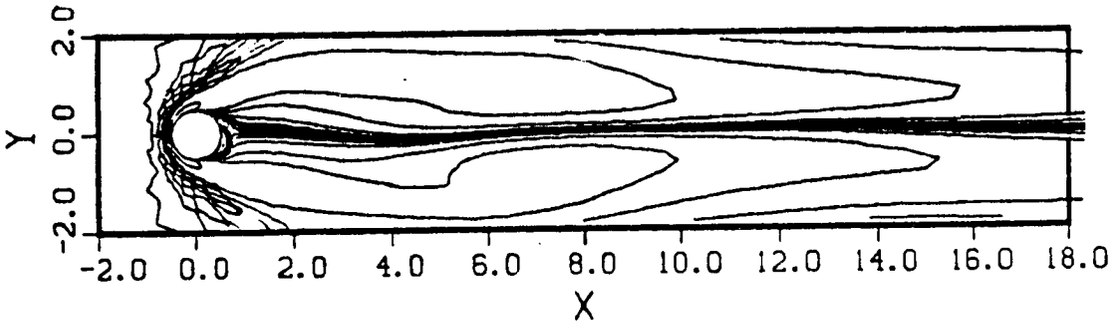

(a) T=1.8

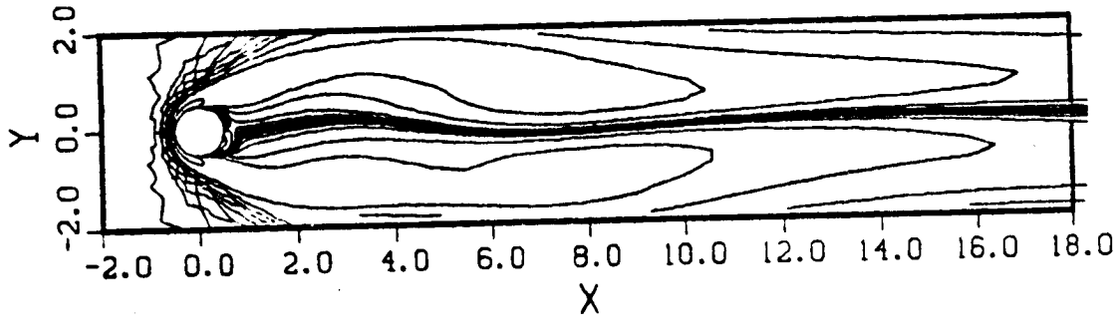

(b) T=4.4

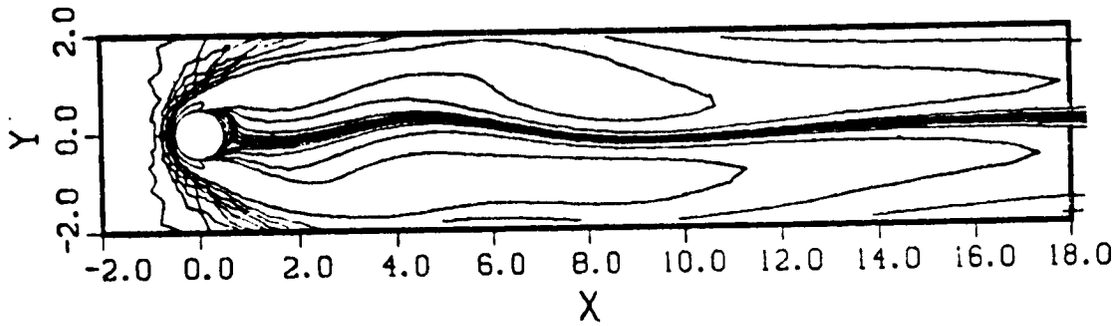

(c) T=6.6

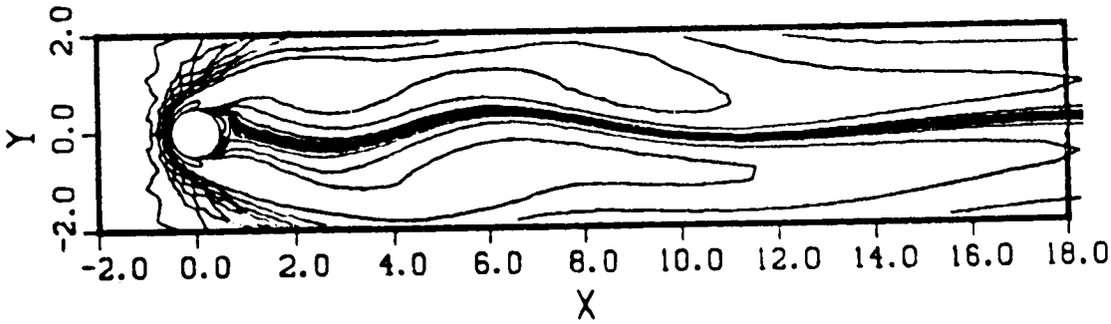

(d) T=8.6

Fig. 6-20 Re=100 (Vorticity function)

ORIGINAL PAGE IS
OF POOR QUALITY

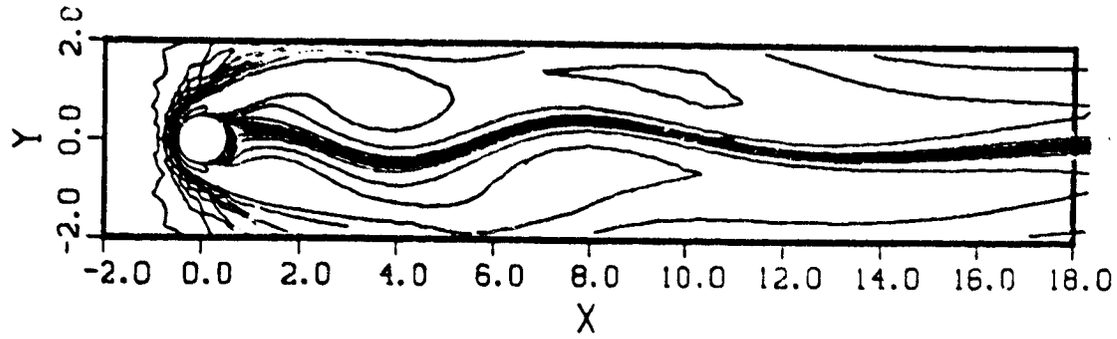

(e) T=10.0

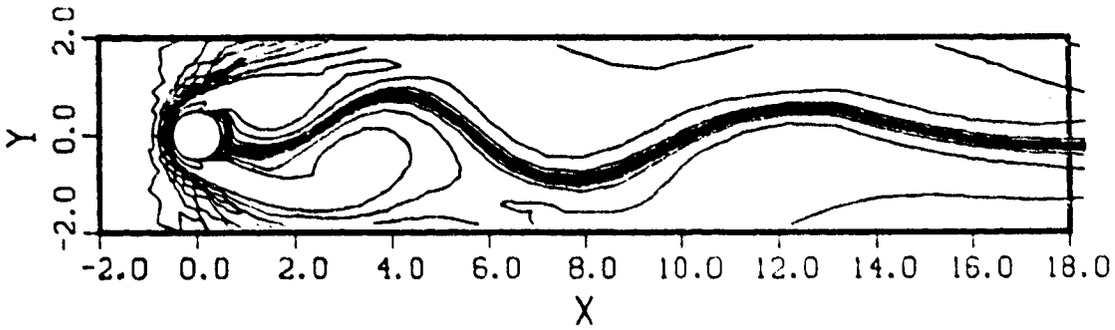

(f) T=13.0

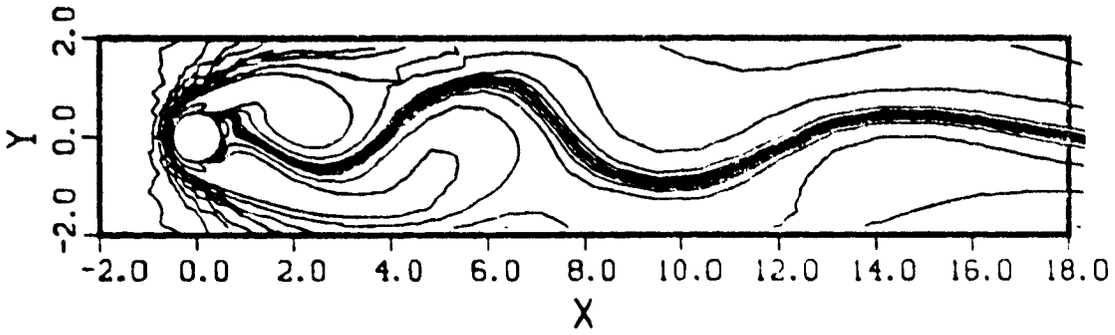

(g) T=15.0

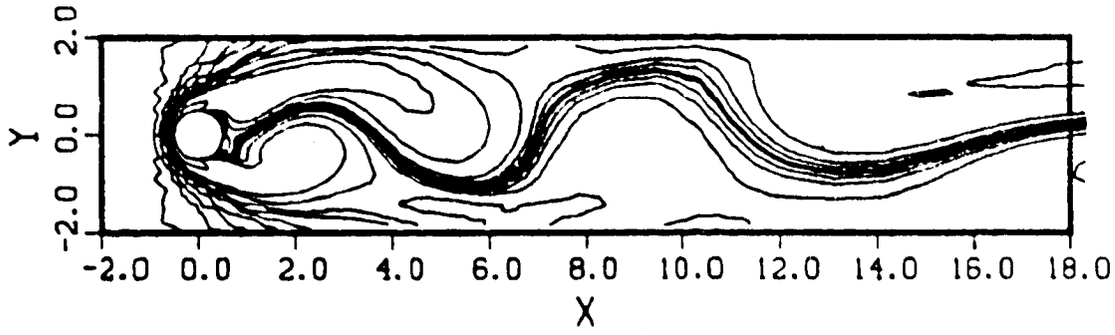

(h) T=17.0

Fig. 6-20 Continued

ORIGINAL PAGE IS
OF POOR QUALITY

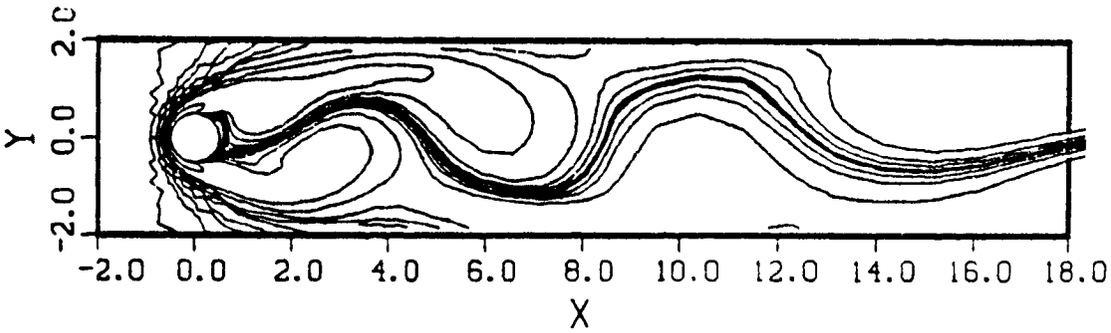

(i) T=18.0

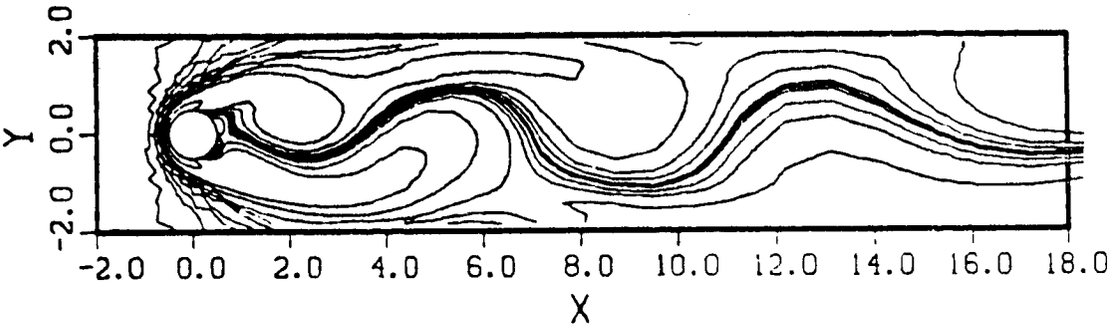

(j) T=19.8

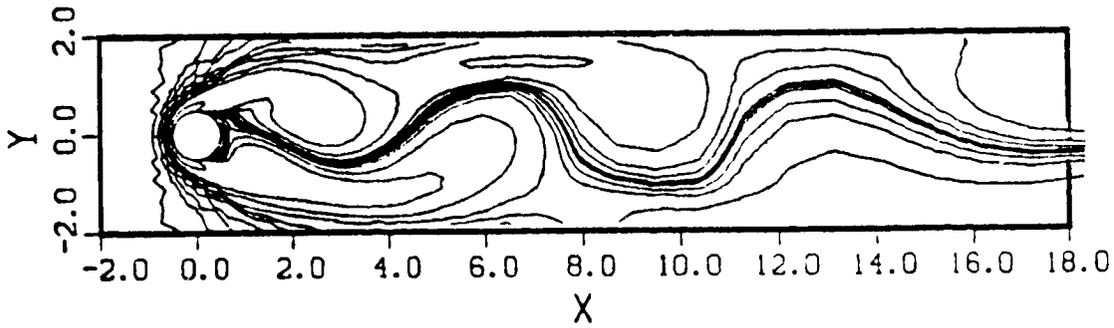

(k) T=21.0

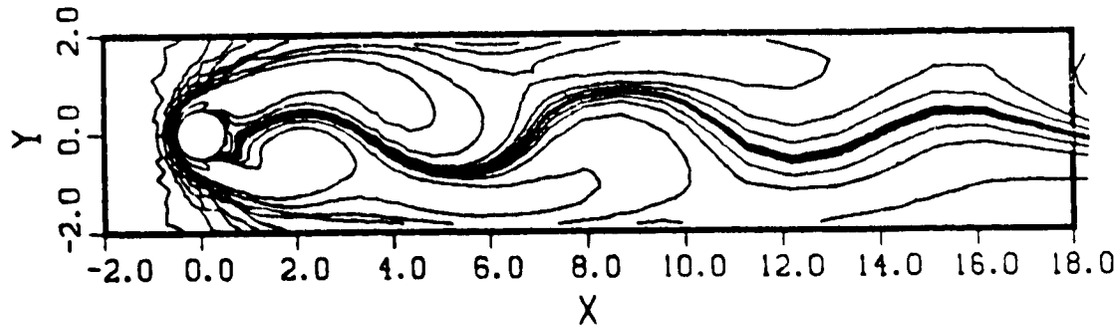

(l) T=23.0

Fig. 6-20 Continued

ORIGINAL PAGE IS
OF POOR QUALITY

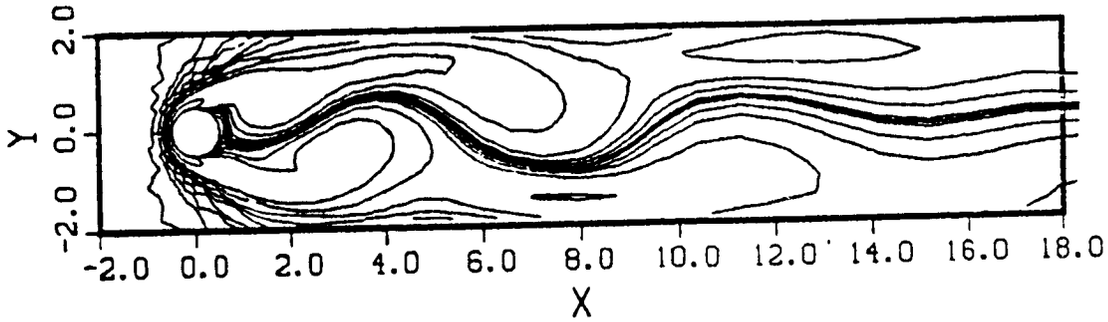

(m) T=24.8

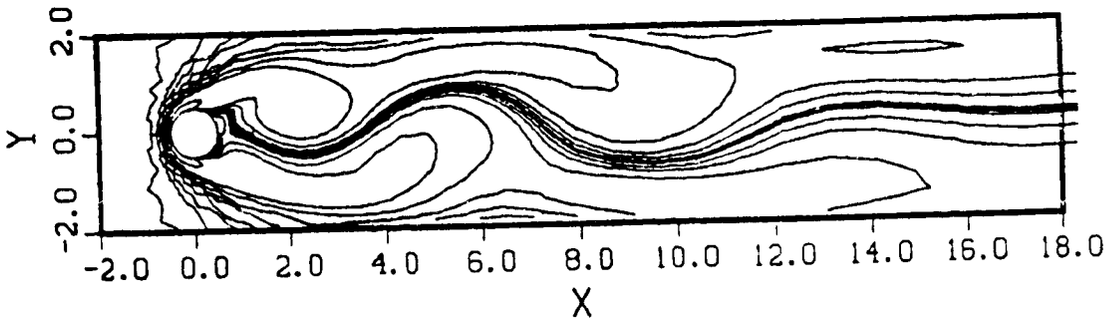

(n) T=26.4

Fig. 6-20 Continued

ORIGINAL PAGE IS
OF POOR QUALITY

(1)Comparison of three numerical solutions for Reynolds number of 100 (see Figs. 6-7, 6-13, and 6-19) shows that case 2 gives the weakest vorticity strength and lowest Strouhal number S=0.125, while the other two results show the similar strength in vorticity value. The reason that case 2 deviates from the other two cases is probably due to the use of Eq.(4-4d-2) as the boundary condition on the downstream boundary. The numerical results of the vortex shedding for case 3 presented in Figs. 6-19 and Figs. 6-20 illustrate the evaluation of the flow from the begining to a stage of steady shedding. Comparison of the flow patterns predicted in the three cases shows that it took a longer time for case 2 to attend a steady shedding. This is due to the use of the boundary condition of Eq.(4-4d-2) $\psi_n^t=\psi_{n-1}^{t-1}, \omega_n^t=\omega_{n-1}^{t-1}$ which tends to delay vortex shedding and as a consequence the vortex grows much larger than it should be, behind the circular cylinder. Thus, it is concluded that Eq.(4-4d-2) is not a good boundary condition for the downstream boundary.

(2)In case 3, although the computational domain is narrower than the first two cases the predicted flow is similar to that of case 1 for each corresponnding Reynolds number. This implies that in order to predicting a vortex shedding phenomena a large computational domain behind the body is more important than top and bottom boundaries. In

the present study it suggests that a minimum distance of 50 diameters of circular cylinder is required.

(3)It is found that the separation angles predicted in the three cases are the same and also agree well with the experimental measurements. One thus may concluded that the use of Eq.(6-1) as the boundary vorticity on the body surface is adequate.

CHAPTER VII

VORTEX SHEDDING BEHIND THE NON CIRCULAR BODY SHAPE

In order to demonstrate the flexibility of the finite analytic solution developed on the boundary fitted coordinates in predicting flows over an arbitrary body shape, the same numerical procedure developed in chapter 6 is used in this chapter to solve flows past a triangle column and a compex arbitrary body shape.

7.1 Flow Over A Triangle Column

There are two reasons in solving the flow over a two dimensional triangle column with the vertex facing the incoming flow (see Fig. 7-1). The first is to demonstrate that the boundary fitted coordinate system can be also generated for a body with linear straight boundaries such as a triangle shape. The second is that there seems no previous numerical prediction of vortex shedding behind the flow past a triangle column. The FA numerical solution will represent a new result in vortex shedding phenomena.

The computational domain and geometry of isosceles triangle is shown in Fig. 7-1 where the vertex of the isosceles triangle is chosen to be a right angle. A total of

ORIGINAL PAGE IS
OF POOR QUALITY

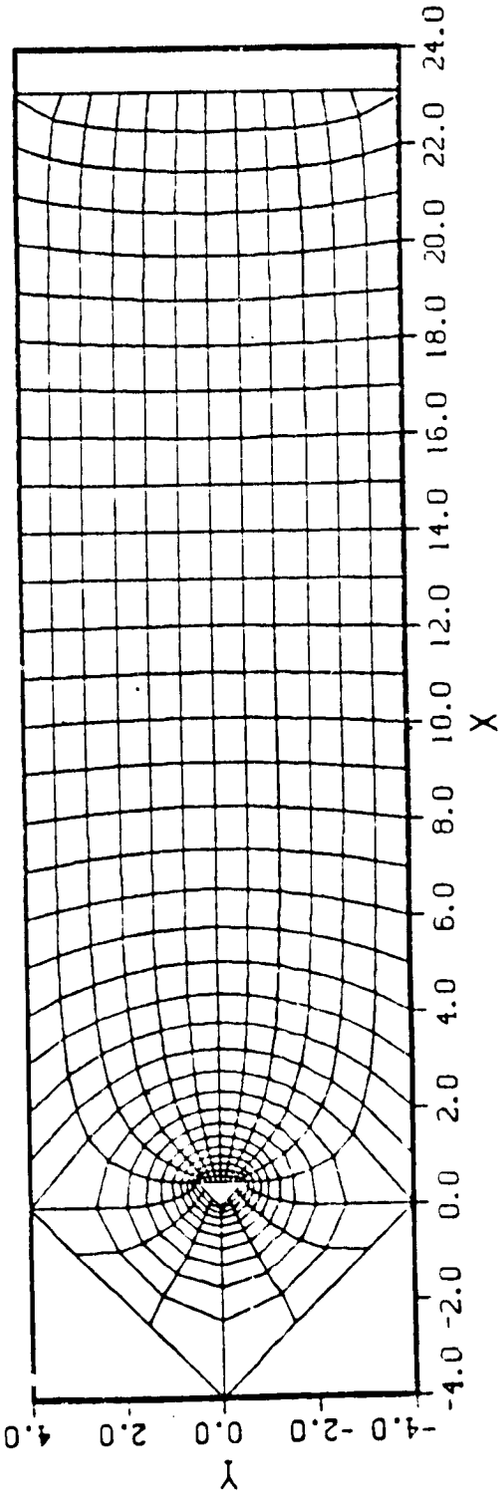

Fig. 7-1 Computational domain of a triangle body

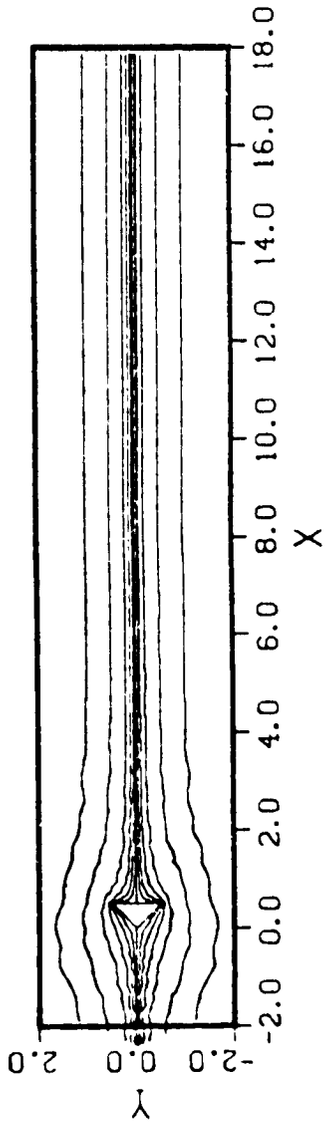

Fig. 7-2 Potential flow

20x35 nodes are used in the computation. The downstream boundary is set at a distance 23 times of the triangle base width. Eq.(4-4d-1) is now used as the boundary condition of the downstream boundary. The finite analytic solution is obtained for Reynolds number of 200 with the potential flow pattern as the initial condition. In this case, the time step Δt is 0.2 and the maximun iteration for each time is 20.

Fig. 7-2 shows the potential flow pattern for the inviscid flow past the isosceles triangle. The ripple show in the figure is due to the plotter connecting the nodal values between relative large grid size used in the present calculation. Figs. 7-3 and 7-4 show the stream line and vorticity function for Re=200 at different time interval during a period of vortex shedding. The shedding frequency or Strohaul number is found to be S=0.156. The Strohaul number is only slightly lower than that of the experimental measurement (S=0.18) [16]. Considering the coarse grid size and few nodes used in the present calculation the prediction is good.

7.2 Flow Over An Irregular Body Shape

The computational domain shown in Fig. 7-5 is the same as that shown in Fig. 6-15. The only change is that the obstacle body, instead of a circular shape is an irregular

ORIGINAL PAGE IS
OF POOR QUALITY

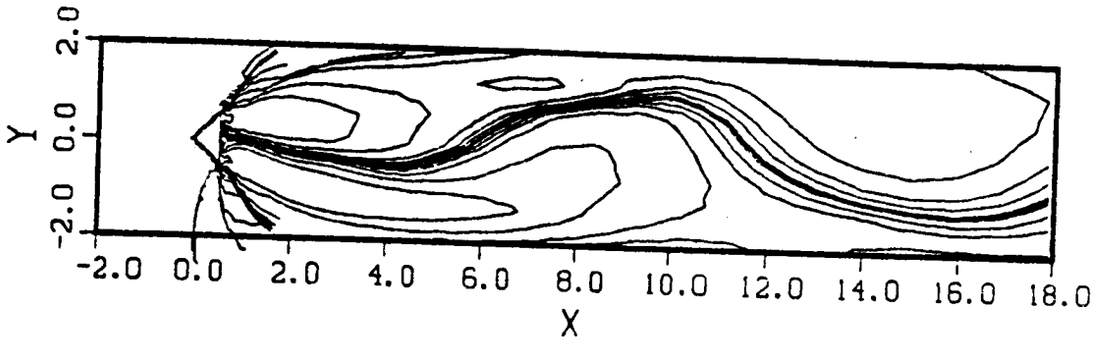

(a) T=13.6

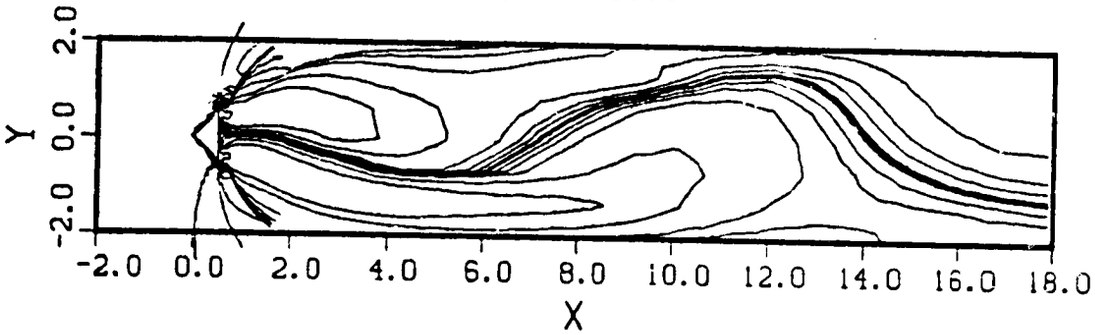

(b) T=15.0

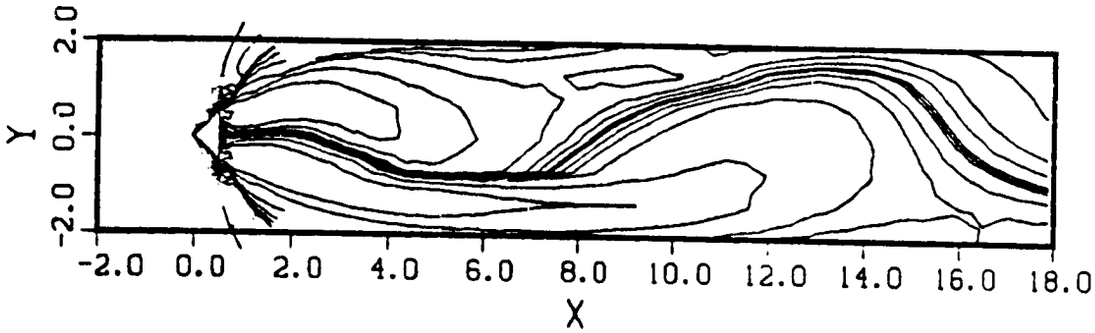

(c) T=16.0

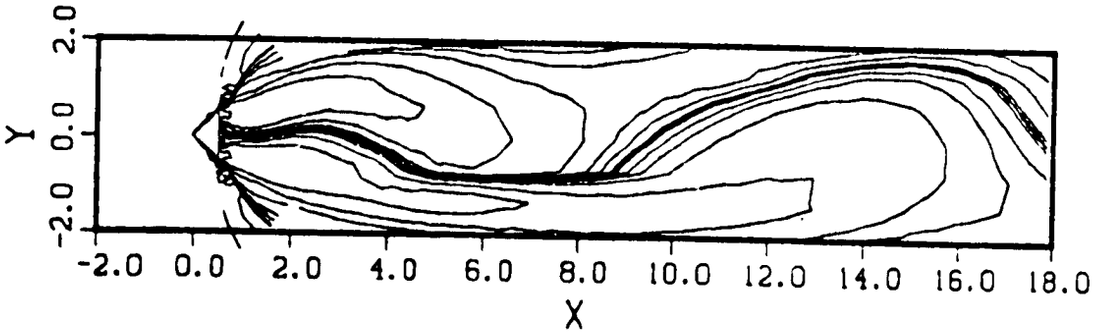

(d) T=17.0

Fig. 7-4 Re=200 (Vorticity function)

ORIGINAL PAGE IS
OF POOR QUALITY

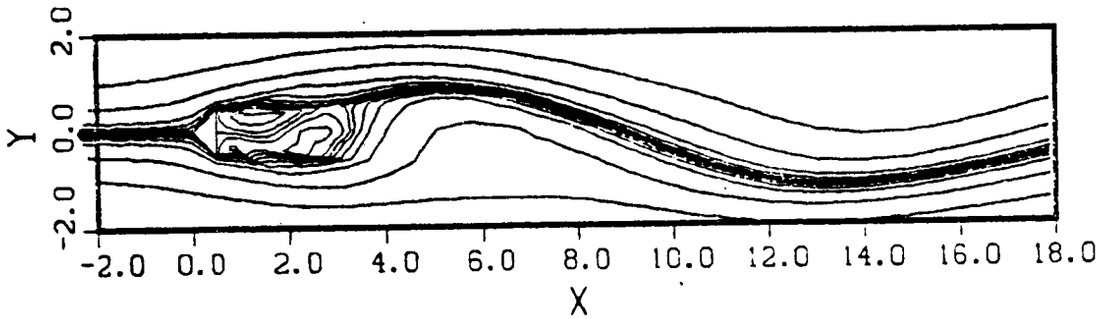

(e) T=17.8

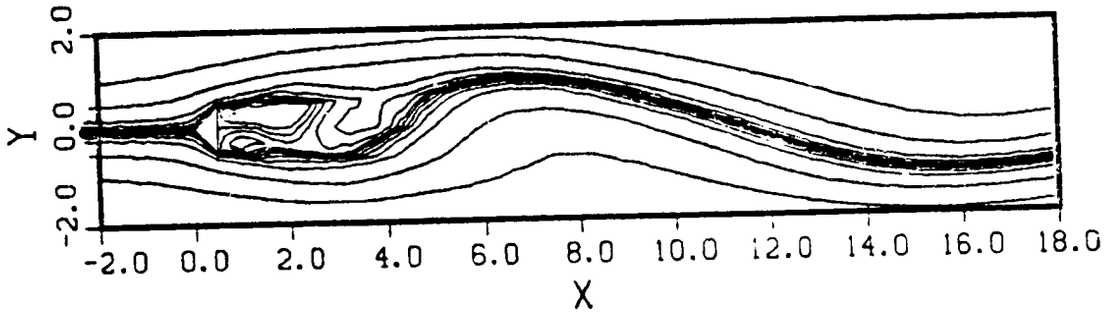

(f) T=19.0

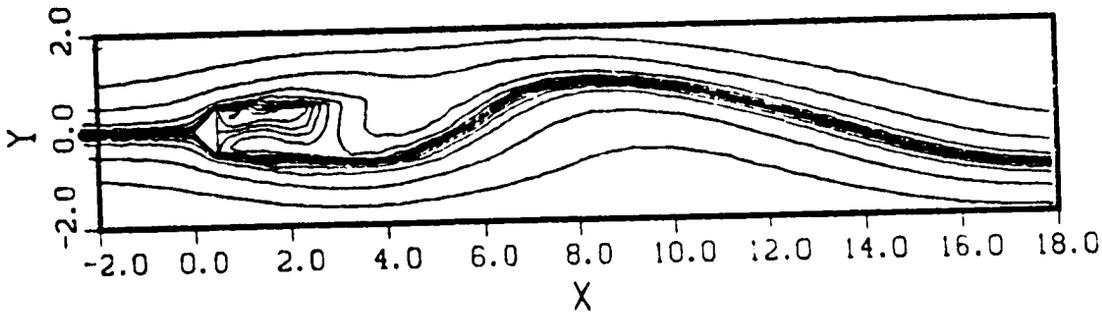

(g) T=20.0

Fig. 7-3 Continued

ORIGINAL PAGE IS
OF POOR QUALITY

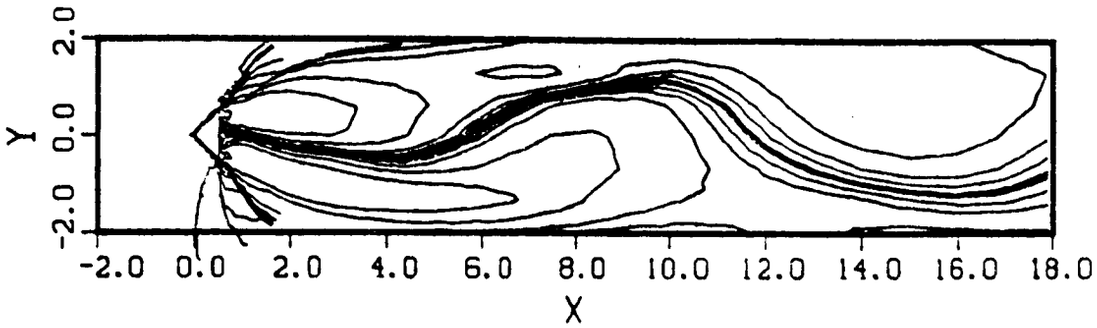

(a) T=13.6

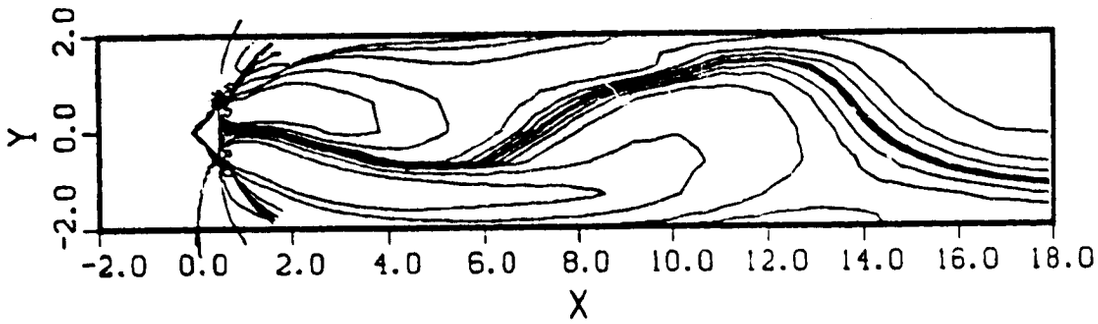

(b) T=15.0

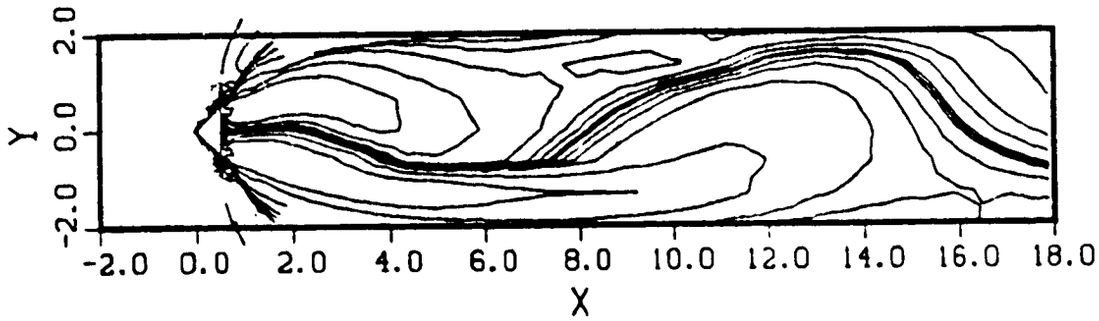

(c) T=16.0

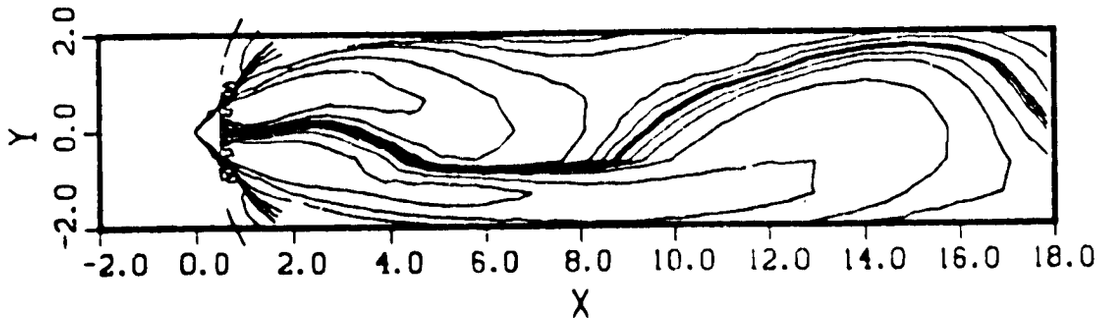

(d) T=17.0

Fig. 7-4 Re=200 (Vorticity function)

ORIG
OF PO

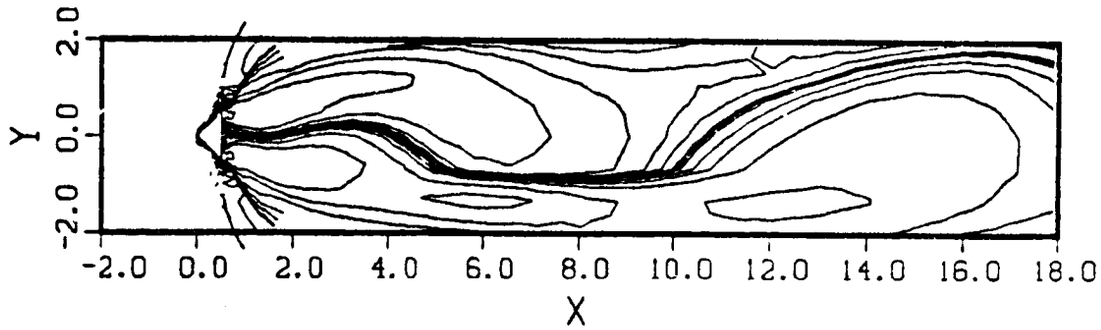

(e) T=17.8

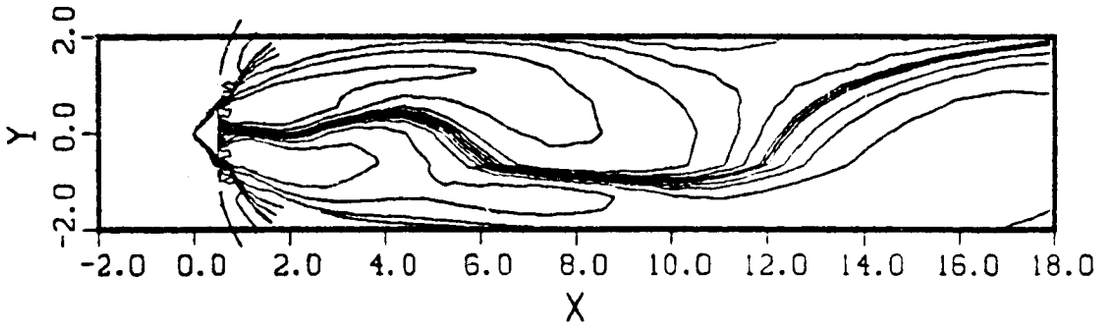

(f) T=19.0

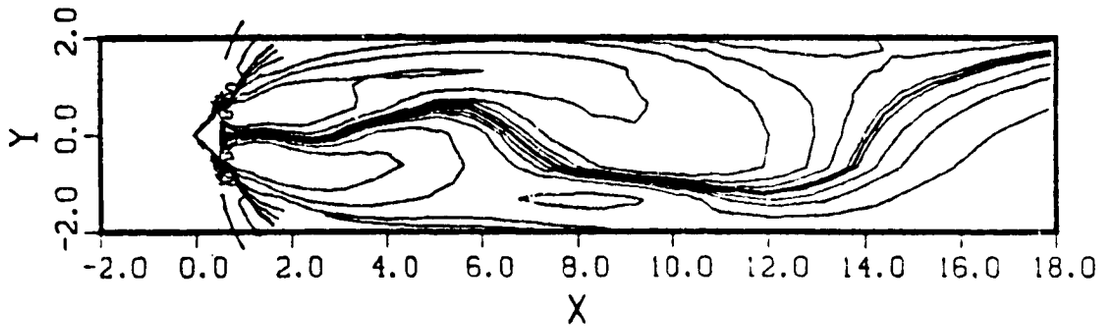

(g) T=20.0

Fig. 7-4 Continued

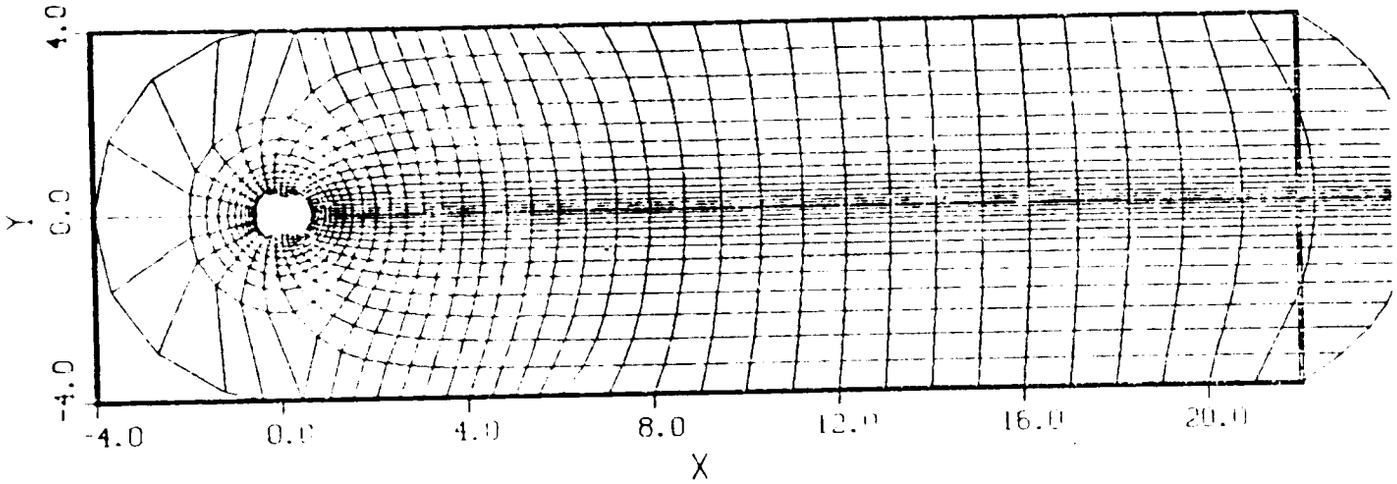

Fig. 7-5 Computional domain of an arbitrary body

ORIGINAL PAGE IS
OF POOR QUALITY

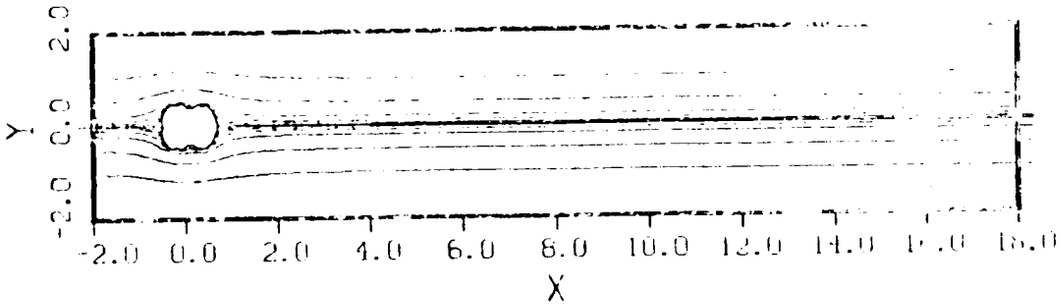

Fig. 7-6 Potential flow

arbitrary shape. The OC-type boundary fitted coordinate is also shown in Fig. 7-5. The same boundary conditions and same numerical procedures as those used in chapter 6 for cylinder case are used here.

Fig. 7-6 shows the stream line pattern of the potential flow over the irregular body shape. Fig. 7-7 shows the stream line and vorticity function at Re=5. Like the flow past a circular cylinder, the flow past the irregular body at Re=5 is still stationary and does not separate. It seems that the local irregularity in shape does not affect the general flow pattern except near the boundary of the body.

Figs. 7-8 and 7-9 present the flow pattern at Re=40. The FA solution predicts a major pair of stationary vortices behind the body which reaches a stable size at a time approximately T=5. A small vortices also appear at the concave region of the body surface.

Figs. 7-10 and 7-11 show the evolution of streamline and vorticity function at Re=100. Now the vortex pair can no longer remain stationary and symmetric, and a vortex shedding is formed behind the body. At the concave region of the body surface there also exist a small vortices. The Strohaul number S=0.11 which is smaler than the case of flow past a circular cylinder.

ORIGINAL PAGE IS
OF POOR QUALITY

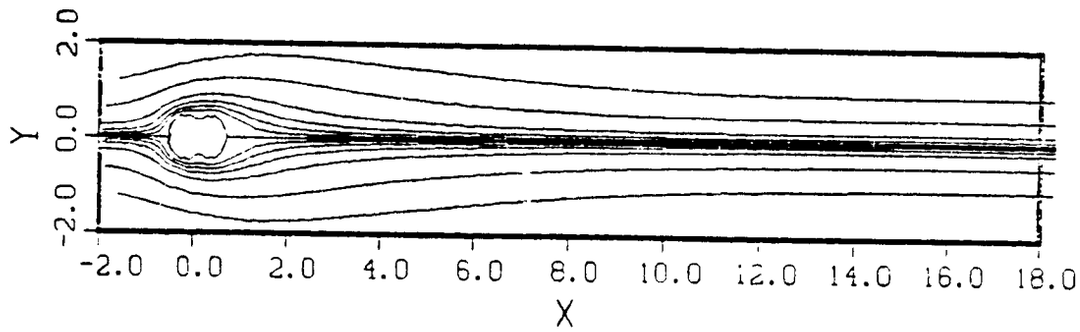

(a) Stream line

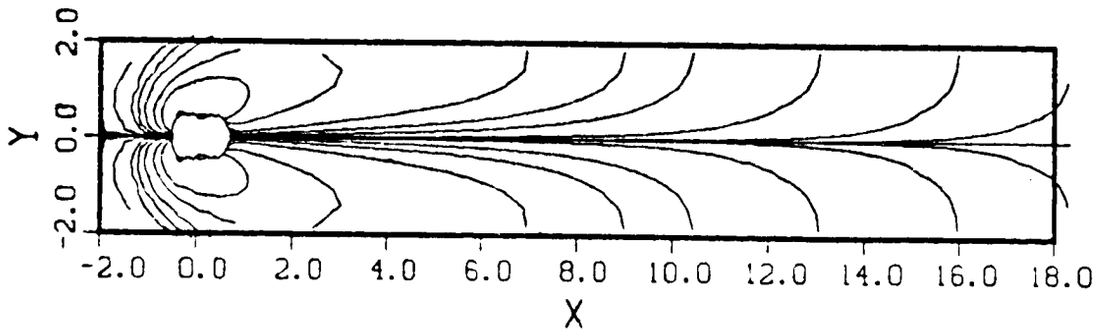

(b) Vorticity function

Fig. 7-7 Re=5

ORIGINAL PAGE IS
OF POOR QUALITY

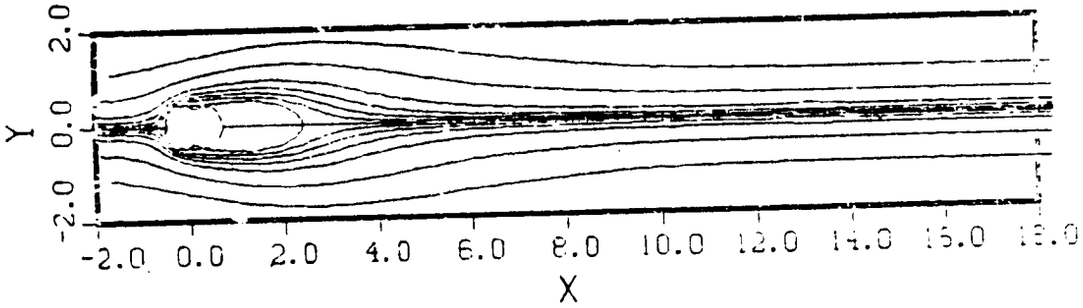

(a) T=0.6

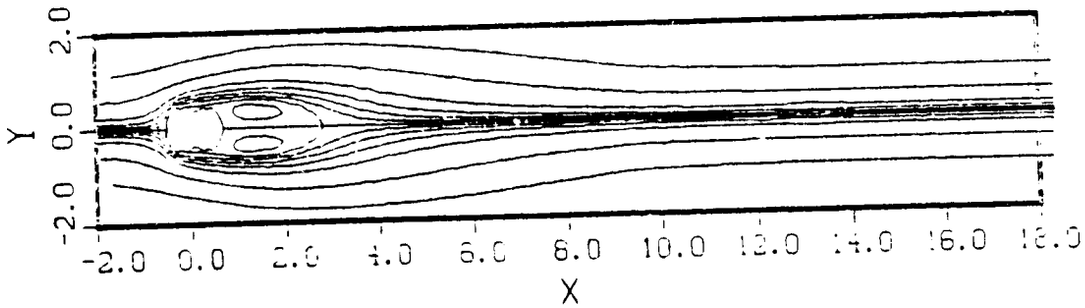

(b) T=1.2

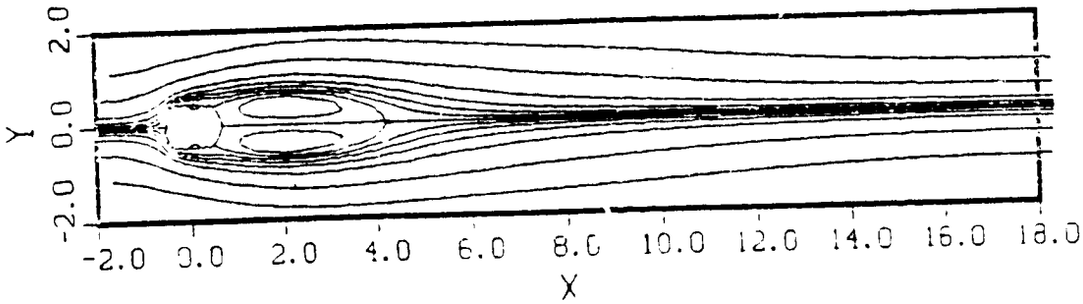

(c) T=5.0

Fig. 7-8 Re=40 (Stream line)

ORIGINAL PAGE IS
OF POOR QUALITY

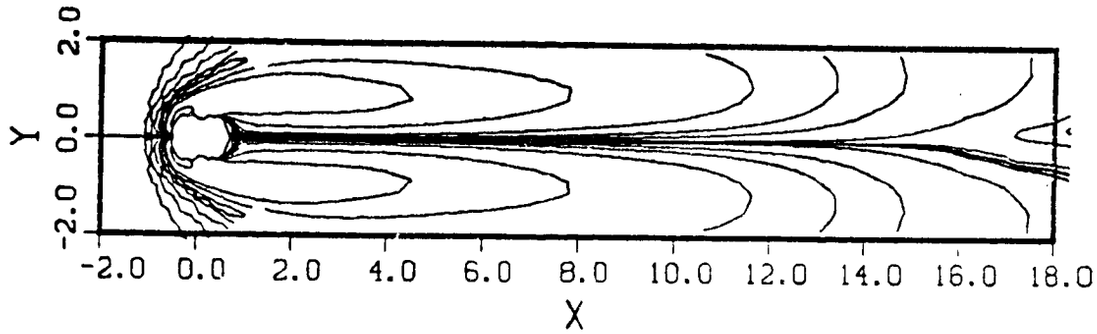

(a) T=1.2

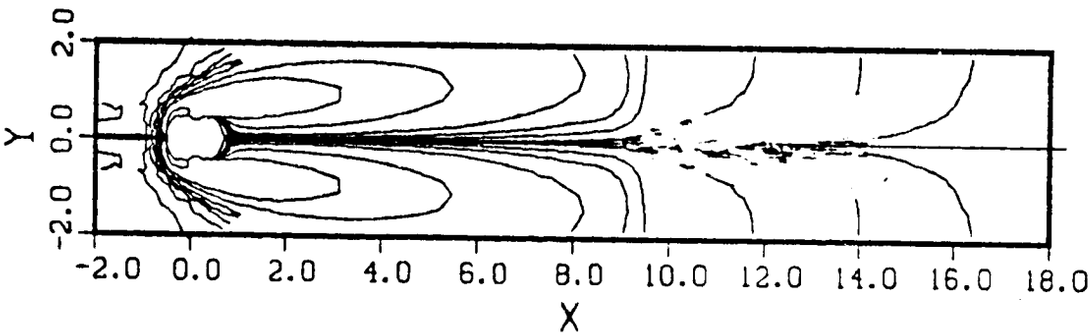

(b) T=5.0

Fig. 7-9 Re=40 (Vorticity function)

ORIGINAL PAGE IS
OF POOR QUALITY

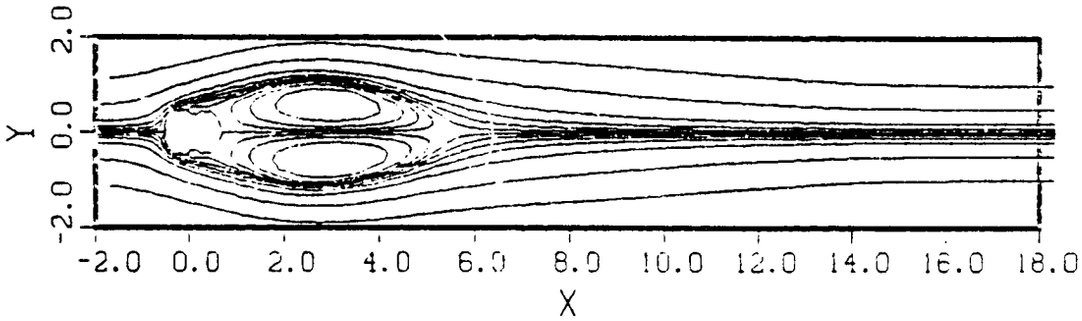

(a) T=1.0

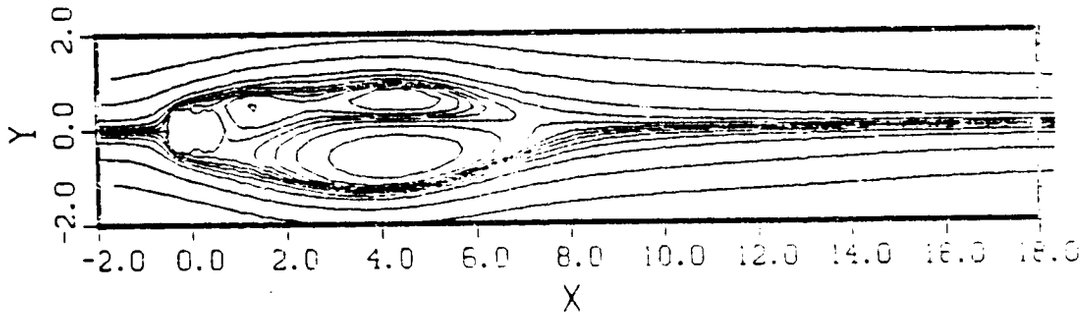

(b) T=2.4

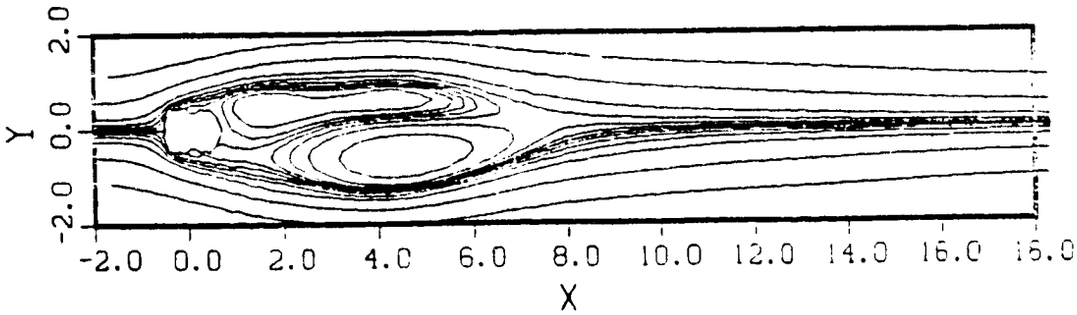

(c) T=3.0

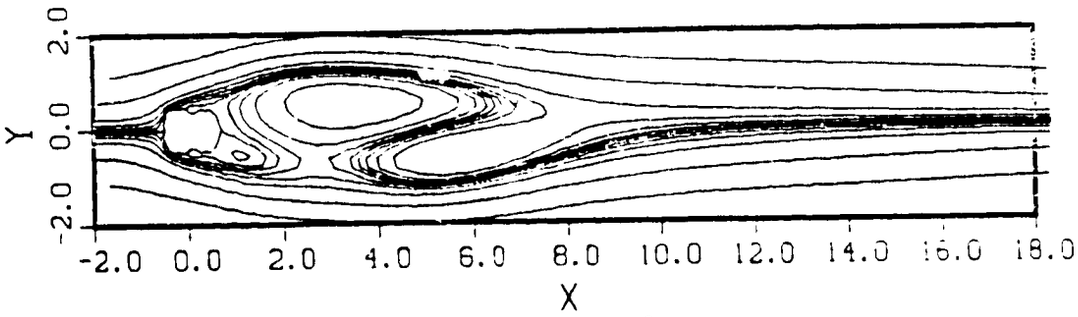

(d) T=5.2

Fig. 7-10 Re=100 (Stream line)

ORIGINAL PAGE IS
OF POOR QUALITY

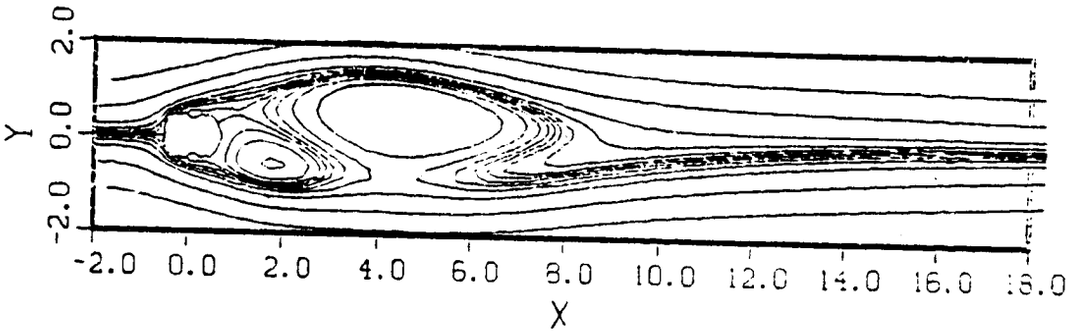

(e) T=7.2

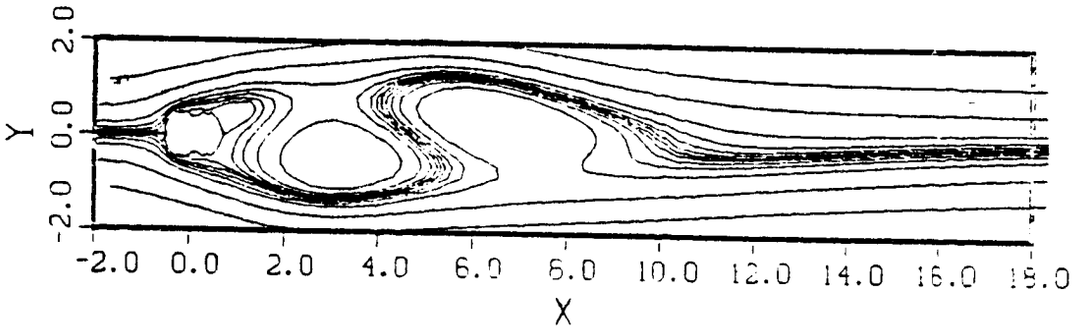

(f) T=9.8

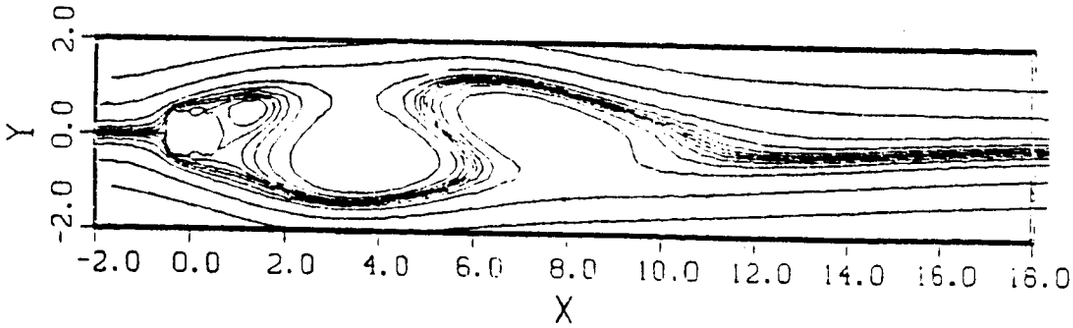

(g) T=10.6

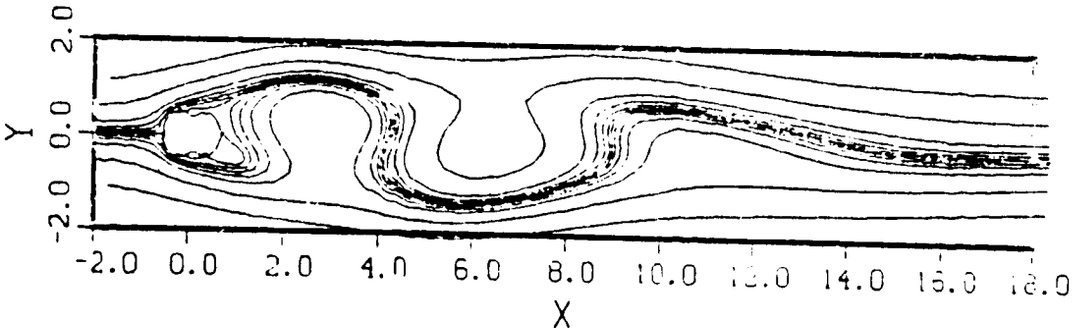

(h) T=14.2

Fig. 7-10 Continued

ORIGINAL PAGE IS
OF POOR QUALITY

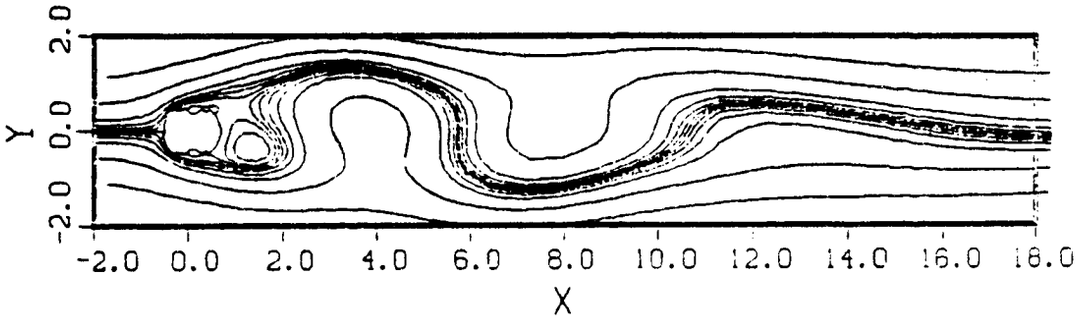

(i) T=15.8

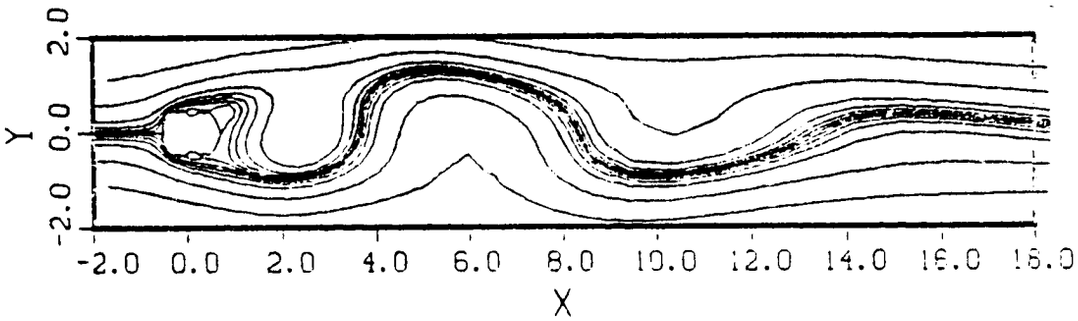

(j) T=18.4

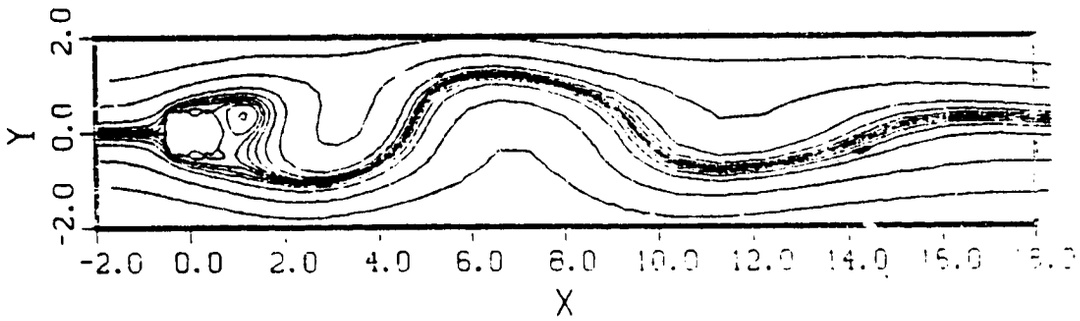

(k) T=19.6

Fig. 7-10 Continued

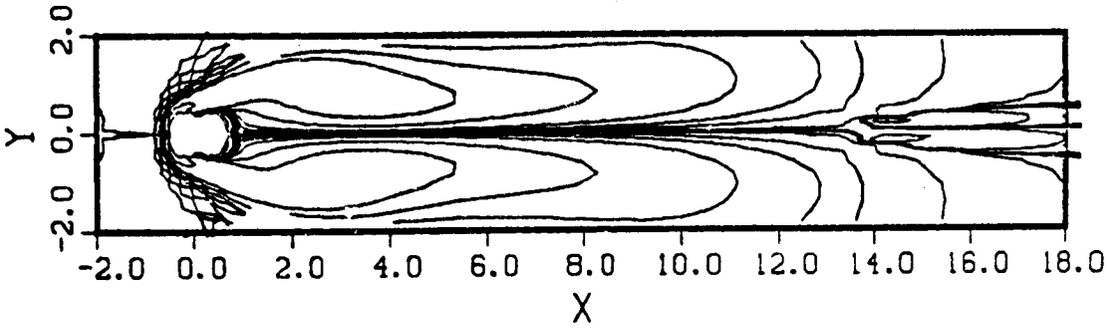

(a) T=1.0

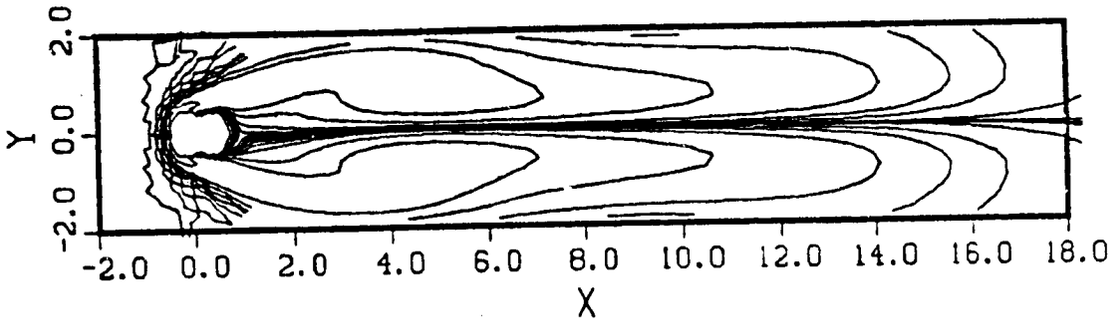

(b) T=2.4

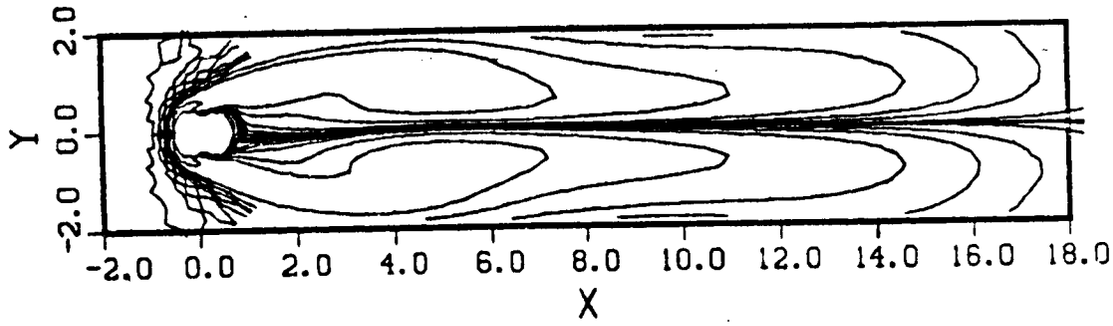

(c) T=3.0

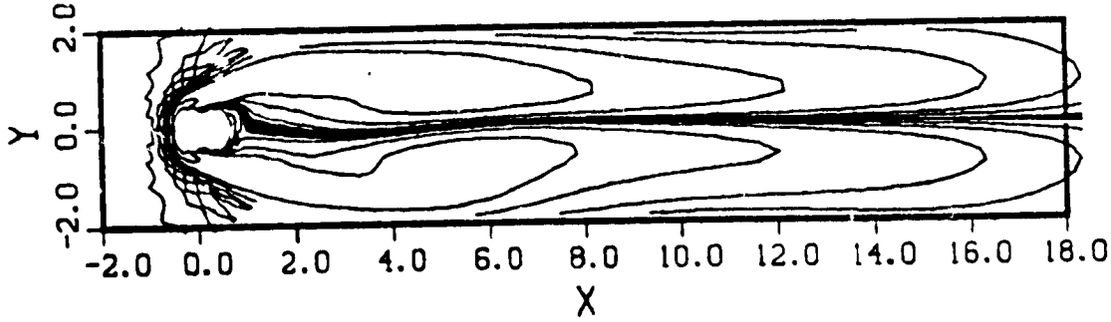

(d) T=5.2

Fig. 7-11 Re=100 (Vorticity function)

ORIGINAL PAGE IS
OF POOR QUALITY

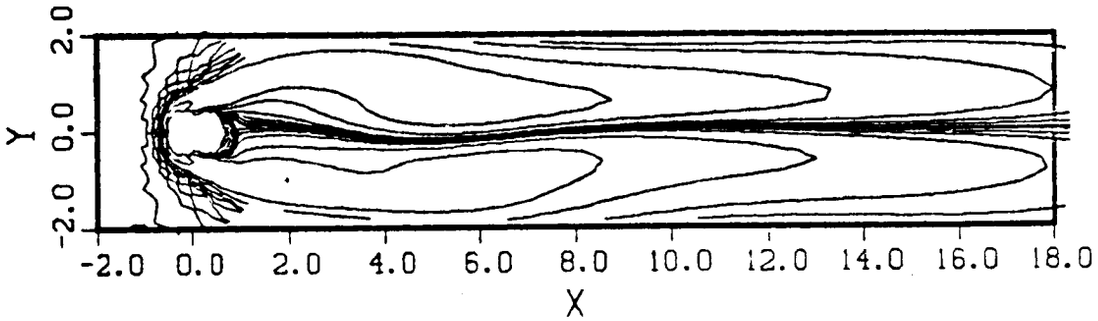

(e) T=7.2

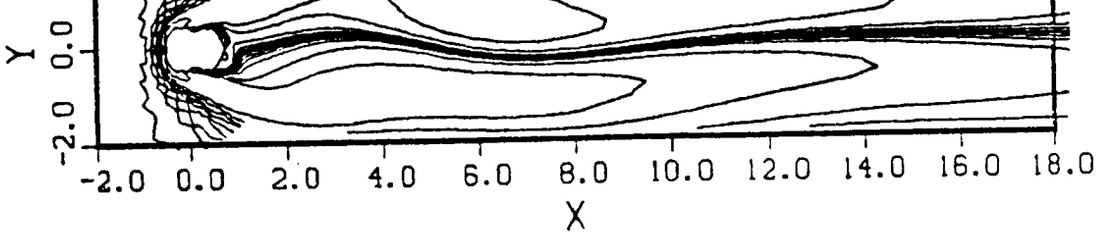

(f) T=9.8

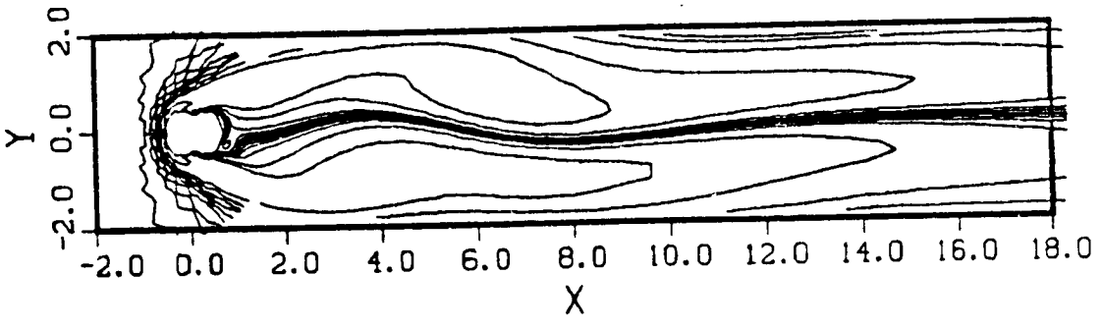

(g) T=10.6

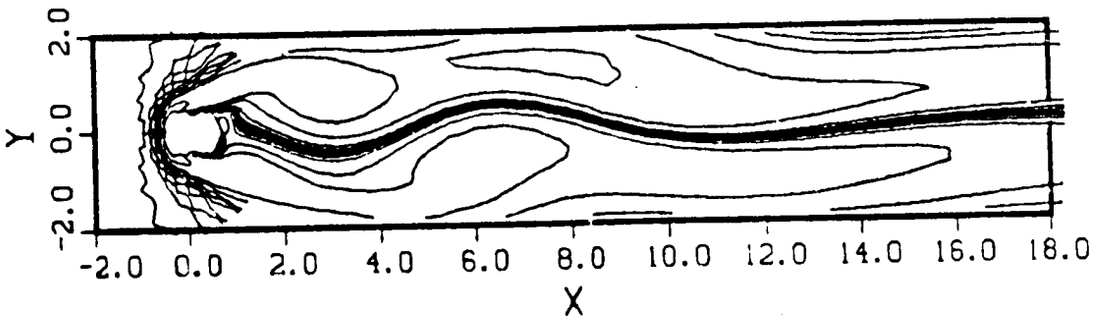

(h) T=14.2

Fig. 7-11 Continued

ORIGINAL PAGE IS
OF POOR QUALITY

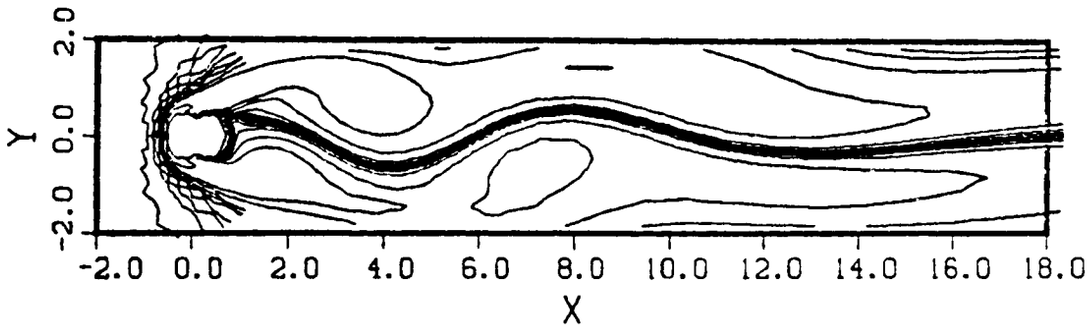

(i) T=15.8

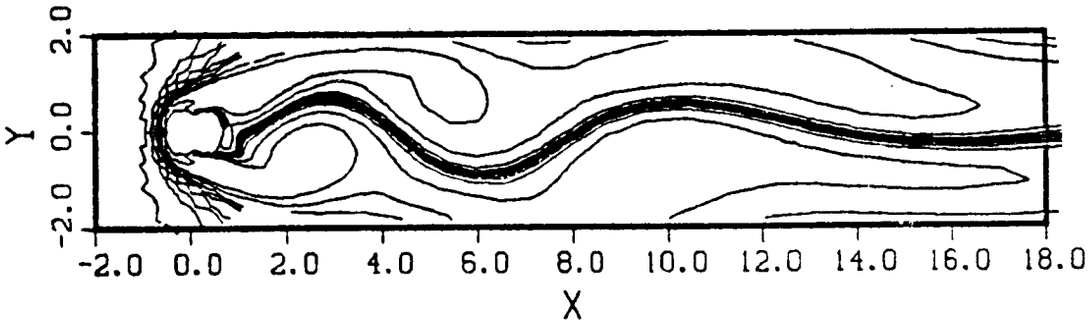

(j) T=18.4

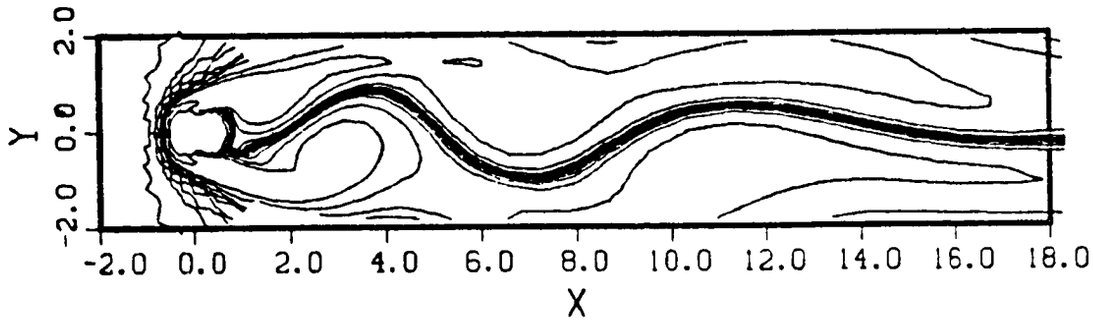

(k) T=19.6

Fig. 7-11 Continued

CHAPTER VIII

CONCLUSIONS AND SUGGESTIONS

In this study a FA numerical method in the boundary fitted coordinate system is developed. This FA method is implimented to solve two dimensional incompressible flows past three obstacles of different body shapes.

As the first problem, the FA solution for flow past a circular cylinder was obtained in chapter 6. The FA solutions were obtained based on both the C-type and the OC-type boundary fitted coordinates so that use of different coordinate type and different approximations to describe the downstream boundary condition can be examined. It is found that in order to predict properly the vortex shedding behind the cylinder, the distance between the body and the downstream boundary should be at least 50 cylinder diameters before the approximation of uniform flow condition can be used. Comparisons of the predicted results and other numerical results and experimental data for Reynolds numbers 5, 40, 100, and 500 were made. Good agreements of the separation angles for steady flow pattern at low Reynolds numbers 5 and 40 were found. The predicted Strohaul number at Re=100 is 0.15 which is also close to the experimental

value of 0.155 to 0.165. However, the predicted Strohaul number at Re=500 is much lower than experimental data. The reason of the discrepancy may be due to the flow is turbulent at Re=500, while the prediction is made under laminar flow assumption.

In chapter 7 the OC-type boundary fitted coordinate system was adapted in solving the flow past a triangle body at Re=200. Although in the computational domain both time step and spatial grid were coarse, the predicted FA results agree reasonably well with the experimental data. From the success of FA solutions in predicting flows past a circular cylinder and an isosceles triangle column, the FA solution for flow past a more complex irregular body shape is obtained to demonstrate the capability of the FA method and the boundary fitted coordinates.

For the further work, improvements for adapting the boundary fitted coordinate system in the finite analytic method are suggested in the following:

(1) The governing Navier-Stokes equations Eq.(4-3) in the transformed plane(ξ,η) are of elliptic type in space. The appearance of the cross second derivative term $-2\beta\omega_{\xi\eta}$ or $-2\beta\psi_{\xi\eta}$ in Eq.(4-3) complicates the solution procedure in obtaining the analytic solution in an element. To simplify Eq.(4-3) we can consider these two cross terms as known values from the previous time step and put them at the right

hand side as the inhomogeneous term as shown in Eq.(4-5). Obviously, if the transformation parameter β which appears in the cross term is small, this approximation creates negligible error. However, if the values of β is of the same or larger order than the values of the coefficients α or γ which appears in other second derivative terms in Eq.(4-5), then the accurancy of the solution may be affected. In order to minimize the error, one observed that the coefficient β vanishes if the transformed coordinate lines ξ and η on the original physical plane are locally orthogonal. Therefore, it is suggested that the boundary fitted coordinate system with nearly orthogonal grid lines should be used when it is possible.

(2) It is found that the value of vorticity on the body surface plays a major roll in obtaining an accurate solution of the problem. This is because the evaluation of the vorticity boundary condition, Eq.(4-4a) $w=-\gamma/J^2\psi_{\eta\eta}$, on the boundary fitted coordinate creates a numerical difficulty, since it is difficult to calculate accurately the transformation parameters γ and J^2 on the body surface. In this study the difficulty is circumvented by deriving an alternative expression, Eq.(6-1), as the vorticity boundary condition instead of Eq.(4-4a). In the future study a means for accurate determination of γ or J^2 is to develop a boundary fitted coordinate system that has extra coordinate

lines devised into the interior region of the solid body. In this way one has an extra reference nodes for accurate evaluation of coefficients γ and J^2.

(3) It should be remarked that the unknown vorticity values on the body surface is in general a function of time in the unsteady flow problem. In this study the boundary vorticity values are determined as part of solution during iteration. Although satisfactory results are obtained, further accurate and simple way of predicting the boundary vorticity values should be investigated in the future study.

REFERENCES

1. Chen, C. J. and Li, P., "Finite Differential Method in Heat Conduction-Application of Analytic Solution Technique," ASME Paper, 79-WA/HT-50, December 2-7, 1979, ASME Winter Annual Meeting, New York, N. Y. (1979).

2. Chen, C. J. and Naseri-Neshat, H. and Ho, K. S., "Finite Analytic Solution of Heat Transfer in Two-Dimensional Cavity Flow," ASME HTD Vol. 13, Momentum and Heat Transfer Processes in Recirculating Flows. Edited by B. E. Launder and J. A. C. Humphrey. Also Journal of Numerical Heat Transfer, Vol. 4, pp. 179-197 (1981).

3. Chen, C. J. and Hamn-Ching Chen, "Development of Finite Analytic Method for Unsteady Two-Dimensional Convective Transport Equation," Proceeding, International Symposium on Refined Modelling of Flows. Paris, September 7-10, (1982).

4. Thompson, J. F., F. C. Thames, and C. W. Mastin, "Automatic Numerical Generation of Body-Fitted Curvilinear Coordinate System for Field Containing Any Number of Arbitrary Two-Dimensional Bodies," Journal of Computational Physis, 15, 299 (1974).

5. Thames, F. C., "Numerical Solution of the Incompressible Navier-Stokes Equation about Arbitrary Two-Dimensional Bodies," Ph. D. Dissertation, Mississippi State University (1975).

6. Thompson, J. F., "Numerical Solution of Flow Problems Using Body-Fitted Coordinate Systems," in "Computational Fluid Dynamics," Edited by Wolfgang Kollmann, pp. 1-98 (1980).

7. "Symposium on the Numerical Generation of Curvilinear Coordinate Systems and use in the Numerical Solution of Partial Differential Equations," Sponsored by NASA & AFOSR, Organized by Mississippi State University, April (1982).

8. A. W. Marris, "A Review on Vortex Streets, Periodic Wakes, and Induced Vibration Phenomena," Journal of Basic Engineering, June (1964).

9. W. A. Main and D. J. Maull, "Bluff Bodies and Vortex Shedding - a report on Euromech 17," Journal of Fluid Mechanics, Vol. 45 part 2, pp. 209-224 (1971).

10. Roshko, A., "On the Drag and Shedding Frequency of Two-Dimensional Bluff Bodies," National Advisory Committee for Aeronautics Report NACA-TN-3169, July (1954).

11. D. J. Tritton, "Experiments on the Flow Past a Circular Cylinder at Low Reynolds Number," Journal of Fluid Mechanics Vol. 6, July-Nov. (1959).

12. Roshko, A., "Experiments on the Flow Past a Cylinder at Very High Reynolds Number," Journal of Fluid Mechanics Vol. 10, pp. 345-356 (1961).

13. J. F. Middlecoff and P. D. Thomas, "Direct Control of the Grid Point Distribution in Meshes Generated by Elliptic Equations," 1979 AIAA Computational Fluid Dynamics Conference, pp. 175-179.

14. Z. U. A. Warsi, R. A. Weed, and J. F. Thompson, "Numerical Generation of Two-Dimensional Orthogonal Coordinates in an Euclidean Space," Mississippi State University, MSSU-EIRS-ASE-80-3.

15. M. Visbal, and D. Knight, "Generation of Orthogonal and Nearly Orthogonal Coordinates with Grid Control near Boundaries," AIAA Journal, Vol. 20, No. 3, March (1982).

16. Blevins, R. D., "Flow-Induced Vibration," Van Nostrand Reinhold Co. Chapter 3 (1977).

17. Von Karman, Th., "Uber den Mechanismus des Widerstandes den ein bewegter Korper in einen Flussigkeit erzeugt," Nachr. Ges. Wiss. Gottingen, Math. Phys. Klasse pp. 509-517 (1911) and pp. 547-556 (1912).

18. Taneda, S., "Experimental Investigation of the Wakes Behind Cylinders and Plates at Low Reynolds Numbers," J. Phys. Soc. Japan 11, pp. 302-307 (1956).

19. Jaime, S. Son and Thomas, J. Hanratty, "Numerical Solution for the Flow Around a Cylinder at Reynolds Number of 40, 200, and 500," Fluid Mech. (1969), Vol. 35, part 2, pp. 369-386.

20. Lienhard, J. H., "Synopsis of Lift, Drag and Vortex Frequency Data for Rigid Circular Cylinders," Washington State University, College of Engineering Research Division, Bulletin 300 (1966).

APPENDIX A

FINITE ANALYTIC SOLUTION OF TWO DIMENSIONAL ELLIPTIC PARTIAL DIFFERENTIAL EQUATION

In this appendix the local finite analytic solution of an elliptic partial differential equation Eq(A-1a) with constants A, B, C and f in a typical finite analytic element (Fig 2-1) is derived.

$$\phi_{\xi\xi}+C\phi_{\eta\eta}-2BC\phi_{\eta}-2A\phi_{\xi}=f \qquad \text{(A-1a)}$$

Eq(A-1a) can be transformed into a homogeneous equation Eq(A-1b) by letting $\phi_h=\phi+\frac{f(A\xi+B\eta)}{2(A^2+B^2C)}$

$$\text{then,}\quad \phi_{h\xi\xi}+C\phi_{h\eta\eta}-2BC\phi_{h\eta}-2A\phi_{h\xi}=0 \qquad \text{(A-1b)}$$

In formulating the boundary conditions for Eq(A-1b), we observed that Eq(A-1b) is an elliptic partial differential equation with constant coefficients and contains only first and second derivatives. Therefore, a constant, a linear function $(A\eta-BC\xi)$ and an exponential function $\exp(2A\xi+2B\eta)$, satisy Eq(A-1b). These functions can be considered as natural or basic modes of the solution form for Eq(A-1b) out of many other possible forms. Thus, it is logical to utilize these basic modes of the solution to form an approximating function for boundary conditions. For example, we may set the northern boundary condition of the Eq(A-1b) as shown in Fig 2-1 to be

$$\phi_{hN}(\xi)=a_N(e^{2A\xi}-1)+b_N\xi+c_N \qquad \text{(A-2)}$$

where the constants a_N, b_N and c_N can be specified by the three nodal values ϕ_{hne}, ϕ_{hnc} and ϕ_{hnw} on the northern boundary that is:

$$\phi_{hnc}=\phi_{hN}(0)=c_N \qquad \text{(A-3a)}$$

$$\phi_{hne}=\phi_{hN}(h)=a_N(e^{2Ah}-1)+b_Nh+c_N \qquad \text{(A-3b)}$$

$$\phi_{hnw}=\phi_{hN}(-h)=a_N(e^{-2Ah}-1)-b_Nh+c_N \qquad \text{(A-3c)}$$

Solving above three equations we get $c_N=\phi_{hnc}$, $b_N=\frac{1}{2h}(\phi_{hne}-\phi_{hnw}-\mathrm{Coth}(Ah)(\phi_{hne}+\phi_{hnw}-2\phi_{hnc}))$, and

$$a_N=(\phi_{hne}+\phi_{hnw}-2\phi_{hnc})/4\mathrm{Sinh}^2(Ah) \qquad \text{(A-4)}$$

The nodal value ϕ_{hne}, ϕ_{hnc} and ϕ_{hnw} etc. in the original variable ϕ are

$$\phi_{hne}=\phi_{ne}+\frac{f}{2(A^2+B^2C)}(Ah+Bk)$$

$$\phi_{hnc}=\phi_{nc}+\frac{f}{2(A^2+B^2C)}(Bk)$$

$$\phi_{hnw}=\phi_{nw}+\frac{f}{2(A^2+B^2C)}(-Ah+Bk) \qquad \text{(A-5)}$$

.

.

.

The other boundary conditions for the south, east and west sides ($\phi_{hS}(\xi)$, $\phi_{hE}(\eta)$ and $\phi_{hW}(\eta)$) can be similarly approximated.

In order to obtain a finite analytic solution of Eq (A-1b) we may set $\phi_h=\phi e^{A\xi+B\eta}$ so that Eq(A-1b) becomes

ORIGINAL PAGE IS
OF POOR QUALITY

$$\phi_{\xi\xi}+C\phi_{\eta\eta}-(A^2+B^2C)\phi=0 \qquad \text{(A-6)}$$

and boundary conditions are:

$$\phi_N(\xi)=e^{-Bk}(a_N e^{A\xi}+b_N\xi e^{-A\xi}+(c_N-a_N)e^{-A\xi}) \qquad \text{(A-7a)}$$

$$\phi_S(\xi)=e^{Bk}(a_S e^{A\xi}+b_S\xi e^{-A\xi}+(c_S-a_S)e^{-A\xi}) \qquad \text{(A-7b)}$$

$$\phi_E(\eta)=e^{-Ah}(a_E e^{B\eta}+b_E\eta e^{-B\eta}+(c_E-a_E)e^{-B\eta}) \qquad \text{(A-7c)}$$

$$\phi_W(\eta)=e^{Ah}(a_W e^{B\eta}+b_W\eta e^{-B\eta}+(c_W-a_W)e^{-B\eta}) \qquad \text{(A-7d)}$$

Eq(A-6) with its boundary conditions (A-7) can be solved analytically by the method of separation of variables. Let $\phi=\phi_1+\phi_2+\phi_3+\phi_4$, where each function satisfies the above Eq(A-6) and following boundary conditions

(1) $\phi_{1N}(\xi)=e^{-Bk}(a_N e^{A\xi}+b_N\xi e^{-A\xi}+(c_N-a_N)e^{-A\xi})$;

$\phi_{1S}(\xi)=0;\ \phi_{1E}(\eta)=0;\ \phi_{1W}(\eta)=0.$ (A-8a)

(2) $\phi_{2S}(\xi)=e^{Bk}(a_S e^{A\xi}+b_S\xi e^{-A\xi}+(c_S-a_S)e^{-A\xi})$;

$\phi_{2N}(\xi)=0;\ \phi_{2E}(\eta)=0;\ \phi_{2W}(\eta)=0.$ (A-8b)

(3) $\phi_{3E}(\eta)=e^{-Ah}(a_E e^{B\eta}+b_E\eta e^{-B\eta}+(c_E-a_E)e^{-B\eta})$;

$\phi_{3N}(\xi)=0;\ \phi_{3S}(\xi)=0;\ \phi_{3W}(\eta)=0.$ (A-8c)

(4) $\phi_{4W}(\eta)=e^{Ah}(a_W e^{B\eta}+b_W\eta e^{-B\eta}+(c_W-a_W)e^{-B\eta})$;

$\phi_{4N}(\xi)=0;\ \phi_{4S}(\xi)=0;\ \phi_{4E}(\eta)=0.$ (A-8d)

From method of separation of variables one finds the series of eigenfunction satisfies those vanishing boundary conditions in Eq(A-8) becomes

$$\phi_1=\sum_{n=1}^{\infty}A_{1n}\text{Sinh}\ \mu_n(\eta+k)\ \text{Sin}\ \lambda_n(\xi+h) \qquad \text{(A-9a)}$$

$$\phi_2=\sum_{n=1}^{\infty}A_{2n}\text{Sinh}\ \mu_n(\eta-k)\ \text{Sin}\ \lambda_n(\xi+h) \qquad \text{(A-9b)}$$

$$\phi_3=\sum_{n=1}^{\infty}A_{3n}\text{Sinh}\ \mu'_n(\xi+h)\ \text{Sin}\ \lambda'_n(\eta+k) \qquad \text{(A-9c)}$$

ORIGINAL PAGE IS
OF POOR QUALITY

$$\phi_4=\sum_{n=1}^{\infty}A_{4n}\text{Sinh}\ \mu_n'(\xi-h)\ \text{Sin}\ \lambda_n'(\eta+k) \qquad \text{(A-9d)}$$

where $\lambda_n=\frac{n\pi}{2h}$, $\lambda_n'=\frac{n\pi}{2k}$, $\mu_n=((A^2+B^2C+\lambda_n^2)/C)^{0.5}$,

$$\mu_n'=((A^2+B^2C+\lambda_n'^2C)^{0.5}, \quad n=1,2,3,4.....$$

The constants A_{1n}, A_{2n}, A_{3n} and A_{4n} can be respectively determined from the no vanishing boundary conditions in Eq (A-8). For example, the determination of A_{1n} can be obtained as follow: Setting Eq(A-9a) at =k, then

$$\phi_1(\xi)=e^{-Bk}(a_Ne^{A\xi}+b_N\xi e^{-A\xi}+(c_N-a_N)e^{-A\xi})=\sum_{n=1}^{\infty}A_{1n}\text{Sinh}\ 2\mu_nk\text{Sin}(\xi+h)\lambda_n$$

from the property of orthogonality of Fourier eigenfunction we have

$$A_{1n}\text{Sinh}\ 2\mu_nk=\frac{1}{n}\int_{-h}^{h}e^{-Bk}(a_Ne^{A\xi}+b_N\xi e^{-A\xi}+(c_N-a_N)e^{A\xi})\text{Sin}\ \lambda_n(\xi+h)d\xi$$

or

$$=\frac{e^{-Bk}}{h}\{a_N\frac{\lambda_n}{A^2+\lambda_n^2}(e^{-Ah}-(-1)^ne^{Ah})+(c_N-a_N)\frac{\lambda_n}{A^2+\lambda_n^2}(e^{Ah}-(-1)^ne^{-Ah})\}$$

$$+\frac{e^{-Bk}}{h}\{b_N(\frac{2A\lambda_n(e^{Ah}-(-1)^ne^{-Ah})}{(A^2+\lambda_n^2)^2}-\frac{\lambda_nh(e^{Ah}+(-1)^ne^{-Ah})}{A^2+\lambda_n^2}\}$$

Substitute the values of a_N, b_N and c_N in Eq(A-4) into the above equation then,

$$A_{1n}e^{Bk}\text{Sinh}\ 2\mu_nk=\frac{\phi_{hne}+\phi_{hnw}-2\phi_{hnc}}{4\text{Sinh}^2Ah}\frac{\lambda_nh}{(Ah)^2+(\lambda_nh)^2}(e^{-Ah}-(-1)^ne^{Ah})$$

$$+(\phi_{hnc}-\frac{\phi_{hne}+\phi_{hnw}-2\phi_{hnc}}{4\text{Sinh}^2Ah})\frac{\lambda_nh}{(Ah)^2+(\lambda_nh)^2}(e^{Ah}-(-1)^ne^{-Ah})$$

ORIGINAL PAGE IS
OF POOR QUALITY

$$+\frac{\phi_{hne}-\phi_{hnw}-\text{Coth } Ah\ (\phi_{hne}+\phi_{hnw}-2\phi_{hnc})}{2}\left\{\frac{2(Ah)(\lambda_n h)}{((Ah)^2+(\lambda_n h)^2)^2}\right.$$

$$\left.(e^{Ah}-(-1)^n e^{-Ah})-\frac{\lambda_n h}{(Ah)^2+(\lambda_n h)^2}(e^{Ah}+(-1)^n e^{-Ah})\right\}$$

Now let $n=2m-1$, $m=1,2,3,4.....$

then, $A_{1m}e^{Bk}\text{Sinh } 2\mu_m k=\frac{\lambda_m h}{(Ah)^2+(\lambda_m h)^2}\{\phi_{hnc}(e^{Ah}+e^{-Ah})-(e^{Ah}-e^{-Ah})$

$$\left(\frac{\phi_{hne}-\phi_{hnw}-\text{Coth } Ah\ (\phi_{hne}+\phi_{hnw}-2\phi_{hnc})}{2}\right)\}+(Ah)(\lambda_m h)$$

$$\frac{(e^{Ah}+e^{-Ah})}{((Ah)^2+(\lambda_m h)^2)^2}(\phi_{hne}-\phi_{hnw}-\text{Coth } Ah\ (\phi_{hne}+\phi_{hnw}-2\phi_{hnc}))$$

(A-10)

Since $\phi_h=\phi e^{A\xi+B\eta}$

then, $\phi_{1h}=\phi_1 e^{A\xi+B\eta}=e^{A\xi+B\eta}\sum_{m=1}^{\infty}A_{1m}\text{Sinh } \mu_m(\eta+k)\ \text{Sin } \lambda_m(\xi+h)$ (A-11a)

Similarly $\phi_{2h}=e^{A\xi+B\eta}\sum_{m=1}^{\infty}A_{2m}\text{Sinh } \mu_m(\eta-k)\ \text{Sin } \lambda_m(\xi+h)$ (A-11b)

$\phi_{3h}=e^{A\xi+B\eta}\sum_{m=1}^{\infty}A_{3m}\text{Sinh } \mu'_m(\xi+h)\ \text{Sin } \lambda'_m(\eta+k)$ (A-11c)

$\phi_{4h}=e^{A\xi+B\eta}\sum_{m=1}^{\infty}A_{4m}\text{Sinh } \mu'_m(\xi-h)\ \text{Sin } \lambda'_m(\eta+k)$ (A-11d)

where $\lambda_m=\frac{n\pi}{2h}$, $\lambda'_m=\frac{n\pi}{2k}$, and $n=2m-1$, $m=1,2,3,4.....$

$\mu_m=((A^2+B^2C+\lambda_m^2)/C)^{0.5}$, $\mu'_m=(A^2+B^2C+\lambda'^2_m C)^{0.5}$.

and $\phi_h(\xi,\eta)=\phi_{1h}+\phi_{2h}+\phi_{3h}+\phi_{4h}$, where ϕ_h is the solution of Eq(A-1b).

The finite analytic algebratic equation relating the center node to the neighboring nodes ne, nc, nw, etc. may be obtained by setting $\xi=0$ $\eta=0$ in Eq(A-11) to give

$$\phi_h(0,0)=\phi_{1h}(0,0)+\phi_{2h}(0,0)+\phi_{3h}(0,0)+\phi_{4h}(0,0)$$

where, for example

C - 5

ORIGINAL PAGE IS
OF POOR QUALITY

$$\phi_{1h}(0,0)=\sum_{m=1}^{\infty}A_{1m}\text{Sinh }\mu_m k\text{ Sin }\lambda_m h$$

and $A_{1m}e^{Bk}\text{Sinh }2\mu_m k=2A_{1m}e^{Bk}\text{Sinh }\mu_m k\text{ Cosh }\mu_m K$

Combining these expressions we have

$$\phi_{1h}(0,0)=e^{-Bk}\sum_{m=1}^{\infty}\frac{-(-1)^m\lambda_m h}{2((Ah)^2+(\lambda_m h)^2)\text{Cosh }\mu_m k}\{\phi_{hnc}(e^{Ah}+e^{-Ah})$$

$$-(e^{Ah}-e^{-Ah})(\frac{\phi_{hne}-\phi_{hnw}}{2}-\text{Coth Ah }(\phi_{hne}+\phi_{hnw}-2\phi_{hnc}))\}$$

$$+e^{-Bk}\sum_{m=1}^{\infty}\frac{-(-1)^m(\lambda_m h)(Ah)}{2((Ah)^2+(\lambda_m h)^2\text{Cosh }\mu_m k}(e^{Ah}+e^{-Ah})$$

$$(\phi_{hne}-\phi_{hnw}-\text{Coth Ah }(\phi_{hne}+\phi_{hnw}-2\phi_{hnc}))$$

or $$\phi_{1h}(0,0)=e^{-Bk}((\tfrac{1}{2}\text{Cosh Ah}-\tfrac{1}{2}\text{Sinh Ah})E_1+(\text{Cosh Ah}-\frac{\text{Cosh}^2\text{Ah}}{\text{Sinh Ah}})$$

$$\text{Ah }E_2)\phi_{hne}+e^{-Bk}((\tfrac{1}{2}\text{Cosh Ah}+\tfrac{1}{2}\text{Sinh Ah})E_1-(\text{Cosh Ah}$$

$$+\frac{\text{Cosh}^2\text{Ah}}{\text{Sinh Ah}})\text{Ah }E_2)\phi_{hnw}+e^{-Bk}(\text{Ah}\frac{2\text{Cosh}^2\text{Ah}}{\text{Sinh Ah}}E_2)\phi_{hnc}\quad\text{(A-12a)}$$

Similarly,

$$\phi_{2h}(0,0)=e^{Bk}((\tfrac{1}{2}\text{Cosh Ah}-\tfrac{1}{2}\text{Sinh Ah})E_1+(\text{Cosh Ah}-\frac{\text{Cosh}^2\text{Ah}}{\text{Sinh Ah}})$$

$$\text{Ah }E_2)\phi_{hse}+e^{Bk}((\tfrac{1}{2}\text{Cosh Ah}+\tfrac{1}{2}\text{Sinh Ah})E_1-(\text{Cosh Ah}+$$

$$\frac{\text{Cosh}^2\text{Ah}}{\text{Sinh Ah}})\text{Ah }E_2)\phi_{hsw}+e^{Bk}(\text{Ah}\frac{2\text{Cosh}^2\text{Ah}}{\text{Sinh Ah}}E_2)\phi_{hsc}\quad\text{(A-12b)}$$

where $$E_1=\sum_{m=1}^{\infty}\frac{-(-1)^m(\lambda_m h)}{((Ah)^2+(\lambda_m h)^2)\text{Cosh }\mu_m k}$$

$$E_2=\sum_{m=1}^{\infty}\frac{-(-1)^m\lambda_m h}{((Ah)^2+(\lambda_m h)^2)^2\text{Cosh }\mu_m k}\quad\text{(A-12c)}$$

ORIGINAL PAGE IS
OF POOR QUALITY

$$\phi_{3h}(0,0)=e^{-Ah}\left(\frac{1}{2}(\text{Cosh } Bk-\text{Sinh } Bk)E_1'+(\text{Cosh } Bk-\frac{\text{Cosh}^2 Bk}{\text{Sinh } Bk})\right.$$

$$\left. Bk\ E_2'\right)\phi_{hne}+e^{-Ah}\left(\frac{1}{2}(\text{Cosh } Bk+\text{Sinh } Bk)E_1'-(\text{cosh } Bk+\right.$$

$$\left.\frac{\text{Cosh}^2 Bk}{\text{Sinh } Bk})Bk\ E_2'\right)\phi_{hse}+e^{-Ah}\left(Bk\frac{2\text{Cosh}^2 Bk}{\text{Sinh } Bk}E_2'\right)\phi_{hec} \quad \text{(A-13a)}$$

$$\phi_{4h}(0,0)=e^{Ah}\left(\frac{1}{2}(\text{Cosh } Bk-\text{Sinh } Bk)E_1'+(\text{Cosh } Bk-\frac{\text{Cosh}^2 Bk}{\text{Sinh } Bk})\right.$$

$$\left. Bk\ E_2'\right)\phi_{hnw}+e^{Ah}\left(\frac{1}{2}(\text{Cosh } Bk+\text{Sinh } Bk)E_1'-(\text{Cosh } Bk+\right.$$

$$\left.\frac{\text{Cosh}^2 Bk}{\text{Sinh } Bk})Bk\ E_2'\right)\phi_{hsw}+e^{Ah}\left(Bk\frac{2\text{Cosh}^2 Bk}{\text{Sinh } Bk}E_2'\right)\phi_{hwc} \quad \text{(A-13b)}$$

where $E_1'=\sum_{m=1}^{\infty}\frac{-(-1)^m\lambda_m'k}{((Bk)^2+(\lambda_m'k)^2)\text{Cosh } \mu_m'h}$

$$E_2'=\sum_{m=1}^{\infty}\frac{-(-1)^m\lambda_m'k}{((Bk)^2+(\lambda_m'k)^2)^2\text{Cosh } \mu_m'h} \quad \text{(A-13c)}$$

Combining Eq(A-12) and Eq(A-13) we have

$$\phi_h(0,0)=C_{ne}\phi_{hne}+C_{nw}\phi_{hnw}+C_{se}\phi_{hse}+C_{sw}\phi_{hsw}+C_{nc}\phi_{hnc}+C_{sc}\phi_{hsc}$$

$$+C_{ec}\phi_{hec}+C_{wc}\phi_{hwc} \quad \text{(A-14)}$$

where $C_{ne}=e^{-Ah-Bk}\left(\frac{1}{2}(E_1+E_1')-Ah\ \text{Coth } Ah\ E_2-Bk\ \text{Coth } Bk\ E_2'\right)$ (A-15a)

$$C_{nw}=e^{Ah-Bk}\left(\frac{1}{2}(E_1+E_1')-Ah\ \text{Coth } Ah\ E_2-Bk\ \text{Coth } Bk\ E_2'\right) \quad \text{(A-15b)}$$

$$C_{se}=e^{-Ah+Bk}\left(\frac{1}{2}(E_1+E_1')-Ah\ \text{Coth } Ah\ E_2-Bk\ \text{Coth } Bk\ E_2'\right) \quad \text{(A-15c)}$$

$$C_{sw}=e^{Ah+Bk}\left(\frac{1}{2}(E_1+E_1')-Ah\ \text{Coth } Ah\ E_2-Bk\ \text{Coth } Bk\ E_2'\right) \quad \text{(A-15d)}$$

$C_{nc}=e^{-Bk}Ah\frac{2\text{Cosh}^2 Ah}{\text{Sinh } Ah}E_2$ (A-15e) $C_{sc}=e^{Bk}Ah\frac{2\text{Cosh}^2 Ah}{\text{Sinh } Ah}E_2$ (A-15f)

$C_{ec}=e^{-Ah}Bk\frac{2\text{Cosh}^2 Bk}{\text{Sinh } Bk}E_2'$ (A-15g) $C_{wc}=e^{Ah}Bk\frac{2\text{Cosh}^2 Bk}{\text{Sinh } Bk}E_2'$ (A-15h)

ORIGINAL PAGE IS
OF POOR QUALITY

The following relations can be used to simplify the coefficients C_{ne}, C_{nw}, C_{se},..... etc.

First, since $_h$=constant is a solution of Eq(A-1b), Eq (A-14) is still true for the case when all nodal values on the element are set equal. In this case one has

$$C_{ne}+C_{nw}+C_{se}+C_{sw}+C_{nc}+C_{sc}+C_{ec}+C_{wc}=1 \qquad \text{(A-16)}$$

Substituting Eq(A-15) into Eq(A-16) we have

$$2\text{Cosh Ah Cosh Bk } (E_1+E_1')=1$$

or

$$E_1+E_1'=1/(2\text{Cosh Ah Cosh Bk}) \qquad \text{(A-17)}$$

Secondly, $\phi_h=A\eta-BC\xi$ is also a solution of Eq(A-1b), so the boundary functions (A-4) should be a linear case, that is $a_N=a_S=a_E=a_W=0$ or $\phi_{hnc}=0.5(\phi_{hne}+\phi_{hnw})$, $\phi_{hsc}=0.5(\phi_{hsw}+\phi_{hse})$,

$$\phi_{hec}=0.5(\phi_{hne}+\phi_{hse}),\ \phi_{hwc}=0.5(\phi_{hnw}+\phi_{hsw}).$$

and $\phi_{hne}=-BCh+Ak$, $\phi_{hnw}=BCh+Ak$, $\phi_{hse}=-BCh-Ak$, $\phi_{hsw}=BCh-Ak$, $\phi_h(0,0)=0$. Substituting these relations into Eq(A-14) we have

$$Ch^2E_2-k^2E_2'=\frac{BCh\ \text{Tanh Ah}-Ak\ \text{Tanh Bk}}{4AB\ \text{Cosh Ah Cosh Bk}} \qquad \text{(A-18)}$$

With relations (A-17) and (A-18) the computation of FA coefficients in Eq(A-1b) requires only one series summation that is either E_2 which given in Eq(A-12c) or E_2' which given in Eq(A-13c). Because the limitation of the present computer in handling large exponential function, the summation E_2 or E_2' may become inaccurate when it contains a larger value. In order to avoid this problem (note: with further advance of computer technology this should not be a problem), it is suggested that if C is greater than 1, one should choose

ORIGINAL PAGE IS
OF POOR QUALITY

to calculate the series summation E_2' firstly, then use relation (A-18) to obtain E_2. If C is less than 1 it is suggested to compute the series summation E_2 firstly, and use relation (A-18) to get E_2'. After the values of E_2 and E_2' have been obtained we define new relations for EA, EB and EC, where

$$EA=2Ah\frac{\text{Cosh}^2 Ah}{\text{Sinh } Ah}E_2; \quad EB=2Bk\frac{\text{Cosh}^2 Bk}{\text{Sinh } Bk}E_2';$$

$$EC=\frac{1}{4\text{Cosh } Ah \text{ Cosh } Bk} - Ah \text{ Coth } Ah\ E_2 - Bk \text{ Coth } Bk\ E_2'$$

Then the finite analytic coefficients become

$$C_{ne}=e^{-Ah-Bk}EC; \quad C_{nw}=e^{Ah-Bk}EC; \quad C_{se}=e^{-Ah+Bk}EC; \quad C_{sw}=e^{Ah+Bk}EC;$$

$$C_{nc}=e^{-Bk}EA; \quad C_{sc}=e^{Bk}EA; \quad C_{ec}=e^{-Ah}EB; \quad C_{wc}=e^{Ah}EB. \qquad \text{(A-19)}$$

To obtain the finite analytic solution of Eq(A-1a) one simply substitute Eq(A-5) into Eq(A-14). However, since $\phi_h(0,0)=\phi(0,0)$ we have the final FA algebratic equation for the node at $\xi=0$ $\eta=0$ as

$$\phi(0,0)=C_{ne}\phi_{ne}+C_{nw}\phi_{nw}+C_{se}\phi_{se}+C_{sw}\phi_{sw}+C_{nc}\phi_{nc}+C_{sc}\phi_{sc}+C_{ec}\phi_{ec}$$

$$+C_{wc}\phi_{wc}+C_f f \qquad \text{(A-20)}$$

where $C_f=\frac{1}{2(A^2+B^2C)}(Ah(C_{ne}+C_{ec}+C_{se}-C_{nw}-C_{wc}-C_{sw})$

$$+Bk(C_{ne}+C_{nc}+C_{nw}-C_{se}-C_{sc}-C_{sw}))$$

In other words Eq(A-20) is the FA algebratic representation of the partial differential equation (A-1a) which we used in this study.

ORIGINAL PAGE IS
OF POOR QUALITY

Next step we derive the finite analytic solution for Eq.(A-1a) in a finite analytic element.

From Eq.(A-1b) and Eq.(A-11) the finite analytic solution for ϕ_h in the element can be written as $\phi_h=\phi_1+\phi_2+\phi_3+\phi_4$ where, for example

$$\phi_{1h}=e^{A\xi+B\eta}\sum_{m=1}^{\infty}A_{1m}\text{Sinh}\ \mu_m(\eta+k)\ \text{Sin}\ \lambda_m(\xi+h)$$

Taking the derivative of this equation one has

$$\phi_{1h\xi}=Ae^{A\xi+B\eta}\sum_{m=1}^{\infty}A_{1m}\text{Sinh}\ \mu_m(\eta+k)\ \text{Sin}\ \lambda_m(\xi+h)$$
$$+e^{A\xi+B\eta}\sum_{m=1}^{\infty}A_{1m}\text{Sinh}\ \mu_m(\eta+k)\ \lambda_m\text{Cos}\ \lambda_m(\xi+h) \qquad \text{(A-21a)}$$

$$\phi_{1h\eta}=Be^{A\xi+B\eta}\sum_{m=1}^{\infty}A_{1m}\text{Sinh}\ \mu_m(\eta+k)\ \text{Sin}\ \lambda_m(\xi+h)$$
$$+e^{A\xi+B\eta}\sum_{m=1}^{\infty}A_{1m}\mu_m\text{Cosh}\ \mu_m(\eta+k)\ \text{Sin}\ \lambda_m(\xi+h) \qquad \text{(A-21b)}$$

$$\phi_{1h\xi\eta}=ABe^{A\xi+B\eta}\sum_{m=1}^{\infty}A_{1m}\text{Sinh}\ \mu_m(\eta+k)\ \text{Sin}\ \lambda_m(\xi+h)$$
$$+Ae^{A\xi+B\eta}\sum_{m=1}^{\infty}A_{1m}\mu_m\text{Cosh}\ \mu_m(\eta+k)\ \text{Sin}\ \lambda_m(\xi+h)$$
$$+Be^{A\xi+B\eta}\sum_{m=1}^{\infty}A_{1m}\text{Sinh}\ \mu_m(\eta+k)\ \lambda_m\text{Cos}\ \lambda_m(\xi+h)$$
$$+e^{A\xi+B\eta}\sum_{m=1}^{\infty}A_{1m}\mu_m\text{Cosh}\ \mu_m(\eta+k)\ \lambda_m\text{Cos}\ \lambda_m(\xi+h) \qquad \text{(A-21c)}$$

When these derivatives are evaluated at the interior node P(0,0) we obtain

$$\phi_{1h\xi}(0,0)=A\sum_{m=1}^{\infty}A_{1m}\text{Sinh}\ \mu_m k\ \text{Sin}\ \lambda_m h+\sum_{m=1}^{\infty}A_{1m}\text{Sinh}\ \mu_m k\ \lambda_m\text{Cos}\ \lambda_m h$$
$$=A\phi_{1h}(0,0) \qquad \text{(A-22a)}$$

$$\phi_{1h\eta}(0,0)=B\sum_{m=1}^{\infty}A_{1m}\text{Sinh}\ \mu_m k\ \text{Sin}\ \lambda_m h+\sum_{m=1}^{\infty}A_{1m}\mu_m\text{Cosh}\ \mu_m k\ \text{Sin}\ \lambda_m h$$
$$=B\phi_{1h}(0,0)+\sum_{m=1}^{\infty}A_{1m}\mu_m\text{Cosh}\ \mu_m k\ \text{Sin}\ \lambda_m h$$

ORIGINAL PAGE IS
OF POOR QUALITY

ORIGINAL PAGE IS
OF POOR QUALITY

Using Eq.(A-10) and the following relation

$$A_{1m}\mu_m \text{Cosh } \mu_m k = \mu_m A_{1m} e^{Bk} \text{Sinh } 2\mu_m k / 2e^{Bk} \text{Sinh } \mu_m k$$

we have

$$\phi_{1h\eta}(0,0) = B\phi_{1h}(0,0) + e^{-Bk}\left(\left(\tfrac{1}{2}(\text{Cosh } Ah - \text{Sinh } Ah)G_1 + \left(\text{Cosh } Ah - \frac{\text{Cosh}^2 Ah}{\text{Sinh } Ah}\right) Ah\ G_2\right)\phi_{hne} + e^{-Bk}\left(\tfrac{1}{2}(\text{Cosh } Ah + \text{Sinh } Ah)G_1 - \left(\text{Cosh } Ah + \frac{\text{Cosh}^2 Ah}{\text{Sinh } Ah}\right) Ah\ G_2\right)\phi_{hnw} + e^{-Bk}\left(Ah \frac{2\text{Cosh}^2 Ah}{\text{Sinh } Ah} G_2\right)\phi_{hnc} \qquad \text{(A-22b)}$$

where

$$G_1 = \sum_{m=1}^{\infty} \frac{-(-1)^m \lambda_m h \mu_m}{((Ah)^2 + (\lambda_m h)^2)\text{Sinh } \mu_m k}$$

$$G_2 = \sum_{m=1}^{\infty} \frac{-(-1)^m \lambda_m h \mu_m}{((Ah)^2 + (\lambda_m h)^2)^2 \text{Sinh } \mu_m k}$$

$$\lambda_m = \frac{n\pi}{2h}, \quad n = 2m-1, \quad m = 1,2,3,4 \ldots\ldots\ldots\ldots$$

$$\mu_m = ((A^2 + B^2 C + {}_m^2)/C)^{0.5}$$

Similarly, one may obtain from the finite analytic solution of ϕ_{2h} as

$$\phi_{2h\xi}(0,0) = A\phi_{2h}(0,0) \qquad \text{(A-23a)}$$

$$\phi_{2h\eta}(0,0) = B\phi_{2h}(0,0) - e^{Bk}\left(\tfrac{1}{2}(\text{Cosh } Ah - \text{Sinh } Ah)G_1 + \left(\text{Cosh } Ah - \frac{\text{Cosh}^2 Ah}{\text{Sinh } Ah}\right) Ah\ G_2\right)\phi_{hse} - e^{Bk}\left(\tfrac{1}{2}(\text{Cosh } Ah + \text{Sinh } Ah)G_1 - \left(\text{Cosh } Ah + \frac{\text{Cosh}^2 Ah}{\text{Sinh } Ah}\right) Ah\ G_2\right)\phi_{hsw} - e^{Bk}\left(Ah \frac{2\text{Cosh}^2 Ah}{\text{Sinh } Ah} G_2\right)\phi_{hsc} \qquad \text{(A-23b)}$$

Similarly,

$$\phi_{3h\xi}(0,0) = A\phi_{3h}(0,0) + e^{-Ah}\left(\tfrac{1}{2}(\text{Cosh } Bk - \text{Sinh } Bk)G_1' + \left(\text{Cosh } Bk - \frac{\text{Cosh}^2 Bk}{\text{Sinh } Bk}\right) Bk\ G_2'\right)\phi_{hne} + e^{-Ah}\left(\tfrac{1}{2}(\text{Cosh } Bk + \text{Sinh } Bk)G_1' - \left(\text{Cosh } Bk + \frac{\text{Cosh}^2 Bk}{\text{Sinh } Bk}\right) Bk\ G_2'\right)\phi_{hse} + e^{-Ah}\left(Bk \frac{2\text{Cosh}^2 Bk}{\text{Sinh } Bk} G_2'\right)\phi_{hec} \qquad \text{(A-24a)}$$

ORIGINAL PAGE IS
OF POOR QUALITY

where $G_1' = \sum_{m=1} \frac{-(-1)^m \lambda_m' k \mu_m'}{((Bk)^2 + (\lambda_m' k)^2) \operatorname{Sinh} \mu_m' h}$

$$G_2' = \sum_{m=1} \frac{-(-1)^m \lambda_m' k \mu_m'}{((Bk)^2 + (\lambda_m' k)^2)^2 \operatorname{Sinh} \mu_m' h}$$

$$\lambda_m' = \frac{n\pi}{2k}, \quad n = 2m-1, \quad m = 1,2,3,4 \ldots\ldots\ldots$$

$$\mu_m' = (A^2 + B^2 C + \lambda_m'^2 C)^{0.5}$$

$$\phi_{3h\eta}(0,0) = B\phi_{3h}(0,0) \tag{A-24b}$$

and $\phi_{4h\xi}(0,0) = A\phi_{4h}(0,0) - e^{Ah}(\frac{1}{2}(\operatorname{Cosh} Bk - \operatorname{Sinh} Bk)G_1' + (\operatorname{Cosh} Bk - \frac{\operatorname{Cosh}^2 Bk}{\operatorname{Sinh} Bk})Bk\ G_2')\phi_{hnw} - e^{Ah}(\frac{1}{2}(\operatorname{Cosh} Bk + \operatorname{Sinh} Bk)G_1' - (\operatorname{Cosh} Bk + \frac{\operatorname{Cosh}^2 Bk}{\operatorname{Sinh} Bk})Bk\ G_2')\phi_{hsw} - e^{Ah}(Bk\frac{2\operatorname{Cosh}^2 Bk}{\operatorname{Sinh} Bk}G_2')\phi_{hwc}$ (A-25a)

$$\phi_{4h\eta}(0,0) = B\phi_{4h}(0,0) \tag{A-25b}$$

then $\phi_{h\xi}(0,0) = \phi_{1h\xi}(0,0) + \phi_{2h\xi}(0,0) + \phi_{3h\xi}(0,0) + \phi_{4h\xi}(0,0)$

$= A\phi_h(0,0) + (\frac{1}{2}(\operatorname{Cosh} Bk - \operatorname{Sinh} Bk)G_1' + (\operatorname{Cosh} Bk - \frac{\operatorname{Cosh}^2 Bk}{\operatorname{Sinh} Bk})Bk\ G_2')(e^{-Ah}\phi_{hne} - e^{Ah}\phi_{hnw}) + (\frac{1}{2}(\operatorname{Cosh} Bk + \operatorname{Sinh} Bk)G_1' - (\operatorname{Cosh} Bk + \frac{\operatorname{Cosh}^2 Bk}{\operatorname{Sinh} Bk})Bk\ G_2')(e^{-Ah}\phi_{hse} - e^{Ah}\phi_{hsw}) + (Bk\frac{2\operatorname{Cosh}^2 Bk}{\operatorname{Sinh} Bk}G_2')(e^{-Ah}\phi_{hec} - e^{Ah}\phi_{hwc})$ (A-26)

ORIGINAL PAGE IS
OF POOR QUALITY

$$\phi_{h\eta}(0,0)=\phi_{1h\eta}(0,0)+\phi_{2h\eta}(0,0)+\phi_{3h\eta}(0,0)+\phi_{4h\eta}(0,0)$$

$$=B\phi_h(0,0)+(\tfrac{1}{2}(\text{Cosh Ah}-\text{Sinh Ah})G_1+(\text{Cosh Ah}-\frac{\text{Cosh}^2\text{Ah}}{\text{Sinh Ah}})$$

$$\text{Ah } G_2)(e^{-Bk}\phi_{hne}-e^{Bk}\phi_{hse})+(\tfrac{1}{2}(\text{Cosh Ah}+\text{Sinh Ah})G_1-$$

$$(\text{Cosh Ah}+\frac{\text{Cosh}^2\text{Ah}}{\text{Sinh Ah}})\text{Ah } G_2)(e^{-Bk}\phi_{hnw}-e^{Bk}\phi_{hsw})+$$

$$(\text{Ah}\frac{2\text{Cosh}^2\text{Ah}}{\text{Sinh Ah}}G_2)(e^{-Bk}\phi_{hnc}-e^{Bk}\phi_{hsc}) \qquad \text{(A-27)}$$

Using the following relations the series summation in G_1, G_2, G_1', G_2' can be simplified.

First, since ϕ_h=constant is a solution of Eq.(A-1b) that all nodal values in the element must be the same constant, and hence $\phi_{h\xi}=0$, $\phi_{h\eta}=0$. Then from Eq.(A-26) and Eq.(A-27) we have

$$A-2\text{Cosh Bk Sinh Ah } G_1'=0$$

$$B-2\text{Cosh Ah Sinh Bk } G_1=0$$

or $$G_1'=\frac{A}{2\text{Sinh Ah Cosh Bk}}; \quad G_1=\frac{B}{2\text{Sinh Bk Cosh Ah}} \qquad \text{(A-28)}$$

Secondly, $\phi_h=-BC\xi+A\eta$ is also a solution of Eq.(A-1b), so $\phi_{h\xi}=-BC$, $\phi_{h\eta}=A$. Substituting boundary functions into Eq. (A-26) and Eq.(A-27) we have

$$G_2'=\frac{1}{4ABk^2\text{Sinh Ah Cosh Bk}}(BC(1-\frac{\text{Ah Cosh Ah}}{\text{Sinh Ah}})+\frac{A^2k\text{ Sinh Bk}}{\text{Cosh Bk}})$$

$$G_2=\frac{1}{4ABCh^2\text{Sinh Bk Cosh Ah}}(A(1-\frac{\text{Bk Cosh Bk}}{\text{Sinh Bk}})+\frac{B^2Ch\text{ Sinh Ah}}{\text{Cosh Ah}}) \qquad \text{(A-29)}$$

It should be remarked here, that one does not need any series summation to calculate G_1, G_1', G_2 and G_2', hence, the computational time involved in the evaluation of the

ORIGINAL PAGE IS
OF POOR QUALITY

finite analytic coefficients for derivatives is indeed very little.

Since $\phi_h=\phi+\frac{f(A\xi+B\eta)}{2(A^2+B^2C)}$, then $\phi_\xi=\phi_{h\xi}-\frac{fA}{2(A^2+B^2C)}$

and $\phi_\xi(0,0)=\phi_{1h\xi}(0,0)+\phi_{2h\xi}(0,0)+\phi_{3h\xi}(0,0)+\phi_{4h\xi}(0,0)-\frac{fA}{2(A^2+B^2C)}$

$$=A\phi_h(0,0)+(\tfrac{1}{2}(\text{Cosh Bk}-\text{Sinh Bk})G_1'+(\text{Cosh Bk}-\frac{\text{Cosh}^2\text{Bk}}{\text{Sinh Bk}})$$

$$\text{Bk } G_2')(e^{-Ah}\phi_{hne}-e^{Ah}\phi_{hnw})+(\tfrac{1}{2}(\text{Cosh Bk}+\text{Sinh Bk})G_1'-$$

$$(\text{Cosh Bk}+\frac{\text{Cosh}^2\text{Bk}}{\text{Sinh Bk}})\text{Bk } G_2')(e^{-Ah}\phi_{hse}-e^{Ah}\phi_{hsw})+$$

$$(\text{Bk}\frac{2\text{Cosh}^2\text{Bk}}{\text{Sinh Bk}}G_2')(e^{-Ah}\phi_{hec}-e^{Ah}\phi_{hwc})-\frac{fA}{2(A^2+B^2C)} \quad \text{(A-30)}$$

Substituting Eq.(A-5) into Eq.(A-30) we have

$$\phi_\xi(0,0)=A\phi(0,0)+e^{-Bk}(\tfrac{1}{2}G_1'-\text{Bk Coth Bk } G_2')(e^{-Ah}\phi_{ne}-e^{Ah}\phi_{nw})$$

$$+e^{Bk}(\tfrac{1}{2}G_1'-\text{Bk Coth Bk } G_2')(e^{-Ah}\phi_{se}-e^{Ah}\phi_{sw})$$

$$+(e^{Bk}+e^{-Bk})(\text{Bk COth Bk } G_2')(e^{-Ah}\phi_{ec}-e^{Ah}\phi_{wc})$$

$$+\frac{f}{2(A^2+B^2C)}\{Ah(e^{-Ah}+e^{Ah})(\tfrac{1}{2}G_1'(e^{Bk}+e^{-Bk}))+\text{Bk}$$

$$(e^{Ah}-e^{-Ah})(e^{Bk}-e^{-Bk})(\tfrac{1}{2}G_1'-\text{Bk Coth Bk } G_2')-A\}$$

or $\phi_\xi(0,0)=A\phi(0,0)+C_{ne}'\phi_{ne}+C_{nw}'\phi_{nw}+C_{se}'\phi_{se}+C_{sw}'\phi_{sw}+C_{ec}'\phi_{ec}$

$$+C_{wc}'\phi_{wc}+C_f'f \quad \text{(A-31)}$$

and $GA=\frac{1}{2}G_1'-\text{Bk Coth Bk } G_2'$; $GB=(e^{Bk}+e^{-Bk})(\text{Bk Coth Bk } G_2')$

$C_{ne}'=e^{-Ah-Bk}GA$; $C_{nw}'=-e^{Ah-Bk}GA$; $C_{se}'=e^{-Ah+Bk}GA$;

$C_{sw}'=-e^{Ah+Bk}GA$; $C_{ec}'=e^{-Ah}GB$; $C_{wc}'=-e^{Ah}GB$;

ORIGINAL PAGE IS
OF POOR QUALITY

$$C_f' = \frac{1}{2(A^2+B^2C)}\{Ah(e^{Ah}+e^{-Ah})(\tfrac{1}{2}G_1'(e^{Bk}+e^{-Bk}))+Bk(e^{Ah}-e^{-Ah})$$
$$(e^{Bk}-e^{-Bk})(\tfrac{1}{2}G_1'-Bk \text{ Coth } Bk\ G_2')-A\} \qquad \text{(A-32)}$$

Similarly, $\phi_\eta(0,0)=B\phi(0,0)+C_{ne}''\phi_{ne}+C_{se}''\phi_{se}+C_{nw}''\phi_{nw}+C_{sw}''\phi_{sw}$

$$+C_{nc}''\phi_{nc}+C_{sc}''\phi_{sc}+C_f''f \qquad \text{(A-33)}$$

and $HA=\frac{1}{2}G_1-Ah \text{ Coth } Ah\ G_2$; $HB=(e^{Ah}+e^{-Ah})(Ah \text{ Coth } Ah\ G_2)$;

$C_{ne}''=e^{-Ah-Bk}HA$; $C_{se}''=-e^{-Ah+Bk}HA$; $C_{nw}''=e^{Ah-Bk}HA$;

$C_{sw}''=-e^{Ah+Bk}HA$; $C_{nc}''=e^{-Bk}HB$; $C_{sc}''=-e^{Bk}HB$;

$$C_f''=\frac{1}{2(A^2+B^2C)}\{Bk(e^{Bk}+e^{-Bk})(\tfrac{1}{2}G_1(e^{Ah}+e^{-Ah})+Ah(e^{Bk}-e^{-Bk})$$
$$(e^{Ah}-e^{-Ah})(\tfrac{1}{2}G_1-Ah \text{ Coth } Ah\ G_2)-B\} \qquad \text{(A-34)}$$

In an attempt to reduce computational time for evaluation of FA coefficients, we found that the form of E_2 or E_2' in Eq.(A-12c) or Eq.(A-13c) is very close connected to series summation of G_2 or G_2' in Eq.(A-22b) or Eq.(A-24a).

After a comparison study between the series summation of G_2 and E_2 or G_2' and E_2' (see Table A-1), it is found that if A>10 B>10, there exist an approximate relation between E_2 and G_2 or E_2' and G_2', that is:

$$E_2 \simeq G_2 \text{Tanh } (\mu_1 h/\mu_1); \quad E_2' \simeq G_2' \text{ Tanh } (\mu_1' k/\mu_1'). \qquad \text{(A-35)}$$

where $\mu_1=((A^2+B^2C+(\frac{\pi}{2h})^2)/C)^{0.5}$;

$\mu_1'=(A^2+B^2C+(\frac{\pi}{2k})^2C)^{0.5}$.

In Table A-1 FAP means approximate FA method.

Table A-1 Comparison of FA and FAP Coefficients

A	B	C		C_{NW}	C_{WC}	C_{SW}	C_{NC}	C_{SC}	C_{NE}	C_{EC}	C_{SE}	C_f
0.	0.	1.	FA	0.04469	0.20531	0.04469	0.20531	0.20531	0.04469	0.20531	0.04469	0.29469
			FAP	0.05538	0.19482	0.05549	0.19443	0.19482	0.05527	0.19443	0.05538	0.30538
			ϕ_x	-0.08334	-0.33366	-0.08350	--	--	0.08317	0.33299	0.08334	0.00017
			ϕ_y	0.08334	--	-0.08350	0.33299	-0.33366	0.08317	--	-0.08334	0.00017
0.	0.	100.	FA	0.00250	0.00000	0.00250	0.49500	0.49500	0.00250	0.00000	0.00250	0.00500
			FAP	0.03913	-0.07260	0.03921	0.49378	0.49477	0.03905	-0.07246	0.03913	0.00573
			ϕ_x	-0.25000	0.00000	-0.25050	--	--	0.24950	0.00000	0.25000	0.00001
			ϕ_y	0.00083	--	-0.00083	0.49784	0.49883	0.00083	--	-0.00083	0.00000
0.	0.	0.001	FA	0.00025	0.49950	0.00025	0.00000	0.00000	0.00025	0.49950	0.00025	0.50000
			FAP	0.03897	0.49992	0.03905	-0.07729	-0.07744	0.03889	0.49892	0.03897	0.57737
			ϕ_x	-0.00008	-0.50033	-0.00008	--	--	0.00008	0.49933	0.00008	0.00017
			ϕ_y	0.25000	--	-0.25050	0.00000	0.00000	0.24950	--	-0.25000	0.00017
1.	1.	1.	FA	0.02363	0.34130	0.17457	0.04619	0.34130	0.00320	0.04619	0.02363	0.23324
			FAP	0.03037	0.31300	0.22442	0.04236	0.31300	0.00411	0.04236	0.03037	0.24548
			ϕ_x	-0.05666	-0.68116	-0.41870	--	--	0.00767	0.09219	0.05666	0.15652
			ϕ_y	0.05666	--	-0.41870	0.09218	-0.68116	0.00767	--	-0.05666	0.15652
50.	50.	1.	FA	**	**	**	**	**	**	**	**	**
			FAP	0.00000	0.00028	0.99943	0.00000	0.00028	0.00000	0.00000	0.00000	0.01000
			ϕ_x	0.00000	-0.02000	-0.98000	--	--	0.00000	0.00000	0.00000	0.00980
			ϕ_y	0.00000	--	-0.98000	0.00000	-0.02000	0.00000	--	0.00000	0.00980
1000.	1000.	1.	FA	**	**	**	**	**	**	**	**	**
			FAP	0.00000	0.00000	1.00000	0.00000	0.00000	0.00000	0.00000	0.00000	0.00050
			ϕ_x	0.00000	-0.00100	-0.99900	--	--	0.00000	0.00000	0.00000	0.00050
			ϕ_y	0.00000	--	-0.99900	0.00000	-0.00100	0.00000	--	0.00000	0.00050
1.	100.	5.	FA	0.00000	0.00000	0.00231	0.00000	0.99737	0.00000	0.00000	0.00031	0.00100
			FAP	0.00000	0.00000	0.00231	0.00000	0.99737	0.00000	0.00000	0.00031	0.00100
			ϕ_x	0.00000	0.00000	-1.15652	--	--	0.00000	0.00000	0.15652	0.00100
			ϕ_y	0.00000	--	-0.00229	0.00000	-0.99740	0.00000	--	-0.00031	0.00099
1000.	1.	50.	FA	0.00783	0.93435	0.05782	0.00000	0.00000	0.00000	0.00000	0.00000	0.00050
			FAP	0.00783	0.93435	0.05783	0.00000	0.00000	0.00000	0.00000	0.00000	0.00050
			ϕ_x	-0.00782	-0.93442	-0.05777	--	--	0.00000	0.00000	0.00000	0.00050
			ϕ_y	0.15652	--	-1.15652	0.00000	0.00000	0.00000	--	0.00000	0.00050

-- no values
** overflow

$\phi_p = \sum_{n=1}^{\infty} C_n \phi_n + C_f f$

$\phi_x = A\phi_p + \sum_{n=1}^{\infty} C_n \phi_n + C_f f$, $\phi_y = B\phi_p + \sum_{n=1}^{\infty} C_n \phi_n + C_f f$

If A>1 then A=1, B>1 then B=1

ORIGINAL PAGE IS OF POOR QUALITY

ORIGINAL PAGE IS
OF POOR QUALITY

APPENDIX B

RELATIONSHIPS BETWEEN PHYSICAL AND TRANSFORMED PLANE

This appendix contains the pertient definitions and relations between the physical (x,y) plane and transformed (ξ,η) plane used in the present study. Basically the relations and the notation used in Ref. [5] is retained here. The function f(x,y,t) is defined as a twice continuously differentiable scalar function of x,y and t and the vector $F(x,y)=F_1(x,y)i+F_2(x,y)j$ is a continuously differentiable vector-valued function where i and j are the conventional cartesian coordinate unit vectors.

It should be noted that all derivative transformations given here are in the geometrically non-conservation form.

Definitions of the transformation relevent to the present study are

$$\alpha=x_\eta^{\ 2}+y_\eta^{\ 2} \tag{B-1}$$

$$\beta=x_\xi x_\eta+y_\xi y_\eta \tag{B-2}$$

$$\gamma=x_\xi^{\ 2}+y_\xi^{\ 2} \tag{B-3}$$

$$D_x=\alpha x_{\xi\xi}-2\beta x_{\xi\eta}+\gamma x_{\eta\eta} \tag{B-4}$$

$$D_y=\alpha y_{\xi\xi}-2\beta y_{\xi\eta}+\gamma y_{\eta\eta} \tag{B-5}$$

$$\sigma=(y_\xi D_x-x_\xi D_y)/J \tag{B-6}$$

$$\tau=(x_\eta D_y-y_\eta D_x)/J \tag{B-7}$$

$$J=x_\xi y_\eta-x_\eta y_\xi \tag{B-8}$$

where J is the determinant of the Jacobian matrix.

Derivative transformations for function f between (x,y) and (ξ,η) coordinate are

$$f_x=(\partial f/\partial x)_{y,t}=(y_\eta f_\xi-y_\xi f_\eta)/J \tag{B-9}$$

$$f_y=(\partial f/\partial y)_{x,t}=(x_\xi f_\eta-x_\eta f_\xi)/J \tag{B-10}$$

$$\begin{aligned} f_{xx}=(\partial^2 f/\partial x^2)_{y,t}&=(y_\eta{}^2 f_{\xi\xi}-2y_\xi y_\eta f_{\xi\eta}+y_\xi{}^2 f_{\eta\eta})/J^2 \\ &+(y_\eta{}^2 y_{\xi\xi}-2y_\xi y_\eta y_{\xi\eta}+y_\xi{}^2 y_{\eta\eta})(x_\eta f_\xi-x_\xi f_\eta)/J^3 \\ &+(y_\eta{}^2 x_{\xi\xi}-2y_\xi y_\eta x_{\xi\eta}+y_\xi{}^2 x_{\eta\eta})(y_\xi f_\eta-y_\eta f_\xi)/J^3 \end{aligned} \tag{B-11}$$

$$\begin{aligned} f_{yy}=(\partial^2 f/\partial x^2)_{x,t}&=(x_\eta{}^2 f_{\xi\xi}-2x_\xi x_\eta f_{\xi\eta}+x_\xi{}^2 f_{\eta\eta})/J^2 \\ &+(x_\eta{}^2 y_{\xi\xi}-2x_\xi x_\eta y_{\xi\eta}+x_\xi{}^2 y_{\eta\eta})(x_\eta f_\xi-x_\xi f_\eta)/J^3 \\ &+(x_\eta{}^2 x_{\xi\xi}-2x_\xi x_\eta x_{\xi\eta}+x_\xi{}^2 x_{\eta\eta})(y_\xi f_\eta-y_\eta f_\xi)/J^3 \end{aligned} \tag{B-12}$$

$$\begin{aligned} f_{xy}=&((x_\xi y_\eta+x_\eta y_\xi)f_{\xi\eta}-x_\xi y_\xi f_{\eta\eta}-x_\eta y_\eta f_{\xi\xi})/J^2 \\ &+(x_\eta y_\eta x_{\xi\xi}-(x_\xi y_\eta+x_\eta y_\xi)x_{\xi\eta}+x_\xi y_\xi x_{\eta\eta})(y_\eta f_\xi-y_\xi f_\eta)/J^3 \\ &+(x_\eta y_\eta y_{\xi\xi}-(x_\xi y_\eta+x_\eta y_\xi)y_{\xi\eta}+x_\xi y_\xi y_{\eta\eta})(x_\xi f_\eta-x_\eta f_\xi)/J^3 \end{aligned} \tag{B-13}$$

ORIGINAL PAGE IS
OF POOR QUALITY

Vector Derivative Transformations for function f and F are

Laplacian:

$$\nabla^2 f=(\alpha f_{\xi\xi}-2\beta f_{\xi\eta}+\gamma f_{\eta\eta})/J^2+((\alpha x_{\xi\xi}-2\beta x_{\xi\eta}+\gamma x_{\eta\eta})(y_\xi f_\eta-y_\eta f_\xi)$$
$$+(\alpha y_{\xi\xi}-2\beta y_{\xi\eta}+\gamma y_{\eta\eta})(x_\eta f_\xi-x_\xi f_\eta))/J^3 \qquad \text{(B-14)}$$

or $$\nabla^2 f=(\alpha f_{\xi\xi}-2\beta f_{\xi\eta}+\gamma f_{\eta\eta}+\sigma f_\eta+\tau f_\xi)/J^2 \qquad \text{(B-15)}$$

Gradient:

$$\nabla f=((y_\eta f_\xi-y_\xi f_\eta)i+(x_\xi f_\eta-x_\eta f_\xi)j)/J \qquad \text{(B-16)}$$

Divergence:

$$\nabla\cdot F=(y_\eta(F_1)_\xi-y_\xi(F_1)_\eta+x_\xi(F_2)_\eta-x_\eta(F_2)_\xi)/J \qquad \text{(B-17)}$$

Curl:

$$\nabla \times F=k(y_\eta(F_2)_\xi-y_\xi(F_2)_\eta-x_\xi(F_1)_\eta+x_\eta(F_1)_\xi)/J \qquad \text{(B-18)}$$

Unit Tangent and Normal Vectors

Normal to η-line

$$n^{(\eta)}=\nabla\eta/|\nabla\eta|=(-y_\xi i+x_\xi j)/\sqrt{\gamma} \qquad \text{(B-19)}$$

Normal to ξ-line

$$n^{(\xi)}=\nabla\xi/|\nabla\xi|=(y_\eta i-x_\eta j)/\sqrt{\alpha} \qquad \text{(B-20)}$$

Tangent to η-line

$$t^{(\eta)}=n^{(\eta)}\times k=(x_\xi i+y_\xi j)/\sqrt{\gamma} \qquad \text{(B-21)}$$

Tangent to ξ-line

$$t^{(\xi)}=n^{(\xi)}\times k=-(x_\eta i+y_\eta j)/\sqrt{\alpha} \qquad \text{(B-22)}$$

ORIGINAL PAGE IS
OF POOR QUALITY

Vector Components Tangent and Normal to ξ and η lines

$$F_n^{(\eta)} = n^{(\eta)} \cdot F = (-y_\xi F_1 + x_\xi F_2)/\sqrt{\gamma} \tag{B-23}$$

$$F_t^{(\eta)} = t^{(\eta)} \cdot F = (x_\xi F_1 + y_\xi F_2)/\sqrt{\gamma} \tag{B-24}$$

$$F_n^{(\xi)} = n^{(\xi)} \cdot F = (y_\eta F_1 - x_\eta F_2)/\sqrt{\alpha} \tag{B-25}$$

$$F_t^{(\xi)} = t^{(\xi)} \cdot F = -(x_\eta F_1 + y_\eta F_2)/\sqrt{\alpha} \tag{B-26}$$

Directional Derivatives:

$$\partial f/\partial n^{(\eta)} = n^{(\eta)} \cdot \nabla f = (\gamma f_\eta - \beta f_\xi)/J\sqrt{\gamma} \tag{B-27}$$

$$\partial f/\partial t^{(\eta)} = t^{(\eta)} \cdot \nabla f = f_\xi/\sqrt{\gamma} \tag{B-28}$$

$$\partial f/\partial n^{(\xi)} = n^{(\xi)} \cdot \nabla f = (\alpha f_\xi - \beta f_\eta)/J\sqrt{\alpha} \tag{B-29}$$

$$\partial f/\partial t^{(\xi)} = t^{(\xi)} \cdot \nabla f = -f_\eta/\sqrt{\alpha} \tag{B-30}$$

ORIGINAL PAGE IS
OF POOR QUALITY

APPENDIX C

CONTOUR PLOT

This appendix presents the basic idea of the methods used to determine contour plots of a function defined on the transformed plane, and graph it back on the physical plane.

Let us consider that $\phi=\phi(\xi,\eta)$ as shown in Fig. C-1 is a function defined on the transformed plane D^*, and that We are interested in the contour curve of constant ϕ value say $C(\phi)$ on the physical(x,y) plane, Graphically, $C(\phi)$ is the curve created by the intersection of the surface $\phi(\xi,\eta)$ and the plane $\phi(\xi,\eta)=c$ For plotting convience this contour curve is usually projected onto the transformed(ξ,η) plane, then one needs to creat a program to locate all pairs of the nodes where this contour curve lies on the transformmed - plane.

To accomplish this, let us consider a portion of computationaal region on D as shown in Fig C-2a where $1\leq I1<I2\leq IMAX$ and $1\leq J1<J2\leq JMAX$. Here each grid block is labeled by the (i,j) coordinate of the lower left hand corner of the block. Let us assumed that a constant line passes through the block (m,n) as shown on a large scale in Fig. C-2b.

ORIGINAL PAGE IS
OF POOR QUALITY

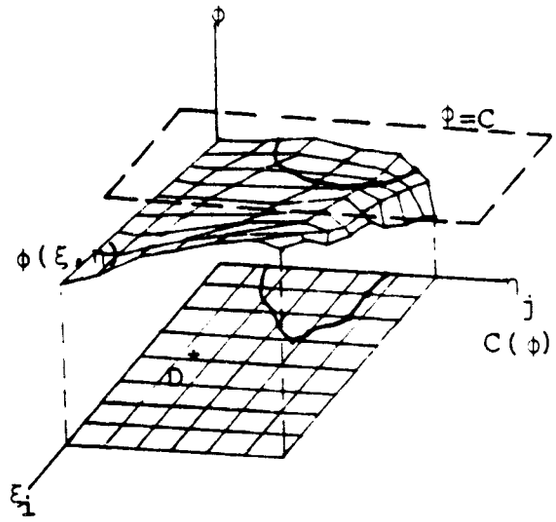

Fig. C-1 Contour of $\phi(\xi_i, \eta_j)$

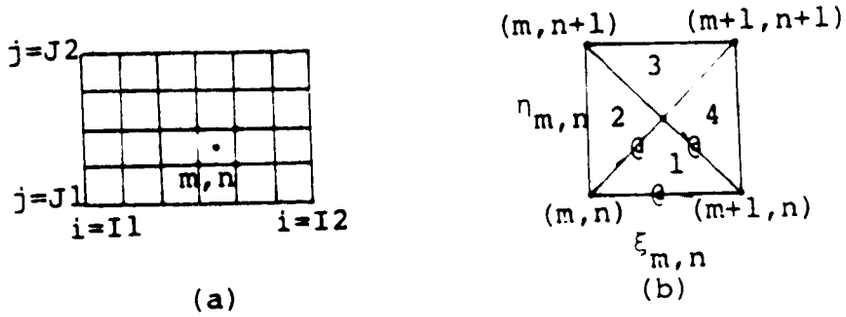

Fig. C-2 Simple grid in set D^*

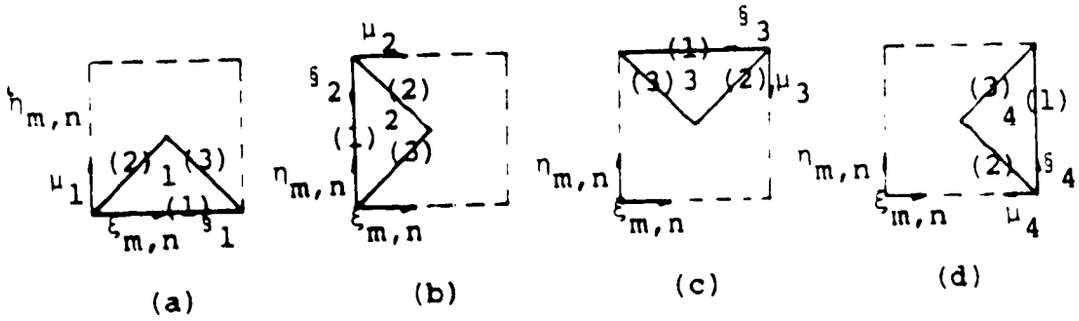

Fig. C-3 Local coordinate system for triangle

ORIGINAL PAGE IS
OF POOR QUALITY

In order to obtain an accurated plot resolution, We subdivid each block into four triangles, as shown. The value of ϕ at (m+1/2,n+1/2) is taken as the four point average or

$$\phi_{m+\frac{1}{2},n+\frac{1}{2}}=(\phi_{m,n}+\phi_{m+1,n}+\phi_{m,n+1}+\phi_{m+1,n+1})/4$$

At a grid block (m,n) as demonstrated in Fig C-2b the interpolation procedures of standard form can be set up by first placing a local coordinate ($\S,\mu$) on each of the subtriangles as illustrated in the series of drawings given in Fig C-3. Interpolation is carried out on each of the four triangles for each grid block in the segment ($I1 \leq i \leq I2$, $J1 \leq j \leq J2$) of the set D^* specified. In each triangle where a desired contour value ϕ is known to lie, interpolations are performed along all three sides of triangle. Let d' be the directed distance from a given triangle vertex to the point on the triangle side where the contour intersects that side (denoted by @) as illustrated in Fig C-2b for triangle 1 and is defined in an analogous manner for the other triangles. Let ϕ_1 and ϕ_2 be respectively the value of ϕ at different triangle vertex, then d' may be expressed as

$$d'=(\text{side length})(\phi-\phi_1)/(\phi_2-\phi_1)$$

For example, along side 1 of triangle 1, d' is given by

$$d'_{1-2}=(1.0)(\phi-\phi_{m+1,n})/(\phi_{m,n}-\phi_{m+1,n})$$

ORIGINAL PAGE IS
OF POOR QUALITY

Noting that the sides of the triangle have lengths 1.0, 0.71 and 0.71 The contour intersections can be expressed in the local triangle coordinate $(\S,\mu)$ as

Side	Coordinates	
	$\S_l$	μ_l
1	1-d	0
2	d/2	d/2
3	(1+d)/2	(1-d)/2

where $d=(\phi-\phi_l)/(\phi_2-\phi_l)$ and where l=1,2,3 or 4 denotes the triangle number.

Once the contour intersections have been located in terms of the local triangle coordinates $(\S_l,\mu_l)$, they must be transformed to the grid block coordinates (ξ_{mn},η_{mn}). This is done in the conventional fashion using orthogonal rotation matrices. If $[\S_{l,p},\mu_{l,p}]$ are the coordinates of an intersection in triangle l, then

$$\begin{vmatrix} (\xi_{m,n})_{l,p} \\ (\eta_{m,n})_{l,p} \end{vmatrix} = A_l \begin{vmatrix} \S_{l,p} \\ \mu_{l,p} \end{vmatrix}$$

where $A_1 \equiv \begin{vmatrix} 1 & 0 \\ 1 & 0 \end{vmatrix}$; $A_2 \equiv \begin{vmatrix} 0 & 1 \\ -1 & 0 \end{vmatrix}$;

ORIGINAL PAGE IS
OF POOR QUALITY

$$A_3 \equiv \begin{vmatrix} -1 & 0 \\ 0 & -1 \end{vmatrix}; \quad A_4 \equiv \begin{vmatrix} 0 & -1 \\ 1 & 0 \end{vmatrix}.$$

Finally, the point $[(\xi_{mn})_{1p}, (\eta_{mn})_{1p}]$ is transformed to (ξ, η) coordinates by a simple linear transformation producing an element $[\bar{\xi}_k, \bar{\eta}_k]$ of the set $C(\phi)$.

Table C-1 of numerical procedure can be used to save the computational time and to set up a smooth plotting.

Since contours on the transformed plane are of little interest, $C(\phi)$ must be transformed to the physical plane. This is made possible through the use of the coordinate transformation function $X(\xi_i, \eta_j)$ and $Y(\xi_i, \eta_j)$. Again interpolation is required since almost all points of $C(\phi)$ are not on the nodes of elements of D^* on which the discrete function $X(\xi_i, \eta_j)$ and $Y(\xi_i, \eta_j)$ are defined. As illustrated in Fig C-4 this implies a dobule linear interpolation must be performed. If $[\bar{\xi}_k, \bar{\eta}_k]$ denotes an point of $C(\phi)$, the first step to locate the ξ and η values. Denoting these by ξ_i, ξ_{i+1} and η_j, η_{j+1} as shown in the Fig C-4, the values of x_k and y_k are calculated as follows:

$$\bar{x}_k = (\bar{\eta}_k - \eta_j)(X_{j+1} - X_j)/(\eta_{j+1} - \eta_j) + X_j$$

where $$X_j = (\bar{\xi}_k - \xi_i)(x_{i+1,j} - x_{i,j})/(\xi_{i+1} - \xi_i) + x_{i,j}$$

Table C-1 Flow Chart of Contour Plot

IT: the subtriangles 1, 2, 3, 4.
ID: denotes the sides of each subtriangle.
yes: means the curve passes the sides of subtriangle.
no: means the curve not passes the sides of subtriangle.

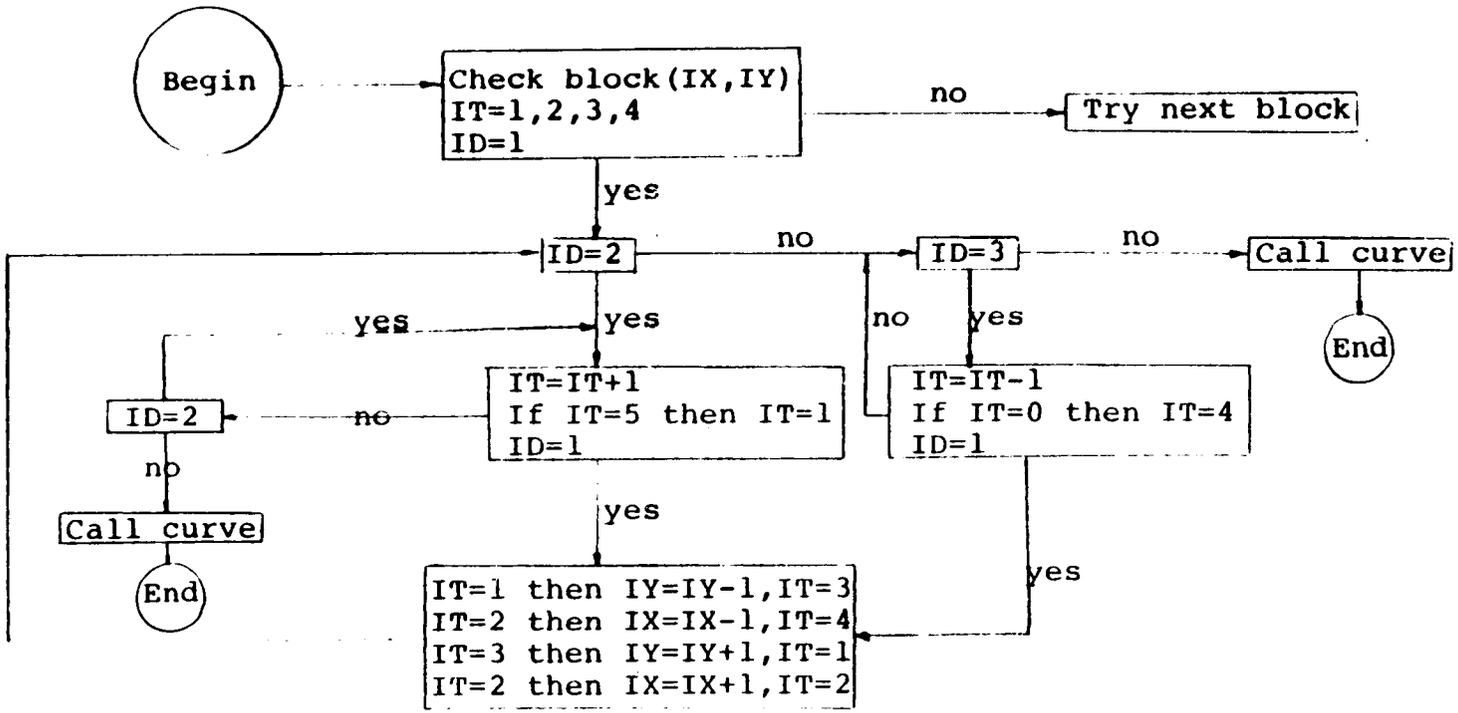

ORIGINAL PAGE IS
OF POOR QUALITY

ORIGINAL PAGE IS
OF POOR QUALITY

$$X_{j+1}=(\bar{\xi}_k-\xi_i)(x_{i+1,j+1}-x_{i,j+1})/(\xi_{i+1}-\xi_i)+x_{i,j+1}$$

for all k=1,2,.....,n. Similar expressions are used to calculate Y .

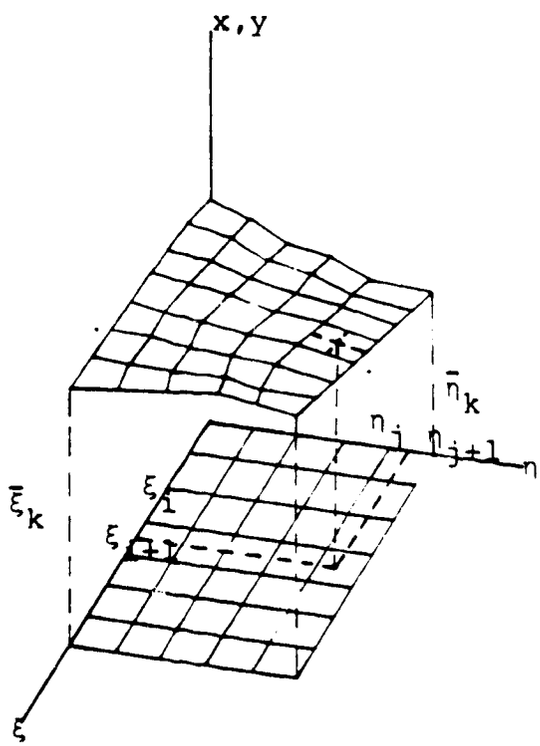

Fig. C-4 Interpolation for x and y

ORIGINAL PAGE IS
OF POOR QUALITY

APPENDIX D

COMPUTER PROGRAM

```
(0001)  C       D-1:BOUNDARY FITTED COORDINATE SYSTEM


(0001)  C       D-1:BOUNDARY FITTED COORDINATE SYSTEM
(0002)  C
(0003)  C
(0004)  C      THIS PROGRAM IS USED TO TRANSFER A PHYSICAL(X,Y)
(0005)  C      DOMAIN INTO A TRANSFORMED(ξ,η) DOMAIN.
(0006)  C
(0007)  C     IXMAX: THE MAXIMUM NODES IN THE ξ DIRECTION
(0008)  C     IYMAX: THE MAXIMUM NODES IN THE η DIRECTION
(0009)  C         P: THE CONCENTRATION VALLES ON THE ξ LINE
(0010)  C         Q: THE CONCENTRATION VALUES ON THE η LINE
(0011)  C     X(I,J): THE X VALUE AT THE POINT(I,J) IN THE TRANSFORMED DOMAIN
(0012)  C     Y(I,J): THE Y VALUE AT THE POINT(I,J) IN THE TRANSFORMED DOMAIN
(0013)  C         AF: α=Xη*Xη+Yη*Yη
(0014)  C         BT: β=Xξ*Xη+Yξ*Yη
(0015)  C         CM: γ=Xξ*Xξ+Yξ*Yξ
(0016)  C        XYJ: J=Xξ*Yη-Xη*Yξ
(0017)  C        SOR: SUCCESSIVE OVER RELATION
(0018)  C         AK: AMPLIFIED FACTOR
(0019)  C         CK: DECAY FACTOR
(0020)  C
(0021)  C     ****************************************************************
(0022)  C
(0023)  $INSERT SYSCOM>ERROR.F
(0024)  $INSERT SYSCOM>KEYS.F
(0025)  $INSERT SYSCOM>ACKEYS
(0026)        IMPLICIT REAL*8 (A-H,O-Z)
(0027)        COMMON/AAA/ X(40,41),Y(40,41)
(0028)        COMMON Q(41),P(40),FX(40,41),FY(40,41)
(0029)        CALL SRCHSS(KSPEAD,'SMAL',4,7,TYPE,CODE)
(0030)        CALL SRCHSS(KSWRIT,'SMAI',4,2,TYPE,CODE)
(0031)  C
(0032)  C     ************************** INPUT KNOWN BOUNDARY VALUES
(0033)  C                                AND INITIAL GUESS OF INTERIOR NODES
(0034)  C                                ----- THE FILE 'SMAL'.
(0035)  C
(0036)        IMAX=40
(0037)        JMAX=41
(0038)        IMAX1=IMAX-1
(0039)        JMAX1=JMAX-1
(0040)        READ(11,200)SOR,AK,CK
(0041)        DO 1 J=1,JMAX
(0042)        READ(11,200)(X(I,J),I=1,IMAX)
(0043)      1 READ(11,200)(Y(I,J),I=1,IMAX)
(0044)  C
(0045)  C     ************************ CONCENTRATION VALUES P&Q
(0046)  C
(0047)        DO 12 J=2,11
(0048)        Q(J)=CONC(J-1,1,AK,CK)
(0049)     12 CONTINUE
(0050)        WRITE(6,200)Q
(0051)        DO 16 K=8,39
(0052)     16 P(K)=CONC(K-21,21,AK,CK)
(0053)        WRITE(6,200)P
(0054)  C
(0055)  C     ********************** NUMERICAL CALCULATION
(0056)  C
(0057)        DO 48 I=1,5
(0058)        N=1
(0059)     80 DO 26 J=1,11
(0060)        X(1,J)=X(IMAX1,J)
```

ORIGINAL PAGE IS
OF POOR QUALITY


```
(0061)          X(IMAX,J)=X(2,J)
(0062)          Y(1,J)=Y(IMAX1,J)
(0063)       26 Y(IMAX,J)=Y(2,J)
(0064)          DO 65 J=2,JMAX1
(0065)          IN1=2
(0066)          INP=IMAX1
(0067)          IF(J.GE.12)IN1=4
(0068)          IF(J.GT.12)INP=34
(0069)   C
(0070)   C      ********************** LAPLACE EQUATION (P=0,Q=0)
(0071)   C
(0072)          DO 70 I=IN1,INP
(0073)          XET=X(I,J+1)-X(I,J-1)
(0074)          XXI=X(I+1,J)-X(I-1,J)
(0075)          YET=Y(I,J+1)-Y(I,J-1)
(0076)          YXI=Y(I+1,J)-Y(I-1,J)
(0077)          XXIET=X(I+1,J+1)-X(I+1,J-1)-X(I-1,J-1)-X(I-1,J+1)
(0078)          YXIET=Y(I+1,J+1)-Y(I+1,J-1)-Y(I-1,J-1)-Y(I-1,J+1)
(0079)          AF=(XET)**2+(YET)**2
(0080)          BT=XXI*XET+YXI*YET
(0081)          GM=(XXI)**2+(YXI)**2
(0082)          FX(I,J)=(AF*(X(I-1,J)+X(I+1,J))-(BT*XXIET/2.)
(0083)         1+GF*(X(I,J+1)+X(I,J-1)))/(2.*(AF+GM))
(0084)          FY(I,J)=(AF*(Y(I-1,J)+Y(I+1,J))-(BT*YXIET/2.)
(0085)         1+GM*(Y(I,J+1)+Y(I,J-1)))/(2.*(AF+GM))
(0086)   C
(0087)   C      ****************** IF P=0 OR Q=0 ADD POISSON SOURCE TERM
(0088)   C
(0089)          XYJ=.25*(XXI*YET-XET*YXI)
(0090)          XAC=((XYJ)**2*(XET*Q(J)+XXI*P(I)))/(AF+GM)
(0091)          YAC=((XYJ)**2*(YET*Q(J)+YXI*P(I)))/(AF+GM)
(0092)          FX(I,J)=FX(I,J)+XAC
(0093)          FY(I,J)=FY(I,J)+YAC
(0094)          X(I,J)=X(I,J)+(FX(I,J)-X(I,J))*SOR
(0095)          Y(I,J)=Y(I,J)+(FY(I,J)-Y(I,J))*SOR
(0096)       70 CONTINUE
(0097)       65 CONTINUE
(0098)          DO 27 J=2,JMAX1
(0099)          Y(2,J)=0.00
(0100)       27 Y(21,J)=0.00
(0101)   C
(0102)   C      ******************** CHECK FOR CONVERGENCE
(0103)   C
(0104)          EPS=0.0
(0105)          DO 77 J=2,JMAX1
(0106)          EPS1=X(8,J)-X(34,J)
(0107)          IF(CABS(EPS1).GT.CABS(EPS))EPS=EPS1
(0108)          EPS3=Y(8,J)-Y(34,J)
(0109)          IF(CABS(EPS3).GT.CABS(EPS))EPS=EPS3
(0110)    77    CONTINUE
(0111)          WRITE(6,202)N,EPS
(0112)   202    FORMAT(1X,'ITERATION AND EPS ARE',I4,F13.7)
(0113)          IF(CABS(EPS).LT.0.0000001)GO TO 85
(0114)          IF(N.GT.30) GO TO 85
(0115)          DO 125 J=2,JMAX1
(0116)          IN1=3
(0117)          INP=20
(0118)          IF(J.GE.12)IN1=4
(0119)          DO 125 I=IN1,INP
(0120)          IJ=42-I
```

ORIGINAL PAGE IS
OF POOR QUALITY

```
(0001)  C       D-1:BOUNDARY FITTED COORDINATE SYSTEM


(0121)          AX=0.500*(X(I,J)+X(IJ,J))
(0122)          AY=0.500*(Y(I,J)-Y(IJ,J))
(0123)          X(I,J)=AX
(0124)          X(IJ,J)=AX
(0125)          Y(I,J)=AY
(0126)      125 Y(IJ,J)=-AY
(0127)          N=N+1
(0128)          GO TO 90
(0129)  C
(0130)  C       *************** OUTPUT DATA ---- THE FILE 'SMAI'
(0131)  C
(0132)       85 WRITE(6,500)N
(0133)          DO 90 J=1,JMAX
(0134)          WRITE(6,100)J
(0135)          WRITE(6,200)(X(I,J),I=1,IMAX)
(0136)          WRITE(6,300)
(0137)       90 WRITE(6,200)(Y(I,J),I=1,IMAX)
(0138)       88 CONTINUE
(0139)      100 FORMAT(,55X,'J=',I2,/,35X,'*** X-COORDINATE ***')
(0140)      200 FORMAT(8F10.5)
(0141)      300 FORMAT(35X,'*** Y-COORDINATE ***')
(0142)      400 FORMAT(8F10.2)
(0143)      500 FORMAT(53X,'****** N=',I3,' ******')
(0144)          CALL EXIT
(0145)          END
PROGRAM SIZES:   PROCEDURE - 001756    LINKAGE - 000332    STACK - 000070
0000 ERRORS [<.MAIN.>FTN-REV1A.3]
```

ORIGINAL PAGE IS
OF POOR QUALITY

```
(0146)  C
(0147)  C     ***********************************************************
(0148)  C
(0149)  C      FUNCTION FOR SOLVING CONCENTRATION VALUES PRO
(0150)  C
(0151)  C         AK: AMPLIFIED FACTOR
(0152)  C         CK: DECAY FACTOR
(0153)  C
(0154)  C
(0155)          FUNCTION CONC(I,J1,J2,A,C)
(0156)          IMPLICIT REAL*8 (A-H,O-Z)
(0157)          DIMENSION AK(74),CK(74)
(0158)          CONC=0.
(0159)          DO 10 J=J1,J2
(0160)          AK(J)=A-(J-J1)*10.
(0161)          CK(J)=C
(0162)       10 CONTINUE
(0163)          DO 20 J=J1,J2
(0164)          M=I-J
(0165)          IF(M)1,2,3
(0166)        1 SIG=-1.
(0167)          L=-M
(0168)          GO TO 4
(0169)        3 SIG=1.
(0170)          L=M
(0171)        4 GP=CK(J)*L
(0172)          XM=DEXP(GP)
(0173)          CON1=(-1.+AK(J)*SIG)/(XM)
(0174)          GO TO 5
(0175)        2 CON1=0.
(0176)        5 CONC=CONC+CON1
(0177)       20 CONTINUE
(0178)          RETURN
(0179)          END
PROGRAM SIZE:   PROCEDURE - 000166    LINKAGE - 001172    STACK - 000062
0000 ERRORS [<CONC  >FTN-REV1P.3]
(0180)  C
(0181)  C     ***********************************************************
(0182)  C
```

ORIGINAL PAGE IS
OF POOR QUALITY

```
(0001)  C         D-2: THE TRANSFORMED COEFFICIENTS


(0001)  C         D-2: THE TRANSFORMED COEFFICIENTS
(0002)  C
(0003)  C
(0004)  C
(0005)  C     THIS PROGRAM IS USED TO CALCULATE THE TRANSFORMED
(0006)  C     COEFFICIENTS A,B,C,.... etc. (SEE TABLE D-1), WHICH
(0007)  C     WILL BE USED AGAIN IN SOLVING THE GOVERNING EQUATIONS
(0008)  C     IN THE TRANSFORMED DOMAIN.
(0009)  C
(0010)  C     ************************************************************
(0011)  C
(0012)  $INSERT SYSSOURCE>READ.F
(0013)  $INSERT SYSCOMM>KEYS.F
(0014)  $INSERT SYSCOMM>ACKEYS
(0015)        IMPLICIT REAL*8 (A-H,O-Z)
(0016)        COMMON A(40,41),Y(40,41),XZ(40,41),XZZ(40,41),YE(40,41),
(0017)       $XEE(40,41),YZ(40,41),YZZ(40,41),YEE(40,41),YZE(40,41),
(0018)       $XB(40,41),XD(40,41),YC(40,41),YBD(40,41),F1(40,41),
(0019)       $F2(40,41),XZE(40,41),YZE(40,41),XXX(40),YYY(40),ZZZ(40)
(0020)       * ,ABD(40),DCB(40),P(40),G(41)
(0021)        CALL SYCMSS(KSREAD,'SMA1',4,7,TYPE,CODE)
(0022)        CALL SSCMSS(KSWRIT,'LAST',4,2,TYPE,CODE)
(0023)  C
(0024)  C     ******************** INPUT KNOWN TRANSFORMED DOMAIN
(0025)  C                                -- THE FILE 'SMA1'
(0026)  C
(0027)        IMAX=40
(0028)        JMAX=41
(0029)        IMAX1=IMAX-1
(0030)        JMAX1=JMAX-1
(0031)        DO 10 IY=1,JMAX
(0032)        READ(11,100)(X(IX,IY),IX=1,IMAX)
(0033)     10 READ(11,100)(Y(IX,IY),IX=1,IMAX)
(0034)        READ(11,100)(G(J),J=1,41)
(0035)        READ(11,100)(P(I),I=1,40)
(0036)  C
(0037)  C     ******************** CALCULATE THE TRANSFORMED COEFFICIENTS
(0038)  C
(0039)        DO 411 IY=2,JMAX1
(0040)        IN1=2
(0041)        INP=IMAX1
(0042)        IF(IY.LE.12)INP=9
(0043)        IF(IY.GE.12)IN1=39
(0044)        DO 411 IX=IN1,INP
(0045)        XZ(IX,IY)=0.5*(X(IX+1,IY)-X(IX-1,IY))
(0046)        XZZ(IX,IY)=X(IX+1,IY)-2.0*X(IX,IY)+X(IX-1,IY)
(0047)        YE(IX,IY)=0.5*(Y(IX,IY+1)-Y(IX,IY-1))
(0048)        YEE(IX,IY)=Y(IX,IY+1)-2.0*Y(IX,IY)+Y(IX,IY-1)
(0049)        YZ(IX,IY)=0.5*(Y(IX+1,IY)-Y(IX-1,IY))
(0050)        YZZ(IX,IY)=Y(IX+1,IY)-2.0*Y(IX,IY)+Y(IX-1,IY)
(0051)        YE(IX,IY)=0.5*(Y(IX,IY+1)-Y(IX,IY-1))
(0052)        YEE(IX,IY)=Y(IX,IY+1)-2.0*Y(IX,IY)+Y(IX,IY-1)
(0053)        XZE(IX,IY)=0.25*(X(IX+1,IY+1)-X(IX+1,IY-1)+X(IX-1,IY-1)
(0054)       1            -X(IX-1,IY+1))
(0055)    411 YZE(IX,IY)=0.25*(Y(IX+1,IY+1)-Y(IX+1,IY-1)+Y(IX-1,IY-1)
(0056)       1            -Y(IX-1,IY+1))
(0057)        DO 413 IX=2,IMAX1
(0058)        XZ(IX,1)=0.5*(X(IX+1,1)-X(IX-1,1))
(0059)        YZ(IX,1)=0.5*(Y(IX+1,1)-Y(IX-1,1))
(0060)        XE(IX,1)=0.5*(4.*X(IX,2)-3.*X(IX,1)-X(IX,3))
```

ORIGINAL PAGE IS
OF POOR QUALITY

```
(0061)     415 YS(IX,1)=0.5*(4.*Y(IX,2)-3.*Y(IX,1)-Y(IX,3))
(0062)         DO 415 IY=2,JMAX1
(0063)         IM1=2
(0064)         IMP=IMAX1
(0065)         IF(IY.GE.12)IM1=8
(0066)         IF(IY.GE.12)IMP=34
(0067)         DO 415 IX=IM1,IMP
(0068)         AF=XE(IX,IY)*XE(IX,IY)+YE(IX,IY)*YE(IX,IY)
(0069)         BT=XZ(IX,IY)*XE(IX,IY)+YZ(IX,IY)*YE(IX,IY)
(0070)         GA=XZ(IX,IY)*XZ(IX,IY)+YZ(IX,IY)*YZ(IX,IY)
(0071)         BJ=XZ(IX,IY)*YE(IX,IY)-XE(IX,IY)*YZ(IX,IY)
(0072)         GZE=GA(IX)*BJ*BJ
(0073)         GTA=BT(IX)*BJ*BJ
(0074)         VA(IX,IY)=-0.5*GTA/AF
(0075)         VZ(IX,IY)=-0.5*GZE/AF
(0076)         VC(IX,IY)=GM/AF
(0077)         VAZ(IX,IY)=0.5*BJ/AF
(0078)         F1(IX,IY)=BJ*BJ/AF
(0079)         F2(IX,IY)=BT/AF
(0080)     415 CONTINUE
(0081)         DO 5 IX=2,IMAX1
(0082)         RTR=DSQRT(X(IX,2)**2+Y(IX,2)**2)-DSQRT(Y(IX,1)**2+Y(IX,1)**2)
(0083)         DCP(IX)=(1.00/RTR)**2
(0084)         AF=XE(IX,1)*XE(IX,1)+YE(IX,1)*YE(IX,1)
(0085)         BT=XZ(IX,1)*XE(IX,1)+YZ(IX,1)*YE(IX,1)
(0086)         BN=YZ(IX,1)*YZ(IX,1)+YZ(IX,1)*YZ(IX,1)
(0087)         ABJ(IX)=XZ(IX,1)*YE(IX,1)-YZ(IX,1)*YZ(IX,1)
(0088)         ABJ2=ABJ(IX)*ABJ(IX)
(0089)         XXX(IX)=AF/ABJ2
(0090)         YYY(IX)=BT/ABJ2
(0091)       5 ZZZ(IX)=GM/ABJ2
(0092)   C
(0093)   C     ******************** OUTPUT DATA -- THE FILE PLOT3D
(0094)   C
(0095)         DO 91 J=2,JMAX1
(0096)    91   WRITE(6,100)(VA(I,J),I=2,IMAX1)
(0097)         DO 92 J=2,JMAX1
(0098)    92   WRITE(6,100)(VZ(I,J),I=2,IMAX1)
(0099)         DO 93 J=2,JMAX1
(0100)    93   WRITE(6,100)(VC(I,J),I=2,IMAX1)
(0101)         DO 94 J=2,JMAX1
(0102)    94   WRITE(6,100)(VAZ(I,J),I=2,IMAX1)
(0103)         DO 95 J=2,JMAX1
(0104)    95   WRITE(6,100)(F1(I,J),I=2,IMAX1)
(0105)         DO 96 J=2,JMAX1
(0106)    96   WRITE(6,100)(F2(I,J),I=2,IMAX1)
(0107)         WRITE(6,100)XXX
(0108)         WRITE(6,100)YYY
(0109)         WRITE(6,100)ZZZ
(0110)         WRITE(6,100)DCP
(0111)         WRITE(6,100)ABJ
(0112)    100  FORMAT(4F10.5)
(0113)    110  FORMAT(7F11.6)
(0114)         CALL EXIT
(0115)         END
PROGRAM SIZE:   PROCEDURES = 0.3024    LIBRARY = 000312    STACK = 000070
5.00 ERRORS [C,MAIN,SYN=PFV1,S]
(0116)   C
(0117)   C     ******************************************************
(0118)   C
```

ORIGINAL PAGE IS
OF POOR QUALITY

```
(0001)  C                    D-3: POTENTIAL FLO.


(0001)  C                    D-3: POTENTIAL FLO.
(0002)  C
(0003)  C
(0004)  C
(0005)  C     THIS PROGRAM IS USED TO CALCULATE POTENTIAL FLO.
(0006)  C
(0007)  C     ***************************************************************
(0008)  C
(0009)  C
(0010)  C     ******************** POTENTIAL FLOW PROGRAM
(0011)  C
(0012)  $INSERT SYSCOM>DEFIN.F
(0013)  $INSERT SYSCOM>DCYS.F
(0014)  $INSERT SYSCOM>ADCKFYS
(0015)        IMPLICIT REAL*4(A-H,O-Z)
(0016)        COMMON/AAA/ AA(62),DC(62),CC(62),DD(62),PSIN(62,61),Z(62)
(0017)        COMMON/BBB/SIA(60,61),SIB(60,61),AA(60,61),
(0018)       *B1(60,61),B2(60,61)
(0019)        COMMON/PSIC/PC1P1(60,61),PC1P2(60,61),PC2P1(60,61),
(0020)       1PC2P2(60,61),PCP01(60,61),PCP1P1(60,61),PCP1P2(60,61),
(0021)       2PCP1Y1(60,61),PCP2P2(60,61)
(0022)        CALL SPCHSS(KSPEAD,'LAST',0,7,TYPE,CODE)
(0023)        CALL SPCHSS(KSPUT,'PSIT',0,2,TYPE,CODE)
(0024)  C
(0025)  C     ******************** INPUT THE TRANSFORMED COEFFICIENTS
(0026)  C                                -- THE FILE 'LAST'
(0027)  C
(0028)        IXMAX=60
(0029)        IYMAX=61
(0030)        IXM1=IXMAX-1
(0031)        IYM1=IYMAX-1
(0032)        HX=1.000
(0033)        HY=1.000
(0034)        SOR=1.400
(0035)   113  FORMAT(4F13.5)
(0036)        DO 122 IY=2,IYM1
(0037)   122  READ(11,113)(SIA(IX,IY),IX=2,IXM1)
(0038)        DO 123 IY=2,IYM1
(0039)   123  READ(11,113)(SIB(IX,IY),IX=2,IXM1)
(0040)        DO 124 IY=2,IYM1
(0041)   124  READ(11,113)(SIC(IX,IY),IX=2,IXM1)
(0042)        DO 125 IY=2,IYM1
(0043)   125  READ(11,113)(A1(IX,IY),IX=2,IXM1)
(0044)        DO 126 IY=2,IYM1
(0045)   126  READ(11,113)(B1(IX,IY),IX=2,IXM1)
(0046)        DO 127 IY=2,IYM1
(0047)   127  READ(11,113)(B2(IX,IY),IX=2,IXM1)
(0048)  C
(0049)  C******************************** GET A.C. A.D INITIAL GUESS
(0050)  C
(0051)        DO 100 IX=1,IXMAX
(0052)        DO 100 IY=1,IYMAX
(0053)        PSIN(IX,IY,1)=0.00
(0054)  100   PSIN(IX,IY,2)=0.00
(0055)        READ(11,113)(PC1P1(IX,2),IX=1,IXMAX)
(0056)        READ(11,113)(PC1P2(IX,2),IX=1,IXMAX)
(0057)        DO 61 IX=3,IXM1
(0058)        PSIN(IX,J,2)=0.00
(0059)     61 PSIN(IX,J,2)=0.002
(0060)        DO 107 IY=1,IYM1
```

ORIGINAL PAGE IS
OF POOR QUALITY

```
(0001)  C                    2-D: POTENTIAL FLO.

(0061)        DO 107 IX=4,34
(0062)    107 PSIN(IX,IY,2)=PSIN(IX,IYMAX,2)
(0063)  C
(0064)  C     ********************** FA 1-POINT COEFFICIENTS IN THE STREAM FUNCTION
(0065)  C                                  COMMIN
(0066)  C
(0067)        DO 251 IY=2,IYM1
(0068)        I1=2
(0069)        IN=I+1
(0070)        IF(IY.GE.12)I1=8
(0071)        IF(IY.GE.12)IN=34
(0072)        DO 251 IX=I1,IN
(0073)        AU=UIA(IX,IY)
(0074)        AV=VIA(IX,IY)
(0075)        CSI=SIG(IX,IY)
(0076)    251 CALL PSICOE(AU,AV,CSI,HX,HY,IX,IY)
(0077)  C
(0078)  C     ********************** NUMERICAL SOLUTION
(0079)  C                              USING LINE-BY-LINE ITERATION
(0080)  C
(0081)        N1=1
(0082)    405 SMPSI=0.0D0
(0083)        DO 406 IY=2,IYM1
(0084)        IN1=2
(0085)        IN=IXM1
(0086)        IF(IY.GE.12)IN1=8
(0087)        IF(IY.GE.12)IN=34
(0088)        DO 421 IX=IN1,IN
(0089)        PSI(2,IY)=0.25*(PSIN(IX+1,IY+1,2)-PSIN(IX-1,IY+1,2)+
(0090)       1                 PSIN(IX-1,IY-1,2)-PSIN(IX+1,IY-1,2))
(0091)        AA(IX)=PCP1P0(IX,IY)
(0092)        AB(IX)=1.0D0
(0093)        CC(IX)=PCP1P0(IX,IY)
(0094)    421 DD(IX)=PCP(P1(IX,IY)*PSIN(IX,IY+1,2)+PCP1M1(IX,IY)*PSI(IX,
(0095)       1IY-1,2)+PCP1P1(IX,IY)*PSIN(IX+1,IY+1,2)+PCP1M1(IX,IY)*PSI(
(0096)       1(IX+1,IY-1,2)+PCM1P1(IX,IY)*PSIN(IX-1,IY+1,2)+PCM1-1(IX,IY)*PSI(
(0097)       1(IX-1,IY-1,2)+PCP0P0(IX,IY)*(-3.0*P2(IX,IY)*PSI(2)
(0098)        DD(IN1)=DD(IN1)-AA(IN1)*PSIN(IN1-1,IY,2)
(0099)        DD(IN)=DD(IN)-CC(IN)*PSIN(IN+1,IY,2)
(0100)        CALL TRIDAG(IN1,IN,AA,AB,CC,DD,T)
(0101)        DO 431 I=IN1,IN
(0102)        PSIN(I,IY,3)=T(I)
(0103)        PSIN(I,IY,2)=PSIN(I,IY,2)+(PSIN(I,IY,3)-PSI(I,IY,2))*.5R
(0104)    431 CONTINUE
(0105)        IF(IY.LE.11)GO TO 43
(0106)        GO TO 433
(0107)     43 PSIN(1,IY,2)=PSIN(5,IY,2)
(0108)        PSIN(2,IY,2)=PSIN(6,IY,2)
(0109)    433 PSIN(21,IY,2)=0.D0
(0110)    406 CONTINUE
(0111)  C
(0112)  C     ********************** CHECK FOR CONVERGENCE
(0113)  C
(0114)        DO 425 IY=2,IY
(0115)        DO 425 IX=2,34
(0116)        DEPSI=PSIN(IX,IY,2)-PSIN(I,IY,1)
(0117)        IF(ABS(DEPSI).LT.ABS(SMPSI))SMPSI=DEPSI
(0118)    425 CONTINUE
(0119)        DO 993 IX=4,34
(0120)        DO 995 IY=3,IY
```

ORIGINAL PAGE IS
OF POOR QUALITY


```
C                D-4 UNSTEADY FLOW PROGRAM

                 D-4 UNSTEADY FLOW PROGRAM
(0001)  C
(0002)  C
(0003)  C
(0004)  C      THIS PROGRAM IS USED TO CALCULATE 2D UNSTEADY NAVIER-STOKES
(0005)  C      EQUATIONS IN STREAM FUNCTION VORTICITY FORM.
(0006)  C
(0007)  C     ***************************************************************
(0008)  C
(0009)  C     ******************************  UNSTEADY FLOW PROGRAM
(0010)  C
(0011)  $INSERT SYSSOM>ERRD.F
(0012)  $INSERT SYSSOM>KEYS.F
(0013)  $INSERT SYSSOM>ASKEYS
(0014)        IMPLICIT REAL*8(A-H,O-Z)
(0015)        COMMON/AAA/ AA(62),BB(62),CC(62),DD(62),T(62),
(0016)       $PSIN(40,41,3),ZETAN(40,41,3)
(0017)        COMMON/BBB/SIA(40,41),SIB(40,41),SIC(40,41),ABW(40,41),
(0018)       $F1(40,41),F2(40,41),XXX(40),YYY(40),ZZZ(40),ABJ(40),DCR(40)
(0019)        COMMON/COEF/CM1P1(40,41),CPCP1(40,41),CP1P1(40,41),CM1P0
(0020)       1(40,41),CP0P0(40,41),CP1P0(40,41),CM1M1(40,41),CP0M1(40,41),
(0021)       2CP1M1(40,41)
(0022)        COMMON/PSIC/PCM1P1(40,41),PCM1P0(40,41),PCM1M1(40,41),
(0023)       1PCPCP1(40,41),PCP0M1(40,41),PCP1P1(40,41),PCP1P0(40,41),
(0024)       2PCP1M1(40,41),PCP0P0(40,41)
(0025)        COMMON DAA(40,41),DFB(40,41),ZT(40,41),PE(40,41),PZ(40,41)
(0026)       $  ,HF(40,41),AF(40,41),U(40),SSS(40)
(0027)        CALL SRCHSS(KSREAD,'BEST',4,7,TYPE,CODE)
(0028)        CALL SRCHSS(KSWRIT,'SLBR',4,2,TYPE,CODE)
(0029)  C
(0030)  C     ***************  INPUT TRANSFORMATION COEFFICIENTS, BOUNDARY
(0031)  C                      CONDITIONS AND INITIAL CONDITIONS.
(0032)  C                       -- THE FILE 'BEST' --
(0033)  C
(0034)        IXMAX=40
(0035)        IYMAX=41
(0036)        IXM1=IXMAX-1
(0037)        IYM1=IYMAX-1
(0038)        LX=12
(0039)        LY=8
(0040)        LZ=34
(0041)        IEND=120
(0042)        HX=1.0D0
(0043)        HY=1.0D0
(0044)   113  FORMAT(9F10.5)
(0045)        DO 122 IY=2,IYM1
(0046)   122  READ(11,113)(SIA(IX,IY),IX=2,IXM1)
(0047)        DO 123 IY=2,IYM1
(0048)   123  READ(11,113)(SIB(IX,IY),IX=2,IXM1)
(0049)        DO 124 IY=2,IYM1
(0050)   124  READ(11,113)(SIC(IX,IY),IX=2,IXM1)
(0051)        DO 125 IY=2,IYM1
(0052)   125  READ(11,113)(ABW(IX,IY),IX=2,IXM1)
(0053)        DO 126 IY=2,IYM1
(0054)   126  READ(11,113)(F1(IX,IY),IX=2,IXM1)
(0055)        DO 127 IY=2,IYM1
(0056)   127  READ(11,113)(F2(IX,IY),IX=2,IXM1)
(0057)        READ(11,113)(XXX(IX),IX=1,IXMAX)
(0058)        READ(11,113)(YYY(IX),IX=1,IXMAX)
(0059)        READ(11,113)(ZZZ(IX),IX=1,IXMAX)
(0060)        READ(11,113)(DCR(IX),IX=1,IXMAX)
```

ORIGINAL PAGE IS
OF POOR QUALITY


```
C                 0-4 UNSTEADY FLOW PROGRAM

(0061)          READ(11,113)(ABJ(IX),IX=1,IXMA))
(0062)          DO 128 IY=1,IYMAX
(0063)     128  READ(11,111)(PSIN(IX,IY,2),IX=1,IXMAX)
(0064)          DO 129 IY=1,IYMAX
(0065)     129  READ(11,111)(ZETAN(IX,IY,3),IX=1,IXMAX)
(0066)          READ(11,113)RE,TIME,TAU,XPS,XZT,REMAX,YY,XIM,XNM,XYMAX,COF
(0067)         $     ,XLL1,XLL2,XLL3
(0068)          IIM=XIM
(0069)          IYY=XYMAX
(0070)          NM=XNM
(0071)          LL1=XLL1
(0072)          LL2=XLL2
(0073)          LL3=XLL3
(0074)          IPS=XPS
(0075)          IZT=XZT
(0076)          DO 100 IX=1,IXMAX
(0077)          DO 100 IY=1,IYMAX
(0078)          ZETAN(IX,IY,2)=ZETAN(IX,IY,3)
(0079)          ZETAN(IX,IY,1)=ZETAN(IX,IY,2)
(0080)     100  PSIN(IX,IY,1)=PSIN(IX,IY,2)
(0081)          DO 110 IY=2,IYM1
(0082)          IN1=2
(0083)            P=IXM1
(0084)          IF(IY.GE.LX)IN1=LY
(0085)          IF(IY.GE.LX)INP=LZ
(0086)          DO 110 IX=IN1,INP
(0087)          DAA(IX,IY)=REMAX*ABN(IX,IY)
(0088)     110  DBB(IX,IY)=DAA(IX,IY)/SIC(IX,IY)
(0089)          NM=0
(0090)  C
(0091)  C       ********************  FA 9-POINT COEFFICIENTS IN THE STREAM
(0092)  C                                 FUNCTION DOMAIN.
(0093)  C
(0094)          DO 251 IY=2,IYM1
(0095)          IN1=2
(0096)          INP=IXM1
(0097)          IF(IY.GE.LX)IN1=LY
(0098)          IF(IY.GE.LX)INP=LZ
(0099)          DO 251 IX=IN1,INP
(0100)          AU=SIA(IX,IY)
(0101)          BV=SIB(IX,IY)
(0102)          CSI=SIC(IX,IY)
(0103)     251  CALL PSICOE(AU,BV,CSI,HX,HY,IX,IY)
(0104)  C
(0105)  C       ***************  FIRST DERIVATIVES OF STREAM FUNCTION ON THE
(0106)  C                        TRANSFORMED DOMAIN.
(0107)  C
(0108)          DO 1200 IT=1,IEND
(0109)          TIME=TIME+TAU
(0110)          WRITE(6,600)TIME
(0111)          NM=NM+1
(0112)          DO 175 IY=2,IIM
(0113)          IN1=2
(0114)          INP=IXM1
(0115)          IF(IY.GE.LX)IN1=LY
(0116)          IF(IY.GE.LY)INP=LZ
(0117)          DO 175 IX=IN1,INP
(0118)          PE(IX,IY)=(PSIN(IX,IY+1,2)-PSIN(IX,IY-1,2))/3.0D0/HY+(PSIN(IX+1,
(0119)         $IY+1,2)+PSIN(IX-1,IY+1,2)-PSIN(IX+1,IY-1,2)-PSIN(IX-1,IY-1,2))/
(0120)         $12.0D0/HY
```

ORIGINAL PAGE IS
OF POOR QUALITY

```
C                C-4 UNSTEADY FLOW PROGRAM

(0121)   175  PZ(IX,IY)=-((PSIN(IX-1,IY+2)-PSIN(IX+1,IY+2))/3.000/HX+(PSIN(IX-1,
(0122)       $IY+1,2)+PSIN(IX-1,IY-1,2)-PSIN(IX+1,IY+1,2)-PSIN(IX+1,IY-1,2))/
(0123)       $12.000/HX)
(0124)  C
(0125)  C     ************** FA 9-POINT COEFFICIENTS IN THE VORTICITY
(0126)  C                      DOMAIN.
(0127)  C
(0128)        DO 200 IY=2,IIM
(0129)        IN1=2
(0130)        INP=IXM1
(0131)        IF(IY.GE.LX)IN1=LY
(0132)        IF(IY.GE.LX)INP=LZ
(0133)        DO 201 IX=IN1,INP
(0134)        LL=LL1
(0135)        IF(IX.GE.20)LL=LL2
(0136)        AU=SIA(IX,IY)+DAA(IX,IY)+PE(IX,IY)
(0137)        BV=SIB(IX,IY)-DPB(IX,IY)+PZ(IX,IY)
(0138)        CSI=SIC(IX,IY)
(0139)        CALL COEFF(AU,BV,CSI,HX,HY,IX,IY,LL)
(0140)    201 CONTINUE
(0141)    200 CONTINUE
(0142)  C
(0143)  C     ********************  VORTICITY BOUNDARY CONDITIONS ON THE
(0144)  C                              BODY SURFACE.
(0145)  C
(0146)        DO 419 IX=2,IXM1
(0147)    419 ZETAN(IX,1,2)=-2.00*DCR(IX)*(PSIN(IX,2,2)-PF(IX,1)*COF)
(0148)       $    *RE/RENAX
(0149)        ZETAN(IXMAX,1,2)=ZETAN(2,1,2)
(0150)        ZETAN(1,1,2)=ZETAN(IXM1,1,2)
(0151)  C
(0152)  C     *****************  VORTICITY FIELD, USING LINE BY LINE ITERATION.
(0153)  C
(0154)        DO 421 IY=2,IIM
(0155)        IN1=2
(0156)        INP=IXM1
(0157)        IF(IY.GE.LX)IN1=LY
(0158)        IF(IY.GE.LX)INP=LZ
(0159)        DO 421 IX=IN1,INP
(0160)    421 ZT(IX,IY)=1.000+CP0P0(IX,IY)*F1(IX,IY)*RENAX/TAU
(0161)        N3=1
(0162)        N4=1
(0163)        N2=1
(0164)    305 SMZET=0.000
(0165)        DO 306 JY=2,IIM
(0166)        IY=2+IIM-JY
(0167)        IF(N4.EQ.2)IY=JY
(0168)        IN1=2
(0169)        INP=IXM1
(0170)        IF(IY.GE.LX)IN1=LY
(0171)        IF(IY.GE.LX)INP=LZ
(0172)        DO 320 JX=IN1,INP
(0173)        IX=IN1+INP-JX
(0174)        IF(N4.EQ.2)IX=JX
(0175)        ZETEZ=0.2500*(ZETAN(IX+1,IY+1,2)-ZETAN(IX-1,IY+1,2)+
(0176)       1                    ZETAN(IX-1,IY-1,2)-ZETAN(IX+1,IY-1,2))
(0177)        AA(IX)=-CM(P0(IX,IY)/ZT(IX,IY)
(0178)        BB(IX)=1.000
(0179)        CC(IX)=-CP1P0(IX,IY)/ZT(IX,IY)
(0180)    320 DD(IX)=(CP0P1(IX,IY)*ZETAN(IX,IY+1,2)+CP0M1(IX,IY)*ZETAN(IX,
```

ORIGINAL PAGE IS
OF POOR QUALITY

```
C                 C-4 UNSTEADY FLOW PROGRAM

((181)        $IY-1,2)+CP1P1(IX,IY)*ZETAN(IX+1,IY+1,2)+CP1M1(IX,IY)*ZETAN
((182)        $(IX+1,IY-1,2)+CM1P1(IX,IY)*ZETAN(IX-1,IY+1,2)+CM1M1(IX,IY)*ZETAN
((183)        $(I)-1,IY-1,2)+(ZT(IX,IY)-1.0)*ZETAN(IX,IY,3)-2.D0*F2(IX,IY)
((184)        $*ZETEZ*CP0P0(IX,IY))/ZT(IX,IY)
((185)         DD(IN1)=DD(IN1)-AA(IN1)*ZETAN(IN1-1,IY,2)
((186)         DD(INP)=DD(INP)-CC(INP)*ZETAN(INP+1,IY,2)
((187)         CALL TRIDAG(IN1,INP,AA,BB,CC,DD,T)
((188)         DO 330 IX=IN1,INP
((189)         ZETAN(IX,IY,2)=T(IX)
((190)   330  CONTINUE
((191)         IF(IY.LE.11)GO TO 554
((192)         GO TO 306
((193)    554 ZETAN(1,IY,2)=ZETAN(IXM1,IY,2)
((194)         ZETAN(2,IY,2)=ZETAN(IXMAX,IY,2)
((195)    306 CONTINUE
((196)  C
((197)  C     ******************** CHECK FOR CONVERGENCE.
((198)  C
((199)         DO 309 IY=2,15
((200)         DO 309 IX=LY,LZ
((201)         DEZET=ZETAN(IX,IY,2)-ZETAN(IX,IY,1)
((202)         IF(DABS(DEZET).GT.DABS(SMZET))SMZET=DEZET
((203)    309 CONTINUE
((204)         DO 500 IY=2,15
((205)         DO 500 IX=LY,LZ
((206)    500 ZETAN(IX,IY,1)=ZETAN(IX,IY,2)
((207)         IF(CABS(SMZET).LT.0.00001)GO TO 1408
((208)         IF(N2.GE.IZT)GO TO 1408
((209)         IF(N4.EQ.2)N4=0
((210)         N2=N2+1
((211)         N4=N4+1
((212)         GO TO 305
((213)   1408 N1=1
((214)         DO 510 IY=2,IIM
((215)         IN1=2
((216)         INP=IXM1
((217)         IF(IY.GE.LX)IN1=LY
((218)         IF(IY.GE.LX)INP=LZ
((219)         DO 510 IX=IN1,INP
((220)    510 AF(IX,IY)=F1(IX,IY)+ZETAN(IX,IY,2)
((221)  C
((222)  C     ************** STREAM FUNCTION FIELD USING LINE BY LINE ITERATION.
((223)  C
((224)   1405 SMPSI=0.000
((225)         DO 1406 JY=2,IIM
((226)         IY=2+IIM-JY
((227)         IF(N3.EQ.2)IY=JY
((228)         IN1=2
((229)         INP=IXM1
((230)         IF(IY.GE.LX)IN1=LY
((231)         IF(IY.GE.LX)INP=LZ
((232)         DO 1421 JX=IN1,INP
((233)         IX=IN1+INP-JX
((234)         IF(N3.EQ.2)IY=JY
((235)         PSIEZ=0.2500*(PSIN(IX+1,IY+1,2)-PSIN(IX-1,IY+1,2)+
((236)        1                 PSIN(IX-1,IY-1,2)-PSIN(IX+1,IY-1,2))
((237)         FF(IX,IY)=2.D0*F2(IX,IY)*PSIEZ-AF(IX,IY)
((238)         AA(IX)=-PCM1P0(IX,IY)
((239)         BB(IX)=1.000
((240)         CC(IX)=-PCP1P0(IX,IY)
```

ORIGINAL PAGE IS
OF POOR QUALITY

```
C                D-4 UNSTEADY FLOW PROGRAM

 1421 DD(IX)=PCP0P1(IX,IY)*PSIN(IX,IY+1,2)+PCP0M1(IX,IY)*PSIN(IX,
     $IY-1,2)+PCP1P1(IX,IY)*PSIN(IX+1,IY+1,2)+PCP1M1(IX,IY)*PSIN
     $(IX+1,IY-1,2)+PCM1P1(IX,IY)*PSIN(IX-1,IY+1,2)+PCM1M1(IX,IY)*PSIN
     $(IX-1,IY-1,2)-PCP0P0(IX,IY)*FF(IX,IY)
      DD(IN1)=DD(IN1)-AA(IN1)*PSIN(IN1-1,IY,2)
      DD(INP)=DD(INP)-CC(INP)*PSIN(INP+1,IY,2)
      CALL TRIDAG(IN1,INP,AA,BB,CC,DD,T)
      DO 1431 IX=IN1,INP
      PSIN(IX,IY,3)=T(IX)
      PSIN(IX,IY,2)=PSIN(IX,IY,2)+(PSIN(IX,IY,3)-PSIN(IX,IY,2))*YY
 1431 CONTINUE
      IF(IY.LE.11)GO TO 1415
      GO TO 1406
 1415 PSIN(1,IY,2)=PSIN(IXM1,IY,2)
      PSIN(2,IY,2)=PSIN(IXMAX,IY,2)
 1406 CONTINUE
C
C     ***************  CHECK FOR CONVERGENCE.
C
      DO 1425 IY=2,15
      DO 1425 IX=LY,LZ
      DEPSI=PSIN(IX,IY,2)-PSIN(IX,IY,1)
      IF(CABS(DEPSI).GT.DABS(SMPSI))SMPSI=DEPSI
 1425 CONTINUE
      DO 1505 IY=2,15
      DO 1505 IX=LY,LZ
 1505 PSIN(IX,IY,1)=PSIN(IX,IY,2)
      IF(CABS(SMPSI).LT.0.00001)GO TO 275
      IF(N1.GE.IPS)GO TO 275
      IF(N3.EQ.2)N3=0
      N1=N1+1
      N3=N3+1
      GO TO 1405
C
C     ***************  THE NUMERICAL RESULTS OF STREAM FUNCTION AND
C                         VORTICITY VALUES AT EACH TIME STEP.
C
  275 WRITE(6,1002)SMZET,N2
      WRITE(6,1002)SMPSI,N1
      DO 501 IY=2,IIM
      IN1=2
      INP=IXM1
      IF(IY.GE.LX)IN1=LY
      IF(IY.GE.LX)INP=LZ
      DO 501 IX=IN1,INP
  501 ZETAN(IX,IY,3)=ZETAN(IX,IY,2)
      IF(IT.EQ.20)NM=4
      IF(IT.EQ.30)NM=3
      IF(IT.EQ.40)NM=2
      IF(IT.EQ.50)NM=1
      IF(MM.LT.NM)GO TO 1200
      MM=0
      IIP=IIM+5
      IF(IIM.GE.IYY)IIM=IYY
      LL1=LL1+1
      LL2=LL2+1
      IF(LL1.GE.LL3)LL1=LL3
      IF(LL2.GE.LL3)LL2=LL3
      RE=RE+2.D0
      IF(RE.GE.REMAX)RE=REMAX
```

ORIGINAL PAGE IS
OF POOR QUALITY


```
C                    C-4 UNSTEADY FLOW PROGRAM

(0301)          DO 700 IY=1,IYMAX
(0302)          IF(IY.GE.3)GO TO 700
(0303)          WRITE(6,112)IY
(0304)      700 WRITE(6,111)(PSIN(IX,IY,2),IX=1,IXMAX)
(0305)          DO 800 IY=1,IYMAX
(0306)          IF(IY.GE.3)GO TO 800
(0307)          WRITE(6,112)IY
(0308)      800 WRITE(6,111)(ZETAN(IX,IY,2),IX=1,IXMAX)
(0309)          WRITE(6,1001)RE
(0310)      111 FORMAT(7F11.6)
(0311)      112 FORMAT(1X,'I2=',I3)
(0312)      600 FORMAT(//,5X,'VAL OF TIME=',F11.6)
(0313)     1002 FORMAT(15X,'ERR=',F15.8,5X,'N=',I5)
(0314)     1001 FORMAT(//,15X,'RE=',F10.5)
(0315)     1200 CONTINUE
(0316)          CALL EXIT
(0317)          END
PROGRAM SIZE:   PROCEDURE - 004330    LINKAGE - 000526    STACK - 000102
0000 ERRORS [<.MAIN.>FTN-REV18.3]
```

ORIGINAL PAGE IS
OF POOR QUALITY

```
(0001)  C                    D-T: POTENTIAL FLD.


(0121)     505 PSIN(IY,IY,1)=PSIN(IX,IY,2)
(0122)         IF(N1.GE.300)GO TO 5000
(0123)         IF(CABS(SMPSI).LT.0.000001)GO TO 5000
(0124)         N1=N1+1
(0125)         GO TO 505
(0126)  C
(0127)  C     ********************** POTENTIAL STREAM FUNCTION
(0128)  C                                 -- THE FILE 'BEST'
(0129)  C
(0130)    5000 WRITE(6,110)N1,SMPSI
(0131)         DO 700 IY=1,IYMAX
(0132)     700 WRITE(6,111)(PSIN(IY,IY,2),IX=1,IXMAX)
(0133)     110 FORMAT('N=',I5,5X,'ERR=',F11.6)
(0134)     111 FORMAT(7F11.6)
(0135)     112 FORMAT(14,'IC=',I3)
(0136)         CALL EXIT
(0137)         END
PROGRAM SIZE:   PROCEDURE = 001712    LINKAGE = 002276    STACK = 00.376
0000 ERRORS [<,MAIN,>FTN-PF/13.32]
```

ORIGINAL PAGE IS
OF POOR QUALITY

```
C

(0138)  C
(0139)  C     ***********************************************************
(0140)  C
(0141)  SUBROUTINE TRIDAG
(0142)  C
(0143)  C     SUBROUTINE FOR SOLVING A SYSTEM OF LINEAR SIMULTANEOUS
(0144)  C     EQUATIONS HAVING A TRIDIAGONAL COEFFICIENT MATRIX.
(0145)  C
(0146)  C     THE EQUATIONS ARE NUMBERED FROM IF THROUGH L, AND THEIR
(0147)  C     SUB-DIAGONAL, DIAGONAL, AND SUPER-DIAGONAL COEFFICIENTS
(0148)  C     ARE STORED IN THE ARRAYS A, B, AND C. THE COMPUTED
(0149)  C     SOLUTION VECTOR V(IF)......V(L) IS STORED IN THE ARRAY V.
(0150)  C
(0151)  C     ***********************************************************
(0152)  C
(0153)        SUBROUTINE TRIDAG(IF,L,A,B,C,D,V)
(0154)        IMPLICIT REAL*8(A-H,O-Z)
(0155)        DIMENSION A(62),B(62),C(62),D(62),V(62),BETA(62),GAMMA(62)
(0156)        BETA(IF)=B(IF)
(0157)        GAMMA(IF)=D(IF)/BETA(IF)
(0158)        IFP1=IF+1
(0159)        DO 1 I=IFP1,L
(0160)        BETA(I)=B(I)-A(I)*C(I-1)/BETA(I-1)
(0161)      1 GAMMA(I)=(D(I)-A(I)*GAMMA(I-1))/BETA(I)
(0162)        V(L)=GAMMA(L)
(0163)        LAST=L-IF
(0164)        DO 2 K=1,LAST
(0165)        I=L-K
(0166)      2 V(I)=GAMMA(I)-C(I)*V(I+1)/BETA(I)
(0167)        RETURN
(0168)        END
PROGRAM SIZE:   PROCEDURE = 000221    LITERAL = 001000    STACK = 000074
0001 ERRORS C:TRIDAG.BETA=REV1.33
```

ORIGINAL PAGE IS
OF POOR QUALITY

```
C
(0169)  C
(0170)  C     ***********************************************************
(0171)  C
(0172)  SUBROUTINE PSICOE(COEFF)
(0173)  C
(0174)  C     SUBROUTINE FOR SOLVING FA 9-POINT COEFFICIENTS.
(0175)  C
(0176)  C     ***********************************************************
(0177)  C
(0178)        SUBROUTINE PSICOE(A,B,C,DM,DK,IY,IY)
(0179)        IMPLICIT REAL*8(A-H,O-Z)
(0180)        COMMON/PSIC/PCM1P1(40,41),PCM1P0(40,41),PCM1M1(40,41),
(0181)       1PCP(P1(40,41),PCP0M1(40,41),PCP1P1(40,41),PCP1P0(40,41),
(0182)       2PCP1M1(40,41),PCP0P0(40,41)
(0183)        PI=3.1415926535897932D0
(0184)        EPE=0.000001
(0185)        AH=2*DM
(0186)        BK=2*DK
(0187)        EPA=EPE
(0188)        IF(AH.LT.0.)EPA=-EPE
(0189)        EPB=EPE
(0190)        IF(BK.LT.0.)EPB=-EPE
(0191)        IF(CABS(AH).LT.EPE)AH=EPA
(0192)        IF(CABS(BK).LT.EPE)BK=EPB
(0193)        AHS=AH*AH
(0194)        BKC=BK*BK
(0195)        BKSC=BKS*C
(0196)        NM=10
(0197)        IF(C.LT.1.0)GO TO 33
(0198)        E2M=0.
(0199)        DO 20 M=1,NM
(0200)        N=2*M-1
(0201)        P.N=(-1.)**M
(0202)        AN=FLOAT(N)
(0203)        ELAM=AN*PI*0.5
(0204)        ELAM2=ELAM*ELAM
(0205)        EXUPK=DSQRT(AHS+BKSC+ELAM2*C)
(0206)        COSHP=.5D0*(DEXP(EXUPK)+DEXP(-EXUPK))
(0207)        E2M=-PMN*ELAM/((BKS+ELAM2)**2.D)/COSHP+E2M
(0208)   20   CONTINUE
(0209)        EXPAM=DEXP(AH)
(0210)        EXPBK=DEXP(BK)
(0211)        COSAH=0.5*EXPAM+0.5/EXPAM
(0212)        COSBK=0.5*EXPBK+0.5/EXPBK
(0213)        COTAH=(EXPAM*EXPAM+1.D)/(EXPAM*EXPAM-1.D)
(0214)        COTBK=(EXPBK*EXPBK+1.D)/(EXPBK*EXPBK-1.D)
(0215)        E2=(E2M+(BK*C/COTAH-AH/COTBK))/(4.D*AH*BK*COSAH*COSBK))/C
(0216)        GO TO 44
(0217)   33   E2=0.
(0218)        DO 30 M=1,NM
(0219)        N=2*M-1
(0220)        P.N=(-1.)**M
(0221)        AN=FLOAT(N)
(0222)        ELAM=AN*PI*0.5
(0223)        ELAM2=ELAM*ELAM
(0224)        EXUPK=DSQRT(ELAM2*C)
(0225)        COSHP=.5D0*(DEXP(EXUPK)+DEXP(-EXUPK))
(0226)        E2=-PMN*ELAM/((AHS+ELAM2)**2.D)/COSHP+E2
(0227)   30   CONTINUE
(0228)        EXPAM=DEXP(AH)
```

ORIGINAL PAGE IS
OF POOR QUALITY

```
C

      EXPBK=DEXP(BK)
      COSAH=0.5*EXPAH+0.5/EXPAH
      COSBK=0.5*EXPBK+0.5/EXPBK
      COTAH=(EXPAH*EXPAH+1.0)/(EXPAH*EXPAH-1.0)
      COTBK=(EXPBK*EXPBK+1.0)/(EXPBK*EXPBK-1.0)
      E2=SC*SC-(BK*C/COTAH-AH/COTBK)/(4.0*AH*BK*COSAH*COSBK)
   44 E3=2.0*AH*COSAH*COTAH*E2
      E0=2.0*BK*COSBK*COTBK*E2P
      E=0.25/(COSAH*COSBK)-AH*COTAH*E0-BK*COTBK*E0P
      PCM1P1(IX,IY)=E*EXPAH/EXPBK
      PCM1P0(IX,IY)=E3*EXPAH
      PCM1M1(IX,IY)=E*EXPAH*EXPBK
      PCPCP1(IX,IY)=E/EXPBK
      PCPCM1(IX,IY)=E*EXPBK
      PCP1P1(IX,IY)=E/EXPAH/EXPBK
      PCP1P0(IX,IY)=E3/EXPAH
      PCP1M1(IX,IY)=E/EXPAH*EXPBK
      PCPCP0(IX,IY)=(0.5*AH*(PCM1P1(IX,IY)+PCM1P0(IY,IY)+PCM1M1(IX,IY)
     1                  -PCP1P1(IX,IY)-PCP1P0(IX,IY)-PCP1M1(IX,IY))+
     2            0.5*BK*(PCM1M1(IX,IY)+PCPCM1(IX,IY)+PCP1M1(IX,IY)
     3                  -PCP1P1(IX,IY)-PCPCP1(IX,IY)-PCM1P1(IY,IY)))/
     4              (AHS+BKS*SC)
      RETURN
      END
PROGRAM SIZE:   PROCEDURE = 001312    LINKAGE = 000242    STACK = 00.104
0001 ERRORS C<PSICOE>FTN-REV19.37
```

ORIGINAL PAGE IS
OF POOR QUALITY

C D-5 CONTOUR PLOT

```
C            D-5 CONTOUR PLOT
C
C
C
C      THIS PROGRAM IS USED TO GRAPH STREAM LINE OR
C      EQUAL-VORTICITY FUNCTION FROM TRANSFORMED
C      PLANE BACK TO PHYSICAL PLANE.
C
C     ***********************************************************
C
MAIN PROGRAM
C
C
//AEGSUNG4 JOB (********,20),*EE /MEAG*,TIME=1
/*PASSWORD      ****
/*ROUTE   PRINT LO/AL
//S1 EXE/ FORCISVT,REGION.GO=380K
//FORT.SYSIN DD *
      COMMON PSIC(30),P00(40,41),XXC(61),YYC(61)
      COMMON/AAA/PSI(40,41),X(40,41),Y(40,41),XC(1000),YC(1000),ITO
      COMMON/BBB/XMKV(40,41)
      CALL VERSTC
      READ(5,1500)(PSIC(I),I=1,14)
      DO 30 J=1,41
      READ(5,1000)(X(I,J),I=1,40)
      READ(5,1000)(Y(I,J),I=1,40)
   30 CONTINUE
      DO 145 LLN=1,1
      DO 135 P=1,4
      READ(5,1100)XPHYS,YPHYS
      IF((XPHYS+YPHYS).LT.0.000001)GO TO 145
      DO 700 IY=1,41
  700 READ(5,1100)(PSI(IX,IY),IX=1,40)
      CALL BGNPL(0)
      CALL SETDEV(0,0)
      CALL NOCROR
      CALL PHYSOR(XPHYS,YPHYS)
      CALL TITLE(* *,1,*XS*,100,*YS*,100,5.0,1.0)
      CALL GRAF(-2.0,2.0,18.0,-2.0,2.5,2.0)
      CALL POLYS
      DO 41 I=1,40
      J=1
      XXC(I)=X(I,J)
   41 YYC(I)=Y(I,J)
      CALL CURVE(XXC,YYC,40,0)
      DO 300 IY=1,41
      DO 300 IX=1,40
  300 XMKV(IX,IY)=0.0
      IY=34
      DO 5100 N=1,14
      DO 5000 IX=11,31
      NP=1
      IT=2
      ID=1
      CALL CHECK(IX,IY,PSIC(N),IT,ID,NP)
      IF(ATO.GT.1)GO TO 5010
 5000 CONTINUE
      GO TO 5100
 5010 CALL PATH(IX,IY,PSIC(N),IT,ID,NP)
 5100 CONTINUE
```

ORIGINAL PAGE IS
OF POOR QUALITY

```
C              -9 CONTOUR PLOT

((061)          IY=2
((062)      20  DO 100 N=1,10
((063)          DO 200 IX=12,30
((064)          IF(XMNV(IX,IY).GT.1.0)GO TO 800
((065)          NP=1
((066)          IT=1
((067)          ID=1
((068)          CALL CHECK(IX,IY,PSIC(N),IT,ID,NP)
((069)          IF(NTO.NT.1)GO TO 810
((070)      80  CONTINUE
((071)          GO TO 130
((072)     810  CALL PATH(IX,IY,PSIC(N),IT,ID,NP)
((073)     100  CONTINUE
((074)          IY=IY+1
((075)          IF(IY.GE.20)GO TO 211
((076)          GO TO 210
((077)     211  CALL FRAME
((078)          CALL ENDSR(0)
((079)     130  CONTINUE
((080)          CALL ENDPL(0)
((081)     140  CONTINUE
((082)          CALL CONEPL
((083)    1000  FORMAT(F10.5)
((084)    1100  FORMAT(7F11.6)
((085)    1200  FORMAT(3I11)
((086)    1500  FORMAT(7F11.7)
((087)          STOP
((088)          END
PROGRAM SIZE:   PROCEDURE - 001002   -LINKAGE - 000156    STACK - 000344
0001 ERRORS [<,PAIN,>FTN-REV1A.3]
```

ORIGINAL PAGE IS
OF POOR QUALITY

C

```
C
C     ***********************************************************
C
SUBROUTINE PATH
C
C      THIS SUBROUTINE IS USED TO FIND OUT THE PATH OF THE CURVE.
C
C     ***********************************************************
C
C
      SUBROUTINE PATH(IX,IY,PSIC,IT,ID,NP)
      COMMON/AAA/PSI(40,41),X(40,41),Y(40,41),XC(1000),YC(1000),ATO
      COMMON/BBB/XMKV(40,41)
      XMKV(IX,IY)=3.0
      IX1=IX
      IY1=IY
      LN=1
      NP=NP+1
  860 ID=2
      CALL CHECK(IX,IY,PSIC,IT,ID,NP)
      IF(ATO.GT.1)GO TO 55
      IF(LN.GT.2)GO TO 850
      GO TO 920
   55 NP=NP+1
      IT=IT+1
      ID=1
      CALL CHECK(IX,IY,PSIC,IT,ID,NP)
      LN=2
      IF(ATO.LT.1)GO TO 860
      LN=1
      NP=NP+1
  850 IF(IT.EQ.1)IY=IY-1
      IF(IT.EQ.2)IX=IX-1
      IF(IT.EQ.3)IY=IY+1
      IF(IT.EQ.4)IX=IX+1
      IF(IT.EQ.1)GO TO 901
      IF(IT.EQ.2)GO TO 902
      IF(IT.EQ.3)GO TO 903
      IF(IT.EQ.4)GO TO 904
  901 IT=3
      GO TO 900
  902 IT=4
      GO TO 900
  903 IT=1
      GO TO 900
  904 IT=2
  900 IF(IY.GE.35)GO TO 850
      IF(AP.GT.220)GO TO 850
      IF(IX.LE.5)GO TO 66
      IF(IX.GE.37)GO TO 46
      GO TO 86
   66 IF(IY.GE.11)GO TO 850
   86 XMKV(IX,IY)=3.0
      IF(IX.EQ.IX1)GO TO 88
      GO TO 87
   88 IF(IY.EQ.IY1)GO TO 850
   87 GO TO 860
  920 ID=3
      CALL CHECK(IX,IY,PSIC,IT,ID,NP)
      IF(ATO.LT.1)GO TO 950
```

ORIGINAL PAGE IS
OF POOR QUALITY

```
C

(0149)          NP=NP+1
(0150)          IT=IT-1
(0151)          ID=1
(0152)          CALL CHECK(IX,IY,PSIC,IT,ID,NP)
(0153)          IF(NTO.LT.1)GO TO 820
(0154)          NP=NP+1
(0155)          GO TO A30
(0156)      850 N1=NP-1
(0157)          CALL CURVE(XC,YC,N1,0)
(0158)          IX=IX1
(0159)          IY=IY1
(0160)      851 RETURN
(0161)          END
PROGRAM SIZE:   PROCEDURE - 000034    LINKAGE - 000054    STACK - 000064
3C01 ERRORS [<PATH  >FTN-REV1R.3]
```

ORIGINAL PAGE IS
OF POOR QUALITY

```
C

C
C     ***********************************************************
C
SUBROUTINE CHECK
C
C      THIS SUBROUTINE IS USED TO CHECK WHETHER  THE CURVE LINE WOULD
C      THROUGH TWO FIXED NODES OR NOT.
C
C     ***********************************************************
C
C
      SUBROUTINE CHECK(IX,IY,PSIC,IT,ID,NP)
      COMMON/AAA/PSI(40,41),Y(40,41),Y(40,41),XC(1000),YC(1000),NTO
      S3=0.25*(PSI(IX,IY)+PSI(IX+1,IY)+PSI(IX,IY+1)+PSI(IX+1,IY+1))
      NTO=0
      IF(IT.GT.4)IT=IT-4
      IF(IT.LT.1)IT=IT+4
      IF(IT.EQ.1)GO TO 11
      IF(IT.EQ.2)GO TO 12
      IF(IT.EQ.3)GO TO 13
      IF(IT.EQ.4)GO TO 14
   11 S1=PSI(IX+1,IY)
      S2=PSI(IX,IY)
      GO TO 15
   12 S1=PSI(IX,IY)
      S2=PSI(IX,IY+1)
      GO TO 15
   13 S1=PSI(IX,IY+1)
      S2=PSI(IX+1,IY+1)
      GO TO 15
   14 S1=PSI(IX+1,IY+1)
      S2=PSI(IX+1,IY)
   15 IF(ID.EQ.1)GO TO 21
      IF(ID.EQ.2)GO TO 22
      IF(ID.EQ.3)GO TO 23
   21 D1=PSIC-S1
      D2=PSIC-S2
      GO TO 24
   22 D1=PSIC-S2
      D2=PSIC-S3
      GO TO 24
   23 D1=PSIC-S3
      D2=PSIC-S1
   24 CK=D1*D2
      IF(CK.GE.0.0)GO TO 113
      D=D1/(D1-D2)
      IF(IT.EQ.1)GO TO 31
      IF(IT.EQ.2)GO TO 32
      IF(IT.EQ.3)GO TO 33
      IF(IT.EQ.4)GO TO 34
   31 IF(ID.EQ.1)GO TO 311
      IF(ID.EQ.2)GO TO 312
      IF(ID.EQ.3)GO TO 313
   32 IF(ID.EQ.1)GO TO 321
      IF(ID.EQ.2)GO TO 322
      IF(ID.EQ.3)GO TO 323
   33 IF(ID.EQ.1)GO TO 331
      IF(ID.EQ.2)GO TO 332
      IF(ID.EQ.3)GO TO 333
   34 IF(ID.EQ.1)GO TO 341
```

ORIGINAL PAGE IS
OF POOR QUALITY

```
C
(0222)          IF(ID.EQ.2)GO TO 342
(0223)          IF(ID.EQ.3)GO TO 343
(0224)      311 ZK=1.-D
(0225)          EK=0.
(0226)          GO TO 45
(0227)      312 ZK=C/2.
(0228)          EK=C/2.
(0229)          GO TO 45
(0230)      313 ZK=(1.+D)/2.
(0231)          EK=(1.-C)/2.
(0232)          GO TO 45
(0233)      321 ZK=0.
(0234)          EK=C
(0235)          GO TO 45
(0236)      322 ZK=C/2.
(0237)          EK=1.-D/2.
(0238)          GO TO 45
(0239)      323 ZK=(1.-C)/2.
(0240)          EK=(1.-D)/2.
(0241)          GO TO 45
(0242)      331 ZK=C
(0243)          EK=1.
(0244)          GO TO 45
(0245)      332 ZK=1.-D/2.
(0246)          EK=1.-D/2.
(0247)          GO TO 45
(0248)      333 ZK=(1.-D)/2.
(0249)          EK=(1.+D)/2.
(0250)          GO TO 45
(0251)      341 ZK=1.
(0252)          EK=1.-D
(0253)          GO TO 45
(0254)      342 ZK=1.-D/2.
(0255)          EK=C/2.
(0256)          GO TO 45
(0257)      343 ZK=(1.+D)/2.
(0258)          EK=(1.+D)/2.
(0259)       45 CALL XY(ZK,EK,IX,IY,NP)
(0260)          NTC=2
(0261)      113 RETURN
(0262)          END
PROGRAM SIZE:   PROCEDURE - 000640    LINKAGE - 000064    STACK - 000066
0(01 ERRORS [<CHECK >FTN-REV18.3]
```

ORIGINAL PAGE IS
OF POOR QUALITY

```
C

(0263)  C
(0264)  C     ***********************************************************
(0265)  C
(0266)  SUBROUTINE XY
(0267)  C
(0268)  C       THIS SUBROUTINE IS USED TO LOCATE THE CURVE LINE ON
(0269)  C       THE PHYSICAL PLANE.
(0270)  C
(0271)  C     ***********************************************************
(0272)  C
(0273)          SUBROUTINE XY(ZK,EK,IX,IY,NF)
(0274)          COMMON/AAA/PSI(40,41),X(40,41),Y(40,41),XC(1000),YC(1000),ATO
(0275)          XJ=ZK*(X(IX+1,IY)-X(IX,IY))+X(IX,IY)
(0276)          XJP1=ZK*(X(IX+1,IY+1)-X(IX,IY+1))+X(IX,IY+1)
(0277)          XC(NP)=EK*(XJP1-XJ)+XJ
(0278)          YJ=ZK*(Y(IX+1,IY)-Y(IX,IY))+Y(IX,IY)
(0279)          YJP1=ZK*(Y(IX+1,IY+1)-Y(IX,IY+1))+Y(IX,IY+1)
(0280)          YC(NP)=EK*(YJP1-YJ)+YJ
(0281)          RETURN
(0282)          END
PROGRAM SIZE:   PROCEDURE - 000110    LINKAGE - 000056    STACK - 000064
0001 ERRORS [<XY    >FTN-REV18.3]
```

END

DATE

FILMED

JUN 29 1983